RESEARCH, DEVELOPMENT AND CLINICAL TRIALS FOR PEPTIDES-BASED VACCINES

EDITED BY: Shisong Jiang, Min Gong and Xiaoning Xu
PUBLISHED IN: Frontiers in Immunology

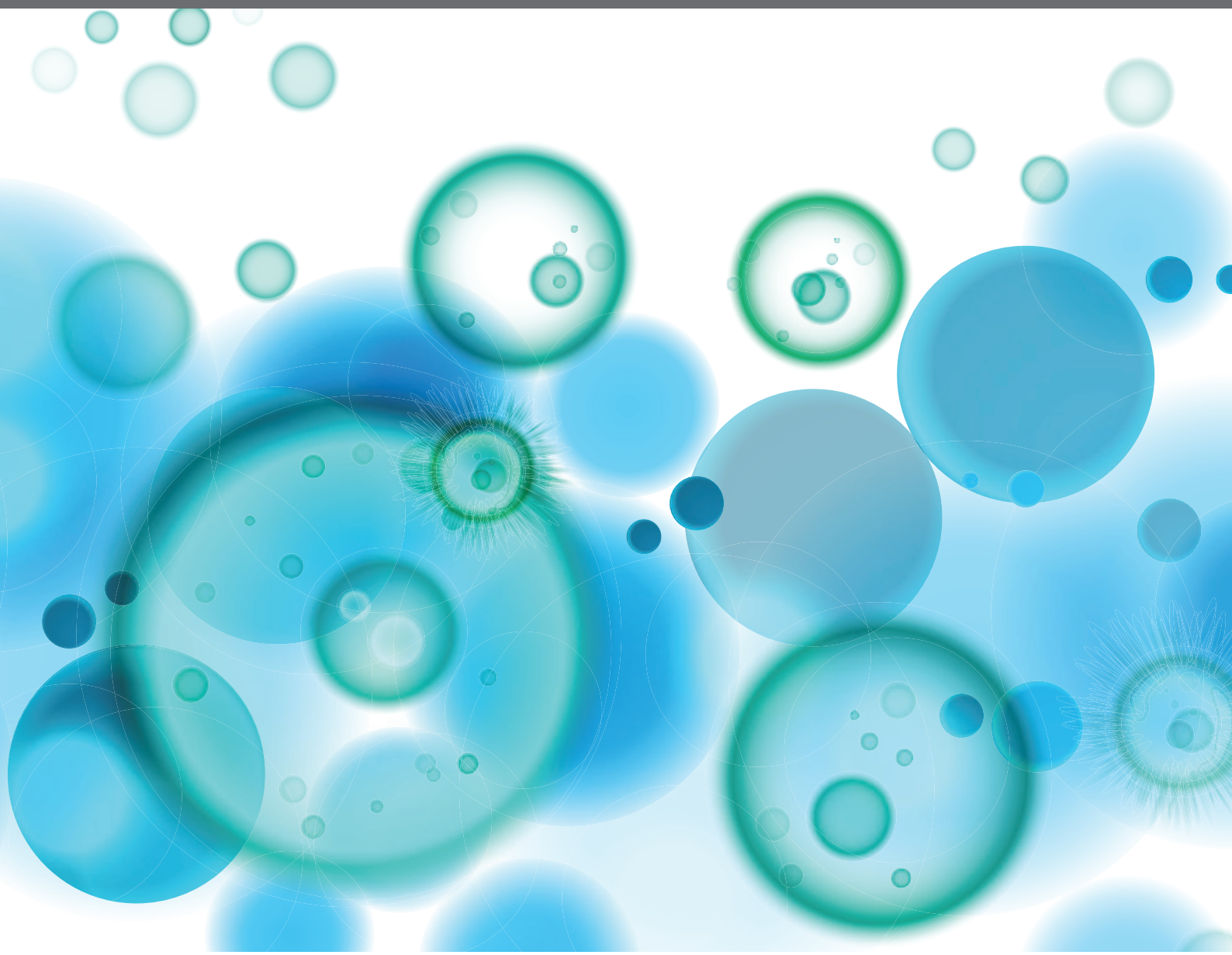

frontiers Research Topics

ISSN 1664-8714
ISBN 978-2-88976-146-3
DOI 10.3389/978-2-88976-146-3

About Frontiers

Frontiers is more than just an open-access publisher of scholarly articles: it is a pioneering approach to the world of academia, radically improving the way scholarly research is managed. The grand vision of Frontiers is a world where all people have an equal opportunity to seek, share and generate knowledge. Frontiers provides immediate and permanent online open access to all its publications, but this alone is not enough to realize our grand goals.

Frontiers Journal Series

The Frontiers Journal Series is a multi-tier and interdisciplinary set of open-access, online journals, promising a paradigm shift from the current review, selection and dissemination processes in academic publishing. All Frontiers journals are driven by researchers for researchers; therefore, they constitute a service to the scholarly community. At the same time, the Frontiers Journal Series operates on a revolutionary invention, the tiered publishing system, initially addressing specific communities of scholars, and gradually climbing up to broader public understanding, thus serving the interests of the lay society, too.

Dedication to Quality

Each Frontiers article is a landmark of the highest quality, thanks to genuinely collaborative interactions between authors and review editors, who include some of the world's best academicians. Research must be certified by peers before entering a stream of knowledge that may eventually reach the public - and shape society; therefore, Frontiers only applies the most rigorous and unbiased reviews.
Frontiers revolutionizes research publishing by freely delivering the most outstanding research, evaluated with no bias from both the academic and social point of view. By applying the most advanced information technologies, Frontiers is catapulting scholarly publishing into a new generation.

What are Frontiers Research Topics?

Frontiers Research Topics are very popular trademarks of the Frontiers Journals Series: they are collections of at least ten articles, all centered on a particular subject. With their unique mix of varied contributions from Original Research to Review Articles, Frontiers Research Topics unify the most influential researchers, the latest key findings and historical advances in a hot research area! Find out more on how to host your own Frontiers Research Topic or contribute to one as an author by contacting the Frontiers Editorial Office: frontiersin.org/about/contact

RESEARCH, DEVELOPMENT AND CLINICAL TRIALS FOR PEPTIDES-BASED VACCINES

Topic Editors:
Shisong Jiang, University of Oxford, United Kingdom
Min Gong, Tianjin Medical University, China
Xiaoning Xu, Imperial College London, United Kingdom

Citation: Jiang, S., Gong, M., Xu, X., eds. (2022). Research, Development and Clinical Trials for Peptides-Based Vaccines. Lausanne: Frontiers Media SA.
doi: 10.3389/978-2-88976-146-3

Table of Contents

frontiers | Frontiers in Immunology

EDITORIAL
published: 22 April 2022
doi: 10.3389/fimmu.2022.894989

Editorial: Research, Development and Clinical Trials for Peptide-Based Vaccines

Shisong Jiang[1]*, *Min Gong*[2] *and Xiao-Ning Xu*[3]

[1] Department of Oncology, University of Oxford, Oxford, United Kingdom, [2] Department of Pharmacy, Tianjin Medical University, Tianjin, China, [3] Faculty of Medicine, Department of Infectious Disease, Imperial College London, London, United Kingdom

Keywords: Peptides, vaccines, epitopes, innate immunity, adoptive immunity, T cells, clinical trials, editorial

Editorial on the Research Topic

Research, Development and Clinical Trials for Peptides-Based Vaccines

From the eradication of smallpox through to the global response to the COVID-19 pandemic, vaccines have been a cornerstone in the fight against infectious diseases in humans and livestock since the 18th century (1). Although vaccines against COVID-19 are unlikely to eradicate the disease in the way that the smallpox vaccine did, they have proved very effective in preventing death and hospitalisation, with enormous societal and economic benefits (2). There is now considerable research effort invested in building on the success of prophylactic vaccines in controlling infectious disease through the development of therapeutic vaccines for chronic diseases such as inflammation and cancer. These approaches are based on down-regulating or up-regulating immune responses for the treatment of inflammatory disease and cancer respectively, through judicious choice of epitopes, adjuvants and mode of the display to the immune system. Though such therapeutic vaccines have shown some early promise, no commercially available products are yet available.

There are six categories of vaccines in use or under development: live attenuated vaccines, inactivated vaccines, subunit vaccines, toxoid vaccines, viral vector-based vaccines, and nucleic acid (DNA or RNA) vaccines (3). In each case, there are multiple examples of vaccines approved for human use. Despite the different modes of delivery of the antigenic payload in these six classes, their common goal is to stimulate one or all of the following types of immune responses: 1) innate immunity, 2) antibody (humoral) immunity, and 3) T cell immunity.

Peptide-based vaccines are a particular type of subunit vaccine usually characterised by a focus on short sequences encompassing single epitopes, normally produced by chemical synthesis. Peptide vaccines have a number of advantages including better defined and more specific immune responses; a good safety profile; simple manufacture and relatively fast drug development (4). Moreover, the sequences of peptide vaccines can be converted into nucleic acids, so they are easily turned into nucleic vaccines or vector-based vaccines. To make peptide vaccines more effective and suitable for industrial manufacture, new forms of peptide-based vaccines are proposed beyond single epitope and beyond chemical synthesis, for example, synthetic long peptide vaccines and recombinant overlapping peptide vaccines (5–7).

OPEN ACCESS

Edited and reviewed by:
Denise L. Doolan,
James Cook University, Australia

***Correspondence:**
Shisong Jiang
shisong.jiang@oncology.ox.ac.uk

Specialty section:
This article was submitted to Vaccines and Molecular Therapeutics, a section of the journal Frontiers in Immunology

Received: *12 March 2022*
Accepted: *01 April 2022*
Published: *22 April 2022*

Citation:
Jiang S, Gong M and Xu X-N (2022) Editorial: Research, Development and Clinical Trials for Peptide-Based Vaccines. Front. Immunol. 13:894989. doi: 10.3389/fimmu.2022.894989

In this collection of eleven articles for Frontiers in Immunology titled "Research, Development, and Clinical Trials for Peptide-based Vaccines" we cover key aspects of peptide vaccine development including epitope selection and vaccine design, conjugation methods and adjuvants, the balance between antibody and T cell immunity, and design of clinical trials.

DESIGN OF PEPTIDE VACCINES AND USE OF EPITOPES

The key starting point for design of peptide vaccines is the choice of epitopes that stimulate humoral and/or T cell immunity. There are several ways of identifying the epitopes.

Overlapping Synthetic Peptides

Jiang et al. used overlapping synthetic peptides covering the target sequence as a library for screening. In this case, they obtained antisera from SARS-CoV-2 receptor binding domain (RBD)-immunised pigs or mice. The antisera were incubated with overlapping peptides covering the RBD to identify those carrying B cell epitopes. The authors then showed that these peptides were immunogenic in their own right and capable of stimulating neutralising antibodies. However, an obvious caveat in the use of this overlapping peptide approach is that it will miss non-sequential conformational epitopes which may play an important role in neutralising targets (8).

Computer Algorithm/Database

Epitopes can be predicted by computer software. Gong et al. picked their potential HLA-DR1 restricted, TB-targeted T cell epitopes from the Immune Epitope Database (IEDB, https://www.iedb.org/) which they then validated using an ELISPOT assay. Instead of using the pooled peptides as a vaccine, they produced a recombinant poly-epitope in which the relevant peptides were joined *via* a flexible linker (GGGGS). In humanised mice, the poly-epitope vaccine generated strong cellular immunity which protected mice from TB infection. The obvious advantage of linking epitopes in this way (over the use of pooled peptides) is that there is only a single product, greatly simplifying quality control during manufacture and regulatory compliance.

Neoantigens: Sequencing + Computer Algorithm

Cancer therapeutic vaccines depend on the identification of tumour-specific neoantigens that can be targeted with peptide-based vaccines. Chen et al. combined next generation sequencing (NGS) with bioinformatics and epitope prediction algorithms to design personalised peptide vaccines. Vaccines designed such way have been tested in seven pancreatic cancer patients with promising results (see clinical study section below).

Processed Pathogens

A novel epitope mapping approach is described by D'haeseleer et al. The authors obtained antisera from mice that had been immunised with a pathogen. The antisera were conjugated to beads which were incubated with trypsinised pathogen as a peptide library. Peptides retained by the beads were subsequently eluted and identified by mass spectroscopy. They validated epitopes identified in this way for two bacterial pathogens (*Francisella tularensis* and *Burkholderia pseudomallei*) and showed that they were immunogenic. Interestingly, they compared their approach with that of computer-based epitope mapping and found that it was more effective at identifying experimentally validated epitopes, even though some computer-picked epitopes gave higher *in silico* scores. However, a necessary limitation of the approach is that it will miss epitopes that carry a tryptic cleavage site.

Recombinant Overlapping Peptides

Zhang et al. used recombinant overlapping peptides (ROPs) from human papilloma virus (HPV) type 16 E7 (ROP-HPV16-E7) as a T cell stimulating agent. Overlapping peptides avoid the boundary problem and must therefore contain all possible T cell epitopes for different MHC phenotypes. As a result, they stimulate broad T cell immunity promiscuously. As ROPs are made as a single protein product in *E.coli*, they benefit from a straightforward manufacturing process and offer a comparatively simple path through preclinical development to regulatory approval.

CONJUGATION AND ADJUVANT OF PEPTIDE VACCINES

In addition to epitopes capable of stimulating B cells, $CD4^+$ and $CD8^+$ T cells, peptide vaccines need strong adjuvants to stimulate innate immunity. Rossi et al. describe results with vaccines based on cell penetrating peptide carrying HPV or ovalbumin (OVA) T cell epitopes combined with stimulator of interferon gamma gene agonist (STINGa) as an adjuvant to elicit a potent innate inflammatory response. This strategy stimulated both $CD8^+$ and Th1 $CD4^+$ T cell responses while inhibiting Treg response. The vaccine was effective in prolonging survival in TC-1 tumour inoculated mice.

Calzas et al. describe a vaccine formulation containing weak but conserved antigens from influenza virus combined with a nanoring comprising elements from respiratory syncytial virus. This 'nanoring' stimulates innate immunity - possibly through TLR5. The vaccine is given *via* the mucosal route and induced strong humoral and cellular immune responses. The vaccine protected mice (but not chickens) from viral challenge.

CLINICAL STUDIES OF PEPTIDE VACCINES

Three of the above articles involved clinical studies. Two of these addressed HPV infection and both show the importance of T cell immunity in recovery and viral clearance. Shibata et al. describe one case in detail emerging from the Phase I clinical trial of their peptide vaccine (PepCan). The patient, who had a high-grade cervical squamous intraepithelial lesion, received four doses of

the peptide vaccine at 4-weeks' interval. While Treg and Th2 cytokine levels remained unchanged, Th1 cytokine levels were enhanced significantly. At twelve weeks (end of the follow-up), the intraepithelial lesion had completely disappeared, potentially due to this enhanced T cell response. Moreover, using single cell sequencing, the authors showed specific $CD3^+$ T cell clonal expansion both systemically and at the lesion site.

In the second HPV-related clinical cohort study, Zhang et al. followed up 131 HPV16-infected patients for 12 months and found that HPV specific T cell immunity is important for the viral clearance.

In the final clinical trial report, Chen et al. investigated the safety and immunogenicity of a neoantigen-based vaccine in seven pancreatic cancer patients. The authors showed that the vaccine was safe and induced both $CD4^+$ and $CD8^+$ T cell responses. One patient exhibiting significant expansion of a reactive T cell clone survived for 21 months, considerably in excess of the expected 6-month average for patients with this stage of disease.

CONCLUSION

Vaccines against infectious disease have to date proved much more successful than vaccines against cancer, essentially because pathogens are non-self and present a much larger immunological target which stimulate strong innate, humoral and cellular immunity. Nonetheless, significant progress has been made in the identification of antigens other than foreign pathogens, e.g., neoantigens and tumour associated antigens (TAA) that can be exploited by vaccine technology, particularly using peptide vaccines. These advances, together with recent developments in the clinical application of IO agents, offer the prospect of personalised combination therapies that could be transformative in the treatment of many cancers.

Note that the research articles collected in this research topic are heavily focused on the design of peptide vaccines. For a border perspective on peptide vaccines especially cancer peptide vaccines, see the review article by Stephens et al.

AUTHOR CONTRIBUTIONS

SJ, MG and XNX drafted this article. All authors contributed to the article and approved the submitted version.

FUNDING

SJ is funded by Innovate UK, grant number 104992 & 133783, and by grants from the CBI and Oxford Vacmedix UK Ltd. MG is supported by Chinese National Natural Science Funding program (81771221, 81870967 and 82071384). The funders were not involved in the study design, collection, analysis, interpretation of data, the writing of this article or the decision to submit it for publication.

REFERENCES

1. Clem AS. Fundamentals of Vaccine Immunology. *J Glob Infect Dis* (2011) 3:73–8. doi: 10.4103/0974-777X.77299
2. Sandmann FG, Davies NG, Vassall A, Edmunds WJ, Jit MCentre for the Mathematical Modelling of Infectious Diseases. The Potential Health and Economic Value of SARS-CoV-2 Vaccination Alongside Physical Distancing in the UK: A Transmission Model-Based Future Scenario Analysis and Economic Evaluation. *Lancet Infect Dis* (2021) 21:962–74. doi: 10.1101/2020.09.24.20200857
3. Iwasaki A, Omer SB. Why and How Vaccines Work. *Cell* (2020) 183:290–5. doi: 10.1016/j.cell.2020.09.040
4. Skwarczynski M, Toth I. Peptide-Based Synthetic Vaccines. *Chem Sci* (2016) 7:842–54. doi: 10.1039/C5SC03892H
5. Jiang S, Song R, Popov S, Mirshahidi S, Ruprecht RM. Overlapping Synthetic Peptides as Vaccines. *Vaccine* (2006) 24:6356–65. doi: 10.1016/j.vaccine.2006.04.070
6. Zhang H, Hong H, Li D, Ma S, Di Y, Stoten A, et al. Comparing Pooled Peptides With Intact Protein for Accessing Cross-Presentation Pathways for Protective CD8+ and CD4+ T Cells. *J Biol Chem* (2009) 284:9184–91. doi: 10.1074/jbc.M809456200
7. Melief CJ, van der Burg SH. Immunotherapy of Established (Pre) Malignant Disease by Synthetic Long Peptide Vaccines. *Nat Rev Cancer* (2008) 8:351–60. doi: 10.1038/nrc2373
8. Gattinger P, Niespodziana K, Stiasny K, Sahanic S, Tulaeva I, Borochova K, et al. Neutralization of SARS-CoV-2 Requires Antibodies Against Conformational Receptor-Binding Domain Epitopes. *Allergy* (2022) 77:230–42. doi: 10.1111/all.15066

Conflict of Interest: SJ and XNX are founder or consultant of Oxford Vacmedix UK Ltd which develops peptide-based vaccines.

The remaining author declares that the research was conducted in the absence of any commercial or financial relationships that could be construed as a potential conflict of interest.

Publisher's Note: All claims expressed in this article are solely those of the authors and do not necessarily represent those of their affiliated organizations, or those of the publisher, the editors and the reviewers. Any product that may be evaluated in this article, or claim that may be made by its manufacturer, is not guaranteed or endorsed by the publisher.

frontiers in Immunology

ORIGINAL RESEARCH
published: 26 April 2021
doi: 10.3389/fimmu.2021.666290

Peptides-Based Vaccine MP3RT Induced Protective Immunity Against *Mycobacterium Tuberculosis* Infection in a Humanized Mouse Model

Wenping Gong[1†], Yan Liang[1†], Jie Mi[1], Zaixing Jia[1,2], Yong Xue[1], Jie Wang[1], Lan Wang[1], Yusen Zhou[3], Shihui Sun[3] and Xueqiong Wu[1]*

[1] Tuberculosis Prevention and Control Key Laboratory/Beijing Key Laboratory of New Techniques of Tuberculosis Diagnosis and Treatment, Institute for Tuberculosis Research, 8th Medical Center, Chinese People's Liberation Army General Hospital, Beijing, China, [2] Graduate School, Hebei North University, Zhangjiakou, China, [3] State Key Laboratory of Pathogen and Biosecurity, Beijing Institute of Microbiology and Epidemiology, Beijing, China

OPEN ACCESS

Edited by:
Min Gong,
Tianjin Medical University, China

Reviewed by:
Hongxia Niu,
Lanzhou University, China
Wayne Robert Thomas,
University of Western Australia, Australia

****Correspondence:***
Xueqiong Wu
xueqiongwu@139.com

[†]These authors have contributed equally to this work

Specialty section:
This article was submitted to Vaccines and Molecular Therapeutics, a section of the journal Frontiers in Immunology

Received: *10 February 2021*
Accepted: *06 April 2021*
Published: *26 April 2021*

Citation:
Gong W, Liang Y, Mi J, Jia Z, Xue Y, Wang J, Wang L, Zhou Y, Sun S and Wu X (2021) Peptides-Based Vaccine MP3RT Induced Protective Immunity Against Mycobacterium Tuberculosis Infection in a Humanized Mouse Model. Front. Immunol. 12:666290. doi: 10.3389/fimmu.2021.666290

Background: Tuberculosis (TB) is still a global infectious disease that seriously threatens human beings. The only licensed TB vaccine Bacille Calmette-Guérin (BCG)'s protective efficacy varies significantly among populations and regions. It is very urgent to develop more effective vaccines.

Methods: In this study, eleven candidate proteins of *Mycobacterium tuberculosis* were selected to predict peptides with high-affinity binding capacity for the HLA-DRB1*01:01 molecule. The immunodominant peptides were identified with the enzyme-linked immunospot assay (ELISPOT) and linked in silico to result in a novel polypeptide vaccine in *Escherichia coli* cells. The vaccine's protective efficacy was evaluated in humanized and wild-type C57BL/6 mice. The potential immune protective mechanisms were explored with Enzyme-linked Immunosorbent Assay (ELISA), flow cytometry, and ELISPOT.

Results: Six immunodominant peptides screened from 50 predicted peptides were used to construct a new polypeptide vaccine named MP3RT. After challenge with *M. tuberculosis*, the colony-forming units (CFUs), lung lesion area, and the number of inflammatory cells in humanized mice rather than wild-type mice vaccinated with MP3RT were significantly lower than these in mice immunized with PBS. The humanized mice vaccinated with MP3RT revealed significant increases in IFN-γ cytokine production, IFN-γ^+ T lymphocytes, $CD3^+$IFN-γ^+ T lymphocytes, and the MP3RT-specific IgG antibody.

Conclusions: Taken together, MP3RT is a promising peptides-based TB vaccine characterized by inducing high levels of IFN-γ and $CD3^+$IFN-γ^+ T lymphocytes in humanized mice. These new findings will lay a foundation for the development of peptides-based vaccines against TB.

Keywords: *Mycobacterium tuberculosis*, epitope peptide, vaccine, Th1-type immune responses, protective efficacy, humanized mice

INTRODUCTION

As an ancient disease, tuberculosis (TB) has been a threat to human beings for thousands of years (1). Even today, with advanced technology, the number of deaths caused by TB still ranks first among the top ten infectious diseases (2). According to the Global Tuberculosis Report 2020 released by the World Health Organization (WHO), 10 million people developed TB and 1.2 million died in 2019 (3). Even more worrying is that Corona Virus Disease 2019 (COVID-19) has significantly impacted the TB epidemic and response. Current studies have reported the potential impact of the COVID-19 pandemic on global TB deaths and suggested that the TB mortality could increase to the levels seen in 2015 or even 2012 (3–5).

Vaccination is the best way to stop TB infection. Bacille Calmette-Guérin (BCG), the only licensed vaccine against TB infection, has been approved for neonatal vaccination in TB high-burden countries, which has made an outstanding contribution to controlling the incidence of TB in children. A previous modeling study estimated that BCG vaccination at birth could reduce TB deaths by 16.5%, but delays might increase TB deaths by 0.2% (6). These data indicate that avoiding BCG shortages and increasing BCG coverages at birth is an effective way to reduce global pediatric TB mortality. However, the duration of BCG protection is only 10-15 years, which is why the BCG vaccine has limited efficacy against pulmonary TB in adults (7).

It is urgent to develop a more effective vaccine to make up for the shortcomings of BCG. Pipelines for new TB vaccines are progressing with more than 25 vaccine candidates evaluated in clinical trials (2). Almost all of these TB candidates belong to first (live attenuated vaccines or inactivated vaccines), second (subunit vaccines), or third (DNA vaccines) generation vaccines. The latest generation of TB vaccine formulations is the development of peptide-based vaccines that emerged in recent years. Peptide-based vaccines consist of the immunodominant peptides of proteins recognized by T or B lymphocytes triggering T and B cell-mediated immune responses (8).

Mycobacterium tuberculosis, the pathogen of TB, is an intracellular parasitic bacterium, and the host's removal or killing of *M. tuberculosis* mainly depends on macrophages and T lymphocytes. It is the widely accepted view that $CD4^+$ T cells play an essential role in mycobacterial clearance. The recognition of $CD4^+$ T cells and antigen-presenting cells (APCs) is limited by the major histocompatibility complex II molecule (MHC II). As a new discipline developed in recent years, immunoinformatics provides a possibility for predicting immunogenic T-cell peptides of *M. tuberculosis* that can be used to develop a peptide-based vaccine (9). According to the Immune Epitope Database (IEDB), up to 63% of epitopes are related to the MHC class II molecule. Previous data have demonstrated that the MHC class II molecule plays an essential role in bridging peptides' presentation and activating T-helper 1 (Th1) immune response (10–13).

Furthermore, the selection of animal models is crucial for the evaluation of peptides-based vaccines, because the recognition of this vaccine and host T lymphocytes depends on MHC restriction. In our previous study, we have constructed a humanized C57BL/6 mice (HLA-$A11^{+/+}$ $DRB1*01:01^{+/+}$H-2-$\beta2m^{-/-}$/$IA\beta^{-/-}$) for Chinese population (14). Herein, we selected this mouse model to develop a novel vaccine based on Th1-type peptides might help fight against TB infection. In this study, the immunodominant peptides were identified from the candidate Th1 peptides predicted by the IEDB database (http://www.iedb.org/) using an enzyme-linked immunospot (ELISPOT) array. The nucleotide sequences of these immunodominant peptides were linked in silico to product a novel polypeptide vaccine named MP3RT in *Escherichia coli*. The protective efficacy of the MP3RT vaccine was evaluated in humanized and wild-type C57BL/6 mice, and its potential mechanism was explored in splenocytes *in vitro*.

Abbreviations: APC, antigen-presenting cell; BCG, Bacille Calmette-Guérin; CFA, complete Freund's adjuvant; COVID-19, Corona Virus Disease 2019; ELISA, enzyme-linked immune sorbent assay; ELISPOT, enzyme-linked immunospot; FBS, fetal bovine serum; H&E, hematoxylin and eosin; IEDB, Immune Epitope Database; IFA, incomplete Freund's adjuvant; IFN-γ, interferon-γ; IL, interleukin; LTBI, latent tuberculosis infection; MHC, major histocompatibility complex; NCBI, National Center for Biotechnology Information; NHFPC, National Health and Family Planning Commission of China; PBMCs, peripheral blood mononuclear cells; PBS, phosphate buffer solution; PHA, phytohemagglutinin; RPMI, Roswell Park Memorial Institute; SEM, standard error of the mean; SFCs, spots forming cells; SI, stimulation index; TB, tuberculosis; Th1, T-helper 1; TNF-α, tumor necrosis factor-α; WHO, World Health Organization; WMA, World Medical Association.

MATERIALS AND METHODS

Ethics Statement

All of the experiments related to animals were performed following the Experimental Animal Regulation Ordinances principles established by the China National Science and Technology Commission. Mice were well cared during their living, and all protocols were approved by the Animal Ethical Committee of the 8th Medical Center of Chinese PLA General Hospital (Approved Number: 309201808171015). All animals were raised in a SPF laboratory in the 8th Medical Center of Chinese PLA General Hospital, and the *M. tuberculosis* virulent strain challenge experiments were conducted in a qualified negative pressure biosafety laboratory level-2 PLUS (negative pressure BSL-2 PLUS) in the 8th Medical Center of Chinese PLA General Hospital.

The collection of human peripheral blood mononuclear cells (PBMCs) in TB patients, volunteers with latent tuberculosis infection (LTBI), and normal volunteers were performed following the principles of the Ethical Review of Biomedical Research Involving Humans established by NHFPC and the Declaration of Helsinki established by the World Medical Association (WMA). All participants signed written informed consent. The clinical investigation related to PBMCs isolation was approved by the Medical Ethics Committee of the 8th Medical Center of Chinese PLA General Hospital (Approved Number: 2018ST011).

Bacterial Strains and Plasmids

M. tuberculosis (H37Rv strain) were cultured on Lowenstein-Jensen culture medium (Baso Biotechnology Co., LTD., Zhuhai, Guangdong province, China) at 37°C for 28 days and isolated from grinding fluid following our previous study (15). *M. tuberculosis*'s number and viability were determined with colony-forming units (CFUs) assay (16). Besides, the plasmid pET32a (+) and *Escherichia coli* BL21 cells were purchased from the Wuhan Institute of Biotechnology (Wuhan, Hubei, China) to express the target gene *in vitro* according to our previous studies (13, 17, 18).

Mice and Subjects

Female wild-type C57BL/6 mice at the age of 7-8 weeks were obtained from Vital River Laboratories (Beijing, China), and female humanized C57BL/6 mice (HLA-A11$^{+/+}$DR1$^{+/+}$H-2-β2m$^{-/-}$/IAβ$^{-/-}$) with similar weight and age were presented by professor Yusen Zhou of Beijing Institute of Microbiology and Epidemiology (Beijing, China) (14). Furthermore, this study included 37 patients with TB, 11 volunteers with LTBI, and 62 normal volunteers. The recruitment was carried out at the 8th Medical Center of Chinese PLA General Hospital between December 2019 and June 2020. The diagnoses of TB and LTBI and the inclusion and exclusion criteria for normal volunteers were followed with the Diagnosis for Pulmonary Tuberculosis (WS288-2017) established by the National Health and Family Planning Commission of China (NHFPC).

HLA-DRB1*01:01 Binding Epitopes Prediction and Peptide Synthesis

Eleven mycobacterial antigens, including Mpt51, Mpt63, Mpt64, Mtb8.4, PPE18, PPE44, PPE68, RpfA, RpfB, RpfE, and TB10.4 (**Table 1**), were selected to predict the dominant epitopes restricted by HLA-DRB1*01:01 molecule. Their amino acid sequences were downloaded from the National Center for Biotechnology Information (NCBI, https://www.ncbi.nlm.nih.gov/) database. The obtained amino acid sequences were imported into the IEDB to predict the potential dominant epitopes with high binding affinity to the human HLA-DRB1*01:01 allele as previously described (20, 21). Seven MHC II binding methods such as IEDB recommended, Consensus method, Combinatorial library, NN-align (netMHCII-2.2), SMM-align (netMHCII-1.1), Sturniolo, and NetMHCIIpan were used to predict the potential dominant epitopes. The selection IEDB Recommended uses the Consensus approach, combining NN-align, SMM-align, Combinatorial library and Sturniolo if any corresponding predictor is available for the molecule. Otherwise, NetMHCIIpan is used. The Consensus approach considers a combination of any three of the four methods, if available, where Sturniolo as a final choice.

The predicted peptides were synthesized *in vitro* by SBS Genetech Co., Ltd. (Beijing, China) using a solid-phase synthesis method. Briefly, FMOC (9-fluorenylmethyloxycarbonyl) is used to protect the α-amino group of amino acids, the peptide is synthesized with TETRAS^{TM} Peptide Synthesizer and cleaved

TABLE 1 | The basic information about vaccine candidate proteins of *M. tuberculosis*.

Protein Name	Accession No.[a]	Locus_tag	Gene Name[b]	Length (aa)	Annotation[b]	Group[c]	Summary Information [b]
Mpt51	CCP46632	Rv3803c	*fbpD/fbpC1/ mpb51/mpt51*	299	Secreted MPT51/MPB51 antigen protein FbpD	NA	One of the major proteins in the culture filtrate of Mycobacterium bovis BCG
Mpt63	CCP44693	Rv1926c	*mpt63/mpb63*	159	Immunogenic protein Mpt63	III	Predicted possible vaccine candidate
Mpt64	CCP44749	Rv1980c	*mpt64/mpb64*	228	Immunogenic protein Mpt64	II	Predicted possible vaccine candidate
Mtb8.4	CCP43930	Rv1174c	*TB8.4*	110	Low molecular weight T-cell antigen TB8.4	II	Predicted to be an outer membrane protein and possible vaccine candidate
PPE18	CCP43952	Rv1196	*PPE18*	391	PPE family protein PPE18	NA	Member of the *Mycobacterium tuberculosis* PPE family
PPE44	CCP45569	Rv2770c	*PPE44*	382	PPE family protein PPE44	NA	Member of the *Mycobacterium tuberculosis* PPE family
PPE68	CCP46702	Rv3873	*PPE68*	368	PPE family protein PPE68	I	A peptide-based vaccine candidate
RpfA	CCP43615	Rv0867c	*rpfA*	407	Possible resuscitation-promoting factor RpfA	I	Predicted possible vaccine candidate
RpfB	CCP43759	Rv1009	*rpfB*	362	Probable resuscitation-promoting factor RpfB	I	Predicted possible vaccine candidate
RpfE	CCP45243	Rv2450c	*rpfE*	172	Probable resuscitation-promoting factor RpfE	I	Predicted possible vaccine candidate
TB10.4	CCP43018	Rv0288	*esxH/cfp7/ TB10.4*	96	Low molecular weight protein antigen 7 EsxH	I	Predicted possible vaccine candidate

[a]*The National Center for Biotechnology Information (NCBI, http://www.ncbi.nlm.nih.gov/). Data were retrieved on 3 Mar 2017.*

[b]*The Gene name, annotation, and summary information are based on the data deposited at the NCBI. Data were retrieved on 3 Mar 2017.*

[c]*The group is based on a previous study (See 19). The antigens are sorted by the qualitative score (Qual Total) and subsequently by the quantitative score (Quant Total). Group I includes all antigens with a qualitative score 8 and above, provided that the quantitative score is not lower than 12. The rest of the antigens having a qualitative score of 8 and those having a qualitative score of 7 and a quantitative score not lower than 9 were clustered into Group II. Group III included antigens with qualitative scores of 7 (and a quantitative score of 8) and 6 (with a quantitative score of 9 and up).*

NA, not available.

from the resin with TFA (trifluoroacetic acid). Finally, the peptide was purified by a high-performance liquid chromatography (HPLC) and analyzed by a mass spec-trometer (MS) to make its purity higher than 75%.

Immunodominant Peptides Screening

The ELISPOT assay was performed to screen the immunodominant peptides according to our previous study (21). The differences were described as follows. Four groups of female humanized mice (five mice per group) were immunized with 5×10^6 CFUs of inactivated *M. tuberculosis* in 100 μl complete Freund's adjuvant (CFA, Cat. No.F5881, Sigma-Aldrich, Missouri, USA), 500 μg lysate of *M. tuberculosis* in 100 μl phosphate buffer solution (PBS), 500 μg lysate of *M. tuberculosis* in 100 μl CFA, and 500 μg lysate of *M. tuberculosis* in 100 μl incomplete Freund's adjuvant (IFA, Cat. No.F5506, Sigma-Aldrich, Missouri, USA), respectively. Fourteen days post-immunization, mice in each group were sacrificed, the splenocyte suspension was centrifuged at 4 °C and 500 g for 5 min, and the supernatant was discarded. The pellet was resuspended gently with 10 ml of 1 × Red Blood Cell Lysis Buffer (Cat. No.00-4333, eBioscience, Shanghai, China) and incubated at room temperature for 5 min. After washing twice with PBS, the splenocytes' concentration was adjusted to 3×10^5/ml with Roswell Park Memorial Institute (RPMI) 1640 Medium (Cat. No. 8115240, Gibco, Shanghai, China). Then, the interferon-γ (IFN-γ)$^+$ T cells were detected by a Mouse IFN-γ ELISOPT^{PLUS} (Cat. No. 3321-4APT-2, Mabtech AB, Nacka Strand, Sweden). In detail, 100 μl of splenocytes and 10 μl of candidate peptide (2 μg) were added into a well of 96-well ELISPOT plate and incubated at 37°C. Twenty-four hours later, the splenocytes in the ELISPOT plate were gently removed, and the plate was washed five times with PBS. Subsequently, 100μl of R4-6A2 labeled monoclonal antibody (1μg/ml) was added to the ELISPOT plate and incubated at room temperature for 2h. After washing five times with PBS, 100 μl of streptavidin-ALP diluted 1:1000 with PBS containing 0.5% fetal bovine serum (FBS) was added to the ELISPOT plate and incubated for one hour at room temperature. After washing five times with PBS, 100 μl substrate solution (BCIP/NBT-plus) filtered with a 0.45 μm filter was added to the ELISPOT plate and stopped color development by washing extensively in tap water. The number of spots forming cells (SFCs) in each well was determined with a CTL-S5 Versa ELISPOT Reader (CTL, Cleveland, OH, USA). The immunodominant peptide was defined with a stimulation index (SI) value great than two following our previous study (21).

Preparation and Three-Dimensional (3D) Structure Prediction of the Recombinant Polypeptide

The amino acid sequences of the immunodominant peptides screened by ELISPOT assay were linked with GGGGS or AAY linker in silico. Their hydrophilicity, amphipathic regions, and antigenic index were analyzed using a bioinformatics software Lasergene Protein (DNASTAR, Inc., Madison, Wisconsin, USA). After codon optimization, the nucleotide sequence of the recombinant polypeptide was synthesized by the Wuhan Institute of Biotechnology (Wuhan, Hubei, China) and inserted into the pET32a (+) plasmid (NCOI and XhoI sites) to transform *E. coli* cells *in vitro*. The expression and purification of MP3RT were performed by the C-terminal 6-his tag following our previous studies (12, 17, 18). The endotoxin of the purified antigen MP3RT were removed with Toxin EraserTM (GenScript, Piscataway, NJ) following our previous study (13). Furthermore, the candidate vaccine's 3D structure was predicted by using the SWISS-MODEL database (https://swissmodel.expasy.org/interactive) according to a previous description (22).

Mice Immunization and Infection

The flow diagram of the immunization was presented in **Figure 1**. Three groups of humanized or wild-type mice (ten mice per group) were immunized subcutaneously with 30 μg CpG-ODN2395 adjuvants (Sangon, Shanghai, China) in 100 μl PBS, 30 μg BCG (Chengdu Institute of Biological Products Co., Ltd., Chengdu, Sichuan province, China) in 100 μl PBS, and 30 μg MP3RT combined with 30 μg CpG-ODN2395 adjuvants in 100 μl PBS, respectively. Twenty-eight and 42 days post primary immunization, the mice in PBS and MP3RT groups were boosted subcutaneously with 20 μg CpG-ODN2395 adjuvants in 100 μl PBS and 20 μg MP3RT in 100 μl PBS, respectively. The mice in the BCG group were not performed any booster immunization. Furthermore, to compare the protective efficacy of MP3RT and an *ag85ab* chimeric DNA vaccine whose immunogenicity and therapeutic effects have been confirmed in our previous study (23), ten humanized or wild-type mice were intramuscularly injected with 100 μg *ag85ab* DNA vaccine and boosted with the same dose on the 28th and 42nd days after the first immunization. Then, all of the mice were challenged with *M. tuberculosis* H37Rv strain (2×10^5 CFUs) *via* tail vein injection on days 56 and killed on days 91.

Mycobacterial Colony Counting

On the 91st day after primary immunization, humanized or wild-type mice in each group were sacrificed, and their livers, lungs, and spleens were collected for efficacy evaluation. Briefly, the left lobe of the lung and half part of the liver were homogenized in normal saline (3 ml per organ), and the grinding fluid was diluted at 1:10, 1:100, and 1:1000 with normal saline. Then, 0.1 ml of the diluted solution was drawn from each diluted sample and inoculated on modified antibiotics-free Lowenstein-Jensen medium plates (Baso Biotechnology Co., LTD., Zhuhai, Guangdong province, China) in duplicate. Finally, CFUs were counted after incubating at 37°C for 28 days.

Histopathology

The right lobe of the lung collected from each mouse was cut into blocks of 2.0 cm × 2.0 cm × 0.3 cm with ophthalmic scissors and then fixed overnight in formaldehyde solution (the required volume was 10 times of the sample volume). The tissue sample was dehydrated by ethanol with a concentration of 80%, 90%, 95%, and 100% (2 hours/time), embedded with paraffin, and cut into tissue sections with thickness 4-6 μm. Finally, these tissue sections were stained with hematoxylin and eosin (H&E) method following our previous studies (12, 13, 17, 18). Five tissue sections for each lung were independently observed by two

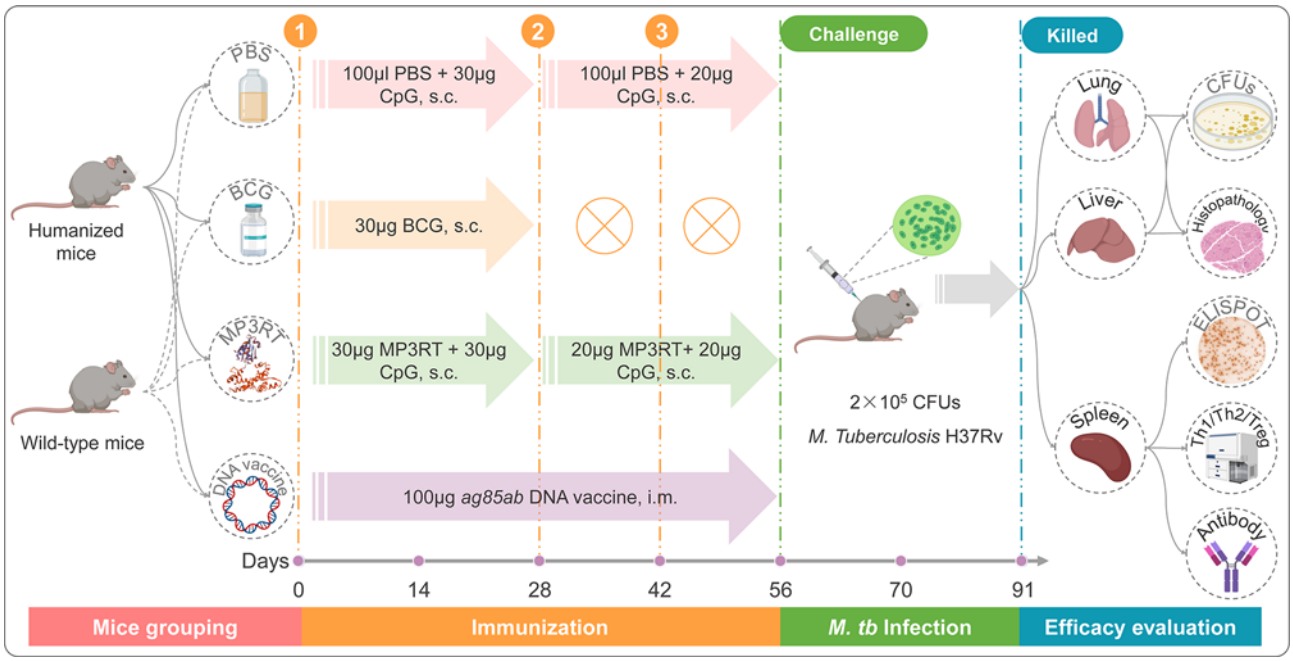

FIGURE 1 | The flow chart of vaccination, infection, and evaluation.

researchers under a microscope of 40 × or 100 × (Olympus Corporation, Tokyo, Japan). The lesion area rate and the number of inflammatory cells were counted by Image-Pro Plus software (Version 6.0, Media Cybernetics, Inc: Bethesda, MD, USA).

ELISPOT

ELISPOT experiment of mouse splenocytes: On 28 days after infection, humanized or wild-type mice were killed. Their spleens were collected to prepare splenocytes suspension according to the method described above. A volume of 100 μl splenocytes (3×10^6/ml) was added into the wall of 96-well ELISPOT plate and incubated with 50 μl of PBS, 50 μl of MP3RT vaccine (60 μg/ml), or 50 μl of phytohemagglutinin (PHA, 60 μg/ml) at 37°C for 24h, respectively. The SFCs were determined according to the methods mentioned above.

ELISPOT experiment of PBMCs: The PBMCs were isolated from blood samples of TB patients, LTBI volunteers, and healthy volunteers using a Human peripheral blood mononuclear cell Isolation Kit (Solarbio, Beijing, China). The isolated PBMCs were added into the 96-well ELISPOT plate wall and incubated with 50 μl of PBS and 50 μl of MP3RT vaccine (60 μg/ml), respectively. Twenty-four hours later, SFCs were determined with a Human IFN-γ ELISpot^{PRO} kit (Cat. No. 3420-2APW-10, Mabtech AB, Nacka Strand, Sweden) following the manufactures' introduction.

Th1/Th2/Th17 Cytokines Analysis

The mice were killed on the 91st day after the first immunization, and the spleens were collected for the preparation of splenocytes suspension following the above methods. A volume of 100μl splenocytes (3×10^6/ml) and 50μl MP3RT vaccine (60 μg/ml) were incubated in a well of 96-well cell culture plate (Mabtech AB, Nacka Strand, Sweden) at 37°C for 48h. Then, the culture solution was transferred into a new tube and centrifugated at 500g for 10 min. Finally, the supernatant was gently transferred into another new tube, and the levels of interleukin -2 (IL-2), IL-4, IL-6, IL-10, IFN-γ, tumor necrosis factor -α (TNF-α), and IL-17A were detected by a Mouse Th1/Th2/Th17 Cytokine Kit (Cat. No. 560485, BD Biosciences, San Jose, CA, USA) following the manufacturer's instruction.

Flow Cytometry

Mouse splenocytes suspension (3×10^7 cells/ml) was prepared according to the above-described method. The frequency of $CD3^+CD4^+$ T cells, $CD3^+IFN\text{-}\gamma^+$ Th1 cells, $CD3^+IL\text{-}4^+$ Th2 cells, and $CD4^+CD25^+FoxP3^+$ regulatory T cells (Treg cells) was quantified with BD IntraSure^{TM} kit (Cat. No. 641776, BD Biosciences, San Jose, CA, USA) according to the manufacturer's instructions. This section contained two independent experiments, one to detect the frequency of $CD3^+IFN\text{-}\gamma^+$ Th1 cells and $CD3^+IL\text{-}4^+$ Th2 cells, and the other to detect the frequency of $CD4^+CD25^+FoxP3^+$ Treg cells.

Experiment 1: Briefly, 100 μl suspension containing 3×10^6 splenocytes was incubated with 10μl of MP3RT vaccine (1mg/ml) at 37°C for 4h. FITC Hamster Anti-Mouse CD3e (Cat. No.553061, BD Biosciences, San Jose, CA, USA) and Percp-cy 5.5 Rat Anti-Mouse CD8a (Cat. No. 561092, BD Biosciences, San Jose, CA, USA) were added into tubes for surface staining for 30 min at 4°C. The cell pellet was

resuspended with 1ml of 1 × Fix/Perm Buffer solution (Cat. No. 51-9008100, BD Biosciences, San Jose, CA, USA), incubated at 4°C for 40 min protected from light, and washed twice with 1ml 1 × Perm/Wash Buffer solution at 4°C and 500g for 6 min. After that, the cells were incubated with 0.9 μl of PE Rat Anti-Mouse IFN-γ (Cat. No. 554412, BD Biosciences, San Jose, CA, USA), 2.4 μl of APC Rat Anti-Mouse IL-4 (Cat. No. 554436, BD Biosciences, San Jose, CA, USA), 1 μl of PE Rat IgG1 κ Isotype Control (Cat. No. 554685, BD Biosciences, San Jose, CA, USA), and 2.5μl of APC Rat IgG1 κ Isotype Control (Cat. No. 554686, BD Biosciences, San Jose, CA, USA) at 4°C for 40 min protected from light, respectively. After washing twice with 1 × Perm/Wash Buffer solution (Cat. No. 51-9008102, BD Biosciences, San Jose, CA, USA), the cells in each tube were resuspended with 350 μl PBS and analyzed on a flow cytometer (Beckman Coulter, Inc., Brea, CA, USA).

Experiment 2: Approximately 3×10^6 prepared splenocytes in 100 μl of RPMI 1640 Medium were added into a tube and incubated with 1 μg of Ms CD16/CD32 Pure 2.4G2 (Cat. No. 553141, BD Biosciences, San Jose, CA, USA) at 4°C for 5min. Then, 2 μl of FITC-CD3 (Cat. No. 553061, BD Biosciences, San Jose, CA, USA), 2 μl of APC-CD4 (Cat. No. 553051, BD Biosciences, San Jose, CA, USA), and 5 μl of PE-CD25 antibodies (Cat. No. 553866, BD Biosciences, San Jose, CA, USA) were added into each sample tube. Then, 2μl of FITC-Ham IgG1 Kap (Cat. No. 553971, BD Biosciences, San Jose, CA, USA), 2μl of APC-Rat IgG2a Kap (Cat. No. 553932, BD Biosciences, San Jose, CA, USA), and 5μl of PE-Rat IgG1 Lam antibodies (Cat. No. 557078, BD Biosciences, San Jose, CA, USA) were added into isotype control tube, respectively. After incubation at 4°C for 40 min protected from light, the samples were washed with 2 ml PBS at 4°C and 500g for 6 min. The samples were incubated with 1ml of 1 × Fix/Perm Buffer solution at 4°C for 40 min protected from light, followed with twice washing with 1ml of 1 × Perm/Wash Buffer solution. Then, the cells in the sample tube and isotype control tube were incubated with 5 μl of BV4212-FoxP3 (Cat. No. 562996, BD Biosciences, San Jose, CA, USA) and 5 μl of Rat IgG2b Kpa ItCl BV4212 antibodies (Cat. No. 562603, BD Biosciences, San Jose, CA, USA) at 4°C for 40 min protected from light, respectively. After twice washing with 2 ml of 1 × Perm/Wash Buffer solution, the samples were resuspended with 350 μl PBS and analyzed on the flow cytometer (Beckman Coulter, Inc., Brea, CA, USA).

Antibody Detection by Enzyme-Linked Immune Sorbent Assay (ELISA)

Blood samples were collected from the mice when they were sacrificed on day 91 after the first immunization. The collected blood sample was centrifuged at 1500rpm for 20 min, and then the supernatant was gently transferred into a new tube. The serum separated from each blood sample was linearly diluted (2 times) with PBS from a minimum dilution of 100 to a maximum dilution of 204800 to determine the optimum dilution by a Mouse ELISA Kit (Solarbio, Beijing, China) following the instruction given by the manufacturer. After that, the rest of the serum was diluted in the optimal dilution, and the levels of MP3RT specific IgG were determined by Goat anti-Mouse IgG/HRP (Cat. No. SE131, Solarbio, Beijing, China). Finally, the OD_{450} values of MP3RT specific IgG were detected with a microplate reader (Thermo Fisher Scientific, Shanghai, China).

Statistical Analysis

All of the results in this study were performed using the GraphPad Prism 8 software (San Diego, CA, USA). The results of efficacy evaluation, pathological lesions, ELISA, ELISPOT on mice, cytokines, and flow cytometry were analyzed with Ordinary one-way ANOVA test or Kruskal-Wallis nonparametric test according to the data normality and homogeneity of variances. The ELISPOT experiment results on the samples collected from TB patients, LTBI, and healthy control were analyzed with an Unpaired *t*-test or nonparametric test (Mann Whitney test) according to the normality. The data was showed as mean ± standard error of the mean (SEM), and P-value < 0.05 was considered as a significant difference. Furthermore, in order to reduce the error caused by multiple comparisons, we also choose the method recommended by the GraphPad Prism 8 software for correction.

RESULTS

Eight Immunodominant Peptides Identified With ELISPOT

The epitopes predicted by the IEDB database were scored by the percentile rank, and the epitopes with scores below 10 in the rank were selected as the dominant Th1 epitopes (the lower the score, the higher the affinity). As a result, a total of 55 potential dominant epitopes were predicted (**Table S1**) and synthesized. After that, the potential immunodominant Th1 peptides were screened by ELISPOT assay, and the results showed that the SI values of eight peptides ($MPT63_{10\text{-}24}$, $Mtb8.4_{69\text{-}83}$, $PPE18_{115\text{-}129}$, $PPE18_{149\text{-}163}$, $PPE68_{138\text{-}152}$, $RpfA_{377\text{-}391}$, $TB10.4_{21\text{-}35}$, and $TB10.4_{23\text{-}37}$) were greater than 2 in at least two independent experiments (**Figure 2**). Our further study found that immunodominant peptide $MPT63_{10\text{-}24}$ was a part of the signal peptide of MPT63 protein, indicating that these amino acid residues would be challenging to express *Escherichia coli* BL21 cells. We also observed that two immunodominant peptides $TB10.4_{21\text{-}35}$ and $TB10.4_{23\text{-}37}$ shared similar amino acid, and the SI value induced by peptide $TB10.4_{21\text{-}35}$ was significantly higher than that of $TB10.4_{23\text{-}37}$. Based on the reasons described above, both immunodominant peptides $MPT63_{10\text{-}24}$ and $TB10.4_{23\text{-}37}$ were not included in our further study.

Sequence Optimization, Construction, and Expression of MP3RT Vaccine

It has been reported that optimizing peptide linkers with length, flexibility, and amino acid composition could improve the thermostability and activity of the displayed enzyme (24). The amino acid sequences of six immunodominant peptides were

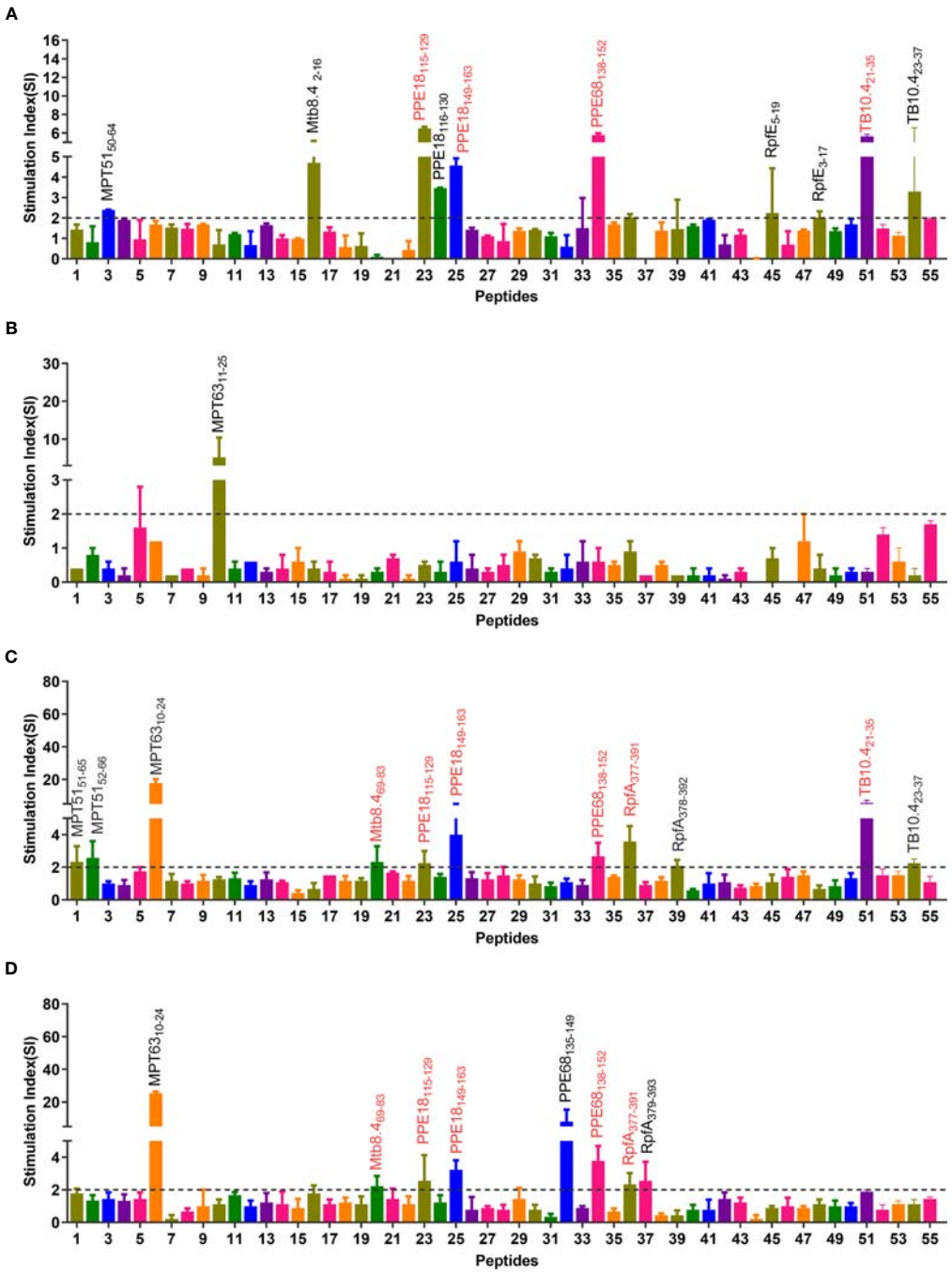

FIGURE 2 | Immunodominant peptides screening *via* four independent ELISPOT experiments. Splenocytes obtained from humanized mice immunized with inactivated *M. tuberculosis* in CFA adjuvant **(A)**, lysate of *M. tuberculosis* in PBS **(B)**, lysate of *M. tuberculosis* in CFA adjuvant **(C)**, and lysate of *M. tuberculosis* in IFA adjuvant **(D)** were stimulated with MP3RT. The SFCs were analyzed by a CTL-S5 Versa ELISPOT Reader. The SI value of 55 peptides was shown as the ratio of SFCs in peptide stimulated cells and medium-stimulated cells. The detailed information of 55 peptides can be found in **Table S1**. SI >2 was considered positive and labeled in the figure. The immunodominant peptides included in the MP3RT vaccine were marked using a red text tag.

linked with flexible GGGGS linker or rigid AAY linker in silico to evaluate the hydrophilicity, antigenic index, and amphipathic regions (**Figure 3A**). The results indicated that the type of linker but not the order and continuity of these immunodominant peptides significantly affected the vaccine's characteristics. Compared with rigid AAY linker, the flexible GGGGS linker significantly decreased the number of α-helices. It increased the antigen index, flexibility, and the number of secondary structures such as the β-sheet, β-turn, and random coils (**Figure 3B**). A recent study also reported that the flexible GGGGS linker

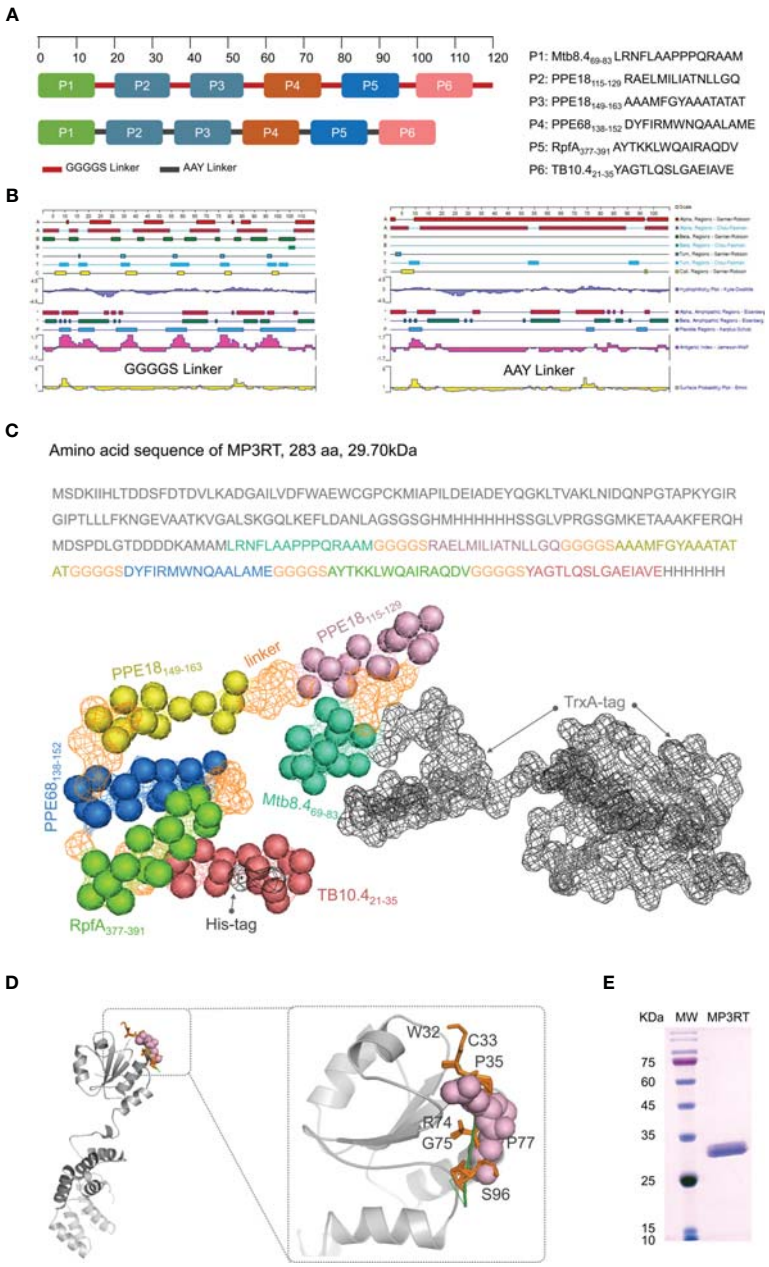

FIGURE 3 | Construction and structural prediction of MP3RT vaccine. Six immunodominant peptides were linked with GGGGS or AAY linkers in silico **(A)**. Their antigenic index, surface probability, hydrophobicity, alpha regions, beta regions, and turn regions were assessed using Lasergene Protein software **(B)**. The length and molecular weight of MP3RT were 283aa and 29.70 kDa, respectively **(C)**. The 3D structure of MP3RT was presented in Cartoon, Spacefill, and Surface **(C, D)**. The MP3RT vaccine was prepared in *E. coli* cells and verified with polyacrylamide gel electrophoresis **(E)**.

provided the best structure and stability for fusion protein (25). Therefore, the GGGGS linker was selected to link the immunodominant peptides together with TrxA-tag and His-tag (**Figure 3C**). The three-dimensional (3D) structure prediction revealed that the MP3RT vaccine consisted of α-helixes and β-sheets, forming a hollow spindle structure (**Figures 3C, D**). Finally, a novel recombinant protein named as MP3RT (283aa in length and 29.7 kDa in molecular weight) was successfully expressed in *E. coli* cells following our previous studies (13, 21) (**Figure 3E**).

Peptide-Based Vaccine MP3RT Elicited Protective Efficacy in Humanized Mice Rather Than Wild-Type Mice

To determine the protective efficacy of the MP3RT vaccine, the humanized mice and wild-type mice were immunized with PBS,

BCG, MP3RT, and *ag85ab* DNA vaccine, respectively. Our results showed that mice's weight in each group decreased during the early *M. tuberculosis* infection stage and increased in the late stage. Interestingly, we found that humanized mice's weight has been on a downward trend and gradually began to rise until the 28th day after infection (**Figure 4A**). In contrast, the weight loss of humanized mice immunized with BCG (**Figure 4A**) and wild-type mice in each group appeared in the first week after infection and then began to increase gradually (**Figure 4B**). In addition, although we found that the weight of MP3RT-immunized mice recovered faster than the PBS negative control and DNA-immunized mice, there was no statistical difference between them (**Figure 4A**, $P > 0.05$). Only the weight of BCG-immunized mice recovered significantly better than that of PBS control group (**Figure 4A**, $P < 0.01$). These results suggested that the protection efficiency induced by MP3RT vaccination does not exceed that of BCG vaccine.

Moreover, five or two humanized mice vaccinated with PBS or DNA vaccine died after *M. tuberculosis* challenge ($P = 0.0123$, **Figure 4C**), respectively. On the contrary, none of the rest humanized mice and all wild-type mice died (**Figures 4C, D**). When the bacterial loads in the organs of humanized mice were compared, the CFUs in the lungs of mice immunized with BCG ($P < 0.0001$) or MP3RT ($P = 0.0108$) was less than that in the lungs of mice immunized with PBS (**Figure 4E**). The CFUs in the livers of mice immunized with BCG ($P = 0.0002$), MP3RT ($P = 0.0285$), or DNA vaccine ($P = 0.0164$) was remarkably lower than that of mice immunized with PBS (**Figure 4G**). As expected, the CFUs in the liver and lungs of MP3RT-immunized wild-type mice were not statistically different from the PBS group (**Figures 4F, H**). However, the CFUs in the lungs and livers collected from wild-type mice immunized with BCG ($P = 0.0019$, **Figure 4F**; $P = 0.0096$, **Figure 4H**) or DNA vaccine ($P = 0.0262$, **Figure 4H**) were lower than that of mice immunized with PBS. These results demonstrated that the MP3RT vaccine had an ability to reduce mycobacterial loads in humanized mice instead of wild-type mice. Moreover, the DNA vaccine may play a potential role in the prevention of TB.

MP3RT Vaccination Significantly Reduced the Pathological Lesions

The reduction of mycobacterial loads was also reflected in the pathological assays. Humanized or wild-type mice's lung lesions were observed under 40 × microscope and determined with Image-Pro Plus software (**Figure 5A**). The results suggested that the lung lesion areas of humanized mice vaccinated with BCG ($P = 0.0006$), MP3RT ($P = 0.0187$), or DNA vaccine ($P = 0.0481$) were significantly less than that of mice immunized with PBS (**Figure 5B**). The lung lesion area of wild-type mice vaccinated with BCG was less than that of wild-type mice immunized with PBS ($P = 0.0001$, **Figure 5C**). Furthermore, the number of inflammatory cells of the lungs obtained from humanized or wild-type mice were observed under 100 × microscope and counted with Image-Pro Plus software (**Figure 5D**). It was found that the number of inflammatory cells in the lungs collected from humanized mice vaccinated with BCG was less than that of mice in the PBS group ($P = 0.0286$, **Figure 5E**). The number of inflammatory cells in the lungs collected from wild-type mice vaccinated with BCG ($P < 0.0001$) and MP3RT ($P = 0.0004$) was less than that of wild-type mice in the PBS or DNA vaccine group (**Figure 5F**).

MP3RT Induced an Increase in Number of IFN-γ^+ T Lymphocytes in Mouse Splenocytes and Human PBMCs

To determine the IFN-γ secreting cells induced by MP3RT vaccine, ELISPOT assays were conducted in splenocytes of mice (**Figure 6A**) and PBMCs of human beings (the spot diagrams are not shown), respectively. The results showed that the number of IFN-γ^+ T lymphocytes (showed as SFCs in **Figure 6**) of humanized mice ($P = 0.0012$, **Figure 6B**) or wild-type mice ($P = 0.0056$, **Figure 6C**) vaccinated with MP3RT was significantly higher than that of mice vaccinated with PBS. Similar results were observed in PBMCs collected from 37 TB patients, 11 LTBI volunteers, and 62 normal controls (**Figure 6D**). With the comparison of PBS stimulation, the stimulation of MP3RT resulted in a significantly higher levels of IFN-γ^+ T lymphocytes in TB patients ($P = 0.0003$), persons with LTBI ($P = 0.0056$), and normal controls ($P < 0.0001$), respectively.

A High Level of IFN-γ Induced by MP3RT Vaccination in Humanized Mice

To determine the cytokines profile induced by the MP3RT vaccine, the Th1/Th2/Th17 cytokines were detected with a Mouse Th1/Th2/Th17 Cytokine Kit. In humanized mice, the level of IFN-γ produced by splenocytes of MP3RT vaccinated mice was significantly higher than that of PBS vaccinated mice ($P = 0.0051$, **Figure 7A**). However, the level of IL-10 secreted by splenocytes of MP3RT vaccinated mice was significantly lower than that of PBS vaccinated mice ($P = 0.0427$, **Figure 7A**). Furthermore, the levels of TNF-α ($P = 0.0422$), IL-4 ($P = 0.0152$), and IL-6 ($P = 0.0009$), and IL-17A ($P = 0.0327$) secreted by splenocytes of BCG vaccinated mice were higher than those of PBS vaccinated mice (**Figure 7A**). In wild-type mice, the levels of IFN-γ ($P = 0.0050$), TNF-α ($P = 0.0051$), IL-4 ($P = 0.0233$), IL-6 ($P = 0.0051$), and IL-10 ($P = 0.0132$) secreted by mice vaccinated with MP3RT were significantly higher than those of mice vaccinated with BCG (**Figure 7B**). Moreover, the level of IL-17A secreted by wild-type mice vaccinated with MP3RT was significantly higher than that of mice vaccinated with PBS ($P = 0.0231$, **Figure 7B**). In contrast, there was no significant difference in the level of IL-2 among groups of humanized (**Figure 7A**) or wild-type mice (**Figure 7B**).

Vaccination With MP3RT Induced a High Rate of Lymphocytes

In order to assess the frequency of lymphocytes such as $CD3^+CD4^+$ T cells, $CD3^+$IFN-γ^+ Th1 cells, $CD3^+$IL-4^+ Th2 cells, and $CD4^+CD25^+FoxP3^+$ Treg cells, flow cytometry was performed. In humanized mice (**Figure 8A**), (1) The frequency of lymphocytes in mice vaccinated with MP3RT was remarkably higher than that in mice vaccinated with PBS ($P = 0.0073$,

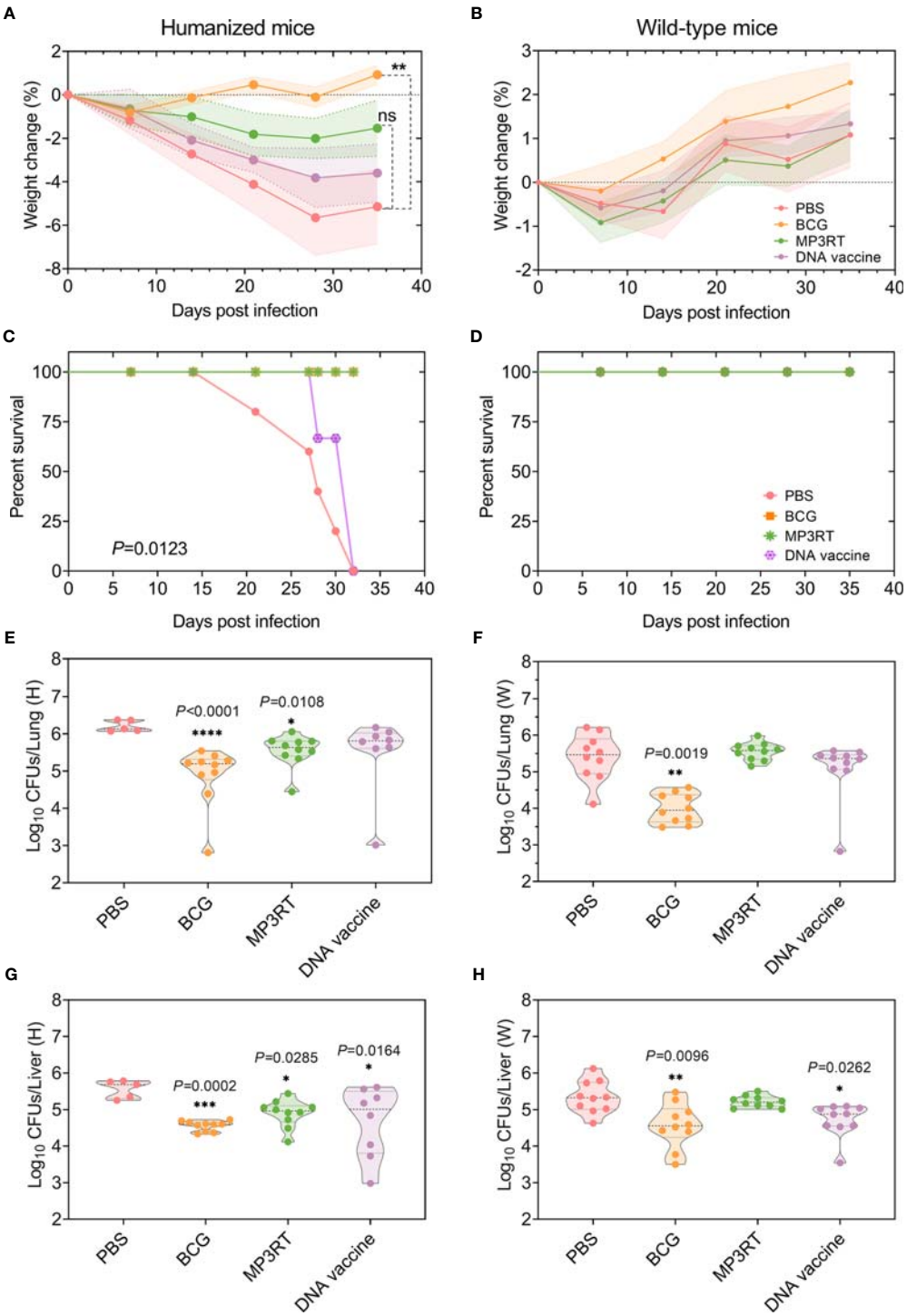

FIGURE 4 | Protective efficacy of MP3RT vaccine in the mouse model. Humanized or wild-type C57BL/6 mice were immunized with PBS, BCG, MP3RT, and *ag85ab* DNA vaccine, respectively. On the 56 days after primary immunization, humanized or wild-type mice were challenged with *M. tuberculosis* H37Rv strain. The weight changes **(A, B)** and deaths **(C, D)** were recorded weekly or daily. Thirty-five days post-infection, mice were sacrificed. The left lobe of the lung **(E** or **F)** and half part of the liver **(G** or **H)** collected from humanized or wild-type mice were used for CFUs counting. The data were expressed as Log_{10} of CFUs and compared with one-way analysis of variance (ANOVA) or Kruskal-Wallis test according to the data normality and homogeneity of variances. All data were shown as mean + SEM (n = 5 in humanized mice vaccinated with PBS and n = 10 in other groups). P<0.05 was considered significantly different. *P < 0.05; **P < 0.01; *** P <0.001; ****P < 0.0001, ns, no significance.

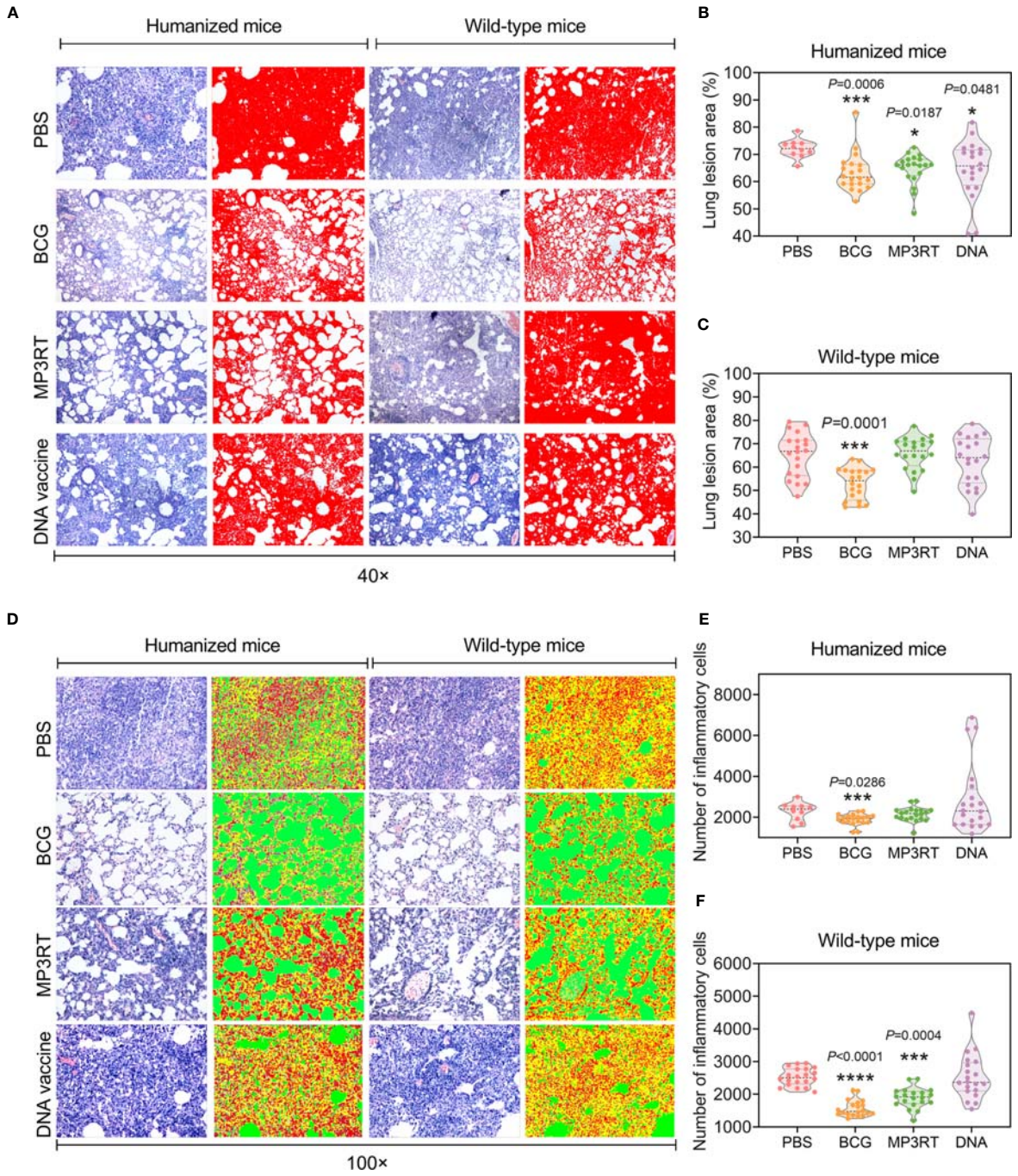

FIGURE 5 | Histopathological characteristics of the lung from mice vaccinated with the MP3RT vaccine. The right lobe of the lung and the rest of the liver obtained from humanized or wild-type mice were used to perform H&E staining and analyzed with software. Each tissue section's pathological changes were observed using a microscope with original magnification times of 40 × **(A)** and 100 × **(D)**. The lung lesion area of tissue section obtained from humanized **(B)** or wild-type mice **(C)** was marked as red and determined using Image-Pro Plus software. The inflammatory cells of the lung tissue section obtained from humanized **(E)** or wild-type mice **(F)** were determined using Image-Pro Plus software. The inflammatory cells were marked in red, alveoli were marked in green, and alveolar walls were marked in yellow. Observations and calculations were done independently by two researchers, and their calculation results were merged. Five tissue sections of each mouse were randomly selected for continuous observation and then took the average value. The results were statistically analyzed with one-way analysis of variance (ANOVA) or Kruskal-Wallis test according to the data normality and homogeneity of variances. All data were shown as mean + SEM (n = 10 in humanized mice vaccinated with PBS and n = 20 in other groups). $P < 0.05$ was considered significantly different. *$P < 0.05$; ***$P < 0.001$; ****$P < 0.0001$.

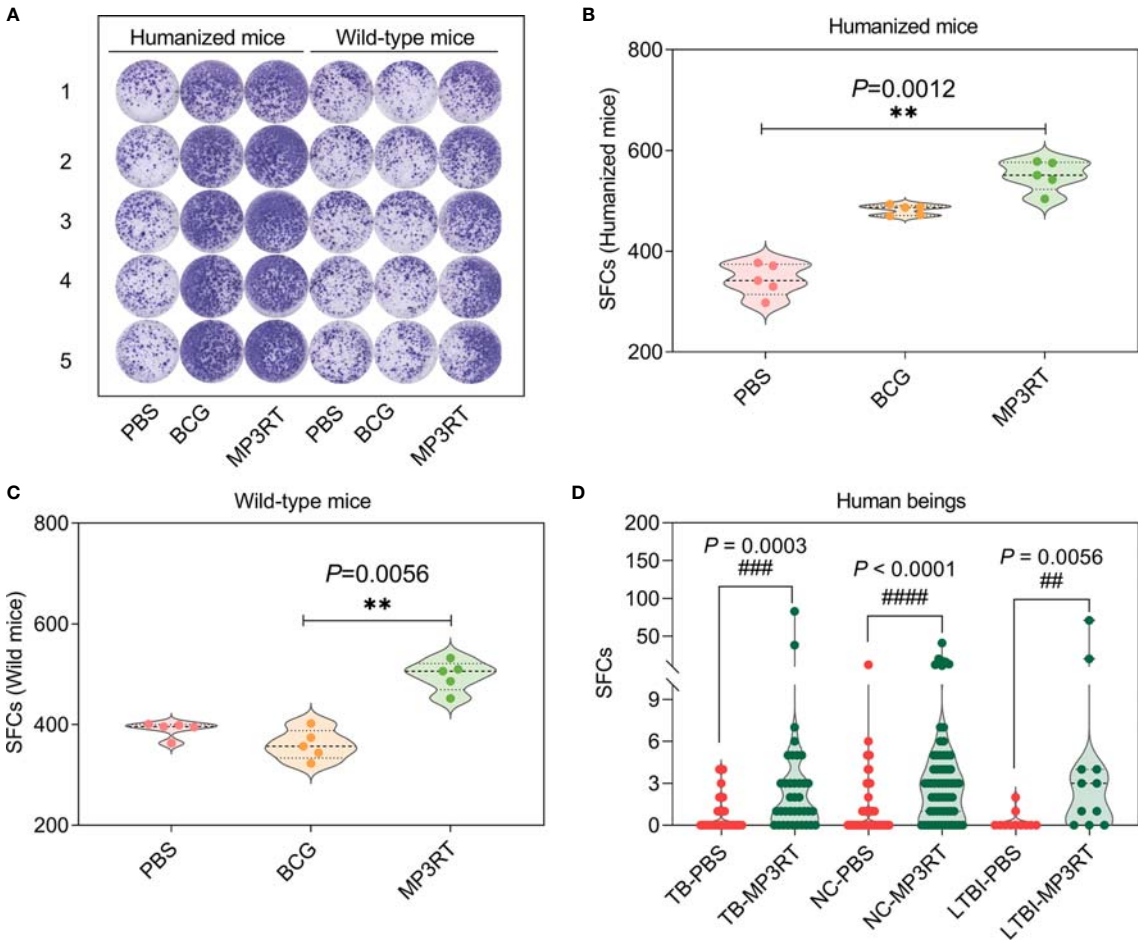

FIGURE 6 | IFN-γ$^+$ T lymphocytes detection with ELISPOT. The MP3RT vaccine was used to stimulate the PBMCs collected from humanized mice or wild-type mice vaccinated with PBS, BCG, and MP3RT *in vitro* **(A)**. The number of IFN-γ$^+$ T lymphocytes (showed as SFCs) in humanized mice **(B)** and wild-type mice **(C)** were determined with a mouse ELISPOT kit. The data were analyzed with a one-way analysis of variance (ANOVA) or Kruskal-Wallis test according to the data normality and homogeneity of variances. All data were shown as mean + SEM (n = 5). $P < 0.05$ was considered significantly different. **, $P < 0.01$. Furthermore, the number of IFN-γ$^+$ T lymphocytes in PBMCs collected from TB patients, LTBI volunteers, and normal controls (NC) were stimulated with the MP3RT vaccine *in vitro*. **(D)** The number of IFN-γ$^+$ T lymphocytes were determined with a human ELISPOT kit. The data were analyzed with the Unpaired *t*-test or nonparametric test (Mann Whitney test) according to the normality. All data were shown as mean + SEM (n = 37, 11, and 62 in TB patients, LTBI volunteers, and normal controls, respectively). $P<0.05$ was considered significantly different. $^{\#\#}P < 0.01$; $^{\#\#\#}P <0.001$; $^{\#\#\#\#}P < 0.0001$.

Figure8B); (2) The frequency of CD3$^+$CD4$^+$ T cells in mice vaccinated with MP3RT was higher than that in mice vaccinated with BCG (P = 0.0361, **Figure 8C**); (3) The frequency of CD3$^+$IFN-γ$^+$ Th1 cells in mice vaccinated with MP3RT was higher than that in mice vaccinated with PBS (P = 0.0046, **Figure 8D**) or BCG (P = 0.0005, **Figure 8D**); (4) The frequency of CD3$^+$IL-4$^+$ Th2 cells (**Figure 8E**) or CD4$^+$CD25$^+$FoxP3$^+$ Treg cells (**Figure 8F**) had no significant differences among groups.

In wild-type mice (**Figure S1A**), the frequency of lymphocytes in mice vaccinated with BCG was higher than that in mice vaccinated with PBS (P = 0.0219, **Figure S1B**). The frequency of CD3$^+$CD4$^+$ T cells (**Figure S1C**), CD3$^+$IFN-γ$^+$ Th1 cells (**Figure S1D**), and CD3$^+$IL-4$^+$ Th2 cells (**Figure S1E**) had no significant differences among groups. The frequency of CD4$^+$CD25$^+$FoxP3$^+$ Treg cells in mice vaccinated with BCG (P = 0.0328) was lower than that in mice vaccinated with PBS (**Figure S1F**).

MP3RT Stimulated High Levels of Antigen-Specific Antibodies

The level of MP3RT-specific IgG was tested with ELISA. Firstly, the optimal dilution of IgG antibody was determined to be 1:400 with cut-off values of 0.157 (**Figure 9A**). Then, the serum samples were diluted at 1:400, and their OD_{450} values were analyzed with a microplate reader. The results indicated that: (1) In humanized mice, the OD_{450} values of MP3RT-special IgG (P = 0.0015, **Figure 9B**) antibody in serum collected from mice vaccinated with MP3RT were significantly higher than those in serum collected from mice vaccinated with PBS or BCG; (2) In wild-type mice, the OD_{450} values of MP3RT-special IgG (**Figure 9C**)

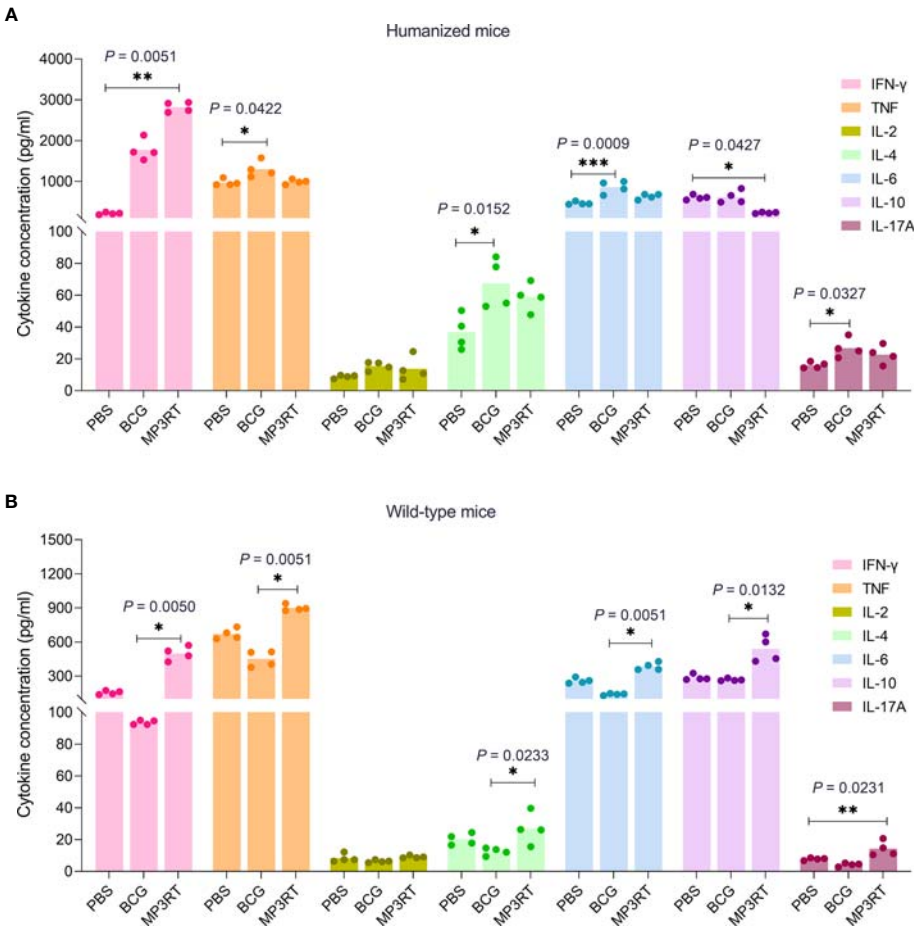

FIGURE 7 | Cytokines. The splenocytes isolated from humanized mice **(A)** or wild-type mice **(B)** immunized with PBS, BCG, or MP3RT were stimulated with the MP3RT vaccine for 48 hours. The levels of IFN-γ, TNF-α, IL-2, IL-4, IL-6, IL-10, and IL-17A cytokines in the supernatant were detected with a Mouse Th1/Th2/Th17 Cytokine Kit. The differences were compared with the one-way analysis of variance (ANOVA) or Kruskal-Wallis test according to the data normality and homogeneity of variances. All data were shown as mean + SEM (n = 4). $P < 0.05$ was considered significantly different. *$P < 0.05$; **$P < 0.01$; ***$P < 0.001$.

antibody in serum collected from mice vaccinated with MP3RT were significantly higher than those in serum collected from mice vaccinated with PBS ($P = 0.0066$) or BCG ($P < 0.0001$).

DISCUSSION

In this study, we reported a novel peptide-based vaccine, MP3RT. The MP3RT vaccine consisted of six immunodominant epitope peptides from five proteins (Mtb8.4, PPE18, PPE68, RpfA, and TB10.4), which were linked in silico by GGGGS linkers. Mtb8.4 (Rv1174c) and TB10.4 (Rv0288) are low molecular weight T-cell antigens and possible vaccine candidates that induced strong cell-mediated and humoral immune responses against *M. tuberculosis* (26–30). PPE18 (Rv1196) and PPE68 (Rv3873) are members of the *M. tuberculosis* PPE family. PPE18 is a crucial virulence factor for the intracellular survival of *M. tuberculosis* and one of the main components of the M72/AS01E vaccine (31, 32). Recently, Komal Dolasia et al. reported that PPE18 protein inhibited MHC class II antigen presentation (33). However, we found that two peptides ($PPE18_{115\text{-}129}$ and $PPE18_{149\text{-}163}$) of PPE18 protein could be recognized and presented by splenolymphocytes from humanized mice. PPE68 involves diversifying selection to evade host immunity and stimulating high levels of IFN-γ in PBMCs isolated from TB patients (34, 35). Both are reported to be attractive vaccine candidates for preventive and therapeutic against TB (31, 32, 34, 35). RpfA (Rv0867c), a possible resuscitation-promoting factor, may influence the outcome of reactivation *via* modulating innate immune responses to *M. tuberculosis* (36). It was reported that RpfA induced a high level of IFN-γ and was a TB vaccine candidate (37).

In previous studies, several immunogenic peptides of these five proteins have been identified, such as $Mtb8.4_{61\text{-}69}$ (ASPVAQSYL) and $Mtb8.4_{33\text{-}43}$ (AVINTTCNYGQ) (38), $PPE68_{118\text{-}135}$ (VLTATNFFGINTIPIALT) (34), $PPE68_{124\text{-}156}$ (ATNFFGINTIPIALTEMDYFIRMWNQAALAMEV) (39),

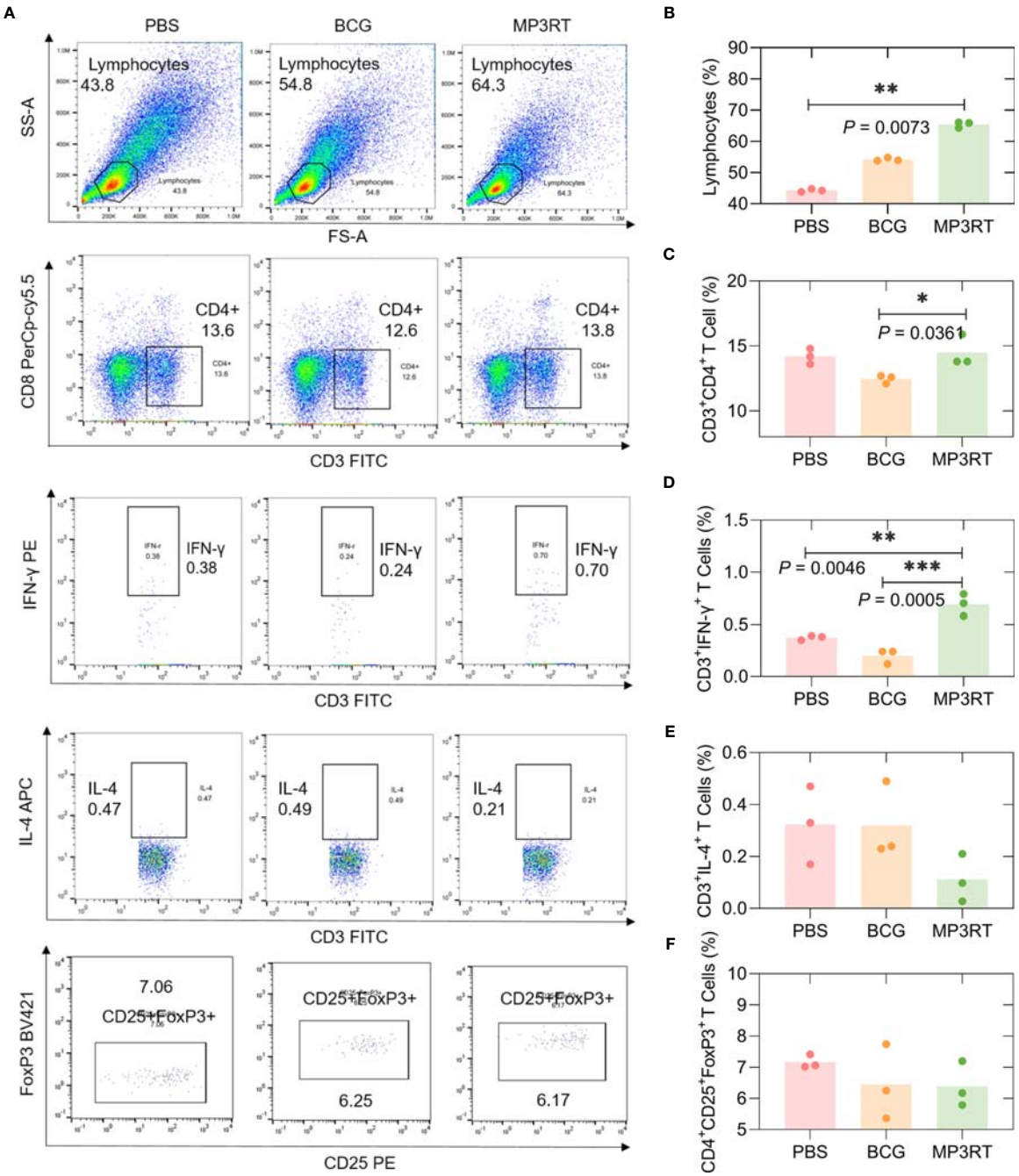

FIGURE 8 | The frequency of lymphocytes, $CD3^+CD4^+$ T cells, $CD3^+IFN\text{-}\gamma^+$ T cells, $CD3^+IL\text{-}4^+$ T cells, and $CD4^+CD25^+FoxP3^+$ Treg T cells in humanized mice. The splenocytes suspension was prepared, and the frequency of lymphocytes **(A, B)**, $CD3^+CD4^+$ T cells **(A, C)**, $CD3^+IFN\text{-}\gamma^+$ T cells **(A, D)**, $CD3^+IL\text{-}4^+$ T cells **(A, E)**, and $CD4^+CD25^+FoxP3^+$ regulatory T cells **(A, F)** was quantified with a BD IntraSure™ kit. The differences in the frequency of cells among PBS, BCG, and MP3RT groups were analyzed with the one-way analysis of variance (ANOVA) or Kruskal-Wallis test according to the data normality homogeneity of variances. All data were shown as mean + SEM (n = 3). $P < 0.05$ was considered significantly different. *$P < 0.05$; **$P < 0.01$; ***$P < 0.001$.

$PPE68_{127\text{-}136}$ (FFGINTIPIA) (40), $RpfA_{41\text{-}60}$ (DGEWDQV ARCESGGNWSINT) (37), $TB10.4_{3\text{-}11}$ (QIMYNYPAM) (41), and $TB10.4_{20\text{-}28}$ (GYAGTLQSL) (42). Herein, using the ELISOPT assays, we identified six immunodominant peptides of above five proteins, including $Mtb8.4_{69\text{-}83}$ (LRNFLAAPPP QRAAM), $PPE18_{115\text{-}129}$ (RAELMILIATNLLGQ), $PPE18_{149\text{-}163}$ (AAAMFGYAAATATAT), $PPE68_{138\text{-}152}$ (DYFIRMW NQAALAME), $RpfA_{377\text{-}391}$ (AYTKKLWQAIRAQDV), and

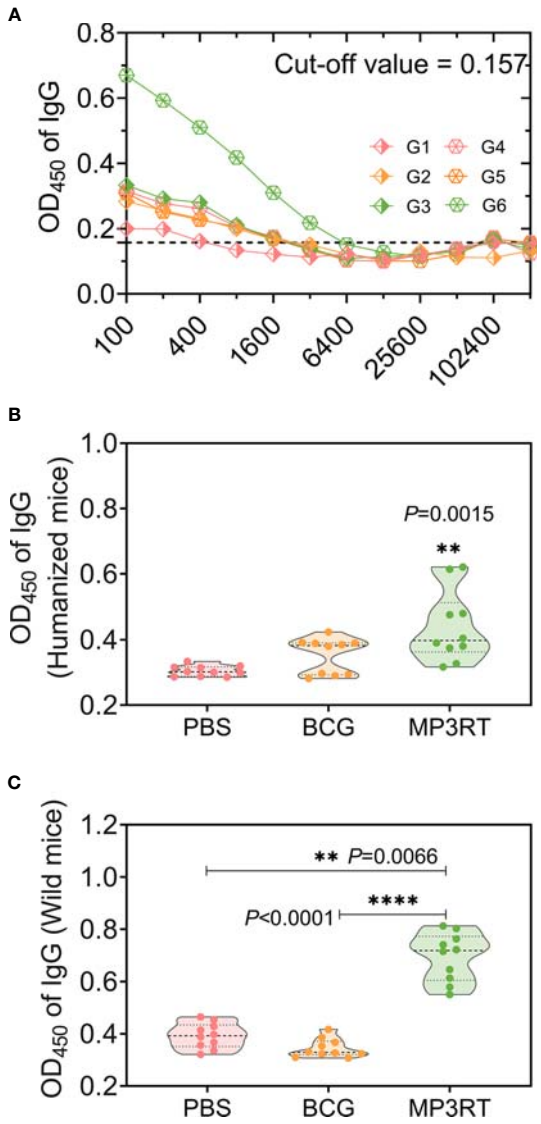

FIGURE 9 | MP3RT-specific IgG antibody. Ninety-one days after the first immunization, the mice in each were killed, and their blood samples were collected for preparing sera. The MP3RT-specific antibodies were detected with ELISA assay. The optimum dilution of IgG **(A)** in sera of humanized or wild-type mice immunized with PBS (G1 or G4 group), BCG (G2 or G5 group), and MP3RT (G3 or G6 group) were determined with a cut-off value. The OD_{450} of IgG antibody in sera of humanized **(B)** or wild-type mice **(C)** was analyzed with a microplate reader. The significant differences of OD_{450} of IgG were analyzed using the one-way analysis of variance (ANOVA) or Kruskal-Wallis test according to the data normality and homogeneity of variances. Data were shown as mean ± SEM (n = 10). P<0.05 was considered significantly different. **P<0.01; ****P<0.0001.

$TB10.4_{21-35}$ (YAGTLQSLGAEIAVE). Interestingly, we found that the peptides $Mtb8.4_{69-83}$, $PPE68_{138-152}$, and $TB10.4_{21-35}$ identified in this study overlapped with the peptides $Mtb8.4_{61-69}$, $PPE68_{124-156}$, and $TB10.4_{20-28}$ previously reported in the literatures (38, 39, 42), respectively. This finding indicates that the IEDB database has unique advantages in predicting Th1-dominant epitopes (8), and it also provides the possibility of using these overlapping epitopes to construct new epitope vaccines in the future.

The most significant difference between MP3RT vaccines and traditional subunit vaccines is that the former are MHC restricted. Therefore, the construction and selection of animal models are the basis for evaluating the protective efficiency of a vaccine. In the current study, we evaluated the protective efficacy of the MP3RT vaccine in humanized C57BL/6 mice (HLA-$A11^{+/+}DR1^{+/+}$H-2-$\beta2m^{-/-}$/$IA\beta^{-/-}$) and wild-type C57BL/6 mice, respectively. This humanized mouse model has been successfully used to evaluate the efficacy of an HIV vaccine restricted by the HLA-DR alleles in the Chinese population in our previous study (14). The clinical manifestations of TB patients often show symptom of weight loss. This phenomenon has also been verified in the animal model used in this study. Our research found that regardless of whether it was a wild-type mouse or a humanized mouse, weight loss occurred within one week after *M. tuberculosis* infection. Interestingly, the bodyweight of humanized mice vaccinated with BCG and MP3RT began to recover rapidly after one week, while that of humanized mice in other groups recovered slowly. In particular, several humanized mice, rather than wild-type mice, immunized with PBS died after the *M. tuberculosis* challenge. These data showed at least two conclusions: First, compared with wild-type mice, humanized mice are more susceptible to *M. tuberculosis* infection, which has been observed in our previous study (14); Second, MP3RT vaccine has a considerable protection effect on humanized mice, but the initial immune response induced by MP3RT vaccine does not appear until two weeks after *M. tuberculosis* infection. The delayed activation of the primary immune response might provide a window period for *M. tuberculosis* to develop infection in lung (43). This delay may be caused by the following factors, such as low-dose mycobacteria, low inflammatory response in the lung itself, or suppressing the activation of the primary immune response caused by *M. tuberculosis*.

Similarly, the MP3RT vaccine's protection was confirmed by CFUs counting experiment and pathological analysis in this study. The results showed that the CFUs in the lungs and livers of humanized mice immunized with MP3RT were significantly reduced and that in the livers of humanized mice and wild-type mice immunized with DNA vaccine were also decreased. The lung is the most common site of initial *M. tuberculosis* infection. The APCs recognize and phagocytose the mycobacteria in the lung and subsequently migrate to the lung-draining lymph nodes to activate T cells (44). Therefore, the lung has essential value in evaluating vaccine protection efficiency. Given this, we further analyzed the lung's pathological lesions. We found that the lesion area and the number of inflammatory cells in the lungs collected from MP3RT vaccinated mice were significantly smaller than these in PBS immunized mice.

The above data indicated that the MP3RT vaccine had potential immune protection advantages in humanized animal models. We can't help asking why this vaccine has protective effect only in humanized mice and no protective effect in wild

mice? As mentioned above, the most obvious difference between peptides-based vaccines and other subunit vaccines is that the former are designed based on MHC restrictions. It has been reported that the MHC class I or II molecule play an important role in the presentation of particular peptides to cytotoxic T lymphocyte (CTL) or helper T lymphocyte (HTL), respectively (45, 46). The epitopes consisted of MP3RT vaccine were determined by ELISPOT assay based on their significantly higher HLA-DR1 binding affinity, which laid a fundament for the protective effect in humanized C57BL/6 mice (HLA-A11$^{+/+}$DR1$^{+/+}$H-2-β2m$^{-/-}$/IAβ$^{-/-}$) rather than wild C57BL/6 mice (HLA-A11$^{-/-}$DR1$^{-/-}$H-2-β2m$^{+/+}$/IAβ$^{+/+}$). These results also remind us that it is necessary to select a suitable transgenic mouse model in the design, protective evaluation, and immune mechanism exploration of peptides-base vaccines.

Subsequently, we have also explored the immune mechanism behind it. *M. tuberculosis* is an intracellular bacterium, and the host's elimination and strangulation of *M. tuberculosis* mainly depend on specific T lymphocytes such as Th1 and Th17 cells (2). Previous studies have shown that Th1 cells activate the protective immunity against *M. tuberculosis* infection by secreting IFN-γ and TNF-α to activate the oxidative burst in macrophages, the expression of nitric oxide (NO) synthase 2, and the production of reactive nitrogen intermediates (47, 48). In contrast, Th2 cell response makes the host more susceptible to *M. tuberculosis* infection, and the role of Th17 cells in *M. tuberculosis* infection has not yet been determined (49, 50). This study observed that the MP3RT vaccine stimulated splenocytes producing a high level of IFN-γ and a low level of IL-10 in the humanized mouse model. Furthermore, we also found that the number of IFN-γ$^+$ T lymphocytes in spleens collected from mice vaccinated with MP3RT vaccine was more than that in the control group. Unexpectedly, the MP3RT protein stimulated a significantly high level of IFN-γ$^+$ T lymphocytes in TB patients, LTBI volunteers and normal controls *in vitro*. However, it is difficult to determine whether the immune response induced by MP3RT is biased towards CD3$^+$CD4$^+$ T lymphocytes, IFN-γ$^+$ T lymphocytes, or CD3$^+$CD8$^+$ T lymphocytes, because CD3$^+$CD8$^+$ T lymphocytes can contribute to mycobacteria control by secretion of IFN-γ (51). This doubt was answered in our subsequent flow cytometry experiments. To confirm which type of lymphocyte plays a crucial role in inducing protective effect, we used flow cytometry to classify the T lymphocytes. We found that T lymphocytes' frequency in the spleens of MP3RT-immunized mice was twice that of the control group. The frequencies of CD3$^+$CD4$^+$ T lymphocytes and CD3$^+$IFN-γ$^+$ T lymphocytes in the spleens of humanized mice vaccinated with MP3RT were significantly higher than these of the control group. However, there was no difference in the frequency of CD3$^+$IL-4$^+$ T lymphocytes and CD4$^+$CD25$^+$FoxP3$^+$ T lymphocytes among the groups. Our data support a positive critical role of MP3RT vaccine in immune protection against *M. tuberculosis* infection depends on up-regulated Th1-type T lymphocytes and down-regulated Treg cells and Th2-type T lymphocytes.

It is generally believed that T cells play an irreplaceable role in eliminating and strangulation of *M. tuberculosis*. Currently, accumulating evidence has suggested that B cells play an important role in resisting *M. tuberculosis*'s respiratory tract infection and inflammation (52, 53). B lymphocytes and T lymphocytes have a wide range of synergy in defending against *M. tuberculosis* infection, and B lymphocytes significantly affect the activation of T lymphocytes (53). To determine the humoral immune response mediated by B cells, we detected the MP3RT-specific IgG titers in serum samples. The results revealed that the MP3RT vaccine induced significantly higher levels of IgG antibody in humanized or wild-type mice.

As exploratory research, this study has some unavoidable shortcomings. First, the epitopes of the MP3RT vaccine were initially designed to bind human HLA-DRB1*01:01 allele instead of HLA-DP, HLA-DQ, HLA-A, HLA-B, and HLA-C alleles, which may lead to the decrease of recognition efficiency of MP3RT vaccine for other alleles. Second, the MP3RT vaccine was composed of Th1 cell epitopes rather than CTL or B cell epitopes, which may weaken this vaccine's protection efficiency. Third, only MP3RT-specific IgG antibody levels were detected but not subtypes such as IgG, IgG2b, and IgG2c antibody levels, which may have missed a strong evidence for elucidating the immune mechanism of MP3RT. Finally, limited to the types of available transgenic animal models, the MP3RT vaccine contains only HLA-DRB1*01:01 binding epitopes and evaluated only on humanized C57BL/6 mice with HLA-A11$^{+/+}$DR1$^{+/+}$H-2-β2m$^{-/-}$/IAβ$^{-/-}$. In future research, we will further enrich the types of epitopes that constitute MP3RT vaccine and verify them on more transgenic animal models.

CONCLUSION

In summary, these data suggested that MP3RT vaccination elicits significant protection against *M. tuberculosis* infection in humanized mice rather than wild-type mice. The potential mechanism of the immune protection depends on MP3RT-specific immune response by triggering the activation of CD3$^+$CD4$^+$ T lymphocytes and CD3$^+$IFN-γ$^+$ T lymphocytes characterized by producing a high level of IFN-γ and IgG antibody. Our research once again proves the role of Th1 epitopes in the fight against TB and the importance of vaccine construction, which will provide a basis for future vaccine design.

DATA AVAILABILITY STATEMENT

The original contributions presented in the study are included in the article/**Supplementary Material**. Further inquiries can be directed to the corresponding author.

ETHICS STATEMENT

The clinical investigation related to PBMCs isolation was approved by the Medical Ethics Committee of the 8th Medical Center of Chinese PLA General Hospital (Approved Number: 2018ST011). The patients/participants provided their written informed consent to participate in this study. The animal study was reviewed and approved by Animal Ethical Committee of the 8th Medical Center of Chinese PLA General Hospital (Approved Number: 309201808171015). Written informed consent was obtained from the owners for the participation of their animals in this study.

AUTHOR CONTRIBUTIONS

Conceptualization: XW, and WG. Methodology: WG, YL, JM, ZJ, YX, LW, JW, YZ, and SS. Data analysis: WG, and JM. Software: WG. Writing original manuscript: WG. Review and revising manuscript: XW, and WG. Funding acquisition: WG, and YZ. All authors contributed to the article and approved the submitted version.

FUNDING

This study was funded by the National Natural Science Foundation of China (Grant No. 81801643), Beijing Municipal Science & Technology Commission (Grant No. Z18110000 1718005 and 19L2152), Chinese PLA General Hospital (Grant No. QNC19047), National Project of Infectious Diseases (Grant No. 2017ZX10304402003007, 2012ZX10003008002, 2018ZX10731301005001, and AWS17J015).

ACKNOWLEDGMENTS

The authors would like to acknowledge Dr. Yumei Liang, Dr. Wen Chen, and Professor Fenghua Wang from the Department of the pathology of the 8th Medical Center of Chinese PLA General Hospital for the preparation of pathological sections.

SUPPLEMENTARY MATERIAL

The Supplementary Material for this article can be found online at: https://www.frontiersin.org/articles/10.3389/fimmu.2021.666290/full#supplementary-material

Supplementary Figure 1 | The frequency of lymphocytes, $CD3^+CD4^+$ T cells, $CD3^+IFN\text{-}\gamma^+$ T cells, $CD3^+IL\text{-}4^+$ T cells, and $CD4^+CD25^+FoxP3^+$ Treg T cells in wild-type mice. The splenocytes suspension was prepared, and the frequency of lymphocytes **(A, B)**, $CD3^+CD4^+$ T cells **(A, C)**, $CD3^+IFN\text{-}\gamma^+$ T cells **(A, D)**, $CD3^+IL\text{-}4^+$ T cells **(A, E)**, and $CD4^+CD25^+FoxP3^+$ regulatory T cells **(A, F)** was quantified with BD IntraSure™ kit. The differences in the frequency of cells among PBS, BCG, and MP3RT groups were analyzed with the one-way analysis of variance (ANOVA) or Kruskal-Wallis test according to the data normality homogeneity of variances. All data were shown as mean + SEM (n = 3). $P<0.05$ was considered significantly different. *, $P<0.05$.

REFERENCES

1. Comas I, Coscolla M, Luo T, Borrell S, Holt KE, Kato-Maeda M, et al. Out-of-Africa Migration and Neolithic Coexpansion of *Mycobacterium Tuberculosis* With Modern Humans. *Nat Genet* (2013) 45:1176–82. doi: 10.1038/ng.2744
2. Gong W, Liang Y, Wu X. The Current Status, Challenges, and Future Developments of New Tuberculosis Vaccines. *Hum Vaccin Immunother* (2018) 14:1697–716. doi: 10.1080/21645515.2018.1458806
3. WHO. *Global Tuberculosis Report 2020*. Geneva: World Health Organization (2020) p. 1–232.
4. Glaziou P. Predicted Impact of the COVID-19 Pandemic on Global Tuberculosis Deaths in 2020. *MedRxiv* (2020), 2020.04.28.20079582. doi: 10.1101/2020.04.28.20079582
5. How to Stop COVID-19 Fuelling a Resurgence of AIDS, Malaria and Tuberculosis. *Nature* (2020) 584:169. doi: 10.1038/d41586-020-02334-0
6. Roy P, Vekemans J, Clark A, Sanderson C, Harris RC, White RG. Potential Effect of Age of BCG Vaccination on Global Paediatric Tuberculosis Mortality: A Modelling Study. *Lancet Global Health* (2019) 7:e1655–e63. doi: 10.1016/S2214-109X(19)30444-9
7. Hussey G, Hawkridge T, Hanekom W. Childhood Tuberculosis: Old and New Vaccines. *Paediatr Respir Rev* (2007) 8:148–54. doi: 10.1016/j.prrv.2007.04.009
8. Reche P, Flower DR, Fridkis-Hareli M, Hoshino Y. Peptide-Based Immunotherapeutics and Vaccines 2017. *J Immunol Res* (2018) 2018:4568239. doi: 10.1155/2018/4568239
9. Ortega-Tirado D, Arvizu-Flores AA, Velazquez C, Garibay-Escobar A. The Role of Immunoinformatics in the Development of T-cell Peptide-Based Vaccines Against *Mycobacterium Tuberculosis*. *Expert Rev Vaccines* (2020) 19:831–41. doi: 10.1080/14760584.2020.1825950
10. Bettencourt P, Müller J, Nicastri A, Cantillon D, Madhavan M, Charles PD, et al. Identification of Antigens Presented by MHC for Vaccines Against Tuberculosis. *NPJ Vaccines* (2020) 5:2. doi: 10.1038/s41541-019-0148-y
11. Gong W, Liang Y, Wu X. Animal Models of Tuberculosis Vaccine Research: An Important Component in the Fight Against Tuberculosis. *BioMed Res Int* (2020) 2020:4263079. doi: 10.1155/2020/4263079
12. Gong W, Qi Y, Xiong X, Jiao J, Duan C, Wen B. *Rickettsia Rickettsii* Outer Membrane Protein YbgF Induces Protective Immunity in C3H/HeN Mice. *Hum Vaccin Immunother* (2015) 11:642–9. doi: 10.1080/21645515.2015.1011572
13. Gong W, Xiong X, Qi Y, Jiao J, Duan C, Wen B. Surface Protein Adr2 of *Rickettsia Rickettsii* Induced Protective Immunity Against Rocky Mountain Spotted Fever in C3H/HeN Mice. *Vaccine* (2014) 32:2027–33. doi: 10.1016/j.vaccine.2014.02.057
14. Zeng Y, Gao T, Zhao G, Jiang Y, Yang Y, Yu H, et al. Generation of Human MHC (HLA-A11/DR1) Transgenic Mice for Vaccine Evaluation. *Hum Vaccin Immunother* (2016) 12:829–36. doi: 10.1080/21645515.2015.1103405
15. Gong W-P, Liang Y, Ling Y-B, Zhang J-X, Yang Y-R, Wang L, et al. Effects of Mycobacterium Vaccae Vaccine in a Mouse Model of Tuberculosis: Protective Action and Differentially Expressed Genes. *Mil Med Res* (2020) 7:25. doi: 10.1186/s40779-020-00258-4
16. Ramos Robles B, Valdez RA, Hernández UJ, Marquina Castillo B, Mata Espinosa D, Barrios Payan J, et al. Immunoendocrine Abnormalities in the Male Reproductive System During Experimental Pulmonary Tuberculosis. *Tuberculosis (Edinburgh Scotland)* (2018) 109:109–16. doi: 10.1016/j.tube.2018.02.005
17. Gong WP, Wang PC, Xiong XL, Jiao J, Yang XM, Wen BH. Chloroform-Methanol Residue of Coxiella Burnetii Markedly Potentiated the Specific Immunoprotection Elicited by a Recombinant Protein Fragment rOmpB-4 Derived From Outer Membrane Protein B of *Rickettsia Rickettsii* in C3H/HeN Mice. *PloS One* (2015) 10:e0124664. doi: 10.1371/journal.pone.0124664
18. Gong WP, Wang PC, Xiong XL, Jiao J, Yang XM, Wen BH. Enhanced Protection Against *Rickettsia Rickettsii* Infection in C3H/HeN

Mice by Immunization With a Combination of a Recombinant Adhesin rAdr2 and a Protein Fragment rOmpB-4 Derived From Outer Membrane Protein B. *Vaccine* (2015) 33:985–92. doi: 10.1016/j.vaccine.2015.01.017

19. Zvi A, Ariel N, Fulkerson J, Sadoff JC, Shafferman A. Whole genome identification of Mycobacterium tuberculosis vaccine candidates by comprehensive data mining and bioinformatic analyses. *BMC Med Genomics* (2008) 1:18. doi: 10.1186/1755-8794-1-18
20. Singh R, Gupta P, Sharma PK, Ades EW, Hollingshead SK, Singh S, et al. Prediction and Characterization of Helper T-cell Epitopes From Pneumococcal Surface Adhesin A. *Immunology* (2014) 141:514–30. doi: 10.1111/imm.12194
21. Wang PC, Xiong XL, Jiao J, Yang XM, Jiang YQ, Wen BH, et al. Th1 Epitope Peptides Induce Protective Immunity Against *Rickettsia Rickettsii* Infection in C3H/HeN Mice. *Vaccine* (2017) 35:7204–12. doi: 10.1016/j.vaccine.2017.09.068
22. Waterhouse A, Bertoni M, Bienert S, Studer G, Tauriello G, Gumienny R, et al. Swiss-MODEL: Homology Modelling of Protein Structures and Complexes. *Nucleic Acids Res* (2018) 46:W296–w303. doi: 10.1093/nar/gky427
23. Liang Y, Wu X, Zhang J, Xiao L, Yang Y, Bai X, et al. Immunogenicity and Therapeutic Effects of Ag85A/B Chimeric DNA Vaccine in Mice Infected With *Mycobacterium Tuberculosis*. *FEMS Immunol Med Microbiol* (2012) 66:419–26. doi: 10.1111/1574-695X.12008
24. Chen H, Wu B, Zhang T, Jia J, Lu J, Chen Z, et al. Effect of Linker Length and Flexibility on the Clostridium Thermocellum Esterase Displayed on *Bacillus Subtilis* Spores. *Appl Biochem Biotechnol* (2017) 182:168–80. doi: 10.1007/s12010-016-2318-y
25. Valiyari S, Salimi M, Bouzari S. Novel Fusion Protein NGR-sIL-24 for Targetedly Suppressing Cancer Cell Growth Via Apoptosis. *Cell Biol Toxicol* (2020) 36:179–93. doi: 10.1007/s10565-020-09519-3
26. Li H, Li R, Zhong S, Ren H. [Plasmid Encoding Human IL-12 Improve Protective Efficacy of Mtb8.4 Gene Vaccine With Signal Sequence Against Infection of *Mycobacterium Tuberculosis*]. *Xi Bao Yu Fen Zi Mian Yi Xue Za Zhi* (2007) 23:291–4.
27. Luo Y, Wang B, Hu L, Yu H, Da Z, Jiang W, et al. Fusion Protein Ag85B-MPT64(190-198)-Mtb8.4 has Higher Immunogenicity Than Ag85B With Capacity to Boost BCG-primed Immunity Against *Mycobacterium Tuberculosis* in Mice. *Vaccine* (2009) 27:6179–85. doi: 10.1016/j.vaccine.2009.08.018
28. Billeskov R, Grandal MV, Poulsen C, Christensen JP, Winther N, Vingsbo-Lundberg C, et al. Difference in TB10.4 T-Cell Epitope Recognition Following Immunization With Recombinant TB10.4, BCG or Infection With *Mycobacterium Tuberculosis*. *Eur J Immunol* (2010) 40:1342–54. doi: 10.1002/eji.200939830
29. Davila J, Zhang L, Marrs CF, Durmaz R, Yang Z. Assessment of the Genetic Diversity of *Mycobacterium Tuberculosis* esxA, esxH, and Fbpb Genes Among Clinical Isolates and its Implication for the Future Immunization by New Tuberculosis Subunit Vaccines Ag85B-ESAT-6 and Ag85B-TB10.4. *J BioMed Biotechnol* (2010) 2010:208371. doi: 10.1155/2010/208371
30. Rashidian S, Teimourpour R, Meshkat Z. Designing and Construction of a DNA Vaccine Encoding Tb10.4 Gene of *Mycobacterium Tuberculosis*. *Iran J Pathol* (2016) 11:112–9.
31. Bhat KH, Ahmed A, Kumar S, Sharma P, Mukhopadhyay S. Role of PPE18 Protein in Intracellular Survival and Pathogenicity of *Mycobacterium Tuberculosis* in Mice. *PloS One* (2012) 7:e52601. doi: 10.1371/journal.pone.0052601
32. Homolka S, Ubben T, Niemann S. High Sequence Variability of the Ppe18 Gene of Clinical *Mycobacterium Tuberculosis* Complex Strains Potentially Impacts Effectivity of Vaccine Candidate M72/AS01E. *PloS One* (2016) 11:e0152200. doi: 10.1371/journal.pone.0152200
33. Dolasia K, Nazar F, Mukhopadhyay S. *Mycobacterium Tuberculosis* PPE18 Protein Inhibits MHC Class II Antigen Presentation and B Cell Response in Mice. *Eur J Immunol* (2021) 51:603–19. doi: 10.1002/eji.201848071
34. Okkels LM, Brock I, Follmann F, Agger EM, Arend SM, Ottenhoff TH, et al. PPE Protein (Rv3873) From DNA Segment RD1 of *Mycobacterium Tuberculosis*: Strong Recognition of Both Specific T-cell Epitopes and Epitopes Conserved Within the PPE Family. *Infect Immun* (2003) 71:6116–23. doi: 10.1128/IAI.71.11.6116-6123.2003
35. Jiang Y, Wei J, Liu H, Li G, Guo Q, Qiu Y, et al. Polymorphisms in the PE35 and PPE68 Antigens in *Mycobacterium Tuberculosis* Strains may Affect Strain Virulence and Reflect Ongoing Immune Evasion. *Mol Med Rep* (2016) 13:947–54. doi: 10.3892/mmr.2015.4589
36. Russell-Goldman E, Xu J, Wang X, Chan J, Tufariello JM. A *Mycobacterium Tuberculosis* Rpf Double-Knockout Strain Exhibits Profound Defects in Reactivation From Chronic Tuberculosis and Innate Immunity Phenotypes. *Infect Immun* (2008) 76:4269–81. doi: 10.1128/IAI.01735-07
37. Commandeur S, van Meijgaarden KE, Lin MY, Franken KL, Friggen AH, Drijfhout JW, et al. Identification of Human T-cell Responses to *Mycobacterium Tuberculosis* Resuscitation-Promoting Factors in Long-Term Latently Infected Individuals. *Clin Vaccine Immunol* (2011) 18:676–83. doi: 10.1128/CVI.00492-10
38. Lewinsohn DA, Winata E, Swarbrick GM, Tanner KE, Cook MS, Null MD, et al. Immunodominant Tuberculosis CD8 Antigens Preferentially Restricted by HLA-B. *PloS Pathog* (2007) 3:1240–9. doi: 10.1371/journal.ppat.0030127
39. Horváti K, Pályi B, Henczkó J, Balka G, Szabó E, Farkas V, et al. A Convenient Synthetic Method to Improve Immunogenicity of *Mycobacterium Tuberculosis* Related T-Cell Epitope Peptides. *Vaccines (Basel)* (2019) 7:101–15. doi: 10.3390/vaccines7030101
40. Mustafa AS, Al-Attiyah R, Hanif SN, Shaban FA. Efficient Testing of Large Pools of *Mycobacterium Tuberculosis* RD1 Peptides and Identification of Major Antigens and Immunodominant Peptides Recognized by Human Th1 Cells. *Clin Vaccine Immunol* (2008) 15:916–24. doi: 10.1128/CVI.00056-08
41. Ashhurst AS, McDonald DM, Hanna CC, Stanojevic VA, Britton WJ, Payne RJ. Mucosal Vaccination With a Self-Adjuvanted Lipopeptide Is Immunogenic and Protective Against *Mycobacterium Tuberculosis*. *J Med Chem* (2019) 62:8080–9. doi: 10.1021/acs.jmedchem.9b00832
42. Majlessi L, Rojas MJ, Brodin P, Leclerc C. Cd8+-T-cell Responses of Mycobacterium-infected Mice to a Newly Identified Major Histocompatibility Complex Class I-restricted Epitope Shared by Proteins of the ESAT-6 Family. *Infect Immun* (2003) 71:7173–7. doi: 10.1128/IAI.71.12.7173-7177.2003
43. Urdahl KB. Understanding and Overcoming the Barriers to T Cell-Mediated Immunity Against Tuberculosis. *Semin Immunol* (2014) 26:578–87. doi: 10.1016/j.smim.2014.10.003
44. Wolf AJ, Desvignes L, Linas B, Banaiee N, Tamura T, Takatsu K, et al. Initiation of the Adaptive Immune Response to *Mycobacterium Tuberculosis* Depends on Antigen Production in the Local Lymph Node, Not the Lungs. *J Exp Med* (2008) 205:105–15. doi: 10.1084/jem.20071367
45. Yang Z, Bogdan P, Nazarian S. An in Silico Deep Learning Approach to Multi-Epitope Vaccine Design: A SARS-CoV-2 Case Study. *Sci Rep* (2021) 11:3238. doi: 10.1038/s41598-021-81749-9
46. Srivastava S, Verma S, Kamthania M, Agarwal D, Saxena AK, Kolbe M, et al. Computationally Validated SARS-CoV-2 CTL and HTL Multi-Patch Vaccines, Designed by Reverse Epitomics Approach, Show Potential to Cover Large Ethnically Distributed Human Population Worldwide. *J Biomol Struct Dyn* (2020) 6:1–20. doi: 10.1080/07391102.2020.1838329
47. Abebe F. Is Interferon-Gamma the Right Marker for Bacille Calmette-Guerin-induced Immune Protection? The Missing Link in Our Understanding of Tuberculosis Immunology. *Clin Exp Immunol* (2012) 169:213–9. doi: 10.1111/j.1365-2249.2012.04614.x
48. Hu Z, Gu L, Li CL, Shu T, Lowrie DB, Fan XY. The Profile of T Cell Responses in Bacille Calmette-Guérin-Primed Mice Boosted by a Novel Sendai Virus Vectored Anti-Tuberculosis Vaccine. *Front Immunol* (2018) 9:1796. doi: 10.3389/fimmu.2018.01796
49. Sayes F, Pawlik A, Frigui W, Groschel MI, Crommelynck S, Fayolle C, et al. Cd4+ T Cells Recognizing Pe/Ppe Antigens Directly or Via Cross Reactivity Are Protective Against Pulmonary *Mycobacterium tuberculosis* Infection. *PloS Pathog* (2016) 12:e1005770. doi: 10.1371/journal.ppat.1005770
50. da Costa AC, Costa-Junior Ade O, de Oliveira FM, Nogueira SV, Rosa JD, Resende DP, et al. A New Recombinant BCG Vaccine Induces Specific Th17 and Th1 Effector Cells With Higher Protective Efficacy Against Tuberculosis. *PloS One* (2014) 9:e112848. doi: 10.1371/journal.pone.0112848

51. Shams H, Wizel B, Weis SE, Samten B, Barnes PF. Contribution of CD8(+) T Cells to Gamma Interferon Production in Human Tuberculosis. *Infect Immun* (2001) 69:3497–501. doi: 10.1128/IAI.69.5.3497-3501.2001
52. Maglione PJ, Xu J, Chan J. B Cells Moderate Inflammatory Progression and Enhance Bacterial Containment Upon Pulmonary Challenge With *Mycobacterium tuberculosis*. *J Immunol (Baltimore Md 1950)* (2007) 178:7222–34. doi: 10.4049/jimmunol.178.11.7222
53. Chan J, Mehta S, Bharrhan S, Chen Y, Achkar JM, Casadevall A, et al. The Role of B Cells and Humoral Immunity in *Mycobacterium tuberculosis* Infection. *Semin Immunol* (2014) 26:588–600. doi: 10.1016/j.smim.2014.10.005

Conflict of Interest: The authors declare that the research was conducted in the absence of any commercial or financial relationships that could be construed as a potential conflict of interest.

frontiers in Immunology

REVIEW
published: 30 June 2021
doi: 10.3389/fimmu.2021.696791

Beyond Just Peptide Antigens: The Complex World of Peptide-Based Cancer Vaccines

Alexander J. Stephens[1,2], *Nicola A. Burgess-Brown*[2] *and Shisong Jiang*[1*]

[1] Department of Oncology, Medical Sciences Division, University of Oxford, Oxford, United Kingdom, [2] Centre for Medicines Discovery, Nuffield Department of Medicine, Medical Sciences Division, University of Oxford, Oxford, United Kingdom

OPEN ACCESS

Edited by:
Jochen Mattner,
University of Erlangen Nuremberg, Germany

Reviewed by:
Shi Hu,
Second Military Medical University, China
María Marcela Barrio,
Fundación Cáncer, Argentina

***Correspondence:**
Shisong Jiang
Shisong.Jiang@oncology.ox.ac.uk

Specialty section:
This article was submitted to Vaccines and Molecular Therapeutics, a section of the journal Frontiers in Immunology

Received: 17 April 2021
Accepted: 17 June 2021
Published: 30 June 2021

Citation:
Stephens AJ, Burgess-Brown NA and Jiang S (2021) Beyond Just Peptide Antigens: The Complex World of Peptide-Based Cancer Vaccines. Front. Immunol. 12:696791. doi: 10.3389/fimmu.2021.696791

Peptide-based cancer vaccines rely upon the strong activation of the adaptive immune response to elicit its effector function. They have shown to be highly specific and safe, but have yet to prove themselves as an efficacious treatment for cancer in the clinic. This is for a variety of reasons, including tumour heterogeneity, self-tolerance, and immune suppression. Importance has been placed on the overall design of peptide-based cancer vaccines, which have evolved from simple peptide derivatives of a cancer antigen, to complex drugs; incorporating overlapping regions, conjugates, and delivery systems to target and stimulate different components of antigen presenting cells, and to bolster antigen cross-presentation. Peptide-based cancer vaccines are increasingly becoming more personalised to an individual's tumour antigen repertoire and are often combined with existing cancer treatments. This strategy ultimately aids in combating the shortcomings of a more generalised vaccine strategy and provides a comprehensive treatment, taking into consideration cancer cell variability and its ability to avoid immune interrogation.

Keywords: peptide, cancer, vaccine, dendritic cells, antigen, cross-presentation, immunotherapy

INTRODUCTION

Antigen Presentation in the Context of Cancer

Vaccines have been used for the treatment of infectious diseases for over 200 years and are based on the original principal of inoculating an individual with a weakened or inactive form of a microbe or its constituent components, with the aim of provoking an adaptive immune response to provide long term acquired immunity to a foreign antigen (1). Cancer vaccines work on the same principal by programming the immune system to recognise cancer antigens as 'foreign', and can be

administered prophylactically to prevent tumour occurrence, or therapeutically as a treatment in individuals who have already contracted the disease.

One of the hallmarks of cancer is its ability to avoid the immune system (2). Normally, aberrant cells are recognised by the immune system through immunosurveillance, where antigen presentation cells recognise and process antigens produced by these cells, presenting them to effector cells and leading to cell death through the adaptive immune response. In cancer however, many factors are at play which prevent the immune system functioning properly. This includes immunoediting, the process by which cancer cells escape the immune system by selective pressure on tumour cells for a non-immunogenic phenotype (3). The tumour microenvironment also plays a part, with its pro-cancer nature promoting tumour growth and preventing a strong anti-tumour response through immunosuppression (4, 5).

The most common treatments for cancers target rapidly dividing cells in a non-discriminatory manner, or by targeting cells with high doses of radiation to damage the DNA of tumour cells and induce cell death. The difficulty however is in the total removal or destruction of cancer cells and inherent or acquired multi-drug resistance, which ultimately leads to tumour recurrence (6, 7). Cancer immunotherapy aims to overcome this by reprogramming the body's immune system to recognise cancer-specific antigens and the tumours producing them, targeting cancer cells for destruction. This can include the production of anti-tumour antibodies by B-cells through humoral immunity, or through T-cell mediated cytotoxicity through the cell-mediated immune response. For this review, the focus will be primarily on the use of cancer vaccines in the context of a cell-mediated response, and the current progress in the field.

Cancer vaccines require the strong activation of the T-cell mediated adaptive immune response to elicit their anti-tumour potential. The adaptive immune response is initiated by the uptake, processing, and presentation of immunogenic antigens by antigen-presenting cells (APC). Dendritic cells (DCs) are one of the primary professional antigen-presenting cells, and act as the link between the antigen non-specific innate immune response and the antigen-specific adaptive immune response (8). Upon encountering an exogenous antigen, dendritic cells internalise them by receptor-mediated endocytosis or macropinocytosis and process the antigen within endosomes to be loaded onto MHC Class II molecules for presentation to $CD4^+$ T cells. This leads to the activation of a Th1 response, including the increased production of cytokines such as IFN-γ, which promotes and maintains macrophages and Cytotoxic T-lymphocyte (CTL) effector functions (9–11). A small proportion of internalised antigen can escape this classical pathway by export into the cytosol of DCs, where they are processed by the proteasome. The resulting peptides are transported to the endoplasmic reticulum, where they are loaded onto MHC class I molecules for presentation to $CD8^+$ T cells, a process known as antigen cross-presentation (12). The recognition and subsequent maturation of $CD8^+$ T cells by antigen cross-presentation results in an antigen-specific response against cells displaying that antigen. In the case of cancer, the $CD8^+$ T cells recognise surface-expressed cancer antigens on tumours and initiate apoptosis through cell-mediated cytotoxicity by releasing apoptotic factors such as Perforin, Fas Ligand and Granzymes (13). The activation of T cells by dendritic cells requires three signals, with any one missing resulting in incomplete activation. The first signal is generated by binding of the T-cell receptor (TCR) to peptide-bound MHC with the aid of the CD4 or CD8 co-receptors, which stabilise the bond and promote TCR signalling (14–16). Signal two is formed from co-stimulatory signals caused by the interaction of cell surface molecules between dendritic cells and T cells, for example by CD28 on T cells with B7 on DCs (17, 18). Finally, the third signal is provided by cytokines released by dendritic cells which drive the T cells into a specific type, for example IL-12 promotes a Th1 phenotype for T-helper cells and promotes the expansion of $CD8^+$ T cells (19–21).

Cancer is however, a complicated disease, with immunosuppressive cells in the tumour microenvironment such as regulatory T cells (Treg) and Myeloid-derived suppressor cells (MDSCs) tempering the immune response and aiding in cancer cell immune escape (22). Ultimately, the aim of a cancer vaccine is to strongly activate the $CD8^+$ T-cell pathway, mediated by $CD4^+$ T cells, thus overcoming self-tolerance and immune suppression, leading to the elimination of cancer cells.

Principals of Peptide-Based Cancer Vaccines

Peptide-based cancer vaccines typically consist of a sequence of amino acids derived from tumour-specific or tumour-associated antigens (TSA/TAA), the difference being whether the antigen is specific to cancer cells (TSA) or whether it can be found both on healthy and cancer cells, but at elevated levels in cancer (TAA). For peptide-based cancer vaccines to be efficacious, they must contain $CD8^+$ epitopes to exploit the antigen cross-presentation pathway, leading to the activation of CTL anti-tumour immunity, along with $CD4^+$ epitopes for T-helper cell activation, which sustains CTLs effector function (23). Therefore, to promote a strong immunogenic response, the sequence length of peptide vaccines is important. If the peptide is too short it can bind to MHC of non-professional APCs, which lack the secondary signalling machinery for complete T cell activation, leading to a poor T cell response or immune tolerance (24). Shorter peptides also tend to be HLA-type restricted due to their length not allowing for the diversity required for the high polymorphism of HLA in the general population (25, 26). Finally, short peptides are also prone to enzymatic digestion and elimination from the body faster unless modified (27, 28). A longer peptide length however allows for a broader population coverage of HLA-types (25, 26), the inclusion of multi-epitope peptides to bolster the $CD4^+$ and $CD8^+$ response, and allows for the inclusion of binding or recognition motifs to bolster immunogenicity.

Peptide-based cancer vaccines have showed promising immunogenicity in a pre-clinical setting, though there is a lot of progress still to be made for them to show strong clinical efficacy – to date no *in vivo* peptide-based cancer vaccine has attained FDA approval (29). There is a multitude of possible reasons for this, including: inappropriate adjuvants (30, 31), tumour heterogeneity (32, 33), tumour antigen loss (34), decreased MHC expression (35, 36), lack of infiltrating T cells in tumour tissue (37), and immune suppression through T cell dysfunction (38, 39).

Peptide-based cancer vaccines stand amongst a plethora of therapeutic strategies for cancer treatment, including DNA/RNA vaccines and adoptive cell transfer (ACT). Like peptide-based cancer vaccines, DNA and RNA-based vaccines are inexpensive to produce, and have the advantage of not being HLA-specific (40). DNA/RNA vaccines are also able to encode multiple antigens that can activate both the adaptive and innate immune responses (41), but DNA vaccines have shown to be poorly immunogenic in humans (42). This is in part due to limited cellular uptake and rapid elimination by the body (43, 44). RNA vaccines are also relatively unstable, and can produce strong unwanted innate immune responses (44, 45), however with modifications to reduce these issues, mRNA vaccines are showing themselves to be promising cancer vaccine candidates (46). ACT on the other hand, functions by taking a patient's cells, expanding, and engineering them *ex vivo*, before transplanting them back into the body. CAR-T and TIL therapies are examples of this, and have proven to be excellent anti-tumour therapies with a strong and highly personalised immunogenic profile (47). ACT is however an expensive, time- and labour-intensive process (48, 49), and can lead to toxic effects, as seen with cytokine release syndrome in CAR-T patients (50). Often ACT is combined with other cancer vaccine types, including pulsing DCs with tumour antigen-derived peptides, or transfecting with tumour-associated antigen mRNA (51). The hope of peptide-based cancer vaccines is in bridging the gap between these two alternative strategies by being highly specific, with a low manufacturing cost, and a proven safety record (52). However, challenges remain in improving their immunogenicity and attaining use in the clinic. The aim of this review is to evaluate recent strategies to improve the immunogenicity of peptide-based cancer vaccines, and to look for trends which could lead to their clinical application. The topics of discussion will be on peptide design, conjugation, formulation, personalised peptide vaccines, and combination therapies (**Figure 1**). We will discuss how each strategy overcomes the issues highlighted and the future of peptide-based cancer vaccines.

DESIGNING PEPTIDE-BASED CANCER VACCINES

Long Peptides and Overlapping Peptides as Cancer Vaccines

Peptide-based cancer vaccines are established on the principle of selecting peptide sequences from TSA/TAAs containing T cell epitopes to use as a template. This can take the form of single epitopes, long-chained polypeptides with multiple epitopes, or pools of peptides. However, to produce a strong immunogenic response, peptide-based cancer vaccines need to include multiple epitopes that are recognised by both $CD8^+$ and $CD4^+$ T cells in a diverse population with different HLA haplotypes. The rationale of this strategy being that, unlike the primarily structural-based recognition of antibodies (53), T-cell receptors recognise short linear peptide sequences derived from an antigen. It is therefore possible to use *in silico* bioinformatics and T cell epitope mapping to predict and select sequences from a target tumour antigen (53–55). By using multi-epitope or overlapping peptide sequences as opposed to short single-epitope peptides, issues such as tumour heterogeneity, tumour antigen down-regulation and the diversity of HLA haplotypes may be overcome.

One type of peptide-based cancer vaccines is synthetic long peptides (SLPs), which are pools of 25-35 amino acid peptides derived from TAA/TSAs. SLPs have successfully shown to elicit a strong immunogenic response since their inception (56–58), and have proven to be more immunogenic compared to the whole antigen in which they are derived from (59). Using long peptides as opposed to short peptides equal in size to T cell epitopes, means that the peptide must be processed within dendritic cells before they can be presented to T cells, rather than binding directly to MHC-I of dendritic cells or non-APCs (60, 61). However, a pool of peptides will need to be quality controlled for each individual peptide within that pool which could hamper its manufacturing capability and cost.

Recently SLPs derived from MELOE-1 melanoma antigen have been developed from Class I and Class II epitopes separated by a cathepsin protease-sensitive linker (62). Cathepsins are key proteases in dendritic cells involved in antigen presentation (63, 64), and it was found that the composition and size of the Cathepsin-sensitive linker had a significant impact on the presentation of the $CD4^+$ and $CD8^+$ T cell epitopes. Of the linker sequences tested, LLSVGG showed the strongest immunogenicity (62). Mouse studies to evaluate SLPs in the prime-boost immunisation strategy using LLSVGG-based vaccine showed a strong $CD8^+$ T cell response, but a lower $CD4^+$ compared to human PBMC tests, which could produce a less well-rounded response, and shows the epitope sensitivity differences between mice and human models (62). Mouse tumour models also revealed a reduction in tumour growth in 4 out of 7 mice when compared to unvaccinated mice but fell outside of significance (62). To help clarify these results, further studies with an alternative antigen model that shows similar epitope reactivity between species, as well as an increased sample size are needed. This study demonstrates the flexibility of SLP technology in peptide vaccine design, through the incorporation of strategic and specific enzymatic cleavage sites to enhance antigen presentation.

Among many others, Survivin is a cancer antigen that has been the target of peptide-based cancer vaccine design. Survivin is an anti-apoptotic protein and a member of the inhibitor of apoptosis family. It is a classic tumour-associated antigen that is

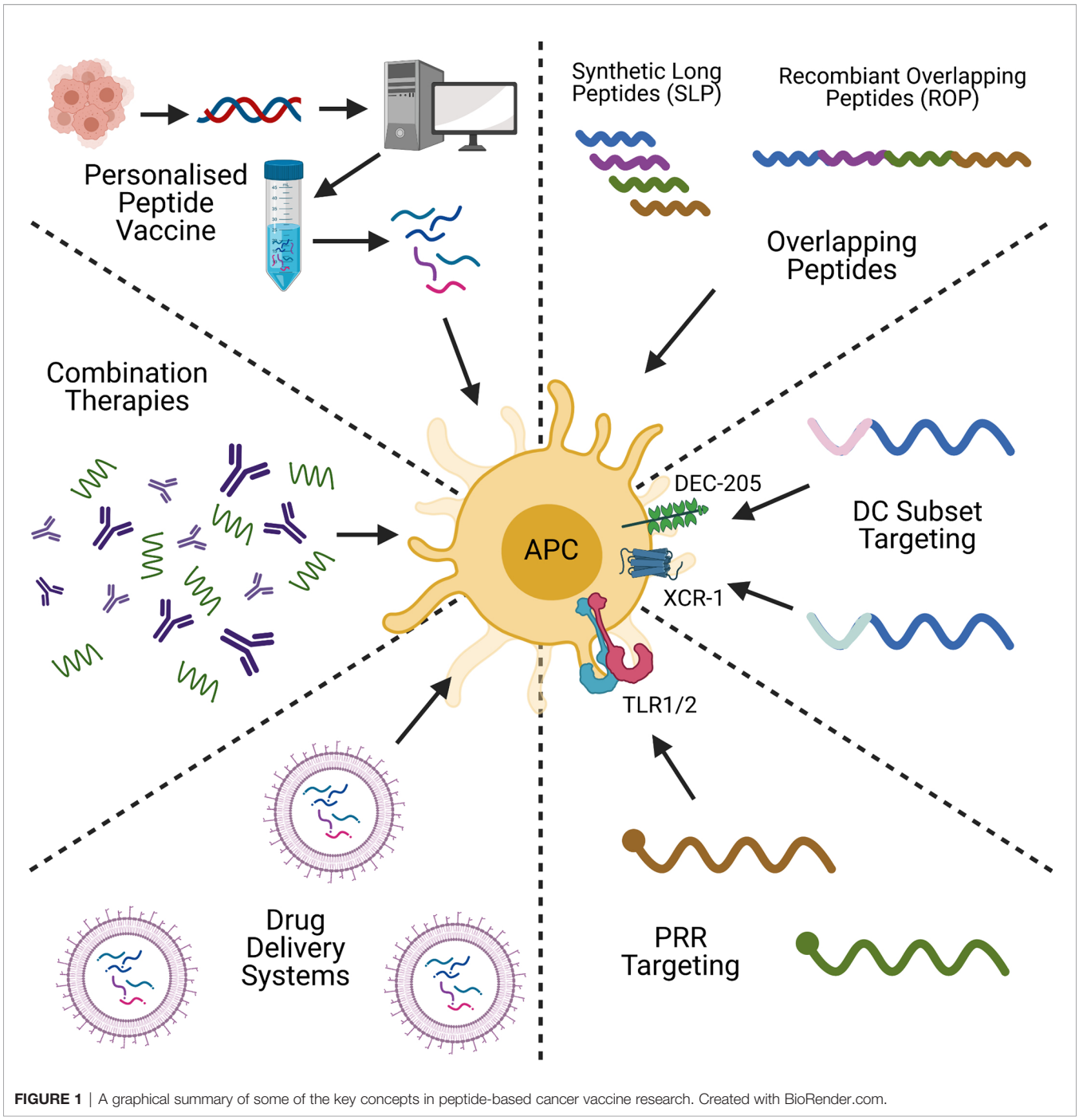

FIGURE 1 | A graphical summary of some of the key concepts in peptide-based cancer vaccine research. Created with BioRender.com.

not normally found in somatic cells but is up-regulated in numerous cancers (65). A Survivin-based vaccine composed of a pool of three SLPs with eight $CD4^+$ epitopes and six $CD8^+$ epitopes was recently developed (66). Although Survivin is found in a large proportion of cancer cells, it is normally immune tolerant (67, 68), the Survivin-SLP vaccine however was shown to activate both $CD4^+$ and $CD8^+$ immune responses through stimulation with autologous dendritic cells, regardless of HLA types in tested populations (66). Following on from this, the SLP vaccine in engrafted mouse models for colorectal cancer and B-lymphoma showed a significant level of tumour eradication, with secondary challenge also demonstrating reduced tumour growth and complete survival up to 60 days (66). The cytokine release profile of $CD4^+$ and $CD8^+$ T cells were enhanced with the vaccine, and with an increase in Perforin and Granzyme B, which forms a part of the CTL response (13, 66).

Recombinant overlapping peptides (ROPs) are another design strategy for peptide vaccines which have shown

promising pre-clinical efficacy. ROPs are comprised of sequential overlapping long peptide sequences covering the whole sequence of a target, with Cathepsin S protease-sensitive linkers between the peptide sequence overlaps (69, 70). The overlapping region allows for diversity in epitope, in particular with MHC-II molecules which have shown different but overlapping recognition of $CD4^+$ epitopes between HLA haplotypes (71). ROPs differ from other synthetic peptide pools as they are produced recombinantly as a single-chain polypeptide with multiple epitopes, giving ROPs potential advantages in manufacturing and drug approval. However, dealing with long peptides also comes with problems in solubility. ROPs have shown to produce strong immunogenic response in both $CD4^+$ and $CD8^+$ T cell over native protein, and are able to break self-tolerance as shown with Survivin ROP, mainly due to its design resulting in reduced homology when compared to native protein (70).

Overcoming immune tolerance is a significant hurdle for peptide-based cancer vaccines, as T cells reactive to self-antigens are eliminated as part of the central and peripheral tolerance mechanisms. But by incorporating multiple epitopes for $CD4^+$ and $CD8^+$ T cell activation, the examples so far have shown to be immunogenic in diverse HLA types which may not be possible with single epitope vaccines.

Personalised Peptide-Based Cancer Vaccines

Peptide vaccine design is key in targeting tumour neoantigens, and with the emergence of whole exome sequencing (WES) and single-cell RNA-Sequencing (RNA-Seq), peptide-based cancer vaccines are increasingly becoming more tailored to an individual's neoantigen repertoire. By creating specific vaccines to each patient and their genetic background, personalised immunotherapy avoids the issues of "off-the-shelf" peptide vaccines which may not take into consideration tumour heterogeneity and HLA haplotype. Reports in this field are promising, for example, by combining WES and RNA-Seq with *in silico* neoepitope predictions, Ott P.A. et al., created 20 unique SLPs specific to patient HLA type (72). *Ex vivo* experiments showed a strong $CD4^+$ antigen specific response while $CD8^+$ response was undetectable until after a round of *in vitro* expansion with the peptides (72). Indeed, the weaker $CD8^+$ T cell response might be explained by only 16% of the peptides containing $CD8^+$ T cell epitopes compared to 60% for $CD4^+$ epitopes (72). This could show a bias in the software for predicting of $CD4^+$ epitope sites or the higher level of promiscuity of MHC-II peptide binding compared to MHC-I (73). Further experiments showed that the $CD4^+$ and $CD8^+$ immune responses were highly specific, with 86% of T cells acting against the mutant antigens but not the wildtype (72). In a phase I vaccination trial, four stage IIB/C patients were disease free after 2 years, with another two patients in Stage IVM1b requiring further treatment with anti-PD-1 therapy to achieve tumour regression (72). Another example is in the clinical study by Hilf N. et al., that looked at personalised vaccination strategies against glioblastoma (74). Glioblastoma is notorious for its bad patient prognosis, with mean survival with Temozolomide and radiotherapy of 14.6 months (75). In the phase I study, a two-pronged vaccine treatment strategy was adopted using a pre-made library of unmutated antigens from glioblastomas and ranking each patient's response to them. This was followed with a second vaccine consisting of either; mutated antigen peptides predicted to bind MHC-I and produce an immune response, or any other unmutated epitopes not included in the first vaccine's library (74). For the first vaccine, around half of the total evaluated peptides were $CD8^+$ and $CD4^+$ immunogenic, with the $CD8^+$ showing a primarily memory phenotype, while the second vaccine was dominated by a Th1 $CD4^+$ response (74). It is worth considering that the original idea of the second vaccine was to use next-generation sequencing to compare the patient's genomic mutations against HLA-bound peptides by mass spectrometry, but that failed to match any (74). What this research demonstrates is the infancy of personalisation strategies, but also showing its promise as a highly specific treatment for individuals. The main issues with neoantigen-based peptide vaccines at present are the cost and time required to produce, but advances in sequencing, software predictions, databasing and manufacturing hope to allow for their use on a larger, more cost-effective scale (76).

PEPTIDE-CONJUGATE VACCINES

Targeting Pattern Recognition Receptors

Peptide-based cancer vaccines alone are poorly immunogenic and require strong adjuvants or immune stimulants to produce an efficacious response. But by combining peptide-based cancer vaccines with conjugates that stimulate or target dendritic cells, peptide-conjugate vaccines have shown a greater potential over peptide vaccines alone. One common method is the inclusion of dendritic cell activation markers such as pathogen associated molecular patterns (PAMPs), or damage associated molecular patterns (DAMPs), to act as adjuvants by binding to pattern recognition receptors (PRRs) on the surface of dendritic cells. Examples of PRRs include the toll-like receptors (TLR), C-type lectin receptors (CLR) and NOD-like receptors (NLR). The activation of PRRs induces the maturation of DCs, causing an upregulation of MHC-II expression, co-stimulatory signalling, and the release of pro-inflammatory cytokines, to bolster the anti-tumour response (77–80). PRRs in the context of peptide-based cancer vaccines varies from a simple adjuvant mixed with the peptide vaccine (81), to PRR ligand-peptide conjugates.

One example of this novel technology is a conjugate formed from the TLR2 ligand Pam3CSK4 covalently bound to TLR1 (82). As TLR1 is TLR2's heterodimeric partner, the conjugate enhances the targeting of TLR1 to TLR2 for dimerization and by proxy the immunogenicity of the SLP it is conjugated to (82). Research from this group showed a significant increase in the frequency of SIINFEKL (an OVA $CD8^+$ epitope) positive H-$2kb^+$ cells with the use of SLP-Conjugate over Pam3CSK4 alone, with significantly more DC maturation markers (83). They also showed greater $CD8^+$ T cell infiltration in a HPV16 TC-1

tumour model, with a reduction in tumour growth and increased survival time (83, 84).

Targeting Dendritic Cell Subsets

A further method of targeting dendritic cells is by incorporating ligands specific to DCs or a subtype of DCs (85). DEC-205 (CD205) is a dendritic cell receptor involved in receptor-mediated endocytosis, and has been associated with antigen cross-presentation in $CD8^+$ dendritic cells (86). Although its natural ligand is not fully understood, there is some evidence of its involvement as a PRR in binding to CpG oligodeoxynucleotides and recognition of apoptotic cells (86, 87). In theory, by conjugating a cancer peptide to a ligand recognised by DEC-205, the vaccines antigen presentation ability could be enhanced. Recently, Liu Z. et al., designed a ScFv that targets the DC marker DEC-205 fused with a HPV E7 SLP, which showed potent targeting effect when compared with the SLP alone (88). However, the author notes that the conjugating motif used in the study stimulates a $CD4^+$ response by itself (88). While this is not necessarily a negative, may have exaggerated the DEC-205 ScFv potency to target DCs.

Along with the PRRs already mentioned, DCs contain many chemokine receptors which are used in their migration or in attraction of other cells of the adaptive immune response. One example is the XCR1 receptor, a chemokine receptor which binds XCL1 to attract DCs to CTLs (89). What is of particular interest about $XCR1^+$ DCs, is their high efficiency at antigen cross-presentation (90). Botelho N.K. et al., investigated XCL1 fused with OVA SLP and a mutated IgG1 Fc which prevents Fc-mediated endocytosis, to evaluate its immunogenic potential in OVA expressing tumour models (91). The inclusion of the XCL1-Fc fused to the OVA peptide showed significant anti-tumour immunity in B16-OVA tumour models, with increased CTL response when compared to OVA SLP alone and OVA with free XCL1 (91). Interestingly the inclusion of OVA SLP with free XCL-Fc showed very similar responses than the full fusion, the author speculates this may be caused by aggregation of the molecules (91). It is worth noting this paper did not consider the equally important $CD4^+$ response, which would provide valuable insight into the viability of this targeted strategy as an anti-cancer treatment.

Multiple-Conjugate Peptide-Based Cancer Vaccines

So far, all the conjugates given as examples have focused on one target or conjugate per peptide vaccine. Logically, by combining multiple conjugates with different effector or targeting motifs, peptide-conjugate vaccines can synergistically boost multiple branches of the adaptive immune response. One example of this was recently developed by a combination of a cell-penetrating peptide (CPP), a TLR2/4 agonist which activates APCs, and a multi-antigenic domain that stimulates $CD4^+$ and $CD8^+$ T cells (92). The TLR agonist promotes DC maturation and activation, while the cell-penetrating peptide allows the antigenic domain to access the cytosolic compartment of DCs where antigen cross-presentation occurs, increasing production of antigen-specific $CD8^+$ T cells and boosting anti-tumour immunity (93). With this strategy, in HPV TC-1 therapeutic mouse tumour models, a significant increase in survival time and reduction in tumour size were observed, and in multiple mouse models an increase in antigen-specific $CD8^+$ T cell tumour infiltration (92). Finally, they found in non-human primates the ability to break self-tolerance by eliciting a T cell response to EPCAM and Survivin (92). It is worth considering though that CPPs are non-specific and will penetrate most cells (94), possibly leading to substantial off-target effects and reduced bioavailability to DCs through absorption by non-professional APCs. Perhaps a method of combing the ability of CPPs to penetrate cells in a more targeted approach to DCs could be beneficial to the creation of an efficacious peptide-based cancer vaccine.

PEPTIDE VACCINE FORMULATION & DRUG DELIVERY SYSTEMS

PLGA and Liposomes as Particulate Drug Delivery Platforms

The shortcomings of peptide-based cancer vaccines can be improved by proper formulation. For example, incorporating drug delivery systems into the vaccine formulation can facilitate peptide delivery to antigen presenting cells. By using drug delivery systems, peptides along with adjuvants and targeting motifs, can be encapsulated, or incorporated onto a surface, allowing for delivery of a single "package" to protect the peptide and deliver a strong T-cell mediated response.

PLGA and liposomes are two examples of drug delivery systems which have been used experimentally for many years, and have a proven track-record in safety and biodegradability, with the FDA approving their use as drug delivery systems (29, 95). Liposomes are highly customizable cell membrane mimics composed of phospholipid bilayers. The charge, size, surface molecules and delivery mechanism of liposomes are all tailorable – this feature allows a liposome to mimic the size and surface markers of a pathogen for example (96, 97). As particulate systems can protect peptides from degradation and control their release, liposomes provide peptides greater access to the spleen and lymph nodes which contain a higher proportion of cross-presenting DCs (98, 99). Upon internalisation, the liposome can continue to promote antigen cross-presentation by enabling its peptide cargo to escape from the lysosome into the cytosol, a key step in antigen cross-presentation and stimulation of a robust $CD8^+$ T cell response (100).

One example of the diversity of liposome-based delivery systems is in nanoliposomes designed by Rueda et. al., which contained multi-antigenic T-helper cell epitopes against LHR hormone, tetanus toxin immunogen as an adjuvant, and external Fc receptor ligands which increases liposome uptake by DCs (101). The adjuvants bolstered DC maturation, and the inclusion of multiple independent TLR agonists worked synergistically to enhance the stimulation of DCs *in vitro* (101). However, the

efficacy of this strategy with tumour models both *in vitro* and *in vivo* was not investigated, which is needed to fully evaluate its anti-tumour response against the self-antigen LHRH for the treatment of prostate cancer.

In another example of the customisability of liposomes, and how the lipid composition can affect antigen uptake, Zamani, P. et al., designed a DOPE-liposome system in combination with monophosphoryl lipid A (MPL), a detoxified LPS adjuvant derivative, and Pan HLA-DR epitope (PADRE) peptide (102). PADRE is considered a 'universal' HLA-DR (MHC class II) restrictive $CD4^+$ epitope, which stimulates a $CD4^+$ response in most patients (103). By using DOPE in the liposome design, the nanoparticle forms a hexagonal structure at low pH, which permits the particle to fuse with the endosomal wall and escape into the cytosolic pathway for MHC Class I cross-presentation (102, 104). The authors combined the DOPE : PADRE : MPL liposome with P5 peptide derived from HER2/neu breast cancer epitopes, and found reduced tumour growth and increased survival time in mice vaccinated with the $P5^+$DOPE : PADRE : MPL liposomes (102). A second study using a different HER2/neu derived peptide, showed similar results with an increased presence of $CD4^+$ tumour-infiltrating lymphocytes as well (105). Together these studies show that by optimising vaccine formulation, it is possible to re-direct antigen presentation pathway from MHC-I to MHC-II. However, optimisation is important and necessary as the weak $CD4^+$ cytokine profile and no apparent reduction in Treg cell numbers within the TME (102), may harm the vaccine's efficacy in the clinic.

In a study that looked at mutant KRAS SLP-Liposomes, the use of KRAS G12 mutant SLPs alone resulted in primarily a $CD4^+$ response (99). It was only upon the SLP being bound to the liposome did the vaccine produce a strong $CD8^+$ response, albeit at the slight expense of $CD4^+$ activity (99). The authors did note an increase in tumour PD-1 and TIL exhaustion markers, which resulted in a therapeutic response that slowed tumour growth but did not lead to regression (99). However, upon combination with PD-1 checkpoint inhibition therapy they saw tumour regression in 5 out of 10 mice with the Neo-lpx vaccine (99). One highlight of the work was the remarkable specificity of the vaccine to the mutant KRAS and not to the wildtype (99), emphasising the safety of formulated peptide-based cancer vaccines.

The importance of formulating an appropriate particle-based delivery system is imperative to the efficacy of a peptide-based cancer vaccine. This was proven by comparing PLGA and liposome with free peptide (106). It was found that although using a particulate based system was better than free peptide with adjuvant, liposomes were consistently better than PLGA at eliciting an anti-tumour immune response (106). The possible reason being the cationic charge of the liposome, and its comparatively smaller size than PLGA, promoting a stronger attraction and elevated uptake of the liposome by DCs (106).

One caveat for formulating vaccine delivery systems is the complications of construction and manufacture. Jacoberger-Foissac, C. et al., demonstrated this by looking to optimise liposome delivery by experimenting with different $CD4^+$ and $CD8^+$ epitopes in combination with adjuvants (107). By experimentation and sequential screening, they displayed the versatility and modular nature of liposomes as a delivery system. However, they also highlighted the empirical nature of its construction and the difficulties in manufacturing and optimisation.

Novel Delivery Systems for Peptide-Based Cancer Vaccines

So far, the focus has been on the use of PLGA and liposomes, but many groups are exploring novel formulations for peptide-based cancer vaccine delivery systems and their composition. For example, it has been shown that simply using the amino acid L-Tyrosine in combination with an adjuvant formula acts as a depot for peptide vaccines. This effect could enhance the duration and effectiveness of the peptides, and was found to work similarly to repeated injection of peptide alone (108). Although ultimately the study showed the strategy to be no better than repeated vaccination, this depot effect still has its benefit in allowing fewer vaccinations to attain the same effect.

Cross-linked polymer networks known as nanogels are also being explored, which can be customised with different sizes, charges and properties that allow the release of their payload by a trigger such as pH or enzymatic cleavage (109–111). Indeed, one group took advantage of this by designing a nanogel that releases its peptide payload in a reducing environment, as is found in endosomes (109). They found in *in vitro* and *in vivo* experiments that the nanogel vaccine was superior to soluble SLP in stimulating $CD4^+$ and $CD8^+$ response with adjuvant, although the $CD4^+$ response was not as strong *in vivo* than *in vitro* (109).

Finally, one group designed an ingenious delivery platform for their PPV consisting of a charge modified TLR7/8a conjugate, that was able to self-assemble into precise 20 nm diameter particles regardless of peptides it was conjugated to (112). The self-assembled particles were able to induce a $CD8^+$ T cell response 20-fold higher than PLGA and liposomes with the same dose (112). *In vivo* experiments also showed a larger accumulation of nanoparticles in the lymph nodes compared with soluble SLP and microparticles (particles greater than 200 nm in diameter), as well as producing a higher $CD8^+$ T cell response and a significant reduction in tumour growth rate in M39 mice (112). As this system seems to work regardless of the peptide load, it could reduce the empirical testing required by traditional carrier systems, while simultaneously reducing the variability of peptide loading and potential damage to peptide integrity.

PEPTIDE-BASED CANCER VACCINE COMBINATION THERAPIES

Peptide-Based Cancer Vaccines and Immune Checkpoint Inhibitors

Peptide-based cancer vaccines as a monotherapy have yet to show an efficacious response in the clinic. However, data to date has shown that peptide-based cancer vaccines can work in

combination with other drugs or therapies to enhance efficacy over individual monotherapies. One prominent example is the combination of peptide-based cancer vaccines with checkpoint inhibitors, such as anti-PD-1. Checkpoint blockades act as the brakes of the immune system to regulate T cell response, and are essential for self-tolerance and prevention of autoimmune disorders. However, the checkpoint blockade also scuppers cancer immunotherapy by supressing effector CTL function on tumours (113, 114). Checkpoint inhibitors block this action, overcoming immune suppression and allowing for greater antigen-specific T cell responses against tumours. By combining checkpoint inhibitors with peptide-based cancer vaccines, the immune system is released from suppression, allowing it to specifically target cancer cells.

Many of groups in this review combined their therapy with checkpoint inhibitors and additional anti-cancer agents to test efficacy in combination therapies. Liu, Z. et al., found their DEC-205- targeting ScFv-HPV E7 SLP fusion resulted in higher PD-L1 expression, and were able to show a more efficacious response when combining anti-PD-L1 antibody with their vaccine (88). Zom, G.G. et al., had a curative rate of 10% with their Pam3CSK4-TLR-SLP fusion as a monotherapy, however when used in combination with the cervical cancer chemotherapy drug Cisplatin survival increased to 71%, and with photodynamic therapy survival increased to 89% (83). The authors cited the possible reasons to be; depletion of immunosuppressive myeloid cells, increased TNF-α sensitivity, or induction of immunogenic cell death (83). Finally, Belnouse, E. et al., found that combining their modular self-adjuvating vaccine strategy, composed of a CPP with a multi-antigenic domain and a TLR2/4 agonist, with anti-PDL1 therapy, achieved greater efficacy than the vaccine alone (92). This perfectly illustrates that even with targeting motifs or PRR agonists to enhance peptide vaccine immunogenicity, peptide-based cancer vaccines as a monotherapy are still inferior to combination with other treatment strategies. This being attributed to the complexity of tumour immunology and the suppressive nature of the tumour microenvironment.

Combining Peptide-Based Cancer Vaccines With Existing Cancer Therapies

Combining peptide-based cancer vaccines with existing anti-cancer therapies is common, as patients are often treated with established chemotherapy, radiotherapy, and immunotherapy as part of standard care practices. Trastuzumab for example is an anti-HER2 monoclonal antibody used to treat breast cancer, and has been shown to make $HER2^+$ tumour cells more susceptible to antibody dependent and T-cell mediated cytotoxicity (115, 116). In one study, anti-HER2 antibodies enabled DCs to expand HER2-derived peptide E75 specific CTLs greater than peptide alone (117). *In vivo* experiments with anti-HER2 antibodies showed similar increases in antigen-specific CTLs with spontaneous and implantable HER2 mouse models (117). In a phase IIb clinical trial combining Trastuzumab with GM-CSF and E75, the vaccine was found to be safe and non-toxic (118).

Another group combined their peptide pool with docetaxel, a standard of care chemotherapy drug for treatment of castration-resistant prostate cancer (119). Docetaxel has been shown to reduce immunosuppression within tumours by reducing Treg cell numbers (120), and it was thought that combining Docetaxel with a peptide vaccine may enhance its efficacy (119). Unfortunately, in a randomised phase II trial, the combination did not show a robust synergistic effect, with no increase in overall survival, even with a decrease in PSA levels and a reduction in the immunosuppressive MDSCs (119).

Cyclophosphamide (CPA) is a chemotherapy agent with direct cytotoxicity in high doses, but has immunomodulatory effects when used at lower doses, including the suppression of Treg cells and the modulation of antigen-specific T cell responses (121). In a randomized phase II trial that investigated the efficacy of combining personalised peptide vaccines (PPVs) with CPA on previously treated advanced biliary tract cancer patients (122), pre-vaccinated PBMCs showed no significant increase in IFN-γ with the use of PPV compared with PPV and CPA combination therapy (122). However, in the clinical context they saw a doubling of progression free and overall survival and a reduction in IL-6 with the PPV/CPA combination compared to PPV alone; lower IL-6 is suggested to be associated with a better prognosis (123, 124). However, the expected Treg reduction shown to occur with low dose CPA treatment did not occur when using PPV/CPA combination, and a mixed picture was observed with frequency and numbers of MDSCs, which did not correlate with an increase in overall survival (121, 122). Taken together, this suggests that although the results related to clinical outcomes were promising, more research is necessary to optimise the combination of PPVs with CPA.

The mixed results between the three studies highlighted, emphasises the need for careful consideration on the design of experiment and the need for empirical investigation into the combinations worth pursuing. Especially when working with combination therapies where changing variables such as dose, administrative route and timing can have drastic implications on a vaccine's capability.

Novel Therapies That Modulate Peptide-Based Cancer Vaccine Function

Some of the drugs being investigated in combination with peptide-based cancer vaccines do not have direct anti-cancer properties, but help to modulate mechanisms required for peptide-based cancer vaccines to function. Avasimibe for example is an ACAT1 inhibitor, which prevents esterification of cholesterol and the attenuation of lipid rafts, which in turn increases the level of cholesterol in $CD8^+$ T cells and promotes T cell receptor signal transduction, enhancing anti-tumour response (125). One group found that by combining Avasimibe with a KRAS multi-peptide vaccine in prophylactic mouse models, a significant decrease in tumour volume was seen compared to monotherapies, with an increase in $CD8^+$ T cell levels in the TME (126). In therapeutic models, the Avasimibe/KRAS combination therapy did not show a significant decrease in tumourigenesis, but did show a reduction in tumour load and delayed tumour progression (126). This again highlights the

TABLE 1 | A summary of Phase I and II peptide-based cancer vaccine clinical trials currently active or recruiting.

Condition	Peptide Vaccine Type	NCT number
Adenocarcinoma	HER2/neu Peptides	NCT02795988
	Personalised Peptide Vaccine	NCT04627246, NCT02600949
Bladder Cancer	Personalised Peptide Vaccine	NCT03359239
Blood Cancer & Leukaemia	Multiple Peptides	NCT04051307
	Personalised Peptide Vaccine Combination Therapy	NCT04688385, NCT03559413, NCT02802943
	WT1 Peptides	NCT04747002, NCT03761914
	IDO Peptides	NCT03939234
	Survivin Peptides	NCT02334865
Brain Cancer	TAA Peptide Combination Therapy	NCT01795313
	IDH1 Peptide	NCT02193347
Breast Cancer	Folate Receptor Peptide Combination Therapy	NCT02593227, NCT03012100
	HER2/neu Peptides	NCT02636582, NCT00194714, NCT04144023, NCT04024800, NCT04197687, NCT03384914
	Novel Peptides	NCT02826434, NCT03362060
	Personalised Peptide Vaccine Combination Therapy	NCT03606967, NCT02427581
	ESR1 Peptide	NCT04270149
Cervical & Ovarian Cancers	HPV E6/E7 Liposomes Combination Therapy	NCT04580771
	WT1 Peptides	NCT02737787
Colorectal Cancer	MUC1 Peptides	NCT02134925
Gastric Cancer	Multiple Peptides Combination Therapy	NCT03784040
Glioblastoma	CMV Peptide targets	NCT02864368
	Novel Peptides	NCT04116658
	Personalised Peptide Vaccine	NCT03223103
	Survivin Peptides	NCT02455557
	Telomerase-derived Peptides	NCT04280848
Glioma	Neoantigen Peptides	NCT04749641, NCT02358187, NCT01130077
	Neoantigen Combination Therapy	NCT03893903, NCT02960230
	Multiple Peptides Combination Therapy	NCT02924038
Head & Neck Cancers	IDO Peptides	NCT04445064
Kidney Cancer	Personalised Peptide Vaccine Combination Therapy	NCT02950766
Liver Cancer	PKA Peptide Combination Therapy	NCT04248569
Lung Cancer (inc. NSCLC)	MUC1 Peptides	NCT03300817, NCT01720836
	P10s-PADRE Peptide	NCT02264236
	Telomerase-derived Peptides	NCT01789099, NCT02818426
	Neoantigen Peptides	NCT04487093
	Personalised Peptide Vaccine	NCT04397926
Lymphoma	Novel Peptides	NCT04669171
	Personalised Peptide Vaccine Combination Therapy	NCT03361852
Melanoma	BRAF/CD4 Epitopes	NCT04364230
	CD4+ Epitope peptides	NCT03617328
	Novel Peptides	NCT02126579
	NY-ESO & gp100 Peptide Combination Therapy	NCT01176474, NCT01176461
	IDO & PD-L1 Peptide Combination Therapy	NCT03047928
	Personalised Peptide Vaccine Combination Therapy	NCT04072900
Multiple Cancers & Solid Tumours	Arginase-1 Peptide	NCT03689192
	HER2/neu Peptides	NCT01376505
	KRAS Peptide Combination Therapy	NCT04117087
	Multiple Peptides	NCT04316689
	Personalised Peptide Vaccine	NCT03715985
	Personalised Peptide Vaccine Combination Therapy	NCT03633110, NCT04266730
	Survivin Peptides Combination Therapy	NCT03879694
	Telomerase-derived Peptides Combination Therapy	NCT03946358
Myeloma	Novel Peptide Combination Therapy	NCT02886065
	PD-L1 Peptides	NCT03850522
Pancreatic Cancer	Neoantigen Peptides	NCT03956056
	Personalised Peptide Vaccine	NCT03558945
Prostate Cancer	Bcl-xl Peptides	NCT03412786
	Novel Peptide-Conjugate	NCT04701021
	RhoC Peptide	NCT04114825
	TARP Peptide	NCT02362464
	Telomerase-derived Peptides	NCT01784913

difference in efficacy that can occur depending on the vaccine setting.

Most of this review has focused on how $CD8^+$ T cell activity is imperative to a strong anti-tumour response, with $CD4^+$ T cells playing a supporting role in activating and maintaining the immune response. However, there is evidence of the importance of $CD4^+$ activity in generating an anti-tumour response directly with so called cytotoxic $CD4^+$ T cells. Cytotoxic $CD4^+$ T cells are characterised by their ability to produce Granzyme B and Perforin (127, 128). Kumai T. et al., focused on inducing an anti-tumour $CD4^+$ response as opposed to $CD8^+$, by combining $CD4^+$ epitope specific peptides with TLR ligands, CD40 monoclonal antibodies and with various co-stimulatory activators to optimise the $CD4^+$ activity (129). OX40 (CD134) was one example of a co-stimulatory activator, which is used to maintain long-term T cell activity by promoting survival and proliferation (130). OX40 agonistic monoclonal antibodies in combination with the $CD4^+$ epitope peptide vaccine showed an enhanced peptide-specific $CD4^+$ T cell response, and a slowing of tumour progression in therapeutic models, with an increase in IFN-γ, TNF-α and Granzyme B production (129). Interestingly, this would point to a possible cytotoxic $CD4^+$ activity, as in $CD8^+$ depleted mice there was still a reduced anti-tumour response (129). This study emphasises the importance of considering both the $CD4^+$ and $CD8^+$ activity when designing a peptide vaccine strategy; it would be interesting to see the results of combining this with a $CD8^+$ specific vaccine to observe its effects.

Oncolytic viruses are an emerging therapy that utilise engineered viruses to target and kill cancer cells, with the first oncolytic virus approved by the FDA in 2015 (131). One group combined a Maraba virus engineered to produce E6 and E7 sequences from HPV16 with SLP peptide derived from epitope mapping of HPV16/18 E6 and E7 wildtype sequences (132). By using the SLP as the 'Prime' in a prime-boost vaccine strategy, they showed an increase in IFN-γ and TNF-α release by $CD8^+$ T cells, but no significant increase in survival time in mouse models compared to SLP prime-boost monotherapy (132). This strategy warrants further investigation into optimising the vaccine and administration strategy, with more trials and differing the peptide target and virus.

CONCLUDING REMARKS

Peptide-based cancer vaccines are a diverse and versatile means of eliciting a cell-mediated anti-tumour response through antigen presentation of tumour antigen epitopes to T cells. The activated T cells then recognise and respond to tumour antigens presented on the surface of cancer cells, initiating an immune response, and subsequently leading to T cell mediated killing of the cancer cells. Many conjugates and polymers are used to enhance the immunogenicity of peptide-based cancer vaccines by targeting the peptides to specific subtypes of immune cells, or by containing stimulatory molecules to increase the activation and maturation of dendritic cells. Many groups have shown promising results combining peptide vaccines with chemotherapy agents, along with drugs not originally designed as anti-cancer agents. Others are incorporating peptide vaccines into highly customisable vaccine carrier systems, bringing together $CD4^+$ and $CD8^+$ epitopes, adjuvants, and targeting motifs into a single particle. In general, peptide-based cancer vaccines as a monotherapy struggle to achieve efficacy, but show great promise as a component of a combinational treatment strategy. Combination therapy is likely to be the approach needed for peptide-based cancer vaccines to gain traction as a viable treatment in the clinic.

As vaccines increasingly become more customised to individual patients, personalised peptide vaccines represent a promising vaccine candidate. The design and manufacture of personalised peptide vaccines are currently an expensive and time-consuming process, but will be a valuable toolkit in the future with the advent of new sequencing technologies, bioinformatics, T cell epitope prediction and improved manufacturing practices. From this review, one can appreciate the complexity involved with designing a peptide-based cancer vaccine and the challenges of striking a fine balance between method and mode of delivery, half-life, epitope selection, and immunogenicity to produce an efficacious vaccine strategy. Although many of the studies outlined in this review were pre-clinical or in the early stages of clinical trials, studies on peptide-based cancer vaccines in the clinic are numerous. As of May 2021, there are approaching 80 phase I or II clinical trials utilising a peptide-based vaccine strategy in cancer, with 20 currently active and 20 having been completed since the start of 2019 (133). **Table 1** summarises the current Phase I & II peptide-based cancer vaccine trials currently active and/or recruiting. Featuring prominently on the list are peptide-based cancer vaccines against breast, lung, blood and brain cancers to name a few (133). Exhibiting the diversity of targets peptide-based cancer vaccines are being trialled upon (133). What is quite apparent though is the lack of trials beyond phase II, illustrating the current issues with efficacy that peptide-based cancer vaccines face. However, encouragingly there is a clear trend towards a more personalised approach to patient neoepitope selection in the current pool of trials, with an increased focus on peptide-based cancer vaccines use in combination with other cancer treatment strategies (133). For a more detailed analysis, Bezu, L. et al., have expertly collated and reviewed trials up until 2018 for peptide-based cancer vaccines (134).

For peptide-based cancer vaccines to make their mark on cancer treatment, future studies will need to ensure a robust combination of *in vivo* $CD4^+$ and $CD8^+$ responses in a package that strongly activates DCs and subsequently T cells in a prolonged fashion, with minimal exhaustion or immune tolerance. They will need to be targeted, multi-faceted and personalised to an individual's neoantigen repertoire, and able to overcome or reduce the immunosuppressive burden of the tumour microenvironment.

AUTHOR CONTRIBUTIONS

AS conceptualised and wrote the first draft of the manuscript. NB-B and SJ supervised. All authors contributed to the article and approved the submitted version.

FUNDING

This research was funded by Innovate UK, grant number 104992 & 133783, and by grants from the CBI and Oxford Vacmedix UK Ltd.

ACKNOWLEDGMENTS

The authors would like to thank members of the Jiang lab for their helpful feedback and discussion.

REFERENCES

1. Clem AS. Fundamentals of Vaccine Immunology. *J Glob Infect Dis* (2011) 3 (1):73–8. doi: 10.4103/0974-777X.77299
2. Hanahan D, Weinberg RA. Hallmarks of Cancer: The Next Generation. *Cell* (2011) 144(5):646–74. doi: 10.1016/j.cell.2011.02.013
3. Mittal D, Gubin MM, Schreiber RD, Smyth MJ. New Insights Into Cancer Immunoediting and Its Three Component Phases–Elimination, Equilibrium and Escape. *Curr Opin Immunol* (2014) 27:16–25. doi: 10.1016/j.coi.2014.01.004
4. Whiteside TL. The Tumor Microenvironment and Its Role in Promoting Tumor Growth. *Oncogene* (2008) 27(45):5904–12. doi: 10.1038/onc.2008.271
5. Balkwill FR, Capasso M, Hagemann T. The Tumor Microenvironment at a Glance. *J Cell Sci* (2012) 125(Pt 23):5591–6. doi: 10.1242/jcs.116392
6. Gillet JP, Gottesman MM. Mechanisms of Multidrug Resistance in Cancer. *Methods Mol Biol* (2010) 596:47–76. doi: 10.1007/978-1-60761-416-6_4
7. Mansoori B, Mohammadi A, Davudian S, Shirjang S, Baradaran B. The Different Mechanisms of Cancer Drug Resistance: A Brief Review. *Adv Pharm Bull* (2017) 7(3):339–48. doi: 10.15171/apb.2017.041
8. Steinman RM. Linking Innate to Adaptive Immunity Through Dendritic Cells. *Novartis Found Symp* (2006) 279:101–9; discussion 109-13, 216-9. doi: 10.1002/9780470035399.ch9
9. Mosmann TR, Coffman RL. TH1 and TH2 Cells: Different Patterns of Lymphokine Secretion Lead to Different Functional Properties. *Annu Rev Immunol* (1989) 7:145–73. doi: 10.1146/annurev.iy.07.040189.001045
10. Bonnerot C, Briken V, Amigorena S. Intracellular Signaling and Endosomal Trafficking of Immunoreceptors. Shared Effectors Underlying MHC Class II-Restricted Antigen Presentation. *Immunol Lett* (1997) 57(1-3):1–4. doi: 10.1016/S0165-2478(97)00054-0
11. Schroder K, Hertzog PJ, Ravasi T, Hume DA. Interferon-Gamma: An Overview of Signals, Mechanisms and Functions. *J Leukoc Biol* (2004) 75 (2):163–89. doi: 10.1189/jlb.0603252
12. Joffre OP, Segura E, Savina A, Amigorena S. Cross-Presentation by Dendritic Cells. *Nat Rev Immunol* (2012) 12(8):557–69. doi: 10.1038/nri3254
13. Halle S, Halle O, Forster R. Mechanisms and Dynamics of T Cell-Mediated Cytotoxicity *In Vivo*. *Trends Immunol* (2017) 38(6):432–43. doi: 10.1016/j.it.2017.04.002
14. Janeway CAJr. The T Cell Receptor as a Multicomponent Signalling Machine: CD4/CD8 Coreceptors and CD45 in T Cell Activation. *Annu Rev Immunol* (1992) 10:645–74. doi: 10.1146/annurev.iy.10.040192.003241
15. Daniels MA, Jameson SC. Critical Role for CD8 in T Cell Receptor Binding and Activation by Peptide/Major Histocompatibility Complex Multimers. *J Exp Med* (2000) 191(2):335–46. doi: 10.1084/jem.191.2.335
16. Artyomov MN, Lis M, Devadas S, Davis MM, Chakraborty AK. CD4 and CD8 Binding to MHC Molecules Primarily Acts to Enhance Lck Delivery. *Proc Natl Acad Sci USA* (2010) 107(39):16916–21. doi: 10.1073/pnas.1010568107
17. McAdam AJ, Schweitzer AN, Sharpe AH. The Role of B7 Co-Stimulation in Activation and Differentiation of CD4+ and CD8+ T Cells. *Immunol Rev* (1998) 165:231–47. doi: 10.1111/j.1600-065X.1998.tb01242.x
18. Chen L, Flies DB. Molecular Mechanisms of T Cell Co-Stimulation and Co-Inhibition. *Nat Rev Immunol* (2013) 13(4):227–42. doi: 10.1038/nri3405
19. Heufler C, Koch F, Stanzl U, Topar G, Wysocka M, Trinchieri G, et al. Interleukin-12 is Produced by Dendritic Cells and Mediates T Helper 1 Development as Well as Interferon-Gamma Production by T Helper 1 Cells. *Eur J Immunol* (1996) 26(3):659–68. doi: 10.1002/eji.1830260323
20. Curtsinger JM, Mescher MF. Inflammatory Cytokines as a Third Signal for T Cell Activation. *Curr Opin Immunol* (2010) 22(3):333–40. doi: 10.1016/j.coi.2010.02.013
21. Keppler SJ, Rosenits K, Koegl T, Vucikuja S, Aichele P. Signal 3 Cytokines as Modulators of Primary Immune Responses During Infections: The Interplay of Type I IFN and IL-12 in CD8 T Cell Responses. *PLoS One* (2012) 7(7): e40865. doi: 10.1371/journal.pone.0040865
22. Hatziioannou A, Alissafi T, Verginis P. Myeloid-Derived Suppressor Cells and T Regulatory Cells in Tumors: Unraveling the Dark Side of the Force. *J Leukoc Biol* (2017) 102(2):407–21. doi: 10.1189/jlb.5VMR1116-493R
23. Tay RE, Richardson EK, Toh HC. Revisiting the Role of CD4(+) T Cells in Cancer Immunotherapy-New Insights Into Old Paradigms. *Cancer Gene Ther* (2020) 28:5–17. doi: 10.1038/s41417-020-0183-x
24. Bijker MS, van den Eeden SJ, Franken KL, Melief CJ, van der Burg SH, Offringa R. Superior Induction of Anti-Tumor CTL Immunity by Extended Peptide Vaccines Involves Prolonged, DC-Focused Antigen Presentation. *Eur J Immunol* (2008) 38(4):1033–42. doi: 10.1002/eji.200737995
25. Sidney J, del Guercio MF, Southwood S, Engelhard VH, Appella E, Rammensee HG, et al. Several HLA Alleles Share Overlapping Peptide Specificities. *J Immunol* (1995) 154(1):247–59.
26. Southwood S, Sidney J, Kondo A, del Guercio MF, Appella E, Hoffman S, et al. Several Common HLA-DR Types Share Largely Overlapping Peptide Binding Repertoires. *J Immunol* (1998) 160(7):3363–73.
27. Diao L, Meibohm B. Pharmacokinetics and Pharmacokinetic-Pharmacodynamic Correlations of Therapeutic Peptides. *Clin Pharmacokinet* (2013) 52(10):855–68. doi: 10.1007/s40262-013-0079-0
28. Di L. Strategic Approaches to Optimizing Peptide ADME Properties. *AAPS J* (2015) 17(1):134–43. doi: 10.1208/s12248-014-9687-3
29. Food and Drug Admistration (FDA). (2021). Available at: www.fda.gov.
30. Khong H, Overwijk WW. Adjuvants for Peptide-Based Cancer Vaccines. *J Immunother Cancer* (2016) 4:56. doi: 10.1186/s40425-016-0160-y
31. Gouttefangeas C, Rammensee HG. Personalized Cancer Vaccines: Adjuvants are Important, Too. *Cancer Immunol Immunother* (2018) 67 (12):1911–8. doi: 10.1007/s00262-018-2158-4
32. Marincola FM, Jaffee EM, Hicklin DJ, Ferrone S. Escape of Human Solid Tumors From T-Cell Recognition: Molecular Mechanisms and Functional Significance. *Adv Immunol* (2000) 74:181–273. doi: 10.1016/S0065-2776(08)60911-6
33. McGranahan N, Swanton C. Clonal Heterogeneity and Tumor Evolution: Past, Present, and the Future. *Cell* (2017) 168(4):613–28. doi: 10.1016/j.cell.2017.01.018
34. Han BS, Ji S, Woo S, Lee JH, Sin JI. Regulation of the Translation Activity of Antigen-Specific mRNA Is Responsible for Antigen Loss and Tumor Immune Escape in a HER2-Expressing Tumor Model. *Sci Rep* (2019) 9 (1):2855. doi: 10.1038/s41598-019-39557-9
35. Romero I, Martinez M, Garrido C, Collado A, Algarra I, Garrido F, et al. The Tumour Suppressor Fhit Positively Regulates MHC Class I Expression on Cancer Cells. *J Pathol* (2012) 227(3):367–79. doi: 10.1002/path.4029
36. Morrison BJ, Steel JC, Morris JC. Reduction of MHC-I Expression Limits T-Lymphocyte-Mediated Killing of Cancer-Initiating Cells. *BMC Cancer* (2018) 18(1):469. doi: 10.1186/s12885-018-4389-3
37. Melero I, Rouzaut A, Motz GT, Coukos G. T-Cell and NK-Cell Infiltration Into Solid Tumors: A Key Limiting Factor for Efficacious Cancer Immunotherapy. *Cancer Discov* (2014) 4(5):522–6. doi: 10.1158/2159-8290.CD-13-0985
38. Betts G, Jones E, Junaid S, El-Shanawany T, Scurr M, Mizen P, et al. Suppression of Tumour-Specific CD4(+) T Cells by Regulatory T Cells is Associated With Progression of Human Colorectal Cancer. *Gut* (2012) 61 (8):1163–71. doi: 10.1136/gutjnl-2011-300970
39. Xia A, Zhang Y, Xu J, Yin T, Lu XJ. T Cell Dysfunction in Cancer Immunity and Immunotherapy. *Front Immunol* (2019) 10:1719. doi: 10.3389/fimmu.2019.01719
40. Walters JN, Ferraro B, Duperret EK, Kraynyak KA, Chu J, Saint-Fleur A, et al. A Novel DNA Vaccine Platform Enhances Neo-Antigen-Like T Cell Responses Against WT1 to Break Tolerance and Induce Anti-Tumor Immunity. *Mol Ther* (2017) 25(4):976–88. doi: 10.1016/j.ymthe.2017.01.022
41. Flingai S, Czerwonko M, Goodman J, Kudchodkar SB, Muthumani K, Weiner DB. Synthetic DNA Vaccines: Improved Vaccine Potency by

Electroporation and Co-Delivered Genetic Adjuvants. *Front Immunol* (2013) 4:354. doi: 10.3389/fimmu.2013.00354
42. Hobernik D, Bros M. DNA Vaccines-How Far From Clinical Use? *Int J Mol Sci* (2018) 19(11):3605. doi: 10.3390/ijms19113605
43. Dupuis M, Denis-Mize K, Woo C, Goldbeck C, Selby MJ, Chen M, et al. Distribution of DNA Vaccines Determines Their Immunogenicity After Intramuscular Injection in Mice. *J Immunol* (2000) 165(5):2850–8. doi: 10.4049/jimmunol.165.5.2850
44. Miao L, Zhang Y, Huang L. mRNA Vaccine for Cancer Immunotherapy. *Mol Cancer* (2021) 20(1):41. doi: 10.1186/s12943-021-01335-5
45. Pardi N, Hogan MJ, Porter FW, Weissman D. mRNA Vaccines - a New Era in Vaccinology. *Nat Rev Drug Discov* (2018) 17(4):261–79. doi: 10.1038/nrd.2017.243
46. Thess A, Grund S, Mui BL, Hope MJ, Baumhof P, Fotin-Mleczek M, et al. Sequence-Engineered mRNA Without Chemical Nucleoside Modifications Enables an Effective Protein Therapy in Large Animals. *Mol Ther* (2015) 23 (9):1456–64. doi: 10.1038/mt.2015.103
47. Rosenberg SA, Restifo NP. Adoptive Cell Transfer as Personalized Immunotherapy for Human Cancer. *Science* (2015) 348(6230):62–8. doi: 10.1126/science.aaa4967
48. Hay AE, Cheung MC. CAR T-Cells: Costs, Comparisons, and Commentary. *J Med Econ* (2019) 22(7):613–5. doi: 10.1080/13696998.2019.1582059
49. Rosenberg SA, Restifo NP, Yang JC, Morgan RA, Dudley ME. Adoptive Cell Transfer: A Clinical Path to Effective Cancer Immunotherapy. *Nat Rev Cancer* (2008) 8(4):299–308. doi: 10.1038/nrc2355
50. Brudno JN, Kochenderfer JN. Toxicities of Chimeric Antigen Receptor T Cells: Recognition and Management. *Blood* (2016) 127(26):3321–30. doi: 10.1182/blood-2016-04-703751
51. Wilgenhof S, Van Nuffel AMT, Benteyn D, Corthals J, Aerts C, Heirman C, et al. A Phase IB Study on Intravenous Synthetic mRNA Electroporated Dendritic Cell Immunotherapy in Pretreated Advanced Melanoma Patients. *Ann Oncol* (2013) 24(10):2686–93. doi: 10.1093/annonc/mdt245
52. Yoshida K, Noguchi M, Mine T, Komatsu N, Yutani S, Ueno T, et al. Characteristics of Severe Adverse Events After Peptide Vaccination for Advanced Cancer Patients: Analysis of 500 Cases. *Oncol Rep* (2011) 25 (1):57–62. doi: 10.3892/or_00001041
53. Sanchez-Trincado JL, Gomez-Perosanz M, Reche PA. Fundamentals and Methods for T- and B-Cell Epitope Prediction. *J Immunol Res* (2017) 2017:2680160. doi: 10.1155/2017/2680160
54. Lehmann PV, Suwansaard M, Zhang T, Roen DR, Kirchenbaum GA, Karulin AY, et al. Comprehensive Evaluation of the Expressed CD8+ T Cell Epitope Space Using High-Throughput Epitope Mapping. *Front Immunol* (2019) 10:655. doi: 10.3389/fimmu.2019.00655
55. Ahmad TA, Eweida AE, El-Sayed LH. T-Cell Epitope Mapping for the Design of Powerful Vaccines. *Vaccine Rep* (2016) 6:13–22. doi: 10.1016/j.vacrep.2016.07.002
56. Zwaveling S, Ferreira Mota SC, Nouta J, Johnson M, Lipford GB, Offringa R, et al. Established Human Papillomavirus Type 16-Expressing Tumors are Effectively Eradicated Following Vaccination With Long Peptides. *J Immunol* (2002) 169(1):350–8. doi: 10.4049/jimmunol.169.1.350
57. Speetjens FM, Kuppen PJ, Welters MJ, Essahsah F, Voet van den Brink AM, Lantrua MG, et al. Induction of P53-Specific Immunity by a P53 Synthetic Long Peptide Vaccine in Patients Treated for Metastatic Colorectal Cancer. *Clin Cancer Res* (2009) 15(3):1086–95. doi: 10.1158/1078-0432.CCR-08-2227
58. van Poelgeest MI, Welters MJ, van Esch EM, Stynenbosch LF, Kerpershoek G, van Persijn van Meerten EL, et al. HPV16 Synthetic Long Peptide (HPV16-SLP) Vaccination Therapy of Patients With Advanced or Recurrent HPV16-Induced Gynecological Carcinoma, a Phase II Trial. *J Transl Med* (2013) 11:88. doi: 10.1186/1479-5876-11-88
59. Rosalia RA, Quakkelaar ED, Redeker A, Khan S, Camps M, Drijfhout JW, et al. Dendritic Cells Process Synthetic Long Peptides Better Than Whole Protein, Improving Antigen Presentation and T-Cell Activation. *Eur J Immunol* (2013) 43(10):2554–65. doi: 10.1002/eji.201343324
60. Melief CJ, van der Burg SH. Immunotherapy of Established (Pre)Malignant Disease by Synthetic Long Peptide Vaccines. *Nat Rev Cancer* (2008) 8 (5):351–60. doi: 10.1038/nrc2373
61. Slingluff CLJr. The Present and Future of Peptide Vaccines for Cancer: Single or Multiple, Long or Short, Alone or in Combination? *Cancer J* (2011) 17 (5):343–50. doi: 10.1097/PPO.0b013e318233e5b2
62. Rabu C, Rangan L, Florenceau L, Fortun A, Charpentier M, Dupre E, et al. Cancer Vaccines: Designing Artificial Synthetic Long Peptides to Improve Presentation of Class I and Class II T Cell Epitopes by Dendritic Cells. *Oncoimmunology* (2019) 8(4):e1560919. doi: 10.1080/2162402X.2018.1560919
63. Shen L, Sigal LJ, Boes M, Rock KL. Important Role of Cathepsin S in Generating Peptides for TAP-Independent MHC Class I Crosspresentation *In Vivo*. *Immunity* (2004) 21(2):155–65. doi: 10.1016/j.immuni.2004.07.004
64. Riese RJ, Chapman HA. Cathepsins and Compartmentalization in Antigen Presentation. *Curr Opin Immunol* (2000) 12(1):107–13. doi: 10.1016/S0952-7915(99)00058-8
65. Schmidt SM, Schag K, Muller MR, Weck MM, Appel S, Kanz L, et al. Survivin Is a Shared Tumor-Associated Antigen Expressed in a Broad Variety of Malignancies and Recognized by Specific Cytotoxic T Cells. *Blood* (2003) 102(2):571–6. doi: 10.1182/blood-2002-08-2554
66. Onodi F, Maherzi-Mechalikh C, Mougel A, Ben Hamouda N, Taboas C, Gueugnon F, et al. High Therapeutic Efficacy of a New Survivin LSP-Cancer Vaccine Containing CD4(+) and CD8(+) T-Cell Epitopes. *Front Oncol* (2018) 8:517. doi: 10.3389/fonc.2018.00517
67. Ambrosini G, Adida C, Altieri DC. A Novel Anti-Apoptosis Gene, Survivin, Expressed in Cancer and Lymphoma. *Nat Med* (1997) 3(8):917–21. doi: 10.1038/nm0897-917
68. Ciesielski MJ, Ahluwalia MS, Munich SA, Orton M, Barone T, Chanan-Khan A, et al. Antitumor Cytotoxic T-Cell Response Induced by a Survivin Peptide Mimic. *Cancer Immunol Immunother* (2010) 59(8):1211–21. doi: 10.1007/s00262-010-0845-x
69. Zhang H, Hong H, Li D, Ma S, Di Y, Stoten A, et al. Comparing Pooled Peptides With Intact Protein for Accessing Cross-Presentation Pathways for Protective CD8+ and CD4+ T Cells. *J Biol Chem* (2009) 284(14):9184–91. doi: 10.1074/jbc.M809456200
70. Cai L, Zhang J, Zhu R, Shi W, Xia X, Edwards M, et al. Protective Cellular Immunity Generated by Cross-Presenting Recombinant Overlapping Peptide Proteins. *Oncotarget* (2017) 8(44):76516–24. doi: 10.18632/oncotarget.20407
71. Greenbaum J, Sidney J, Chung J, Brander C, Peters B, Sette A. Functional Classification of Class II Human Leukocyte Antigen (HLA) Molecules Reveals Seven Different Supertypes and a Surprising Degree of Repertoire Sharing Across Supertypes. *Immunogenetics* (2011) 63(6):325–35. doi: 10.1007/s00251-011-0513-0
72. Ott PA, Hu Z, Keskin DB, Shukla SA, Sun J, Bozym DJ, et al. An Immunogenic Personal Neoantigen Vaccine for Patients With Melanoma. *Nature* (2017) 547(7662):217–21. doi: 10.1038/nature22991
73. Nielsen M, Lund O, Buus S, Lundegaard C. MHC Class II Epitope Predictive Algorithms. *Immunology* (2010) 130(3):319–28. doi: 10.1111/j.1365-2567.2010.03268.x
74. Hilf N, Kuttruff-Coqui S, Frenzel K, Bukur V, Stevanovic S, Gouttefangeas C, et al. Actively Personalized Vaccination Trial for Newly Diagnosed Glioblastoma. *Nature* (2019) 565(7738):240–5. doi: 10.1038/s41586-018-0810-y
75. Stupp R, Mason WP, van den Bent MJ, Weller M, Fisher B, Taphoorn MJ, et al. Radiotherapy Plus Concomitant and Adjuvant Temozolomide for Glioblastoma. *N Engl J Med* (2005) 352(10):987–96. doi: 10.1056/NEJMoa043330
76. Blass E, Ott PA. Advances in the Development of Personalized Neoantigen-Based Therapeutic Cancer Vaccines. *Nat Rev Clin Oncol* (2021) 18:215–229. doi: 10.1038/s41571-020-00460-2
77. Fang H, Ang B, Xu X, Huang X, Wu Y, Sun Y, et al. TLR4 is Essential for Dendritic Cell Activation and Anti-Tumor T-Cell Response Enhancement by DAMPs Released From Chemically Stressed Cancer Cells. *Cell Mol Immunol* (2014) 11(2):150–9. doi: 10.1038/cmi.2013.59
78. Dalod M, Chelbi R, Malissen B, Lawrence T. Dendritic Cell Maturation: Functional Specialization Through Signaling Specificity and Transcriptional Programming. *EMBO J* (2014) 33(10):1104–16. doi: 10.1002/embj.201488027
79. Oth T, Vanderlocht J, Van Elssen CH, Bos GM, Germeraad WT. Pathogen-Associated Molecular Patterns Induced Crosstalk Between Dendritic Cells, T Helper Cells, and Natural Killer Helper Cells Can Improve Dendritic Cell Vaccination. *Mediators Inflamm* (2016) 2016:5740373. doi: 10.1155/2016/5740373
80. Oth T, Van Elssen CH, Schnijderberg MC, Senden-Gijsbers BL, Germeraad WT, Bos GM, et al. Potency of Both Human Th1 and NK Helper Cell

Activation is Determined by IL-12p70-Producing PAMP-Matured DCs. *J Interferon Cytokine Res* (2015) 35(9):748–58. doi: 10.1089/jir.2015.0022
81. Yang Y, Che Y, Zhao Y, Wang X. Prevention and Treatment of Cervical Cancer by a Single Administration of Human Papillomavirus Peptide Vaccine With CpG Oligodeoxynucleotides as an Adjuvant *In Vivo*. *Int Immunopharmacol* (2019) 69:279–88. doi: 10.1016/j.intimp.2019.01.024
82. Willems MM, Zom GG, Khan S, Meeuwenoord N, Melief CJ, van der Stelt M, et al. N-Tetradecylcarbamyl Lipopeptides as Novel Agonists for Toll-Like Receptor 2. *J Med Chem* (2014) 57(15):6873–8. doi: 10.1021/jm500722p
83. Zom GG, Willems M, Khan S, van der Sluis TC, Kleinovink JW, Camps MGM, et al. Novel TLR2-Binding Adjuvant Induces Enhanced T Cell Responses and Tumor Eradication. *J Immunother Cancer* (2018) 6(1):146. doi: 10.1186/s40425-018-0455-2
84. Zom GG, Welters MJ, Loof NM, Goedemans R, Lougheed S, Valentijn RR, et al. TLR2 Ligand-Synthetic Long Peptide Conjugates Effectively Stimulate Tumor-Draining Lymph Node T Cells of Cervical Cancer Patients. *Oncotarget* (2016) 7(41):67087–100. doi: 10.18632/oncotarget.11512
85. Macri C, Dumont C, Johnston AP, Mintern JD. Targeting Dendritic Cells: A Promising Strategy to Improve Vaccine Effectiveness. *Clin Transl Immunol* (2016) 5(3):e66. doi: 10.1038/cti.2016.6
86. Shrimpton RE, Butler M, Morel AS, Eren E, Hue SS, Ritter MA. CD205 (DEC-205): A Recognition Receptor for Apoptotic and Necrotic Self. *Mol Immunol* (2009) 46(6):1229–39. doi: 10.1016/j.molimm.2008.11.016
87. Lahoud MH, Ahmet F, Zhang JG, Meuter S, Policheni AN, Kitsoulis S, et al. DEC-205 is a Cell Surface Receptor for CpG Oligonucleotides. *Proc Natl Acad Sci U S A* (2012) 109(40):16270–5. doi: 10.1073/pnas.1208796109
88. Liu Z, Zhou H, Wang W, Fu YX, Zhu M. A Novel Dendritic Cell Targeting HPV16 E7 Synthetic Vaccine in Combination With PD-L1 Blockade Elicits Therapeutic Antitumor Immunity in Mice. *Oncoimmunology* (2016) 5(6): e1147641. doi: 10.1080/2162402X.2016.1147641
89. Dorner BG, Dorner MB, Zhou X, Opitz C, Mora A, Guttler S, et al. Selective Expression of the Chemokine Receptor XCR1 on Cross-Presenting Dendritic Cells Determines Cooperation With CD8+ T Cells. *Immunity* (2009) 31(5):823–33. doi: 10.1016/j.immuni.2009.08.027
90. Kroczek RA, Henn V. The Role of XCR1 and its Ligand XCL1 in Antigen Cross-Presentation by Murine and Human Dendritic Cells. *Front Immunol* (2012) 3:14. doi: 10.3389/fimmu.2012.00014
91. Botelho NK, Tschumi BO, Hubbell JA, Swartz MA, Donda A, Romero P. Combination of Synthetic Long Peptides and XCL1 Fusion Proteins Results in Superior Tumor Control. *Front Immunol* (2019) 10:294. doi: 10.3389/fimmu.2019.00294
92. Belnoue E, Mayol JF, Carboni S, Di Berardino Besson W, Dupuychaffray E, Nelde A, et al. Targeting Self and Neo-Epitopes With a Modular Self-Adjuvanting Cancer Vaccine. *JCI Insight* (2019) 5:e127305. doi: 10.1172/jci.insight.127305
93. Wu H, Zhuang Q, Xu J, Xu L, Zhao Y, Wang C, et al. Cell-Penetrating Peptide Enhanced Antigen Presentation for Cancer Immunotherapy. *Bioconjug Chem* (2019) 30(8):2115–26. doi: 10.1021/acs.bioconjchem.9b00245
94. Zahid M, Robbins PD. Cell-Type Specific Penetrating Peptides: Therapeutic Promises and Challenges. *Molecules* (2015) 20(7):13055–70. doi: 10.3390/molecules200713055
95. Makadia HK, Siegel SJ. Poly Lactic-Co-Glycolic Acid (PLGA) as Biodegradable Controlled Drug Delivery Carrier. *Polymers (Basel)* (2011) 3(3):1377–97. doi: 10.3390/polym3031377
96. Wang N, Wang T, Zhang M, Chen R, Niu R, Deng Y. Mannose Derivative and Lipid A Dually Decorated Cationic Liposomes as an Effective Cold Chain Free Oral Mucosal Vaccine Adjuvant-Delivery System. *Eur J Pharm Biopharm* (2014) 88(1):194–206. doi: 10.1016/j.ejpb.2014.04.007
97. De Serrano LO, Burkhart DJ. Liposomal Vaccine Formulations as Prophylactic Agents: Design Considerations for Modern Vaccines. *J Nanobiotechnol* (2017) 15(1):83. doi: 10.1186/s12951-017-0319-9
98. Stark B, Andreae F, Mosgoeller W, Edetsberger M, Gaubitzer E, Koehler G, et al. Liposomal Vasoactive Intestinal Peptide for Lung Application: Protection From Proteolytic Degradation. *Eur J Pharm Biopharm* (2008) 70(1):153–64. doi: 10.1016/j.ejpb.2008.04.015
99. Arbelaez CA, Estrada J, Gessner MA, Glaus C, Morales AB, Mohn D, et al. A Nanoparticle Vaccine That Targets Neoantigen Peptides to Lymphoid Tissues Elicits Robust Antitumor T Cell Responses. *NPJ Vaccines* (2020) 5 (1):106. doi: 10.1038/s41541-020-00253-9
100. Chatin B, Mevel M, Devalliere J, Dallet L, Haudebourg T, Peuziat P, et al. Liposome-Based Formulation for Intracellular Delivery of Functional Proteins. *Mol Ther Nucleic Acids* (2015) 4:e244. doi: 10.1038/mtna.2015.17
101. Rueda F, Eich C, Cordobilla B, Domingo P, Acosta G, Albericio F, et al. Effect of TLR Ligands Co-Encapsulated With Multiepitopic Antigen in Nanoliposomes Targeted to Human DCs via Fc Receptor for Cancer Vaccines. *Immunobiology* (2017) 222(11):989–97. doi: 10.1016/j.imbio.2017.06.002
102. Zamani P, Navashenaq JG, Nikpoor AR, Hatamipour M, Oskuee RK, Badiee A, et al. MPL Nano-Liposomal Vaccine Containing P5 HER2/neu-Derived Peptide Pulsed PADRE as an Effective Vaccine in a Mice TUBO Model of Breast Cancer. *J Control Release* (2019) 303:223–36. doi: 10.1016/j.jconrel.2019.04.019
103. Alexander J, Sidney J, Southwood S, Ruppert J, Oseroff C, Maewal A, et al. Development of High Potency Universal DR-Restricted Helper Epitopes by Modification of High Affinity DR-Blocking Peptides. *Immunity* (1994) 1 (9):751–61. doi: 10.1016/S1074-7613(94)80017-0
104. Du Z, Munye MM, Tagalakis AD, Manunta MD, Hart SL. The Role of the Helper Lipid on the DNA Transfection Efficiency of Lipopolyplex Formulations. *Sci Rep* (2014) 4:7107. doi: 10.1038/srep07107
105. Zamani P, Teymouri M, Nikpoor AR, Navashenaq JG, Gholizadeh Z, Darban SA, et al. Nanoliposomal Vaccine Containing Long Multi-Epitope Peptide E75-AE36 Pulsed PADRE-Induced Effective Immune Response in Mice TUBO Model of Breast Cancer. *Eur J Cancer* (2020) 129:80–96. doi: 10.1016/j.ejca.2020.01.010
106. Varypataki EM, Silva AL, Barnier-Quer C, Collin N, Ossendorp F, Jiskoot W. Synthetic Long Peptide-Based Vaccine Formulations for Induction of Cell Mediated Immunity: A Comparative Study of Cationic Liposomes and PLGA Nanoparticles. *J Control Release* (2016) 226:98–106. doi: 10.1016/j.jconrel.2016.02.018
107. Jacoberger-Foissac C, Saliba H, Seguin C, Brion A, Kakhi Z, Frisch B, et al. Optimization of Peptide-Based Cancer Vaccine Compositions, by Sequential Screening, Using Versatile Liposomal Platform. *Int J Pharm* (2019) 562:342–50. doi: 10.1016/j.ijpharm.2019.03.002
108. Khong H, Volmari A, Sharma M, Dai Z, Imo CS, Hailemichael Y, et al. Peptide Vaccine Formulation Controls the Duration of Antigen Presentation and Magnitude of Tumor-Specific CD8(+) T Cell Response. *J Immunol* (2018) 200(10):3464–74. doi: 10.4049/jimmunol.1700467
109. Kordalivand N, Tondini E, Lau CYJ, Vermonden T, Mastrobattista E, Hennink WE, et al. Cationic Synthetic Long Peptides-Loaded Nanogels: An Efficient Therapeutic Vaccine Formulation for Induction of T-Cell Responses. *J Control Release* (2019) 315:114–25. doi: 10.1016/j.jconrel.2019.10.048
110. Wei P, Gangapurwala G, Pretzel D, Leiske MN, Wang L, Hoeppener S, et al. Smart pH-Sensitive Nanogels for Controlled Release in an Acidic Environment. *Biomacromolecules* (2019) 20(1):130–40. doi: 10.1021/acs.biomac.8b01228
111. Klinger D, Aschenbrenner EM, Weiss CK, Landfester K. Enzymatically Degradable Nanogels by Inverse Miniemulsion Copolymerization of Acrylamide With Dextran Methacrylates as Crosslinkers. *Polymer Chem* (2012) 3(1):204–16. doi: 10.1039/C1PY00415H
112. Lynn GM, Sedlik C, Baharom F, Zhu Y, Ramirez-Valdez RA, Coble VL, et al. Peptide-TLR-7/8a Conjugate Vaccines Chemically Programmed for Nanoparticle Self-Assembly Enhance CD8 T-Cell Immunity to Tumor Antigens. *Nat Biotechnol* (2020) 38(3):320–32. doi: 10.1038/s41587-019-0390-x
113. Chikuma S. Basics of PD-1 in Self-Tolerance, Infection, and Cancer Immunity. *Int J Clin Oncol* (2016) 21(3):448–55. doi: 10.1007/s10147-016-0958-0
114. Topalian SL, Drake CG, Pardoll DM. Immune Checkpoint Blockade: A Common Denominator Approach to Cancer Therapy. *Cancer Cell* (2015) 27 (4):450–61. doi: 10.1016/j.ccell.2015.03.001
115. Petricevic B, Laengle J, Singer J, Sachet M, Fazekas J, Steger G, et al. Trastuzumab Mediates Antibody-Dependent Cell-Mediated Cytotoxicity and Phagocytosis to the Same Extent in Both Adjuvant and Metastatic HER2/neu Breast Cancer Patients. *J Transl Med* (2013) 11:307. doi: 10.1186/1479-5876-11-307
116. Kono K, Sato E, Naganuma H, Takahashi A, Mimura K, Nukui H, et al. Trastuzumab (Herceptin) Enhances Class I-Restricted Antigen Presentation Recognized by HER-2/Neu-Specific T Cytotoxic Lymphocytes. *Clin Cancer Res* (2004) 10(7):2538–44. doi: 10.1158/1078-0432.CCR-03-0424

117. Gall VA, Philips AV, Qiao N, Clise-Dwyer K, Perakis AA, Zhang M, et al. Trastuzumab Increases HER2 Uptake and Cross-Presentation by Dendritic Cells. *Cancer Res* (2017) 77(19):5374–83. doi: 10.1158/0008-5472.CAN-16-2774
118. Hickerson A, Clifton GT, Hale DF, Peace KM, Holmes JP, Vreeland TJ, et al. Final Analysis of Nelipepimut-S Plus GM-CSF With Trastuzumab Versus Trastuzumab Alone to Prevent Recurrences in High-Risk, HER2 Low-Expressing Breast Cancer: A Prospective, Randomized, Blinded, Multicenter Phase IIb Trial. *J Clin Oncol* (2019) 37(8_suppl):1–1. doi: 10.1200/JCO.2019.37.8_suppl.1
119. Noguchi M, Arai G, Egawa S, Ohyama C, Naito S, Matsumoto K, et al. Mixed 20-Peptide Cancer Vaccine in Combination With Docetaxel and Dexamethasone for Castration-Resistant Prostate Cancer: A Randomized Phase II Trial. *Cancer Immunol Immunother* (2020) 69:847–57. doi: 10.1007/s00262-020-02498-8
120. Roselli M, Cereda V, di Bari MG, Formica V, Spila A, Jochems C, et al. Effects of Conventional Therapeutic Interventions on the Number and Function of Regulatory T Cells. *Oncoimmunology* (2013) 2(10):e27025. doi: 10.4161/onci.27025
121. Scurr M, Pembroke T, Bloom A, Roberts D, Thomson A, Smart K, et al. Low-Dose Cyclophosphamide Induces Antitumor T-Cell Responses, Which Associate With Survival in Metastatic Colorectal Cancer. *Clin Cancer Res* (2017) 23(22):6771–80. doi: 10.1158/1078-0432.CCR-17-0895
122. Shirahama T, Muroya D, Matsueda S, Yamada A, Shichijo S, Naito M, et al. A Randomized Phase II Trial of Personalized Peptide Vaccine With Low Dose Cyclophosphamide in Biliary Tract Cancer. *Cancer Sci* (2017) 108(5):838–45. doi: 10.1111/cas.13193
123. Cheon YK, Cho YD, Moon JH, Jang JY, Kim YS, Kim YS, et al. Diagnostic Utility of Interleukin-6 (IL-6) for Primary Bile Duct Cancer and Changes in Serum IL-6 Levels Following Photodynamic Therapy. *Am J Gastroenterol* (2007) 102(10):2164–70. doi: 10.1111/j.1572-0241.2007.01403.x
124. Hogdall D, O'Rourke CJ, Dehlendorff C, Larsen OF, Jensen LH, Johansen AZ, et al. Serum IL6 as a Prognostic Biomarker and IL6R as a Therapeutic Target in Biliary Tract Cancers. *Clin Cancer Res* (2020) 26(21):5655–67. doi: 10.1158/1078-0432.CCR-19-2700
125. Yang W, Bai Y, Xiong Y, Zhang J, Chen S, Zheng X, et al. Potentiating the Antitumour Response of CD8(+) T Cells by Modulating Cholesterol Metabolism. *Nature* (2016) 531(7596):651–5. doi: 10.1038/nature17412
126. Pan J, Zhang Q, Palen K, Wang L, Qiao L, Johnson B, et al. Potentiation of Kras Peptide Cancer Vaccine by Avasimibe, a Cholesterol Modulator. *EBioMedicine* (2019) 49:72–81. doi: 10.1016/j.ebiom.2019.10.044
127. Quezada SA, Simpson TR, Peggs KS, Merghoub T, Vider J, Fan X, et al. Tumor-Reactive CD4(+) T Cells Develop Cytotoxic Activity and Eradicate Large Established Melanoma After Transfer Into Lymphopenic Hosts. *J Exp Med* (2010) 207(3):637–50. doi: 10.1084/jem.20091918
128. Xie Y, Akpinarli A, Maris C, Hipkiss EL, Lane M, Kwon EK, et al. Naive Tumor-Specific CD4(+) T Cells Differentiated *In Vivo* Eradicate Established Melanoma. *J Exp Med* (2010) 207(3):651–67. doi: 10.1084/jem.20091921
129. Kumai T, Lee S, Cho HI, Sultan H, Kobayashi H, Harabuchi Y, et al. Optimization of Peptide Vaccines to Induce Robust Antitumor CD4 T-Cell Responses. *Cancer Immunol Res* (2017) 5(1):72–83. doi: 10.1158/2326-6066.CIR-16-0194
130. Croft M, So T, Duan W, Soroosh P. The Significance of OX40 and OX40L to T-Cell Biology and Immune Disease. *Immunol Rev* (2009) 229(1):173–91. doi: 10.1111/j.1600-065X.2009.00766.x
131. Oncology Times. *FDA Approves First Oncolytic Virus Therapy: Imlygic for Melanoma* Vol. 37. United States: Oncology Times (2015). p. 36.
132. Atherton MJ, Stephenson KB, Nikota JK, Hu QN, Nguyen A, Wan Y, et al. Preclinical Development of Peptide Vaccination Combined With Oncolytic MG1-E6E7 for HPV-Associated Cancer. *Vaccine* (2018) 36(16):2181–92. doi: 10.1016/j.vaccine.2018.02.070
133. ClinicalTrials.gov. (2021). [cited 2021 31st May] Available at: www.clinicaltrials.gov.
134. Bezu L, Kepp O, Cerrato G, Pol J, Fucikova J, Spisek R, et al. Trial Watch: Peptide-Based Vaccines in Anticancer Therapy. *Oncoimmunology* (2018) 7 (12):e1511506. doi: 10.1080/2162402X.2018.1511506

Conflict of Interest: SJ receives grants from CBI and Oxford Vacmedix UK Ltd, a spin-out from University of Oxford who develop recombinant overlapping peptide (ROP) cancer vaccines. NB-B consults for Oxford Vacmedix UK Ltd.

frontiers in Immunology

ORIGINAL RESEARCH
published: 01 July 2021
doi: 10.3389/fimmu.2021.695056

STING Agonist Combined to a Protein-Based Cancer Vaccine Potentiates Peripheral and Intra-Tumoral T Cell Immunity

Matteo Rossi[1,2], *Susanna Carboni*[1,2], *Wilma Di Berardino-Besson*[1,2], *Erika Riva*[1,2], *Marie-Laure Santiago-Raber*[1,2], *Elodie Belnoue*[1,2†] *and Madiha Derouazi*[1,2*†]

[1] AMAL Therapeutics, Geneva, Switzerland, [2] Boehringer Ingelheim International GmbH, Ingelheim, Germany

OPEN ACCESS

Edited by:
Shisong Jiang,
University of Oxford, United Kingdom

Reviewed by:
Laura Rogers,
Mayo Clinic, United States
Sultan Gulce Iz,
Eindhoven University of Technology, Netherlands

***Correspondence:**
Madiha Derouazi
madiha.derouazi@boehringer-ingelheim.com

†These authors share senior authorship

Specialty section:
This article was submitted to Vaccines and Molecular Therapeutics, a section of the journal Frontiers in Immunology

Received: 14 April 2021
Accepted: 16 June 2021
Published: 01 July 2021

Citation:
Rossi M, Carboni S, Di Berardino-Besson W, Riva E, Santiago-Raber M-L, Belnoue E and Derouazi M (2021) STING Agonist Combined to a Protein-Based Cancer Vaccine Potentiates Peripheral and Intra-Tumoral T Cell Immunity. Front. Immunol. 12:695056. doi: 10.3389/fimmu.2021.695056

Combining different immunotherapy approaches is currently building the future of immunotherapy, with the view to maximize anti-tumoral efficacy for larger patient population. The KISIMA™ platform allows the development of protein-based cancer vaccines able to induce tumor-specific T cell response resulting in anti-tumoral efficacy in various mouse models. Intra-tumoral administration of stimulator of interferon gene agonists (STINGa) was shown to induce a potent inflammatory response leading to the development of tumor-specific immunity. Here, we explored the efficacy and mechanisms of action of subcutaneous STINGa treatment combined with therapeutic vaccination in various mouse tumor models. This combinatory treatment highly enhanced frequency and effector function of both peripheral and intra-tumoral antigen-specific CD8 T cells, promoting potent IFNγ and TNFα production along with increased cytotoxicity. Moreover, combination therapy favorably modulated the tumor microenvironment by dampening immune-suppressive cells and increasing CD4 T cell infiltration together with their polarization toward Th1 phenotype. Combination with STINGa treatment improved the effect of therapeutic vaccination, resulting in a prolonged control and slower growth of B16-OVA and TC-1 tumors. Altogether, the results presented here highlight the potential of combining STINGa with a therapeutic protein vaccine for cancer treatment.

Keywords: STING agonist, protein cancer vaccine, combination immunotherapy, CD8 T cells functionality, Th1 CD4 T cells, tumor microenvironment

INTRODUCTION

It is now established that modulating the immune system of cancer patients to specifically recognize and eliminate tumor cells is a promising therapeutic modality. As of September 2020, 4,400 clinical trials investigating the efficacy of PD-1/PD-L1 blockade were open (1). The initial enthusiasm for the impressive efficacy of checkpoint inhibitors (CPIs) was nevertheless dampened by the restricted patient population responding to therapy and by acquired treatment resistance (2).

In parallel to immune checkpoints, immune co-stimulators —molecules transiently expressed or up-regulated by T cells during the priming to potently increase their activation such as OX40 or Glucocorticoid-induced TNFR-related protein (GITR) —are promising immunotherapy targets. OX40- and GITR-agonists have been shown to potently stimulate anti-tumoral immune response in pre-clinical studies, resulting in an inhibition of tumor growth (3, 4). Another very promising strategy is the targeting of the stimulator of interferon genes (STING) pathway. STING is an adaptor protein activated by the binding to cyclic GAMP—a by-product of cytosolic DNA degradation by DNA sensors (5, 6)—which upon activation induces the secretion of high levels of type I interferons and other pro-inflammatory cytokines such as IL-6 and TNFα (7–9). Activation of STING was shown to enhance NK cell recruitment and activation (10) and to promote CD4 and CD8 T cell chemotaxis (11). In addition, STING signaling was found to be inhibited in patient derived colorectal adenocarcinoma cells, supporting its anti-tumoral role (12). Due to these properties, synthetic STING agonists have been tested in pre-clinical and clinical studies with the intent of inflaming the tumor and eliciting an anti-tumoral immune response. Intra-tumoral injection of STING agonist was shown to induce tumor regression as well as a systemic, tumor-specific memory immune response in different murine tumor models (13). Moreover, STING agonist formulated within a GM-CSF-producing cancer cell vaccine was shown to delay tumor progression in different murine models, demonstrating that intra-tumoral administration is not the only effective route (14). Currently, multiple phase 1/2 clinical trials investigate the use of STING agonists—alone or in combination with CPIs—in different solid tumors and lymphoma patients (15).

As for CPIs, the impact of immune-modulators is however limited by the need for a pre-existing immune response able to infiltrate the core of the tumor, while cancer cells are master of immune evasion and suppression. Combination of immune modulators with therapeutic cancer vaccines could support T cell-mediated immunity and infiltration in the tumor despite a detrimental suppressive tumor micro-environment (16, 17).

We previously described an original chimeric protein vaccine platform, named KISIMA™, composed of three elements: a ZEBRA-derived cell-penetrating peptide (Z13) (18), a multiantigenic domain (Mad) with epitopes restricted by multiple MHC alleles, and a TLR2/4 agonist (Anaxa) conferring self-adjuvanticity. This vaccine platform was shown to elicit both CD8 and CD4 antigen-specific T cell responses in preclinical tumor models, leading to immunological memory and high vaccine efficacy (19, 20). Here, we sought to take advantage of both cancer vaccine and immune-modulator properties to impact not only the quantity but also the quality of both CD8 and CD4 T cells, establishing a combination immunotherapy able to effectively tackle different types of cancers. We assessed the combination of KISIMA-derived vaccines with subcutaneously administered STING agonist. Improved tumor growth control in mouse tumor models was associated with higher frequency of CD8 and CD4 T cells, improved effector functions, re-polarization of CD4 toward Th1, and modulation of the tumor microenvironment (TME).

MATERIALS AND METHODS

Mice

Female C57BL/6J mice were purchased from Charles River Laboratories (L'arbresle, France). All animals used in this study were between 6 and 10 weeks old at the time of experiments.

Vaccines

Vaccine constructs were designed in-house and produced in *E. coli* by Genscript. Vaccines were prepared by dilution in vaccine buffer (50 mM TRIS-HCl, 150 mM NaCl, 10% Glycerol, 1 M L-Arg, 1mM DTT, 0.2% Tween20, pH 8) and administered by subcutaneous (s.c.) injection of 10 nmoles in 100 µl volume. The different constructions used are illustrated in **Figure S1**.

STING Agonist

STING agonist (ML-RR-S2 CDA, ADU-S100, Med Chem Express) was resuspended in DMSO at a concentration of 6.9 mg/ml and diluted in 1× phosphate buffer saline (PBS, Gibco) prior to injection.

Tumor-Free Mice Vaccination Experiments

C57BL/6 mice were vaccinated twice (at days 0 and 14 for Z13Mad25Anaxa and days 0 and 7 for Z13Mad39Anaxa) by s.c. injection of 10 nmoles of vaccine at the tail base. At the same time of vaccination, mice received 25 µg of STING agonist administered *via* 2× 50 µl s.c. injections in each side of the low back, in proximity of the vaccination site. Serum was collected 4 and 24 h after the first vaccination and IFN-α concentration was measured by ELISA. Whole blood was collected one week after the last vaccination and used for antigen-specific CD8 T cell measurement by multimer flow cytometry staining. At the same time, spleens were harvested, and splenocytes were used for *ex vivo* stimulation, and intracellular cytokine production was analyzed by flow cytometry. Alternatively, splenocytes were used for TCR avidity assay.

Tumor Cell Line

The TC-1 cell line was obtained from ATCC. This cell line, derived from lung epithelial cells transfected with HPV16 E6/E7 and c-H-ras oncogenes, was maintained in RPMI 1640 Glutamax™ supplemented with 10% heat-inactivated fetal calf serum (FCS), 100 U/ml penicillin/streptomycin (P/S), 1 mM sodium pyruvate, MEM NEAA, and 0.4 mg/ml geneticin G418.

The B16-OVA cell line was provided by Bertrand Huard (University of Grenoble-Alpes, France). This cell line, derived from mouse melanoma cells transfected with OVA, was maintained in RPMI 1640 Glutamax™ supplemented with 10% heat-inactivated fetal calf serum (FCS), 100 U/ml penicillin/streptomycin (P/S), 1 mM sodium pyruvate, MEM NEAA and 1 mg/ml geneticin G418.

In Vivo Tumor Experiments

C57BL/6J mice were implanted s.c. with 1×10^5 TC-1 tumor cells in the back, and mice were stratified according to tumor size on day 6 of tumor implantation. Alternatively, C57BL/6J mice were injected i.v. with 1×10^5 B16-OVA cells. Mice were vaccinated two times by s.c. injection of 10 nmoles of KISIMA vaccine at the tail base. At the same time of vaccination, mice received 25 µg of STING agonist administered *via* 2× 50 µl s.c. injections in each side of the low back, in proximity of the vaccination site. TC-1 tumor size was measured with a caliper, and mice were euthanized when tumor reached a volume of 1,000 mm^3. Tumor volume was calculated with the following formula: $V = length \times length \times width \times Pi/6$. B16-OVA tumor bearing mice were sacrificed at day 20; lungs were perfused with a saline solution, and the number of lung metastasis was counted.

Ex Vivo Cell Preparation

TC-1 tumors were harvested at day 20 post implantation, and tumor-infiltrating leucocytes (TILs) were purified using mouse tumor dissociation kit from Miltenyi, following manufacturer's instructions. Briefly, tumor tissues were chopped into small pieces and resuspended in DMEM medium containing tumor dissociating enzymes (Miltenyi). Tumors were digested on a Gentle MACS with heating system (Miltenyi) using solid tumor program. Enzymatic digestion was stopped by adding cold PBS 0.5% BSA solution and keeping cells on ice. Digested tumors were passed through a 70 µm cell strainer to eliminate remaining undigested tissue. CD45+ cells were purified using CD45 TIL microbeads (Miltenyi) following manufacturer's protocol. Purified CD45+ cells were used for flow cytometry staining or *ex vivo* T cell stimulation.

B16-OVA tumor bearing mice were perfused with a saline solution to eliminate blood from the lungs before their collection. Lung-infiltrating leucocytes (LILs) were purified using mouse tumor dissociation kit from Miltenyi, following manufacturer's instructions.

Peripheral blood and spleen mononuclear cell suspensions from mice were isolated using Ficoll–Paque gradient (GE Healthcare) before flow cytometry analysis, *ex vivo* stimulation, or TCR avidity assay.

Ex Vivo T Cell Stimulation

TILs, LILs, or splenocytes were numerated, and 1×10^5 or 2×10^6 cells were plated per condition, respectively. Cells were incubated with HPV-CD8, OVA-CD8, or OVA-CD4 epitope peptide, or without any stimulant as a negative control in the presence of Golgi stop (BD biosciences) and a fluorochrome coupled anti-CD107α for 6 h. After washing, cells were stained for cell surface antigens and fixable viability dye, then, after fixation and permeabilization according to manufacturer's instructions (BD biosciences), cells were stained for intracellular cytokines.

In Vivo Cytotoxicity Assay

Naive splenocytes were harvested and incubated for 1.5 h in DMEM complete medium at 37°C with or without HPV-E7 CD8 epitope peptide. Then, loaded and non-loaded splenocytes were stained with cell tracer violet (CTV) or CFSE (both from ThermoFisher Scientific), respectively, following manufacturer's instructions. Splenocytes were then mixed at a 1:1 ratio, and a total of 5×10^6 cells were transferred by intravenous injection into previously vaccinated mice. Then 20 h post cell transfer, splenocytes were harvested, and the survival of CTV or CFSE stained cells was assessed by flow cytometry. The percentage of antigen-specific killing was calculated with the following formula: % antigen-specific killing = (1−(ratio $peptide^+$: $peptide^-$ vaccinated/ratio $peptide^+$: $peptide^-$ naive)) * 100.

Ex Vivo TCR Avidity Assay

One week after the second vaccination, spleens were harvested, and splenocytes were isolated (see above). Then 1×10^6 cells/well were seeded in an IFN-γ ELISpot plate (Diaclone) and stimulated overnight with decreasing concentrations of RAHYNIVTF or SIINFEKL peptide. ELISpot plates were then revealed following manufacturer's instructions, and the percentage of maximal response was calculated relatively to the highest concentration of stimulating peptide.

Antibodies and Flow Cytometry

The following antibodies were used: CD45 (clone 30-F11), CD11b (M1/70), KLRG1 (2F1), CD103 (M290), NKg2a (20d5), Ly6C (AL-21), Ly6G (1A8), PD-L1 (MIH5), I-A/I-E (M5/114), CD11c (HL3), PDCA1 (927), CD64 (X54-5/7.1), B220 (RA3-6B2), CD24 (M1/69), CD4 (GK1.5), CD25 (3C7), CD3 (500A2), NKp46 (29A1.4), TNF-α (MP6-XT22), IFN-γ (XMG1.2), H2-Kb (AF6-88.5), and H2-Db (28–14–8) were from BD Biosciences; Tim3 (RMT3-23), PD-1 (29F.1A12), CD38 (90), Gr-1 (RB6-8C5), CD206 (C068C2), CD68 (FA-11) were from BioLegend; FoxP3 (FJK-16s), T-bet (4B10), GATA-3 (TWAJ), and RORγt (AFKJS-9) were from ThermoFisher Scientific; Granzyme B (REA226) was from Miltenyi; CD8 (KT15) was from MBL. Dead cells were stained with LIVE/DEAD Yellow or Aqua fluorescent reactive dye (Life Technologies) and excluded from analyses. Murine MHC-peptide multimers were from Immudex (Copenhagen, Denmark). Cells were analyzed using an Attune NxT flow cytometer (ThermoFisher Scientific), and results were analyzed with Kaluza (Beckman Coulter) software.

Quantification of Serum Interferon-α

Blood was collected from mouse tail vein, and serum was isolated by centrifugation using Starstedt tubes. The concentration of IFN-α cytokine was measured using commercial ELISA kits according to the manufacturer's recommendations (PBL Assay Science).

HPV-16 E7 mRNA Extraction and Sequencing

A tumor sample of 4 mm^2 was snap dry frozen in liquid nitrogen and RNA was extracted using the RNwasy Plus Mini kit (Qiagen) following manufacturer's instructions. cDNA was generated by RT-PCR, and HPV-16 E7 DNA was then amplified using the following primers: Forward 5′-ATGCATGGAGATACAC

CTAC-3′; Reverse 5′-TTATGGTTTCTGAGAACAGATG-3′. The amplified cDNA was then sequenced by Sanger sequencing (Microsynth).

Statistical Analysis

Statistical analyses were performed using Prism software (GraphPad). *Mann–Whitney Student's t-test*, *Log-rank Mantel–Cox test* or *ANOVA* was used depending on the experiment, and groups were considered statistically significant if $p < 0.05$. In TC-1 tumor model, mice were stratified according to tumor size on the day of the first vaccination. In other experiments, mice were randomly assigned to the treatment on the day of the first vaccination.

Ethic Approval

These studies have been reviewed and approved by the institutional and cantonal veterinary authorities in accordance with Swiss Federal law on animal protection.

RESULTS

Combination of STING Agonist Treatment With a Protein Vaccine Modulates Peripheral CD8 and CD4 T Cell Response

We previously reported that therapeutic subcutaneous (s.c.) vaccination with different KISIMA constructions elicits antigen-specific CD8 T cell response and promotes their infiltration within the tumor (19). In this study, therapeutic vaccination was combined with subcutaneous STING agonist (STINGa) administration. In preclinical tumor model and ongoing clinical trials, STINGa is generally administered intratumorally (i.t.) in order to inflame the tumor microenvironment (TME). Subcutaneous STINGa injection in proximity of the vaccination site would allow for expanding its clinical application to non-accessible tumors while still exploiting the potent immune-stimulatory effect. In order to evaluate the impact of the combination on the T cells' compartment, tumor-free mice were vaccinated twice at 2 weeks interval, with concomitant STINGa treatment (**Figure 1A**) and Z13Mad25Anaxa, a KISIMA-derived construct containing one human papilloma virus (HPV)-derived CD8 epitope (**Figure S1**). First, the systemic inflammatory response upon subcutaneous STINGa administration was analyzed. STINGa s.c. treatment induced a potent but transient systemic type I interferon response, characterized by high IFN-α serum level 4 h post-injection and already decreasing 24 h later (**Figure 1B**). The systemic interferon response was not affected by concomitant injection of the protein vaccine. Combination of Z13Mad25Anaxa and STINGa treatment further increased by two-fold the frequency of antigen-specific CD8 T cells (**Figure 1C**, left). In addition to their frequency, STINGa–Z13Mad25Anaxa combination treatment also highly enhanced the effector function of antigen-specific CD8 T cells. *In vivo* killing assay performed one week after vaccination revealed a significant 2.5-fold increase of antigen-specific cytotoxicity in STINGa–Z13Mad25Anaxa combination treated mice (**Figure 1C**, middle). Furthermore, *ex vivo* stimulation with decreasing concentration of HPV-CD8 peptide showed significantly higher TCR avidity on STINGa–Z13Mad25Anaxa primed T cells (**Figure 1C**, right). STINGa–protein vaccine combination modulated also bystander CD4 T cells response, deeply changing their polarization (**Figure 1D**). Significantly higher proportion of T helper 1 (Th1, T-bet$^+$) and lower proportion of Treg (Foxp3$^+$) and Th2 (GATA-3$^+$) CD4 T cells were quantified in combination with STINGa, resulting in higher Th1/Th2 ratio. Similar modulation of CD8 and CD4 T cell response was observed using a different KISIMA construct containing CD4 and CD8 epitopes derived from ovalbumin (OVA), Z13Mad39Anaxa (**Figure S1**), suggesting that the modulation of the T cell response does not depend on the antigenic cargo (**Figure S2**). Z13Mad39Anaxa vaccination elicited polyfunctional CD8 and CD4 antigen-specific T cells, which produced IFNγ and TNFα following *ex vivo* stimulation with the specific peptide (**Figure S2**). Altogether, addition of STINGa to a protein vaccine profoundly impacts frequency and quality of CD8 T cell response along with polarization of CD4 T cell toward Th1.

STINGa–Protein Vaccine Combination Inhibits B16-OVA Tumor Growth

The anti-tumoral efficacy of therapeutic STINGa–protein vaccine combination treatment was then evaluated in the B16-OVA pulmonary metastases tumor model. Starting three days post tumor cell intravenous injection, mice were vaccinated twice at one-week interval, and the number of pulmonary metastasis was counted 10 days after the last vaccination (**Figure 2A**). Z13Mad39Anaxa vaccination resulted in a significant reduction of the number of metastasis, and while STINGa monotherapy had no effect, in combination with Z13Mad39Anaxa, it significantly further lowered the number of metastasis (**Figure 2B**). In addition, the presence and functionality of lung infiltrating lymphocytes (LILs) were analyzed by flow cytometry. The vaccination induced polyfunctional OVA-specific CD8 T cell infiltration, characterized by the expression of granzyme B (GzB), IFNγ and TNFα (**Figure 2C**), which were significantly increased with STINGa combination. Similar increase in T cell phenotype and functionality was observed in the periphery (blood and spleen) with a lower magnitude, suggesting that antigen-specific T cells are prevalently recruited to the tumor site (**Figures S3A, B**). As observed in tumor-free mice, KISIMA–STINGa combination treatment modulated the polarization of intra-tumoral CD4 T cells, decreasing the presence of Tregs while increasing the Th1/Th2 ratio (**Figure 2D**). *Ex vivo* stimulation with OVA peptide highlighted the presence of functional antigen-specific CD4 T cells in the spleen but not in the lungs, suggesting that helping CD8 T cell response is prevalently happening in the secondary lymphoid organ (**Figures 2D**, **S3C**).

Taken together these results show that combination treatment of a protein vaccine and a STINGa promotes both

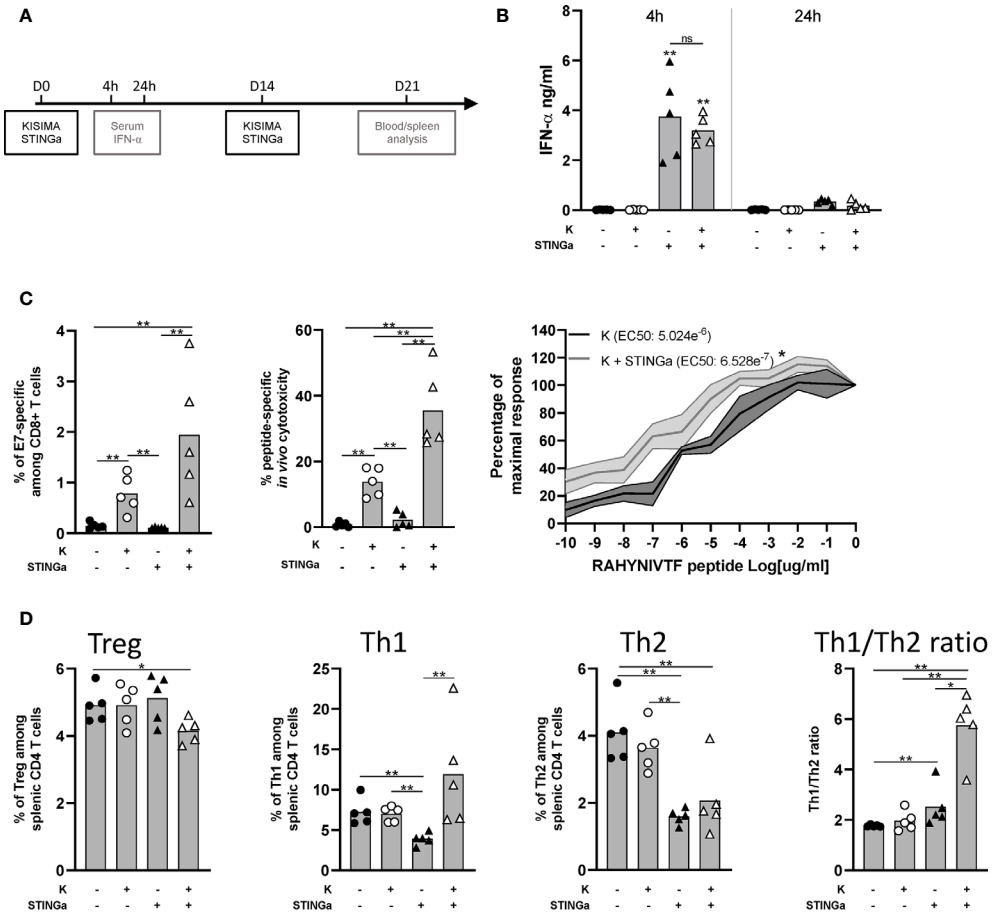

FIGURE 1 | Protein vaccine combination treatment with STING agonist enhances functionality of CD8 T and CD4 T cell peripheral responses in tumor-free mice. C57BL/6 mice were treated with two administrations of Z13Mad25Anaxa vaccine, STING agonist or a combination of the two at two weeks interval. **(A)** Vaccination schedule. **(B)** Serum IFN-a level was measured 4 and 24 h post first vaccination. **(C)** One week after the second vaccination, circulating RAHYNIVTF (HPV-E7)-specific CD8 T cells were measured by multimer staining (left); *in vivo* cytotoxicity of RAHYNIVTF-specific CD8 T cells was measured by transfer of RAHYNIVTF peptide loaded splenocytes (middle); RAHYNIVTF-specific CD8 T cell TCR avidity was measured by *ex vivo* ELISpot (right). **(D)** Frequency of Treg (FoxP3$^+$), Th1 (T-bet$^+$), Th2 (GATA-3$^+$) splenic CD4 T cells and Th1/Th2 ratio was measured by flow cytometry one week after the second vaccination. **(B–D)** One representative of two experiments is shown (n = 5/group/replicate), *Mann–Whitney test*, *p < 0.05, **p < 0.01; ns, not significant.

intra-tumoral infiltration of antigen-specific effector CD8 T cells and the functionality of peripheral CD4 T cells, resulting in the inhibition of B16-OVA tumor growth.

Anti-Tumoral Effect of STINGa–Protein Vaccine Combination in TC-1 Tumor Model

The anti-tumoral effect of therapeutic STINGa–protein vaccine combination treatment was then assessed in TC-1 tumor—a cell line derived from mouse lung epithelial cells and transfected with HPV-16 E6/E7 and c-H-ras oncogenes. When tumors were palpable (day 6), mice were vaccinated twice at one-week interval, and tumor growth was monitored (**Figure 3A**). Z13Mad25Anaxa therapeutic vaccination of TC-1 tumor-bearing mice resulted in a significant delay of tumor development and a 27-day increase in median survival (**Figures 3B, C**). While STINGa monotherapy had no effect on tumor growth, in combination with Z13Mad25Anaxa vaccination, it further delayed tumor development and enhanced median survival by 15 days compared to vaccination alone. Of note, neither single nor combination treatment caused significant variation of body temperature or weight shortly after administration to TC-1 tumor-bearing mice, indicating good safety and tolerability of the combination (**Figure S4**). Thus, therapeutic vaccination with a protein vaccine effectively delays TC-1 tumor growth, and concomitant STINGa treatment enhances the vaccine efficacy.

Profound Impact of STINGa–Protein Vaccine Combination Treatment on the Composition of TC-1 Tumor Microenvironment

Despite T cells being the principal target of immunotherapy, due to their ability to directly kill cancer cells, the TME is a very complex network constituted by different immune cell types able

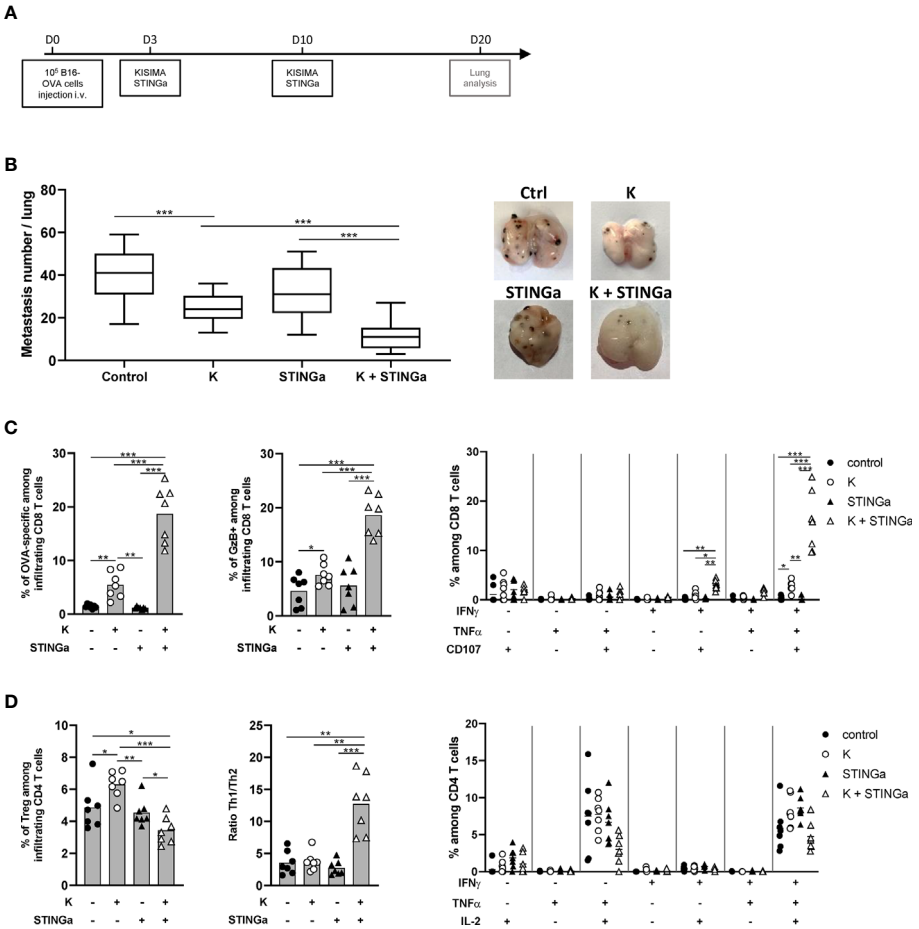

FIGURE 2 | Combining protein vaccine with STING agonist inhibits B16-OVA tumor growth. 10^5 B16-OVA cells were injected intravenously into C57BL/6 mice. At days 3 and 10 post tumor injection, mice were treated with two administrations of KISIMA vaccine, STING agonist or a combination of the two. At day 20, the number of lung metastasis was counted, and lung infiltrating lymphocytes were analyzed. **(A)** Vaccination schedule. **(B)** Number of metastatic nodules per lung and representative pictures. **(C)** Frequency of SIINFEKL (OVA)-specific CD8 T cells among tumor infiltrating leukocytes and expression of Granzyme B was measured by flow cytometry. Antigen-specific cytokine production by CD8 T cells was measured by intracellular staining after *ex vivo* stimulation with SIINFEKL peptide in presence of Golgi inhibitor. Antigen-specific cytokine production was measured by intracellular staining; frequency of cytokine-producing among CD8 T cells is shown. **(D)** Frequency of Treg (FoxP3$^+$) and Th1/Th2 ratio was measured by flow cytometry. Antigen-specific cytokine production by CD4 T cells was measured by intracellular staining after *ex vivo* stimulation with ISQAVHAAHAEINEAGR (OVA-CD4) peptide in the presence of Golgi inhibitor. Antigen-specific cytokine production was measured by intracellular staining; frequency of cytokine-producing among CD4 T cells is shown. **(B–D)** One representative of two experiments is shown (n = 7/group/replicate), *Mann–Whitney test*, $^*p < 0.05$, $^{**}p < 0.01$, $^{***}p < 0.001$.

to promote or inhibit cancer growth. Thus, the composition of TC-1 TME was dissected in order to have a complete view of its immunological status. TC-1 being a cold tumor model, CD4 and CD8 T cell infiltration combined represented less than 2% of tumor infiltrating CD45+ cells in vehicle treated mice (**Figures 3D**, **S5**). The most prominent cell type was tumor associated macrophages (TAMs), representing up to 75% of the infiltrate, and in particular the immunosuppressive TAM2. Myeloid derived suppressor cells (MDSCs) represent another 15%, with the monocytic type (mMDSC) being prevalent. Other cell types found with lower frequency were dendritic cells (DCs, 7%), B cells (2%), NK and NKT cells (1.5%), and neutrophils (1%). Therapeutic protein vaccine treatment induced a profound modification of the TME, characterized by a strong increase in CD8 T cells and DC frequency and the appearance of non-Treg CD4 T cells. Interestingly, the increase of DC infiltration was also characterized by an increase of monocytic DC (moDC) proportion (**Figures 3E**, **S6**), a particular subset which has been described to differentiate only in inflammatory conditions and has been shown to activate anti-tumoral T cell responses (21). While the TAM1 compartment remained mostly unaltered, TAM2 frequency was strongly decreased resulting in a higher TAM1/TAM2 ratio. In contrast, the frequency of mMDSC was increased by Z13Mad25Anaxa vaccination, while granulocytic MDSC and neutrophils remained mostly unchanged. STINGa monotherapy did not affect the composition of TME, which was essentially identical to vehicle treated mice. However, in combination with protein vaccine treatment, it further

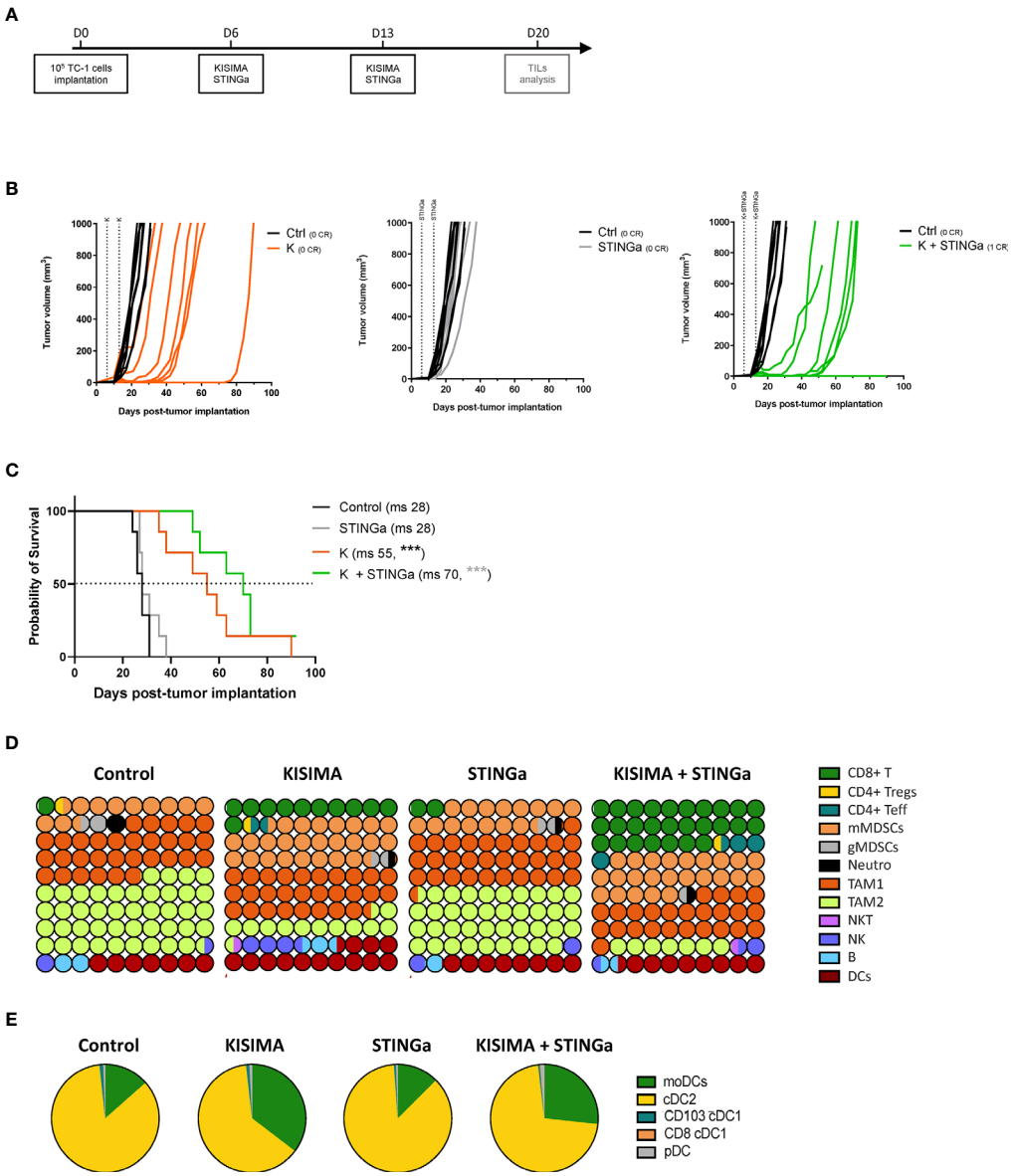

FIGURE 3 | Combining protein vaccine with STING agonist delays TC-1 tumor growth and profoundly impacts tumor microenvironment. 10^5 TC-1 cells were implanted subcutaneously on the back of C57BL/6 mice. When tumors were visible, mice were treated with two administrations of KISIMA vaccine, STING agonist or a combination of the two at one-week interval and tumor growth was monitored. **(A)** Vaccination schedule. Tumor growth **(B)** and median survival **(C)** were followed. CR, complete regression; ms, median survival. **(D)** 10 × 10 dot plot chart showing 100 circles, corresponding to 100%, and representing the proportion of different cell populations among CD45+ tumor-infiltrating cells; every circle represents 1% of the CD45+ population (see **Figure S11** for gating strategy). **(B)** Pie chart representing different tumor infiltrating dendritic cell populations, moDCs ($CD11b^+MHCII^{hi}CD11c^{hi}Ly6C^+$), cDC2 ($CD11b^+MHCII^{hi}CD11c^{hi}Ly6C^+CD103^-$), cDC1 ($CD11b\text{-}MHCII^{hi}CD11c^{hi}CD24^+$ and $CD103^+$ or $CD8^+$), pDC ($CD11b^-Ly6C^+CD11c^{int}B220^+PDCA1^+$). One representative of three experiments (n = 7/group/replicate) **(B, C)** or a pool of two experiments (n = 7/group) **(D, E)** are shown. *Log-rank Mantel–Cox test*, ***$p < 0.001$.

expanded both CD8 and non-Treg CD4 T cell infiltration by 2.5-fold, while decreasing TAM2 frequency.

In addition to TME cellular composition, the intra-tumoral expression of MHC-I and MHC-II was monitored. Both H2-Kb and H2-Db MHC-I allele expression was up-regulated by tumor cells in Z13Mad25Anaxa vaccinated or combination treated mice, compared to both vehicle and STINGa treatment (**Figure S7A**), suggesting that therapeutic protein vaccine treatment could even promote tumor cell recognition by CD8 T cells. At the same time, Z13Mad25Anaxa vaccination also increased MHC-II expression on CD11b+ cells (**Figure S7B**, right), thus promoting the presentation of epitopes to CD4 T cells.

Altogether, these results highlight the profound modulation of TME induced by therapeutic protein vaccine treatment, which is

able to turn a cold tumor into hot tumor favoring the effect of STINGa treatment which further increases anti-tumoral immunity.

Therapeutic STINGa–Protein Vaccine Combination Treatment Improves Antigen-Specific CD8 T Cell Response in TC-1 Tumor Bearing Mice

The effect of Z13Mad25Anaxa–STINGa combination on CD8 T cell response in TC-1 tumor-bearing mice was then analyzed. Protein vaccine treatment significantly increased peripheral HPV-specific response, and as expected, combination with STINGa further enhanced antigen-specific CD8 T cell number (**Figure S8A**). Very low levels of total or HPV-specific CD8 T cells were found in control mice, either considering proportion—they represented less than 1% of tumor infiltrating leukocytes—or total number (**Figure 4A**), a typical trait of cold tumors. Z13Mad25Anaxa vaccination induced a significant increase of CD8 T cell tumor infiltration, of which over 60% was HPV-specific. Notably, HPV-specific CD8 T cells were massively present within the tumor in contrast to the level observed in the blood, suggesting that measurement of peripheral responses can only partially predict the intra-tumoral outcome. While STINGa monotherapy did not modulate CD8 T cell tumor infiltration nor the proportion of HPV-specific, Z13Mad25Anaxa–STINGa combination significantly increased both CD8 T cell infiltration and HPV-specific proportion. In addition, the functionality of tumor-infiltrating HPV-specific CD8 T cells was monitored by measuring IFNγ, TNFα, and degranulating marker CD107α expression after HPV-specific *ex vivo* stimulation of TILs; a significant increase of HPV-specific cytokine-producing and degranulating CD8 T cells was found in Z13Mad25Anaxa-vaccinated mice compared to that in control or STINGa monotherapy group (**Figure 4B**). Combination with STINGa significantly further increased not only CD8 T cell functionality but also the frequency of multifunctional cells. Higher frequency and

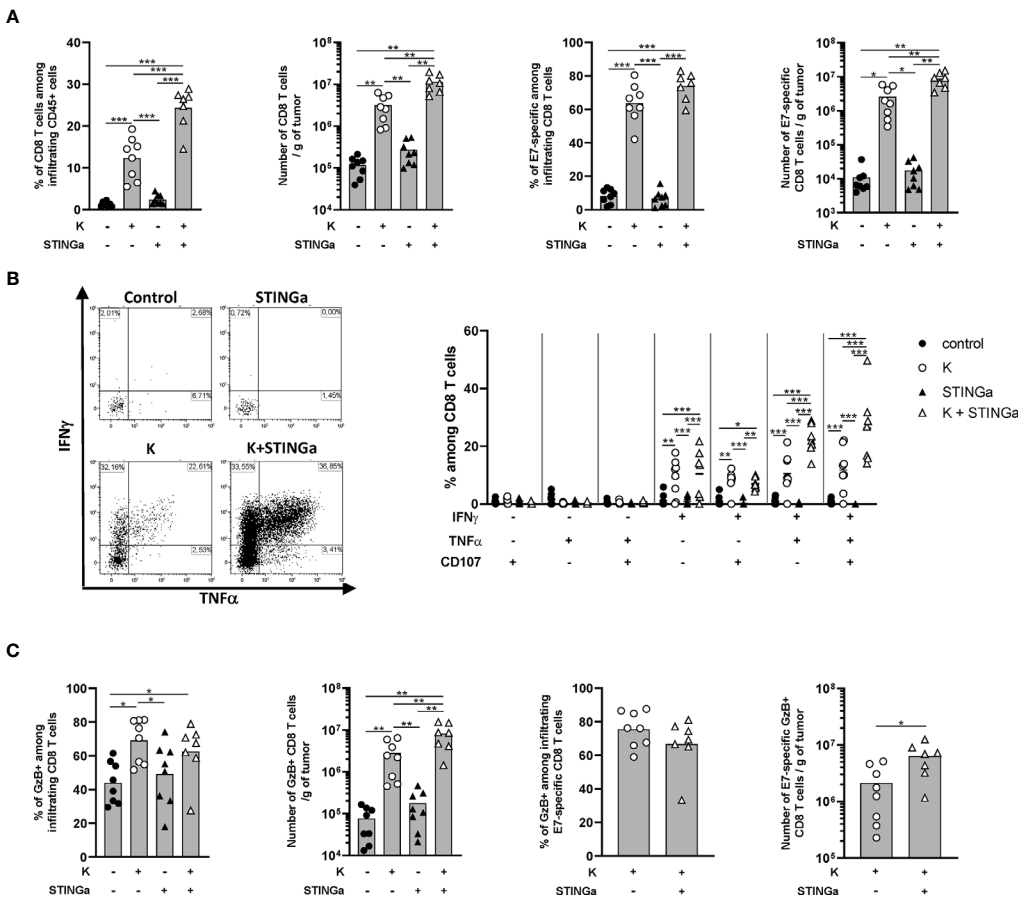

FIGURE 4 | Combining protein vaccine treatment with STING agonist enhances functionality of intra-tumoral CD8 T cells in TC-1 model. 10^5 TC-1 cells were implanted subcutaneously on the back of C57BL/6 mice. When tumors were visible, mice were treated with two administrations of KISIMA vaccine, STING agonist or a combination of the two at one-week interval. One week after the last treatment, mice were sacrificed, tumor harvested, and CD8 T cells' presence and phenotype were analyzed by flow cytometry. **(A)** Frequency and number of total and RAHYNIVTF (E7)-specific CD8 T cells among tumor infiltrating leukocytes. **(B)** Tumor infiltrating CD45+ cells were stimulated *ex vivo* with RAHYNIVTF peptide in the presence of Golgi inhibitor. Antigen-specific cytokine production was measured by intracellular staining; representative FACS plots and frequency of cytokine-producing among CD8 T cells are shown. **(C)** CD45+ tumor infiltrating cells were cultured *ex vivo* with Golgi inhibitor and granzyme B production was monitored by intracellular staining. Frequency and total number of granzyme B-producing total and RAHYNIVTF-specific CD8 T cells are shown. **(A–C)** A pool of two experiments is shown (n ≥7/group), *Mann–Whitney test*, *p < 0.05, **p < 0.01, ***p < 0.001.

number of GzB-producing CD8 T cells in Z13Mad25Anaxa vaccinated mice were observed compared to vehicle or STINGa monotherapy (**Figure 4C**). Combination with STINGa did not impact the frequency of GzB-positive among HPV-specific CD8 T cells but further increased their total number (**Figure 4C**). In contrast to the intra-tumoral compartment, very low frequency of cytokine- or GzB-producing splenic HPV-specific CD8 T cells was observed in all the different treatments (**Figure S8B**).

Despite high activation, the majority of tumor infiltrating CD8 T cells in protein vaccine treated mice expressed PD-1, Tim-3, CD38, and NKG2a markers associated with T cell exhaustion (22, 23) (**Figures S9A–C**). Interestingly, in the combination group, a lower proportion of CD8 T cells co-expressed PD-1 and Tim-3, suggesting a less exhausted phenotype, which correlated with the higher proportion of cytokine-secreting cells. Similar to functionality analysis, peripheral CD8 T cells showed a less-exhausted phenotype (**Figure S8A** right), suggesting that exhaustion is acquired within the TME.

Taken together these results show that therapeutic protein vaccine treatment highly increases HPV-specific CD8 T cells tumor infiltration and functionality and while STINGa monotherapy has no effect, the combination further enhances vaccination efficacy.

Therapeutic STINGa–Protein Vaccine Combination Treatment Modulates Intra-Tumoral CD4 T Cell Responses

The importance of CD4 T cells, in particular the Th1 subset, for the development of a proper anti-tumoral CD8 T cell response is now established (24, 25). Thus, intra-tumoral CD4 T cells were monitored and a significantly increased infiltration was observed in Z13Mad25Anaxa–STINGa combination treated mice compared to the other groups (**Figure 5A**). The ratio between intra-tumoral CD8 and CD4 T cells is often used as a predictive value for the immunological state of TME (26) and was found to be increased in protein vaccine or combination treated mice (**Figure 5A**). Interestingly, the increased CD4 T cell infiltration was led by effector rather than regulatory CD4 T cells (**Figure 5A**). Further analysis revealed that in combination treated mice, most of intra-tumoral CD4 T cells were Th1 (T-bet^{+}), whose number significantly increased over 50-fold compared to that of the control group, while CD4 Tregs only slightly increased and just a minimal part was Th2 (GATA-3^{+}) cells (**Figure 5B**). This modulation of bystander CD4 T cell polarization resulted in increased CD8/Treg and Th1/Th2 ratio, highlighting a less immunosuppressive TME (**Figure 5C**).

TME Modulation and Epitope Mutation in Relapsing Tumors

Although STINGa–protein vaccine combination treatment was able to induce tumor regression in over 80% of mice and prolonged disease control, the majority (over 95%) of animals developed tumor relapses between two and four weeks after the last vaccination (**Figure 6A**). In order to understand the mechanism of tumor relapse, the expression of intra-tumoral MHC-I was measured, as its down-regulation by tumor cells is one of the tumor escape mechanisms (27). Indeed, MHC-I expression was down-regulated on relapsing tumor cells compared to that of regressing tumors (**Figure 6B**). In addition, the expression of MHC-II on CD11b+ cells was also down-regulated, suggesting that antigen-presentation to CD4 T cells was reduced (**Figure 6B**). To address the impact of decreased intra-tumoral antigen-presentation, the TME composition of escaping tumors was monitored. In contrast to regressing tumors, the TME was largely dominated by TAM-2, which represented over 45% of the total CD45+ infiltrates, followed by TAM-1 and mMDSC (**Figure 6C**), and resembled very closely to mock treated tumor (**Figure 3C**). CD8 T cells represented only the 5% of the immune infiltrate, a drastic reduction compared to the over 25% of regressing tumors. While the total number of antigen-specific CD8 T cells decreased by 10-fold in relapsing tumors (**Figure S10A**), their functionality was not impacted, with most of the cells still able to produce IFNγ, TNFα, and granzyme B following brief *ex vivo* peptide-specific stimulation (**Figure S10B**). The polarization of intra-tumoral CD4 T cells was impacted as well; the proportion of t-bet+ Th1 CD4 T cells remained unchanged; however, the frequency of anti-inflammatory Tregs and Th2 cells significantly increased, resulting in a less favorable Th1/Th2 ratio (**Figure S10C**).

Finally, as a prerogative of cancer cell is to be inclined to acquire new mutations, the HPV-16 E7 mRNA expressed by tumor cells, which contains the epitope encoded by Z13Mad25Anaxa vaccine, was sequenced. Surprisingly, in 80% of the mice the HPV-16 E7 transcript contained a single amino-acid mutation in the CD8 epitope region (RAHYNIVTF) (**Figure 6D**), which allowing tumor to escape recognition by Z13Mad25Anaxa elicited HPV-E7 specific CD8 T cells, and proliferate despite the presence of functional CD8 T cells. Taken together, these results highlight different tumor cell intrinsic and extrinsic immune evasion mechanisms which allow TC-1 tumor to finally escape from the protective tumor-specific response elicited by therapeutic STINGa–protein vaccine combination treatment.

DISCUSSION

The efficacy of KISIMA platform for development of protein based cancer vaccines which showed high immunogenicity and anti-tumoral efficacy in different preclinical tumor models was previously reported (19, 20). In preclinical studies, STING agonists have been mainly assessed using intra-tumoral injection, with the goal of directly inflame the tumor, which showed a potent anti-tumoral activity (13). The promising preclinical studies have been recently translated into the initiation of several clinical studies focusing on different tumor types, aiming to use STINGa as a universal cancer treatment. However, current reported clinical data do not corroborate the pre-clinical results (28).

In preclinical studies, STINGa anti-tumoral activity was shown to require intra-tumoral administration (29). Nevertheless, STINGa i.t. treatment induces also a systemic interferon response, which can result in abscopal efficacy on untreated tumors (29). This highlights

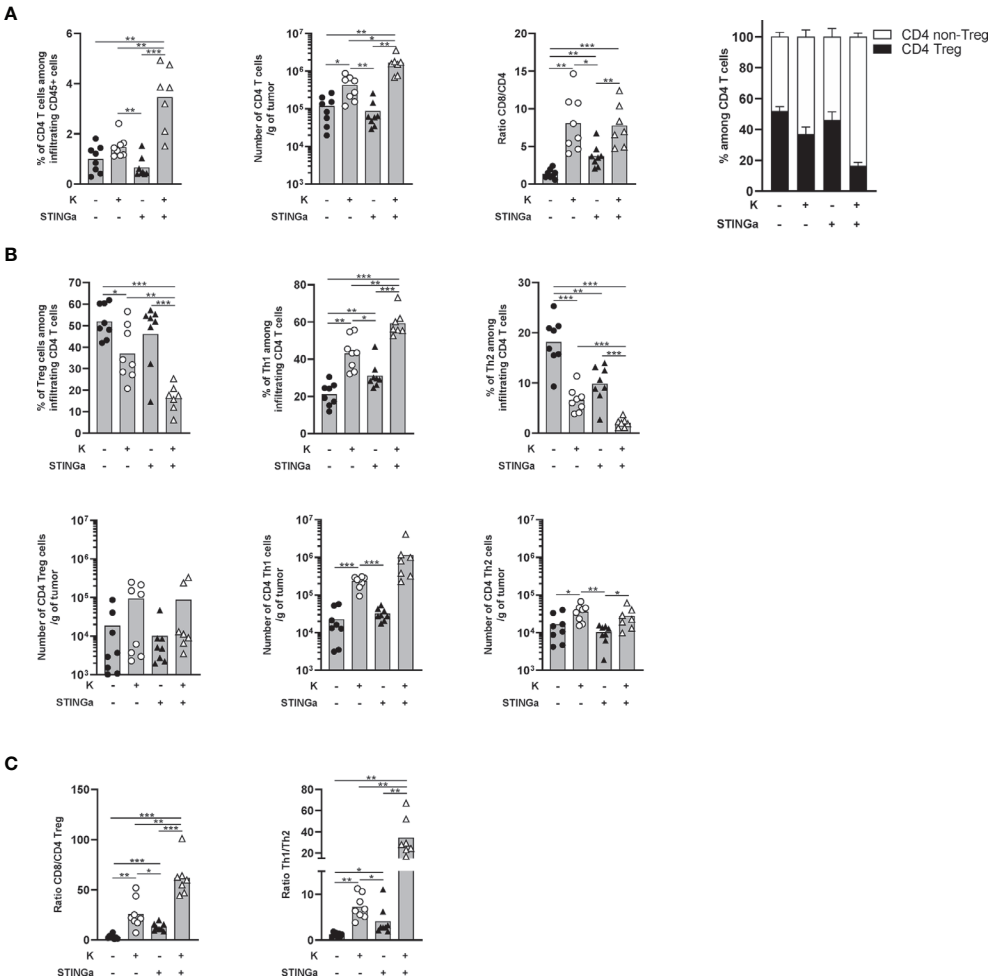

FIGURE 5 | Combination of protein vaccine with STING agonist positively modulates the polarization of intra-tumoral CD4 T cells in TC-1 model. 10^5 TC-1 cells were implanted on the back of C57BL/6 mice. When tumors were visible, mice were treated with two administrations of KISIMA vaccine, STING agonist, or a combination of the two at one-week interval. One week post the last treatment, mice were sacrificed, tumor harvested, and CD4 T cells' presence and phenotype were analyzed by FACS staining. **(A)** Frequency and number of total CD4 T cells among tumor infiltrating leukocytes, ratio between tumor infiltrating CD8 T cells and CD4 T cells, frequency of Treg and non-Treg among tumor infiltrating CD4 T cells. **(B)** Frequency (top) and total number normalized to tumor weight (bottom) of Treg, Th1, and Th2 among tumor infiltrating CD4 T cells. **(C)** Ratio between tumor infiltrating CD8 T cells and CD4 Treg cells, and between Th1 and Th2 tumor infiltrating CD4 T cells. **(A–C)** A pool of two experiment is shown (n ≥7/group), *Mann–Whitney test*, *p < 0.05, **p < 0.01, ***p < 0.001.

the possibility of using STINGa in combination with a cancer vaccine, exploiting its potent immune-modulator properties in addition to the vaccine induced antigen-specific T cell response. In this combination setting, STINGa would not necessarily require i.t. administration, thus expanding its possible human indication to non-accessible tumors. We showed here that combination of KISIMA vaccination therapeutic protein vaccine with subcutaneous STINGa treatment profoundly impacts both quantity and quality of CD8 and CD4 T cells, which resulted in a prolonged control of tumor growth in both B16-OVA and TC-1 tumor models.

While treatment with a protein vaccine induced only a local inflammatory response, STINGa s.c. administration caused high level of systemic IFN-α, which impacted both CD8 and CD4 T cell responses. Combination with STINGa not only increased the frequency of splenic CD4 T cells, but also drove their polarization toward the inflammatory Th1 type and at the same time decreased Treg and Th2 frequency. Importantly, while the increase of total CD4 T cell frequency was strictly STINGa dependent, the different polarization required combination with protein-based vaccination, highlighting a combinatory effect on this cell type. CD4 T cell response has been widely overlooked in cancer immunotherapy, but recently gained more attention as Th1 and Th17 CD4 T cells have been shown to contribute to anti-tumoral immune responses by promoting CD8 T cell recruitment and activation or by secreting inflammatory cytokines (24, 25). It was recently reported that utilization of STINGa as adjuvant formulated

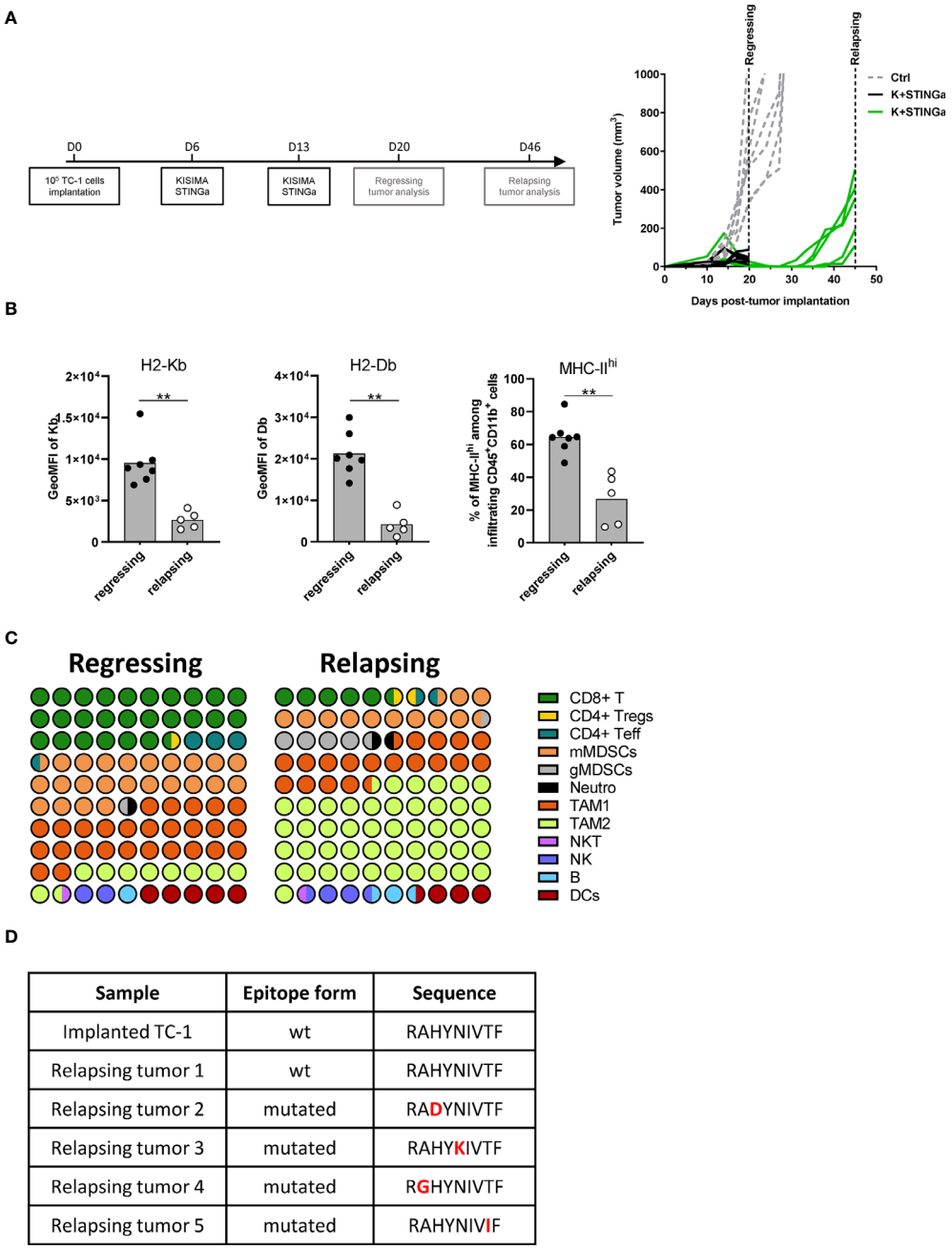

D

Sample	Epitope form	Sequence
Implanted TC-1	wt	RAHYNIVTF
Relapsing tumor 1	wt	RAHYNIVTF
Relapsing tumor 2	mutated	RADYNIVTF
Relapsing tumor 3	mutated	RAHYKIVTF
Relapsing tumor 4	mutated	RGHYNIVTF
Relapsing tumor 5	mutated	RAHYNIVIF

FIGURE 6 | Comparison of regressing and relapsing tumor microenvironment. 10^5 TC-1 cells were implanted on the back of C57BL/6 mice. When tumors were visible, mice were treated with two administrations of a combination of KISIMA vaccine and STING agonist at one-week interval. **(A)** Vaccination schedule and tumor growth. **(B)** Expression level of H2-Kb, H2-Db on CD45-tumor infiltrating cells and frequency of MHC-II^{hi} among CD11b+ cells. **(C)** One (regressing) or four (relapsing) tumors. One (regressing) or four (relapsing) weeks post the last treatment, mice were sacrificed, tumor harvested, and tumor microenvironment was analyzed by FACS staining. Proportion of different cell populations among CD45+ tumor-infiltrating cells is shown; every circle represents 1% of the CD45+ population (see **Figure S11** for gating strategy). **(D)** Sequence of HPV-E7 CD8 epitope expressed by implanted and relapsing tumors. **(B–D)** One representative of two experiments is shown (n ≥5/group/replicate), *Mann–Whitney test*, **p < 0.01.

within a *M. tuberculosis* protein subunit vaccine results in increased Th1 and Th17 *M. tuberculosis*-specific response (30); however to our knowledge this is the first report of a STINGa-dependent modulation of CD4 T cell polarization in a cancer immunotherapy context. In addition to the peripheral effects, the intra-tumoral T cell response was particularly increased after protein vaccine–STINGa treatment, highlighting the ability of the combination to promote tumor infiltration overcoming

immune evasion and/or exclusion typical of TC-1 tumors. CD4 T cell frequency was highly increased upon combination treatment in TC-1 tumors, while it remained unchanged in STINGa monotherapy, highlighting again that vaccination is required for tumor infiltration in this tumor model. Intra-tumoral CD4 T cells have often been linked to immune-suppression due to their regulatory phenotype; however this was not the case in this combination, as Tregs represent only a minority of the infiltrating CD4 T cells, while the majority show a Th1 phenotype in both B16-OVA and TC-1 tumor models. However, following *ex vivo* stimulation with SIINFEKL peptide IFN-γ, TNF-α nor IL-2 production was increased in combination treated mice spleen but not tumor compartment, suggesting that antigen-specific CD4 T cells reside prevalently in secondary lymphoid organ. Nevertheless, the peripheral activity of antigen-specific CD4 T cells may be sufficient to help establish a more powerful CD8 T cell response.

In addition to CD4 T cells, therapeutic protein vaccine treatment highly enhanced CD8 T cell tumor infiltration and improved their TCR avidity and functionality—an effect further enhanced by combination with STINGa—while simultaneously increasing the expression of exhaustion markers PD-1 and Tim-3. Exhaustion being a multi-phased progressive process, intra-tumoral CD8 T cells could be in an early exhaustion phase and still maintain functionality, in particular as TILs were analyzed while tumor growth was controlled in vaccinated mice. Concordantly, antigen-specific CD8 T cells maintained their functionality weeks later in relapsing TC-1 tumors. An important difference was observed between the modest response induced by Z13Mad25Anaxa vaccination in peripheral blood and the magnitude of HPV-specific CD8 T cells observed within the tumor. This indicate that blood analysis is only partially representative of the anti-tumoral response induced by cancer vaccines, and its relevance in the prediction of vaccine immunogenicity in human patient should be carefully evaluated.

In addition to T lymphocytes, combination with STINGa induced profound changes of the TME, promoting the development of an inflammatory environment. The most evident modulation was the decrease of TAM2 frequency, which could be related to a lower tumor infiltration and/or to a different polarization of monocytes into mMDSCs, as their presence is increased by protein vaccine treatment. TAMs, in particular TAM2, have been associated with poor prognosis in several cancer types, promoting immune suppression, tumor growth and metastasis development (31). In preclinical models, TAM depletion or re-polarization towards the more inflammatory TAM1 type, was shown to favor tumor control and response to immunotherapy in different tumor models (32, 33). In addition to TAMs, Z13Mad25Anaxa vaccination also increased DC infiltration and their differentiation. The presence of intra-tumoral DCs is fundamental to maintain an active immune response, as they are able to pick up tumor antigens, migrate to the draining lymph node, and present them to T cells. Particularly important in cancer immune response are monocyte-derived (moDCs) cross-presenting DCs, which are able to activate tumor specific CD8 T cells and have been shown to play a primary role in the initiation of anti-tumoral immune responses (21). Protein vaccine treatment with or without STINGa combination increased the frequency of moDCs, suggesting that it can prolong the extent of the induction of immune response well past vaccination. Thus, therapeutic protein vaccine treatment in combination with STINGa bears additional beneficial effects to the induction of a potent antigen-specific CD8 T cells response.

Mechanistically, the impact of STINGa treatment in combination with a protein vaccine on T cell response is probably mediated by innate immune sensing, as direct STING activation in T cells was shown to induce cell death (34). In preclinical mouse studies, the anti-tumoral effect of STING signaling was closely associated with the potent induction of type I IFNs, which promoted the activation of cross-presenting Batf3-DCs resulting in increased CD8 T cells activation (35). In addition, activation of intra-tumoral Batf3-DCs was required for optimal trafficking of CD8 T cells into the core of the tumor, a process mediated by CXCL9 secretion (36). In the present study, STINGa monotherapy did not expand intra-tumoral DCs nor improved CD8 T cell infiltration, likely due to the distal administration route. Nevertheless, in combination with KISIMA vaccination, STINGa strongly enhanced CD8 T cell response, suggesting that a similar improvement of cross-presentation could take place at the vaccine draining lymph node. In addition, the STINGa-dependent polarization of CD4 T cells into Th1 is likely driven by the strong type I IFN response, which was also shown to impact CD4 T cell polarization (37).

While protein vaccine–STINGa combination treatment was able to control TC-1 tumor early growth and induce tumor regression, in the majority of the case, tumors were finally able to escape immune surveillance. TC-1 tumor escape following therapeutic vaccination was previously observed and was associated with a decreased tumor infiltration by inflammatory myeloid cells (38). Moreover, tumor regrowth was observed despite the presence of functional antigen-specific CD8 T cells. Similarly, in this study tumor relapses were associated with increased infiltration of immunosuppressive TAM-2 and MDSCs and a decrease of TAM-1, while CD8 T cells maintained their functionality despite the reduction in number. However, in addition, tumor relapse was associated with single amino-acid mutations in the HPV-16 E7 CD8 epitope contained in Z13Mad25Anaxa vaccine, highlighting the importance of including different antigen targets in human vaccine candidates. In this study, protein vaccine–STINGa combinatory treatment was administered only twice; however, the observation of mutations in the targeted epitope suggests that additional vaccinations using the same vaccine construction would not prevent tumor escape. Importantly, tumor escape associated with a single epitope mutation suggests that, despite the profound modulation of the tumor microenvironment induced by protein vaccine–STINGa combinatorial treatment, epitope spreading might be limited. The mutation within the epitope region differed from tumor to tumor, suggesting that it is the result of a random mutation rather than a driver mutation.

Further studies are required to expand the sequencing of E7 antigen in relapsing tumor to a larger sample size allowing identification of the most recurrent mutations to be included in a new vaccine strategy which could potentially prevent tumor escape. In addition, in relapsing tumors, the expression of both MHC-I on tumor cells and MHC-II on CD11b+ cells were reduced, highlighting a decreased antigen presentation.

In conclusion, it is nowadays clear that an effective cancer immunotherapy cannot focus on a single treatment but must combine different approaches to target different aspects of tumor biology (39). Our findings highlight the promising combination of protein-based cancer vaccine with STING agonists and could offer opportunity for bimodal treatment of patients with innate resistance to immune check point blockade.

DATA AVAILABILITY STATEMENT

The raw data supporting the conclusions of this article will be made available by the authors, without undue reservation.

ETHICS STATEMENT

The animal study was reviewed and approved by the institutional and cantonal veterinary authorities in accordance with Swiss Federal law on animal protection.

AUTHOR CONTRIBUTIONS

MD and EB conceived and designed the study. MR, SC, WB-B, and ER performed, processed, and analyzed *in vivo* mouse tumor studies and data. MD, EB, MR, and M-LS-R contributed to discussions and writing of the manuscript. All authors contributed to the article and approved the submitted version.

SUPPLEMENTARY MATERIAL

The Supplementary Material for this article can be found online at: https://www.frontiersin.org/articles/10.3389/fimmu.2021.695056/full#supplementary-material

REFERENCES

1. Upadhaya S, Neftelino ST, Hodge JP, Oliva C, Campbell JR, Yu JX. Combinations Take Centre Stage in PD1/PDL1 Inhibitor Clinical Trials. *Nat Rev Drug Discov* (2021) 20(3):168–9. doi: 10.1038/d41573-020-00204-y
2. Sharma P, Hu-Lieskovan S, Wargo JA, Ribas A. Primary, Adaptive, and Acquired Resistance to Cancer Immunotherapy. *Cell* (2017) 168(4):707–23. doi: 10.1016/j.cell.2017.01.017
3. Linch SN, McNamara MJ, Redmond WL. Ox40 Agonists and Combination Immunotherapy: Putting the Pedal to the Metal. *Front Oncol* (2015) 5:34. doi: 10.3389/fonc.2015.00034
4. Mahne AE, Mauze S, Joyce-Shaikh B, Xia J, Bowman EP, Beebe AM, et al. Dual Roles for Regulatory T-Cell Depletion and Costimulatory Signaling in Agonistic Gitr Targeting for Tumor Immunotherapy. *Cancer Res* (2017) 77 (5):1108–18. doi: 10.1158/0008-5472.CAN-16-0797
5. Ablasser A, Goldeck M, Cavlar T, Deimling T, Witte G, Rohl I, et al. cGAS Produces a 2'-5'-Linked Cyclic Dinucleotide Second Messenger That Activates STING. *Nature* (2013) 498(7454):380–4. doi: 10.1038/nature12306
6. Ishikawa H, Barber GN. STING Is an Endoplasmic Reticulum Adaptor That Facilitates Innate Immune Signalling. *Nature* (2008) 455(7213):674–8. doi: 10.1038/nature07317
7. Ishikawa H, Ma Z, Barber GN. STING Regulates Intracellular DNA-Mediated, Type I Interferon-Dependent Innate Immunity. *Nature* (2009) 461(7265):788–92. doi: 10.1038/nature08476
8. Saitoh T, Fujita N, Hayashi T, Takahara K, Satoh T, Lee H, et al. Atg9a Controls dsDNA-Driven Dynamic Translocation of STING and the Innate Immune Response. *Proc Natl Acad Sci USA* (2009) 106(49):20842–6. doi: 10.1073/pnas.0911267106
9. Sokolowska O, Nowis D. Sting Signaling in Cancer Cells: Important or Not? *Arch Immunol Ther Exp (Warsz)* (2018) 66(2):125–32. doi: 10.1007/s00005-017-0481-7
10. Takashima K, Takeda Y, Oshiumi H, Shime H, Okabe M, Ikawa M, et al. STING in Tumor and Host Cells Cooperatively Work for NK Cell-Mediated Tumor Growth Retardation. *Biochem Biophys Res Commun* (2016) 478 (4):1764–71. doi: 10.1016/j.bbrc.2016.09.021
11. Parkes EE, Walker SM, Taggart LE, McCabe N, Knight LA, Wilkinson R, et al. Activation of STING-Dependent Innate Immune Signaling By s-Phase-Specific DNA Damage in Breast Cancer. *J Natl Cancer Inst* (2017) 109(1): djw199. doi: 10.1093/jnci/djw199
12. Xia X, Mai J, Xu R, Perez JET, Guevara ML, Shen Q, et al. Porous Silicon Microparticle Potentiates Anti-Tumor Immunity by Enhancing Cross-Presentation and Inducing Type I Interferon Response. *Cell Rep* (2015) 11 (6):957–66. doi: 10.1016/j.celrep.2015.04.009
13. Corrales L, Glickman LH, McWhirter SM, Kanne DB, Sivick KE, Katibah GE, et al. Direct Activation of STING in the Tumor Microenvironment Leads to Potent and Systemic Tumor Regression and Immunity. *Cell Rep* (2015) 11 (7):1018–30. doi: 10.1016/j.celrep.2015.04.031
14. Fu J, Kanne DB, Leong M, Glickman LH, McWhirter SM, Lemmens E, et al. STING Agonist Formulated Cancer Vaccines Can Cure Established Tumors Resistant to PD-1 Blockade. *Sci Transl Med* (2015) 7(283):283ra52. doi: 10.1126/scitranslmed.aaa4306
15. Le Naour J, Zitvogel L, Galluzzi L, Vacchelli E, Kroemer G. Trial Watch: STING Agonists in Cancer Therapy. *Oncoimmunology* (2020) 9(1):1777624. doi: 10.1080/2162402X.2020.1777624
16. Melief CJ, van Hall T, Arens R, Ossendorp F, van der Burg SH. Therapeutic Cancer Vaccines. *J Clin Invest* (2015) 125(9):3401–12. doi: 10.1172/JCI80009
17. Song Q, Zhang CD, Wu XH. Therapeutic Cancer Vaccines: From Initial Findings to Prospects. *Immunol Lett* (2018) 196:11–21. doi: 10.1016/j.imlet.2018.01.011
18. Belnoue E, Di Berardino-Besson W, Gaertner H, Carboni S, Dunand-Sauthier I, Cerini F, et al. Enhancing Antitumor Immune Responses by Optimized Combinations of Cell-Penetrating Peptide-Based Vaccines and Adjuvants. *Mol Ther* (2016) 24(9):1675–85. doi: 10.1038/mt.2016.134
19. Belnoue E, Mayol JF, Carboni S, Di Berardino Besson W, Dupuychaffray E, Nelde A, et al. Targeting Self and Neo-Epitopes With a Modular Self-Adjuvanting Cancer Vaccine. *JCI Insight* (2019) 4(11):e127305. doi: 10.1172/jci.insight.127305
20. Derouazi M, Di Berardino-Besson W, Belnoue E, Hoepner S, Walther R, Benkhoucha M, et al. Novel Cell-Penetrating Peptide-Based Vaccine Induces Robust CD4+ and CD8+ T Cell-Mediated Antitumor Immunity. *Cancer Res* (2015) 75(15):3020–31. doi: 10.1158/0008-5472.CAN-14-3017
21. Kuhn S, Yang J, Ronchese F. Monocyte-Derived Dendritic Cells Are Essential for CD8(+) T Cell Activation and Antitumor Responses After Local Immunotherapy. *Front Immunol* (2015) 6:584. doi: 10.3389/fimmu.2015.00584
22. van Montfoort N, Borst L, Korrer MJ, Sluijter M, Marijt KA, Santegoets SJ, et al. Nkg2a Blockade Potentiates Cd8 T Cell Immunity Induced by Cancer Vaccines. *Cell* (2018) 175(7):1744–55.e15. doi: 10.1016/j.cell.2018.10.028
23. Zhou J, Wang W, Liang Z, Ni B, He W, Wang D. Clinical Significance of CD38 and CD101 Expression in PD-1(+)CD8(+) T Cells in Patients With Epithelial Ovarian Cancer. *Oncol Lett* (2020) 20(1):724–32. doi: 10.3892/ol.2020.11580

24. Melssen M, Slingluff CL Jr. Vaccines Targeting Helper T Cells for Cancer Immunotherapy. *Curr Opin Immunol* (2017) 47:85–92. doi: 10.1016/j.coi.2017.07.004
25. Muranski P, Boni A, Antony PA, Cassard L, Irvine KR, Kaiser A, et al. Tumor-Specific Th17-Polarized Cells Eradicate Large Established Melanoma. *Blood* (2008) 112(2):362–73. doi: 10.1182/blood-2007-11-120998
26. Diederichsen AC, Hjelmborg J, Christensen PB, Zeuthen J, Fenger C. Prognostic Value of the CD4+/CD8+ Ratio of Tumour Infiltrating Lymphocytes in Colorectal Cancer and HLA-DR Expression on Tumour Cells. *Cancer Immunol Immunother* (2003) 52(7):423–8. doi: 10.1007/s00262-003-0388-5
27. Bubenik J. Tumour MHC Class I Downregulation and Immunotherapy (Review). *Oncol Rep* (2003) 10(6):2005–8. doi: 10.3892/or.10.6.2005
28. Gauthier K, Desbien A, Reiner G, Corrales L, Deng W, Glickman L, et al. 33rd Annual Meeting & Pre-Conference Programs of the Society for Immunotherapy of Cancer (Sitc 2018): Washington, D.C., USA. 7-11 November 2018. *J Immunother Cancer* (2018) 6(Suppl 1):114. doi: 10.1186/s40425-018-0422-y
29. Sallets A, Robinson S, Kardosh A, Levy R. Enhancing Immunotherapy of STING Agonist for Lymphoma in Preclinical Models. *Blood Adv* (2018) 2 (17):2230–41. doi: 10.1182/bloodadvances.2018020040
30. Van Dis E, Sogi KM, Rae CS, Sivick KE, Surh NH, Leong ML, et al. Sting-Activating Adjuvants Elicit a Th17 Immune Response and Protect Against Mycobacterium Tuberculosis Infection. *Cell Rep* (2018) 23(5):1435–47. doi: 10.1016/j.celrep.2018.04.003
31. Lin Y, Xu J, Lan H. Tumor-Associated Macrophages in Tumor Metastasis: Biological Roles and Clinical Therapeutic Applications. *J Hematol Oncol* (2019) 12(1):76. doi: 10.1186/s13045-019-0760-3
32. Pyonteck SM, Akkari L, Schuhmacher AJ, Bowman RL, Sevenich L, Quail DF, et al. Csf-1R Inhibition Alters Macrophage Polarization and Blocks Glioma Progression. *Nat Med* (2013) 19(10):1264–72. doi: 10.1038/nm.3337
33. Zhu Y, Knolhoff BL, Meyer MA, Nywening TM, West BL, Luo J, et al. CSF1/CSF1R Blockade Reprograms Tumor-Infiltrating Macrophages and Improves Response to T-Cell Checkpoint Immunotherapy in Pancreatic Cancer Models. *Cancer Res* (2014) 74(18):5057–69. doi: 10.1158/0008-5472.CAN-13-3723
34. Larkin B, Ilyhukha V, Sorokin M, Buzdin A, Vannier E, Poltorak A. Activation of STING in T Cells Induces Type-I IFN Responses and Cell Death. *J Immunol* (2017) 199:397–402. doi: 10.4049/jimmunol.1601999
35. Woo SR, Fuertes MB, Corrales L, Spranger S, Furdyna MJ, Leung MYK, et al. Gajewski: STING-Dependent Cytosolic DNA Sensing Mediates Innate Immunity Recognition of Immunogenic Tumors. *Immunity* (2014) 41 (5):830–42. doi: 10.1016/j.immuni.2014.10.017
36. Spranger S, Dai D, Horton B, Gajewski TF. Tumor-Residing Batf3 Dendritic Cells Are Required for Effector T Cell Trafficking and Adoptive T Cell Therapy. *Cancer Cell* (2017) 31(5):711–23. doi: 10.1016/j.ccell.2017.04.003
37. Way SS, Havenar-Daughton C, Koluman GA, Orgun NN, Murali-Krishna K. IL-12 and Type-I IFN Synergize for IFN-g Production by CD4 T Cells, Whereas Neither Are Required for IFN-g Production by CD8 T Cells After Listeria Monocytogenes Infection. *J Immunol* (2007) 178:4498–505. doi: 10.4049/jimmunol.178.7.4498
38. Beyranvand Nejad E, Labrie C, Abdulrahman Z, van Elsas MJ, Rademaker E, Kleinovink JW, et al. Lack of Myeloid Cell Infiltration as an Acquired Resistance Strategy to Immunotherapy. *J Immunother Cancer* (2020) 8(2): e001326. doi: 10.1136/jitc-2020-001326
39. Ott PA, Hodi FS, Kaufman HL, Wigginton JM, Wolchok JD. Combination Immunotherapy: A Road Map. *J Immunother Cancer* (2017) 5:16. doi: 10.1186/s40425-017-0218-5

Conflict of Interest: All authors were employed by company Boehringer Ingelheim International GmbH and AMAL Therapeutics.

frontiers in Immunology

CLINICAL TRIAL
published: 13 August 2021
doi: 10.3389/fimmu.2021.691605

A Neoantigen-Based Peptide Vaccine for Patients With Advanced Pancreatic Cancer Refractory to Standard Treatment

Zheling Chen[1†], Shanshan Zhang[2,3†], Ning Han[2†], Jiahong Jiang[1†], Yunyun Xu[4], Dongying Ma[2], Lantian Lu[2], Xiaojie Guo[2], Min Qiu[2], Qinxue Huang[2], Huimin Wang[2], Fan Mo[2,5,6,7], Shuqing Chen[2,3,5*] and Liu Yang[1*]*

[1] Cancer Center, Department of Medical Oncology, Zhejiang Provincial People's Hospital, People's Hospital of Hangzhou Medical College, Hangzhou, China, [2] Hangzhou Neoantigen Therapeutics Co., Ltd., Hangzhou, China, [3] Zhejiang California International Nanosystems Institute, Zhejiang University, Hangzhou, China, [4] Department of Gastrointestinal and Pancreatic Surgery, Zhejiang Provincial People's Hospital, People's Hospital of Hangzhou Medical College, Hangzhou, China, [5] College of Pharmaceutical Sciences, Zhejiang University, Hangzhou, China, [6] Vancouver Prostate Centre, University of British Columbia, Vancouver, BC, Canada, [7] Hangzhou AI-Force Therapeutics Co., Ltd., Hangzhou, China

OPEN ACCESS

Edited by:
Shisong Jiang,
University of Oxford, United Kingdom

Reviewed by:
Wayne Robert Thomas,
University of Western Australia, Australia
Cristina Maccalli,
Sidra Medicine, Qatar

***Correspondence:**
Liu Yang
yangliu@hmc.edu.cn;
yangliuqq2003@163.com
Shuqing Chen
chenshuqing@zju.edu.cn
Fan Mo
mofan_hz@163.com

[†]These authors have contributed equally to this work

Specialty section:
This article was submitted to Vaccines and Molecular Therapeutics, a section of the journal Frontiers in Immunology

Received: 06 April 2021
Accepted: 29 July 2021
Published: 13 August 2021

Citation:
Chen Z, Zhang S, Han N, Jiang J, Xu Y, Ma D, Lu L, Guo X, Qiu M, Huang Q, Wang H, Mo F, Chen S and Yang L (2021) A Neoantigen-Based Peptide Vaccine for Patients With Advanced Pancreatic Cancer Refractory to Standard Treatment. Front. Immunol. 12:691605. doi: 10.3389/fimmu.2021.691605

Background: Neoantigens are critical targets to elicit robust antitumor T-cell responses. Personalized cancer vaccines developed based on neoantigens have shown promising results by prolonging cancer patients' overall survival (OS) for several cancer types. However, the safety and efficacy of these vaccine modalities remains unclear in pancreatic cancer patients.

Methods: This retrospective study enrolled 7 advanced pancreatic cancer patients. Up to 20 neoantigen peptides per patient identified by our in-house pipeline iNeo-Suite were selected, manufactured and administered to these patients with low tumor mutation burden (TMB) (less than 10 mutations/Mb). Each patient received multiple doses of vaccine depending on the progression of the disease. Peripheral blood samples of each patient were collected pre- and post-vaccination for the analysis of the immunogenicity of iNeo-Vac-P01 through ELISpot assay and flow cytometry.

Results: No severe vaccine-related adverse effects were witnessed in patients enrolled in this study. The mean OS, OS associated with vaccine treatment and progression free survival (PFS) were reported to be 24.1, 8.3 and 3.1 months, respectively. Higher peripheral IFN-γ titer and $CD4^+$ or $CD8^+$ effector memory T cells count post vaccination were found in patients with relatively long overall survival. Remarkably, for patient P01 who had a 21-month OS associated with vaccine treatment, the abundance of antigen-specific TCR clone drastically increased from 0% to nearly 100%, indicating the potential of iNeo-Vac-P01 in inducing the activation of a specific subset of T cells to kill cancer cells.

Conclusions: Neoantigen identification and selection were successfully applied to advanced pancreatic cancer patients with low TMB. As one of the earliest studies that addressed an issue in treating pancreatic cancer with personalized vaccines, it has been

demonstrated that iNeo-Vac-P01, a personalized neoantigen-based peptide vaccine, could improve the currently limited clinical efficacy of pancreatic cancer.

Clinical Trial Registration: ClinicalTrials.gov, identifier (NCT03645148). Registered August 24, 2018 - Retrospectively registered

Keywords: neoantigen, pancreatic cancer, vaccine, peptide, immunotherapy

INTRODUCTION

Pancreatic cancer is one of the top-leading causes of cancer-related death in the world, with a 5-year survival rate of only 9.3% (1). Most of the pancreatic cancer patients are diagnosed at an advanced stage (2). The poor prognosis of pancreatic cancer mainly results from the lack of early detection strategies such as a screening test, as no screening test has yet been shown to lower the risk of dying from pancreatic cancer. Even for those initially diagnosed at an early stage and subsequently received standard treatments such as surgical resection in combination with systemic radiotherapy or chemotherapy, their 5-year OS rate is still below 25% (3). According to the 2018 International Cancer Research Institute (IARC) GLOBOCAN statistics, there were 458,918 new cases and 432,242 deaths of pancreatic cancer, accounting for 2.5% of total new cancer cases and 4.5% of total deaths caused by all cancer types respectively in 2018 (4). Greater efforts should be addressed to the development of more promising therapies for pancreatic cancer.

With the development of chimeric antigen receptor T cell (CAR-T) immunotherapy and immune checkpoint inhibitors (ICIs) such as anti-PD-1/PD-L1 antibodies, cancer immunotherapy has shown attractive potential in the treatment of various solid tumors (5, 6). However, for pancreatic cancer, ICIs alone or combined with chemotherapy have not achieved evident positive outcomes in clinical studies (7, 8). Therapeutic neoantigen cancer vaccines belong to another important category of cancer immunotherapy. Several clinical studies have been launched recently to study their safety, tolerability and efficacy amongst patients diagnosed with different cancer types (9–11). Mostly generated from non-synonymous mutations specific in cancer cells, neoantigens are usually exempted from central tolerance. Personalized peptide neoantigen vaccines designed to train a patient's immune system can target and kill tumor cells specifically through following steps: deliver neoantigens to antigen-presenting cells (APCs); present tumor-specific neoantigens to T cells and activate cytotoxic T cells to recognize and eliminate tumor cells (12). Activated tumor-specific cytotoxic T-lymphocytes could infiltrate into tumors, turning "cold" tumors into "hot" ones, thereby eliciting a stronger antitumor immune response. Neoantigens of high immunogenicity and abundant $CD8^+$ T-cell infiltrates have been detected in long-term survivors of pancreatic ductal adenocarcinoma, suggesting that neoantigen-based cancer immunotherapies could benefit the survival of pancreatic cancer patients (13).

Recently, studies by Wu and Sahin et al. have demonstrated that peptide- or RNA-based neoantigen vaccines not only induce significant regression of advanced melanoma, but also provide long-term protection against tumor relapse and metastasis (14, 15). Sustained T cell response and increase in the number of tumor-infiltrating T cells were also reported in newly diagnosed glioblastoma patients after personalized peptide neoantigen vaccination (16). Studies focusing on colon and esophageal cancer also confirmed the effectiveness of neoantigen vaccination (17, 18). Moreover, combination treatment of personalized peptide neoantigen vaccines with ICIs has demonstrated good feasibility, safety and immunogenicity in patients with advanced melanoma, non-small cell lung cancer as well as bladder cancer in a phase Ib study (11). Although tumor-associated antigen (TAA)-based vaccines have been extensively investigated for their efficacy for pancreatic cancer (19–21), the anticancer effects of personalized neoantigen vaccines remain unclear.

Herein, we retrospectively assessed the anticancer effects of a personalized peptide neoantigen cancer vaccine, iNeo-Vac-P01, in patients with advanced pancreatic cancer from a clinical study (trial number: NCT03645148). Comprehensive analysis of these patients' immune response after vaccination was done to investigate its safety, tolerability and anticancer efficacy.

METHODS

Patients

Eligible patients with advanced pancreatic cancer confirmed histologically or cytologically were aged at least 18 years. Only patients who developed chemotherapy intolerance or disease progression after second-line treatments, with at least one measurable lesion in accordance with investigator-assessed Response Evaluation Criteria in Solid Tumors (RECIST; version 1.1), an Eastern Cooperative Oncology Group (ECOG) performance status of 0 or 1, as well as physiologically functional healthy organs such as heart, liver and kidney were considered. All patients selected for this study provided sufficient tumor tissue and blood samples for whole exome sequencing (WES) and RNA sequencing (when fresh tumor tissue is available).

Patients who had other malignant tumors except for cured basal cell carcinoma, thyroid carcinoma or cervical dysplasia, who lacked identified neoantigens by sequencing, who had received bone marrow or stem cell transplant or were allergic to polypeptides or other immunotherapies were excluded from this study.

Study Design and Treatment

We retrospectively investigated the clinical response of advanced pancreatic cancer patients upon receiving a personalized neoantigen peptide vaccine from a single-arm, open-label and

investigator-initiated clinical study at Zhejiang Provincial People's Hospital in China (NCT03645148). The primary endpoints of this clinical study were safety and feasibility, which were assessed based on the occurrence of adverse events (AEs) and whether the identification of neoantigens by our in-house pipeline iNeo-Suite and the subsequent peptide synthesis could be accomplished for clinical use. Whereas the secondary endpoint was efficacy which was evaluated through progression-free survival (PFS), overall survival (OS) and neoantigen-specific immune responses.

All patients received neoantigen vaccine iNeo-Vac-P01 comprising 5~20 peptides of varying length of 15 to 35 amino acids multiple times depending on the progression of the disease. Based on their HLA typing, affinity and allele frequency, these peptides were grouped into 2~4 pools and administered subcutaneously (s.c.) at the dose of 100 μg per peptide to patients at their upper arms and paraumbilical area. Each patient was primed with iNeo-Vac-P01 on day 1, 4, 8, 15 and 22, and boosted with the same vaccine formulation on day 78 and 162. Additional booster shots were scheduled to some patients to maximize the clinical benefits in accordance with the clinical research protocol. Thirty minutes prior to each immunization, 40 μg granulocyte-macrophage colony-stimulating factor (GM-CSF) was administered subcutaneously to patients around the injection site as an adjuvant (14, 16, 22–24). Poly-IC was tested in our previous study, however, due to the observation of AEs in patients, GM-CSF was chosen as an adjuvant for this study. Application of concomitant medical therapy such as ICIs during neoantigen vaccination was determined by clinicians to improve each patient's clinical response in accordance with the clinical research protocol. The treatment regimen for each patient was summarized in **Supplementary Table 1**.

Clinical assessment, monitoring and follow-up consisted of physical examination such as ECOG performance, vital sign, blood test and urinalysis for safety evaluation, imaging examination at baseline and post-vaccination for efficacy assessment, as well as immune response testing such as IFN-γ Enzyme-Linked Immunospot (ELISpot) assay and flow cytometry (T cell subsets and cytokines) at pre- and post-vaccination stages.

A retrospective assessment of tumors was conducted by investigators at each time point (baseline and approximately every 8 weeks thereafter) according to RECIST v1.1 criterion. The clinical response of each patient was evaluated not only throughout the vaccination, but also at regular intervals of 3 months post-vaccination until the development of cumulative toxic effects, disease progression or discontinuation of treatment. The occurrence of adverse events (AEs) were recorded, with the severity graded in accordance with National Cancer Institute Common Terminology Criteria for Adverse Events (version 4.0) throughout the treatment.

The study protocol was approved by the Institutional Review Board and Independent Ethics Committee and implemented in accordance with the Declaration of Helsinki and the International Conference on Harmonization Guidelines for Good Clinical Practice. All patients had signed informed consent forms before immunization.

Generation of Personalized Peptide Neoantigen Vaccines

To identify mutation-derived neoantigens, whole exome sequencing was conducted on samples obtained from patients by surgery, biopsy or intravenous blood sampling using Hiseq 4000 NGS platforms (Illumina) with coverage depths of 500x for tumor cells and 100x for blood cells (Novogene Biotech Co., Ltd., Beijing, China) (25–29). In addition, formalin-fixed paraffin-embedded (FFPE) samples were used for WES when fresh tumor samples were unavailable.

Bioinformatic analysis was performed by our in-house pipeline iNeo-Suite consisting of multiple modules including sequencing read filtering, genome alignment, mutation calling, HLA typing, MHC affinity prediction, gene expression profiling, vaccine peptide sequence design and mutation-centered prioritization based on therapeutic potency (Supplementary Methods).

Customized clinical-grade long peptides were manufactured through chemical synthesis at GMP-like standard (bacteria-free, > 95.0% purity with endotoxin less than 10 EU/mg) to generate iNeo-Vac-P01. The water solubility of synthesized peptides was tested, and water insoluble peptides were excluded from the final formulation.

IFN-γ Enzyme-Linked Immunospot Assay

To confirm the immunogenicity of iNeo-Vac-P01, ELISpot assays were performed for each patient at multiple time points pre- and post-vaccination. Peripheral blood (10-30 mL) was obtained from each patient for the isolation of peripheral blood mononuclear cells (PBMCs). PBMCs were then co-incubated (2×10^5 cells per well) with peptides for 16-24 hours using human IFN-γ pre-coated ELISpot kit following the standard protocol. Spots in ELISpot plates were counted using an automatic plate reader with proper parameters (Supplementary Methods).

T Cell Receptor Sequencing

To monitor the change of T cell population for each patient, T cell receptor (TCR) β chains were sequenced before and after vaccination. RNA extraction of PBMCs was performed using RNeasy Plus Mini Kit (Qiagen). Samples were analyzed by High-throughput sequencing of TCR using ImmuHub TCR profiling system at a deep level (ImmuQuad Biotech). Briefly, a 5' RACE unbiased amplification protocol was used. Unique molecular identifiers (UMIs) introduced to the course of cDNA synthesis were used to control bottlenecks and eliminate the errors of PCR and sequencing. Sequencing was performed on an Illumina HiSeq system with PE150 mode (Illumina). One common adaptor with UMI was added to the 5' of cDNA during the synthesis of first-strand cDNA. One reverse primer corresponding to the constant (C) regions of each TCRα and β was designed to facilitate PCR amplification of cDNA sequences in a less biased manner. The UMIs attached to each raw sequence reads were applied for sequencing error correction and PCR duplication removal. V, D, J and C segments were mapped with

IMGT. CDR3 regions were extracted, and clonotype assembled for all clones. The special nucleotide/amino acid sequences of CDR3 region of TCRβ subunit were determined. Those with out-of-frame or stop codon sequences were removed from the identified TCRβ repertoire. The total number of TCRβ clones sharing the same nucleotide sequence of CDR3 region was defined as the amount of each TCRβ clonotype.

Cytometric Analysis of T-Lymphocyte and Cytometric Bead Array Analysis of Cytokines

To quantify the activation of T cells after vaccination, peripheral T cells extracted from each patient were labeled with several different antibodies (CD279, CD197, CD4, CD8, CD45RA, CD38, CD45, CD3, HLA-DR and CD152) for flow cytometry analysis. To examine the cytokines secreted from activated T cells after vaccination, cytokine titers in peripheral blood were measured by CBA following manufacturer's protocol (Supplementary Methods).

Statistical Analysis

Data from the patients who received at least one dose of iNeo-Vac-P01 was analyzed for safety and clinical efficacy assessment. Descriptive statistics was applied to determine the characteristics of baseline and assess the safety of iNeo-Vac-P01. The target lesions of each patient were measured before the treatment and then every two months during the treatment to monitor the changes in lesion sizes. All tumors were sized by MRI and CT. Disease control rate (DCR) was defined as the proportion of patients who had complete response (CR), partial response (PR) and stable disease (SD) for best clinical response. Standard RECISTv1.1 guideline was followed for the analysis of all clinical data. The survival curves were plotted by GraphPad Prism 5 (v5.01).

RESULTS

Patients and Demographics

A total of 7 eligible advanced pancreatic cancer patients, enrolled between January 1, 2018 to March 31, 2020, were included in this retrospective study. All patients had previously received surgery or standard chemotherapy, and experienced cancer relapse or metastasis. Patients baseline characteristics were summarized in **Table 1**. Six (85.71%) patients had adenocarcinoma and one (14.29%) had squamous cell carcinoma. Four (57.14%) patients had liver metastases and three (42.86%) had peritoneum metastases. In addition, four (57.14%) patients had higher CA19-9 levels at baseline compared to the other three (42.86%) with normal levels.

Feasibility of Preparation and Application of Neoantigen in Patients With Advanced Pancreatic Cancer

WES results of both tumor tissues and peripheral blood samples were shown in **Supplementary Table 2**. Neoantigens were predicted and prioritized using our in-house pipeline iNeo-Suite, in consideration of allelic frequency of mutation, affinity between mutated peptide and HLA class I and II, as well as feasibility of peptide synthesis (**Supplementary Tables 3**, **4**). Clinical-grade long peptides (15-35 amino acids) incorporating multiple neo-epitopes of both HLA class I and II were synthesized (**Supplementary Table 3**). Depending on the quantities of tumor samples as well as the sequences of long peptides, the turnaround time of the whole process varied from 1.5 to 3 months.

Based on the analysis of 1061 pancreatic cancer samples from cBioPortal for Cancer Genomics, KRAS, TP53, SMAD4 and CDKN2A are the most common mutations in tumor-related genes, and all detected in over 10% patient samples. In this study, the numbers of the patients with TP53, KRAS, SMAD4 and CDKN2A mutations were seven (100%), five (71.43%), three (42.86%) and one (14.29%). Importantly, among patients with KRAS mutations, there were two with G12V mutation, two with G12D and one with Q61H. Despite of the lower tumor mutation burden (TMB) in pancreatic cancers, sufficient neoantigens were identified, followed by successful manufacture of corresponding personalized long peptides for each patient in this study. Different from other clinical studies published prior to this study (14, 16), no organic solvent such as DMSO was applied to enhance the water solubility of personalized long peptides due to the disapproval of its use in clinics. Among the total 94 long peptides that were designed and synthesized successfully, 70 peptides with good water solubility were further selected for vaccination (**Supplementary Table 5**). The median number of peptides administered to each patient was 12. Most patients (5 out of 7) received vaccines consisted of more than 10 peptides (**Supplementary Tables 3**, **5**), which contained a median of 9 class I neo-epitopes and 20 class II neo-epitopes per peptide.

Treatment and Follow-Up of Patients

Patients were scheduled to receive iNeo-Vac-P01 together with GM-CSF as adjuvant (**Figure 1**). The median follow-up duration for all patients was 9.7 months, ranging from 2 months to 21 months before the deadline March 31, 2020. All patients completed the prime phase of immunization (**Figure 1**). The average duration of treatment was 2.57 months, ranging from 1 month to 5 months. Patients P02, P03, P06 and P07 had stable disease during vaccination. Patients P01 and P04 showed partial response during vaccination and had good disease control for a period after vaccination. Patients P05 had progressive disease (PD) during the boost phase of vaccination.

Safety and Side Effects

During the vaccine treatment, none of the patients had grade 3-4 adverse events associated with iNeo-Vac-P01 defined by NCI CTCAE 4.03. One of the patients (P06) experienced a mild rash after vaccine injection but recovered within one week. To be noted, all seven patients had experienced different degrees of adverse reactions due to chemotherapy before scheduled for vaccination. The most common serious adverse events of chemotherapy among these patients were hematological toxic events including neutropenia (7/7) and anemia (5/7). Other chemotherapy-related adverse reactions including gastrointestinal reactions, rashes and fever were summarized in **Table 2**.

TABLE 1 | Baseline characteristics of each patient.

Characteristics	Patient (N=7)	
	n	%
Sex		
Male	5	71.43
Female	2	28.57
Age		
<60	3	42.86
>=60	4	57.14
Tumor location		
Pancreatic head	2	28.57
Pancreatic body and tail	5	71.43
Histopathology		
Adenocarcinoma	6	85.71
Others	1	14.29
Metastatic sites		
Liver	4	57.14
Peritoneum	3	42.86
ECOG score		
0	3	42.86
1	4	57.14
CA19-9 level(first visit)		
<37.0	3	42.86
>=37.0	4	57.14

ECOG, Eastern cooperative oncology group; CA19-9, Carbohydrate antigen 19-9.

Clinical Response

RECIST 1.1 criteria were used to assess target lesions in all patients. The OS of all patients was summarized in **Figure 2A**. The mean OS of the 7 patients was 24.1 months (11 to 31.4 months), and the mean PFS was 3.1 months (**Table 3**). Calculated from each patient's first immunization, the mean OS associated with peptide vaccination was 8.3 months (3 to 21 months). All patients had died except for Patient P04. The survival rate was around 50% at 24 months according to **Table 3**. Clinical response of all patients in this study was shown in **Figure 2B**. Three out of seven patients showed tumor reduction at the target lesions. Patients P01 and P04 were evaluated as PR, as the sizes of their target lesions reduced by 54% and 57% respectively compared to those of baseline, while patient P06 maintained stable disease with the size of target lesion only reduced by 5%. Although different degrees of size increase at target lesions was observed for the other four patients (P02, P03, P05 and P07), patients P02, P03 and P07 were assessed as SD with less than 20% increase. Only patient P05 was evaluated as PD for a 40% increase in target lesion. The disease control rate (DCR) of the 7 patients was 85.71%.

Case Report of Patient P01

Patient P01 was first diagnosed with pancreatic cancer with liver metastasis in July 2017. From July 2017 to February 2018, she was given AG regimen (paclitaxel albumin plusS-1) for 8 cycles as first-line conversion chemotherapy. Under general anesthesia, laparoscopic radical pancreatectomy was performed on March 5th, 2018. No chemotherapy was given after surgery due to the patient's poor physical condition. However, in less than three months, lymph node metastasis was found. From 6th June 2018 to 7th November 2018, Patient P01 received 8 doses of iNeo-Vac-P01 in total, including 5 prime and 3 boost immunizations. In addition, to maximize the patient's clinical benefits, 5-cycle AS

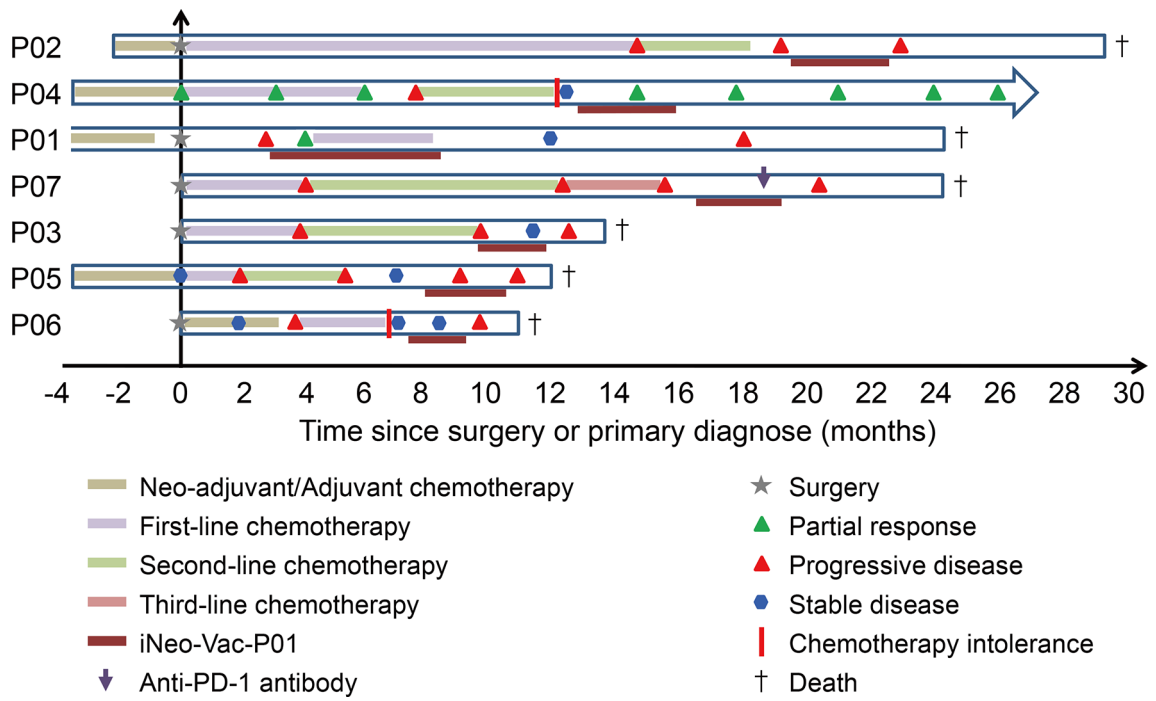

FIGURE 1 | Clinical treatment process for each patient from surgery or primary visit until the end of follow-up.

TABLE 2 | Comparison of adverse reactions between peptide therapy and chemotherapy in treated patients.

Adverse Effects	Any grade		Grades 3 to 4	
	Chemotherapy	Neoantigen vaccine	Chemotherapy	Neoantigen vaccine
	N (%)	N (%)	N (%)	N (%)
Gastrointestinal reaction	7 (100.0)	0 (0.0)	2 (28.6)	0 (0.0)
Thrombocytopenia	5 (71.4)	0 (0.0)	2 (28.6)	0 (0.0)
Rash	2 (28.6)	1 (14.3)	0 (0.0)	0 (0.0)
Fever	1 (14.3)	0 (0.0)	0 (0.0)	0 (0.0)
Neutropenia	7 (100.0)	0 (0.0)	4 (57.1)	0 (0.0)
Peripheral nerve abnormalities	3 (42.9)	0 (0.0)	0 (0.0)	0 (0.0)
Anemia	5 (71.4)	0 (0.0)	1 (14.3)	0 (0.0)
Elevated transaminase	3 (42.9)	0 (0.0)	0 (0.0)	0 (0.0)
Fatigue	7 (100.0)	0 (0.0)	1 (14.3)	0 (0.0)

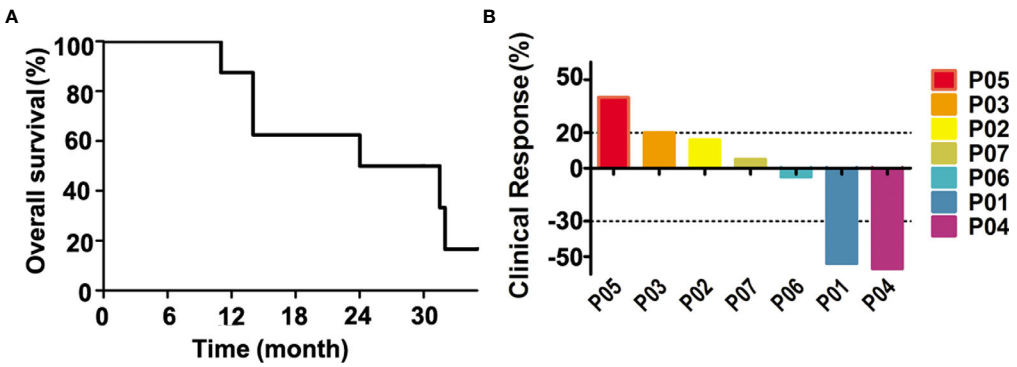

FIGURE 2 | The clinical response and prognosis of treated patients. **(A)** The overall survival curve of each patient. **(B)** The percentage changes of tumor lesion in size from baseline. The changes in lesions between a positive value of 25% and a negative value of 50% are considered stable disease.

TABLE 3 | The survival and objective response rate of each patient.

Survival	Months
mOS	24.1
mPFS	3.1
mOS*	8.3
Objective response rate	**n/N**
CR	0/7
PR	2/7
SD	4/7
PD	1/7

*mOS, mean Overall survival; mPFS, mean Progression-free survival; CR, Complete remission; PR, Partial response; SD, Stable disease; PD, Progressive disease; *Calculated from the time the patient received the peptide vaccine.*

second-line treatment was given from July 2018 to November 2018 as a concomitant therapy. In February 2019, a tumor marker was detected while CT imaging showed no tumor recurrence. In response, the patient soon received 2-cycle AS systemic chemotherapy. After the treatment, the patient's disease was considered to be well controlled until bone metastasis and pleural effusion occurred in September 2019. Since then, the disease progressed rapidly. After supportive treatment and chemotherapy, Patient P01 died in March 2020. The OS and PFS of Patient P01 were 32 and 8 months. It is noteworthy that the OS associated with iNeo-Vac-P01 treatment of Patient P01 was 21 months. The whole treatment regimen was shown in **Figure 3A**. MRI images showed the regression of pancreaticogastric nodule 4 months after first immunization when compared to baseline level (**Figure 3B**). No iNeo-Vac-P01-related serious AEs occurred during the whole vaccine treatment. *Ex vivo* IFN-γ ELISpot of PBMCs confirmed robust *de novo* immune response against all neoantigen peptides since vaccination, with a peak at Week 3 (**Figures 3C, D**). TCR sequencing of peripheral T cells revealed that the abundance of the TCR clone (CASSPGQGVYNEQFF) considerably increased after vaccination. Moreover, a new TCR clone (CASSLGTGYNEQFF) was detected after vaccination (**Figure 3E**). These data suggested that a subset of T cells with neoantigen specificities were induced by iNeo-Vac-P01 in Patient P01. However, no enough blood sample left could be applied to evaluate whether these TCR clones recognize the same peptide. The concomitant iNeo-Vac-P01 therapy and chemotherapy might have generated synergetic benefits to prolong the OS and PFS of Patient P01.

Immune Response

Ex vivo IFN-γ ELISpot assay was performed with autologous PBMCs after vaccination. ELISpot assay results demonstrated the potentials of iNeo-Vac-P01 to induce the activation of T cells in 5 out of 7 (71.4%) patients (**Figure 4A** and **Supplementary Table 6**).

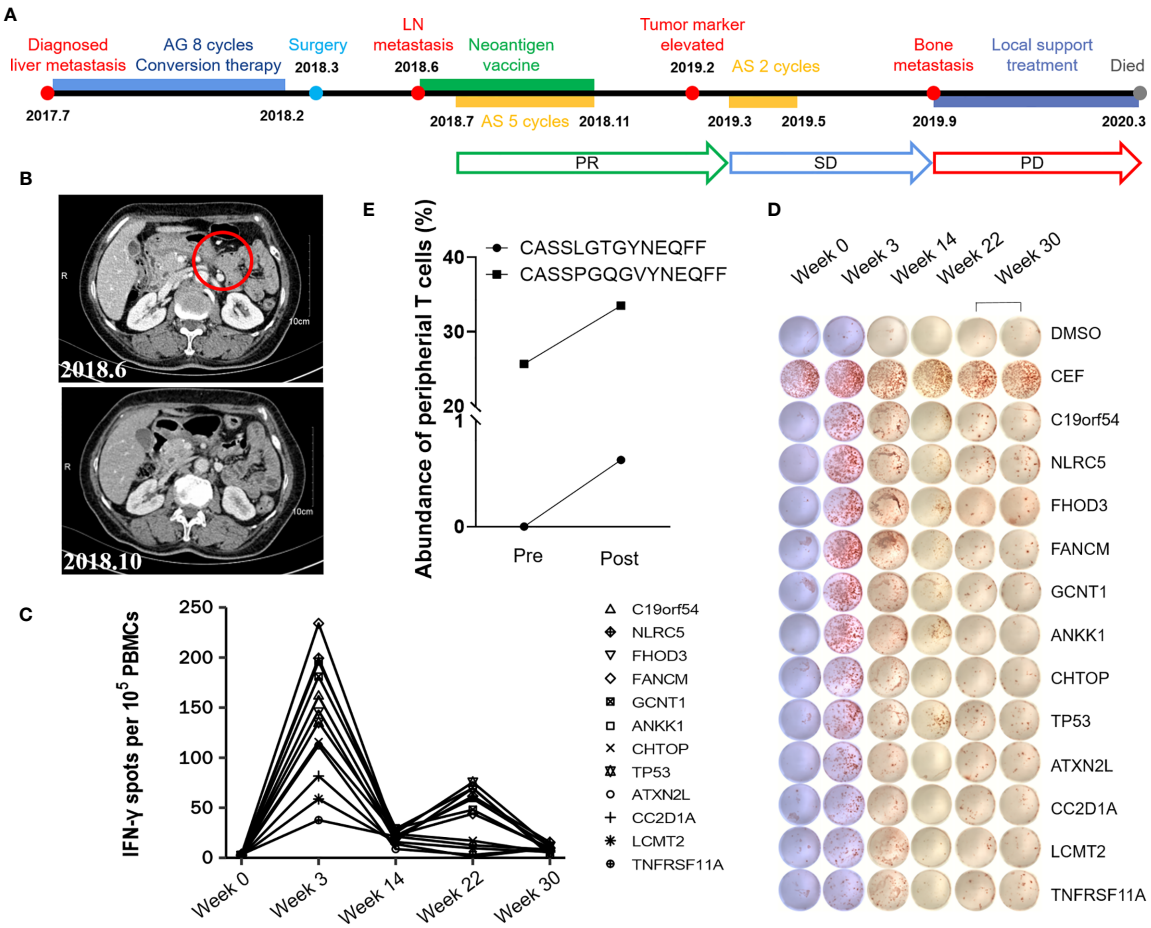

FIGURE 3 | A case report of Patient P01. **(A)** Treatment timeline of P01. **(B)** Comparison of lymph node before & after vaccination by imaging. **(C, D)** *Ex vivo* IFN-γ ELISpot of PBMCs was performed with peptides at different time points. The dimethyl sulfoxide (DMSO) group was used as the negative control and mixed peptides from CEF (including peptides of cytomegalovirus, Epstein–Barr virus and influenza virus) were used as the positive control. **(E)** Increased abundance of peripheral T cell clones after vaccination was detected by TCR sequencing.

For each patient, the number of IFN-γ spots per 10^5 PBMCs of the peptide or peptide pool with best response was shown in **Figure 4A**. For patients P05 and P07, no evident response was found pre- and post-vaccination. Overall, 31 out of 70 (44.3%) individual long peptides elicited measurable peptide-specific immune responses (positive results in ELISpot assay after vaccination). No correlation between IL-2, IL-6, IL-10, TNF-α and clinical response was found, as the titers of these cytokines did not change drastically after vaccination. However, for patients who had a relatively long OS (P01, P04 and P07), their IFN-γ titer in the peripheral blood increased to a much larger extent after vaccination, compared to patients who had relatively short OS (P03, P05 and P06) (**Supplementary Table 7**). This phenomenon suggested that IFN-γ titer in the peripheral blood could be a potential biomarker for clinical response. It is noted that not every patient managed to provide sufficient blood sample for cytokine studies due to their poor physical conditions at the designated time points (P04). Moreover, for all 7 patients, the proportions of CD4+ CTLA4+ T cells and CD8+ CTLA4+ T cells in peripheral blood increased during vaccination (**Figure 5**), suggesting that combined treatment with anti-CTLA-4 immunotherapy might help achieve stronger antitumoral immune response. It is noteworthy that not all patients provided enough blood samples for analysis due to their poor physical conditions at the designated time points (e.g. P03 and P05). In addition, changes in the T cell subsets post vaccination also suggested that $CD4^+$ or $CD8^+$ effector memory T cells in the peripheral blood could be a potential biomarker for clinical response. Before treatment, patients with relatively long OS (P01, P02, P04 and P07) had more $CD4^+$ or $CD8^+$ central memory T cells (T_{CM}) and $CD4^+$ or $CD8^+$ effector memory T cells (T_{EM}) than patients with relatively short OS (P03, P05 and P06); however, only the difference in T_{CM} showed statistical significance ($p<0.05$). Post vaccination, longer OS patients still had more T_{CM} and T_{EM}, while only T_{EM} showed statistical significance ($p<0.05$) (**Figure 4B** and **Supplementary Table 8**). This phenomenon indicated that upon antigenic stimulation,

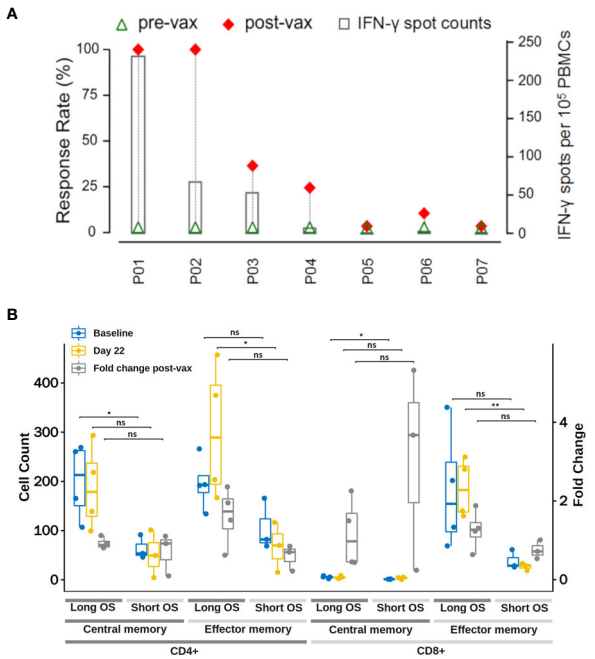

FIGURE 4 | Immune Response induced by iNeo-Vac-P01. **(A)** iNeo-Vac-P01 induced specific T cell response. For each patient marked in X-axis, green triangle and red diamond represent the response rates pre- and post-vaccination, defined as the ratios of the numbers of peptides (or peptide pools) with positive ELISpot results before and after vaccination to the total number of peptides (or peptide pools) in vaccine, respectively. The bar chart with secondary Y-axis represented the IFN-γ spots per 10^5 PBMCs of the peptide with best response for each patient. **(B)** Change in T cell subsets count at baseline and 22 days post iNeo-Vac-P01 vaccination. Blue and yellow dots represent the cell counts at baseline and 22 days post iNeo-Vac-P01, respectively. Grey dots represent the fold change of corresponding cell count, which can be read at the right Y-axis. Counts of T cell subsets including $CD4^+$ central memory, $CD4^+$ effector memory, $CD8^+$ central memory and $CD8^+$ effector memory T cells were compared in long OS patients (shown in dark grey) and short OS patients (shown in light grey). *: significant, p=0.01 to 0.05; **: very significant, p=0.001 to 0.01; ns: not significant.

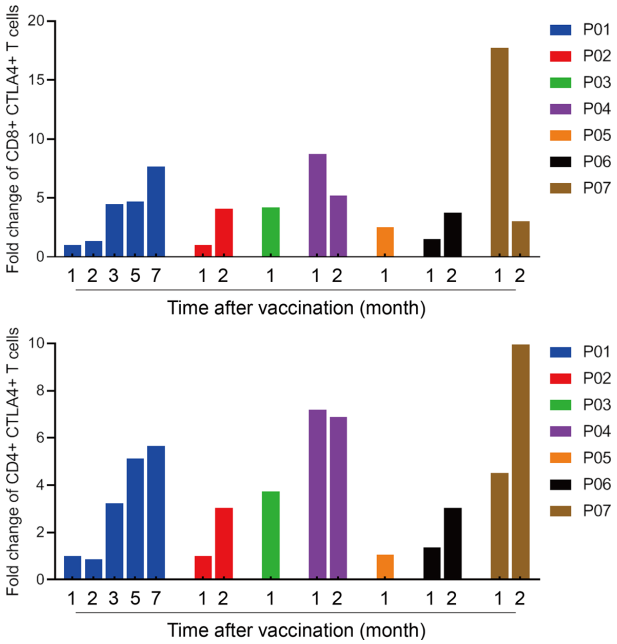

FIGURE 5 | The proportion of CTLA4+ T cells in peripheral blood increased after vaccination. The proportions of CD8+ CTLA-4+ T cells and CD4+ CTLA-4+ T cells ratio to total T cells in peripheral blood were determined by flow cytometry. Fold changes of post vaccination compared with baseline were calculated.

differentiation of central memory T cells to effector memory T cells might be activated (30).

DISCUSSION

In this study, we retrospectively analyzed the safety and tolerability of neoantigen-based peptide vaccine iNeo-Vac-P01 in pancreatic cancer patients. Although mRNA vaccines have gained much research interest since the approval of mRNA-based COVID-19 vaccines under Emergency Use Authorization for COVID-19, no mRNA therapy was approved during the time this study was conducted. Thus, well-investigated peptide-based vaccine approach was used in this study. None of the patients enrolled in this study showed SAE during vaccination, while only one patient showed vaccine-related AE (slight rash) which recovered without any nursing.

Currently, the median overall survival time for advanced pancreatic cancer patients is only 6 to 9 months (31). Albumin paclitaxel combined with gemcitabine or mFOLFIRINOX regimen [5-fluorouracil (5-FU), irinotecan and oxaliplatin] is recommended as the standard first-line treatment by the guidelines (32, 33). Meanwhile, there is no standard chemotherapy regimen after second-line treatment. A stratified analysis of the posterior survival of pancreatic cancer patients showed that the median survival time of patients with high-risk pancreatic cancer was only 1.4 months, and that of low-risk patients was less than 12 months (34). To our knowledge, advanced pancreatic cancer patients tend to have larger tumor burdens than patients diagnosed with other cancer types, therefore, instead of applying monotherapy of neoantigen vaccination, chemotherapy or ICI (i.e. anti-PD-1) therapy were scheduled to several patients (P01 and P07) to maximize the clinical benefits for them. The treatment regimen for each patient was listed in **Supplementary Table 1**. The mean OS and PFS of advanced pancreatic cancer patients in this retrospective study were 24.1 and 3.1 months, longer than most of the clinical data reported in other clinical studies. In addition, the mean OS associated with the vaccine treatment was 8.3 months. Although this retrospective study has a relatively small sample size, the results here demonstrated promising potentials of using personalized neoantigen-based peptide vaccine as a second-line or later treatment to prolong the survival duration of an advanced pancreatic cancer patient.

GM-CSF was used as a molecular adjuvant for personalized vaccine in this study due to ethical concerns, as choices of approved vaccine adjuvants in China were limited. No GM-CSF control group was set since this study was a retrospective cohort study with a small sample size, instead of a randomized controlled trial. However, in future phase 2 study, GM-CSF could be used as control.

KRAS mutation is a common driver mutation for several cancer types including pancreatic cancer. It is usually incorporated in the "shared" tumor antigen combinations as "off-the-shelf" tumor vaccines. In a study of patients with advanced cancer (pancreatic cancer, cholangiocarcinoma and colorectal cancer), Rahma et al. demonstrated that the patients could achieve a mean PFS and OS of 3.6 months and 16.9 months respectively, with an immune response rate of 54% when treated with the vaccine formulation containing KRAS G12D, G12V and G12C peptides (35). Although it is a promising strategy to treat the patients with KRAS mutations, the "off-the-shelf" tumor vaccines cannot fulfill the clinical needs for those who do not harbor the mutations. Different from the vaccines based on "shared" antigens, personalized neoantigen-based peptide cancer vaccines are customized for each patient. In this retrospective study, only 5 out of 7 patients had KRAS mutations (**Supplementary Table 9**). KRAS mutations were also included in the design of personalized iNeo-Vac-P01 for these 5 patients to maximize the clinical benefits. For Patient P01 who did not have KRAS mutation had a significant extension of survival duration as a result of concomitant iNeo-Vac-P01 vaccine therapy with chemotherapy (**Figure 3** and **Table 1**).

It is also noteworthy that Patient P01 started the personalized peptide vaccination only three months after the primary tumor resection, leading to relatively lower tumor burden compared to other patients. The iNeo-Vac-P01-related OS of Patient P01 was 21 months which was longer than that of any other patients in this study. More studies should be conducted in the future to investigate whether a pancreatic cancer patient could achieve longer survival duration if neoantigen tumor vaccine is given when the tumor burden is low. Previously, a case report had described a pancreatic cancer patient who began SVN-2B peptide vaccine treatment during the adjuvant treatment stage (20). After the vaccine regimen, isolated lung metastases were observed in this patient but subsequently well controlled by surgery. It was reported that this patient had a survival duration of more than 10 years (20). In light of this case report together with our clinical findings with Patient P01, we believe that it is important to investigate the "perfect" timing for the administration of neoantigen tumor vaccine, for instance, when the tumor burden is low.

In addition, several T cell subsets and cytokines in peripheral blood were evaluated in this study to identify potential biomarkers for clinical response. The drastic fold-change of IFN-γ titer in peripheral blood observed in patients with relatively long OS (P01, P02 and P07), in comparison with patients with relatively short OS that did not experience significant IFN-γ change (P03, P05 and P06), has suggested that peripheral IFN-γ titer could be a biomarker for clinical response. Interestingly, these patients with short OS happened to have very short vaccine-associated OS as well. Although P02 and P07 had relatively long OS compared to P03, P05 and P06, the vaccine-associated OS for them was short. This could be attributed to the late administration of vaccines for them, which again, emphasizes the point of interventional vaccination scheduled at an earlier time point after first-line or second-line chemotherapy can be more beneficial to achieve better clinical response. As a result of induction by peptide vaccines, both CD4+ CTLA4+ T cell and CD8+ CTLA4+ T cell populations in peripheral blood had increased in all 7 patients. Therefore, combined treatment of personalized neoantigen-based peptide vaccines with anti-CTLA-4 antibody could potentially be a promising treatment modality for pancreatic cancer patients. A shift from $CD4^+$ or $CD8^+$ T_{CM} to $CD4^+$ or $CD8^+$ T_{EM} was observed in long OS patients (P01, P02, P04 and P07) upon vaccination, showing significant differences with relatively short OS patients (P03, P05 and P06). This indicated the successfully antigenic stimulation that led to the differentiation of T_{CM} to T_{EM}. In all, further studies with special considerations of the time for neoantigen vaccine administration should be conducted to achieve better clinical benefits for cancer patients such as pancreatic cancer patients.

CONCLUSIONS

This retrospective study demonstrated the feasibility of neoantigen selection for pancreatic cancer patients with low TMB (less than 10 mutations/Mb), as well as the tolerability of personalized neoantigen-based peptide vaccine, iNeo-Vac-P01, for treating pancreatic cancer. Our findings were important and complementary to previously published studies in neoantigen cancer vaccines treating other types of cancers. The development and implementation of personalized neoantigen-based peptide cancer vaccines might provide a new strategy to improve the limited clinical efficacy of traditional treatments for pancreatic cancer.

DATA AVAILABILITY STATEMENT

The datasets presented in this study can be found in online repositories. The names of the repository/repositories and accession number(s) can be found below: https://ngdc.cncb.ac.cn/gsa-human/s/UHnoE84R.

ETHICS STATEMENT

The studies involving human participants were reviewed and approved by Ethics Committee of Zhejiang Provincial People's Hospital. The patients/participants provided their written informed consent to participate in this study.

AUTHOR CONTRIBUTIONS

ZC, SZ, SC, LY, and FM contributed to the conception and design of the work. ZC, NH, DM and XG conducted the studies.

JJ, YX, HW, and MQ contributed to data processing and analysis. ZC, QH, FM, and NH helped with the statistical analysis. ZC, SZ, LL, SC, and LY prepared most part of the manuscript with FM. NH revised it critically. All authors contributed to the article and approved the submitted version.

FUNDING

This work was supported by National Natural Science Foundation of China (U20A20409 to SC, 81772575 and 81972455 to Liu Yang, and 81802623 to ZC).

ACKNOWLEDGMENTS

The authors are grateful for all patients participated in the trial and their families, as well as Zhejiang Provincial People's Hospital as the clinical site.

SUPPLEMENTARY MATERIAL

The Supplementary Material for this article can be found online at: https://www.frontiersin.org/articles/10.3389/fimmu.2021.691605/full#supplementary-material

REFERENCES

1. Idachaba S, Dada O, Abimbola O, Olayinka O, Uma A, Olunu E, et al. A Review of Pancreatic Cancer: Epidemiology, Genetics, Screening, and Management. *Open Access Macedonian J Med Sci* (2019) 7(4):663–71. doi: 10.3889/oamjms.2019.104
2. Bliss LA, Witkowski ER, Yang CJ, Tseng JF. Outcomes in Operative Management of Pancreatic Cancer. *J Surg Oncol* (2014) 110(5):592–8. doi: 10.1002/jso.23744
3. Vincent A, Herman J, Schulick R, Hruban RH, Goggins M. Pancreatic Cancer. *Lancet* (2011) 378(9791):607–20. doi: 10.1016/S0140-6736(10)62307-0
4. Bray F, Ferlay J, Soerjomataram I, Siegel RL, Torre LA, Jemal A. Global Cancer Statistics 2018: GLOBOCAN Estimates of Incidence and Mortality Worldwide for 36 Cancers in 185 Countries. *CA: Cancer J Clin* (2018) 68 (6):394–424. doi: 10.3322/caac.21492
5. Nair R, Westin J. CAR T-Cells. *Adv Exp Med Biol* (2020) 1244:215–33. doi: 10.1007/978-3-030-41008-7_10
6. Han Y, Liu D, Li L. PD-1/PD-L1 Pathway: Current Researches in Cancer. *Am J Cancer Res* (2020) 10(3):727–42.
7. Weiss GJ, Waypa J, Blaydorn L, Coats J, McGahey K, Sangal A, et al. A Phase Ib Study of Pembrolizumab Plus Chemotherapy in Patients With Advanced Cancer (PembroPlus). *Br J Cancer* (2017) 117(1):33–40. doi: 10.1038/bjc.2017.145
8. Aglietta M, Barone C, Sawyer MB, Moore MJ, Miller WH Jr, Bagala C, et al. A Phase I Dose Escalation Trial of Tremelimumab (CP-675,206) in Combination With Gemcitabine in Chemotherapy-Naive Patients With Metastatic Pancreatic Cancer. *Ann Oncol* (2014) 25(9):1750–5. doi: 10.1093/annonc/mdu205
9. Bansal D, Beck R, Arora V, Knoche EM, Picus J, Reimers MA, et al. A Pilot Trial of Neoantigen DNA Vaccine in Combination With Nivolumab/Ipilimumab and Prostvac in Metastatic Hormone-Sensitive Prostate Cancer (mHSPC). *J Clin Oncol* (2021) 39(6_suppl):TPS192–TPS. doi: 10.1200/JCO.2021.39.6_suppl.TPS192
10. Ding Z, Li Q, Zhang R, Xie L, Shu Y, Gao S, et al. Personalized Neoantigen Pulsed Dendritic Cell Vaccine for Advanced Lung Cancer. *Signal Transduct Targeted Ther* (2021) 6(1):26. doi: 10.1038/s41392-020-00448-5
11. Ott PA, Hu-Lieskovan S, Chmielowski B, Govindan R, Naing A, Bhardwaj N, et al. A Phase Ib Trial of Personalized Neoantigen Therapy Plus Anti-PD-1 in Patients With Advanced Melanoma, Non-Small Cell Lung Cancer, or Bladder Cancer. *Cell* (2020) 183(2):347–62 e24. doi: 10.1016/j.cell.2020.08.053
12. Yadav M, Jhunjhunwala S, Phung QT, Lupardus P, Tanguay J, Bumbaca S, et al. Predicting Immunogenic Tumour Mutations by Combining Mass Spectrometry and Exome Sequencing. *Nature* (2014) 515(7528):572–6. doi: 10.1038/nature14001
13. Balachandran VP, Łuksza M, Zhao JN, Makarov V, Moral JA, Remark R, et al. Identification of Unique Neoantigen Qualities in Long-Term Survivors of Pancreatic Cancer. *Nature* (2017) 551(7681):512–6. doi: 10.1038/nature24462
14. Ott PA, Hu Z, Keskin DB, Shukla SA, Sun J, Bozym DJ, et al. An Immunogenic Personal Neoantigen Vaccine for Patients With Melanoma. *Nature* (2017) 547(7662):217–21. doi: 10.1038/nature22991
15. Sahin U, Derhovanessian E, Miller M, Kloke BP, Simon P, Lower M, et al. Personalized RNA Mutanome Vaccines Mobilize Poly-Specific Therapeutic Immunity Against Cancer. *Nature* (2017) 547(7662):222–6. doi: 10.1038/nature23003
16. Keskin DB, Anandappa AJ, Sun J, Tirosh I, Mathewson ND, Li S, et al. Neoantigen Vaccine Generates Intratumoral T Cell Responses in Phase Ib Glioblastoma Trial. *Nature* (2019) 565(7738):234–9. doi: 10.1038/s41586-018-0792-9
17. Forghanifard MM, Gholamin M, Moaven O, Farshchian M, Ghahraman M, Aledavood A, et al. Neoantigen in Esophageal Squamous Cell Carcinoma for Dendritic Cell-Based Cancer Vaccine Development. *Med Oncol* (2014) 31 (10):191. doi: 10.1007/s12032-014-0191-5
18. Kuai R, Ochyl LJ, Bahjat KS, Schwendeman A, Moon JJ. Designer Vaccine Nanodiscs for Personalized Cancer Immunotherapy. *Nat Mater* (2017) 16 (4):489–96. doi: 10.1038/nmat4822
19. Middleton G, Silcocks P, Cox T, Valle J, Wadsley J, Propper D, et al. Gemcitabine and Capecitabine With or Without Telomerase Peptide Vaccine GV1001 in Patients With Locally Advanced or Metastatic Pancreatic Cancer (TeloVac): An Open-Label, Randomised, Phase 3 Trial. *Lancet Oncol* (2014) 15(8):829–40. doi: 10.1016/S1470-2045(14)70236-0
20. Shima H, Kutomi G, Satomi F, Imamura M, Kimura Y, Mizuguchi T, et al. Case Report: Long-Term Survival of a Pancreatic Cancer Patient Immunized With an SVN-2B Peptide Vaccine. *Cancer Immunol Immunother: CII* (2018) 67(10):1603–9. doi: 10.1007/s00262-018-2217-x
21. Suzuki N, Hazama S, Iguchi H, Uesugi K, Tanaka H, Hirakawa K, et al. Phase II Clinical Trial of Peptide Cocktail Therapy for Patients With Advanced Pancreatic Cancer: VENUS-PC Study. *Cancer Sci* (2017) 108(1):73–80. doi: 10.1111/cas.13113
22. Weden S, Klemp M, Gladhaug IP, Moller M, Eriksen JA, Gaudernack G, et al. Long-Term Follow-Up of Patients With Resected Pancreatic Cancer Following Vaccination Against Mutant K-Ras. *Int J Cancer* (2011) 128 (5):1120–8. doi: 10.1002/ijc.25449
23. Gjertsen MK, Buanes T, Rosseland AR, Bakka A, Gladhaug I, Soreide O, et al. Intradermal Ras Peptide Vaccination With Granulocyte-Macrophage Colony-Stimulating Factor as Adjuvant: Clinical and Immunological Responses in Patients With Pancreatic Adenocarcinoma. *Int J Cancer* (2001) 92(3):441–50. doi: 10.1002/ijc.1205
24. Kirner A, Mayer-Mokler A, Reinhardt C. IMA901: A Multi-Peptide Cancer Vaccine for Treatment of Renal Cell Cancer. *Hum Vaccin Immunother* (2014) 10(11):3179–89. doi: 10.4161/21645515.2014.983857
25. Bais P, Namburi S, Gatti DM, Zhang X, Chuang JH. CloudNeo: A Cloud Pipeline for Identifying Patient-Specific Tumor Neoantigens. *Bioinformatics* (2017) 33(19):3110–2. doi: 10.1093/bioinformatics/btx375
26. Hundal J, Miller CA, Griffith M, Griffith OL, Walker J, Kiwala S, et al. Cancer Immunogenomics: Computational Neoantigen Identification and Vaccine Design. *Cold Spring Harb Symp Quant Biol* (2016) 81:105–11. doi: 10.1101/sqb.2016.81.030726
27. Schenck RO, Lakatos E, Gatenbee C, Graham TA, Anderson ARA. NeoPredPipe: High-Throughput Neoantigen Prediction and Recognition Potential Pipeline. *BMC Bioinf* (2019) 20(1):264. doi: 10.1186/s12859-019-2876-4
28. Tappeiner E, Finotello F, Charoentong P, Mayer C, Rieder D, Trajanoski Z. TIminer: NGS Data Mining Pipeline for Cancer Immunology and Immunotherapy. *Bioinformatics* (2017) 33(19):3140–1. doi: 10.1093/bioinformatics/btx377
29. Torres-Garcia W, Zheng S, Sivachenko A, Vegesna R, Wang Q, Yao R, et al. PRADA: Pipeline for RNA Sequencing Data Analysis. *Bioinformatics* (2014) 30(15):2224–6. doi: 10.1093/bioinformatics/btu169

30. Sallusto F, Geginat J, Lanzavecchia A. Central Memory and Effector Memory T Cell Subsets: Function, Generation, and Maintenance. *Annu Rev Immunol* (2004) 22:745–63. doi: 10.1146/annurev.immunol.22.012703.104702
31. Ryan DP, Hong TS, Bardeesy N. Pancreatic Adenocarcinoma. *New Engl J Med* (2014) 371(22):2140–1. doi: 10.1056/NEJMc1412266
32. Conroy T, Desseigne F, Ychou M, Bouche O, Guimbaud R, Becouarn Y, et al. FOLFIRINOX Versus Gemcitabine for Metastatic Pancreatic Cancer. *New Engl J Med* (2011) 364(19):1817–25. doi: 10.1056/NEJMoa1011923
33. Von Hoff DD, Ervin T, Arena FP, Chiorean EG, Infante J, Moore M, et al. Increased Survival in Pancreatic Cancer With Nab-Paclitaxel Plus Gemcitabine. *New Engl J Med* (2013) 369(18):1691–703. doi: 10.1056/NEJMoa1304369
34. Vienot A, Beinse G, Louvet C, de Mestier L, Meurisse A, Fein F, et al. Overall Survival Prediction and Usefulness of Second-Line Chemotherapy in Advanced Pancreatic Adenocarcinoma. *J Natl Cancer Inst* (2017) 109(10). doi: 10.1093/jnci/djx037
35. Rahma OE, Hamilton JM, Wojtowicz M, Dakheel O, Bernstein S, Liewehr DJ, et al. The Immunological and Clinical Effects of Mutated Ras Peptide Vaccine in Combination With IL-2, GM-CSF, or Both in Patients With Solid Tumors. *J Trans Med* (2014) 12:55. doi: 10.1186/1479-5876-12-55

Conflict of Interest: FM is an employee for Hangzhou Neoantigen Therapeutics Co., Ltd and Hangzhou Al-Force Therapeutics. SZ, NH, DM, HW, XG, KL, MQ, QH, LL, and SC are employees for Hangzhou Neoantigen Therapeutics Co., Ltd.

The remaining authors declare that the research was conducted in the absence of any commercial or financial relationships that could be construed as a potential conflict of interest.

Publisher's Note: All claims expressed in this article are solely those of the authors and do not necessarily represent those of their affiliated organizations, or those of the publisher, the editors and the reviewers. Any product that may be evaluated in this article, or claim that may be made by its manufacturer, is not guaranteed or endorsed by the publisher.

frontiers in Immunology

ORIGINAL RESEARCH
published: 21 September 2021
doi: 10.3389/fimmu.2021.707977

Epitope Profiling Reveals the Critical Antigenic Determinants in SARS-CoV-2 RBD-Based Antigen

*Min Jiang[1], Gaiping Zhang[1], Hongliang Liu[1,2], Peiyang Ding[1], Yunchao Liu[2,3], Yuanyuan Tian[1,2], Yanwei Wang[1,2] and Aiping Wang[1]**

[1] School of Life Sciences, Zhengzhou University, Zhengzhou, China, [2] Henan Zhongze Bioengineering Co., Ltd., Zhengzhou, China, [3] Key Laboratory of Animal Immunology, Henan Academy of Agricultural Sciences, Zhengzhou, China

The ongoing COVID-19 pandemic caused by SARS-CoV-2 is a huge public health crisis for the globe. The receptor-binding domain (RBD) of SARS-CoV-2 spike (S) protein plays a vital role in viral infection and serves as a major target for developing neutralizing antibodies. In this study, the antibody response to the RBD of SARS-CoV-2 S protein was analyzed by a panel of sera from animals immunized with RBD-based antigens and four linear B-cell epitope peptides (R345, R405, R450 and R465) were revealed. The immunogenicity of three immunodominant peptides (R345, R405, R465) was further accessed by peptide immunization in mice, and all of them could induced potent antibody response to SARS-CoV-2 S protein, indicating that the three determinants in the RBD were immunogenic. We further generated and characterized monoclonal antibodies (15G9, 12C10 and 10D2) binding to these epitope peptides, and finely mapped the three immunodominant epitopes using the corresponding antibodies. Neutralization assays showed that all three monoclonal antibodies had neutralization activity. Results from IFA and western blotting showed that 12C10 was a cross-reactive antibody against both of SARS-CoV-2 and SARS-CoV. Results from conservative and structural analysis showed that ^{350}VYAWN^{354} was a highly conserved epitope and exposed on the surface of SARS-CoV-2 S trimer, whereas ^{473}YQAGSTP^{479} located in the receptor binding motif (RBM) was variable among different SARS-CoV-2 strains. ^{407}VRQIAP^{412} was a highly conserved, but cryptic epitope shared between SARS-CoV-2 and SARS-CoV. These findings provide important information for understanding the humoral antibody response to the RBD of SARS-CoV-2 S protein and may facilitate further efforts to design SARS-CoV-2 vaccines and the target of COVID-19 diagnostic.

Keywords: SARS-CoV-2, spike protein, RBD, monoclonal antibody, epitope

OPEN ACCESS

Edited by:
Shisong Jiang, University of Oxford, United Kingdom

Reviewed by:
Marion E. G. Brunck, Monterrey Institute of Technology and Higher Education (ITESM), Mexico
Thorsten Demberg, Marker Therapeutics, United States

***Correspondence:**
Aiping Wang
pingaw@126.com

Specialty section:
This article was submitted to Vaccines and Molecular Therapeutics, a section of the journal Frontiers in Immunology

Received: *11 May 2021*
Accepted: *03 September 2021*
Published: *21 September 2021*

Citation:
Jiang M, Zhang G, Liu H, Ding P, Liu Y, Tian Y, Wang Y and Wang A (2021) Epitope Profiling Reveals the Critical Antigenic Determinants in SARS-CoV-2 RBD-Based Antigen. Front. Immunol. 12:707977. doi: 10.3389/fimmu.2021.707977

INTRODUCTION

Common coronaviruses (CoVs) have been circulating in humans for a long time, which usually cause mild to moderate diseases, like the common cold. However, three beta-CoVs (SARS-CoV, MERS-CoV and SARS-CoV-2) infections have caused large outbreaks in recent years (1–3). Especially, SARS-CoV-2 has caused a global pandemic, namely the coronavirus disease in 2019

(COVID-19) (4). According to real-time data from Worldometer (updated on August 12, 2021), 220 countries and territories around the world have reported a total of 205,512,912 confirmed cases of the coronavirus COVID-19 and a death toll of 4,337,588 deaths (https://www.worldometers.info/coronavirus/countries-where-coronavirus-has-spread/). Unfortunately, the first COVID-19 wave has never really ended in some countries, and a new COVID-19 surge is on track this fall and winter, meaning more severe COVID-19 cases and potentially higher mortality (https://www.cdc.gov/coronavirus/2019-ncov/covid-data/covidview/index.html). Various modalities of vaccines against SARS-CoV-2, based on different routes and immunization procedures, have been approved for marketing worldwide (5). However, the antigen epitopes in these vaccines are poorly understood.

Similar to SARS-CoV in genome structure, SARS-CoV-2 has a single-stranded positive-sense (+ss) RNA genome varies from 29.8 kb to 29.9 kb in length, including two large ORFs (ORF1a and ORF1ab) encoding the polyproteins (pp1a, and pp1ab), four structural protein genes encoding proteins envelope (E), membrane (M), nucleocapsid (N) and spike (S), and some accessary protein genes (i.e., ORF3a, ORF6, ORF7a, ORF7b, ORF8, ORF10) (6, 7).The entry of SARS-CoV-2 into its host cells depends on interaction between the S protein with the angiotensin-converting enzyme 2 (ACE2) receptor on host cells and virus-host membrane fusion mediated by S protein (8). As other CoVs, the S protein of SARS-CoV-2 is cleaved into two functional subunits, S1 and S2, *via* the furin site (682-685 aa) (9). Binding with ACE2 triggers membrane fusion activation, in which S is further cleaved by a second proteolytic site (S2′) to release fusion peptide (10, 11). Therefore, hindering viral engagement with ACE2 is an efficient strategy to prevent the virus entry. In addition, the S glycoprotein of CoVs is surface-exposed. Multiple studies have been launched to assess the immunogenicity of structural domains of S protein. Currently, most of the potent antibodies are against CoVs RBD (11–14). This makes the RBD of SARS-CoV-2 S protein is the primary candidate for clinical interventions and vaccine design (15, 16).

The high-resolution structure of SARS-CoV-2 RBD bound with ACE2 suggested that the overall ACE2-binding mode of SARS-CoV-2 is similar to SARS-CoV (17–19). According to amino acid alignment, the RBDs of SARS-CoV and SARS-CoV-2 share 73.5% homology (20). Because of the high similarity in structure and sequence, the RBDs of the two viruses may have cross-reactive epitopes which can induce cross-reactive antibodies. The serum of SARS-CoV convalescent patients and several SARS-CoV antibodies have been shown to confer react to SARS-CoV-2 as well (21–25). However, there is a gap in knowledge on the broad cross-protective epitopes shared between SARS-CoV-2 and SARS-CoV. Currently, findings on SARS-CoV-2 B cell epitopes mainly include the determination of antigen-antibody structural complex, bioinformatics prediction and Pepscan (26–29). Undoubtedly, determination the complex structure is the most accurate method for epitope identification, but it is not readily applicable to many antigens and antibodies, for its laborious efforts with a low success rate. The accuracy of bioinformatics prediction is unclear and the obtained epitopes need further experimental verification. The sera (polyclonal antibodies) from COVID-19 convalescent individuals were mostly used to identify SARS-CoV-2 epitopes by the Pepscan method (30–32). Further studies that involve the determination of the minimum functional motif for antibody binding and the isolation of the monoclonal antibodies (mAbs) targeting these linear epitopes will be needed.

Here, we attempted to analyze the antibody response to the RBD of SARS-CoV-2. We screened the linear B-cell epitope peptides in a panel of sera from animals (swine/mouse) immunized with RBD-based antigens using overlapping peptides spanning the RBD of SARS-CoV-2 S protein. After synthesis and conjugation, the immunogenicity of these immunodominant epitope peptides was further validated by immunizing mice. Furthermore, the monoclonal antibodies binding to these immunodominant epitope peptides were generated and characterized. In addition, the variable regions of these antibodies were sequenced and the immunodominant epitopes in the SARS-CoV-2 RBD were finely mapped. The conservation of these epitopes was analyzed across various virus isolates. The spatial distribution and structural property of these epitopes were analyzed by mapping to the structures of SARS-CoV-2 RBD-ACE2 complex and S trimer.

MATERIALS AND METHODS

Cells and Serum

Human embryonic kidney 293T (HEK293T) cells were obtained from ATCC (Manassas, VA, USA) and maintained in Dulbecco's modified Eagle's medium (DMEM, Solarbio, Beijing, China) supplemented with 10% (v/v) fetal bovine serum (FBS, Gibco, USA). The sera of animals used to screen the linear B-cell epitope peptides and SP2/0 myeloma cells were kindly provided by Henan Provincial Key Laboratory of Animal Immunology, Henan Academy of Agricultural Sciences (Zhengzhou, China). These animals were vaccinated with the recombinant proteins designed based on SARS-CoV-2 RBD containing adjuvants (aluminum hydroxide/CpG1018). SP2/0 cells were maintained in Roswell Park Memorial Institute 1640 (RPMI1640, Solarbio, Beijing, China) medium supplemented with 10% (v/v) FBS (Gibco, USA).

Peptide Design and Synthesis

To analyze the humoral response to SARS-CoV-2 RBD, 22 overlapping peptides with 5 amino acids offsets covering the RBD were synthesized based on the reference sequence of SARS-CoV-2 S protein (GenBank: YP_009724390) (**Figure 1A** and **Table 1**). To obtain higher mapping resolution, the truncation library was designed through a systematic truncation of the identified epitope peptides (**Table 4**). All peptides which were designed with cysteine residues at the N-terminus were synthesized by Sangon Biotech Co., Ltd. (Shanghai, China). The purity of the synthetic peptides was equal to or greater than 95%.

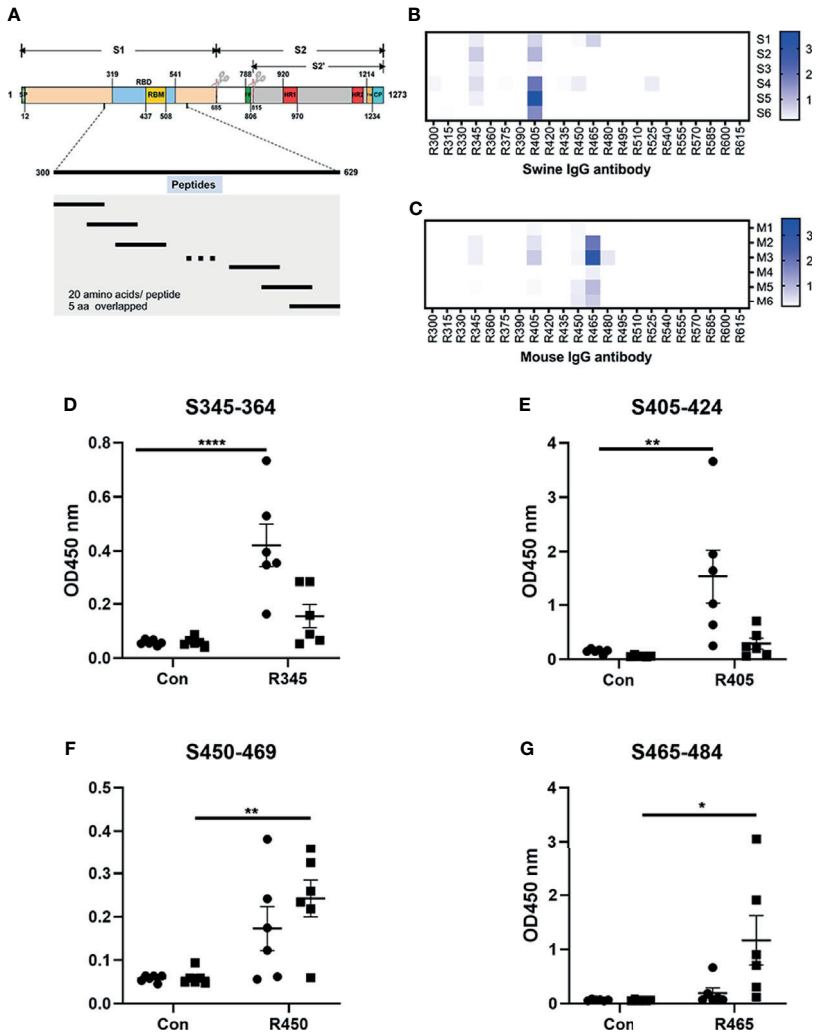

FIGURE 1 | Analysis of B-cell epitope peptides of serum antibodies against SARS-CoV-2 RBD. **(A)** Schematic representation of the functional domains of S protein of SARS-CoV2 and the overlapped peptides spanning the RBD of SARS-CoV2. The S protein consist of two functional subunits (S1 and S2). The S1/S2 cleavage sites are indicated by the scissors. SP, signal peptide. FP, fusion peptide. HR1, heptad repeat 1. HR2, heptad repeat 2. TM, transmembrane domain. CP, cytoplasm domain. RBD, receptor-binding domain. RBM, receptor-binding motif. The amino acid residues number in each domain indicates their position in the S protein. **(B, C)** The reactivity of sera from immunized animals with peptide array was determined by ELISA. S1-S6, sera from swine immunized with RBD-based antigens. M1-M6, sera from mice immunized with RBD-based antigens. R300-R615, 20-mer overlapped peptides covering the RBD. The shade of blue is directly proportional to OD450 value. **(D–G)** Immunodominant epitope peptides binding with the antibodies in sera from swine/mouse immunized with RBD-based antigens. Closed circle, sera from swine immunized with RBD-based antigens. Closed square, sera from mice immunized with RBD-based antigens. Data was shown as mean ± SEM. *$p < 0.05$; **$p < 0.01$; ****$p < 0.0001$. Graphs were made in GraphPad Prism version 8.0.2.

Peptide-Based ELISA

Peptide-based ELISA were performed according to described previously (33). Briefly, the 96-well plates were coated with the peptides (250 ng/well) in 0.05 M carbonate–bicarbonate buffer (CBS, pH 9.6) and incubated overnight at 4°C. After washing thrice with PBST (1× PBS with 0.05% Tween 20, pH 7.4), the plates were blocked with 5% skim milk at 37°C for 2h. Mouse serum samples diluted at 1:100 and swine serum samples diluted at 1:1000 were added to each well and incubated at 37°C for 30 min. The wells were washed thrice with PBST and incubated with HRP-conjugated goat anti-mouse IgG or goat anti-swine IgG diluted at 1:5000 at 37°C for 30 min. The reactions were developed using TMB. The OD values of each well were measured at 450 nm using an ELISA microplate reader.

Monoclonal Antibodies Generation and Characterization

In order to prepare mAbs against these identified epitope peptides, the peptides (R345, R405, R465) designed with cysteine residues at the N-terminus were conjugated to the carrier protein, bovine serum albumin (BSA, Jackson ImmunoResearch Inc., USA), using the sulfosuccinimidyl 4-[N-maleimidomethyl] cyclohexane-1-

TABLE 1 | Overlapped peptides spanning the RBD of SARS-CoV-2 S protein in this work.

Name	Peptides	Name	Peptides
R300	KCTLKSFTVEKGIYQTSNFR	R465	ERDISTEIYQAGSTPCNGVE
R315	TSNFRVQPTESIVRFPNITN	R480	CNGVEGFNCYFPLQSYGFQP
R330	PNITNLCPFGEVFNATRFAS	R495	YGFQPTNGVGYQPYRVVVLS
R345	TRFASVYAWNRKRISNCVAD	R510	VVVLSFELLHAPATVCGPKK
R360	NCVADYSVLYNSASFSTFKC	R525	CGPKKSTNLVKNKCVNFNFN
R375	STFKCYGVSPTKLNDLCFTN	R540	NFNFNGLTGTGVLTESNKKF
R390	LCFTNVYADSFVIRGDEVRQ	R555	SNKKFLPFQQFGRDIADTTD
R405	DEVRQIAPGQTGKIADYNYK	R570	ADTTDAVRDPQTLEILDITP
R420	DYNYKLPDDFTGCVIAWNSN	R585	LDITPCSFGGVSVITPGTNT
R435	AWNSNNLDSKVGGNYNYLYR	R600	PGTNTSNQVAVLYQDVNCTE
R450	NYLYRLFRKSNLKPFERDIS	R615	VNCTEVPVAIHADQL

carboxylate (Sulfo-SMCC, Thermo Scientific, USA). Peptide–BSA conjugates were served as the immunogens. The recombinant SARS-CoV-2 S1 protein (Sino Biological, Beijing, China) was used as the coating antigen in ELISA to determine serum titer of mice and screen for positive hybridomas. Twenty 6- to 8-week-old female BALB/c mice were randomly into four groups. The immunization scheme was as schematic **Figure 2A**. Mice were subcutaneously immunized with 20 μg of each immunogen emulsified with Freund's adjuvant (Sigma-Aldrich, Shanghai, China) at 0, 14, and 28 days post prime-immunization (dpi). Mice from groups 1-3 were immunized with R345-BSA, R405-BSA, R465-BSA, respectively. Mice from group 4 were immunized with BSA as the negative control. All four groups were immunized three times at an interval of 2 weeks (0, 14, 28 dpi), while serum samples were collected 2 weeks after each immunization (14, 28, 42 dpi). The mice with the highest antibody titers in group 1-3 were given the last boost (at 42 dpi) with 40μg immunogens (without any adjuvant) by intravenous injection to prepare mAbs by hybridoma technology. Four days after the last boost (46 dpi), splenocytes from the mice were collected and fused with SP2/0 myeloma cells using PEG 1500. The unconjugated peptides (≥ 20 aa) could be used directly in the peptide-based ELISA (34). In order to obtain the specific mAbs against the B-cell epitope peptides, both the unconjugated peptides and SARS-CoV-2 S1 protein were used to screen for positive hybridomas, respectively. The positive hybridomas were further subcloned more than three times by the limiting dilution method. After subcloning, the positive hybridoma cells were injected into BALB/c mice and the ascites were collected. The subtypes of these mAbs were determined by mouse monoclonal antibody subtype identification kit (Proteintech, Wuhan, China). The antibody titers of these mAbs were detected by ELISA. Briefly, 96-well plates were coated with SARS-CoV-2 S1 protein. Hybridoma clone supernatants or ascites fluid were used as the primary antibody. The other steps refer to the peptide-based ELISA

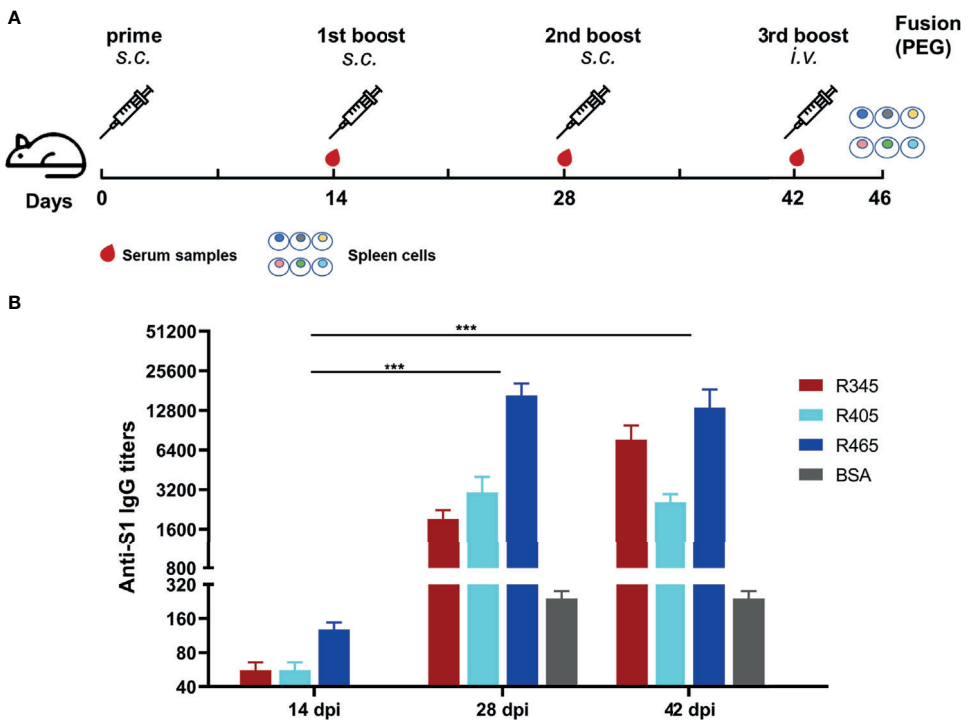

FIGURE 2 | Immunization strategies and antibody responses in mice. **(A)** Scheme of immunization and sampling. Serum samples were collected 2 weeks after each immunization. Each immunogen plus with Freund's adjuvant by subcutaneous (*s.c.*) injection for the immunizations at 0, 14, and 28 dpi. The mice with the highest antibody titers in each group were given the 3rd boost by intravenous (*i.v.*) injection at 42 dpi for mAbs preparation. **(B)** Titers of serum samples at 14, 28, and 42 dpi were detected by ELISA. Data was shown as mean ± SEM. ***$p < 0.001$. Graphs were made in GraphPad Prism version 8.0.2.

protocol. The neutralization capacity of these mAbs was assessed with a commercial SARS-CoV-2 Surrogate Virus Neutralization Test (sVNT) kit (GenScript, Nanjing, China) according to the manufacturer's instruction. Negative control was a mAb against African swine fever virus p54 protein.

Immunofluorescence Assay

The specific binding of these mAbs to SARS-CoV-2 S protein was further confirmed by IFA. Briefly, HEK293T cells were seeded at 2.5×10^5 cells/well into a 24-well plate one day prior to transfection. When the cells in each well were 70–80% confluent, the cells were transfected with the recombinant plasmid pLVX-S that contained the full-length S protein gene (GenBank: YP_009724390). At 24 h post-transfection, the plates were fixed with methanol containing 1% H2O2 (precooled to −20°C) for 15 min at room temperature (RT). Then, the plates were washed with PBST and blocked with 5% skim milk. Next, the plates were incubated with the identified mAbs for 30 min at 37°C. Subsequently, the plates were washed for three times and incubated with goat anti-mouse IgG (H+L)-Alexa Fluor 488 (Invitrogen, Rockford, IL, USA). At last, the plates were stained by 4′,6-diamidino-2-phenylindole (DAPI, Solarbio, Beijing, China) and the fluorescence signals were developed by fluorescence microscopy (ZEISS, Jena, Germany).

Western Blotting Analysis

The reactivity of these mAbs with the S proteins of SARS-CoV-2, SARS-CoV and MERS-CoV was determined by western blotting analysis. SARS-CoV-2 S1 subunit (YP_009724390.1, Val16-Arg685), SARS-CoV S1 subunit (AAX16192.1, Met1-Arg667) and MERS-CoV S1 subunit (AFS88936.1, Met1-Glu725) were purchased from Sino Biological Inc. The proteins were subjected to 10% NuPAGE™ Bis-Tris gels (Invitrogen, Rockford, IL, USA) and performed by blotting from the gels with iBlot™ 2 Transfer Stacks (Invitrogen, Rockford, IL, USA). The membranes were blocked with 5% skim milk and incubated with the identified mAbs, respectively. HRP-conjugated goat anti-mouse IgG was used with a 1:10000 dilution as the secondary antibody. The blots were exposed with enhanced chemiluminescent (ECL) substrate (NCM Biotech, China).

Sequencing and Analysis of the mAb Variable Regions

The total RNA of hybridoma cell lines secreting the mAbs was isolated using TRIzol reagent (Invitrogen, USA) and the cDNA was synthesized using PrimeScript™ II 1st strand cDNA synthesis kit (Takara Biomedical Technology (Beijing) Co.) according to the manufacture's protocols. The light- and heavy-chain (VL and VH) variable domains of the mAbs were amplified in two separate polymerase chain reaction (PCR) tests by two mouse Ig-Primer sets according to the previous methods (35, 36). The heavy chain amplification cycles were 95°C for 5 min; 35 cycles of 95°C for 30 sec, 55°C for 30 sec, 72°C for 1 min, and further extension at 72°C for 10 min. The light chain amplification reaction was similar to that of the heavy chain, except that the annealing temperature was replaced by 60°C. The PCR products were gel purified and sequenced by Sangon Biotech Co., Ltd (Shanghai, China). The VH and VL sequences were analyzed using IgBlast and IMGT/V-QUEST (37, 38). Based on results from the tools, the complementarity-determining regions (CDRs) were labeled. The amino acid sequences of the variable regions were aligned by ClustalW method. Tertiary structures of these mAbs were built using SWISS-MODEL and analyzed by the PyMOL Molecular Graphics System (Version 2.3.0, Schrödinger, LLC.).

Conservation Analysis of the Identified Linear Epitopes

To assess the potential cross-reactive epitopes with its close relatives, the RBD sequence of SARS-CoV-2 (Wuhan-Hu-1) S protein was aligned with the consensus sequences from SARS-CoV (WH20) and MERS-CoV (HCoV-EMC). The multiple alignment was created with MegAlign. To deeply analyze the conservation of the identified linear epitopes in the currently circulating SARS-CoV-2 strains, all receptor binding site changes that occurred in different SARS-CoV-2 virus strains were extracted from GISAID database (https://www.gisaid.org/hcov19-mutation-dashboard/), where a total of 431,752 SARS-CoV-2 virus data was collected (updated on 2021-01-28).

RESULTS

Analysis of B-Cell Epitope Peptides of Antibodies in the Sera From Animals Immunized With RBD-Based Antigens

The linear B-cell epitope peptides recognized by sera from animals immunized with RBD-based antigens were screened using 22 overlapping peptides with 5 amino acids offsets spanning the RBD of SARS-CoV-2 S protein (GenBank: YP_009724390) (**Figure 1A** and **Table 1**). Four linear B-cell epitope peptides (R345, R405, R450 and R465) of SARS-CoV-2 RBD were screened (**Figures 1B–G**). Three B-cell epitope peptides, R345, R405, and R465 strongly reacted with sera from some of the animals. The B-cell epitope peptide, R450, mildly reacted with all serum samples. Interestingly, two epitope peptides (R345, R405) were strongly recognized by swine sera, but weaker by mouse sera (**Figures 1D, E**). The epitope peptides (R450 and R465) were strongly recognized by mouse sera, but weaker by swine sera (**Figures 1F, G**). We speculated that this may be due to differences in ACE2 receptors between pigs and mice (39).

Mouse Immunizations, Antibody Responses, and Generation of mAbs Targeting the Identified Linear B-Cell Epitope Peptides

The SARS-CoV-2 S protein-specific antibodies were detected by ELISA (**Figure 2B**). As shown in **Figure 2B**, the antibody titers at 28 dpi and 42 dpi were significantly higher than those at 14 dpi, indicating that potent antibody responses were induced. The antibody titer of group 1 (R345) at 42 dpi was slightly higher than that at 28 dpi, while the antibody titers of groups 2 (R405) and 3 (R465) at 42 dpi were slightly lower than their antibody titers at 28 dpi, indicating that the antibody titers had approximately

reached the peak after three immunizations (**Figure 2B**). The mice with the highest antibody titers (12800 for R345, 3200 for R405, 25600 for R465) in each group were used as spleen donors for further mAbs preparation. The hybridoma cell lines stably secreting specific mAbs against the identified linear B-cell epitope peptides were screened by ELISA based on the peptides and SARS-CoV-2 S protein, and were named as 15G9 (anti-R345), 12C10 (anti-R405) and 10D2 (anti-R465). The antibody titers of these mAbs reached 409600, 819200 and 409600, respectively (**Table 2**). Subtype analysis revealed all mAbs are IgG1, and the light chain types are Kappa (**Table 2**).

Binding and Neutralization Activity of These mAbs

Binding analysis of the mAbs (15G9, 12C10 and 10D2) by IFA revealed that all three mAbs can specifically bind to the SARS-CoV-2 S protein expressed by HEK293T cells (**Figure 3A**). Results from western blotting showed that 15G9 and 10D2 reacted strongly with SARS-CoV-2 S protein, but did not react with SARS-CoV and MERS-CoV S proteins, indicating that the two mAbs specifically recognize SARS-CoV-2 S protein (**Figures 3B, D**). MAb 12C10 reacted strongly with the S proteins of both SARS-CoV-2 and SARS-CoV, indicating that the mAb is cross-reactive between the two coronaviruses, and implying that there may be a cross-reactive epitope in R405 (**Figure 3C**). The neutralization capacity of the mAbs was assessed by a commercial sVNT kit based on antibody-mediated blockage of ACE2-S protein interaction. The results of neutralization analysis showed that all three mAbs could inhibit the interaction between the SARS-CoV-2 S protein with the ACE2 receptor, indicating that they have neutralization activity (**Figure 3E** and **Table 2**).

Detection of VH and VL of mAbs 15G9, 12C10 and 10D2

To further characterize 15G9, 12C10 and 10D2, the variable region of each mAb was amplified and sequenced. Results from sequencing showed that each mAb only has one sequence, further confirming the monoclonality of the hybridoma cell lines (**Figure 4**). Sequence

TABLE 2 | Characteristics of mAbs.

Mab name	Immunogen	Epitope type	Mab type	Titers		IFA	‡SVN
				Supernatants	Ascitic fluid		
15G9	R345-BSA	Linear	IgG1, Kappa	6400	409600	†+	+
12C10	R405-BSA	Linear	IgG1, Kappa	6400	819200	+	+
10D2	R465-BSA	Linear	IgG1, Kappa	800	409600	+	+

†*Positive result.*

‡*Neutralization activity of the mAbs were assessed by a commercial SARS-CoV-2 surrogate virus neutralization test kit (Genscript, Nanjing, China).*

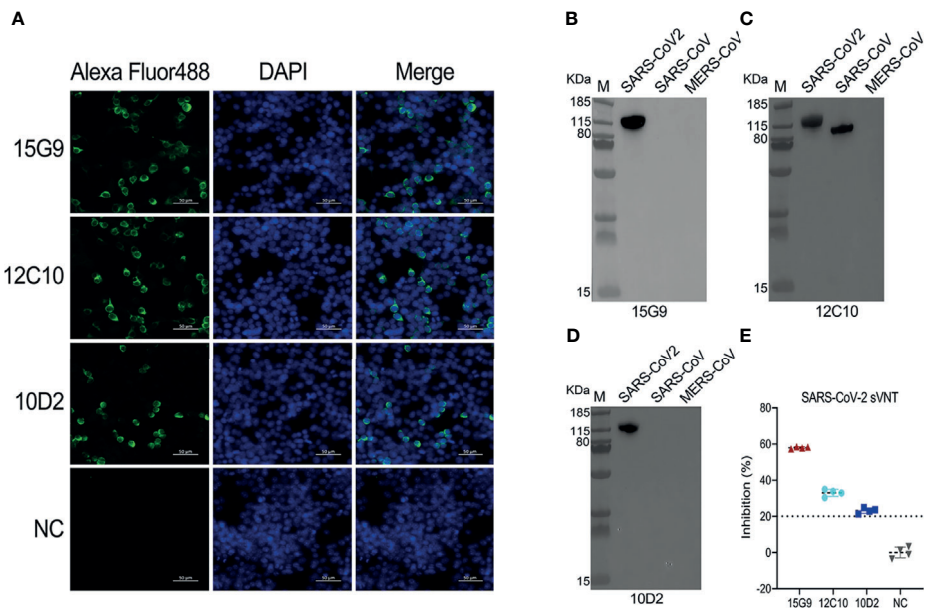

FIGURE 3 | Characterization of the isolated mAbs (15G9, 12C10, 10D2). **(A)** Binding of the mAbs with SARS-CoV-2 S protein expressed in HEK293T cells. MAbs anti-SARS-CoV-2 S protein (green). Nuclei (blue). NC, Negative control. Scale bars, 50 μm. **(B–D)** The reactivity of mAbs with S1 proteins of SARS-CoV-2, SARS-CoV and MERS-CoV was measured by western blotting. **(E)** The neutralization capacity of the mAbs. NC, Negative control.

analysis revealed that 15G9 and 10D2 have the same VL, but the VHs have some difference. Mab 12C10 has vastly different V domains (VL and VH) with 15G9 and 10D2 (**Figure 4A**). Structural alignment further revealed that 15G9 and 10D2 have the identical VL and similar VH. But, 12C10 has distinct tertiary structures with 15G9 and 10D2, especially for CDR-H3 region (**Figures 4B, C**). By comparison with the published mouse sequences, the closest germline gene that the mAbs might originate from were identified, indicating that all three mAbs were derived from productively rearranged sequences. The closest germline genes encoded variable regions of these mAbs were shown in **Table 3**. The closest genes and alleles for the V and J gene of the kappa light chains are same in mAb 15G9 and mAb 10D2, while mAb 12C10 are different. Interestingly, the VL of 12C10 is minimally mutated with only one residue change from the germline gene, and the residue (Asn→Tyr) is located in the CDR-L1 region.

Identification of Minimal Motifs of the Identified Epitope Peptides Using the mAbs

In order to determine the minimal motif of the identified epitope peptides, the peptides (R345, R405, R465) were further truncated and characterized (**Table 4**). The results of peptide-based ELISA showed the reactivity of these truncated peptides with the corresponding mAbs (**Figure 5**). For peptide R345, the N-truncated peptide (^{350}VYAWNRKRISNCVAD^{364}) could be effectively bind to mAb 15G9, while the N-truncated peptide (^{351}YAWNRKRISNCVAD^{364}) had weaker reactivity, compared with peptide (^{350}VYAWNRKRISNCVAD^{364}). In addition, any peptide that was further truncated from the N-terminus of the peptide (^{351}YAWNRKRISNCVAD^{364}) could not bind to mAb 15G9 (**Figure 5A**). The C-truncated peptide (^{345}TRFASV YAWN^{354}) could be effectively recognized by mAb 15G9, while deletion any amino acids at the C-terminus of the peptide showed no reactivity (**Figure 5B**). These results suggested that the motif (^{350}VYAWN^{354}) is the minimal residues required for antibody recognition. For R405, the N-truncated peptide (^{407}VRQIAPGQTGKIADYNYK^{424}) could be well recognized by mAb 12C10, but the binding capability of truncated peptides was completely lost when ^{407}Val was deleted (**Figure 5C**). The C-truncated peptides of R405 were shown to bind mAb 12C10 strongly until ^{412}Gln was removed (**Figure 5D**). This indicated that the motif ^{407}VRQIAP^{412} is a precise linear epitope for antibody binding. MAb 10D2 specific to R465 effectively recognized the N-truncated peptides until the deletion of ^{473}Tyr, while the C-truncated peptides shown to bind mAb 10D2 strongly until ^{479}Pro was removed, indicating that the linear B-cell epitope in R465 is ^{473}YQAGSTP^{479} and both of ^{473}Tyr and ^{479}Pro are critical residues for epitope- antibody interaction (**Figures 5E, F**).

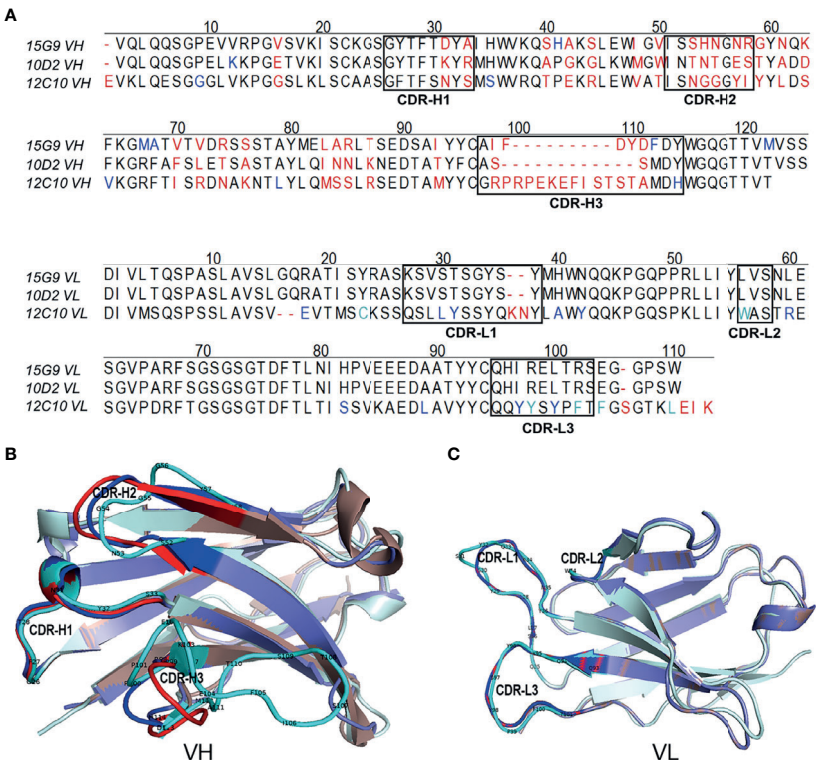

FIGURE 4 | Sequence characteristics of the mAbs. **(A)** Multiple alignment of the variable regions of 15G9, 12C10 and 10D2. The black boxes indicated the complementarity-determining regions (CDRs). **(B)** Structural alignment of VHs for 15G9, 12C10 and 10D2. **(C)** Structural alignment of VLs for 15G9, 12C10 and 10D2. 15G9 (darksalmon), 12C10 (palecyan), 10D2 (slate). The CDRs of 15G9, 12C10, 10D2 were marked as red, cyan and blue, respectively. The variable region sequences of these mAbs had been submitted to GenBank and the accession numbers were MZ751046, MZ751047, MZ751048, MZ751049 and MZ751050, respectively.

TABLE 3 | Sequence characteristics of the SARS-CoV-2 mAbs.

Mab Name		CDRs			Closest germline gene and allele		
		CDR1	CDR2	CDR3	V	D	J
VH	15G9	GYTFTDYA	ISSHNGNR	AIFDYDFDY	IGHV1-67*01	IGHD2-4*01	IGHJ2*01
	10D2	GYTFTKYR	INTNTGES	ASSMDY	IGHV9-3*02	IGHD3-3*01	IGHJ4*01
	12C10	GFTFSNYS	ISNGGGYI	GRPRPEKEFISTSTAMDH	IGHV5-9-3*01	IGHD1-2*01	IGHJ4*01
VL	15G9	KSVSTSGYSY	LVS	QHIRELTRS	IGKV3-12*01	–	IGKJ2*01
	10D2	KSVSTSGYSY	LVS	QHIRELTRS	IGKV3-12*01	–	IGKJ2*01
	12C10	QSLLYSSYQKNY	WAS	QQYYSYPFT	IGKV8-30*01	–	IGKJ4*01

*The number *01 signifies that any new polymorphic sequence will be described by comparison to that allele *01.*

TABLE 4 | Truncation library of the identified epitope peptides used in this work.

Name	Location (aa)	N-term truncations	Name	Location (aa)	C-term truncations
R345-N2	**347-364**	**CFASVYAWNRKRISNCVAD**	**R345-C2**	**345-362**	**CTRFASVYAWNRKRISNCV**
R345-N4	**349-364**	**CSVYAWNRKRISNCVAD**	**R345-C4**	**345-360**	**CTRFASVYAWNRKRISN**
R345-N6	**351-364**	**CYAWNRKRISNCVAD**	**R345-C6**	**345-358**	**CTRFASVYAWNRKRI**
R345-N8	353-364	CWNRKRISNCVAD	**R345-C8**	**345-356**	**CTRFASVYAWNRK**
R345-N10	355-364	CRKRISNCVAD	**R345-C10**	**345-354**	**CTRFASVYAWN**
R405-N2	**407-424**	**CVRQIAPGQTGKIADYNYK**	**R405-C2**	**405-422**	**CDEVRQIAPGQTGKIADYN**
R405-N4	409-424	CQIAPGQTGKIADYNYK	**R405-C4**	**405-420**	**CDEVRQIAPGQTGKIAD**
R405-N6	411-424	CAPGQTGKIADYNYK	**R405-C6**	**405-418**	**CDEVRQIAPGQTGKI**
R405-N8	413-424	CGQTGKIADYNYK	**R405-C8**	**405-416**	**CDEVRQIAPGQTG**
R405-N10	415-424	CTGKIADYNYK	**R405-C10**	**405-414**	**CDEVRQIAPGQ**
R465-N2	**467-484**	**CDISTEIYQAGSTPCNGVE**	**R465-C2**	**465-482**	**CERDISTEIYQAGSTPCNG**
R465-N4	**469-484**	**CSTEIYQAGSTPCNGVE**	**R465-C4**	**465-480**	**CERDISTEIYQAGSTPC**
R465-N6	**471-484**	**CEIYQAGSTPCNGVE**	R465-C6	465-478	CERDISTEIYQAGST
R465-N8	**473-484**	**CYQAGSTPCNGVE**	R465-C8	465-476	CERDISTEIYQAG
R465-N10	475-484	CAGSTPCNGVE	R465-C10	465-474	CERDISTEIYQ
R345-N5	**350-364**	**CVYAWNRKRISNCVAD**	R345-C11	345-353	CTRFASVYAW
R345-N7	352-364	CAWNRKRISNCVAD	**R405-C11**	**405-413**	**CDEVRQIAPG**
R405-N3	408-424	CRQIAPGQTGKIADYNYK	**R405-C12**	**405-412**	**CDEVRQIAP**
R465-N9	474-484	CQAGSTPCNGVE	R405-C13	405-411	CDEVRQIA
			R465-C5	**465-479**	**CERDISTEIYQAGSTP**

The truncated peptides that reacted with the corresponding mAbs.

The Conservation of the Identified Linear B-Cell Epitopes

All residues of epitope ^{407}VRQIAP^{412} were conserved between SARS-CoV-2 and SARS-CoV, explaining the cross-reactivity of mAb 12C10 and indicating that epitope ^{407}VRQIAP^{412} is a cross-reactive epitope for SARS-CoV and SARS-CoV-2 (**Figure 3C** and **Figure 6A**). Out of 5 residues in the epitope ^{350}VYAWN^{354} of SARS-CoV-2, four were conserved between SARS-CoV-2 and SARS-CoV, only one substitution (^{341}E→^{354}N) (**Figure 6A**). Nonetheless, mAb 15G9 targeting the linear epitope ^{350}VYAWN^{354} reacted with SARS-CoV-2 S1, but not with SARS-CoV S1 protein (**Figure 3B**). The results indicated that the difference in reactivity of mAb 15G9 between SARS-CoV-2 and SARS-CoV S proteins was likely due to the residue change (^{341}E→^{354}N). The sequence of epitope ^{473}YQAGSTP^{479} located in RBM, a critical region for ACE2-binding, was vastly different to SARS-CoV and MERS-CoV, revealing the molecular basis of mAb 10D2 specific binding to SARS-CoV-2 (**Figure 3D** and **Figure 6A**). To deeply analyze the conservation of the identified linear epitopes in the currently circulating SARS-CoV-2 strains, all receptor binding site changes obtained from GISAID database which contained a total of 431,752 virus data (updated on 2021-01-28) were labeled (**Figure 6B**). It could be seen that epitope ^{350}VYAWN^{354} and epitope ^{407}VRQIAP^{412} were highly conserved among different SARS-CoV-2 strains. Epitope ^{473}YQAGSTP^{479} overlapped with ACE2-binding residues (^{473}Y, ^{475}A and ^{476}G) was variable, especially for residues ^{477}S and ^{478}T. Currently, ^{477}S had 7 forms of mutations: S477N, S477R, S477I, S477G, S477N, S477T. S477K and S477N was the dominant mutation with a frequency of 21465, second only to N501Y, which has raised public concerns. There were four mutations at site 478: T478I, T478K, T478R, T478A, and the frequency of each mutation was 218, 69, 30, 2, respectively.

Structural Analysis of the Identified Linear B-Cell Epitopes

The spatial distribution and structural property of the experimentally identified epitopes were analyzed by mapping to the SARS-CoV-2 RBD-ACE2 complex (PDB ID: 6M0J) and S trimer (PDB ID: 7A95). Epitope ^{350}VYAWN^{354} and epitope ^{407}VRQIAP^{412} were located in distinct face of SARS-CoV-2

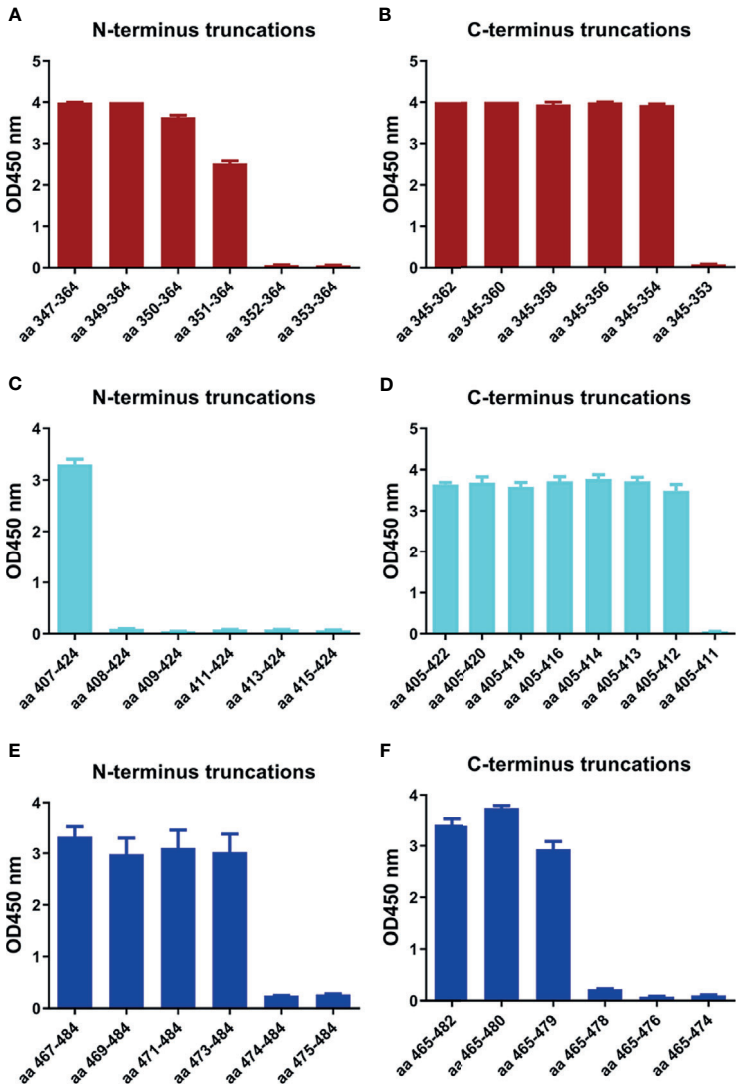

FIGURE 5 | Minimal motifs recognized by the mAbs against the identified linear B-cell peptides. **(A, B)** N-terminal and C-terminal truncations of peptide R345. **(C, D)** N-terminal and C-terminal truncations of peptide R405. **(E, F)** N-terminal and C-terminal truncations of peptide R465.

RBD, and epitope ^{473}YQAGSTP^{479} was located at the RBD loop that bound with the ACE2 receptor (**Figure 7A**). The superposed structure of SARS-CoV RBD-ACE2 complex (PDB ID: 2AJF) and SARS-CoV-2 RBD-ACE2 complex (PDB ID: 6M0J) showed that all the three epitopes contained loop region and epitope ^{407}VRQIAP^{412} was identical between SARS-CoV and SARS-CoV-2, implying that the three epitopes were easily accessible to the antibodies and further confirming that epitope ^{407}VRQIAP^{412} was a common epitope of SARS-CoV and SARS-CoV-2 (**Figure 7B**). Like other coronaviruses, SARS-CoV-2 RBD switches between "up" and "down" conformations by hinge-like movements and can interact with ACE2 only when it is in the "up" configuration (10, 40). Epitope ^{350}VYAWN^{354} located at the exposed surface of S trimer, implying it was accessible to the antibody in both the "down" and "up" forms of S protein (**Figure 7C**). Interestingly, the cross-reactive epitope (^{407}VRQIAP^{412}) of SARS-CoV and SARS-CoV-2 was buried and inaccessible to the antibody when the RBD existed in a "down" conformation (**Figure 7C**). Epitope ^{473}YQAGSTP^{479} located in RBM region of the spike head and overlapped with the ACE2-binding sites, further showing that it was a potential target for stimulating neutralizing antibody that interfere with virus–receptor interactions (**Figure 7C**).

DISCUSSION

The ongoing COVID-19 pandemic caused by SARS-CoV-2 poses a huge threat to global public health and is disrupting societies and economies worldwide. The RBD of SARS-CoV-2 S

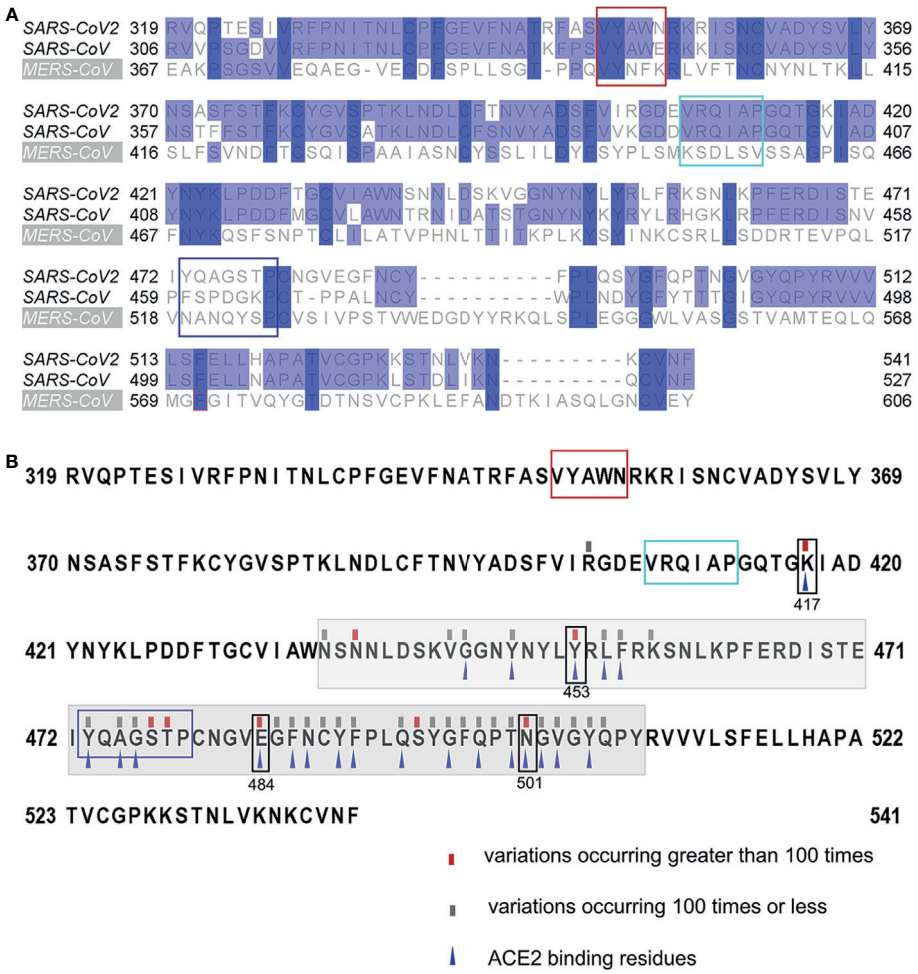

FIGURE 6 | Conservation of the identified linear B-Cell epitopes. **(A)** Multiple sequence alignments of the RBDs of SARS-CoV-2 (Wuhan-Hu-1), SARS-CoV (WH20) and MERS-CoV (HCoV-EMC). **(B)** Mutations found in the RBDs of the currently circulating SARS-CoV-2 strains. All receptor binding site changes reported in GISAID (updated on 2021-01-28) were listed in the figure. The red rectangles indicated variations occurring greater than 100 times at the site. The grey rectangles indicated variations occurring 100 times or less at the site. The grey shading indicated the sequence of the RBM. The blue triangles indicated the residues that interact with ACE2. The box indicated the identified epitopes, epitope ^{351}YAWN^{354} (red), epitope ^{407}VRQIAP^{412} (cyan), epitope ^{473}YQAGSTP^{479} (blue). The black boxes indicated the mutation sites in RBD, included K417N, E484K and N501Y of the novel variant 501Y.V2, N501Y of the B.1.1.7 variant, and Y453F of mink-associated variant strains.

protein plays an essential role in viral infection and is considered as a major antigen for vaccine design (41, 42). Understanding the humoral response to the RBD of SARS-CoV-2 S protein may help find more targeted biomarkers for COVID-19 detect and vaccine development. In this study, the humoral response to RBD-based antigen was profiled by screening the linear B-cell epitopes in a panel of sera from animals (swine/mouse) immunized with RBD-based antigens. Mice are the most commonly used animals in the laboratory for preliminary evaluation of antigen. However, the previous reports had shown that ACE2, the receptor for SARS-CoV-2, from human, *Rhinolophus sinicus* (bat), civet, swine but not mouse mediate SARS-CoV-2 infection *in vitro* (39, 43). Therefore, the swine was also chosen for immunization and evaluation. Furthermore, mAbs (15G9, 12C10, 10D2) binding to the linear B-cell peptides were generated and characterized, and three immunodominant linear B-cell epitopes, ^{350}VYAWN^{354}, ^{407}VRQIAP^{412} and ^{473}YQAGSTP^{479}, on the RBD of SARS-CoV-2 S protein, were finely mapped using the mAbs. These findings may facilitate further understanding the antigenic structure in the SARS-CoV-2 RBD and development of vaccines and immune-based diagnosis.

Analysis of serum antibodies induced by RBD-based antigens revealed four linear antigenic targets (R345, R405, R450 and R465) (**Figure 1**). Previous reports had identified that the peptides S456-460 and S455-469 containing an identical linear B-cell epitope overlap with ACE2-binding residues (31, 44, 45). In addition, the epitope partially overlaps the binding sites of the neutralizing antibody CB6 and the antibody induced by S455-469 had a neutralizing effect on the pseudovirus of SARS-CoV-2, suggesting that it is a neutralizing epitope (44, 45).Consistent with the previous reports, R450 (S450-469) includes the same

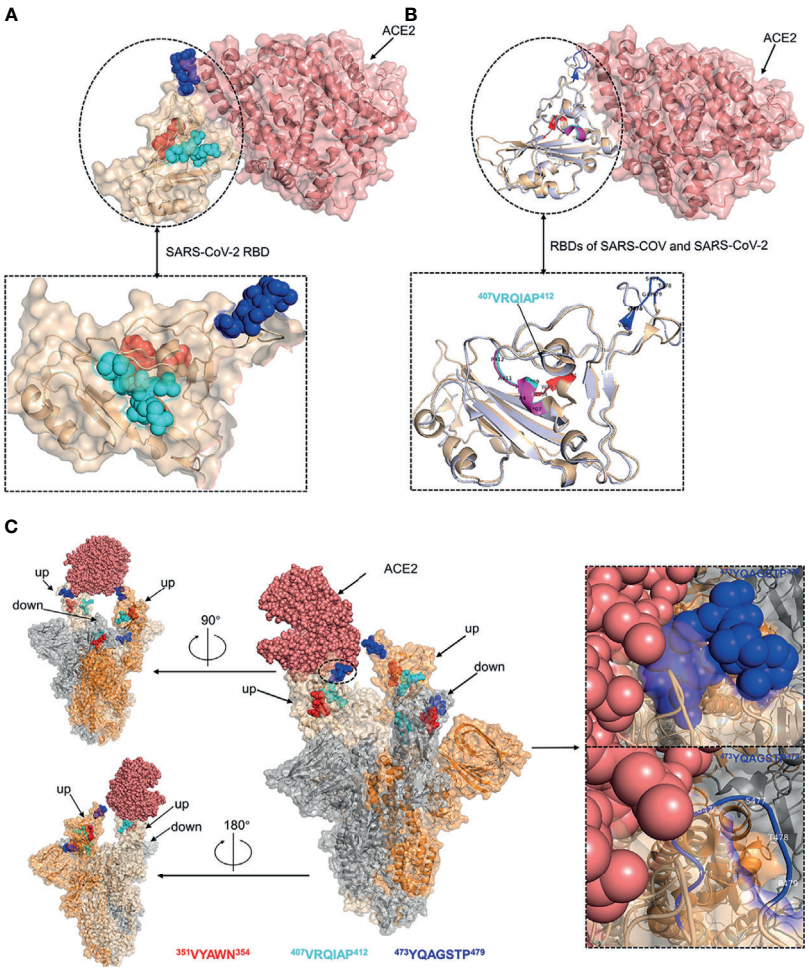

FIGURE 7 | Structural analysis of the identified linear B-cell epitopes. **(A)** The linear B-cell epitopes were mapped on the structure of SARS-CoV-2 RBD-ACE2 complex (PDB ID: 6M0J). Inset was a zoomed-in view of the SARS-CoV-2 RBD. **(B)** The structure of SARS-CoV RBD-ACE2 complex (PDB ID: 2AJF) was superimposed with the structure of SARS-CoV-2 RBD-ACE2 complex (PDB ID: 6M0J). Cartoon representation of the RBDs of SARS-CoV and SARS-CoV-2. Inset was a zoomed-in view of the RBDs of SARS-CoV and SARS-CoV-2. **(C)** The localization of identified epitopes mapped on SARS-CoV-2 S trimer (PDB ID: 7A95). Two RBDs in the open state and one RBD in the closed state. The S monomer configured 'up' and complexed with ACE2 was colored as wheat. The other 'up' configured S monomer was colored as orange. The S monomer in the closed state was colored as grey. Insets were zoomed-in views of the localization of epitope ^{473}YQAGSTP^{479}. Throughout the whole figure, SARS-CoV RBD (whiteblue), SARS-CoV-2 RBD (wheat), ACE2 (salmon pink), epitope ^{407}VRQIAP^{412} on SARS-CoV RBD (magentas), epitope ^{407}VRQIAP^{412} on SARS-CoV-2 RBD (cyan), epitope ^{350}VYAWN^{354} (red), epitope ^{473}YQAGSTP^{479} (blue).

linear B-Cell epitope with the peptides S456-460 and S455-469, indicating that it is a potential neutralizing epitope peptides and can be used as a SARS-CoV-2 vaccine candidate. Peptide immunization *in vivo* showed that the peptides (R345, R405, R465) could induce strong and specific immune responses to SARS-CoV-2 S protein, confirming that they are linear B-cell epitope peptides of SARS-CoV-2 S protein (**Figure 2B**). Furthermore, three hybridoma cell lines secreting the mAbs (15G9, 12C10 and 10D2) that targeted the peptides (R345, R405 and R465) were generated and characterized, respectively (**Figure 3** and **Table 2**). Both of 15G9 and 10D2 specifically recognized the S protein of SARS-CoV-2 (**Figures 3B, D**), whereas mAb12C10 could strongly bind to both of SARS-CoV-2 and SARS-CoV S proteins (**Figure 3C**), indicating that 12C10 is a cross-reactive antibody between SARS-CoV-2 and SARS-CoV. Neutralization analysis showed that all three mAbs had neutralization activity. Consistent with a previous report, mAb 12C10 of R405 and mAb 10D2 of R465 inhibited the RBD-ACE2 interaction with an inhibition rate of 20%–40% (**Figure 3E**), suggesting that R405 and R465 were able to elicit neutralizing antibodies (45).

The amino acid sequence of an antibody, especially the CDRs, is the core of its biological function, and responsible for antibody-antigen response (46, 47). Hybridoma cell lines secreting mAbs may be lost or mutated due to storage accidents, gene drift, or contamination. To protect and characterize the mAbs, we further sequenced and analyzed the variable regions of these antibodies (15 G9, 12C10 and 10D2).

Only one sequence was found for each mAb, further confirming the monoclonality of the hybridoma cell lines. Sequence analysis revealed that all three mAbs were derived from productively rearranged sequences. The CDRs of heavy chain and kappa light chain were also characteristically annotated (**Figure 4** and **Table 3**). A recent study reported that the average CDR-H3 length of SARS-CoV-2 mAb was longer compared to the IgG repertoires of three healthy human donors, consistent with our study (48). The previous report also showed that the predominant subtype of mAbs against SARS-CoV-2 spike is IG1, while all the three mAbs are IgG1 in our work (**Table 2**). In addition, the sequencing analysis of these mAbs may facilitate further antibody engineering, such as species, isotype and subtype switching, and antibody humanization by methods of speciation and affinity maturation.

In order to determine the minimal binding motif of the mAbs (15G9, 12C10 and 10D2), the peptides (R345, R405, R465) were further truncated. As shown in **Figure 5**, ^{350}VYAWN^{354}, ^{407}VRQIAP^{412} and ^{473}YQAGSTP^{479} are the precise epitopes for mAbs binding. Epitope ^{350}VYAWN^{354} overlaps with epitope S348-357 identified by serological analysis of COVID-19 patients, suggesting that it is a natural linear epitope and can be used as a candidate for COVID-19 diagnosis (44). Up to now, no mutation located in epitope ^{350}VYAWN^{354} had been found in a total of 431,752 SARS-CoV-2 virus strains, indicating that it was highly conserved among different SARS-CoV-2 strains (**Figure 6B**). Epitope ^{407}VRQIAP^{412} is consistent with some identified neutralizing epitopes, such as S406-415, S406–420 and S404-426 (44, 45, 49). MAb 12C10 binding to epitope ^{407}VRQIAP^{412} had cross-reactivity between SARS-CoV-2 and SARS-CoV, implying that epitope ^{407}VRQIAP^{412} is a cross-reactive epitope for SARS-CoV-2 and SARS-CoV. Further alignment analysis of SARS-CoV-2 (Wuhan-Hu-1), SARS-CoV (WH20) and MERS-CoV (HCoV-EMC) validated that ^{407}VRQIAP^{412} is the common epitope of SARS-CoV-2 and SARS-Co-V, explaining the mechanism of mAb 12C10 cross-reaction between SARS-CoV-2 and SARS-CoV (**Figure 6A**). Interesting, epitope ^{407}VRQIAP^{412} overlaps with the epitope of a potent therapeutic antibody, H104, that efficiently neutralized SARS-CoV-2 and SARS-CoV pseudoviruses as well as authentic SARS-CoV-2, suggesting that ^{407}VRQIAP^{412} would also a common neutralizing epitope of SARS-CoV-2 and SARS-CoV (25). In addition, ^{407}VRQIAP^{412} was highly conserved across various virus isolates. Therefore, it was considered to be a promising candidate for structure-based universal vaccine design. Like CR3022, epitope ^{407}VRQIAP^{412} was located in the trimeric interface and was only exposed on the "up" conformation (**Figure 7C**), implying mAb 12C10 would sterically block ACE2 receptor binding (21). Epitope ^{473}YQAGSTP^{479} also partially overlaps the binding sites of the human neutralizing mAb CB6, indicating that the epitope is a neutralizing epitope (13). Similar to CB6, it may be inferred that the antibody targeting epitope ^{473}YQAGSTP^{479} may interfere with virus–receptor interactions through both steric hindrance and direct competition with interface residues. By comparing with the mutations documented in 431,752 SARS-CoV-2 strains (GISAID), we found that five (^{473}Y, ^{475}A, ^{476}G, ^{477}S and ^{478}T) out of 7 residues in epitope ^{473}YQAGSTP^{479} were variable (**Figure 6B**). Epitope ^{473}YQAGSTP^{479} is localized in RBM and the residues 473, 475 and 476 are ACE2-binding sites (**Figure 7**). Some novel SARS-CoV-2 variants has been found to harbor mutations in the S protein, and increase the affinity between SARS-CoV-2 and the ACE2 receptor, accelerate the transmission of the virus and exhibit substantial or complete escape from therapeutically relevant mAbs/convalescent plasma (https://virological.org/t/preliminary-genomic-characterisation-of-an-emergent-sars-cov-2-lineage-in-the-uk-defined-by-a-novel-set-of-spike-mutations/563) (50–52). Most neutralizing epitopes in the RBD of SARS-CoV S protein could be completely disrupted by single amino acid substitutions (e.g., D429A, R441A or D454A) or by deletions of several amino acids at the N-terminal or C-terminal region of the RBD (53). Although the mutations at sites 473, 475 and 476 presented in a few virus strains at present, but they should still cause a great concern of the potential to reduce the binding affinity and effectiveness of antibodies. Currently, no evidence showed that the mutations at sites 477 and 478 of SARS-CoV-2 S protein result in reducing the protection of antibodies and affecting virus-host interaction. However, the mutations occurred in epitope ^{473}YQAGSTP^{479}, which located in RBM and overlapped with ACE2-binding residues, probably beneficial for the virus in some way that has not been revealed. In addition, the mutations frequency of site 477 was 21465, second only to N501Y (with a frequency of 26174). It may be also beneficial for the virus when the same mutation is independently selected multiple times. Actual effects of these mutations will require further efforts.

Overall, four linear B-cell epitope peptides of SARS-CoV-2 (R345, R405, R450 and R465) were screened utilizing sera from animals vaccinated with RBD-based antigens and strong responses to three linear B-cell epitope peptides (R345, R405 and R465) were observed. The immunogenicity of the three peptides was further accessed by peptide immunization in mice and all of them could induced potent antibody response to SARS-CoV-2 S protein. Furthermore, three potential neutralizing mAbs (15G9, 12C10 and 10D2) binding to the antigenic peptides (R345, R405, R465) were further generated and characterized. Among of these antibodies, 12C10 is a cross-reactive antibody against SARS-CoV-2 and SARS-CoV. In addition, the variable regions of these antibodies were sequenced and three immunodominant epitopes in the SARS-CoV-2 RBD were finely mapped using these mAbs. Among of these epitopes, ^{350}VYAWN^{354} is specific for SARS-CoV-2 S protein and highly conserved in different SARS-CoV-2 strains; ^{407}VRQIAP^{412} is a cross-reactive epitope shared between SARS-CoV-2 and SARS-CoV; ^{473}YQAGSTP^{479} located in RBM is variable among different SARS-CoV-2 strains. Aside from scientific significance for understanding the antigenic structure, function, antibody–antigen interaction, these findings may facilitate further efforts to design SARS-CoV-2 vaccines and the target of COVID-19 diagnostic.

DATA AVAILABILITY STATEMENT

The original contributions presented in the study are included in the article/supplementary material. Further inquiries can be directed to the corresponding author.

ETHICS STATEMENT

The animal study was reviewed and approved by the Ethical and Animal Welfare Committee of Henan Academy of Agricultural Sciences (Approval number SYXK 2021-0003).

AUTHOR CONTRIBUTIONS

GZ, AW and MJ conceptualized and designed this study. MJ, PD, YT and YW conducted the most experiments. YL collected and prepared the serum samples. MJ and HL performed figure preparation and prepared the manuscript. AW revised the manuscript. All authors contributed to the article and approved the submitted version.

FUNDING

This work was supported by the National Natural Science Foundation of China (Grant No. 32072944); Henan Scientific Research Project on Prevention and Control of COVID-19 epidemic (Grant No. 211100310200).

REFERENCES

1. van den Brand JM, Smits SL, Haagmans BL. Pathogenesis of Middle East Respiratory Syndrome Coronavirus. *J Pathol* (2015) 235(2):175–84. doi: 10.1002/path.4458
2. Lee PI, Hsueh PR. Emerging Threats From Zoonotic Coronaviruses-From SARS and MERS to 2019-Ncov. *J Microbiol Immunol Infect* (2020) 53(3):365–7. doi: 10.1016/j.jmii.2020.02.001
3. Liu J, Zheng X, Tong Q, Li W, Wang B, Sutter K, et al. Overlapping and Discrete Aspects of the Pathology and Pathogenesis of the Emerging Human Pathogenic Coronaviruses SARS-CoV, MERS-CoV, and 2019-Ncov. *J Med Virol* (2020) 92(5):491–4. doi: 10.1002/jmv.25709
4. Mahase E. Covid-19: WHO Declares Pandemic Because of "Alarming Levels" of Spread, Severity, and Inaction. *BMJ* (2020) 368:m1036. doi: 10.1136/bmj.m1036
5. Chen M, Yuan Y, Zhou Y, Deng Z, Zhao J, Feng F, et al. Safety of SARS-CoV-2 Vaccines: A Systematic Review and Meta-Analysis of Randomized Controlled Trials. *Infect Dis Poverty* (2021) 10(1):94. doi: 10.1186/s40249-021-00878-5
6. Song Z, Xu Y, Bao L, Zhang L, Yu P, Qu Y, et al. From SARS to MERS, Thrusting Coronaviruses Into the Spotlight. *Viruses* (2019) 11(1):59. doi: 10.3390/v11010059
7. Khailany RA, Safdar M, Ozaslan M. Genomic Characterization of a Novel SARS-CoV-2. *Gene Rep* (2020) 19:100682. doi: 10.1016/j.genrep.2020.100682
8. Walls AC, Park YJ, Tortorici MA, Wall A, McGuire AT, Veesler D. Structure, Function, and Antigenicity of the SARS-CoV-2 Spike Glycoprotein. *Cell* (2020) 181(2):281–92.e6. doi: 10.1016/j.cell.2020.02.058
9. Ou X, Liu Y, Lei X, Li P, Mi D, Ren L, et al. Characterization of Spike Glycoprotein of SARS-CoV-2 on Virus Entry and Its Immune Cross-Reactivity With SARS-CoV. *Nat Commun* (2020) 11(1):1620. doi: 10.1038/s41467-020-15562-9
10. Benton DJ, Wrobel AG, Xu P, Roustan C, Martin SR, Rosenthal PB, et al. Receptor Binding and Priming of the Spike Protein of SARS-CoV-2 for Membrane Fusion. *Nature* (2020) 588(7837):327–30. doi: 10.1038/s41586-020-2772-0
11. Ju B, Zhang Q, Ge J, Wang R, Sun J, Ge X, et al. Human Neutralizing Antibodies Elicited by SARS-CoV-2 Infection. *Nature* (2020) 584(7819):115–9. doi: 10.1038/s41586-020-2380-z
12. Huo J, Le Bas A, Ruza RR, Duyvesteyn HME, Mikolajek H, Malinauskas T, et al. Neutralizing Nanobodies Bind SARS-CoV-2 Spike RBD and Block Interaction With ACE2. *Nat Struct Mol Biol* (2020) 27(9):846–54. doi: 10.1038/s41594-020-0469-6
13. Shi R, Shan C, Duan X, Chen Z, Liu P, Song J, et al. A Human Neutralizing Antibody Targets the Receptor-Binding Site of SARS-CoV-2. *Nature* (2020) 584(7819):120–4. doi: 10.1038/s41586-020-2381-y
14. Tortorici MA, Beltramello M, Lempp FA, Pinto D, Dang HV, Rosen LE, et al. Ultrapotent Human Antibodies Protect Against SARS-CoV-2 Challenge *via* Multiple Mechanisms. *Science* (2020) 370(6519):950–7. doi: 10.1126/science.abe3354
15. Wang N, Shang J, Jiang S, Du L. Subunit Vaccines Against Emerging Pathogenic Human Coronaviruses. *Front Microbiol* (2020) 11:298. doi: 10.3389/fmicb.2020.00298
16. Yang S, Li Y, Dai L, Wang J, He P, Li C, et al. Safety and Immunogenicity of a Recombinant Tandem-Repeat Dimeric RBD-Based Protein Subunit Vaccine (ZF2001) Against COVID-19 in Adults: Two Randomised, Double-Blind, Placebo-Controlled, Phase 1 and 2 Trials. *Lancet Infect Dis* (2021) 21(8):1107–19. doi: 10.1016/S1473-3099(21)00127-4
17. Lan J, Ge J, Yu J, Shan S, Zhou H, Fan S, et al. Structure of the SARS-CoV-2 Spike Receptor-Binding Domain Bound to the ACE2 Receptor. *Nature* (2020) 581(7807):215–20. doi: 10.1038/s41586-020-2180-5
18. Shang J, Ye G, Shi K, Wan Y, Luo C, Aihara H, et al. Structural Basis of Receptor Recognition by SARS-CoV-2. *Nature* (2020) 581(7807):221–4. doi: 10.1038/s41586-020-2179-y
19. Yan R, Zhang Y, Li Y, Xia L, Guo Y, Zhou Q. Structural Basis for the Recognition of SARS-CoV-2 by Full-Length Human ACE2. *Science* (2020) 367(6485):1444–8. doi: 10.1126/science.abb2762
20. Yi C, Sun X, Ye J, Ding L, Liu M, Yang Z, et al. Key Residues of the Receptor Binding Motif in the Spike Protein of SARS-CoV-2 That Interact With ACE2 and Neutralizing Antibodies. *Cell Mol Immunol* (2020) 17(6):621–30. doi: 10.1038/s41423-020-0458-z
21. Yuan M, Wu NC, Zhu X, Lee CD, So RTY, Lv H, et al. A Highly Conserved Cryptic Epitope in the Receptor Binding Domains of SARS-CoV-2 and SARS-CoV. *Science* (2020) 368(6491):630–3. doi: 10.1126/science.abb7269
22. Casadevall A, Henderson JP, Joyner MJ, Pirofski LA. SARS-CoV-2 Variants and Convalescent Plasma: Reality, Fallacies, and Opportunities. *J Clin Invest* (2021) 131(7):e148832. doi: 10.1172/JCI148832
23. Shen C, Wang Z, Zhao F, Yang Y, Li J, Yuan J, et al. Treatment of 5 Critically Ill Patients With COVID-19 With Convalescent Plasma. *JAMA* (2020) 323(16):1582–9. doi: 10.1001/jama.2020.4783
24. Wang C, Li W, Drabek D, Okba NMA, van Haperen R, Osterhaus A, et al. A Human Monoclonal Antibody Blocking SARS-CoV-2 Infection. *Nat Commun* (2020) 11(1):2251. doi: 10.1038/s41467-020-16256-y
25. Lv Z, Deng YQ, Ye Q, Cao L, Sun CY, Fan C, et al. Structural Basis for Neutralization of SARS-CoV-2 and SARS-CoV by a Potent Therapeutic Antibody. *Science* (2020) 369(6510):1505–9. doi: 10.1126/science.abc5881
26. Yoshida S, Ono C, Hayashi H, Fukumoto S, Shiraishi S, Tomono K, et al. SARS-CoV-2-Induced Humoral Immunity Through B Cell Epitope Analysis in COVID-19 Infected Individuals. *Sci Rep* (2021) 11(1):5934. doi: 10.1038/s41598-021-85202-9
27. Fu D, Zhang G, Wang Y, Zhang Z, Hu H, Shen S, et al. Structural Basis for SARS-CoV-2 Neutralizing Antibodies With Novel Binding Epitopes. *PloS Biol* (2021) 19(5):e3001209. doi: 10.1371/journal.pbio.3001209
28. Ahmed SF, Quadeer AA, McKay MR. Preliminary Identification of Potential Vaccine Targets for the COVID-19 Coronavirus (SARS-CoV-2) Based on SARS-CoV Immunological Studies. *Viruses* (2020) 12(3):254. doi: 10.3390/v12030254
29. Oliveira SC, de Magalhaes MTQ, Homan EJ. Immunoinformatic Analysis of SARS-CoV-2 Nucleocapsid Protein and Identification of COVID-19 Vaccine Targets. *Front Immunol* (2020) 11:587615. doi: 10.3389/fimmu.2020.587615
30. Amrun SN, Lee CY, Lee B, Fong SW, Young BE, Chee RS, et al. Linear B-Cell Epitopes in the Spike and Nucleocapsid Proteins as Markers of SARS-CoV-2

Exposure and Disease Severity. *EBioMedicine* (2020) 58:102911. doi: 10.1016/j.ebiom.2020.102911
31. Wang H, Wu X, Zhang X, Hou X, Liang T, Wang D, et al. SARS-CoV-2 Proteome Microarray for Mapping COVID-19 Antibody Interactions at Amino Acid Resolution. *ACS Cent Sci* (2020) 6(12):2238–49. doi: 10.1021/acscentsci.0c00742
32. Poh CM, Carissimo G, Wang B, Amrun SN, Lee CY, Chee RS, et al. Two Linear Epitopes on the SARS-CoV-2 Spike Protein That Elicit Neutralising Antibodies in COVID-19 Patients. *Nat Commun* (2020) 11(1):2806. doi: 10.1038/s41467-020-16638-2
33. Jiang M, Guo J, Zhang G, Jin Q, Liu Y, Jia R, et al. Fine Mapping of Linear B Cell Epitopes on Capsid Protein of Porcine Circovirus 3. *Appl Microbiol Biotechnol* (2020) 104(14):6223–34. doi: 10.1007/s00253-020-10664-2
34. Dubois ME, Hammarlund E, Slifka MK. Optimization of Peptide-Based ELISA for Serological Diagnostics: A Retrospective Study of Human Monkeypox Infection. *Vector Borne Zoonotic Dis* (2012) 12(5):400–9. doi: 10.1089/vbz.2011.0779
35. Xiao S, Yu L, Gu Z. Amplification, Cloning and Sequence Analysis of the Variable Region Genes of Monoclonal Antibody Against Human Bladder Carcinoma. *Zhonghua Wai Ke Za Zhi* (1996) 34(1):13–5.
36. Dang VT, Mandakhalikar KD, Ng OW, Tan YJ. A Simple Methodology for Conversion of Mouse Monoclonal Antibody to Human-Mouse Chimeric Form. *Clin Dev Immunol* (2013) 2013:716961. doi: 10.1155/2013/716961
37. Ye J, Ma N, Madden TL, Ostell JM. IgBLAST: An Immunoglobulin Variable Domain Sequence Analysis Tool. *Nucleic Acids Res* (2013) 41:W34–40. doi: 10.1093/nar/gkt382
38. Ehrenmann F, Kaas Q, Lefranc MP. IMGT/3Dstructure-DB and IMGT/DomainGapAlign: A Database and a Tool for Immunoglobulins or Antibodies, T Cell Receptors, MHC, IgSF and MhcSF. *Nucleic Acids Res* (2010) 38:D301–7. doi: 10.1093/nar/gkp946
39. Li R, Qiao S, Zhang G. Analysis of Angiotensin-Converting Enzyme 2 (ACE2) From Different Species Sheds Some Light on Cross-Species Receptor Usage of a Novel Coronavirus 2019-Ncov. *J Infect* (2020) 80(4):469–96. doi: 10.1016/j.jinf.2020.02.013
40. Gui M, Song W, Zhou H, Xu J, Chen S, Xiang Y, et al. Cryo-Electron Microscopy Structures of the SARS-CoV Spike Glycoprotein Reveal a Prerequisite Conformational State for Receptor Binding. *Cell Res* (2017) 27(1):119–29. doi: 10.1038/cr.2016.152
41. Tai W, He L, Zhang X, Pu J, Voronin D, Jiang S, et al. Characterization of the Receptor-Binding Domain (RBD) of 2019 Novel Coronavirus: Implication for Development of RBD Protein as a Viral Attachment Inhibitor and Vaccine. *Cell Mol Immunol* (2020) 17(6):613–20. doi: 10.1038/s41423-020-0400-4
42. Yang J, Wang W, Chen Z, Lu S, Yang F, Bi Z, et al. A Vaccine Targeting the RBD of the S Protein of SARS-CoV-2 Induces Protective Immunity. *Nature* (2020) 586(7830):572–7. doi: 10.1038/s41586-020-2599-8
43. Zhou P, Yang XL, Wang XG, Hu B, Zhang L, Zhang W, et al. A Pneumonia Outbreak Associated With a New Coronavirus of Probable Bat Origin. *Nature* (2020) 579(7798):270–3. doi: 10.1038/s41586-020-2012-7
44. Shrock E, Fujimura E, Kula T, Timms RT, Lee IH, Leng Y, et al. Viral Epitope Profiling of COVID-19 Patients Reveals Cross-Reactivity and Correlates of Severity. *Science* (2020) 370(6520):eabd4250. doi: 10.1126/science.abd4250
45. Lu S, Xie XX, Zhao L, Wang B, Zhu J, Yang TR, et al. The Immunodominant and Neutralization Linear Epitopes for SARS-CoV-2. *Cell Rep* (2021) 34(4):108666. doi: 10.1016/j.celrep.2020.108666
46. Maynard J, Georgiou G. Antibody Engineering. *Annu Rev BioMed Eng* (2000) 2:339–76. doi: 10.1146/annurev.bioeng.2.1.339
47. Steiniger SC, Dunkle WE, Bammert GF, Wilson TL, Krishnan A, Dunham SA, et al. Fundamental Characteristics of the Expressed Immunoglobulin VH and VL Repertoire in Different Canine Breeds in Comparison With Those of Humans and Mice. *Mol Immunol* (2014) 59(1):71–8. doi: 10.1016/j.molimm.2014.01.010
48. Liu L, Wang P, Nair MS, Yu J, Rapp M, Wang Q, et al. Potent Neutralizing Antibodies Against Multiple Epitopes on SARS-CoV-2 Spike. *Nature* (2020) 584(7821):450–6. doi: 10.1038/s41586-020-2571-7
49. Li L, Zhao Z, Yang X, Li W, Chen S, Sun T, et al. Identification of Four Linear B-Cell Epitopes on the SARS-CoV-2 Spike Protein Able to Elicit Neutralizing Antibodies. *bioRxiv* (2020). doi: 10.1101/2020.12.13.422550
50. Galloway SE, Paul P, MacCannell DR, Johansson MA, Brooks JT, MacNeil A, et al. Emergence of SARS-CoV-2 B.1.1.7 Lineage - United States, December 29, 2020-January 12, 2021. *MMWR Morb Mortal Wkly Rep* (2021) 70(3):95–9. doi: 10.15585/mmwr.mm7003e2
51. Tang JW, Toovey OTR, Harvey KN, Hui DDS. Introduction of the South African SARS-CoV-2 Variant 501Y.V2 Into the UK. *J Infect* (2021) 82(4):e8–10. doi: 10.1016/j.jinf.2021.01.007
52. Wibmer CK, Ayres F, Hermanus T, Madzivhandila M, Kgagudi P, Lambson BE, et al. SARS-CoV-2 501y.V2 Escapes Neutralization by South African COVID-19 Donor Plasma. *Nat Med* (2021) 27(4):622–5. doi: 10.1038/s41591-021-01285-x
53. He Y, Li J, Du L, Yan X, Hu G, Zhou Y, et al. Identification and Characterization of Novel Neutralizing Epitopes in the Receptor-Binding Domain of SARS-CoV Spike Protein: Revealing the Critical Antigenic Determinants in Inactivated SARS-CoV Vaccine. *Vaccine* (2006) 24(26):5498–508. doi: 10.1016/j.vaccine.2006.04.054

Conflict of Interest: HL, YL, YT and YW were employed by Henan Zhongze Bioengineering Co., Ltd.

The remaining authors declare that the research was conducted in the absence of any commercial or financial relationships that could be construed as a potential conflict of interest.

frontiers in Immunology

ORIGINAL RESEARCH
published: 24 September 2021
doi: 10.3389/fimmu.2021.725240

Identification of Unique Peptides for SARS-CoV-2 Diagnostics and Vaccine Development by an *In Silico* Proteomics Approach

Veerbhan Kesarwani[1], *Rupal Gupta*[1,2], *Ramesh Raju Vetukuri*[3]*, *Sandeep Kumar Kushwaha*[1]* and *Sonu Gandhi*[1]*

[1] DBT-National Institute of Animal Biotechnology (NIAB), Hyderabad, India, [2] Amity Institute of Biotechnology, Amity University, Mumbai, India, [3] Department of Plant Breeding, Swedish University of Agricultural Sciences, Alnarp, Sweden

OPEN ACCESS

Edited by:
Min Gong,
Tianjin Medical University, China

Reviewed by:
Said Dermime,
National Center for Cancer Care and Research, Qatar
Narendra Verma,
NYU Grossman School of Medicine, United States
Jitender Kumar,
Amity University, India

***Correspondence:**
Ramesh Raju Vetukuri
Ramesh.Vetukuri@slu.se
Sandeep Kumar Kushwaha
sandeep@niab.org
Sonu Gandhi
gandhi@niab.org.in;
sonugandhi@gmail.com

Specialty section:
This article was submitted to Vaccines and Molecular Therapeutics, a section of the journal Frontiers in Immunology

Received: 15 June 2021
Accepted: 10 September 2021
Published: 24 September 2021

Citation:
Kesarwani V, Gupta R, Vetukuri RR, Kushwaha SK and Gandhi S (2021) Identification of Unique Peptides for SARS-CoV-2 Diagnostics and Vaccine Development by an In Silico Proteomics Approach. Front. Immunol. 12:725240. doi: 10.3389/fimmu.2021.725240

Ongoing evolution of severe acute respiratory syndrome coronavirus 2 (SARS-CoV-2) virus strains is posing new COVID-19 diagnosis and treatment challenges. To help efforts to meet these challenges we examined data acquired from proteomic analyses of human SARS-CoV-2-infected cell lines and samples from COVID-19 patients. Initially, 129 unique peptides were identified, which were rigorously evaluated for repeats, disorders, polymorphisms, antigenicity, immunogenicity, toxicity, allergens, sequence similarity to human proteins, and contributions from other potential cross-reacting pathogenic species or the human saliva microbiome. We also screened SARS-CoV-2-infected NBHE and A549 cell lines for presence of antigenic peptides, and identified paratope peptides from crystal structures of SARS-CoV-2 antigen-antibody complexes. We then selected four antigen peptides for docking with known viral unbound T-cell receptor (TCR), class I and II peptide major histocompatibility complex (pMHC), and identified paratope sequences. We also tested the paratope binding affinity of SARS-CoV T- and B-cell peptides that had been previously experimentally validated. The resultant antigenic peptides have high potential for generating SARS-CoV-2-specific antibodies, and the paratope peptides can be directly used to develop a COVID-19 diagnostics assay. The presented genomics and proteomics-based *in-silico* approaches have apparent utility for identifying new diagnostic peptides that could be used to fight SARS-CoV-2.

Keywords: SARS-CoV-2, COVID-19 vaccines, diagnostic peptides, docking, paratopes, TCR, MHC

INTRODUCTION

According to a World Health Organization report issued in May 2021, the SARS-CoV-2 virus has infected more than 158 million people, causing more than 3.3 million deaths worldwide (1, 2). Moreover, ongoing evolution of SARS-CoV-2 strains is posing constant challenges to develop new COVID-19 diagnoses and treatments for shifting life-threatening symptoms, *inter alia*, fever,

respiratory distress, stomach ache and pneumonia (1–3). The SARS-CoV-2 virus has a 50–200 nm diameter and 27–30 Kb long single-stranded positive-sense RNA genome. This genome encodes large polyproteins (Orf 1a and 1b), four structural proteins (spike glycoprotein, envelope protein, membrane protein, and nucleocapsid protein), and five accessory proteins: Orf3a, Orf6, Orf7a, Orf8, and Orf10 (4). The spike protein is a key protein in host cell membrane attachment, as its S1 subunit binds to the human Angiotensin-Converting Enzyme 2 (ACE2 receptor) and activates the adhesion process (5, 6).

This involves a temporary hinge-like conformational movement of S1 receptor-Binding Domain (RBD) that enables binding to a protease domain (PD) of ACE2, which includes its alpha1-helix with inputs from its alpha2-helix and both β3 and β4 sheets (7, 8). Therefore, the spike protein appears to be the most suitable target for disease prevention, diagnosis, and treatment strategies.

Various molecular techniques such as Reverse Transcriptase Polymerase Chain Reaction (RT-PCR) analysis, Enzyme-Linked Immunosorbent Assays (ELISA), Western Blotting, Lateral Flow Immunoassays (LFIA), and Clustered Regularly Interspaced Short Palindromic Repeats (CRISPR)-based approaches have been used for SARS-CoV-2 diagnosis. However, these techniques are time-consuming, labor-intensive, and require substantial expertise. Currently, RT-PCR is widely considered the gold standard for confirmatory diagnosis (9–12). However, recent advances in proteomics have significantly contributed to disease diagnosis, elucidation of the host-pathogen interaction, disease biomarkers, antigens, and detection of antibodies in patient samples (13–17). Mass spectrometry (MS)-based proteomic methods have been used to detect SARS-CoV-2 viral proteins in human, animal, and cell line studies (*in-vitro* and *in-vivo*), and the virus at low loads in human samples (18, 19). In addition, targeted proteomic techniques have detected polypeptides of the SARS-CoV-2 nucleoprotein (20, 21), and several *in-silico* efforts have been made to identify antigenic peptides, T- and B-cell epitopes of SARS-CoV-2 proteins, and proteome sequences (22–25). Furthermore, transcriptomic studies have identified T- and B-cell epitopes (26) and the efficacy of the antiviral drug cepharanthine for COVID-19 treatment (27).

Since the pandemic began, numerous groups have studied COVID-19, generating enormous genomic and proteomic archives in the public domain. Therefore, we have developed a strategy, presented here, for identifying SARS-CoV-2 antigenic peptides and potential paratope peptides to detect viral antigens using publicly available resources. This involves an *in silico* approach for identifying and validating diagnostic peptides with the following steps. First, collection of genomic and MS-based proteomic data on the virus. Second, cataloging identified peptides' antigenicity, immunogenicity, and toxicity. Third, selection of diagnostic peptides by removing potentially cross-reacting interfering peptides associated with human saliva and other pathogens. Fourth, verification of selected peptides' expression in another infected cell line. Fifth, identification of paratopes for viral antigens. Finally, docking of the selected peptides with known viral TCR, class I and II pMHC, and the identified paratope peptides.

MATERIALS AND METHODS

Collection of SARS-CoV-2 Virus Sequences to Explore Genomic Variability in the Spike and Nucleocapsid Proteins

All available SARS-CoV-2 spike and nucleocapsid nucleotide and protein sequences were extracted from the NCBI database using combinations of the keywords "COVID-19", "SARS-CoV-2", "spike," and "nucleocapsid" both singly and in combinations with the Boolean operator AND. To generate a protein dataset, a local BLAST database was searched to find sequences with ≥ 95% similarity using protein sequences of Wuhan-Hu-1 isolates of SARS-CoV-2 (MN908947.3) as references. Sequences with non-standard amino acids were removed, and the remaining sequences were clustered using CD-HIT software with 100% sequence identity setting (28). To explore the genomic variability among the sequenced isolates, we applied multiple sequence alignment with ClustalW (29). Conserved and variable regions of the spike protein were identified using Gblocks software (30). To avoid selecting peptides with poor diagnostic potential, mutations in the protein detected in variants in all countries that had reported more than 10 spike protein sequences were analyzed. A binary matrix was generated for clustering based on the presence and absence of each identified mutation in the spike protein with respect to countries. This was done using the Clustvis web tool (31) and the following parameters. Clustering distance for rows and columns: binary. Clustering method for rows and columns: average. Tree ordering: tightest cluster first.

Peptide Cataloging of the SARS-CoV-2 Proteome From Mass Spectrometric Proteome Data

The ProteomeXchange database was explored to extract SARS-CoV-2 mass spectrometric proteomic data using various keywords such as "SARS-CoV-2", "COVID-19", and "spike." Two cell-line proteomes (PXD017710 and PXD018581) and four naturally infected patient proteomes (PXD019686, PXD021328, PXD018682, and PXD019423) were used to identify expressed SARS-CoV-2 peptides with Proteome Discoverer software (32–35). The extracted SARS-CoV-2 protein sequences and raw proteome files were the initial input for peptide identification with the following settings: 5% max. false discovery rate (FDR) at the protein level, at most one missed cleavage (1), 2–3 charge range (2–3), and 396–1,600 m/z range. A mass tolerance of 10 ppm was set for parent ions and 0.8 Da for fragment ions. The cell-line and patient sample proteomes were processed separately using human and virus reference sequences to explore differences between the two kinds of proteomes associated with infection by the virus.

Network Analysis to Identify Hub and Bottleneck Genes

Immune system-related genes were identified to explore the protective immune response to infection by the virus in humans. A protein-interaction network analysis was constructed to identify

key immune regulator genes among the identified proteins using the STRING 11.0 database with a threshold confidence score of 0.4 (36). The resulting interaction network was imported into Cytoscape 3.8.0 software for visualization. The Cytoscape plugin Cytohubba with an implemented 11-node ranking method was used to analyze the protein-interaction network. In addition, the degree of association and bottleneck approach was used to identify hubs and bottlenecks in the interaction network generated by the Network Analyzer plugin of Cytoscape (37).

Filtering of Cross-Reacting Peptides

All the peptides in the generated catalogs similar to peptides of humans and other pathogens were removed to avoid misleading results from cross-reactive antibodies. Expressed human and human saliva microbiome peptides were extracted from The Human Protein Atlas (https://www.proteinatlas.org/) and proteomeXchange database (PXD003028), respectively. SARS-COV-2 peptides similar to peptides of host origin were filtered out using the phmmer program with default parameters (38). Peptides similar to those of pathogens inducing a clinical presentation similar to COVID-19, such as SARS-CoV, Influenza, Middle East Respiratory virus, Pneumoniae, Respiratory syncytial virus, Rhinovirus, *Staphylococcus aureus*, and *Streptococcu*s species in the Uniprot database were also filtered out using phmmer. The SARS-CoV-2 infected NHBE and A549 cell line proteomes were then explored for evidence of the selected peptides' presence (26). Peptides expressed in all three experimentally generated data sources (cell lines, human patients, and proteome generated from cell-line RNA-Seq data) were retained for further study.

Assessment of Antigenicity and Potential Immunogenicity of the Generated Peptides

In accordance with widely accepted definitions, the antigenicity of a peptide is regarded here as its capacity to bind specifically with a paratope, and its immunogenicity as its ability to induce an immune response, specifically production of antibodies against the antigenic protein (26). We used the Predicted Antigenic Peptides server (http://imed.med.ucm.es/Tools/antigenic.pl) to explore identified peptides' antigenic potential and the Immune Epitope Database (IEDB) toolkit to explore their class-I pMHC immunogenicity (http://tools.iedb.org/immunogenicity), CD4 T-cell immunogenicity (http://tools.iedb.org/CD4episcore/), and binding to both class–I MHC (http://tools.iedb.org/mhci/), and class-II MHC (http://tools.iedb.org/mhcii/). A peptide inhibitory concentration (IC_{50}) ≤ 900 nM was considered diagnostic of MHC class-I and II binding genes and alleles (39). B-cell epitopes for the spike protein RBD domain were identified using the Bepipred2.0 server with default parameter settings. All predicted epitopes were compared with those predicted by other tools for B-cell epitope prediction (BcePred, ABCpred, and SVM Trip) (40).

Paratope Identification: Antigen-Binding Peptide Sequences

Complementarity determining regions (CDRs) are antibodies' main antigen-binding domains, and most antigen-binding residues (ca. 80%) in paratopes are in CDR regions (41). To explore the SARS-CoV-2 antigen-binding peptide sequences, available crystal structures of antibody-antigen complexes involved in SARS-CoV-2 infection (PDB id: 7BWJ, 7BZ5, 7B3O, and 6W41) were downloaded from the RCSB Protein Data Bank (PDB) to extract light and heavy chain protein sequences. Paratome (42) and Parapred server (43) tools were used in conjunction with the extracted sequences to identify paratopes. Parapred applies a deep-learning architecture to integrate functionality from all local neighborhoods, while Paratome applies a machine learning approach based on multiple structure alignment (MSTA) of all available Ab-Ag complexes in the RCSB database. Only paratope sequences including sequences predicted by both tools were selected. The identified paratope peptides were assembled using the synthetic peptide linker GSGSGS to prevent undesired interactions between the discrete domains (44).

Three-Dimensional Interaction Analysis of Selected Antigenic Peptides With Known Viral TCR, Class I and II MHC, and Paratope Peptides

Next, structural information on 19 well-known T-cell receptors (TCR) and 28 pMHC structures for different viruses were downloaded from the TCR3d database (45) for use in docking studies to assess the identified antigenic peptides' structural compatibility with them. The antigen binding affinity of peptides of SARS-CoV-2 were identified by docking with selected paratopes of B cell and T-cell peptides (46, 47). 3D structures of B- and T-cell epitopes and those of the paratope peptides were predicted using the PEP-FOLD3 server (48). The identified SARS-CoV-2 peptides were docked with TCR and pMHC proteins using Cluspro 2.0, while paratopes were docked with the identified antigens, the independently predicted antigens of the RBD protein, and whole spike and RBD proteins using Cluspro 2.0 in antibody mode (49). Protein-paratope complexes were visualized and hydrogen bonds analyzed using the UCSF chimera (50) and LIGPLOT software (51).

RESULTS

Numerous groups have studied the severity of COVID-19 since the pandemic began, resulting in massive genomics and proteomics resources in the public domain. Therefore, we have developed a strategic approach to identify unique SARS-CoV-2 antigenic peptides and potential paratope peptides to detect viral antigens using publicly available experimental resources. This involves a multi-step genomic and proteomic approach (**Figure 1**) for diagnostic peptide identification, and validation. Our study demonstrates a practical and precise approach for identifying diagnostic peptides when access to experimental sample data is limited. The identification of SARS-CoV-2 viral proteins highlights the value of today's protein informatics resources in responses to a public health emergency.

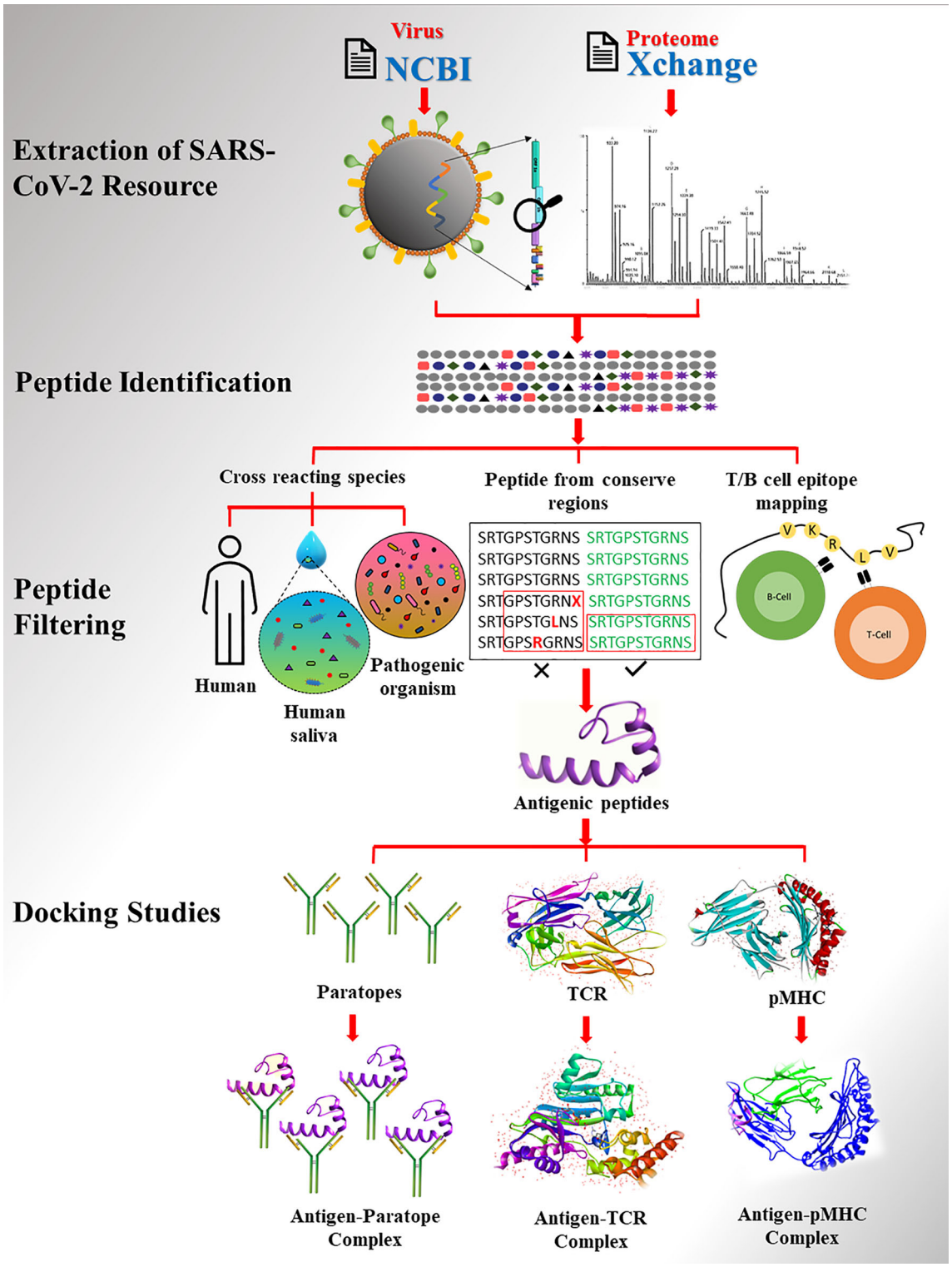

FIGURE 1 | The workflow of study. SARS-CoV2 proteome extracted from database followed by peptide identification and filtering.

Meta-Analysis of the Genomic Diversity of the SARS-CoV-2 Virus

Recently, various studies have reported genomic variation in SARS-CoV-2 viral strains and their severity. Thus, it is crucial to consider genomic variability when identifying and selecting peptides to develop robust diagnostic assays. To meet this need, we performed a large-scale meta-analysis of the variations in 358,558 protein sequences of SARS-CoV-2 detected in samples from 42 countries. A protein dataset was generated for each SASR-CoV-2 protein for sequence conservation analysis. We identified five regions [1–75, 79–197, 219–367, 374–390, and 398–423] and 14 regions [1–67, 77–138, 149–199, 201–209, 211–240, 244–255, 259–263, 267–520, 522–655, 657–679, 693–861, 863–1205, 1207–1246, and 1248–1277] for the nucleocapsid and spike proteins, respectively. Conserved regions of the spike protein are shown in **Figure 2**. In total, 149 spike mutations were identified in samples from all the countries. Mutation G614D, which increases transmissibility (52), was found in samples from 40 countries, while mutations F5L and F12S were found in samples from seven countries (Australia, Bahrain, Bangladesh, Canada, France, India, USA), and three countries (Egypt, Hong Kong, The Philippines), respectively. The numbers of protein sequences before and after clustering and heat map illustrating distributions of mutations in them are presented in **Supplementary File 1** (**Table S1**, **Figures S1**, **S2**). Distribution of the mutations in countries and a binary matrix are provided in **Supplementary File 2** (**Tables S1**, **S2**).

SARS-CoV-2 Peptide Identification From Proteomic Data

Two cell lines and four naturally infected human patient proteomes were selected for the high-confidence identification of peptides using viral and human protein sequences as references. In total, 361 and 81 peptides of viral origin were identified in the cell lines and patient samples, respectively. Only three viral peptides in the cell-line and patient samples were identical. Analysis of the peptides revealed that they are encoded by various parts of the viral genome, such as the ORF1ab, nucleocapsid, envelope, and spike gene regions. Multiple peptides with varying lengths from different parts of the same proteins were found, including 57 component peptides of the spike protein. Of these 57 peptides, 28, 29, and one are components of the S1 (14–685), S2 (686–1273), and RBD (319–541) regions of the spike protein, respectively. The selected proteomes, samples, numbers of peptides, and identified viral proteins are briefly described in **Table 1** and **Supplementary File 2** (**Tables S3–S5**).

Functional Analysis of the Proteomes From Infected Cell Lines and Samples From Naturally Infected Patients

Like any virus, SARS-CoV-2 must enter host cells and manipulate host responses to enable its replication. Therefore, exploration of protective immune responses to infection can provide important insights regarding viral pathogenesis. Thus, we explored host responses to the virus in both cell lines (Colon Carcinoma-2 and H1299) and naturally infected COVID-19 patients' samples (mouth gargle, nasal swab, and respiratory tract). In total, 323 and 143 human peptides were identified in the cell line and patient samples, respectively. Only five (MDGA1, PIK3C2A, FOXP2, DCAF5, and IVD) were detected in both sets of samples. MDGA1 plays a role in formation or maintenance of inhibitory synapses (53), whereas PIK3C2A is involved in several intracellular trafficking and signaling

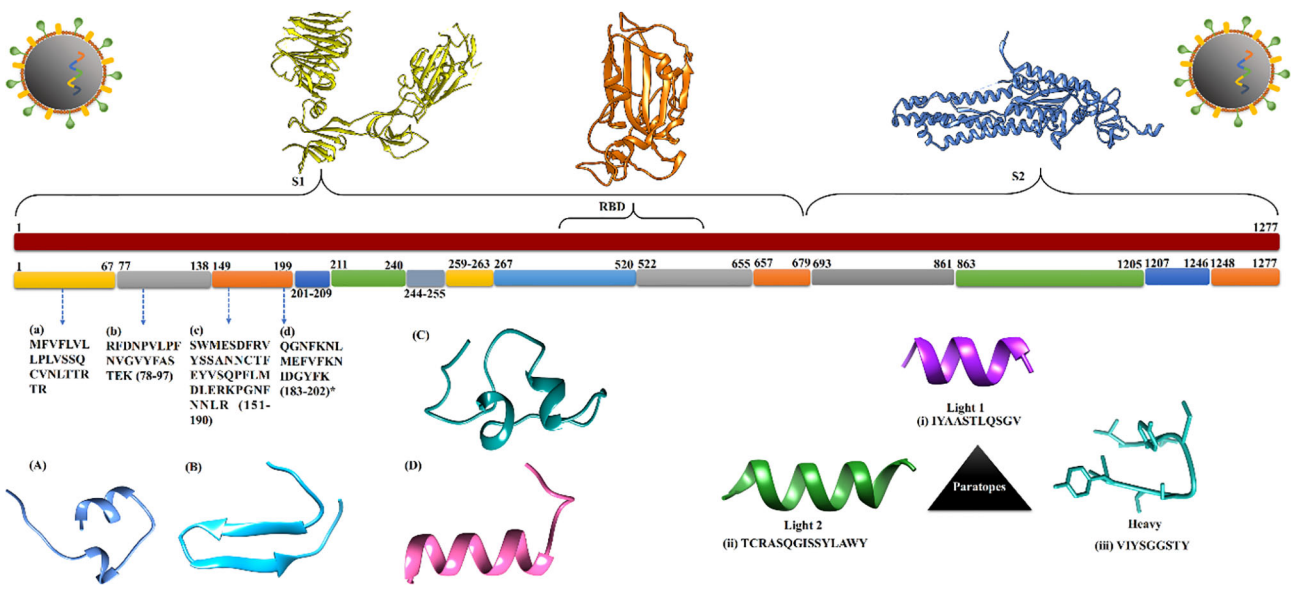

FIGURE 2 | The conserved regions of spike protein extracted from protein data set of SARS-CoV-2. **(A–D)** Identified diagnostics peptide sequences with respect to their genomic location and 3D structure. **(i–iii)** Extracted paratopes sequence with their 3D structure.

TABLE 1 | Summary of studied proteomes, number of uniquely identified peptides, and reference proteins.

Proteome Ids	Sample	Unique Peptide	Identified proteins	Proteome Ids
PXD017710	Colon Carcinoma-2 (Cell line)	148	ORF1ab, ORF3a, N, ORF10, S, ORF7a, ORF6, ORF1a, ORF8, ORF9b	PXD017710
PXD018581	H1299 (Cell line)	213	ORF10, ORF7a, N, ORF3a, ORF1ab, ORF8, S, ORF7b, ORF6, M, ORF6, NS, ORF1a, E	PXD018581
PXD021328	Naso and Oropharyngeal swabs (Human patient)	36	ORF10, ORF1ab, S, N, ORF7a, ORF3a, M	PXD021328
PXD019686	Nasal swab (Human patient)	25	ORF1ab, ORF10, S, N, ORF1a, ORF7a	PXD019686
PXD018682	Mouth Gargle (Human patient)	11	ORF10, ORF1ab, S	PXD018682
PXD019423	Mouth Gargle (Human patient)	9	ORF1ab, ORF3a, S	PXD019423

pathways (54). FOXP2 is a transcription factor that may regulate hundreds of genes in several tissues, including the brain (55). DCAF5 is a receptor of CUL4-DDB1 E3 ubiquitin-protein ligase (56), and IVD is an essential enzyme for mitochondrial fatty acid beta-oxidation. Many of the other proteins are involved in immune system-related biological processes such as regulation of immune responses, autophagy, immune system development, leukocyte migration, antigen processing and presentation, or leukocyte-mediated cytotoxicity, and were detected in both cell line and naturally infected patient proteomes. Proteins involved in biological processes such as production of molecular mediators of immune response and myeloid cell homeostasis were only found in the cell-line proteome. As anticipated, peptides associated with the immune response and leukocyte activation were only found in the proteome of infected patients. In total, 58 and 23 unique genes related to immune system biological processes were found in the cell line and naturally infected patient proteomes, (**Supplementary File 3**: **Tables S1**–**S4**).

The human innate immune system, which plays a crucial role in preventing infection and killing pathogens, involves various kinds of cells, including natural killer cells, macrophages, neutrophils, dendritic cells, and mast cells. Therefore, identifying proteins associated with both these cells and SARS-CoV-2 infection through analysis of experimental resources such as cell-line and patient datasets can improve understanding of interactions between the virus and human hosts. We found 33 innate proteins that matched entries in the InnateDB database. Most of these proteins are involved in immune-related functions such as protein binding (TAB1, SREBF2, HSP90AA1, RB1, STAT3, DCN, IL1R1, BNT3A2, PIK3R2, CCR6), transferase activity (TREM2, ABL1, S100A12, C4BPB), protein dimerization (UBE2N, CSF1R), and lipopeptide binding (EPS8, CD36). TAB1 may be involved in up-regulation of TAK1, IRF7, and IFN signaling during activation of the antiviral innate immune system (57). STAT3 has a well-known role in inflammation and immunity (58), and IL-1R signaling in CD4+ T-cells promotes Th17 immunity and atherosclerosis (59). TREM2 controls phagocytic pathways, which are involved in removal of neuronal debris (60). ABL1 is involved in regulating release of filoviruses through VP40 protein phosphorylation and might also be involved in the virus life cycle (61). EPS8 is a key regulator of the LPS-stimulated TLR4-MyD88 interaction and contributes to macrophage phagocytosis (62), while CD36 is a known scavenger receptor involved in immunity, metabolism, and angiogenesis (63). The major challenge was to identify key expressed immune genes in a complex network of the immune system. Therefore, the identified proteins related to the immune system process from cell-line and patient proteomes were used to generate a protein-interaction network **(Figure 3) (Supplementary File 1- Tables S2**, **S3)**. The generated protein-interaction network, which includes 403 nodes and 671 edges, was used to identify the top rank hubs and bottlenecks **(Supplementary File 1**, **Table S2)**.

Selection of Diagnostic Peptides From the Generated Peptide Catalog

Antigenic peptides must, by definition, have sufficient antigenicity and immunogenicity to bind detectably to antigen-specific receptors on lymphocytes or the Fab region of antibodies. The antigenicity of a peptide is determined by surface epitopes of 5–7 amino acid residues, whereas four intrinsic properties of peptides determine their immunogenicity: chemical composition, molecular size, foreignness, and heterogenicity for processing and presentation on the surface of antigen-presenting cells (APCs). Therefore, we applied multi-step filtering to identify potential diagnostic peptides. Initially, to avoid future cross-reactivity, the identified peptides (442) were filtered to exclude human and human saliva microbiome peptides (418) and subsequently peptides of a targeted group of pathogenic bacteria and viruses (129). Next, to avoid selection of poor peptides for diagnostic purposes, the selected peptides' expression was checked, using results of the infected cell-lines RNA-Seq data analysis. Finally, four peptides (**Table 2** and **Figure 2**), present in the NHBE and A549 cell lines, infected patient samples, and the RNA-Seq-derived proteome were selected after conservation analysis (**Supplementary File 4**: **Tables S1**–**S3**, and **S7**). A sequence alignment of all matched peptides from the three types of sources is provided in **Figure S3** of **Supplementary File 1**.

MHC genes, containing a set of closely linked polymorphic genes, encode crucial cell surface proteins that bind antigens, thereby alerting the immune system. Therefore, we evaluated the identified peptides' antigenicity and CD4 immunogenicity to enable potency-based selection (**Table 3**). The average immunogenicity and antigenicity scores of peptides were approximately 89.06 and 1, respectively, which clearly showed the potential of selected peptides.

Class I and II MHC molecules have small grooves that present self-antigens and pathogen-derived peptides. Members of class I present intracellular antigens such as viruses, intracellular bacteria, or parasites to T cells, whereas the MHC class II presents exogenous antigens to professional APC, including

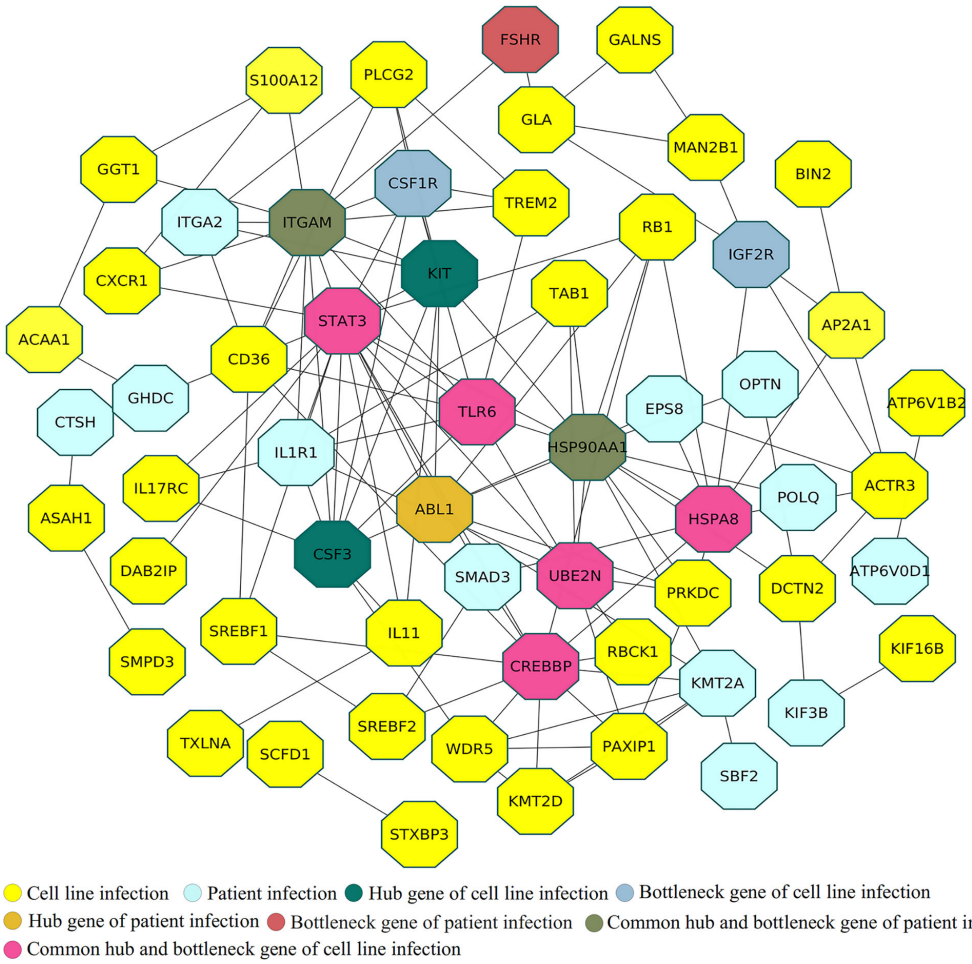

FIGURE 3 | Protein interaction analysis among uniquely identified immune system genes in cell-line and patient proteomes.

TABLE 2 | List of selected peptides for SARS-CoV-2 diagnosis.

Data sources	Peptide ids	Length	Sequence	Protein accessions	Peptide positions
CL+NI+RNA	A26	40	SWMESDFRVYSSANNCTFEYVSQPFLMDLERKPGNFNNLR	QOD59281.1	S-S1 [151-190]
CL+RNA	A349	20	RFDNPVLPFNVGVYFASTEK	QOT61311.1	S-S1 [78-97]
	A194	23	MFVFLVLLPLVSSQCVNLTTRTR	QPG83544.1	S-S1 [1-23]
	A343	20	QGNFKNLMEFVFKNIDGYFK	QOI61545.1	S-S1 [183-202]

CL, Cell-line infected proteome; NI, Natural infected human patients; RNA, Transcriptome; S, Spike.

lymphocytes, macrophages, dendritic cells, and Langerhans cells. Hence, information on MHC alleles' binding of foreign peptide is crucial. The class I and II MHC alleles were evaluated by screening IEDB entries associated with the selected virus peptides. In MHC-I allele analysis, HLA-A and B type alleles were found to be the most frequently occurring (HLA-B*35:01; HLA-B*53:01; HLA-B*40:01; HLA-A*11:01; HLA-A*03:01; HLA-A*24:02; HLA-A*26:01; HLA-A*26:01; HLA-A*23:01; HLA-B*35:01; HLA-B*35:01; HLA-A*01:01; HLA-A*24:02; HLA-B*51:01; HLA-A*03:01; HLA-B*51:01; HLA-A*23:01; HLA-A*30:02; HLA-A*24:02; HLA-B*15:01; HLA-A*01:01; HLA-A*23:01; HLA-A*11:01; HLA-B*53:01). Similarly, MHC-II gene alleles were explored using the stabilized matrix-based method (SMM in IEDB analysis resources (**Supplementary File 4**: **Tables S4–S6**). The identified MHC class-II alleles for peptides are very common for exogenous antigens (HLA-DQA1*05:01, DQB1*03:01, HLA-DPA1*02:01, HLA-DRB1*04:01, HLA-DRB4*01:01) (64).

Paratope Identification for Selected Peptides

Paratopes, sequences of 5–10 amino acids on antibodies that bind specific antigens, are preset at the three CDR regions (CDR1,

TABLE 3 | CD4 immunogenicity and antigenicity of selected peptides.

Peptide id	Peptide Sequence	Peptide core	Immunogenicity Score	Combined Score
CD4 Immunogenicity				
A26	SWMESDFRVYSSANN	FRVYSSANN	91.1108	49.64432
A26	DFRVYSSANNCTFEY	FRVYSSANN	82.9956	46.39824
A194	MFVFLVLLPLVSSQCVNLTTRTR	FNVGVYFAS	91.22	48.125
A349	RFDNPVLPFNVGVYFASTEK	LLPLVSSQC	83.4206	47.64304
A343	NLMEFVFKNIDGYFK	FKNIDGYFK	77.9889	42.59556
Antigenicity				
Peptide id	**Peptide Sequence**	**Antigenic motifs**	**Length**	**Antigenic propensity**
A26	SWMESDFRVYSSANNCTFEYVSQPFLMDLERKPGNFNNLR	DFRVYSS, TFEYVSQPFLM	40	0.9981
A194	MFVFLVLLPLVSSQCVNLTTRTR	FLVLLPLVSSQCVNL	23	1.1110
A349	RFDNPVLPFNVGVYFASTEK	NPVLPFNVGVYFA	20	1.0446
A343	QGNFKNLMEFVFKNIDGYFK	LMEFVFK	20	0.9867
B-cell linear epitopes				
Peptide id	**Peptide Sequence**	**Epitope core**	**Length**	
A26	SWMESDFRVYSSANNCTFEYVSQPFLMDLERKPGNFNNLR	FRVYSSANN, DLERKPGNFN	40	
A194	MFVFLVLLPLVSSQCVNLTTRTR	RF	23	
A349	RFDNPVLPFNVGVYFASTEK	LVSSQCVNLT	20	
A343	QGNFKNLMEFVFKNIDGYFK	QG	20	

CDR2, and CDR3), which are thus key regions for paratope identification. Two light chain (L1 and L2: IYAASTLQSGV and TCRASQGISSYLAWY, respectively) and one heavy chain (H: VIYSGGSTY) paratope sequences were identified using two prediction approaches (**Supplementary File 5**, **Table S3**). The 3D structure of all three paratopes is shown in **Figure 2**. To increase the specificity of paratope sequences for the SARS-CoV-2 antigen, three paratope peptides were linked with a peptide linker (GSGSGS) to ensure that each assembled paratope peptide could work protein-independently, thus reducing unspecific antigen binding. Therefore, the light chain paratope L1 and heavy chain paratope H were stitched at the N and C termini of the first linker, and the second linker was attached to the C terminus of the heavy chain paratope (H) and N terminus of light chain paratope L2. In addition, we used a glycine-serine dimer (GSGSGS) triplet to assemble paratope peptides (IYAASTLQSGVGSGSGSVIY SGGSTYGSGSGSTCRASQGISSYLAWY).

Docking Analysis of Peptides With the TCR and MHC

Cellular immunity systems are activated once MHC molecules present endogenous or exogenous antigens at the cell surface to T cells. Therefore, we evaluated the affinity of well-known TCR receptors of viruses, class I and II MHC, and the identified paratope peptides, for the identified antigens in docking studies. Evaluation of docked complexes of the selected epitopes' peptides A26, A194, A343, and A34919 with 19 MHC molecules and 28 TCR receptors yielded binding affinities ranging from -1138.9 to -741.4 and -1360.3 to -692.7 kcal/mol, respectively. A detailed description of all 19 TCR and 28 pMHC is provided in **Supplementary File 5**, **Tables S1**, **S2**. The molecular interaction of each antigen with each paratope was evaluated, the results are summarized in **Table 4**, and a detailed description is provided in **Supplementary File 5**, **Table S4**. The binding energies of paratopes for each antigen fell into three ranges (L1-antigens, -136.1 to -163.2 kcal/mol; L2-antigens, -199.9 to -242.3 kcal/mol; H-antigens, -181.6 to -202.6 kcal/mol) and all docked complex poses as well as the binding residues are presented in **Supplementary File 1**, **Figure S4**. The binding potential of the paratopes for the independently identified RBD antigens was also explored (**Supplementary File 5**, **Table S5**). To evaluate the assembled paratopes' binding specificity, docking was done with each identified antigen, whole RBD, and spike protein, and the experimentally verified SARS-CoV T-cell and B-cell epitopes (derived binding energies: -196.8 to -235.2, -96.2 to -248, -303.3, -175.1 to -190.9 and -145.2 to -158.4 kcal/mol, respectively). The best-docked poses and several hydrogen bonds are shown in **Figure 4**. Our analysis indicates that the assembled paratope has strong binding affinity for the four identified antigens, RBD protein antigen, and whole spike protein. Moreover, the assembled paratope showed lower binding affinity for SARS-CoV T-cell (KCYGVSATKL, and NYNYKYRYLR) and B-cell (ISPYNTIVAKLR, and LSPLGALVACYK) epitopes.

DISCUSSION

RT-PCR is a widely accepted method for COVID-19 detection that involves sample collection, RNA extraction, reverse transcription, and targeted amplification of cDNA using appropriate primers for conserved regions: procedures that require high technical expertise. In addition to the long processing time (24–48 hours), RT-PCR also requires continuous monitoring of the genomic evolution of the virus to ensure that the primers are still valid. For these reasons, several COVID-19 diagnosis kits are available for testing. However, most kits lack field applicability, lack sufficient sensitivity, have long processing times, and provide undesirably high false-positive results. Globally, the number of cases is increasing due to various mutant strains. Therefore, fast, simple, and reliable diagnosis methods that can be applied used readily portable equipment are required for large-scale screening.

To assist efforts to develop such methods, we applied *in-silico* method techniques to identify unique SARS-CoV-2 peptides using experimentally generated data. The data explored in this

TABLE 4 | Antigen and paratope docking studies.

Antigens	Antigen-Paratope Binding energy	Hydrogen bonds	Interacting residues
A26	L1 (-145.8)	5	ILE1-PHE25, TYR2-PHE25, TYR2-GLU4, ALA3-GLN23, ARG40-THR6
	L2 (-242.3)	7	TYR11-LEU18, TRP14-HR22, TYR15-CYS15, TYR 15-MET1, TYR15-PHE2, TYR11-THR 19, TRP14-THR22
	H (-202.6)	3	TYR3-SER12, SER7-ASN15, THR8-ASN15
A194	L1(-163.2)	3	TYR2-LEU18,THR20-TYR2, THR20-TYR2
	L2 (-233.6)	3	TYR11-LEU18, TYR15-THR22, TYR11-THR22
	H (-190.1)	5	THR8-THR22, TYR9-VAL16, SER4-ARG21, TYR3-ARG21, GLY5-ARG23
A343	L1(-136.1)	3	TYR2-PHE10, GLY10-ASN3, SER9-ASN6
	L2 (-199.9)	3	ARG3-ASP16, ARG3-ASP16, TYR11-GLN1
	H (-181.6)	2	ASN14-TYR9, LYS20-TYR 3
A349	L1 (-156.9)	8	TYR2-ASN4, SER5-GLU19, SER5-GLU19, THR6-ARG1, ARG1-THR6, THR6- ARG1, TYR2-PHE2, GLY10-ASN10
	L2 (-219.6)	3	ARG3-ASP3, TYR11-ASN10, TYR11-ASN10
	H (-193.9)	5	TYR3-ASN4, SER7-ASP3, TYR9-PRO8, TYR9-ARG1, SER4-ASN4
Docking studies of assembled paratopes (AP)			
A26	AP (-235.2)	5	TYR 20-MET 3, SER 37-TYR 10, ALA 36-ARG 8, GLY 22-SER 12, TYR 47-LYS 32
A194	AP (-196.8)	7	ARG 35-GLN 14, ARG 35-GLN 14, TYR 47-THR 19, ALA 36-THR 19, TYR 20-ARG 21, VAL 18-ARG 21, VAL 18-ARG 21
A343	AP (-201.6)	4	TYR 20-MET 8, GLY 23-LYS 20, TRP 46-LYS 5, TYR 47-LYS 13
A349	AP (-211.2)	9	TYR 20-ASN 4, GLY 23-GLU 19, SER 37-THR 18, TYR 47-LYS 20, VAL 18-ARG 1, TYR 20-ARG 1, TYR 20-ARG 1, ALA 36-LYS 20, ILE 40-LYS 20
RBD	AP (-227.3)	7	TYR 2-TYR 449, GLY 22-GLY 485, ALA 45-TYR 449, SER 21-TYR 489, TYR 20-PHE 490, GLY 16-GLN 493, TRP 46-GLN 493
Spike	AP (-303.3)	11	ASN 556-SER 28, ASN 556-GLY 29, LYS 557-THR 33, ASN 616-GLY 16, ASN 616-TRP 46, GLN 644-TYR 47, ARG 646-LEU 44, ARG 646-LEU 44, GLU 619-VAL 18, ASP 574-TYR 26

study were originally generated with specific objectives. The PXD017710 cell line proteome was first used to identify drug targets and host cellular response players (34), the PXD018581 proteome was generated to compare SARS-CoV and SARS-CoV-2 virus disease progression, and the PXD021328, PXD019686, and PXD019423 proteomes were generated from infected human samples (mouth gargle, nasal and oral swab). Our primary objective was to develop robust, convenient, diagnostic methods for large-scale screening of human patient samples (20, 32, 33). However, none of the studies aligned with our aim and objectives. In this study, extracted virus protein and human proteome sequences were used to identify peptides from mass spectrometry data by exclusive data-processing flow (PWF_QE_Precursor_Quan and LFQ_MPS_SequestHT_Percolator). Several peptides of different lengths were identified from the whole genome of SARS-CoV-2 from both the cell line and patient proteomics data (**Table 1**). These results indicated that the trypsin digestion originally used was an appropriate choice for detecting viral peptides. To select mutation-free peptides, spike protein sequences were subjected to mutation analysis, and three major mutations (F5L, F12S, and G641D) were identified in samples from several countries. The G641D mutation, found in samples from all the countries, might be involved in viral conformational plasticity, increasing viral fitness (65). F5L and F12S mutations were also found in samples from several countries, but their impact on infection and disease progression is unclear. In a recent study (66), the E484K mutation was detected in a new variant (B.1.1.33) of the SARS-CoV-2 virus in Brazil. The E484K mutation has raised concern because it may increase the transmissibility of the virus. In our study, the E484K mutation was found in the Bahrain spike protein dataset.

The SARS-CoV-2 spike protein is one of the crucial targets for disease prevention, diagnosis and therapeutic antibody development. Its S1 region is responsible for binding to the host ACE2 receptor, and the S2 region is responsible for membrane fusion (67). Our results highlight four immunodominant SARS-CoV-2 peptides of the S1 region (A26, A349, A194, and A343**).** The identified peptides have high diagnostic potential due to appropriate proportions of hydrophilic residues (lysine, arginine, histidine, aspartic acid, glutamic acid, serine, threonine, tyrosine, asparagine, and glutamine) and immunogenic residues (lysine, arginine, glutamic acid, aspartic acid, glutamine, and asparagine), low number of internal cysteine residues, and absence of the arginine-glycine (RGD) tripeptide motif. Moreover, analysis of RNA-Seq data confirmed that the identified peptides are expressed in NHBE and A549 cells. The identified antigens were expressed in four cell lines (Colon Carcinoma-2, H1229, NHBE, and A549) and three types of human patient samples (mouth gargle, nasal, and oral swab) corroborating their expression in various cell types.

The SARS-CoV-2 virus binds to the human ACE2 receptor through the spike protein's RBD (**Figure 5A**), and enters cells *via* a mechanism involving a series of conformational changes in both viral and cell membrane proteins followed by an endocytic process. The identified expressed human genes reflect a protective immune response to SARS-CoV-2. Combined cell-line and human proteome data analysis captured immune proteins involved in different phases of the protective immune response, including antigen processing and presentation, and autophagy (**Figures 5B, C**). Various identified proteins such as DCTN2, KIF3B, and AP2A1 are involved in antigen processing for MHC class II molecules and the binding of antigen MHC-II

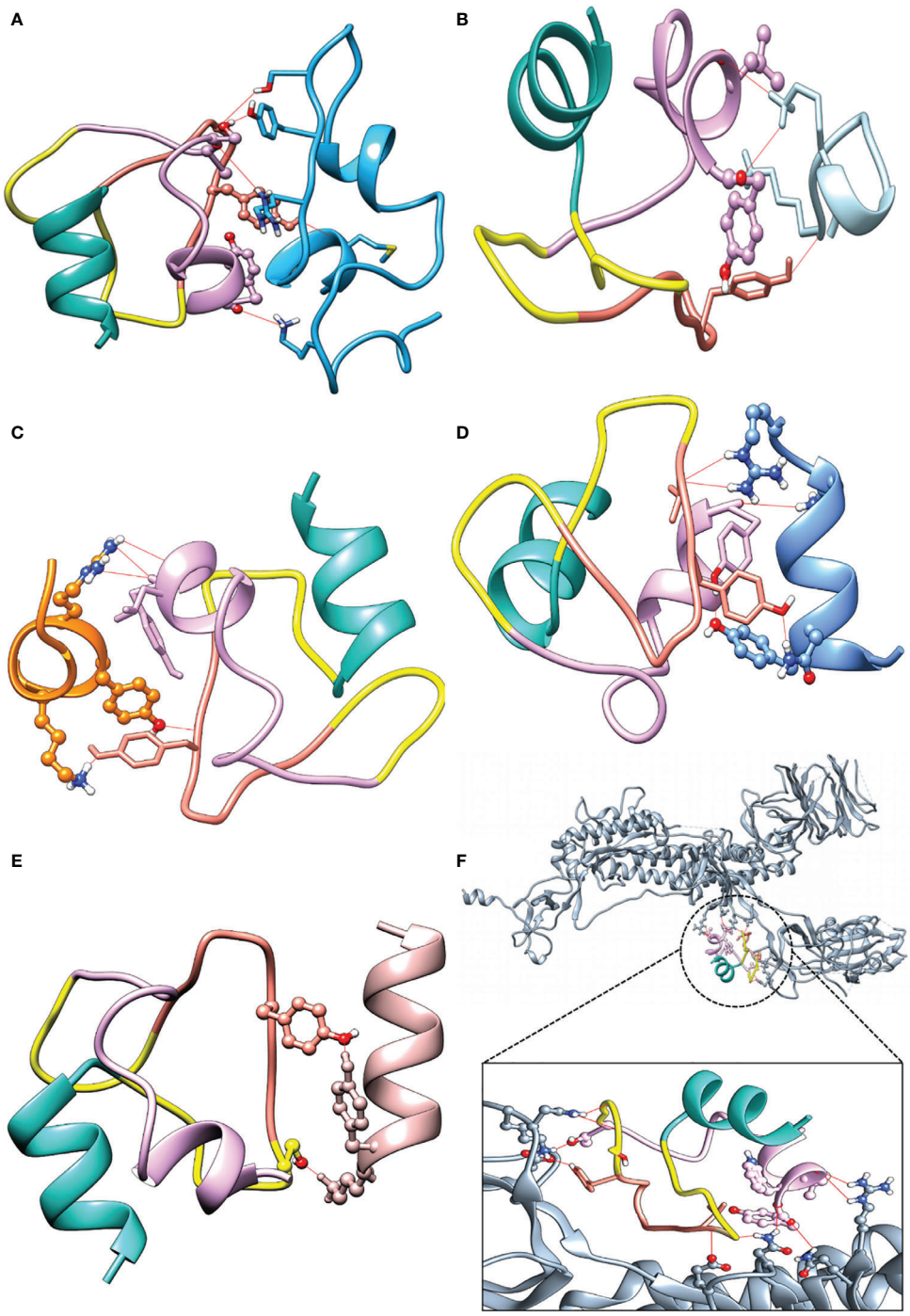

FIGURE 4 | Docking complexes with assembled paratopes (AP) and its respective hydrogen bond numbers. **(A)** (AP - A26, 5). **(B)** (AP – SARS-CoV T-cell1, 3). **(C)** (AP – SARS-CoV T-cell2, 5). **(D)** (AP – SARS-CoV B-cell1, 5). **(E)** (AP – SARS-CoV B-cell2, 2). **(F)** (AP - whole spike, 10). AP color L1 (light sea green), L2 (Plum), H (salmon), and Linker (yellow).

complexes to TCR receptors (68, 69). Other proteins, like STAT3, ABL1, and IL1R1, help in the activation and multiplication of helper T-cells (**Figure 5D**) (70, 71). Activation of helper T-cells leads to B-cell activation and differentiation with OPTN, PLCG2, KLHL6, and TXLNA followed by production of B-cell antibodies (**Figure 5E**) (72, 73). Key immune hub and bottleneck genes were identified through protein-interaction network analysis. According to gene ontology analysis, most of the key genes are

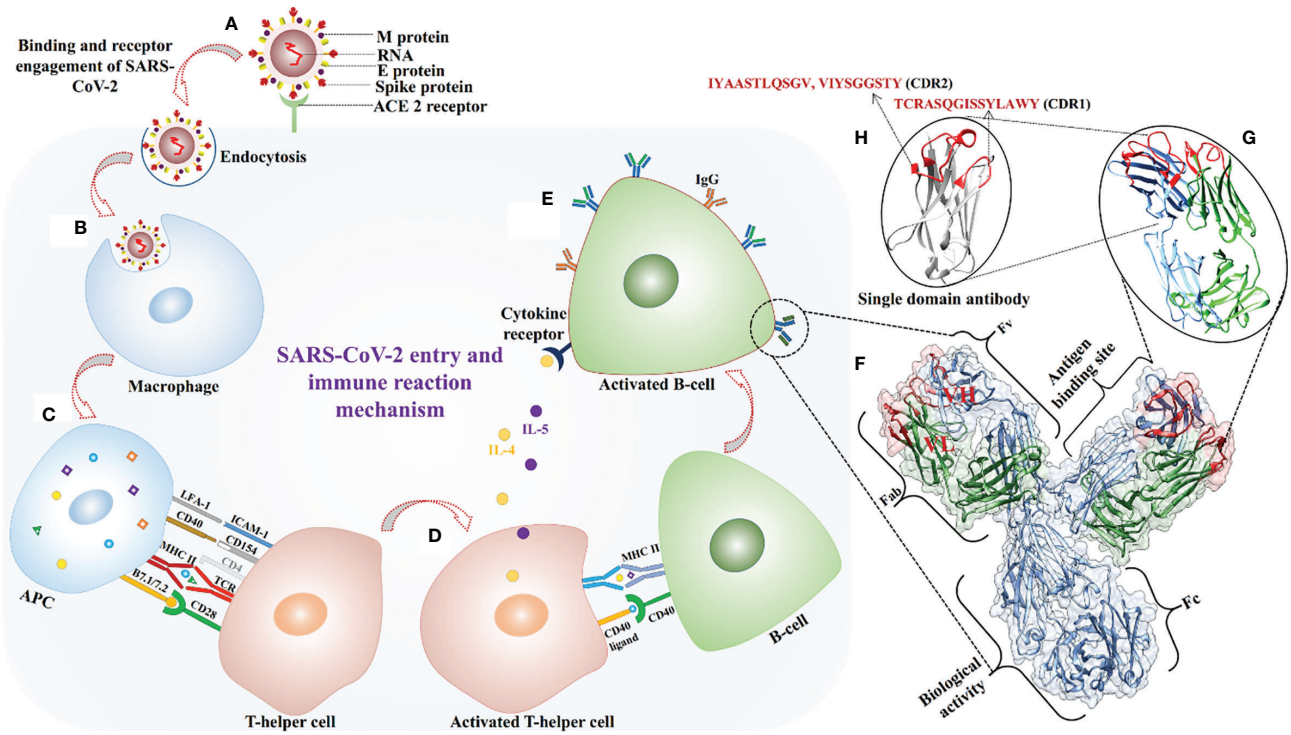

FIGURE 5 | SARS-CoV-2 virus entry in the host cell and antigen-paratopes interaction. **(A)** Recognition of ACE-2 receptor and virus fusion. **(B)** Virus engulfment by a macrophage. **(C)** Antigens from digested SARS-CoV-2 proteins are presented with MHC-II on the cell surface and engagement of helper T-cell for its activation. **(D, E)** Activated helper T-cell interacted with B-cell *via* CD40 ligand and released cytokines for activation of B-cell for secretion of antibodies. **(F)** Enlarge view of antibody structure on the right side, heavy **(H)** and light (L) chains are shown in blue, and green respectively, CDRs are colored in red and light variable domains (V_H and V_L) are labelled in red. **(G, H)** The identified paratopes of light (IYAASTLQSGV, TCRASQGISSYLAWY) and heavy (VIYSGGSTY) chain sequences are shown in red color.

involved in host-virus interaction (*STAT3*, *CREBBP*, *HSPA8*, and *HSP90AA1*), innate immunity, T-cell differentiation, and the inflammatory response. (**Supplementary File 3**, **Tables S2**, **S3**).

Three paratopes [one heavy chain paratope from the CDR2 region (VIYSGGSTY), two light chain paratopes from CDR2 (IYAASTLQSGV), and a CDR1 paratope (TCRASQGIS SYLAWY)] were identified from available X-ray crystallographic structures of antibodies (**Figures 5F–H**). Docking methods enable evaluation of the strength and nature of binding between biomolecules and hence validation of putative *in vitro* or *in vivo* interactions. Therefore, all four antigenic peptides were docked with 19 TCR receptors and MHC receptors, and the results clearly indicate that they had high binding affinity. Three paratope peptides were identified for diagnostic purposes, and most showed high binding affinity with all antigens. However, paratope L2 had the strongest binding affinity and formed several interacting hydrogen bonds (**Table 4**). To increase the diagnostic specificity for SARS-CoV-2 antigens, all the paratopes were then linked with commercially available glycine-serine-rich linkers. Docking studies showed that the designed paratope combination (IYAASTLQSGVGSGSGSVIYSGGSTYGSGSG STCRASQGISSYLAWY) had stronger better binding affinity to different antigens and whole SARS-CoV-2 RBD and spike protein than the individual paratopes. The binding affinity of the assembled paratope peptide was also evaluated for experimentally validated B-and T-cell epitopes of SARS-CoV. The assembled paratopes showed higher binding affinity for SARS-CoV-2 antigens and proteins than for SARS-CoV. (**Supplementary File 5**, **Tables S5–S7**). Hence, the three identified paratopes and their assembled configuration with a glycine-serine rich linker were

CONCLUSION

Various experimental and *in silico* efforts have provided valuable knowledge and resources (including massive genomic and proteomic datasets) to explore (*inter alia*) structural mechanisms of host-pathogen interactions, immune responses, drug candidates, antibodies, epitopes, genomic sequences and variation, infection rates, genome sequences. In this study we explored, available *in silico* resources, namely the cell-line and naturally infected COVID-19 patient's proteomes, and identified four SARS-CoV-2 antigens and three antigen-binding peptides that could be used to develop diagnostic assays. The proposed antigenic peptides can be used for antibody generation, and the paratope sequences can be used directly for COVID-19 diagnostic assay and vaccine development. Moreover, the

developed method and approaches can also be used to explore other infectious diseases

DATA AVAILABILITY STATEMENT

The RNA-Seq data used are available in the NCBI SRA database under project accession number PRJNA615032. Proteomic data are available in the ProteomeXchange database (cell-line proteomes PXD017710 and PXD018581; naturally infected patient proteomes PXD019686, PXD021328, PXD018682, and PXD019423).

AUTHOR CONTRIBUTIONS

SG conceptualized and provided overall guidance. SG, SK, RV, VB, and RG were involved in data curation, analysis, and interpretation. SK, SG, RV, VB, and RG wrote the manuscript. All authors contributed to the article and approved the submitted version.

FUNDING

This work was supported by the Science and Engineering Research Board (SERB), New Delhi, *via* the Intensification of Research in High Priority Area (IRHPA) program (Grant Number IPA/2020/000069), FORMAS (2019-01316), and the Swedish Research Council (2019-04270)].

ACKNOWLEDGMENTS

We gratefully acknowledge assistance from the bioinformatics facility at NIAB and Swedish University of Agricultural Sciences, Sweden for the bioinformatic data analysis.

SUPPLEMENTARY MATERIAL

The Supplementary Material for this article can be found online at: https://www.frontiersin.org/articles/10.3389/fimmu.2021.725240/full#supplementary-material

REFERENCES

1. Lai CC, Shih TP, Ko WC, Tang HJ, Hsueh PR. Severe Acute Respiratory Syndrome Coronavirus 2 (SARS-CoV-2) and Coronavirus Disease-2019 (COVID-19): The Epidemic and the Challenges. *Int J Antimicrob Agents* (2020) 55:105924–34. doi: 10.1016/j.ijantimicag.2020.105924
2. *WHO Coronavirus (COVID-19) Dashboard | WHO Coronavirus (COVID-19) Dashboard With Vaccination Data*. Available at: https://covid19.who.int/ (Accessed June 7, 2021).
3. Zhou P, Yang XL, Wang XG, Hu B, Zhang L, Zhang W, et al. A Pneumonia Outbreak Associated With a New Coronavirus of Probable Bat Origin. *Nature* (2020) 579:270–3. doi: 10.1038/s41586-020-2012-7
4. Chen Y, Liu Q, Guo D. Emerging Coronaviruses: Genome Structure, Replication, and Pathogenesis. *J Med Virol* (2020) 92:418–23. doi: 10.1002/jmv.25681
5. Mousavizadeh L, Ghasemi S. Genotype and Phenotype of COVID-19: Their Roles in Pathogenesis. *J Microbiol Immunol Infect* (2021) 54:159–63. doi: 10.1016/j.jmii.2020.03.022
6. Teng S, Sorbitan A, Rhoades R, Liu D, Tang Q. Systemic Effects of Missense Mutations on SARS-CoV-2 Spike Glycoprotein Stability and Receptor-Binding Affinity. *Brief Bioinform* (2021) 22:1239–53. doi: 10.1093/bib/bbaa233
7. Wrapp D, Wang N, Corbett KS, Goldsmith JA, Hsieh C-L, Abiona O, et al. *Cryo-EM Structure of the 2019-Ncov Spike in the Prefusion Conformation* (2019). Available at: http://science.sciencemag.org/.
8. Yan R, Zhang Y, Li Y, Xia L, Guo Y, Zhou Q. Structural Basis for the Recognition of SARS-CoV-2 by Full-Length Human ACE2. *Science (80-)* (2020) 367:1444–8. doi: 10.1126/science.abb2762
9. Yip TTC, Cho WCS, Cheng WW, Chan JWM, Ma VWS, Yip TT, et al. Application of ProteinChip Array Profiling in Serum Biomarker Discovery for Patients Suffering From Severe Acute Respiratory Syndrome. *Methods Mol Biol* (2007) 382:313–31. doi: 10.1007/978-1-59745-304-2_20
10. Ahirwar R, Gandhi S, Komal K, Dhaniya G, Tripathi PP, Shingatgeri VM, et al. Biochemical Composition, Transmission and Diagnosis of SARS-CoV-2. *Biosci Rep* (2021) 41:20211238. doi: 10.1042/BSR20211238
11. Cheng MP, Papenburg J, Desjardins M, Kanjilal S, Quach C, Libman M, et al. Diagnostic Testing for Severe Acute Respiratory Syndrome-Related Coronavirus 2: A Narrative Review. *Ann Intern Med* (2020) 172:726–34. doi: 10.7326/M20-1301
12. Giri B, Pandey S, Shrestha R, Pokharel K, Ligler FS, Neupane BB. Review of Analytical Performance of COVID-19 Detection Methods. *Anal Bioanal Chem* (2021) 413:35–48. doi: 10.1007/s00216-020-02889-x
13. Eliuk S, Makarov A. *Evolution of Orbitrap Mass Spectrometry Instrumentation* (2015). Available at: http://dx.doi.org/101146/annurev-anchem-071114-040325.
14. Grebe SK, Singh RJ. LC-MS/MS in the Clinical Laboratory – Where to From Here? *Clin Biochem Rev* (2011) 32:5–31.
15. Rauniyar N. Parallel Reaction Monitoring: A Targeted Experiment Performed Using High Resolution and High Mass Accuracy Mass Spectrometry. *Int J Mol Sci* (2015) 16:28566–81. doi: 10.3390/ijms161226120
16. Ying W, Hao Y, Zhang Y, Peng W, Qin E, Cai Y, et al. Proteomic Analysis on Structural Proteins of Severe Acute Respiratory Syndrome Coronavirus. *Proteomics* (2004) 4:492–504. doi: 10.1002/pmic.200300676
17. Kim HJ, Lin D, Lee HJ, Li M, Liebler DC. Quantitative Profiling of Protein Tyrosine Kinases in Human Cancer Cell Lines by Multiplexed Parallel Reaction Monitoring Assays. *Mol Cell Proteomics* (2016) 15:682–91. doi: 10.1074/mcp.O115.056713
18. Zecha J, Lee CY, Bayer FP, Meng C, Grass V, Zerweck J, et al. Data, Reagents, Assays and Merits of Proteomics for SARS-CoV-2 Research and Testing. *Mol Cell Proteomics* (2020) 19:1503–22. doi: 10.1074/mcp.RA120.002164
19. Gouveia D, Grenga L, Gaillard JC, Gallais F, Bellanger L, Pible O, et al. Shortlisting SARS-CoV-2 Peptides for Targeted Studies From Experimental Data-Dependent Acquisition Tandem Mass Spectrometry Data. *Proteomics* (2020) 20:4389–92. doi: 10.1002/pmic.202000107
20. Ihling C, Tänzler D, Hagemann S, Kehlen A, Hüttelmaier S, Arlt C, et al. Mass Spectrometric Identification of SARS-CoV-2 Proteins From Gargle Solution Samples of COVID-19 Patients. *J Proteome Res* (2020) 19:4389–92. doi: 10.1021/acs.jproteome.0c00280
21. Gallien S, Duriez E, Crone C, Kellmann M, Moehring T, Domon B. Targeted Proteomic Quantification on Quadrupole-Orbitrap Mass Spectrometer. *Mol Cell Proteomics* (2012) 11:1709–23. doi: 10.1074/mcp.O112.019802
22. Rencilin CF, Rosy JC, Mohan M, Coico R, Sundar K. Identification of SARS-CoV-2 CTL Epitopes for Development of a Multivalent Subunit Vaccine for COVID-19. *Infect Genet Evol* (2021) 89:104712. doi: 10.1016/j.meegid.2021.104712
23. Lee E, Sandgren K, Duette G, Stylianou VV, Khanna R, Eden J-S, et al. Identification of SARS-CoV-2 Nucleocapsid and Spike T-Cell Epitopes for Assessing T-Cell Immunity. *J Virol* (2021) 95:e02002-20. doi: 10.1128/jvi.02002-20
24. Sohail MS, Ahmed SF, Quadeer AA, McKay MR. In Silico T Cell Epitope Identification for SARS-CoV-2: Progress and Perspectives. *Adv Drug Deliv Rev* (2021) 171:29–47. doi: 10.1016/j.addr.2021.01.007

25. Poh CM, Carissimo G, Wang B, Amrun SN, Lee CYP, Chee RSL, et al. Two Linear Epitopes on the SARS-CoV-2 Spike Protein That Elicit Neutralising Antibodies in COVID-19 Patients. *Nat Commun* (2020) 11:1–7. doi: 10.1038/s41467-020-16638-2
26. Kushwaha SK, Kesarwani V, Choudhury S, Gandhi S, Sharma S. SARS-CoV-2 Transcriptome Analysis and Molecular Cataloguing of Immunodominant Epitopes for Multi-Epitope Based Vaccine Design. *Genomics* (2020) 112:5044–54. doi: 10.1016/j.ygeno.2020.09.019
27. Li S, Liu W, Chen Y, Wang L, An W, An X, et al. Transcriptome Analysis of Cepharanthine Against a SARS-CoV-2-Related Coronavirus. *Brief Bioinform* (2021) 22:1378–86. doi: 10.1093/bib/bbaa387
28. Fu L, Niu B, Zhu Z, Wu S, Li W. CD-HIT: Accelerated for Clustering the Next-Generation Sequencing Data. *Bioinformatics* (2012) 28:3150–2. doi: 10.1093/bioinformatics/bts565
29. Thompson JD, Higgins DG, Gibson TJ. CLUSTAL W: Improving the Sensitivity of Progressive Multiple Sequence Alignment Through Sequence Weighting, Position-Specific Gap Penalties and Weight Matrix Choice. *Nucleic Acids Res* (1994) 22:4673–80. doi: 10.1093/nar/22.22.4673
30. Talavera G, Castresana J. Improvement of Phylogenies After Removing Divergent and Ambiguously Aligned Blocks From Protein Sequence Alignments. *Syst Biol* (2007) 56:564–77. doi: 10.1080/10635150701472164
31. Metsalu T, Vilo J. ClustVis: A Web Tool for Visualizing Clustering of Multivariate Data Using Principal Component Analysis and Heatmap. *Nucleic Acids Res* (2015) 43:W566–70. doi: 10.1093/nar/gkv468
32. Cardozo KHM, Lebkuchen A, Okai GG, Schuch RA, Viana LG, Olive AN, et al. Establishing a Mass Spectrometry-Based System for Rapid Detection of SARS-CoV-2 in Large Clinical Sample Cohorts. *Nat Commun* (2020) 11:1–13. doi: 10.1038/s41467-020-19925-0
33. Gouveia D, Miotello G, Gallais F, Gaillard JC, Debroas S, Bellanger L, et al. Proteotyping SARS-CoV-2 Virus From Nasopharyngeal Swabs: A Proof-Of-Concept Focused on a 3 Min Mass Spectrometry Window. *J Proteome Res* (2020) 19:4407–16. doi: 10.1021/acs.jproteome.0c00535
34. Bojkova D, Klann K, Koch B, Widera M, Krause D, Ciesek S, et al. Proteomics of SARS-CoV-2-Infected Host Cells Reveals Therapy Targets. *Nature* (2020) 583:469–72. doi: 10.1038/s41586-020-2332-7
35. *Proteome Discoverer™ Software* (2021). Available at: https://www.thermofisher.com/order/catalog/product/OPTON-30945#/OPTON-30945 (Accessed June 7, 2021). (10 May 2021, date last accessed).
36. Szklarczyk D, Morris JH, Cook H, Kuhn M, Wyder S, Simonovic M, et al. The STRING Database in 2017: Quality-Controlled Protein-Protein Association Networks, Made Broadly Accessible. *Nucleic Acids Res* (2017) 45:D362–8. doi: 10.1093/nar/gkw937
37. Shannon P, Markiel A, Ozier O, Baliga NS, Wang JT, Ramage D, et al. Cytoscape: A Software Environment for Integrated Models of Biomolecular Interaction Networks. *Genome Res* (2003) 13:2498–504. doi: 10.1101/gr.1239303
38. Eddy SR. Accelerated Profile HMM Searches. *PloS Comput Biol* (2011) 7:1002195. doi: 10.1371/journal.pcbi.1002195
39. Vita R, Mahajan S, Overton JA, Dhanda SK, Martini S, Cantrell JR, et al. The Immune Epitope Database (IEDB): 2018 Update. *Nucleic Acids Res* (2019) 47:D339–43. doi: 10.1093/nar/gky1006
40. Galanis KA, Nastou KC, Papandreou NC, Petichakis GN, Pigis DG, Iconomidou VA. Linear B-Cell Epitope Prediction for in Silico Vaccine Design: A Performance Review of Methods Available *via* Command-Line Interface. *bioRxiv* (2021) 833418. doi: 10.1101/833418
41. Sela-Culang I, Kunik V, Ofran Y. The Structural Basis of Antibody-Antigen Recognition. *Front Immunol* (2013) 4:302–15. doi: 10.3389/fimmu.2013.00302
42. Kunik V, Ashkenazi S, Ofran Y. Paratome: An Online Tool for Systematic Identification of Antigen-Binding Regions in Antibodies Based on Sequence or Structure. *Nucleic Acids Res* (2012) 40:W521–4. doi: 10.1093/nar/gks480
43. Liberis E, Velickovic P, Sormanni P, Vendruscolo M, Lio P. Parapred: Antibody Paratope Prediction Using Convolutional and Recurrent Neural Networks. *Bioinformatics* (2018) 34:2944–50. doi: 10.1093/bioinformatics/bty305
44. Reddy Chichili VP, Kumar V, Sivaraman J. Linkers in the Structural Biology of Protein-Protein Interactions. *Protein Sci* (2013) 22:153–67. doi: 10.1002/pro.2206
45. Gowthaman R, Pierce BG. TCR3d: The T Cell Receptor Structural Repertoire Database. *Bioinformatics* (2019) 35:5323–5. doi: 10.1093/bioinformatics/btz517
46. Liu IJ, Hsueh PR, Lin CT, Chiu CY, Kao CL, Liao MY, et al. Disease-Specific B Cell Epitopes for Serum Antibodies From Patients With Severe Acute Respiratory Syndrome (SARS) and Serologic Detection of SARS Antibodies by Epitope-Based Peptide Antigens. *J Infect Dis* (2004) 190:797–809. doi: 10.1086/422753
47. Huang J, Cao Y, Du J, Bu X, Ma R, Wu C. Priming With SARS CoV S DNA and Boosting With SARS CoV S Epitopes Specific for CD4+ and CD8+ T Cells Promote Cellular Immune Responses. *Vaccine* (2007) 25:6981–91. doi: 10.1016/j.vaccine.2007.06.047
48. Lamiable A, Thévenet P, Rey J, Vavrusa M, Derreumaux P, Tufféry P. PEP-FOLD3: Faster De Novo Structure Prediction for Linear Peptides in Solution and in Complex. *Nucleic Acids Res* (2016) 44:W449–54. doi: 10.1093/nar/gkw329
49. Kozakov D, Hall DR, Xia B, Porter KA, Padhorny D, Yueh C, et al. The ClusPro Web Server for Protein-Protein Docking. *Nat Protoc* (2017) 12:255–78. doi: 10.1038/nprot.2016.169
50. Pettersen EF, Goddard TD, Huang CC, Couch GS, Greenblatt DM, Meng EC, et al. UCSF Chimera - A Visualization System for Exploratory Research and Analysis. *J Comput Chem* (2004) 25:1605–12. doi: 10.1002/jcc.20084
51. Wallace AC, Laskowski RA, Thornton JM. Ligplot: A Program to Generate Schematic Diagrams of Protein-Ligand Interactions. *Protein Eng Des Sel* (1995) 8:127–34. doi: 10.1093/protein/8.2.127
52. Zhang L, Jackson CB, Mou H, Ojha A, Peng H, Quinlan BD, et al. SARS-CoV-2 Spike-Protein D614G Mutation Increases Virion Spike Density and Infectivity. *Nat Commun* (2020) 11:1–9. doi: 10.1038/s41467-020-19808-4
53. Takeuchi A, O'Leary DDM. Radial Migration of Superficial Layer Cortical Neurons Controlled by Novel Ig Cell Adhesion Molecule MDGA1. *J Neurosci* (2006) 26:4460–4. doi: 10.1523/JNEUROSCI.4935-05.2006
54. Domin J, Pages F, Volinia S, Rittenhouse SE, Zvelebil MJ, Stein RC, et al. Cloning of a Human Phosphoinositide 3-Kinase With a C2 Domain That Displays Reduced Sensitivity to the Inhibitor Wortmannin. *Biochem J* (1997) 326:139–47. doi: 10.1042/bj3260139
55. Lai CSL, Fisher SE, Hurst JA, Vargha-Khadem F, Monaco AP. A Forkhead-Domain Gene Is Mutated in a Severe Speech and Language Disorder. *Nature* (2001) 413:519–23. doi: 10.1038/35097076
56. Jin J, Arias EE, Chen J, Harper JW, Walter JC. A Family of Diverse Cul4-Ddb1-Interacting Proteins Includes Cdt2, Which Is Required for S Phase Destruction of the Replication Factor Cdt1. *Mol Cell* (2006) 23:709–21. doi: 10.1016/j.molcel.2006.08.010
57. Zou Z, Xie X, Li W, Song X, Tan Y, Wu H, et al. Black Carp TAB1 Up-Regulates TAK1/IRF7/IFN Signaling During the Antiviral Innate Immune Activation. *Fish Shellfish Immunol* (2019) 89:736–44. doi: 10.1016/j.fsi.2019.04.040
58. Yu H, Pardoll D, Jove R. STATs in Cancer Inflammation and Immunity: A Leading Role for STAT3. *Nat Rev Cancer* (2009) 9:798–809. doi: 10.1038/nrc2734
59. Engelbertsen D, Rattik S, Wigren M, Vallejo J, Marinkovic G, Schiopu A, et al. IL-1R and MyD88 Signalling in CD4 + T Cells Promote Th17 Immunity and Atherosclerosis. *Cardiovasc Res* (2018) 114:180–7. doi: 10.1093/cvr/cvx196
60. Jiang T, Yu JT, Zhu XC, Tan L. TREM2 in Alzheimer's Disease. *Mol Neurobiol* (2013) 48:180–5. doi: 10.1007/s12035-013-8424-8
61. García M, Cooper A, Shi W, Bornmann W, Carrion R, Kalman D, et al. Productive Replication of Ebola Virus Is Regulated by the C-Abl1 Tyrosine Kinase. *Sci Transl Med* (2012) 4:1–23. doi: 10.1126/scitranslmed.3003500
62. Chen YJ, Hsieh MY, Chang MY, Chen HC, Jan MS, Maa MC, et al. Eps8 Protein Facilitates Phagocytosis by Increasing TLR4-MyD88 Protein Interaction in Lipopolysaccharide-Stimulated Macrophages. *J Biol Chem* (2012) 287:18806–19. doi: 10.1074/jbc.M112.340935
63. Silverstein RL, Febbraio M. CD36, a Scavenger Receptor Involved in Immunity, Metabolism, Angiogenesis, and Behavior. *Sci Signal* (2009) 2:1–16. doi: 10.1126/scisignal.272re3
64. Duffy EB, Drake JR, Harton JA. Evolving Insights for MHC Class II Antigen Processing and Presentation in Health and Disease. *Curr Pharmacol Rep* (2017) 3:213–20. doi: 10.1007/s40495-017-0097-y

65. Al-Zyoud W, Haddad H. Mutational Sensitivity of D614G in Spike Protein of SARS-CoV-2 in Jordan. *Biochem Biophys Rep* (2021) 25:100896. doi: 10.1016/j.bbrep.2020.100896
66. Cristina Resende P, Gräf T, Carolina Dias Paixão A, Appolinario L, Serrano Lopes R, Carolina da Fonseca Mendonça A, et al. A Potential SARS-CoV-2 Variant of Interest (VOI) Harboring Mutation E484K in the Spike Protein was Identified Within Lineage B.1.1.33 Circulating in Brazil. *bioRxiv* (2021). doi: 10.1101/2021.03.12.434969 2021.03.12.434969.
67. Waqas M, Haider A, Sufyan M, Siraj S, Sehgal SA. Determine the Potential Epitope Based Peptide Vaccine Against Novel SARS-CoV-2 Targeting Structural Proteins Using Immunoinformatics Approaches. *Front Mol Biosci* (2020) 7:227. doi: 10.3389/fmolb.2020.00227
68. Oh DS, Lee HK. Autophagy Protein ATG5 Regulates CD36 Expression and Anti-Tumor MHC Class II Antigen Presentation in Dendritic Cells. *Autophagy* (2019) 15:2091–106. doi: 10.1080/15548627.2019.1596493
69. Srivastava S, Grace PS, Ernst JD. Antigen Export Reduces Antigen Presentation and Limits T Cell Control of M. Tuberculosis. *Cell Host Microbe* (2016) 19:44–54. doi: 10.1016/j.chom.2015.12.003
70. Kang FB, Wang L, Jia HC, Li D, Li HJ, Zhang YG, et al. B7-H3 Promotes Aggression and Invasion of Hepatocellular Carcinoma by Targeting Epithelial-to-Mesenchymal Transition *via* JAK2/STAT3/Slug Signaling Pathway. *Cancer Cell Int* (2015) 15:45–56. doi: 10.1186/s12935-015-0195-z
71. Benwell RK, Lee DR. Essential and Synergistic Roles of IL1 and IL6 in Human Th17 Differentiation Directed by TLR Ligand-Activated Dendritic Cells. *Clin Immunol* (2010) 134:178–87. doi: 10.1016/j.clim.2009.09.013
72. Demberg T, Mohanram V, Musich T, Brocca-Cofano E, McKinnon KM, Venzon D, et al. Loss of Marginal Zone B-Cells in SHIVSF162P4 Challenged Rhesus Macaques Despite Control of Viremia to Low or Undetectable Levels in Chronic Infection. *Virology* (2015) 484:323–33. doi: 10.1016/j.virol.2015.06.022
73. Choi J, Zhou N, Businо L. KLHL6 Is a Tumor Suppressor Gene in Diffuse Large B-Cell Lymphoma. *Cell Cycle* (2019) 18:249–56. doi: 10.1080/15384101.2019.1568765

Conflict of Interest: The authors declare that the research was conducted in the absence of any commercial or financial relationships that could be construed as a potential conflict of interest.

The reviewer JK declared a shared affiliation with one of the authors, RG, to the handling editor at the time of review.

Publisher's Note: All claims expressed in this article are solely those of the authors and do not necessarily represent those of their affiliated organizations, or those of the publisher, the editors and the reviewers. Any product that may be evaluated in this article, or claim that may be made by its manufacturer, is not guaranteed or endorsed by the publisher.

frontiers in Immunology

ORIGINAL RESEARCH
published: 29 September 2021
doi: 10.3389/fimmu.2021.716676

Shotgun Immunoproteomic Approach for the Discovery of Linear B-Cell Epitopes in Biothreat Agents *Francisella tularensis* and *Burkholderia pseudomallei*

Patrik D'haeseleer[1]*, *Nicole M. Collette*[1], *Victoria Lao*[1], *Brent W. Segelke*[1], *Steven S. Branda*[2] and *Magdalena Franco*[1]

[1] Biosciences and Biotechnology Division, Lawrence Livermore National Laboratory, Livermore, CA, United States,
[2] Molecular and Microbiology Department, Sandia National Laboratories, Livermore, CA, United States

OPEN ACCESS

Edited by:
Shisong Jiang,
University of Oxford, United Kingdom

Reviewed by:
Carolyn M. Nielsen,
University of Oxford, United Kingdom
Wayne Robert Thomas,
University of Western Australia, Australia

***Correspondence:**
Patrik D'haeseleer
dhaeseleer2@llnl.gov

Specialty section:
This article was submitted to Vaccines and Molecular Therapeutics, a section of the journal Frontiers in Immunology

Received: *29 May 2021*
Accepted: *02 September 2021*
Published: *29 September 2021*

Citation:
D'haeseleer P, Collette NM, Lao V, Segelke BW, Branda SS and Franco M (2021) Shotgun Immunoproteomic Approach for the Discovery of Linear B-Cell Epitopes in Biothreat Agents Francisella tularensis and Burkholderia pseudomallei. Front. Immunol. 12:716676. doi: 10.3389/fimmu.2021.716676

Peptide-based subunit vaccines are coming to the forefront of current vaccine approaches, with safety and cost-effective production among their top advantages. Peptide vaccine formulations consist of multiple synthetic linear epitopes that together trigger desired immune responses that can result in robust immune memory. The advantages of linear compared to conformational epitopes are their simple structure, ease of synthesis, and ability to stimulate immune responses by means that do not require complex 3D conformation. Prediction of linear epitopes through use of computational tools is fast and cost-effective, but typically of low accuracy, necessitating extensive experimentation to verify results. On the other hand, identification of linear epitopes through experimental screening has been an inefficient process that requires thorough characterization of previously identified full-length protein antigens, or laborious techniques involving genetic manipulation of organisms. In this study, we apply a newly developed generalizable screening method that enables efficient identification of B-cell epitopes in the proteomes of pathogenic bacteria. As a test case, we used this method to identify epitopes in the proteome of *Francisella tularensis* (Ft), a Select Agent with a well-characterized immunoproteome. Our screen identified many peptides that map to known antigens, including verified and predicted outer membrane proteins and extracellular proteins, validating the utility of this approach. We then used the method to identify seroreactive peptides in the less characterized immunoproteome of Select Agent *Burkholderia pseudomallei* (Bp). This screen revealed known Bp antigens as well as proteins that have not been previously identified as antigens. Although B-cell epitope prediction tools Bepipred 2.0 and iBCE-EL classified many of our seroreactive peptides as epitopes, they did not score them significantly higher than the non-reactive tryptic peptides in our study, nor did they assign higher scores to seroreactive peptides from known Ft or Bp antigens, highlighting the need for experimental data instead of relying on computational epitope predictions alone. The present workflow is easily adaptable to

detecting peptide targets relevant to the immune systems of other mammalian species, including humans (depending upon the availability of convalescent sera from patients), and could aid in accelerating the discovery of B-cell epitopes and development of vaccines to counter emerging biological threats.

Keywords: *Francisella*, *Burkholderia*, immunoproteome, B-cell epitope, antigen, peptide vaccine

INTRODUCTION

Development of an effective vaccine against a biothreat agent or emerging pathogen is a costly and cumbersome process that can take years to decades to complete. The identification of antigens that stimulate protective immunity against a pathogen can represent a significant bottleneck in the vaccine development process, especially for bacterial or fungal pathogens, eukaryotic parasites, or even large DNA viruses, which can contain hundreds to thousands of potential antigens. Our study addressed the need to accelerate this process by testing the feasibility of a screening platform for efficient identification of immunoreactive peptides that could be utilized as candidates for development of peptide-based vaccines.

Peptide-based vaccines represent a potential solution to provide protection against biothreat and emerging pathogens to which current vaccine development strategies have failed. Peptide vaccine formulations consist of multiple synthetic linear epitopes that together trigger immune responses resulting in robust immune memory. This multi-epitope, multi-target approach has the potential to be broadly protective across divergent strains (e.g., the first universal influenza vaccine to enter phase III clinical trials was a peptide vaccine), and could be effective for pathogens with complex life cycles (e.g., several malaria peptide vaccines are currently in clinical trials) (1–3). Although it has been reported that conformational (discontinuous) epitopes make up the majority of B-cell epitopes (4), linear epitopes possess several advantages for vaccine design over conformational epitopes. Due to their short sequence and lack of complex secondary and tertiary structure, short antigenic peptides can be easily synthesized, and multiplexed into vaccine formulations, for high-throughput assessment of efficacy. Consequently, peptide-based vaccines are potentially powerful medical countermeasures that would seem amenable to rapid development in responding to infectious disease outbreaks.

Current strategies for epitope identification depend upon detection of epitopes within an individual full-length protein, a low-throughput approach that requires prior knowledge of the antigenic protein, its sequence, and its conformational structure. Technologies to screen for epitopes at the whole proteome level have been developed (e.g., proteomic microarrays, phage and yeast display); however, these technologies require extensive use of synthetic biology and other time-consuming methodologies (e.g., library construction, peptide/protein array preparation, heterologous protein expression) (3, 5–11). Another major disadvantage of display technologies and use of non-native expression systems is that these methods do not reliably replicate the native properties of the antigenic proteins, including their post-translational modifications, which can lead to inaccurate identification of epitopes.

In this study, proteome-wide screening for linear B-cell epitopes was achieved using total protein extracts isolated from the pathogen of interest, affinity purified using antibodies from convalescent sera from infected animals. This strategy holds several advantages over the currently available methods for epitope discovery: It does not require prior knowledge of antigenicity or antigen structure, and obviates need for complex and laborious experimental techniques such as preparation of display libraries and heterologous protein expression. As with other methods for epitope discovery from serum, it may be less well suited for pathogens for which natural infection does not confer immunity, such as HIV, malaria and TB, although even in those cases protective antibodies may be found in some subsets of patients or animal models (12–14).

Our approach was designed to enable identification of the protein antigen and, importantly, the antigenic regions within the identified antigen, such that these short linear peptides can be immediately synthesized and tested for efficacy in vaccine formulations. Note that several strategies have been previously developed for the identification of T-cell peptide epitopes (15, 16), including techniques similar to that presented here involving purification of MHC-bound peptides and their subsequent identification *via* LC/MS/MS (17).

In this study, we focused on two intracellular bacterial pathogens, *Francisella tularensis* (Ft) and *Burkholderia pseudomallei* (Bp), organisms which pose a high risk for misuse as bioweapons and therefore are considered Tier 1 Select Agents by the US Centers for Disease Control and Prevention. The mortality rates of both pathogens are high, and there is currently no licensed vaccine available for either agent (18–20). Humoral immunity plays an important role in developing immune protection to both of these intracellular pathogens, making them good model organisms for the purposes of this study (21–26). In addition, the immunoproteome of Ft has been thoroughly characterized (19, 27, 28), such that the previously published data could be compared to the datasets generated in our study. We leveraged a merged dataset of 164 previously identified antigens, corresponding to ~10% of Ft proteome. The Bp immunoproteome is not as well characterized compared to that of Ft: our reference dataset contained only 61 previously identified seroreactive proteins, corresponding to ~1% of the Bp proteome (29, 30). Consequently, analysis of the dataset resulting from the Bp screen has revealed many proteins that have not been previously categorized as antigens.

MATERIALS AND METHODS

Bacterial Strains and Culture Conditions

Francisella tularensis SCHU S4ΔclpB ("Ft-ΔclpB") was a generous gift from Dr. Wayne Conlan (National Research Council Canada). Stock cultures were prepared by growing Ft-ΔclpB on Chocolate II Agar plates supplemented with hemoglobin and isovitalex (BD 221169) for 48 hours at 37°C. Bacteria were harvested by scraping confluent lawns into Mueller Hinton (MH) broth containing 20% (w/v) sucrose, and stored at -80°C at a concentration 108 - 109 CFU/mL. *Burkholderia pseudomallei* mutant ΔpurM ("Bp82") was obtained from BEI resources (NR-51280). Frozen stocks were prepared by growing the bacteria to log phase in Luria-Bertani (LB) broth, adding glycerol to achieve 20% (w/v) with the bacteria at a final concentration of 10^8 - 10^9 CFU/mL, and storing aliquots at -80°C. For immunizations, the Ft-ΔclpB and Bp82 bacterial stocks were thawed and diluted in sterile phosphate-buffered saline (PBS) to the specified concentrations used for dosing. For protein extraction purposes, Ft-ΔclpB and Bp82 were propagated to log phase in MH and LB broth, respectively. Both bacterial strains used in this study are classified as Risk Group 2 organisms. All biological materials were handled under standard institutional biosafety and biosecurity procedures, as outlined in an approved Institutional Biosafety Committee (IBC) protocol.

Protein Extraction and Peptide Preparation

Ft-ΔclpB and Bp82 were grown to log phase in 300 mL of MH broth or LB broth, respectively, at 37°C with shaking (250 rpm). The bacteria were harvested by centrifugation at 3200 x g for 10 min at 4°C, washed once with 10 mL of PBS, and the pellet flash frozen using dry ice. The bacteria in the pellet were lysed by subjecting them to two freeze-thaw cycles (alternating between room temperature and dry ice). For protein extraction, the lysate was mixed with Bper Complete Bacterial Protein Extraction Reagent (Thermo Fisher Scientific cat# 89822), and the mixture incubated at room temperature for 15 min with rotational shaking. The mixture was then subjected to two rounds of sonication (1 sec pulses, timed output 10 sec, at 50% power) using a Heat Systems Ultrasonics sonicator (model W-385), and centrifuged at 16,000 x g for 10 min. Proteins were precipitated with acetone and washed twice with ethanol. Air-dried protein pellets were solubilized using 8M urea and Protease Max surfactant (Promega cat# V2071), then digested with trypsin (Promega cat# V5111) using the in-solution digestion protocol provided by the manufacturer (Promega cat# TB373). Completion of the trypsinization reaction was confirmed by gel electrophoresis. The trypsin-digested proteins were filtered using 10K MWCO concentrators (Pierce) at 10,000 x g for 20 min at 20°C, and the filtrates (purified peptides) stored at -20°C. These purified peptides preparations were used as inputs in subsequent experiments.

Mice and Immunizations

Mouse immunization studies were carried out in strict accordance with the recommendations in the Guide for the Care and Use of Laboratory Animals and the National Institutes of Health. Standard institutional safety and biosecurity procedures were followed for *in vivo* experiments. Appropriate efforts were made to minimize suffering of animals. All animals were housed in ABSL2 conditions in an AAALAC-accredited facility, and the protocol (Protocol 270, renumbered 284) was approved by the LLNL Institutional Animal Care and Use Committee (IACUC). For immunization, 6 week-old female specific-pathogen-free BALB/c-Elite and C57BL/6J-Elite mice (Charles River) were injected subcutaneously with 10^6 CFU Ft-ΔclpB (BALB/c and C57BL/6J), or intradermally with 10^7 CFU Bp82 (BALB/c), and boosted at 2 weeks. No adjuvants were used. Matched PBS-dosed controls were included for each injection route. Course of infection was monitored by performing daily health scoring and weight measurements. Mice that developed infection wounds (Ft only) were topically treated with Dakin's solution to encourage wound healing, and allowed to remain on test so long as they did not meet humane endpoint criteria (any mice with ~20% body weight loss or overt signs of morbidity were humanely euthanized). Sera from euthanized mice were excluded from analysis due to lack of immunity to the pathogen. Convalescent sera were harvested from resilient mice at 4 weeks post-infection, *via* cardiac puncture terminal bleeding under inhaled isoflurane anesthesia followed by blood fractionation [centrifugation at 3800 x g for 15 min in microtainer serum separator tubes (BD)]. Sera were stored at -80°C.

SDS-PAGE and Western Analysis

Western analysis was performed to confirm seropositivity of infected mice. Bacterial lysates were prepared using Bper Complete Bacterial Protein Extraction Reagent (Thermo Fisher Scientific cat# 89822), combined with Laemmli loading buffer (BioRad), and boiled at 95°C for 5 min. Samples were loaded onto 4-15% acrylamide gels (Mini-Protean TGX, BioRad) and separated by electrophoresis at 120 V for 1 hr. The proteins were transferred from the gels to nitrocellulose membranes (BioRad). Membranes were blocked with Tris-buffered saline plus 0.05% Tween 20 (TBS-T) plus 5% nonfat dry milk, at room temperature for 1 hr or at 4°C for 16 hrs. The membranes were hybridized with mouse sera at 1:500 dilution in TBS-T plus 5% milk, at room temperature for 2 hrs; washed three times with TBS-T; and then incubated with goat anti-mouse antibodies conjugated to HRP (Pierce cat# 1858413), at 1:5000 dilution in TBS-T plus 5% milk, at room temperature for 1 hr. After three TBS-T washes, the membranes were developed using SuperSignal™ West Pico PLUS Chemiluminescent Substrate (Thermo Fisher Scientific).

Enzyme-Linked Immunosorbent Assay

ELISA was performed to assess the level of seropositivity of infected mice. Wells were coated with bacterial lysates and incubated at 4°C for 16 hrs. After three washes with PBS plus 0.1% Tween-20 (PBS-T), sera from infected mice diluted to 1:100 with PBS were added to the wells and incubated at room temperature for 1 hr. Following four PBS-T washes, the wells were incubated for 1 hr with Recombinant Protein A/G peroxidase (Pierce cat# 32490) diluted at 1:5000 with PBS.

After four PBS-T washes, 1-Step ABTS Substrate Solution (Pierce cat# 37615) was added, and after 15 min incubation any colorimetric changes in the wells were detected using a microplate reader (Tecan M200 Pro).

Affinity Purification of Immunoreactive Peptides

Magnetic beads coated with protein G (Invitrogen cat# 10007D) were used to capture antibodies from pools of sera obtained from either infected (experiment) mice or mock-infected (control) mice, following the manufacturer's protocol (MAN0017348). Each pool was comprised of sera recovered from 3-5 mice, with equal volumes used for each experiment-control pair. The antibody-coated beads were then incubated with peptide preparations (inputs) at room temperature for 45 min. Antibody-coated beads from each experiment-control pair were incubated with the same input peptides; in total, 6 input peptide preparations were used with the 8 Ft experiment-control pairs, and 5 with the 9 Bp experiment-control pairs. Following three PBS washes, immunoreactive peptides were eluted from the beads using citrate buffer (pH 3). Input, unbound, and eluted (output) peptides were flash frozen with dry ice and stored at -20°C.

Mass Spectrometry

The input, unbound, and eluted (output) peptides recovered from the antibody-coated beads (see preceding section) were desalted using an Empore SD solid phase extraction plate; lyophilized; reconstituted in 0.1% TFA; and analyzed *via* LC-MS/MS by MS Bioworks (Ann Arbor, Michigan), using a Waters M-Class UPLC system interfaced to a ThermoFisher Fusion Lumos mass spectrometer. Peptides were loaded on a trapping column and eluted over a 75 μm analytical column at 350 nL/min. Both columns were packed with Luna C18 resin (Phenomenex). A 2 hr gradient was employed. The mass spectrometer was operated in a data dependent HCD mode, with MS and MS/MS performed in the Orbitrap at 60,000 FWHM resolution and 15,000 FWHM resolution, respectively. The instrument was run with a 3 sec cycle for MS and MS/MS.

MS Data Processing

Data were analyzed using Mascot (Matrix Science) with the following parameters: Enzyme: Trypsin/P; Database: UniProt *F. tularensis* SCHU S4 or UniProt *B. pseudomallei* strain 1026b (forward and reverse appended with common contaminants and mouse IgG sequences); Fixed modification: Carbamidomethyl (C); Variable modifications: Oxidation (M), Acetyl (N-term), Pyro-Glu (N-term Q), Deamidation (N/Q); Mass values: Monoisotopic; Peptide Mass Tolerance: 10 ppm; Fragment Mass Tolerance: 0.02 Da; Max Missed Cleavages: 2; Mascot DAT files were parsed into Scaffold Proteome Software for validation, filtering and to create a non-redundant list per sample. Data were filtered using 1% protein and peptide FDR and requiring at least one unique peptide per protein.

Bioinformatic Analysis

Each experiment typically consisted of three sets of data: "Input" (total bacterial peptides without affinity purification), "Control" (peptides purified from beads coated with antibodies from uninfected mice), and "Experiment" (peptides purified from beads coated with antibodies from infected mice).

LC-MS/MS data were analyzed at the peptide level, rather than rolling up peptide scores into a protein abundance metric as would be done in standard proteomics. We used the Total Ion Current (TIC, total area under the MS2 curve) as a metric for the abundance of the peptide in each sample. Input datasets were first normalized against each other based on median ratios for the peptides occurring in every Input dataset. The sparser Control and Experiment datasets were then normalized against their respective Input dataset based on median ratios as well. Since each animal can be expected to raise a different set of antibodies, we counted how often specific output peptides occurred more abundantly in the Experiment *vs* Control, rather than focusing on the average log fold change in abundance. For each peptide and each Experiment sample, we assigned an enrichment score of +1, 0, or -1 depending on whether the normalized peptide abundance was greater than, equal to, or lower in the Experiment than in the corresponding Control sample, creating a score matrix of peptides × Experiments. The total enrichment score for each peptide is then the sum of its enrichment scores across each Experiment. Statistical significance was evaluated by generating a number of randomized score matrices, where each peptide was randomly assigned a +1, 0, or -1 score for each Experiment, with the same probabilities as in the real matrix, and calculating how frequently peptides reach an specific total enrichment score. This gives us a background level of how many high-scoring peptides we would expect to see even if there was no correlation in peptide abundance across the different experiments, which can then be used to calculate the significance level of observing a given number of high scoring peptides in the real data, using a simple binomial test comparing expected *vs* observed number of peptides exceeding a given score.

Amino Acid Conservation Scores were calculated using the ConSurf web server (31) with default parameter values, using near full-length protein structure homology models from SWISS-MODEL or crystal structures from PDB where available. These scores are normalized position-specific evolutionary rates, with negative scores indicating the most conserved amino acids. The Average Amino Acid Conservation Score (AAACS), proposed by Ren et al. as a useful tool to identify conserved epitopes that may be targeted by broadly neutralizing antibodies, is the average of the conservation score for the residues in an epitope, with negative scores indicating more highly conserved regions (32).

In addition to AAACS, we also scored peptides based on how many complete sequenced genomes of pathogenic *B. pseudomallei* and *F. tularensis* they occurred in, similar to the conservation analysis in EpitoCore (33). We downloaded proteomes for all 110 *B. pseudomallei* strains with complete genome sequences available through NCBI. For *F. tularensis*, 36 strains with complete genomes were available through NCBI, but

several of these corresponded to the less-pathogenic *novicida*, *holartica* and *mediasiatica* subspecies, so we decided to focus exclusively on the 17 available *F. tularensis* subsp. *tularensis* complete genomes. We identified homologs with ≥90% sequence identity to the proteins containing our top scoring peptides in **Tables 1**, **2**, and then scored each peptide based on how often they had a 100% identical hit in each homolog.

We used two state-of-the-art computational B-cell epitope prediction tools to evaluate all of the peptides in our proteomic data that match the proteins in **Tables 1**, **2**. Peptides were submitted to the iBCE-EL web server for scoring (34). iBCE-EL is an ensemble-based method based on extremely randomized tree and gradient boosting classifiers, trained on 5,550 experimentally validated B-cell epitopes and 6,893 non-epitopes from the Immune Epitope Database, to identify linear B-cell epitopes. In addition, proteins were submitted to the Bepipred Linear Epitope Prediction 2.0 tool on the IEDB website (35), and peptides were then scored based on their average predicted residue score. Bepipred 2.0 is a random forest classifier trained on 160 non-redundant antigen-antibody crystal structures, to predict the probability that a given antigen residue is part of an epitope.

TABLE 1 | List of top scoring immunoreactive peptides identified for *Francisella tularensis*.

Protein name	Accession	Peptide	Scores
Aminotransferase AspC1	Q5NGG1	LPIDDAEK[2]	
Glutamate dehydrogenase Gdh	Q5NHR7[a]	FHPSVYSGIIK	
Pyruvate dehydrogenase acetyltransferase AceF	Q5NEX3[a]	VSQGSLILK[2]	
60 kDa chaperonin GroL	Q5NEE1[a]	DRVDDALHATR[2]	
Chaperone protein DnaK	Q5NFG7[a]	NTADNLIHSSR	
Chaperone protein DnaK	Q5NFG7[a]	SSSGLSEEDIEK	
60 kDa chaperonin GroL	Q5NEE1[a]	DNTTIIDGAGEK	
60 kDa chaperonin GroL	Q5NEE1[a]	EGVITVEEGK	
Catalase-peroxidase KatG	Q5NGV7[a]	AVAQVYAENGNEQK	
Malate dehydrogenase Mdh	Q5NHC8[a]	FSGVPDNK[1]	
Outer membrane protein 26 Omp26	Q5NES2[o]	EIPADQLGTIK	
Succinate dehydrogenase flavoprotein SdhA	Q5NIJ3[a,i]	ITILATGGAGR	
ATP synthase subunit alpha AtpA	Q5NIK5[a]	GEVATDLTSPIEK	
Elongation factor Ts Tsf	Q5NHX9[a]	ESGKPAEIIEK	
Elongation factor Ts Tsf	Q5NHX9[a]	TVEAETLGAYIHGSK	
Chaperone protein DnaK	Q5NFG7[a]	IAGLEVK[1]	
Cell division protein FtsZ	Q5NI93[a]	KETEVVTGASNAPK	
Trigger factor Tig	Q5NH48	GGVDTFENEIK	
ATP synthase subunit alpha AtpA	Q5NIK5[a]	SVDQALQTGIK	
Catalase-peroxidase KatG	Q5NGV7[a]	NDNLSPQSVDLSPLR	
Isocitrate dehydrogenase [NADP] Idh	Q5NET6[a]	VADIELETK[2]	
Fructose-1,6-bisphosphate aldolase FbaB	Q5NF78[a]	KINIDTDLR	
Glutamate dehydrogenase Gdh	Q5NHR7[a]	GFVHDPEGITTDEK	
Succinate–CoA ligase [ADP-forming] beta SucC	Q5NHF3[a]	PANFLDVGGGATK[1]	
Chaperone protein DnaK	Q5NFG7[a]	KVPYAVIK[2]	
Malonyl CoA-ACP transacylase	Q5NF69[a]	EPTTAVVQNFDAK	
Peroxiredoxin	Q5NHA9[a]	KVPNVTFK[2]	
Chaperone protein DnaK	Q5NFG7[a]	IINEPTAAALAYGVDSK	
Conserved hypothetical lipoprotein LpnA	Q5NGE4[a,o]	ATVYTTYNNNPQGSVR	
Elongation factor Tu Tuf	Q5NID9[a]	TTVTGVEMFR	
Succinate–CoA ligase [ADP-forming] beta SucC	Q5NHF3[a]	EVAESLIGK[1]	
30S ribosomal protein S1 RpsA	Q5NI98[a]	KIELWDR[2]	
Elongation factor Tu Tuf	Q5NID9[a]	HYAHVDCPGHADYVK[1]	
Transcription elongation factor GreA	Q5NFC6[a]	IVGEDEADIDNQK	
60 kDa chaperonin GroL	Q5NEE1[a]	SFGTPTITK[2]	
Aconitate hydratase AcnA	Q5NII1[a]	GIPLVILAGK[1]	
Chaperone protein DnaK	Q5NFG7[a]	AYAEQAQAAVAQGGAK	
Chaperone protein DnaK	Q5NFG7[a]	FHDLVTAR[2]	
Outer membrane protein 26 Omp26	Q5NES2	DGSVGWVK[1]	
3-oxoacyl-ACP reductase FabG	Q5NF68	VALVTGASR[1]	
Chaperone protein DnaK	Q5NFG7[a]	ALEDAGLSK[2]	
Enoyl-ACP reductase [NADH] FabI	Q5NGQ3[i]	TLAASGISNFK	
Aconitate hydratase AcnA	Q5NII1[a]	TAHTTTFEALAR	
Elongation factor Ts Tsf	Q5NHX9[a]	LDVGEGIEK[1]	

The columns under "scores" indicate whether the peptide was over or underrepresented in each of the 8 experimental samples compared to its control sample. Blue: experiment>control. Red: experiment<control. White: peptide undetected in both experiment and control. Dark colors indicate >2-fold difference in relative abundance. Proteins with multiple top scoring peptides are highlighted in bold. See also ***Supplementary Table S1*** *for an extended version of this table.*

[a]*known antigen,* [i]*inner membrane,* [o]*outer membrane.*

[1]*peptide sequence is only a single amino acid away from a human or mouse peptide.* [2]*peptide is only two amino acids away from a human or mouse peptide.*

TABLE 2 | List of top scoring immunoreactive peptides identified for *Burkholderia pseudomallei*.

Protein name	Accession	Peptide	Scores
Aspartate–tRNA(Asp/Asn) ligase AspS	A0A0H3HT48	TGAQDGDIIFFAADR	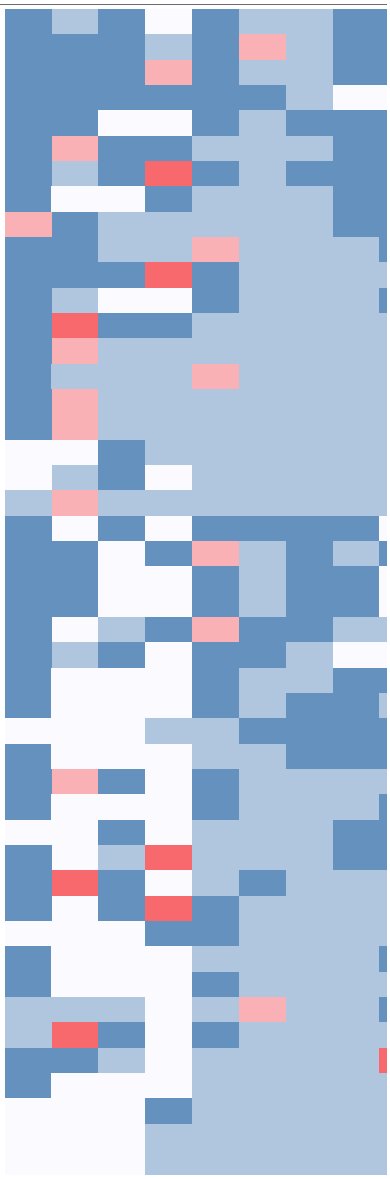
Adenylosuccinate synthetase PurA	A0A0H3HJJ2	QDQIGITLANVGK	
Dihydrolipoyl dehydrogenase OdhL	A0A0H3HQK7	FPFSINGR[2]	
Ankyrin repeat-containing protein	A0A0H3HJC7	IGDAPAPNAQK	
Phosphoribosylformylglycinamidine synthase PurL	A0A0H3HPH9	GATETFVVLPR	
DNA-directed RNA polymerase subunit beta RpoB	A0A0H3HT47	STGPYSLVTQQPLGGK	
50S ribosomal protein L6 RplF	A0A0H3HQ22	GYRPPEPYK	
DNA-directed RNA polymerase subunit beta RpoC	A0A0H3HP07	ISLYATTVGR	
Enolase Eno	A0A0H3HLA6	GIANSILIK[2]	
Uncharacterized protein	A0A0H3HWA2	IDCLTNAYTAR	
DNA gyrase subunit A GyrA	A0A0H3HKL0	INVVLPVR[2]	
Aspartate-semialdehyde dehydrogenase Asd	A0A0H3HW74	VTGTLSVPVGR	
Malic enzyme	A0A0H3HP28	AALLSNSNFGSAPSASSR	
50S ribosomal protein L10 RplJ	A0A0H3HUR4	AQTVVLAEYR	
50S ribosomal protein L6 RplF	A0A0H3HQ22	AIIANAVHGVTK	
Glutamine synthetase GlnA	A0A0H3HL61	ALNAITNPTTNSYK	
Nucleoside diphosphate kinase Ndk	A0A0H3HJK0[e]	NVIGQIYSR[2]	
Antioxidant protein LsfA	A0A0H3HGZ9	LIITYPASTGR	
UDP-glucose 4-epimerase	A0A0H3HFV2	GYSVLEVVR	
Enolase Eno	A0A0H3HLA6	SAIVDIIGR[2]	
Acetyl-CoA acetyltransferase	A0A0H3HTT4	LPLSVGCTTINK	
KHG/KDPG aldolase Eda	A0A0H3HGE0	FGVSPGLTR[2]	
10 kDa chaperonin GroES	A0A0H3HH83[a]	TASGIVIPDAAAEKPDQGEVLAIGPGKR	
Saccharopine dehydrogenase	A0A0H3HIF5	HGQLVQDVFTR	
Citrate synthase GltA	A0A0H3HYU5	YSIGQPFVYPR	
Aspartate–tRNA(Asp/Asn) ligase AspS	A0A0H3HT48	YVAAHHPFTSPK	
Gamma-aminobutyraldehyde dehydrogenase	A0A0H3HQU5	SVLAAAAGNLK[2]	
Peptide chain release factor 2 PrfB	A0A0H3HL96	SYVLDQSR[2]	
Polyketide non-ribosomal peptide synthase	A0A0H3HWL5[i]	AWFIPLSAR[2]	
Transcription termination/antitermination NusG	A0A0H3HPU8	VTGFVGGAR[2]	
Beta sliding clamp DnaN	A0A0H3HFM1	FTFGQVELVSK	
Malate synthase AceB	A0A0H3HIT5	IATLIVRPR[2]	
PTS system, EIIA component	A0A0H3HRL4	ISGHHLEVTPAIR	
Phosphoenolpyruvate synthase PpsA	A0A0H3HJ13	IFILQARPETVK	
Thiol:disulfide interchange protein DsbA	A0A0H3HTS6[p]	NYNIDGVPTIVVQGK	
RND family efflux transporter MFP subunit BpeA	A0A0H3HQZ3[i]	AQANLATQNALVAR	
Inosine-5'-monophosphate dehydrogenase GuaB	A0A0H3HJ23	LVGIVTNR[1]	
Periplasmic maltose-binding protein MalE	A0A0H3HG39[p]	VNWLYINK	
Putative extracellular ligand binding protein	A0A0H3HWC6[p]	VVATDAQQGPALADYAK	
Acid phosphatase AcpA	A0A0H3HV11[e]	NIVVIYAENR	
NADH-quinone oxidoreductase subunit F NuoF	A0A0H3HPW5	EGTGWLYR[2]	
Type VI secretion system Hcp-1	A0A0H3HE88[e]	IGGNQGGNTQGAWSLTK	
50S ribosomal protein L23 RplW	A0A0H3HT35	AAVELLFK[2]	
50S ribosomal protein L6 RplF	A0A0H3HQ22	LTLVGVGYR	
50S ribosomal protein L17 RplQ	A0A0H3HPQ2	LFDVLGPR[2]	
Aconitate hydratase	A0A0H3HVV9	IVLESVLR[1]	

The columns under "scores" indicate whether the peptide was over or underrepresented in each of the 9 experimental samples compared to its control sample. Blue: experiment>control. Red: experiment<control. White: peptide undetected in both experiment and control. Dark colors indicate >2-fold difference in relative abundance. Proteins with multiple top scoring peptides are highlighted in bold. See also ***Supplementary Table S2*** *for an extended version of this table.*

[a]known antigen, [i]inner membrane, [p]periplasmic, [e]extracellular.

[1]peptide sequence is only a single amino acid away from a human or mouse peptide. [2]peptide is only two amino acids away from a human or mouse peptide.

RESULTS

Overview of Immunoproteome Screen

In this study, we tested the feasibility of proteome-wide screening for linear B-cell epitopes using peptide extracts from target bacteria and sera from infected animals. The method requires: (1) isolation of peptides from lysates generated from the target bacteria; (2) challenge of the host (in this case, mouse) with the target bacteria, followed by collection of convalescent serum; (3) mixing of the bacterial peptides and convalescent serum, to allow peptide antigens to bind to their cognate antibodies in the serum; and (4) recovery of bound peptides for identification through mass spectrometry (**Figure 1**). We applied this method to two bacterial Select Agent pathogens: *Francisella tularensis* and *Burkholderia pseudomallei*. Infection with attenuated strains of these pathogens [*F. tularensis* SCHU S4ΔclpB and *B. pseudomallei* ΔpurM (strain Bp82)] has been shown to stimulate development of protective immunity against their corresponding fully-virulent parental strains (*F. tularensis* SCHU S4 and *B. pseudomallei* K96245, respectively) (36, 37), suggesting that convalescent sera

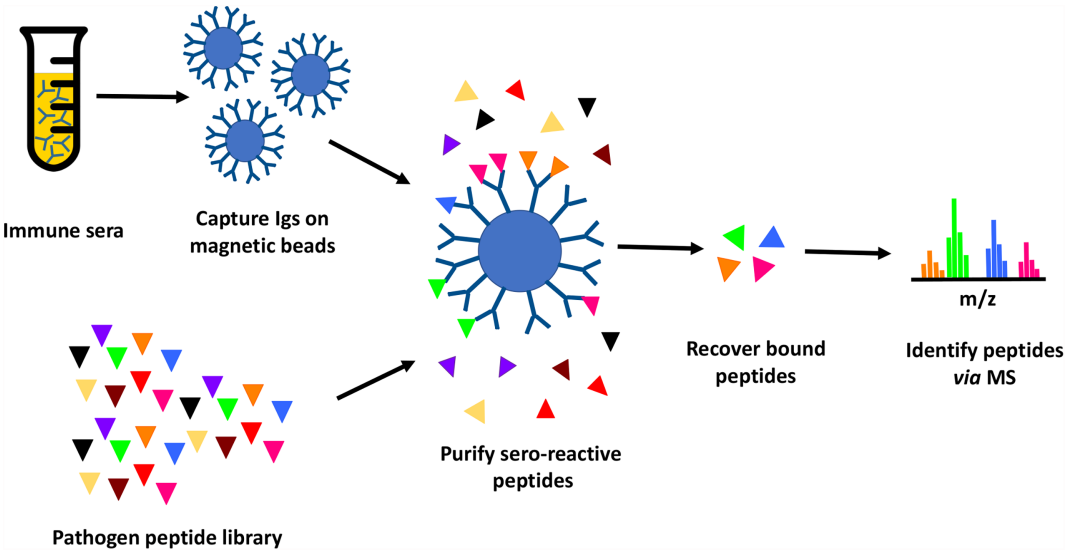

FIGURE 1 | Immunoproteome screening workflow. Schematic overview of high throughput approach for identification of seroreactive peptides in the proteomes of pathogens.

recovered from hosts infected with these attenuated pathogens must contain protective antibodies.

Briefly, proteins purified from pathogen lysates were digested with trypsin to generate a peptide library. Mice were infected with a sublethal dose of Ft-ΔclpB or Bp82, and immune status assessed through observed weight loss and measurement of seroreactivity of mouse sera to pathogen lysates *via* enzyme-linked immunosorbent assay (ELISA) or Western blot analysis (**Figure 2**). Antibodies purified from the convalescent sera of infected mice were immobilized on magnetic beads and then incubated with pathogen-derived peptides to allow formation of antigen-antibody complexes. Peptides recovered from the immobilized antibodies were identified *via* liquid chromatography coupled with tandem mass spectrometry.

Bioinformatic Identification of Enriched Antigenic Peptides

The peptides recovered using pooled sera from infected mice (Experiment peptidome) were compared to those recovered from mock-infected mice (Control peptidome); a total of 8 pairs of Experiment-Control peptidomes were collected for Ft, and 9 pairs for Bp. For Ft, we found that out of the 1923 peptides that were recovered in at least two Experiment peptidomes, 44 had an enrichment score of 6 or greater (**Table 1**), whereas only 20.1 +/- 6.1 peptides would be expected at random ($p=1x10^{-6}$). For Bp, out of 2902 peptides that were recovered in at least two Experiment peptidomes, 46 peptides had an enrichment score of 6 or greater (**Table 2**), whereas only 17.8 +/- 4.3 peptides would be expected at random ($p=1.9x10^{-9}$). If a more stringent enrichment cutoff is desired, we found 16 Ft peptides with an enrichment score of 7 or greater, *versus* 3.5+/-1.6 expected at random ($p=1.8x10^{-7}$), and 20 Bp peptides with an enrichment score of 7 or greater, *versus* 4.1+/-2.1 expected at random ($p=3.9x10^{-9}$). The enriched peptides included some that were derived from protective antigens identified in previous studies, as well as predicted outer membrane and extracellular proteins (**Tables 1**, **2**). There were many examples of multiple enriched peptides originating from the same protein (highlighted in bold in the tables), a further indication that enrichment was not random but rather due to immune response to a discrete set of bacterial proteins.

Note that we used C57BL/6J mice for two of the eight Ft experimental samples, because of previously reported differences in protection and antibody response after immunization of C57BL/6J and BALB/c mice with Ft-ΔclpB by Twine et al. (38). Analyzing the BALB/c Ft samples separately yielded a very similar set of results as in **Table 1**, but with lower p-value for the enrichment due to the smaller number of samples (data not shown). Therefore, we decided to combine the data and focus on antibody responses in common between both strains of mice. Although Twine et al. reported an antibody response against chaperonin protein GroL only in BALB/c mice, our data shows that there are several GroL epitopes that are enriched in samples from both mouse strains (see **Table 1** and **Figure 4**).

Prior immunoproteomics analysis of the antibody response to *F. tularensis* using human or mouse sera has identified 164 antibody targets out of a total of 1667 proteins (~10% of the entire Ft proteome) (19, 27, 28). Out of the 1923 peptides that have hits in at least two Ft datasets, 876 peptides match known antigenic proteins. Given those numbers, we would expect only 20 such peptides to show up at random in our list of 44 in **Table 1**, but instead we observe that 38/44 peptides in the list correspond to known antigens - an almost two-fold enrichment ($p=2.79x10^{-9}$). Note that despite the extensive literature on

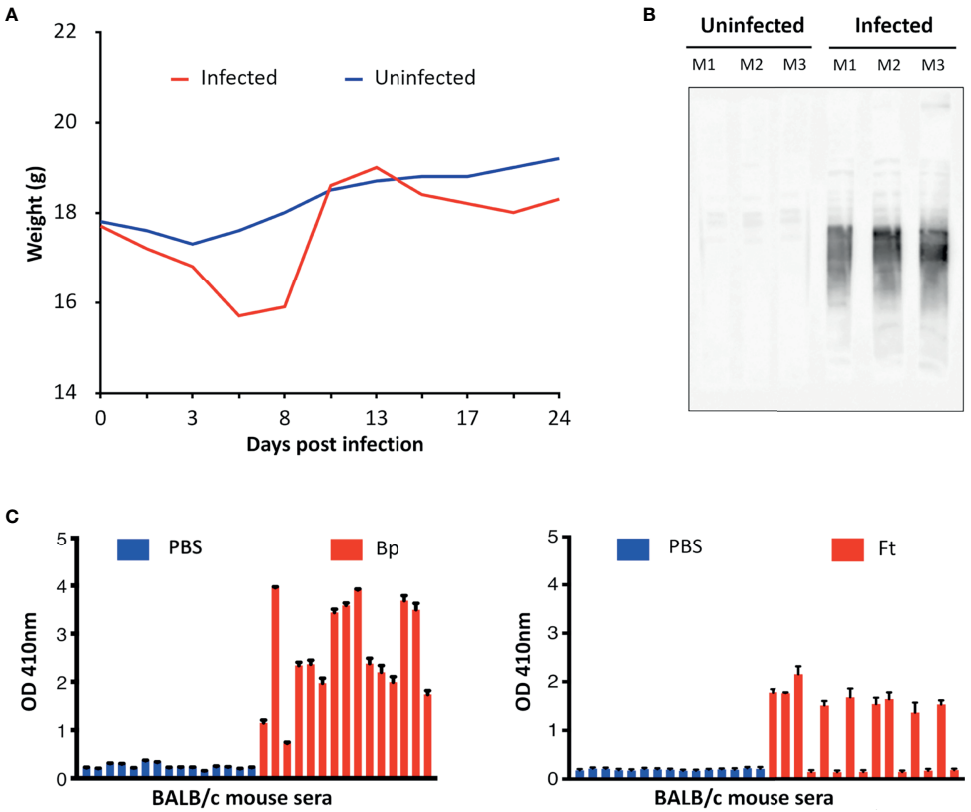

FIGURE 2 | **(A)** Representative course of mouse infection to obtain immune sera. Mice were infected with a sublethal dose of Bp and their weight monitored. Weight was monitored throughout the course of infection. **(B)** Representative Western blot of sera from infected *vs* uninfected mice. Bp protein lysates were analyzed by Western blotting using sera from infected and uninfected mice (Mouse 1–3) and bound antibodies detected using anti-mouse HRP. **(C)** Representative ELISA results obtained from mice infected with Bp and Ft (red) in comparison with uninfected mice (PBS-treated mice, blue). Seroreactivity of mice sera to microwells coated with corresponding pathogen lysate was assessed using protein-A/G-HRP and measuring sample absorbance (optical density). Sera of some mice infected with Ft did not yield positive results because Ft infection led to lethal outcome and mice had to be euthanized during the course of immunization. Graphs represent two technical replicates for sera collected from each mouse. Antibodies from sera with the strongest Western blot and ELISA signals were purified in this study and used to screen for immunogenic peptides.

antigens in Ft, only five B-cell epitopes have been experimentally determined (**Figure 4B**), justifying the need for a simple experimental epitope screening method. The immune response to *B. pseudomallei* has not been studied in as much depth as for *Francisella*. So even though Bp with 6203 protein coding genes has a genome that is more than three times as large as that of Ft, we found only 61 known antigens identified in previous studies (29, 30) (~1% of the entire proteome). Our list of 46 top Bp peptides in **Table 1** includes one known antigen, which does not qualify as a statistically significant enrichment primarily because of the much smaller total number of known antigens for Bp.

Figure 3 shows all 46 Ft DnaK peptides that were detected in at least two Experiment samples, regardless of their degree of enrichment. Eight of these DnaK peptides are in our list of 44 enriched Ft peptides (**Table 1** and red line segments in **Figure 3A**), including two that are enriched in all 8 Experiments (red line segments in **Figure 3A**). Note the lack of correlation between our experimental enrichment scores and the iBCE-EL and Bepipred scores (**Figures 3B, C**). All but one of the 8 enriched peptides are conserved in all 17 fully sequenced Ft strains (**Figure 3E**), but some of the peptides towards the C-terminal show a greater evolutionary rate as measured by their Average Amino Acid conservation Score (AAACS, **Figure 3D**) and thus may be more prone to immune escape mutants.

Figure 4 shows all 32 Ft GroL peptides that were detected in at least two Experiment samples in our study, regardless of the degree of their enrichment. Four of these GroL peptides are in our list of 44 enriched Ft peptides (**Table 1** and red line segments in **Figure 4A**), including three that are enriched in all eight Experiments. Lu et al. (39) used hydrogen/deuterium exchange–mass spectrometry (DXMS) to experimentally identify one discontinuous and four linear B-cell epitopes for a selection of mouse monoclonal antibodies against GroL (**Figure 4B**). Note that one of the four enriched peptides in **Figure 4A** (DNTTIIDGAGEK) overlaps with a linear epitope (NTTIIDGAGEKEAIAKRINVIK) and a discontinuous epitope (SEDLSMKLEETNM—NTTIIDGAGEKEAIA) identified by DXMS in **Figure 4B**, while a second enriched peptide

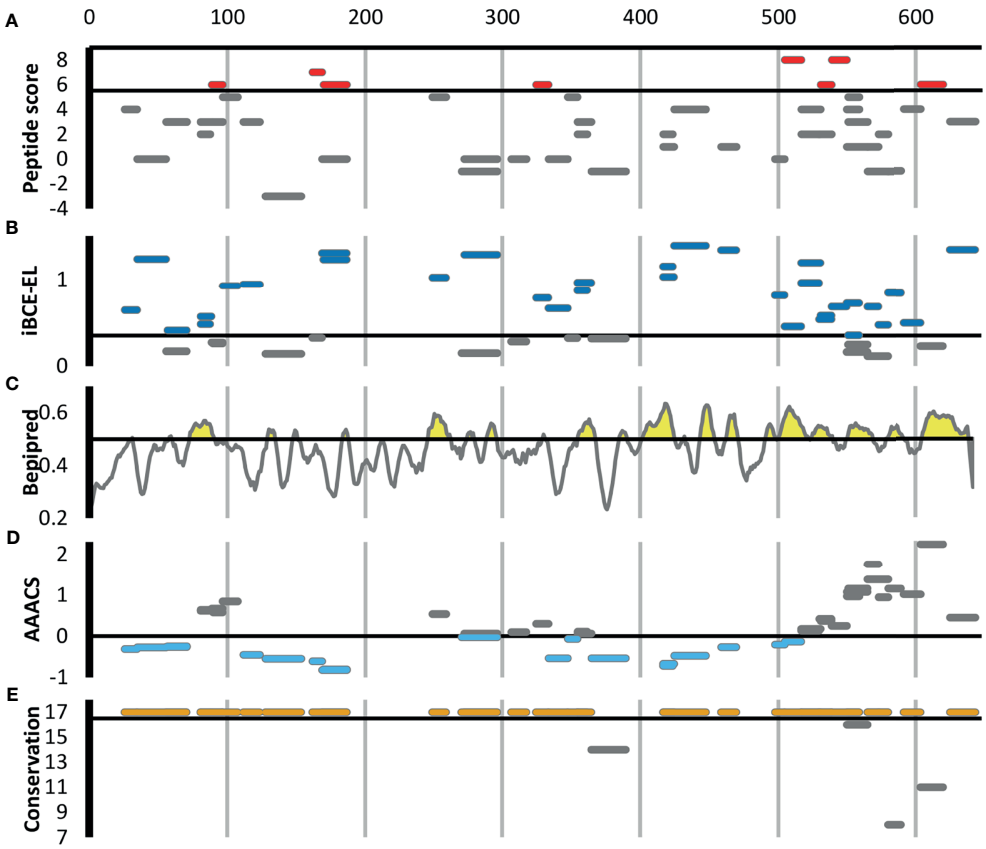

FIGURE 3 | Scoring for the 46 *F. tularensis* DnaK peptides detected in at least two Experiment samples. The short horizontal line segments in A, B, E and F indicate the position of a peptide along the length of the 642aa DnaK protein, and its vertical position within each figure panel indicates its score for the metric indicated. The default score threshold for each tool is shown with a horizontal line, and the peptides or per-amino acid scores exceeding that threshold are shown in color. **(A)** Peptide enrichment score based on our proteomics results. An enrichment score of 8 indicates that the peptide was detected in greater abundance in all 8 Experiment samples relative to their respective Control samples. The threshold for inclusion in **Table 1** was an enrichment score of ≥6 (shown in red). **(B)** B-cell epitope prediction score generated using iBCE-EL. At the default iBCE-EL score threshold of 0.35, nearly three quarter of all peptides were predicted to be likely B-cell epitopes (shown in dark blue). **(C)** B-cell epitope prediction score generated using Bepipred 2.0. The per-amino acid scores are indicated by the line graph. At the default iBCE-EL score threshold of 0.35, 37% of all amino acids were predicted to be in B-cell epitopes (regions of the graph shown in yellow). **(D)** Average Amino Acid Conservation Score (AAACS) based on Consurf analysis. Negative scores indicate greater degrees of evolutionary conservation (shown in light blue). **(E)** Number of fully sequenced *F. tularensis* subsp. tularensis genomes (17 analyzed) in which each peptide occurs. Almost all of the DnaK peptides considered were conserved in all 17 Ft genomes (shown in orange).

(EGVITVEEGK) is directly adjacent to another of the linear DXMS epitopes (FEDEL). According to the Immune Epitope Database (IEDB) (40), these are the only experimentally validated B-cell epitopes for Ft (IEDB also lists four B. pseudomallei antigens that have been assayed for B-cell epitopes, none of which overlap with the proteins in **Table 1**).

DISCUSSION

We have developed a widely applicable shotgun immunoproteomic method that enables efficient identification of B-cell epitopes in the proteomes of pathogens. The results of this study have revealed a significant enrichment of peptides derived from previously identified antigens and vaccine candidates, validating the method's efficacy. This method was designed to identify linear epitopes efficiently without the need of genetic manipulation or other experimental techniques that can be costly and labor intensive. Attenuated strains made the optimization of this proof-of-concept study more efficient; however, the availability of an attenuated strain for the target organism does not represent a limitation, as our strategy could be applied to fully virulent strains of pathogens as well. Although the present study was performed using a mouse model, the workflow could be easily adapted to detecting targets relevant to the human immune system, using convalescent sera from patients.

Utilizing peptide antigens for vaccine development has several advantages over typical vaccine development efforts. Similar to other types of subunit vaccines, peptide vaccines represent a safer alternative to attenuated vaccines due to lack of any potentially infectious materials in the vaccine formulation. Use of short peptides sufficient for stimulation of immune response favors

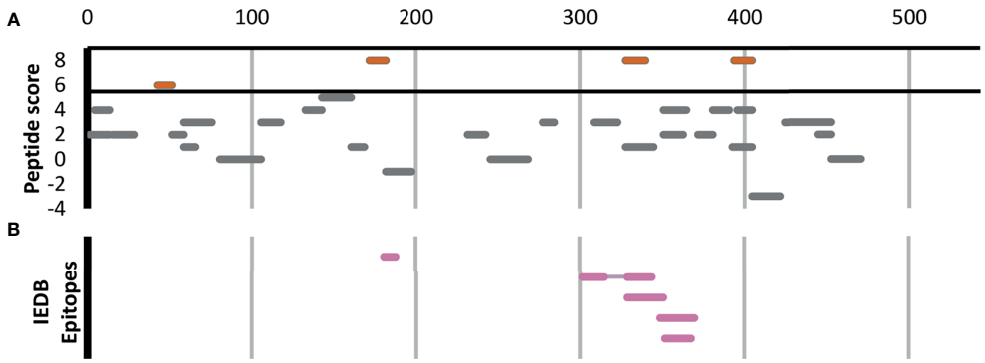

FIGURE 4 | The 32 *F. tularensis* GroL peptides detected in at least two Experiment samples. Horizontal line segments indicate the position of each peptide along the length of the 544aa GroL protein sequence. **(A)** Peptide enrichment score based on our proteomics results, with a score of 8 indicating that the peptide was found in greater abundance in all 8 Experiment samples relative to their respective Control samples. The threshold for inclusion in **Table 1** was a score of ≥6 or better (shown in red). **(B)** Five B-cell epitopes identified by DXMS by Lu et al. (39), including one discontinuous epitope.

exclusion of deleterious sequences that may be present in full length antigenic proteins. Peptide vaccine formulations are defined and their contents fully synthetic, which simplifies quality control procedures and thereby streamlines the regulatory approval process. Production of peptide vaccines is expected to be relatively fast and inexpensive, due to ease of synthesis and recent advances in improved peptide stability (3, 41, 42). Moreover, once antigenic peptides are identified, evaluation of their efficacy could represent a lesser challenge due to the possibility of multiplexing peptides during *in vivo* trials, rather than use of one-at-a-time testing

Among Ft proteins, the present screen identified multiple peptides for two well-characterized antigens, 60kDa chaperonin GroL (Q5NEE1) and chaperone protein DnaK (Q5NFG7). Both chaperonins have been previously implicated in virulence of Francisella (43–45), and are known to induce antibody production in mice and humans (27, 46, 47). These chaperonin proteins are important for facilitating folding of nascent proteins as well as post-translational modifications. They are also known as heat-shock proteins, as they protect cellular proteins from environmental stresses such as high temperature and low pH (47, 48). Although their cellular localization is predicted to be cytoplasmic, they reportedly also associate with membrane proteins and are released into host cells during infection (47, 49–51) perhaps contributing to their ability to stimulate various immune functions, including innate immunity, humoral immunity and cell-mediated immunity (43, 47, 52–55). Heat-shock proteins are good candidates for subunit vaccine design due to their ability to stimulate various immune responses without the need of adjuvant; in fact, both GroL and DnaK have been exploited for vaccine development efforts targeting *Francisella* and other pathogens (39, 47, 56, 57).

Highly virulent Type A *Francisella* strains such as SCHU S4 can bind host plasminogen to the bacterial cell surface where it can be converted to plasmin, a serine protease that degrades opsonizing antibodies, inhibiting antibody-mediated uptake by macrophages (58, 59). Among the 25 Ft proteins listed in **Table 1**, we find at least 3 that are known to be involved in plasminogen binding in *Francisella* or other pathogens, including conserved hypothetical lipoprotein LpnA (Q5NGE4) (59), fructose-1,6-bisphosphate aldolase (Q5NF78) (60), and elongation factor Tu (Q5NID9) (61). These proteins could make for particularly attractive vaccine targets, because if we can interfere with their function before the pathogen has activated its plasmin-mediated antibody evasion, that would make it more susceptible to other antibodies as well.

Among the antigenic peptides identified in the Bp proteome are those belonging to Type VI secretion system component Hcp-,1 and previously identified antigen 10kDa chaperonin GroES (62). Hcp-1 was previously found to be a major virulence determinant in *Burkholderia* and recognized by sera from infected human patients and animals (63–65). Due to this, Hcp-1 has been interrogated as a potential candidate for *Burkholderia* vaccine development (63–65). Additionally, a peptide from an ankyrin repeat-containing protein (A0A0H3HJC) came up as one of the highest scoring peptides in our study. Ankyrin repeats are typically eukaryotic protein domains involved in protein-protein interactions (66), but have been co-opted by many bacterial pathogens as type IV secreted effector proteins to mimic or manipulate various host functions (67).

Recovery of peptides derived from several supposedly cytosolic enzymes may seem puzzling. However several "housekeeping" enzymes are known to be displayed on the surface of pathogens where they play a role in virulence (68). For example, our top scoring peptides from *B. pseudomallei* include two derived from enolase (A0A0H3HLA6). While enolase is primarily thought of as a key glycolytic enzyme, it is also expressed on the surface of a wide variety of bacterial and fungal pathogens, where it interacts with host plasminogen and is associated with invasion and virulence (69). Antibodies against enolase have been detected in a large variety of infectious and autoimmune diseases (70). It is as yet unknown whether enolase plays the same role in Burkholderia, but the protein is predicted to be present both in the cytoplasm and on the cell surface, and

its production was found to be upregulated upon exposure to human lung epithelial cells (71). Other housekeeping proteins in our top scoring results whose homologs in other pathogens are known to play a role in adhesion, invasion, or virulence include elongation factor Tu (Q5NID9), malic enzyme/malate dehydrogenase (A0A0H3HP28, Q5NHC8), and fructose-1,6-bisphosphate aldolase (Q5NF78) (68).

Overall, this immunoproteomic workflow has identified numerous peptides mapping to previously identified antigens and subunit vaccine targets, predicted membrane-associated proteins, as well as uncharacterized proteins. The Ft datasets revealed a significant enrichment of peptides belonging to previously identified antigenic proteins in Experiment samples relative to their respective Control samples, providing validation to this approach. Interestingly, several of these known antigens also yielded multiple top scoring peptides in our analysis. Despite the large amount of prior immunoproteomic analysis on Ft, covering ~10% of the genome, experimentally validated B-cell epitopes are available for only a single protein, and our analysis captures two out of its five known epitopes. Due to the much smaller number of previously identified antigens for Burkholderia, we were not able to tell whether the enrichment in the Bp datasets was significant. Improved proteome coverage and more comprehensive immunogenic profiles could be achieved with the use of alternative enzymes with different specificities, since there is a risk of ablating epitopes that contain cut sites recognized by specific enzymes such as trypsin. Alternatively, performing incomplete digestion with one enzyme, or a cocktail of enzymes with different specificities, could increase the number of overlapping peptides and thereby improve the yield and diversity of identified epitopes. In addition, since the presented method is dependent upon extraction of proteins from whole cell lysates, it is conceivable that the proteome coverage could be biased toward highly abundant proteins or those proteins that are easier to extract, despite this disadvantage we have detected several membrane-bound antigens in this study.

A variety of computational B-cell epitope prediction tools have been developed to identify epitopes in antigens. However accurate computational prediction of B-cell epitopes still poses a major challenge (72), with sensitivity or specificity typically below 60% (35, 73–76), leading some recent in-silico multi-epitope vaccine design efforts to look at the consensus of up to 8 or 9 B-cell epitope prediction tools simultaneously (77, 78). The recent development of prediction tools using state-of-the-art machine learning models that claim significantly higher performance on large benchmarking datasets seems promising (34, 79). Here we compare the performance of Bepipred 2.0 (35), one of the most widely used B-cell prediction tools, and iBCE-EL (34). Interestingly, we find no significant correlation between the peptides experimentally identified using the method described here and computationally predicted linear B-cell epitope scores generated by Bepipred 2.0 and iBCE-EL, even for those antibody-binding peptides belonging to known Ft or Bp antigens, nor do we find any significant correlation between the Bepipred 2.0 and iBCE-EL scores themselves (see **Supplementary Tables S1, S2**, as well as **Figures 3A–C** for Ft DnaK), highlighting the value of an unbiased experimental method to screen for antibody targets, as presented here. At their default score thresholds, iBCE-EL correctly predicts 34/44 of the Ft peptides, and 39/46 of the Bp peptides, while Bepipred 2.0 correctly predicts 21/44 Ft peptides and 13/46 Bp peptides, but that is not actually significantly more than would be expected at random given their hit rates on other un-enriched tryptic peptides in our dataset. Part of the discrepancy between the computational Bepipred 2.0 predictions and our experimental results may be due to the fact that Bepipred 2.0 is trained on antigen-antibody 3D structures, which likely contain a mix of conformational and linear epitopes. In addition, Bepipred 2.0 has a relatively low self-reported 58.6% sensitivity and 57.2% specificity at the default score threshold of 0.5 (80), and thus is expected to exhibit a large number of false positives and false negative predictions. iBCE-EL is reported to have better sensitivity and specificity [73.2% and 72.4% (34)], but explicitly takes into account sequence features at the beginning and end of the epitope that may be missing in the tryptic peptides generated here, affecting their score. In cases where the tryptic peptide is too short to be used directly as a vaccine candidate (some are as short as 6 residues), we may in fact be able to use these computational tools to guide us in how to extend the boundaries of the peptide beyond its flanking trypsin cleavage sites.

Note that computational B-cell prediction tools such as these are trained to distinguish epitopes from non-epitopes in known antigens, but are not an effective alternative to experimentally screening for epitopes across an entire bacterial proteome. For example, on a random selection of 100 Ft and Bp proteins, Bepipred-2.0 using its default epitope threshold of 0.5 classified 40% of all amino acids as being part of an epitope, including an average of 5.5 peptides of length 9 or longer per protein (data not shown). Likewise, on a random selection of 1000 tryptic peptides from all our proteomics data, iBCE-EL classified 81% as B-cell epitopes using its default score threshold of 0.35 (data not shown). Applied across the entire proteome, the computational approach would predict tens of thousands of putative B-cell epitopes, likely with a high false-positive rate and, regardless, providing little guidance in winnowing the possibilities for experimental verification.

If so desired, peptides can be downselected for vaccine development by focusing only on those with the most stringent enrichment scores, or based on consensus with computational epitope prediction tools. Further downselection may include prioritizing highly conserved epitopes that can induce broadly protective immunity, and reduce the risk that emergence of pathogen variants will render the vaccine ineffective (81). ~90% of the top scoring peptides were found to be present in 90% or more of the fully sequenced pathogenic F. tularensis and B. pseudomallei strains (see **Supplementary Tables S1, S2**, and **Figure 3F** for the case of Ft DnaK). In addition, we can target peptides that show even deeper evolutionary conservation based on their Average Amino Acid Conservation Score (AAACS), reflecting parts of the protein that may be important for its function (31) (see **Supplementary Tables S1, S2**, and **Figure 3E** for the case of Ft DnaK). Peptides that are only one or two amino

acids different from human or mouse versions are likely less suitable as vaccine candidates and are marked with a subscript 1 or 2 respectively in **Tables 1**, **2**. Note that while some of the proteins in **Tables 1**, **2** have homologs in human and mouse (e.g. mitochondrial DnaK), the peptides recovered here are unique to the bacterial versions. For vaccine design, we may also want to prioritize peptides which do not tend to occur in healthy human microbiomes, by comparing them against some of the large human metaproteomics datasets recently generated (82–86).

Further confirmation that the identified sequences are B-cell epitopes could be achieved through additional *in vitro* and *in vivo* experimentation (e.g., testing the reactivity of immune sera with synthesized candidate epitopes *via* ELISA or immunization studies). High throughput screening of peptides for efficacy is feasible due to recent advancements in solid phase peptide synthesis (SPPS), which enables efficient and cost-effective production of peptide candidates (3). For immunization studies, pools of multiple peptides could be incorporated into vaccine delivery systems containing adjuvants and T-helper epitopes known to stimulate the induction of adaptive immune response against peptide antigens, as reviewed in Skwarczynski et al. (3).

The method presented here identifies peptides that are immunoreactive, that is, they interact with antibodies in serum from previously infected individuals. Further experimental test would be needed to confirm immunogenicity, that is, whether they can stimulate antibody production themselves, and protectivity, that is, whether they can protect against infection or disease after immunization. Our immunoproteomic method represents a new tool for precise mapping of linear B-cell epitopes. Generation of such immunogenic profiles for pathogens could provide an ample pool of candidates for further experimental validation and efficient vaccine development. Accelerating the discovery of B-cell epitopes in the proteomes of pathogens will help fuel the development of peptide-based vaccines that have the potential to provide rapid solutions to biothreat agents and emerging pathogens.

DATA AVAILABILITY STATEMENT

The datasets presented in this study can be found in online repositories. The names of the repository/repositories and accession number(s) can be found below: https://www.ebi.ac.uk/pride/archive/, PXD026300 (87).

ETHICS STATEMENT

The animal study was reviewed and approved by LLNL Institutional Animal Care and Use Committee.

AUTHOR CONTRIBUTIONS

PD'h, NC, and MF contributed to the conception and design of the study. NC performed the *in vivo* experiments. VL provided laboratory support. VL and MF performed *in vitro* experimentation. PD performed the bioinformatics analysis. BS and SB provided critical input. All authors contributed to the article and approved the submitted version.

FUNDING

This work was supported by Lawrence Livermore National Laboratory Directed Research and Development Program (LLNL LDRD) Labwide grant (18-LW-039) to MF, and by the LDRD program (grant 218309) at Sandia National Laboratories, a multi-mission laboratory managed and operated by National Technology and Engineering Solutions of Sandia, LLC, a wholly owned subsidiary of Honeywell International, Inc., for the U.S. Department of Energy's National Nuclear Security Administration under contract DE-NA0003525. Work at LLNL was performed under the auspices of the U.S. Department of Energy by Lawrence Livermore National Laboratory under Contract DE-AC52-07NA27344. LLNL IM release number LLNL-JRNL-822446. The funders were not involved in the study design, collection, analysis, interpretation of data, the writing of this article or the decision to submit it for publication.

ACKNOWLEDGMENTS

We thank Dr. Wayne Conlan (National Research Council Canada) for providing *Francisella tularensis* SCHU S4ΔclpB strain. Bp 82 reagent was obtained through BEI Resources, NIAID, NIH: *Burkholderia pseudomallei*, Strain Bp82 (Δ*purM*), NR-51280. Our thanks go to Michael Ford and MS Bioworks team for help with sample preparation troubleshooting and specialized mass spectrometry analyses. We also thank past and present members of our laboratories - Drs. Sahar El-Etr, José Peña, Amy Rasley, and Emilio Garcia - for useful discussions and critical input.

SUPPLEMENTARY MATERIAL

The Supplementary Material for this article can be found online at: https://www.frontiersin.org/articles/10.3389/fimmu.2021.716676/full#supplementary-material

REFERENCES

1. Li W, Joshi MD, Singhania S, Ramsey KH, Murthy AK. Peptide Vaccine: Progress and Challenges. *Vaccines Basel* (2014) 2(3):515–36. doi: 10.3390/vaccines2030515
2. Malonis RJ, Lai JR, Vergnolle O. Peptide-Based Vaccines: Current Progress and Future Challenges. *Chem Rev* (2020) 120(6):3210–29. doi: 10.1021/acs.chemrev.9b00472
3. Skwarczynski M, Toth I. Peptide-Based Synthetic Vaccines. *Chem Sci* (2016) 7 (2):842–54. doi: 10.1039/C5SC03892H
4. Sun P, Ju H, Liu Z, Ning Q, Zhang J, Zhao X, et al. Bioinformatics Resources and Tools for Conformational B-Cell Epitope Prediction. *Comput Math Methods Med* (2013) 2013:943636. doi: 10.1155/2013/943636
5. Dudek NL, Perlmutter P, Aguilar MI, Croft NP, Purcell AW. Epitope Discovery and Their Use in Peptide Based Vaccines. *Curr Pharm Des* (2010) 16(28):3149–57. doi: 10.2174/138161210793292447

6. Wang AP, Li N, Zhou JM, Chen YM, Jiang M, Qi YH, et al. Mapping the B Cell Epitopes Within the Major Capsid Protein L1 of Human Papillomavirus Type 16. *Int J Biol Macromol* (2018) 118:1354–61. doi: 10.1016/j.ijbiomac.2018.06.094
7. Zhao DM, Han KK, Huang XM, Zhang LJ, Wang HL, Liu N, et al. Screening and Identification of B-Cell Epitopes Within Envelope Protein of Tembusu Virus. *Virol J* (2018) 15:142. doi: 10.1186/s12985-018-1052-1
8. Bi Y, Jin Z, Wang Y, Mou S, Wang W, Wei Q, et al. Identification of Two Distinct Linear B Cell Epitopes of the Matrix Protein of the Newcastle Disease Virus Vaccine Strain LaSota. *Viral Immunol* (2019) 32(5):221–9. doi: 10.1089/vim.2019.0007
9. Jaenisch T, Heiss K, Fischer N, Geiger C, Bischoff FR, Moldenhauer G, et al. High-Density Peptide Arrays Help to Identify Linear Immunogenic B-Cell Epitopes in Individuals Naturally Exposed to Malaria Infection. *Mol Cell Proteomics* (2019) 18(4):642–56. doi: 10.1074/mcp.RA118.000992
10. Yang W-J, Lai J-F, Peng K-C, Chiang H-J, Weng C-N, Shiuan D. Epitope Mapping of Mycoplasma Hyopneumoniae Using Phage Displayed Peptide Libraries and the Immune Responses of the Selected Phagotopes. *J Immunol Methods* (2005) 304(1–2):15–29. doi: 10.1016/j.jim.2005.05.009
11. Mullen LM, Nair SP, Ward JM, Rycroft AN, Henderson B. Phage Display in the Study of Infectious Diseases. *Trends Microbiol* (2006) 14(3):141–7. doi: 10.1016/j.tim.2006.01.006
12. Ndam NT, Denoeud-Ndam L, Doritchamou J, Viwami F, Salanti A, Nielsen MA, et al. Protective Antibodies Against Placental Malaria and Poor Outcomes During Pregnancy, Benin. *Emerg Infect Dis* (2015) 21(5):813–23. doi: 10.3201/eid2105.141626
13. Gonzales SJ, Reyes RA, Braddom AE, Batugedara G, Bol S, Bunnik EM. Naturally Acquired Humoral Immunity Against *Plasmodium Falciparum* Malaria. *Front Immunol* (2020) 11:594653. doi: 10.3389/fimmu.2020.594653
14. Li H, Wang X-X, Wang B, Fu L, Liu G, Lu Y, et al. Latently and Uninfected Healthcare Workers Exposed to TB Make Protective Antibodies Against Mycobacterium Tuberculosis. *Proc Natl Acad Sci USA* (2017) 114(19):5023–8. doi: 10.1073/pnas.1611776114
15. Sharma G, Holt RA. T-Cell Epitope Discovery Technologies. *Hum Immunol* (2014) 75(6):514–9. doi: 10.1016/j.humimm.2014.03.003
16. Sharma G, Rive CM, Holt RA. Rapid Selection and Identification of Functional CD8+ T Cell Epitopes From Large Peptide-Coding Libraries. *Nat Commun* (2019) 10:4553. doi: 10.1038/s41467-019-12444-7
17. Caron E, Kowalewski DJ, Chiek Koh C, Sturm T, Schuster H, Aebersold R. Analysis of Major Histocompatibility Complex (MHC) Immunopeptidomes Using Mass Spectrometry. *Mol Cell Proteomics MCP* (2015) 14(12):3105–17. doi: 10.1074/mcp.O115.052431
18. Dienst FT. Tularemia: A Perusal of Three Hundred Thirty-Nine Cases. *J State Med Soc* (1963) 115:114–27.
19. Fulton KM, Zhao X, Petit MD, Kilmury SLN, Wolfraim LA, House RV, et al. Immunoproteomic Analysis of the Human Antibody Response to Natural Tularemia Infection With Type A or Type B Strains or LVS Vaccination. *Int J Med Microbiol IJMM* (2011) 301(7):591–601. doi: 10.1016/j.ijmm.2011.07.002
20. Gibney KB, Cheng AC. Reducing the Melioidosis Burden: Public Health, Chronic Disease Prevention, or Improved Case Management? *Lancet Infect Dis* (2019) 19(8):800–2. doi: 10.1016/S1473-3099(19)30303-2
21. Mara-Koosham G, Hutt JA, Lyons CR, Wu TH. Antibodies Contribute to Effective Vaccination Against Respiratory Infection by Type A Francisella Tularensis Strains. *Infect Immun* (2011) 79(4):1770–8. doi: 10.1128/IAI.00605-10
22. Ray HJ, Cong Y, Murthy AK, Selby DM, Klose KE, Barker JR, et al. Oral Live Vaccine Strain-Induced Protective Immunity Against Pulmonary Francisella Tularensis Challenge Is Mediated by CD4+ T Cells and Antibodies, Including Immunoglobulin a. *Clin Vaccine Immunol CVI* (2009) 16(4):444–52. doi: 10.1128/CVI.00405-08
23. Rhinehart-Jones TR, Fortier AH, Elkins KL. Transfer of Immunity Against Lethal Murine Francisella Infection by Specific Antibody Depends on Host Gamma Interferon and T Cells. *Infect Immun* (1994) 62(8):3129–37. doi: 10.1128/iai.62.8.3129-3137.1994
24. Hogan RJ, Lafontaine ER. Antibodies Are Major Drivers of Protection Against Lethal Aerosol Infection With Highly Pathogenic *Burkholderia* spp. *mSphere* (2019) 4:e00674–18. doi: 10.1128/mSphere.00674-18
25. Jones SM, Ellis JF, Russell P, Griffin KF, Oyston PCF. Passive Protection Against *Burkholderia Pseudomallei* Infection in Mice by Monoclonal Antibodies Against Capsular Polysaccharide, Lipopolysaccharide or Proteins. *J Med Microbiol* (2002) 51(12):1055–62. doi: 10.1099/0022-1317-51-12-1055
26. Khakhum N, Bharaj P, Myers JN, Tapia D, Kilgore PB, Ross BN, et al. *Burkholderia Pseudomallei* ΔtonB Δhcp1 Live Attenuated Vaccine Strain Elicits Full Protective Immunity Against Aerosolized Melioidosis Infection. *mSphere* (2019) 4:e00670-18. doi: 10.1128/mSphere.00570-18
27. Kilmury SLN, Twine SM. The Francisella Tularensis Proteome and its Recognition by Antibodies. *Front Microbiol* (2010) 1:143. doi: 10.3389/fmicb.2010.00143
28. Nakajima R, Escudero R, Molina DM, Rodríguez-Vargas M, Randall A, Jasinskas A, et al. Towards Development of Improved Serodiagnostics for Tularemia by Use of Francisella Tularensis Proteome Microarrays. *J Clin Microbiol* (2016) 54(7):1755–65. doi: 10.1128/JCM.02784-15
29. Felgner PL, Kayala MA, Vigil A, Burk C, Nakajima-Sasaki R, Pablo J, et al. A *Burkholderia Pseudomallei* Protein Microarray Reveals Serodiagnostic and Cross-Reactive Antigens. *Proc Natl Acad Sci U S A* (2009) 106(32):13499–504. doi: 10.1073/pnas.0812080106
30. Yi J, Simpanya MF, Settles EW, Shannon AB, Hernandez K, Pristo L, et al. Caprine Humoral Response to Burkholderia Pseudomallei Antigens During Acute Melioidosis From Aerosol Exposure. *PloS Negl Trop Dis* (2019) 13(2):e0006851. doi: 10.1371/journal.pntd.0006851
31. Ashkenazy H, Abadi S, Martz E, Chay O, Mayrose I, Pupko T, et al. ConSurf 2016: An Improved Methodology to Estimate and Visualize Evolutionary Conservation in Macromolecules. *Nucleic Acids Res* (2016) 44(W1):W344–50. doi: 10.1093/nar/gkw408
32. Ren J, Ellis J, Li J. Influenza A Ha's Conserved Epitopes and Broadly Neutralizing Antibodies: A Prediction Method. *J Bioinform Comput Biol* (2014) 12(5):1450023. doi: 10.1142/S0219720014500231
33. Fiuza TS, Lima JPMS, de Souza GA. EpitoCore: Mining Conserved Epitope Vaccine Candidates in the Core Proteome of Multiple Bacteria Strains. *Front Immunol* (2020) 11:816. doi: 10.3389/fimmu.2020.00816
34. Manavalan B, Govindaraj RG, Shin TH, Kim MO, Lee G. iBCE-EL: A New Ensemble Learning Framework for Improved Linear B-Cell Epitope Prediction. *Front Immunol* (2018) 9:1695. doi: 10.3389/fimmu.2018.01695
35. Jespersen MC, Peters B, Nielsen M, Marcatili P. BepiPred-2.0: Improving Sequence-Based B-Cell Epitope Prediction Using Conformational Epitopes. *Nucleic Acids Res* (2017) 45(W1):W24–9. doi: 10.1093/nar/gkx346
36. Conlan JW, Shen H, Golovliov I, Zingmark C, Oyston PC, Chen W, et al. Differential Ability of Novel Attenuated Targeted Deletion Mutants of Francisella Tularensis Subspecies Tularensis Strain SCHU S4 to Protect Mice Against Aerosol Challenge With Virulent Bacteria: Effects of Host Background and Route of Immunization. *Vaccine* (2010) 28(7):1824–31. doi: 10.1016/j.vaccine.2009.12.001
37. Propst KL, Mima T, Choi KH, Dow SW, Schweizer HP. A Burkholderia Pseudomallei deltapurM Mutant is Avirulent in Immunocompetent and Immunodeficient Animals: Candidate Strain for Exclusion From Select-Agent Lists. *Infect Immun* (2010) 78(7):3136–43. doi: 10.1128/IAI.01313-09
38. Twine S, Shen H, Harris G, Chen W, Sjostedt A, Ryden P, et al. BALB/c Mice, But Not C57BL/6 Mice Immunized With a ΔclpB Mutant of Francisella tularensis Subspecies Tularensis are Protected Against Respiratory Challenge With Wild-Type Bacteria: Association of Protection With Post-Vaccination and Post-Challenge Immune Responses. *Vaccine* (2012) 30(24):3634–45. doi: 10.1016/j.vaccine.2012.03.036
39. Lu Z, Rynkiewicz MJ, Madico G, Li S, Yang CY, Perkins HM, et al. B-Cell Epitopes in GroEL of Francisella tularensis. *PloS One* (2014) 9(6):e99847. doi: 10.1371/journal.pone.0099847
40. Vita R, Mahajan S, Overton JA, Dhanda SK, Martini S, Cantrell JR, et al. The Immune Epitope Database (IEDB): 2018 Update. *Nucleic Acids Res* (2019) 47(D1):D339–43. doi: 10.1093/nar/gky1006
41. Purcell AW, McCluskey J, Rossjohn J. More Than One Reason to Rethink the Use of Peptides in Vaccine Design. *Nat Rev Drug Discovery* (2007) 6(5):404–14. doi: 10.1038/nrd2224
42. Sun T, Han H, Hudalla GA, Wen Y, Pompano RR, Collier JH. Thermal Stability of Self-Assembled Peptide Vaccine Materials. *Acta Biomater* (2016) 30:62–71. doi: 10.1016/j.actbio.2015.11.019

43. Noah CE, Malik M, Bublitz DC, Camenares D, Sellati TJ, Benach JL, et al. GroEL and Lipopolysaccharide From Francisella Tularensis Live Vaccine Strain Synergistically Activate Human Macrophages. *Infect Immun* (2010) 78(4):1797–806. doi: 10.1128/IAI.01135-09
44. Pechous RD, McCarthy TR, Zahrt TC. Working Toward the Future: Insights Into Francisella tularensis Pathogenesis and Vaccine Development. *Microbiol Mol Biol Rev* (2009) 73(4):684–711. doi: 10.1128/MMBR.00028-09
45. Weiss DS, Brotcke A, Henry T, Margolis JJ, Chan K, Monack DM. *In Vivo* Negative Selection Screen Identifies Genes Required for Francisella Virulence. *Proc Natl Acad Sci USA* (2007) 104(14):6037–42. doi: 10.1073/pnas.0609675104
46. Havlasova J, Hernychova L, Brychta M, Hubalek M, Lenco J, Larsson P, et al. Proteomic Analysis of Anti-Francisella Tularensis LVS Antibody Response in Murine Model of Tularemia. *Proteomics* (2005) 5(8):2090–103. doi: 10.1002/pmic.200401123
47. Huntley JF, Conley PG, Hagman KE, Norgard MV. Characterization of Francisella tularensis Outer Membrane Proteins. *J Bacteriol* (2007) 189 (2):561–74. doi: 10.1128/JB.01505-06
48. Ericsson M, Tarnvik A, Kuoppa K, Sandstrom G, Sjostedt A. Increased Synthesis of DnaK, GroEL, and GroES Homologs by Francisella Tularensis LVS in Response to Heat and Hydrogen Peroxide. *Infect Immun* (1994) 62 (1):178–83. doi: 10.1128/iai.62.1.178-183.1994
49. Henderson B, Allan E, Coates AR. Stress Wars: The Direct Role of Host and Bacterial Molecular Chaperones in Bacterial Infection. *Infect Immun* (2006) 74(7):3693–706. doi: 10.1128/IAI.01882-05
50. Hickey TB, Thorson LM, Speert DP, Daffe M, Stokes RW. Mycobacterium Tuberculosis Cpn60.2 and DnaK are Located on the Bacterial Surface, Where Cpn60.2 Facilitates Efficient Bacterial Association With Macrophages. *Infect Immun* (2009) 77(8):3389–401. doi: 10.1128/IAI.00143-09
51. Lee BY, Horwitz MA, Clemens DL. Identification, Recombinant Expression, Immunolocalization in Macrophages, and T-Cell Responsiveness of the Major Extracellular Proteins of Francisella tularensis. *Infect Immun* (2006) 74 (7):4002–13. doi: 10.1128/IAI.00257-06
52. Ashtekar AR, Zhang P, Katz J, Deivanayagam CC, Rallabhandi P, Vogel SN, et al. TLR4-Mediated Activation of Dendritic Cells by the Heat Shock Protein DnaK From Francisella tularensis. *J Leukoc Biol* (2008) 84(6):1434–46. doi: 10.1189/jlb.0308215
53. Kol A, Bourcier T, Lichtman AH, Libby P. Chlamydial and Human Heat Shock Protein 60s Activate Human Vascular Endothelium, Smooth Muscle Cells, and Macrophages. *J Clin Invest* (1999) 103(4):571–7. doi: 10.1172/JCI5310
54. Wallin RP, Lundqvist A, More SH, von Bonin A, Kiessling R, Ljunggren HG. Heat-Shock Proteins as Activators of the Innate Immune System. *Trends Immunol* (2002) 23(3):130–5. doi: 10.1016/S1471-4906(01)02168-8
55. Valentino MD, Maben ZJ, Hensley LL, Woolard MD, Kawula TH, Frelinger JA, et al. Identification of T-Cell Epitopes in Francisella Tularensis Using an Ordered Protein Array of Serological Targets. *Immunology* (2011) 132 (3):348–60. doi: 10.1111/j.1365-2567.2010.03387.x
56. Ashtekar AR, Katz J, Xu Q, Michalek SM. A Mucosal Subunit Vaccine Protects Against Lethal Respiratory Infection With Francisella tularensis LVS. *PloS One* (2012) 7(11):e50460. doi: 10.1371/journal.pone.0050460
57. Khan MN, Shukla D, Bansal A, Mustoori S, Ilavazhagan G. Immunogenicity and Protective Efficacy of GroEL (Hsp60) of Streptococcus Pneumoniae Against Lethal Infection in Mice. *FEMS Immunol Med Microbiol* (2009) 56 (1):56–62. doi: 10.1111/j.1574-695X.2009.00548.x
58. Crane DD, Warner SL, Bosio CM. A Novel Role for Plasmin Mediated Degradation of Opsonizing Antibody in the Evasion of Host Immunity by Virulent, But Not Attenuated, Francisella tularensis. *J Immunol Baltim Md 1950* (2009) 183(7):4593–600. doi: 10.4049/jimmunol.0901655
59. Clinton SR, Bina JE, Hatch TP, Whitt MA, Miller MA. Binding and Activation of Host Plasminogen on the Surface of Francisella tularensis. *BMC Microbiol* (2010) 10:76. doi: 10.1186/1471-2180-10-76
60. Shams F, Oldfield NJ, Wooldridge KG, Turner DPJ. Fructose-1,6-Bisphosphate Aldolase (FBA)-A Conserved Glycolytic Enzyme With Virulence Functions in Bacteria: "Ill Met by Moonlight." *Biochem Soc Trans* (2014) 42(6):1792–5. doi: 10.1042/BST20140203
61. Kunert A, Losse J, Gruszin C, Hühn M, Kaendler K, Mikkat S, et al. Immune Evasion of the Human Pathogen Pseudomonas Aeruginosa: Elongation Factor Tuf is a Factor H and Plasminogen Binding Protein. *J Immunol Baltim Md 1950* (2007) 179(5):2979–88. doi: 10.4049/jimmunol.179.5.2979
62. Varga JJ, Vigil A, DeShazer D, Waag DM, Felgner P, Goldberg JB. Distinct Human Antibody Response to the Biological Warfare Agent Burkholderia mallei. *Virulence* (2012) 3(6):510–4. doi: 10.4161/viru.22056
63. Burtnick MN, Brett PJ, Harding SV, Ngugi SA, Ribot WJ, Chantratita N, et al. The Cluster 1 Type VI Secretion System Is a Major Virulence Determinant in Burkholderia pseudomallei. *Infect Immun* (2011) 79(4):1512–25. doi: 10.1128/IAI.01218-10
64. Schell MA, Ulrich RL, Ribot WJ, Brueggemann EE, Hines HB, Chen D, et al. Type VI Secretion is a Major Virulence Determinant in Burkholderia mallei. *Mol Microbiol* (2007) 64(6):1466–85. doi: 10.1111/j.1365-2958.2007.05734.x
65. Whitlock GC, Deeraksa A, Qazi O, Judy BM, Taylor K, Propst KL, et al. Protective Response to Subunit Vaccination Against Intranasal Burkholderia mallei and B. pseudomallei Challenge. *Proc Vaccinol* (2010) 2:73–7. doi: 10.1016/j.provac.2010.03.013
66. Li J, Mahajan A, Tsai M-D. Ankyrin Repeat: A Unique Motif Mediating Protein-Protein Interactions. *Biochemistry* (2006) 45(51):15168–78. doi: 10.1021/bi062188q
67. Pan X, Lührmann A, Satoh A, Laskowski-Arce MA, Roy CR. Ankyrin Repeat Proteins Comprise a Diverse Family of Bacterial Type IV Effectors. *Science* (2008) 320(5883):1651–4. doi: 10.1126/science.1158160
68. Pancholi V, Chhatwal GS. Housekeeping Enzymes as Virulence Factors for Pathogens. *Int J Med Microbiol IJMM* (2003) 293(6):391–401. doi: 10.1078/1438-4221-00283
69. Lottenberg R, Minning-Wenz D, Boyle MD. Capturing Host Plasmin(Ogen): A Common Mechanism for Invasive Pathogens? *Trends Microbiol* (1994) 2 (1):20–4. doi: 10.1016/0966-842X(94)90340-9
70. Terrier B, Degand N, Guilpain P, Servettaz A, Guillevin L, Mouthon L. Alpha-Enolase: A Target of Antibodies in Infectious and Autoimmune Diseases. *Autoimmun Rev* (2007) 6(3):176–82. doi: 10.1016/j.autrev.2006.10.004
71. Al-Maleki AR, Mariappan V, Vellasamy KM, Tay ST, Vadivelu J. Altered Proteome of Burkholderia Pseudomallei Colony Variants Induced by Exposure to Human Lung Epithelial Cells. *PloS One* (2015) 10(5):e0127398. doi: 10.1371/journal.pone.0127398
72. Sun P, Guo S, Sun J, Tan L, Lu C, Ma Z. Advances in In-Silico B-Cell Epitope Prediction. *Curr Top Med Chem* (2019) 19(2):105–15. doi: 10.2174/1568026619666181130111827
73. Larsen JEP, Lund O, Nielsen M. Improved Method for Predicting Linear B-Cell Epitopes. *Immunome Res* (2006) 2:2. doi: 10.1186/1745-7580-2-2
74. Ponomarenko J, Bui H-H, Li W, Fusseder N, Bourne PE, Sette A, et al. ElliPro: A New Structure-Based Tool for the Prediction of Antibody Epitopes. *BMC Bioinf* (2008) 9:514. doi: 10.1186/1471-2105-9-514
75. Kringelum JV, Lundegaard C, Lund O, Nielsen M. Reliable B Cell Epitope Predictions: Impacts of Method Development and Improved Benchmarking. *PloS Comput Biol* (2012) 8(12):e1002829. doi: 10.1371/journal.pcbi.1002829
76. Singh H, Ansari HR, Raghava GPS. Improved Method for Linear B-Cell Epitope Prediction Using Antigen's Primary Sequence. *PloS One* (2013) 8(5): e62216. doi: 10.1371/journal.pone.0062216
77. Safavi A, Kefayat A, Mahdevar E, Abiri A, Ghahremani F. Exploring the Out of Sight Antigens of SARS-CoV-2 to Design a Candidate Multi-Epitope Vaccine by Utilizing Immunoinformatics Approaches. *Vaccine* (2020) 38 (48):7612–28. doi: 10.1016/j.vaccine.2020.10.016
78. Devi YD, Devi A, Gogoi H, Dehingia B, Doley R, Buragohain AK, et al. Exploring Rotavirus Proteome to Identify Potential B- and T-Cell Epitope Using Computational Immunoinformatics. *Heliyon* (2020) 6(12):e05760. doi: 10.1016/j.heliyon.2020.e05760
79. Liu T, Shi K, Li W. Deep Learning Methods Improve Linear B-Cell Epitope Prediction. *BioData Min* (2020) 13:1. doi: 10.1186/s13040-020-00211-0
80. *B Cell Help*. Available at: http://tools.iedb.org/bcell/help/#Bepipred-2.0.
81. Eickhoff CS, Terry FE, Peng L, Meza KA, Sakala IG, Van Aartsen D, et al. Highly Conserved Influenza T Cell Epitopes Induce Broadly Protective Immunity. *Vaccine* (2019) 37(36):5371–81. doi: 10.1016/j.vaccine.2019.07.033
82. Grassl N, Kulak NA, Pichler G, Geyer PE, Jung J, Schubert S, et al. Ultra-Deep and Quantitative Saliva Proteome Reveals Dynamics of the Oral Microbiome. *Genome Med* (2016) 8:44. doi: 10.1186/s13073-016-0293-0
83. Zhang X, Chen W, Ning Z, Mayne J, Mack D, Stintzi A, et al. Deep Metaproteomics Approach for the Study of Human Microbiomes. *Anal Chem* (2017) 89(17):9407–15. doi: 10.1021/acs.analchem.7b02224
84. Blakeley-Ruiz JA, Erickson AR, Cantarel BL, Xiong W, Adams R, Jansson JK, et al. Metaproteomics Reveals Persistent and Phylum-Redundant Metabolic

Functional Stability in Adult Human Gut Microbiomes of Crohn's Remission Patients Despite Temporal Variations in Microbial Taxa, Genomes, and Proteomes. *Microbiome* (2019) 7:18. doi: 10.1186/s40168-019-0631-8
85. Long S, Yang Y, Shen C, Wang Y, Deng A, Qin Q, et al. Metaproteomics Characterizes Human Gut Microbiome Function in Colorectal Cancer. *NPJ Biofilms Microbiomes* (2020) 6:14. doi: 10.1038/s41522-020-0123-4
86. Park SK (Robin), Jung T, Thuy-Boun PS, Wang AY, Yates JR, Wolan DW. ComPIL 2.0: An Updated Comprehensive Metaproteomics Database. *J Proteome Res* (2019) 18(2):616–22. doi: 10.1021/acs.jproteome.8b00722
87. Perez-Riverol Y, Csordas A, Bai J, Bernal-Llinares M, Hewapathirana S, Kundu DJ, et al. The PRIDE Database and Related Tools and Resources in 2019: Improving Support for Quantification Data. *Nucleic Acids Res* (2019) 47 (Database issue):D442–50. doi: 10.1093/nar/gky1106

Conflict of Interest: MF, NC, and PD'h are inventors on a provisional patent application for the method for rapid detection of immunogenic epitopes, filed by Lawrence Livermore National Security, LLC.

The remaining authors declare that the research was conducted in the absence of any commercial or financial relationships that could be construed as a potential conflict of interest.

Publisher's Note: All claims expressed in this article are solely those of the authors and do not necessarily represent those of their affiliated organizations, or those of the publisher, the editors and the reviewers. Any product that may be evaluated in this article, or claim that may be made by its manufacturer, is not guaranteed or endorsed by the publisher.

frontiers in Immunology

ORIGINAL RESEARCH
published: 30 September 2021
doi: 10.3389/fimmu.2021.645299

Expansion of Human Papillomavirus-Specific T Cells in Periphery and Cervix in a Therapeutic Vaccine Recipient Whose Cervical High-Grade Squamous Intraepithelial Lesion Regressed

*Takeo Shibata[1,2], Sumit Shah[1], Teresa Evans[1], Hannah Coleman[1], Benjamin J. Lieblong[1], Horace J. Spencer[3], Charles M. Quick[1], Toshiyuki Sasagawa[2], Owen W. Stephens[4], Erich Peterson[4], Donald Johann Jr.[5], Yong-Chen Lu[1] and Mayumi Nakagawa[1]**

[1] Department of Pathology, University of Arkansas for Medical Sciences, Little Rock, AR, United States, [2] Department of Obstetrics and Gynecology, Kanazawa Medical University, Uchinada, Japan, [3] Department of Biostatistics, University of Arkansas for Medical Sciences, Little Rock, AR, United States, [4] Department of Biomedical Informatics, University of Arkansas for Medical Sciences, Little Rock, AR, United States, [5] Department of Internal Medicine (Hematology-Oncology Division), University of Arkansas for Medical Sciences, Little Rock, AR, United States

Advances in high-throughput sequencing have revolutionized the manner with which we can study T cell responses. We describe a woman who received a human papillomavirus (HPV) therapeutic vaccine called PepCan, and experienced complete resolution of her cervical high-grade squamous intraepithelial lesion. By performing bulk T cell receptor (TCR) β deep sequencing of peripheral blood mononuclear cells before and after 4 vaccinations, 70 putatively vaccine-specific clonotypes were identified for being significantly increased using a beta-binomial model. In order to verify the vaccine-specificity of these clonotypes, T cells with specificity to a region, HPV 16 E6 91-115, previously identified to be vaccine-induced using an interferon-γ enzyme-linked immunospot assay, were sorted and analyzed using single-cell RNA-seq and TCR sequencing. HPV specificity in 60 of the 70 clonotypes identified to be vaccine-specific was demonstrated. TCR β bulk sequencing of the cervical liquid-based cytology samples and cervical formalin-fixed paraffin-embedded samples before and after 4 vaccinations demonstrated the presence of these HPV-specific T cells in the cervix. Combining traditional and cutting-edge immunomonitoring techniques enabled us to demonstrate expansion of HPV-antigen specific T cells not only in the periphery but also in the cervix. Such an approach should be useful as a novel approach to assess vaccine-specific responses in various anatomical areas.

Keywords: cervical intraepithelial neoplasia, human papillomavirus, T cell receptor, therapeutic vaccine, clonal expansion

OPEN ACCESS

Edited by:
Min Gong,
Tianjin Medical University, China

Reviewed by:
Maria Issagouliantis,
Riga Stradiņš University, Latvia
Wathsala Wijayalath,
Naval Medical Research Center, United States

***Correspondence:**
Mayumi Nakagawa
mnakagawa@uams.edu

Specialty section:
This article was submitted to Vaccines and Molecular Therapeutics, a section of the journal Frontiers in Immunology

Received: *22 December 2020*
Accepted: *31 August 2021*
Published: *30 September 2021*

Citation:
Shibata T, Shah S, Evans T, Coleman H, Lieblong BJ, Spencer HJ, Quick CM, Sasagawa T, Stephens OW, Peterson E, Johann D Jr, Lu Y-C and Nakagawa M (2021) Expansion of Human Papillomavirus-Specific T Cells in Periphery and Cervix in a Therapeutic Vaccine Recipient Whose Cervical High-Grade Squamous Intraepithelial Lesion Regressed. Front. Immunol. 12:645299. doi: 10.3389/fimmu.2021.645299

INTRODUCTION

Human papillomavirus (HPV) is best known as the causative agent of cervical cancer, but it can also cause cancers at other mucosal sites including the anus, oropharynx, penis, vagina, and vulva. It is estimated that HPV is responsible for 42,700 cancers in the US each year (1), including more than 90% of anal and cervical cancers and about 70% of oropharyngeal, vaginal, and vulvar cancers (1). Incidences of HPV-associated anal and oropharyngeal cancers have increased notably, and although incidence of cervical cancer has stabilized after significant decreases over the past several decades (2), this remains the fourth most common cancer among women globally (3). The available prophylactic vaccines are effective for preventing HPV infections, but they cannot eliminate established infections; therapeutic vaccines could fill this need. Such vaccines would benefit young women (narrowly, those ≤24 years old), and broadly, any woman who plans to become pregnant (4) because increased incidence of preterm delivery (from 4.4% to 8.9%) is associated with surgical treatments (e.g., loop electrical excision procedure [LEEP]) for high-grade squamous intraepithelial lesion (HSIL) (4, 5). Furthermore, HPV infection has been shown to be associated with inability to conceive (6, 7), spontaneous abortion (8), and male infertility (9, 10). With the goal of circumventing these adverse obstetrics and reproductive outcomes as well as for treating cervical cancer, a variety of HPV therapeutic vaccines are in development including DNA-based (11), peptide-based (12, 13), and bacterial vector-based (14) delivery.

We evaluated the safety of an HPV therapeutic vaccine (PepCan) in a single-center, single-arm, dose-escalation Phase I clinical trial treating women with biopsy-proven HSILs (NCT01653249) (15, 16). PepCan consists of four current good manufacturing practice (cGMP)-grade peptides covering the human papillomavirus type 16 (HPV 16) E6 protein (amino acids 1-45, 46-80, 81-115, and 116-158) and *Candida albicans* skin test reagent (Candin®, Nielsen Biosciences, San Diego, CA). PepCan was shown to be safe, and resulted in a histological regression rate of 45% which is roughly double that of a historical placebo (22%) (17). In addition, circulating, peripheral T-helper type 1 (Th1) cells (p=0.0004) were increased, and the HPV 16 viral load was significantly decreased (p=0.008) (15).

Recent advances in high-throughput sequencing technology have enhanced our ability to appreciate how the T cell receptor (TCR) repertoire may reveal the role of T cells in immunotherapy for HPV-related diseases (18–20). The actual diversity present in a human body is estimated to be around 10^{13} unique TCRs (21). Next generation sequencing can facilitate the simultaneous analysis of millions of TCR sequences. Understanding the cytotoxic T cell repertoire, in parallel with observing clinical responses, would be insightful for revealing immune mechanisms behind immunotherapies for chronic infectious diseases or cancer (18, 22–25). However, the use of high-throughput sequencing technology alone can only identify putatively vaccine-specific T cells on a statistical basis, but it is not able to verify their specificity on an immunological basis. In this article, we utilize multiplexed PCR-based TCR sequencing using genomic DNA to characterize TCR repertoires in peripheral blood mononuclear cells (PBMCs), stimulated CD3+ T cells, cervical formalin-fixed paraffin-embedded (FFPE) tissues, and cervical liquid-based cytology (LBC) samples from one subject who was a histologic responder from the Phase I clinical trial mentioned above. In addition, single-cell RNA-seq and TCR sequencing approaches were utilized to reveal the TCR sequences of HPV-specific T cells with a specificity to the HPV 16 E6 91-115 amino acid region revealed by the enzyme-linked immunospot (ELISPOT) assay. We provide proof-of-principle that a traditional assay, such as ELISPOT, can be combined with a cutting-edge technology to better characterize the specificities of T cells generated by vaccination.

Abbreviations: CIN 3, cervical intraepithelial neoplasia 3; cGMP, current good manufacturing practice; ELISPOT, enzyme-linked imunospot; FFPE, formalin-fixed paraffin-embedded; HNC, head and neck cancer; HPV, human papillomavirus; HPV 16, human papillomavirus type 16; HSIL, high-grade squamous intraepithelial lesion; IFN-γ, interferon-γ; IL-4, interleukin-4; LBC, liquid-based cytology; LEEP, loop electrical excision procedure; PBMCs, peripheral blood mononuclear cells; TCR, T cell receptor; Th1, T-helper type 1; TNF, tumor necrosis factor.

RESULTS

Clinical Trial Design and Vaccine Response

The subject, a 41-year old Caucasian woman, participated in a single-arm, open-label Phase I clinical trial of an HPV therapeutic vaccine, PepCan, for treating biopsy-proven cervical HSILs (**Figure 1A**) (15, 16). At study entry, she had cervical intraepithelial neoplasia 3 (CIN 3), and was positive for HPV types 16, 31, and 58. At study exit (12 weeks after vaccination series completion), her LEEP biopsy was benign but was noted to have marked lymphocytic infiltration. Furthermore, she was noted to have leukocytosis and lymphocytosis (**Table 1**), and was positive for HPV 40 at exit. ELISPOT assay showed CD3+ IFN-γ+ T cell responses specific to multiple regions of HPV 16 E6 and E7 protein before and after the vaccinations. The response to one region, HPV 16 E6 91-115, was significantly increased after 4 vaccinations (**Figure 1B**, p=0.023). Peripheral immune cell profiling showed an increased percentage of Th1 cells, but unchanged levels of Tregs and Th2 cells (**Figure 1C**). Her HLA types were HLA-A*24/A*30, B*15/B*51, C*01/C*03, DPB1*02/DPB1*02, DQB1*03/DQB1*06, and DRB1*11/DRB1*13.

Multiplexed PCR-Based TCR β Chain Deep Sequencing

All samples examined (n=10: PBMCs and stimulated CD3+ T cell samples at pre-, post-2, and post-4 vaccinations; and FFPE and LBC samples at pre- and post-4 vaccinations) yielded sufficient quantities of DNA for bulk TCR sequencing. In total, 749,417 clonotypes, and 1,256,277 T cells were identified in these 10 samples (**Table 2**). The numbers of total T cells and clonotypes were higher in PBMCs than in stimulated CD3+

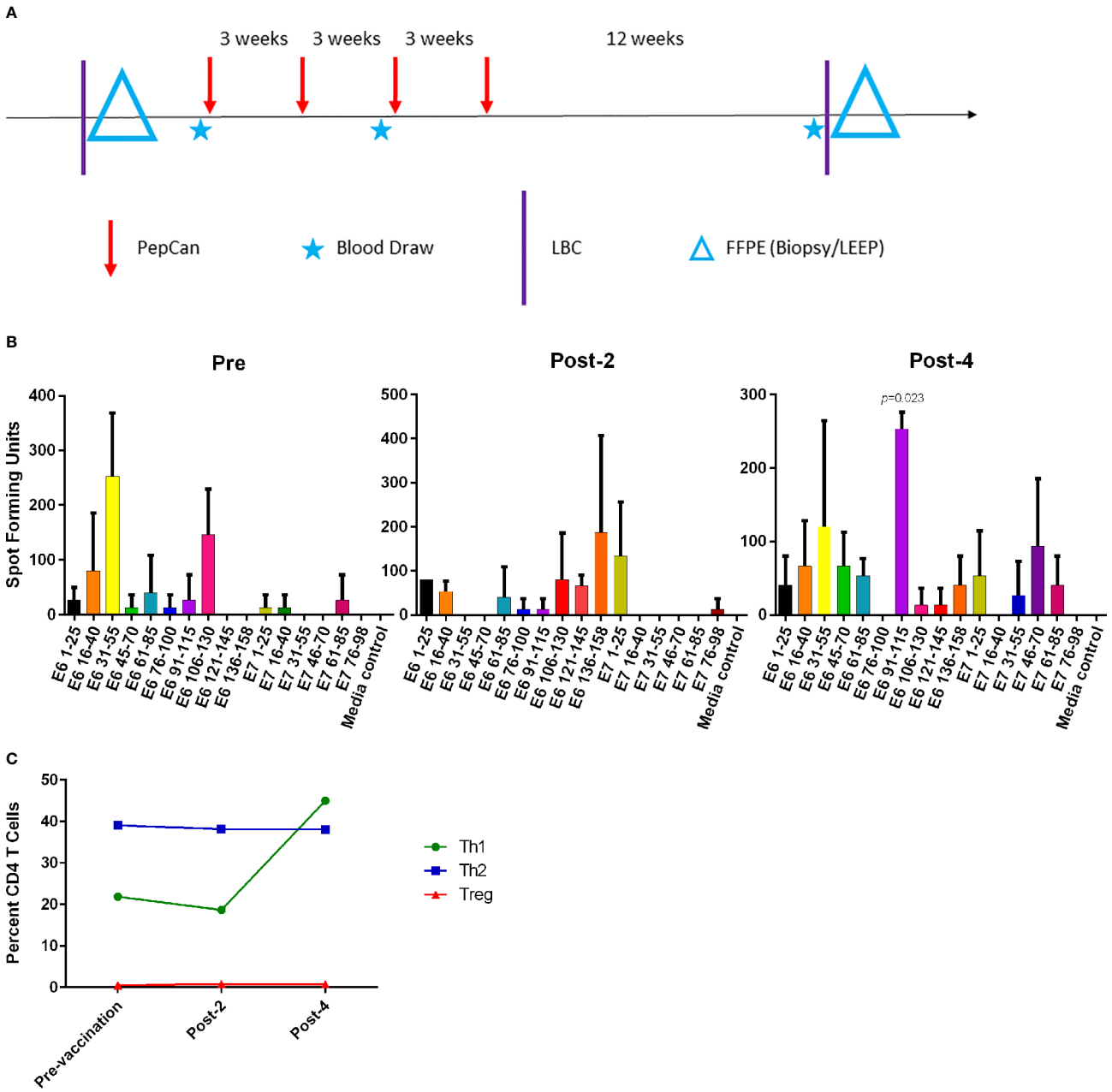

FIGURE 1 | The Phase I clinical trial design and routine immune monitoring assays. **(A)** Clinical trial design of the Phase I study. Vaccination (PepCan) visits were scheduled 3 weeks apart for patients who had biopsy-confirmed cervical high-grade squamous intraepithelial lesions (HSILs, i.e. CIN grade 2 or 3). Blood draws were performed pre-vaccination, and post-2 and post-4 vaccinations. Cervical local samples (LBC and FFPE) were collected pre-vaccination and post-4 vaccinations. FFPE samples were prepared from a pre-vaccination cervical biopsy and from loop electrical excision procedure (LEEP) biopsy post-4 vaccinations. **(B)** Immunogenic HPV16 E6 and E7 regions were determined for each vaccine phase using IFN-γ ELISPOT assay. In pre-vaccine phase, positive responses (i.e., at least twice the media control) were detected in the E6 16-40, E6 31-55, and E6 106-130 regions. Positive responses were seen in the E6 1-25, E6 106-130, E6 136-158, and E7 1-25 regions in the post-2 vaccination sample, and in the E6 31-55, E6 91-115, and E7 46-70 regions in the post-4 vaccination sample. The increase in the response to the HPV16 E6 91-115 regions was statistically significant (paired *t*-test, p=0.023) after 4 vaccinations. Phytohemagglutinin was used as a positive control (not shown). The y-axis represents mean spot forming units of triplicates per 1 x 10^6 CD3+ T cells, and error bars represent standard error of means. **(C)** The fluorescent cell sorter analysis of PBMCs revealed that the Th1 (CD4+Tbet+) level expressed as the percentage of CD4+ T cells increased after 4 vaccinations, but Treg (CD4+CD25+FoxP3+) and Th2 (CD4+GATA3) levels were minimally changed.

TABLE 1 | Complete blood count with differentials.

Test	Reference range	Pre	Post-2	Post-4
WBC (K/μL)	3-12	7.92	8.14	**13.94**
Hemoglobin (g/dL)	11.5-16	12.9	13.4	13.9
Hematocrit (%)	34-47	39.1	41.2	42.7
Platelet (K/μL)	150-500	225	225	237
Neutrophils (K/μL)	2.5-8.2	4.5	5	7
Lymphocyte (K/μL)	1-4.8	2.5	2.3	**5.5**
Monocytes (K/μL)	0.1-1	0.6	0.6	0.9
Eosinophils (K/μL)	0-0.4	0.3	0.2	0.4
Basophils (K/μL)	0-0.22	0.02	0.02	0.03

Bold texts indicate values outside of the reference range.

T cell samples (**Figure 2**). In cervical samples, the clonotypes and total T cells were detected in FFPE (pre- and post-4) and LBC (pre- and post-4). The productive clonality was increased after 4 vaccinations in PBMC, stimulated CD3+ T cell, and LBC samples, and the maximum productive frequencies at least doubled in all sample types (**Figure 2**). The T cell fraction was highest in stimulated CD3+ T cells, and lowest in LBCs. DNA per cell was similar among PBMCs, stimulated CD3+ T cells, and LBC (ranging from 0.0061 ng/cell to 0.011 ng/cell), but much higher in FFPE samples (0.714 ng/cell for pre-vaccination and 1.27 ng/cell for post-4 vaccinations).

The percentages of the top 15 most frequent clonotypes were significantly increased after 4 vaccinations in all sample types except for FFPE (**Figure 3A**). Venn diagrams of clonotypes detected in PBMCs, LBC, and FFPE at pre-vaccination and post-4 vaccinations revealed that some clonotypes can be detected in all sample types, reflecting the capacity of at least a subset of T cells to traffic to the cervix (**Figure 3B**). The presence of T cells in peripheral blood and cervix was shown. Both LBC and FFPE samples from the cervix were analyzed. However, the quality of DNA from FFPE may have been low as approximately one hundred fold larger quantity of DNA per nucleated cell was reported (**Table 2**). This may possibly have led to incomplete identification of TCRs because TCR DNA split in multiple fragments cannot be identified. So, the overlap between FFPE and peripheral blood may not be as reliable as an overlap between LBC and peripheral blood. A beta-binomial model, which accounts for variance due to random sampling from a highly diverse repertoire and time-dependent variance for identifying clinically relevant expansion of T cells (26), was used to identify putatively vaccine-specific TCRs using pre- and post-4 vaccination PBMC samples. Seventy putatively vaccine-specific TCRs were identified using the CDR3 nucleotide sequences (**Supplementary Table 1**). The numbers of such clonotypes and total T cells in pre- and post-4 vaccination FFPE (1 and 9 clonotypes, and 1 and 13 total T cells, respectively) and pre- and post-4 vaccination LBC [14 and 47 clonotypes (**Figure 3C**), and 33 and 1,523 total T cells respectively] showed that LBC may be more an informative sample type compared to FFPE because of a greater T cell abundance and better DNA quality.

Single-Cell RNA-Seq and TCR Sequencing

Of 8.5 x 10^6 peptide (three 15-mer peptides covering the HPV 16 E6 91-115 region)-stimulated and IFN-γ labeled cells from monocyte depleted post-4 vaccination PBMCs, 1.3 x 10^6 (15.3%) were positively sorted. For the TCR sequencing, the estimated number of cells was 12,240 with mean read pairs of 13,678 per cell. Most (10,246 of 12,240 or 83.7%) cells contained productive V-J spanning pairs. The TCR β amino acid sequences of the 4 clonotypes with a frequency of ≥5% among the IFN-γ positive cells are shown in **Table 3**.

The single-cell RNA-seq analysis revealed an estimated 15,114 total number of cells, 32,659 mean reads per cell, and 2,047 median number of genes per cell. After filtering and normalization, cells were clustered into 9 separated populations (**Figure 4A**). Notably, abundant expression of IFN-γ and tumor necrosis factor (TNF), but not interleukin-4 (IL-4), was detected in cluster #1, #2 and #3 within the CD8+ T-cell populations, as shown in violin and feature plots (**Figures 4B, C**). These results corroborate the importance of the role of the Th1 cells play as previously demonstrated using the fluorescent-activated cell sorter analysis (**Figure 1C**).

TABLE 2 | Sample characteristics.

Sample types	Vaccine time point	Used sample amount	Input DNA (ng)	T cells by nucleotide sequence	Clonotypes by nucleotide sequence	T cells by amino acid sequence	Clonotypes by amino acid sequence
PBMC	Pre	8×10^6 cells	2,852	252,926	195,744	252,926	187,972
	Post-2	8×10^6 cells	2,861	253,155	199,650	253,155	191,481
	Post-4	8×10^6 cells	3,428	313,245	149,604	313,245	144,519
Stimulated CD3+	Pre	6.8×10^6 cells	1,204	166,173	88,391	166,173	85,767
T cells	Post-2	6.5×10^6 cells	1,202	158,747	78,715	158,747	76,644
	Post-4	2×10^6 cells	1,202	99,701	29,150	99,701	28,643
LBC	Pre	1,200 μL	318	814	699	814	694
	Post-4	800 μL	930	10,731	6748	10,731	6,693
FFPE	Pre	Five 5μm scrolls	392	403	372	403	359
	Post-4	Five 5μm scrolls	934	382	344	382	331

T cell clone abundances were counted using complementarity determining region 3 (CDR3) nucleotide or amino acid sequences. PBMC, peripheral blood mononuclear cells; CD3+ T cells, CD3+ T cells stimulated with HPV16 E6 and E7 antigens expressed by recombinant vaccinia viruses and in GST-fusion proteins; LBC, liquid-based cytology; FFPE, formalin-fixed paraffin-embedded.

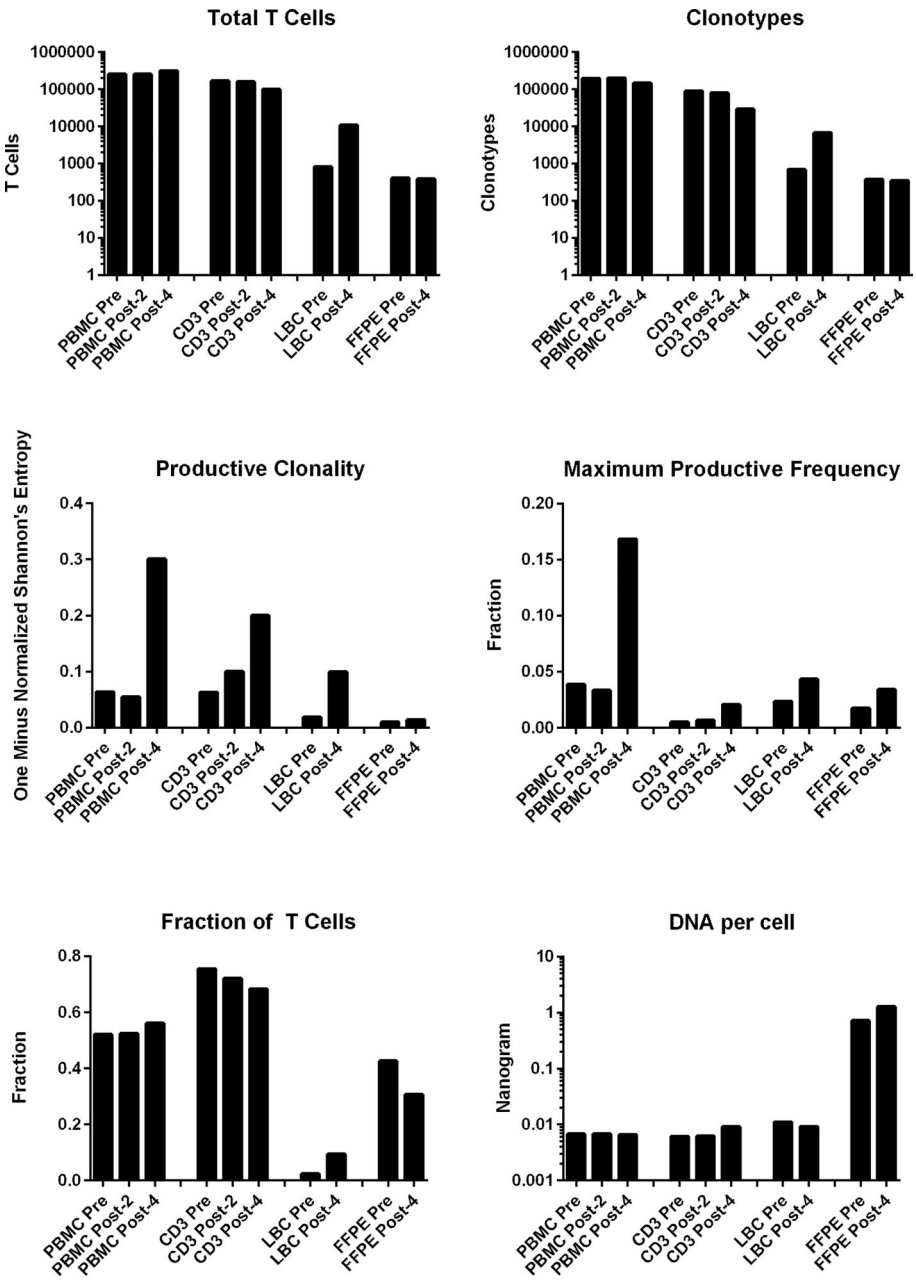

FIGURE 2 | T cell structures of PBMCs stimulated CD3+ T cells, LBC, and FFPE samples described with multiplexed PCR-based TCR sequencing using genomic DNA. The T cell structures of the 4 sample types (PBMCs, stimulated CD3+ T cells, LBC, and FFPE) are shown as the total number of T cells defined by nucleotide sequence, productive clonality (one minus normalized Shannon's entropy for all productive rearrangements), fraction of T cells (the number of productive templates divided by the number of nucleated cells), number of clonotypes defined by nucleotide sequence, maximum productive frequency (the most frequent specific productive rearrangement among all productive rearrangements within a sample), and the quantity of DNA (ng) per nucleated cell. The number of nucleated cells were determined using amplification of reference gene primers.

Tracking of the HPV 16 E6 91-115 Specific T Cells

Using the TCR β CDR3 sequences of the 4 clonotypes specific for HPV 16 E6 91-115, their frequencies in PBMCs, LBC, and FFPE samples were determined using TCR β chain sequencing (**Figure 5**). All 4 clonotypes were detectable in PBMCs and LBC prior to vaccination, and their expansion after 4 vaccinations is shown. Only one T cell of clonotype 2 is detectable prior to vaccination in FFPE. All 4 clonotypes were detectable after 4 vaccinations, but only at 2 T cells for clonotypes 1, 3, and 4, and 1 T cell for clonotype 2. As much fewer cells were detected in FFPE, LBC was a better source for assessing T cell

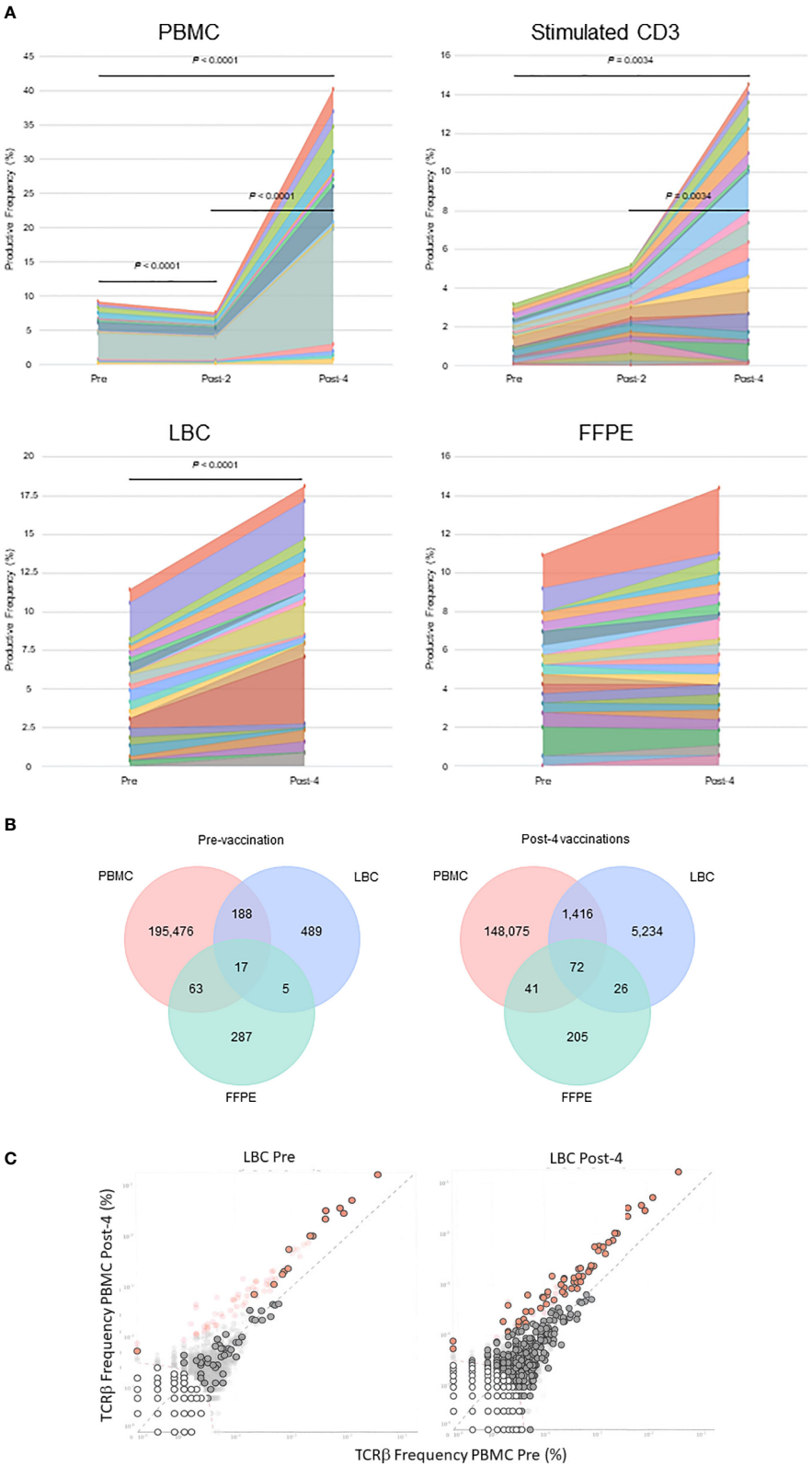

FIGURE 3 | Continued

FIGURE 3 | Tracking of clonotypes in the peripheral blood and cervix. **(A)** Tracking of the top 15 clonotypes defined by nucleotide sequence are shown in productive frequency. The top 15 highest frequency clonotypes were significantly decreased after 2 vaccinations (Wilcoxon matched-pairs signed-ranks test, p=0.0012), but significantly increased after 4 vaccinations (p<0.0001) in PBMC samples calculated using the numbers of T cells. For stimulated CD3+ T cell samples, significant increases were seen between pre-vaccination and post-4 vaccinations (p=0.034) and between post-2 and post-4 vaccinations samples (p=0.0034). A significant increase was seen in LBC samples (p<0.0001) but not in FFPE samples. **(B)** Venn diagrams of clonotypes defined by nucleotides in PBMC, LBC, and FFPE samples pre-vaccination and post-4 vaccinations. Most clonotypes appear only in one sample type, but there are 17 TCRs present in PBMCs, LBC, and FFPE at the pre-vaccination visit and 72 TCRs at the post-4 vaccination visit. **(C)** Putatively vaccine-specific clonotypes in LBC samples before and after 4 vaccinations. Seventy putatively vaccine-specific clonotypes were identified through a comparison of post-4 PBMC and pre PBMC samples using the beta-binomial model (shown as red dots with and without black circular borders). Red dots with black circular borders represent these putatively vaccine-specific TCRs present in pre-vaccination LBC sample (n=15) and in post-4 vaccination LBC sample (n=57). Dark grey dots are not significantly different between pre-vaccination and post-4 vaccinations PBMC samples. Dark grey dots with black circular borders are not significantly increased but are present in the respective LBC sample. Light grey dots without black circular borders are not present in the respective LBC sample.

populations, at least in this subject. All 4 clonotypes were represented in the top 15 most frequent clonotypes for PBMCs, LBC, and stimulated CD3+ T cells, but only clonotype 1 was present in FFPE (**Figure 3A**). Of the 70 clonotypes identified to be putatively vaccine-specific using the beta-biomial model, 60 clonotypes were shown to be HPV 16 E6 91-115 specific (**Supplementary Table 1**). Clonotype 1 was the most abundant clonotype in PBMCs and LBC, and the second most abundant clonotype in stimulated CD3+ T cells.

DISCUSSION

This was a proof-of-concept study to demonstrate the utility of TCR analyses using high-throughput sequencing technology in the context of HPV therapeutic vaccine trials. The earliest evidence of the link between HPV and cervical cancer was discovered in 1983 by Harald zur Hausen and his colleagues (27) to whom a Nobel Prize was later awarded. To date, over 200 HPV types have been described (28). HPV antigens are ideal targets for cancer immunotherapy because they are foreign. Various versions of investigational HPV therapeutic vaccines have been in clinical trials for about the last 30 years, but none has been approved by the United States Food and Drug Administration. Investigational HPV therapeutic vaccines have been tested for many indications including clearance of HPV 16 and/or 18 infection (29), HSIL regression (11, 15, 16), prevention of recurrence of squamous cell carcinoma of head and neck (HNC)(NCT03821272), treatment of advanced stage cervical cancer (13, 14), and treatment of advanced stage HNC (30). The assessment of vaccine efficacy depends on the indication being tested. For HPV 16 infection clearance, HPV-DNA typing was used (29), and biopsies were utilized to evaluate HSIL regression (11, 15, 16). Lack of recurrence within a 2 year period is being used for assessing prevention of recurrence (NCT03821272). Antitumor efficacy was examined using the numbers of patients with complete and partial response, tumor shrinkage, duration of response (13).

Unlike the HPV prophylactic vaccines which work by inducing production of neutralizing antibodies (31, 32), the HPV therapeutic vaccines are believed to cast their effects through stimulation of cell-mediated immunity, mainly T cells. Therefore, assessments of T cell immune response should be included in the endpoints of clinical trials. Such implementation varies widely among the clinical trials because T cell assays are technically challenging. In a Phase I clinical trial, Maciag et al. (14) examined the safety of Lm-LLO-E7 vaccine which is a live-attenuated *Listeria monocytogenes* engineered to secrete HPV 16 E7 protein fused with a *Listeria monocytogenes* protein listeriolysin. Fifteen patients with invasive carcinoma of the cervix were enrolled. In order to demonstrate immune responses, the investigators attempted to perform IFN-γ ELISPOT assay using pooled peptides, but most samples were not suitable due to low yield and viability after thawing. Of the 3 patients having a sufficient number of cells available to perform the assay, only one demonstrated an HPV-specific T cell response after vaccination. HPV 16 E7 short and long peptides were pooled before testing, so no information as to which portion of the protein contained immunogenic epitopes was obtained (14). In the GTL001 trial, van Damme et al. performed *ex vivo* IFN-γ ELISPOT assay with pooled HPV 16 E7 peptides or HPV 18 E7 peptides. GTL001 was made of recombinant HPV 16 and HPV 18 E7 proteins which were fused with catalytically inactive CyaA protein of *Bordetella pertussis*. A total of 47 women with HPV 16 or HPV 18 infection were studied in 4 cohorts. Overall, 18 of 31 patients (58.1%) who received any dose of GTL001 with imiquimod demonstrated positive ELISPOT results to either protein (29). Trimble et al. also tested immune responses using IFN-γ ELISPOT assay and intracellular cytokine staining for assessment of T cell immunity. Significantly higher responses were reported for patients with HSIL who received the VGX-3100 vaccine (synthetic DNA designed to express HPV 16 and 18 E6 and E7 proteins) compared to those who received placebo. As peptides were pooled for each protein tested (HPV 16 E6, HPV 16 E7, HPV 18 E6, and HPV 18 E7), information on which portion of the protein contained the immunogenic epitopes was not determined (11). In the clinical trial which treated advanced-stage HNC patients with ISA101 (a synthetic

TABLE 3 | TCR β CDR3 sequences of clonotypes with specificity to HPV 16 E6 91-115 and ≥5% frequency.

Clonotype	Number	Frequency (%)	Amino acid sequence
1	2,615	33.3	CASSPTSGGLTWDEQYF
2	1,340	17.0	CASSHNSGREGNEQFF
3	772	9.8	CASSFPGENEQFF
4	678	8.6	CASSWEAGQETQYF

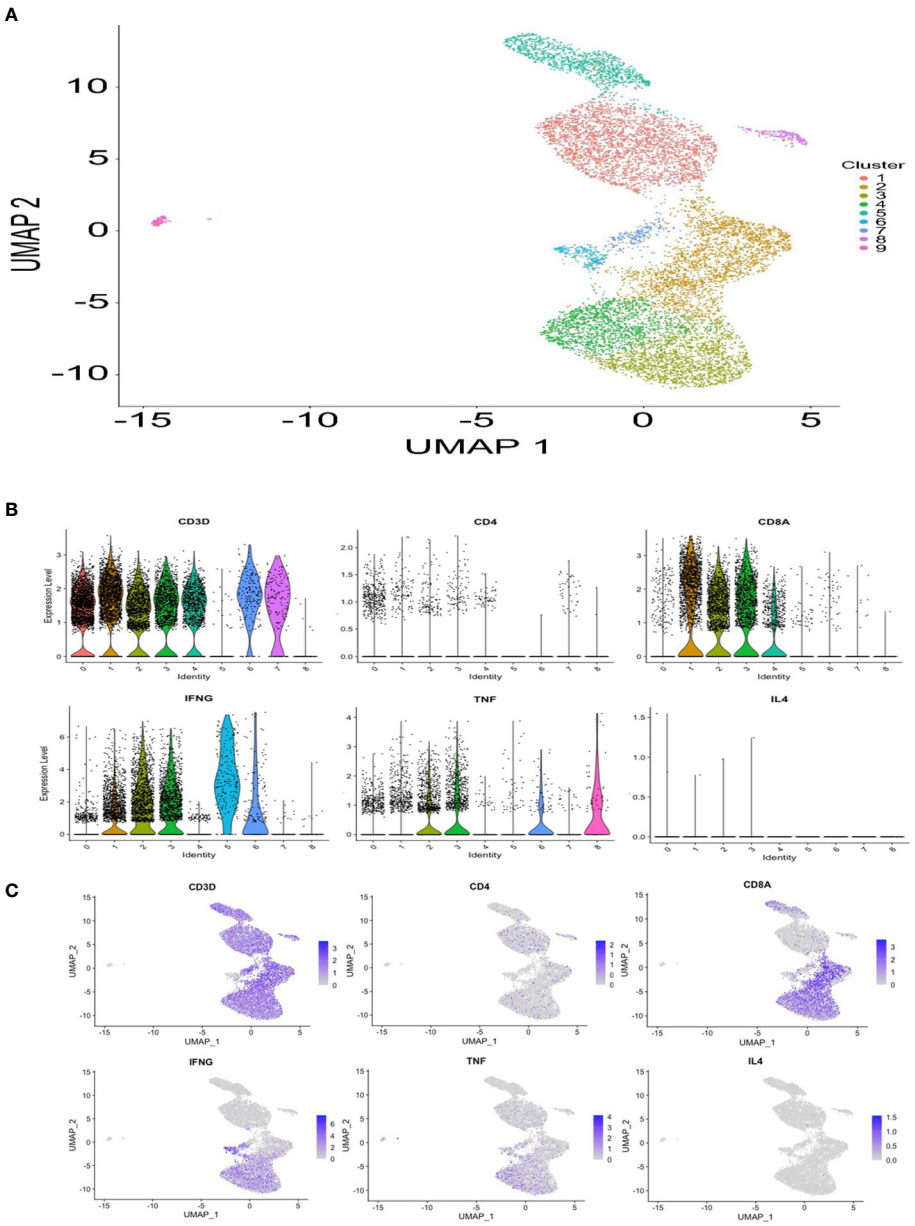

FIGURE 4 | Single-cell gene expression profile of HPV 16 E6 91-115 specific T cells. **(A)** A UMAP plot showing 9 clusters based on gene expression profiles. **(B)** Violin plots showing CD3D, CD4, CD8A, IFN-γ, TNF, and IL-4 gene expression. **(C)** Feature plots showing CD3D, CD4, CD8A, IFN-γ, TNF, and IL-4 gene expression.

long-peptide HPV 16 vaccine) and nivolumab (an anti-PD-1 checkpoint inhibitor), the investigators performed IFN-γ ELISPOT assay for HPV 16 E6 and E7 again using peptide pools. Variable increases in the number of HPV-specific T cells were observed after vaccination in both responders and nonresponders, making the role of vaccine-induced T cells uncertain. Furthermore, the immune response did not correlate with efficacy endpoints (30). In addition to IFN-γ ELISPOT assay, Melief et al. performed lymphocyte stimulation test, intracellular cytokine staining, and cytometric bead arrays to assess immune responses for a clinical trial studying the effects of ISA101 vaccination during chemotherapy in patients with advanced, recurrent, or metastatic cervical cancer (13). In all 64 patients who received ISA101 vaccination, HPV 16 E6 and/or E7-specific T cell responses to one or more of 6 peptide pools (4 pools for HPV 16 E6 and 2 pools for HPV 16 7 protein) were demonstrated.

Our IFN-γ ELISPOT protocol distinguishes itself among others in that we tested for 10 HPV 16 E6 peptides pools and 6 HPV 16 E7 peptide pools (**Figure 1B**) (15, 16). Therefore, the locations of the antigenic epitopes can be narrowed down to 25 amino acid regions. This characteristic of our ELISPOT assay

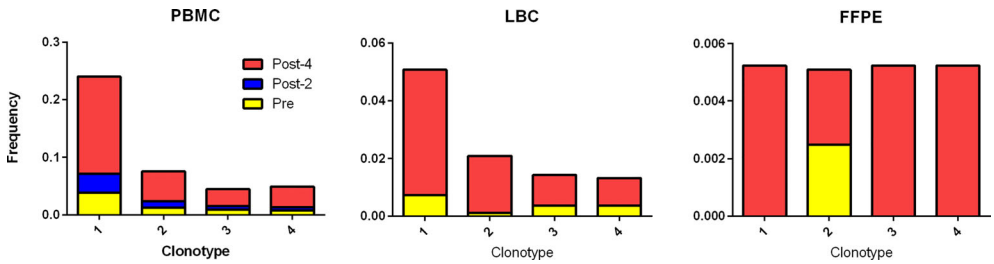

FIGURE 5 | Tracking HPV 16 E6 91-115 specific T cells in PBMC, LBC, and FFPE. The TCR Vα and Vβ sequences of HPV 16 E6 91-115 specific T cells were determined by sorting and sequencing such cells based on IFN-γ secretion upon peptide stimulation. The TCR Vβ CDR3 sequences of top 4 clonotypes (≥ 5% of IFN-γ secreting cells) are shown in **Table 3**. The frequencies of these clonotypes in PBMC, LBC, and FFPE at pre-vaccination (yellow), post-2 vaccinations (blue), and post-4 vaccinations (red) time points are shown. All 4 vaccine-specific clonotypes in PBMC and LBC increased in frequency after 4 vaccinations. On the other hand, data from FFPE were not as informative.

was key to identifying a significant response to the HPV 16 E6 91-115 region, and subsequent isolation of antigen-specific T cells based on IFN-γ secretion. In this clinical trial, 61% (19 of 31) of vaccine recipients demonstrated a new CD3+ T cell response in ELISPOT assay using peripheral blood sample to at least one region of the HPV 16 E6 protein which was not present prior to vaccination (15, 16). Furthermore, these increased responses were statistically significant in 42% (13 of 31) of the subjects when ELISPOT results after vaccination were compared to those prior to vaccination (15, 16). However, the presence of such peripheral T cell responses to HPV after vaccination did not correlate with cervical HSIL regression. Therefore, ELISPOT data alone may not be a good correlate of clinical response, and that they should be combined with advanced technologies such as TCR sequencing for more critical evaluation of local protection at the site of lesion.

It is intriguing that our prior work demonstrated the HPV 16 E6 91-115 region as one of areas in which significantly increased CD4+ T cell responses were demonstrated among regressors of cervical lesions compared to persistors (33). The single-cell RNA-seq data in the current work suggest that the HPV-specific T cells are CD8+ T cells. These data combined raises a possibility that the HPV 16 E6 91-115 region may be an epitope hotspot just like the HPV 16 E6 52-62 regions which we described to be a T cell eptiope hotspot containing both CD4 and CD8 epitopes (34).

TCRs are highly diverse heterodimers consisting of α and β chains in the majority of T cells. However, 1-5% of T cells express γδ chains (35). Similar to B cell receptors, the TCR chains contains a variable region responsible for antigen recognition, and a constant region. The variable region of the α and δ chains is encoded by recombined variable (V) and joining (J) genes. Additionally for the β and γ chains, diversity (D) genes are also recombined (i.e., VDJ recombination). Therefore, the β and γ chains are more diverse than the α and δ chains. The advent of high-throughput sequencing made it possible to probe into the complexity of such TCRs. In the current study, we employed TCR β chain deep sequencing using bulk DNA and single-cell RNA-based TCR analysis using mRNA. The former has the advantage of using DNA, which can be extracted from LBC and FFPE samples; therefore, live cells are not necessary. The latter was utilized to analyze IFN-γ secreting HPV 16 E6 91-115 specific T cells from monocyte-deprived PBMCs after 4 vaccinations. Information on TCR α and β sequences and their pairings was obtained, and the gene expression profiles of individual cells was examined. We demonstrated that using the information from a traditional IFN-γ ELISPOT assay in combination with TCR sequencing enables us to demonstrate the expansion of HPV-specific CD3+ T cells and their presence in the cervix. In addition to demonstrating the information on TCR α and β chain pairings, the single-cell RNA-based method has the advantage of yielding the entire sequences of the α and β chains. This would enable construction of the TCRs in viral vectors with which their specificities can be verified (36, 37). Furthermore, such engineered T cells can be used for immunotherapy as demonstrated by Draper and colleagues (38). They used T cells genetically engineered to express the TCR of HPV 16 E6 29-38 (TIHDIILECV) epitope restricted by HLA-A*02:01. These engineered T cells were shown to be cytotoxic to HPV 16-positive cervical and HNC cell lines (38). The limitation of our current study was that we only examined one subject in this proof-of-concept study. As the Phase II clinical trial of PepCan is ongoing (NCT02481414), additional analyses of Phase II participants would aid in determining the generalizability of the findings of this study. As the participants are being randomized in a blinded fashion to PepCan arm and adjuvant only arm, making comparisons between these two arms as well as between responders and non-responders would be possible.

METHODS

Subject, Clinical Trial Design, and Laboratory Analyses

This open-label single center dose-escalation Phase I clinical trial of PepCan was reported previously (15, 16). Subject 6 was selected for

the current study because she was a vaccine responder, and sufficient amounts of her samples were available for further analyses. Briefly, subjects qualified for vaccination if they had biopsy-proven CIN 2 and/or CIN 3 (**Figure 1**). PepCan (subject 6 received 50 μg/peptide dose) was given 4 times 3 weeks apart, and LEEP was performed 12 weeks after the last vaccination. Cervical LBC samples (ThinPrep, Hologic, Marborough, MA) were collected for HPV typing before vaccination at the time of qualifying biopsy, and after 4 vaccinations at the time of LEEP. Blood was drawn before vaccination, after 2 vaccinations, and after 4 vaccinations to isolate PBMCs. Routine clinical laboratory tests (complete blood count, sodium, potassium, chloride, carbon dioxide, blood urea nitrogen, creatinine, aspartate transaminase, alanine transaminase, lactate dehydrogenase, γ-glutamyl transpeptidase, total bilirubin, and direct bilirubin) were performed. PBMCs were isolated using the ficoll density gradient method. Cells were stored in liquid nitrogen tanks while LBC samples were kept in - 80°C freezers. Cervical FFPE samples were stored at room temperature.

Research laboratory analyses performed (15, 16) as a part of the clinical trial included HPV typing (Linear Array HPV Genotyping Test, Roche Molecular Diagnostics, Pleasanton, CA), IFN-γ ELISPOT assay, fluorescent-activated cell sorter analysis of peripheral Th1, Th2, and Treg cells, and HLA class I and class II low-resolution typing (One Lambda, West Hills, CA). The Linear Array HPV Genotyping Test detects 37 individual HPV types (6, 11, 16, 18, 26, 31, 33, 35, 39, 40, 42, 45, 51, 52, 53, 54, 55, 56, 58, 59, 61, 62, 64, 66, 67, 68, 69, 70, 71, 72, 73, 81, 82, 83, 84, IS 39, and CP6108). For the ELISPOT assay, magnetically selected CD3+ T cells (Pan T Cell Isolation Kit, Miltenyi Biotec, Auburn CA) were stimulated with autologous monocyte-derived dendritic cells pulsed with HPV 16 E6 or E7 using recombinant vaccinia viruses (39) and recombinant GST fusion proteins (39) twice with a one-week duration for each stimulation (15, 16). The assay was performed in triplicates using overlapping HPV 16 E6 and E7 peptide pools covering HPV 16 E6 1-25, 16-40, 31-55, 45-70, 61-85, 76-100, 91-115, 106-130, 121-145, 136-158 and HPV 16 E7 16-40, 31-55, 46-70, 61-85, and 76-98 regions. Each peptide pool contained three peptides which were 15 amino acids in length with 10 amino acid overlap. PBMCs were stained for CD4+, CD25+, T-bet, GATA3, and Foxp3 (15, 16). The percentage of CD4+ cells positive for T-bet represented Th1 cells, those positive for GATA3 represented Th2 cells, and those positive for CD25+ and FoxP3 represented Tregs.

Multiplexed PCR-Based TCR Sequencing

The TCR β CDR3 regions were PCR-amplified and sequenced (immunoSEQ, Adaptive Biotechnologies, Seattle, WA) (40) using genomic DNA from PBMCs (pre-, post-2, and post-4), CD3+ T cells stimulated with HPV 16 E6 and E7 expressed by recombinant vaccinia viruses and in a form of GST-proteins (pre-, post-2, and post-4), LBC (pre- and post-4), and FFPE (pre- and post-4). Using bias-controlled V and J gene primers, the rearranged V(D)J segments were amplified and sequenced. A clustering algorithm was used to correct for sequencing errors, and the CDR3 segments were annotated according to the International ImMunoGeneTicsCollaboration (41, 42) to identify the V, D, and J genes that contributed to each rearrangement. A mixture of synthetic TCR analogs was used in PCR to estimate the number of cells bearing each unique TCR sequence (43). "Detailed rearrangements", "Track Rearrangements", "Venn Diagram", "Differential Abundance", and "Scatterplot with Annotation" features of the immunoSeq analyzer (44) were used to analyze data.

Single-Cell RNA-Seq of HPV-Specific T Cells

In order to obtain TCR Vα and Vβ sequences of T cells specific for HPV 16 E6 91-115 (**Figure 1B**), such T cells were selected using a human IFN-γ Secretion Assay – Cell Enrichment and Detection Kit (Miltenyi Biotec) following the manufacturer's instructions as previously described (34, 45–48). Post-4 vaccination PBMC sample cryopreserved after monocyte depletion (CD14 MicroBeads, Miltenyi Biotec) was thawed and cultured overnight in Yssel's media (Gemini Bio Products, West Sacramento, CA) with 1% human serum and 1,200 IU/mL of recombinant human interleukin-2 (R&D Systems, Inc., Minneapolis, MN). As a positive control, healthy donor PBMCs mixed with 1% HPV 16 E6 52-61 (FAFRDLCIVY)-specific CD8+ T cell clone cells (46) were processed in the same manner. The cells were stimulated for 3 h with 10 μM each of peptides in RPMI1640 media plus 5% human serum: FAFRDLCIVY for the positive control, and the three 15-mer overlapping peptides covering the HPV 16 E6 91-115 region (91-105, YGTTLEQQYNKPLCD; 96-110, EQQYNKPLCDLLIRC; 101-115, KPLCDLLIRCINCQK; RS Synthesis, Louiville, KY; ≥ 70% purity) (49). IFN-γ secreting cells were labeled using the IFN-γ catch reagent and phycoerythrin (PE)-labeled IFN-γ detection antibody. The positive control sample and healthy donor PBMCs stained with mouse IgG1K isotype labeled with PE (eBiosciences) were used as a negative control to set the gate. The cells were sorted for IFN-γ positivity only using FACS Aria (BD Biosciences, Franklin Lakes, New Jersey).

A Next GEM Chip G was loaded with approximately 10,000 cells and Chromium Next GEM Single Cell 5' Library Gel Bead Kit v1.1 reagent (10X Genomics, Pleasanton, CA). An emulsion was generated with the Chromium Controller (10X Genomics). Gene expression (GEX) libraries were prepared with the Chromium Single Cell 5' Library Construction Kit and TCR libraries were prepared with the Chromium Single Cell V(D)J Enrichment Kit, Human T Cell (10X Genomics). A low-pass surveillance sequencing run of both libraries were performed on separate Illumina mid-output MiniSeq flow cells (GEX library Read1:26bp, Read2:91bp, TCR library Read1:150bp, Read2:150bp). Sequencing was scaled up on an Illumina NextSeq 500 with a high-output 150-cycle v2.5 kit for the GEX library and a mid-output 300-cycle v2.5 kit for the TCR library; both runs used identical read lengths as on the MiniSeq. Data was aggregated from both runs.

Sequencing data were first processed by a Cell Ranger pipeline (v3.1.0; 10X Genomics). Gene expression sequencing data were

mapped to human reference (GRCh38-3.0.0) dataset. The raw single-cell data were processed by R package Seurat v. 3.2.2, by following the recommended steps and settings. The low-quality cells and doublets were filtered out by the following recommended setting: percentage of mitochondrial genes > 5%, number of detected genes < 200 and number of detected genes > 2500. The clustering was performed with the resolution setting at 0.4. The UMAP (Uniform Manifold Approximation and Projection) plot, violin plots and feature plots were also generated by Seurat (**Figure 4**).

TCR sequencing data were mapped to human TCR reference (GRCh38-alts-ensembl-3.1.0) dataset, and they were further analyzed by Loupe V(D)J Browser (v3.0.0; 10X Genomics). T cell clonotypes were defined based on TCR Vβ CDR3 nucleotide sequences after removing single cells containing only α chains and those containing two different TCR Vβ CDR3 nucleotide sequences (likely doublets). For calculating the frequencies of ≥ 5% clonotypes (**Table 3**), clonotypes with two or more single cells were included. Full-length TCRα β amino acid sequences were obtained by the Loupe V(D)J Browser.

Statistical Analysis

A paired *t*-test was performed to assess the significant changing of spot forming units (i.e., IFN-γ secreting cells) before and after vaccination in ELISPOT assay. The number of T cells between study visits in PBMC, stimulated CD3+ T cells, LBC, and FFPE were compared using Wilcoxon matched-pairs signed-ranks test (GraphPad Instat 3, GraphPad Software, San Diego, CA). A p value < 0.05 was considered statistically significant.

DATA AVAILABILITY STATEMENT

The datasets presented in this study can be found in online repositories. The names of the repository/repositories and accession number(s) can be found below: https://doi.org/10.21417/TS2020HPV, immuneACCESS, and https://www.ncbi.nlm.nih.gov/geo/query/acc.cgi?=GSE184703, National Center for Biotechnology Information's Gene Expression Omnibus (28).

ETHICS STATEMENT

The studies involving human participants were reviewed and approved by University of Arkansas for Medical Sciences Institutional Review Board. The patients/participants provided their written informed consent to participate in this study.

AUTHOR CONTRIBUTIONS

MN, DJ, ToS, and Y-CL developed the concepts and designed this project. TaS, SS, TE, OS, CQ, HC, and MN performed the experiments. TaS, BL, and MN wrote the manuscript, and all authors edited it. TaS, SS, HS, EP, and MN performed statistical and bioinformatics analyses. All authors contributed to the article and approved the submitted version.

FUNDING

This work was supported by the grant from the National Institutes of Health (R01CA143130, USA), Drs. Mae and Anderson Nettleship Endowed Chair of Oncologic Pathology (31005156, USA), and the Arkansas Biosciences Institute (the major component of the Tobacco Settlement Proceeds Act of 2000, AWD00053655, USA).

SUPPLEMENTARY MATERIAL

The Supplementary Material for this article can be found online at: https://www.frontiersin.org/articles/10.3389/fimmu.2021.645299/full#supplementary-material

REFERENCES

1. *HPV-Associated Cancer Statistics* Vol. 2019. Atlanta, GA: Centers for Disease Control and Prevention (2019).
2. *Cancer Facts & Figures 2019*. Atlanta, GA: American Cancer Society (2019).
3. de Martel C, Plummer M, Vignat J, Franceschi S. Worldwide Burden of Cancer Attributable to HPV by Site, Country and HPV Type. *Int J Cancer* (2017) 141:664–70. doi: 10.1002/ijc.30716
4. Massad LS, Einstein MH, Huh WK, Katki HA, Kinney WK, Shiffman M, et al. Updated Consensus Guidelines for the Management of Abnormal Cervical Cancer Screening Tests and Cancer Precursors. *Obstet Gynecol* (2013) 121:829–46. doi: 10.1097/AOG.0b013e3182883a34
5. Bruinsma FJ, Quinn MA. The Risk of Preterm Birth Following Treatment for Precancerous Changes in the Cervix: A Systematic Review and Meta-Analysis. *BJOG* (2011) 118:1031–41. doi: 10.1111/j.1471-0528.2011.02944.x
6. Spandorfer SD, Bongiovanni AM, Fasioulotis S, Resenwaks Z, Ledger WJ, Witkin SS, et al. Prevalence of Cervical Human Papillomavirus in Women Undergoing In Vitro Fertilization and Association With Outcome. *Fertil Steril* (2006) 86:765–7. doi: 10.1016/j.fertnstert.2006.01.051
7. Depuydt CE, Verstraete L, Berth M, Beert J, Bogers JP, Salembier G, et al. Human Papillomavirus Positivity in Women Undergoing Intrauterine Insemination Has a Negative Effect on Pregnancy Rates. *Gynecol Obstet Invest* (2016) 81:41–6. doi: 10.1159/000434749
8. Hermonat PL, Han L, Wendel PJ, Quirk JG, Stern S, Lowery CL, et al. Human Papillomavirus Is More Prevalent in First Trimester Spontaneously Aborted Products of Conception Compared to Elective Specimens. *Virus Genes* (1997) 14:13–7. doi: 10.1023/A:1007975005433
9. Garolla A, Engl B, Pizzol D, Ghezzi M, Bertoldo A, Bottacin A, et al. Spontaneous Fertility and In Vitro Fertilization Outcome: New Evidence of Human Papillomavirus Sperm Infection. *Fertil Steril* (2016) 105:65–72.e61. doi: 10.1016/j.fertnstert.2015.09.018
10. Garolla A, Pizzol D, Foresta C. The Role of Human Papillomavirus on Sperm Function. *Curr Opin Obstet Gynecol* (2011) 23:232–7. doi: 10.1097/GCO.0b013e328348a3a4
11. Trimble CL, Morrow MP, Kraynyak KA, Shen X, Dallas M, Yan J, et al. Safety, Efficacy, and Immunogenicity of VGX-3100, A Therapeutic Synthetic DNA Vaccine Targeting Human Papillomavirus 16 and 18 E6 and E7 Proteins for Cervical Intraepithelial Neoplasia 2/3: A Randomised, Double-Blind, Placebo-

Controlled Phase 2b Trial. *Lancet* (2015) 386(10008):2078–88. doi: 10.1016/S0140-6736(15)00239-1
12. Kenter GG, Welters MJ, Valentijin AR, Lowik MJ, Berends-van der Meer DM, Vloon AP, et al. Vaccination Against HPV-16 Oncoproteins for Vulvar Intraepithelial Neoplasia. *N Engl J Med* (2009) 361:1838–47. doi: 10.1056/NEJMoa0810097
13. Melief CJM, Welters MJP, Vergote I, Kroep JR, Kenter GG, Ottevanger PB, et al. Strong Vaccine Responses During Chemotherapy Are Associated With Prolonged Cancer Survival. *Sci Transl Med* (2020) 12. doi: 10.1126/scitranslmed.aaz8235
14. Maciag PC, Radulovic S, Rothman J. The First Clinical Use of a Live-Attenuated Listeria Monocytogenes Vaccine: A Phase I Safety Study of Lm-LLO-E7 in Patients With Advanced Carcinoma of the Cervix. *Vaccine* (2009) 27:3975–83. doi: 10.1016/j.vaccine.2009.04.041
15. Coleman HN, Greenfield WW, Stratton SL, Vaughn R, Kieber A, Moerman-Herzog AM, et al. Human Papillomavirus Type 16 Viral Load Is Decreased Following a Therapeutic Vaccination. *Cancer Immunol Immunother* (2016) 65:563–73. doi: 10.1007/s00262-016-1821-x
16. Greenfield WW, Stratton SL, Myrick RS, Vaughn R, Donnalley LM, Coleman HN, et al. A Phase I Dose-Escalation Clinical Trial of a Peptide-Based Human Papillomavirus Therapeutic Vaccine With Skin Test Reagent as a Novel Vaccine Adjuvant for Treating Women With Biopsy-Proven Cervical Intraepithelial Neoplasia 2/3. *Oncoimmunology* (2015) 4:e1031439. doi: 10.1080/2162402X.2015.1031439
17. Nieminen P, Harper DM, Einstein MH, Garcia F, Donders G, Huh W, et al. Efficacy and Safety of RO5217990 Treatment in Patients With High Grade Cervical Intraepithelial Neoplasia (CIN2/3). In: *28th International Papillomavirus Conference*. Puerto Rico (2012).
18. Cui JH, Lin KR, Yuan SH, Jin YB, Chen XP, Su XK, et al. TCR Repertoire as a Novel Indicator for Immune Monitoring and Prognosis Assessment of Patients With Cervical Cancer. *Front Immunol* (2018) 9:2729. doi: 10.3389/fimmu.2018.02729
19. Lang Kuhs KA, Lin SW, Hua X, Schiffman M, Burk RD, Rodriguez AC, et al. T Cell Receptor Repertoire Among Women Who Cleared and Failed to Clear Cervical Human Papillomavirus Infection: An Exploratory Proof-of-Principle Study. *PloS One* (2018) 13:e0178167. doi: 10.1371/journal.pone.0178167
20. Morrow MP, Kraynyak KA, Sylvester AJ, Shen X, Amante D, Sakata L, et al. Augmentation of Cellular and Humoral Immune Responses to HPV16 and HPV18 E6 and E7 Antigens by VGX-3100. *Mol Ther Oncolytics* (2016) 3:16025. doi: 10.1038/mto.2016.25
21. Laydon DJ, Bangham CR, Asquith B. Estimating T-Cell Repertoire Diversity: Limitations of Classical Estimators and a New Approach. *Philos Trans R Soc Lond B Biol Sci* (2015) 370:1–11. doi: 10.1098/rstb.2014.0291
22. Fink K. Can We Improve Vaccine Efficacy by Targeting T and B Cell Repertoire Convergence? *Front Immunol* (2019) 10:110. doi: 10.3389/fimmu.2019.00110
23. Hopkins AC, Yarchoan M, Durham JN, Yusko EC, Rytlewski JA, Robins HS, et al. T Cell Receptor Repertoire Features Associated With Survival in Immunotherapy-Treated Pancreatic Ductal Adenocarcinoma. *JCI Insight* (2018) 3. doi: 10.1172/jci.insight.122092
24. Inoue H, Park JH, Kiyotani K, Zewde M, Miyashita A, Jinnin M, et al. Intratumoral Expression Levels of PD-L1, GZMA, and HLA-A Along With Oligoclonal T Cell Expansion Associate With Response to Nivolumab in Metastatic Melanoma. *Oncoimmunology* (2016) 5:e1204507. doi: 10.1080/2162402X.2016.1204507
25. Tumeh PC, Harview CL, Yearley JH, Shintaku IP, Taylor EJ, Robert L, et al. PD-1 Blockade Induces Responses by Inhibiting Adaptive Immune Resistance. *Nature* (2014) 515:568–71. doi: 10.1038/nature13954
26. Rytlewski J, Deng S, Xie T, Davis C, Robins H, Yusko E, et al. Model to Improve Specificity for Identification of Clinically-Relevant Expanded T Cells in Peripheral Blood. *PloS One* (2019) 14:e0213684. doi: 10.1371/journal.pone.0213684
27. Durst M, Gissmann L, Ikenberg H, zur Hausen H. A Papillomavirus DNA From a Cervical Carcinoma and Its Prevalence in Cancer Biopsy Samples From Different Geographic Regions. *Proc Natl Acad Sci USA* (1983) 80:3812–5. doi: 10.1073/pnas.80.12.3812
28. Schiffman M, Doorbar J, Wentzensen N, de Sanjose S, Fakhry C, Monk BJ, et al. Carcinogenic Human Papillomavirus Infection. *Nat Rev Dis Primers* (2016) 2:16086. doi: 10.1038/nrdp.2016.86
29. Van Damme P, Bouillette-Marussig M, Hens A, De Coster I, Depuydt C, Goubier A, et al. GTL001, A Therapeutic Vaccine for Women Infected With Human Papillomavirus 16 or 18 and Normal Cervical Cytology: Results of a Phase I Clinical Trial. *Clin Cancer Res* (2016) 22:3238–48. doi: 10.1158/1078-0432.CCR-16-0085
30. Massarelli E, William W, Johnson F, Kies M, Ferrarotto R, Guo M, et al. Combining Immune Checkpoint Blockade and Tumor-Specific Vaccine for Patients With Incurable Human Papillomavirus 16-Related Cancer: A Phase 2 Clinical Trial. *JAMA Oncol* (2019) 5:67–73. doi: 10.1001/jamaoncol.2018.4051
31. Godi A, Panwar K, Haque M, Cocuzza CE, Andrews N, Southern J, et al. Durability of the Neutralizing Antibody Response to Vaccine and Non-Vaccine HPV Types 7 Years Following Immunization With Either Cervarix (R) or Gardasil(R) Vaccine. *Vaccine* (2019) 37:2455–62. doi: 10.1016/j.vaccine.2019.03.052
32. Sankaranarayanan R, Prabhu PR, Pawlita M, Gheit T, Bhatla N, Muwonge R, et al. Immunogenicity and HPV Infection After One, Two, and Three Doses of Quadrivalent HPV Vaccine in Girls in India: A Multicentre Prospective Cohort Study. *Lancet Oncol* (2016) 17:67–77. doi: 10.1016/S1470-2045(15)00414-3
33. Kim KH, Greenfield WW, Cannon MJ, Coleman HN, Spencer HJ, Nakagawa M. CD4+ T-Cell Response Against Human Papillomavirus Type 16 E6 Protein Is Associated With a Favorable Clinical Trend. *Cancer Immunol Immunother* (2012) 61:63–70. doi: 10.1007/s00262-011-1092-5
34. Coleman HA, Wang X, Greenfield WW, Nakagawa M. A Human Papillomavirus Type 16 E6 52-62 CD4 T-Cell Epitope Restricted by the HLA-DR11 Molecule Described in an Epitope Hotspot. *MOJ Immunol* (2014) 1:00018. doi: 10.15406/moji.2014.01.00018
35. Lo Presti E, Dieli F, Meraviglia S. Tumor-Infiltrating Gammadelta T Lymphocytes: Pathogenic Role, Clinical Significance, and Differential Programing in the Tumor Microenvironment. *Front Immunol* (2014) 5:607. doi: 10.3389/fimmu.2014.00607
36. Lu YC, Zheng Z, Robbins PF, Tran E, Prickett TD, Gartner JJ, et al. An Efficient Single-Cell RNA-Seq Approach to Identify Neoantigen-Specific T Cell Receptors. *Mol Ther* (2018) 26:379–89. doi: 10.1016/j.ymthe.2017.10.018
37. Morgan RA, Dudley ME, Wunderlich JR, Hughes MS, Yang JC, Sherry RM, et al. Cancer Regression in Patients After Transfer of Genetically Engineered Lymphocytes. *Science* (2006) 314:126–9. doi: 10.1126/science.1129003
38. Draper LM, Kwong ML, Gros A, Stevanovic S, Tran E, Kerkar S, et al. Targeting of HPV-16+ Epithelial Cancer Cells by TCR Gene Engineered T Cells Directed Against E6. *Clin Cancer Res* (2015) 21:4431–9. doi: 10.1158/1078-0432.CCR-14-3341
39. Nakagawa M, Stites DP, Farhat S, Sisler JR, Moss B, Kong F, et al. Cytotoxic T Lymphocyte Responses to E6 and E7 Proteins of Human Papillomavirus Type 16: Relationship to Cervical Intraepithelial Neoplasia. *J Infect Dis* (1997) 175:927–31. doi: 10.1086/513992
40. Robins HS, Campregher PV, Srivastava SK, Wacher A, Turtle CJ, Kahsai O, et al. Comprehensive Assessment of T-Cell Receptor Beta-Chain Diversity in Alphabeta T Cells. *Blood* (2009) 114:4099–107. doi: 10.1182/blood-2009-04-217604
41. Lefranc MP, Giudicelli V, Duroux P, Jabado-Michaloud J, Folch G, Aouinti S, et al. IMGT(R), the International ImMunoGeneTics Information System(R) 25 Years on. *Nucleic Acids Res* (2015) 43:D413–22. doi: 10.1093/nar/gku1056
42. Yousfi Monod M, Giudicelli V, Chaume D, Lefranc MP. IMGT/JunctionAnalysis: The First Tool for the Analysis of the Immunoglobulin and T Cell Receptor Complex V-J and V-D-J JUNCTIONs. *Bioinformatics* (2004) 20(Suppl 1):i379–85. doi: 10.1093/bioinformatics/bth945
43. Wu D, Emerson RO, Shwerwood A, Loh ML, Angiolillo A, Howie B, et al. Detection of Minimal Residual Disease in B Lymphoblastic Leukemia by High-Throughput Sequencing of IGH. *Clin Cancer Res* (2014) 20:4540–8. doi: 10.1158/1078-0432.CCR-13-3231
44. immunoSEQ Analyzer https://www.immunoseq.com/analyzer.
45. Nakagawa M, Kim KH, Gillam TM, Moscicki AB. HLA Class I Binding Promiscuity of the CD8 T-Cell Epitopes of Human Papillomavirus Type 16 E6 Protein. *J Virol* (2007) 81:1412–23. doi: 10.1128/JVI.01768-06
46. Nakagawa M, Kim KH, Moscicki AB. Different Methods of Identifying New Antigenic Epitopes of Human Papillomavirus Type 16 E6 and E7 Proteins.

Clin Diagn Lab Immunol (2004) 11:889–96. doi: 10.1128/CDLI.11.5.889-896.2004

47. Wang X, Greenfield WW, Coleman HN, James LE, Nakagawa M. Use of Interferon-Gamma Enzyme-Linked Immunospot Assay to Characterize Novel T-Cell Epitopes of Human Papillomavirus. *J Vis Exp* (2012) 61:1–8. doi: 10.3791/3657
48. Wang X, Santin AD, Bellone S, Gupta S, Nakagawa M. A Novel CD4 T-Cell Epitope Described From One of the Cervical Cancer Patients Vaccinated With HPV 16 or 18 E7-Pulsed Dendritic Cells. *Cancer Immunol Immunother* (2009) 58:301–8. doi: 10.1007/s00262-008-0525-2
49. Baker CC, Phelps WC, Lindgren V, Braun MJ, Gonda MA, Howley PM. Structural and Transcriptional Analysis of Human Papillomavirus Type 16 Sequences in Cervical Carcinoma Cell Lines. *J Virol* (1987) 61:962–71. doi: 10.1128/jvi.61.4.962-971.1987

Author Disclaimer: The contributions of BL to this study were completed in their entirety while he was affiliated with the University of Arkansas for Medical Sciences, and he now is employed by Adaptive Biotechnologies (Seattle, WA, USA). This manuscript was submitted for publication prior to his employment with Adaptive Biotechnologies.

Conflict of Interest: MN is one of the inventors named in the patents and patent applications for the HPV therapeutic vaccine (PepCan).

The remaining authors declare that the research was conducted in the absence of any commercial or financial relationships that could be construed as a potential conflict of interest.

Publisher's Note: All claims expressed in this article are solely those of the authors and do not necessarily represent those of their affiliated organizations, or those of the publisher, the editors and the reviewers. Any product that may be evaluated in this article, or claim that may be made by its manufacturer, is not guaranteed or endorsed by the publisher.

frontiers in Immunology

ORIGINAL RESEARCH
published: 11 November 2021
doi: 10.3389/fimmu.2021.772550

Immunogenicity and Protective Potential of Mucosal Vaccine Formulations Based on Conserved Epitopes of Influenza A Viruses Fused to an Innovative Ring Nanoplatform in Mice and Chickens

Cynthia Calzas[1], Molida Mao[1], Mathilde Turpaud[1], Quentin Viboud[1], Joelle Mettier[1], Thomas Figueroa[2], Pierre Bessière[2], Antoine Mangin[1,3], Laura Sedano[1], Pierre-Louis Hervé[1†], Romain Volmer[2], Mariette F. Ducatez[2], Steve Bourgault[4], Denis Archambault[5], Ronan Le Goffic[1] and Christophe Chevalier[1]**

[1] Institut National de Recherche pour l'Agriculture, l'Alimentation et l'Environnement (INRAE) Molecular and Virology Unit VIM-Unité Mixte de Recherche (UMR) 892, University Paris-Saclay, Jouy-en-Josas, France, [2] Institut National de Recherche pour l'Agriculture, l'Alimentation et l'Environnement (INRAE) Unité Mixte de Recherche (UMR1225), Interactions Hôtes-Agents Pathogénes-Ecole Nationale Vétérinaire de Toulouse (IHAP-ENVT)-University of Toulouse, Toulouse, France, [3] Dementia Research Institute, Cardiff University, Cardiff, United Kingdom, [4] Chemistry Department, Université du Québec à Montréal, Montreal, QC, Canada, [5] Department of Biological Sciences, Université du Québec à Montréal, Montreal, QC, Canada

Current inactivated vaccines against influenza A viruses (IAV) mainly induce immune responses against highly variable epitopes across strains and are mostly delivered parenterally, limiting the development of an effective mucosal immunity. In this study, we evaluated the potential of intranasal formulations incorporating conserved IAV epitopes, namely the long alpha helix (LAH) of the stalk domain of hemagglutinin and three tandem repeats of the ectodomain of the matrix protein 2 (3M2e), as universal mucosal anti-IAV vaccines in mice and chickens. The IAV epitopes were grafted to nanorings, a novel platform technology for mucosal vaccination formed by the nucleoprotein (N) of the respiratory syncytial virus, in fusion or not with the C-terminal end of the P97 protein (P97c), a recently identified Toll-like receptor 5 agonist. Fusion of LAH to nanorings boosted the generation of LAH-specific systemic and local antibody responses as well as cellular immunity in mice, whereas the carrier effect of nanorings was less pronounced towards 3M2e. Mice vaccinated with chimeric nanorings bearing IAV epitopes in fusion with P97c presented modest LAH- or M2e-specific IgG titers in serum and were unable to generate a mucosal humoral response. In contrast, N-3M2e or N-LAH nanorings admixed with Montanide™ gel (MG) triggered strong specific humoral responses, composed of serum type 1/type 2 IgG and mucosal IgG and IgA, as well as cellular responses dominated by type 1/type 17 cytokine profiles. All mice vaccinated with the [N-3M2e + N-LAH + MG] formulation survived an H1N1 challenge and the combination of both N-3M2e and N-LAH nanorings with MG enhanced the clinical and/or virological protective potential of the

OPEN ACCESS

Edited by:
Shisong Jiang, University of Oxford, United Kingdom

Reviewed by:
Wen-Chun Liu, Academia Sinica, Taiwan
Irina V. Kiseleva, Institute of Experimental Medicine (RAS), Russia

***Correspondence:**
Cynthia Calzas
cynthia.calzas@inrae.fr
Christophe Chevalier
christophe.chevalier@inrae.fr

†Present address:
Pierre-Louis Hervé, DBV Technologies, Montrouge, France

Specialty section:
This article was submitted to Vaccines and Molecular Therapeutics, a section of the journal Frontiers in Immunology

Received: *08 September 2021*
Accepted: *25 October 2021*
Published: *11 November 2021*

Citation:
Calzas C, Mao M, Turpaud M, Viboud Q, Mettier J, Figueroa T, Bessière P, Mangin A, Sedano L, Hervé P-L, Volmer R, Ducatez MF, Bourgault S, Archambault D, Le Goffic R and Chevalier C (2021) Immunogenicity and Protective Potential of Mucosal Vaccine Formulations Based on Conserved Epitopes of Influenza A Viruses Fused to an Innovative Ring Nanoplatform in Mice and Chickens. Front. Immunol. 12:772550. doi: 10.3389/fimmu.2021.772550

preparation in comparison to individual nanorings. Chickens vaccinated parenterally or mucosally with N-LAH and N-3M2e nanorings admixed with Montanide™ adjuvants developed a specific systemic humoral response, which nonetheless failed to confer protection against heterosubtypic challenge with a highly pathogenic H5N8 strain. Thus, while the combination of N-LAH and N-3M2e nanorings with Montanide™ adjuvants shows promise as a universal mucosal anti-IAV vaccine in the mouse model, further experiments have to be conducted to extend its efficacy to poultry.

Keywords: influenza A viruses, highly pathogenic avian influenza virus, mucosal vaccines, adjuvants, nanoparticles, M2e/HA2 subunit vaccines

INTRODUCTION

Avian influenza A viruses (AIV) remain one of the most important respiratory pathogens in humans and various animal species, including poultry. According to the disease severity in poultry, AIV can broadly be categorized as either highly pathogenic (HPAIV) or low pathogenic (LPAIV) AIV. In poultry, infection with LPAIV is asymptomatic or causes low to mild pathophysiological damages to the respiratory, digestive, and reproductive systems (resulting in a drop in egg production), while infection with HPAIV is characterized by high morbidity and mortality rates. AIV can not only dramatically impact the poultry industry by causing severe economic losses, but can also pose a serious threat to public health worldwide through their high rates of zoonotic infection and pandemic potential (1, 2).

Vaccination is the most efficient and cost-effective approach to protect human and animal populations against IAV. Current vaccines are primarily designed to generate an immune response directed towards surface hemagglutinin (HA) (especially the immunodominant HA head domain HA1) or neuraminidase (NA) glycoproteins. However, circulating IAV are continuously evolving, leading to the emergence of strains with new antigenic properties. Point mutations occurring in the HA protein caused by the error-prone viral RNA-dependent RNA polymerase ("antigenic drift") lead to strains which can escape pre-existing host immune responses. In addition, the segmented nature of the viral genome allows for exchanges of viral segments in host cells co-infected with distinct IAV strains, resulting in reassortant viruses with new combinations of HA or NA surface glycoproteins ("antigenic shift"). These genetic reassortments could contribute to the emergence of novel IAV subtypes with pandemic potential (3). These antigenic drift and shift events occurring in circulating IAV may strongly reduce the efficiency of influenza vaccines (4, 5).

Owing to the high variability of IAV, an active area of research focuses on developing subunit vaccines containing conserved "universal" viral antigens, including epitopes located in the membrane proximal stalk domain of HA (HA2) and the ectodomain of the matrix protein 2 (M2e) (4, 6–8). Multiple vaccine candidates and platforms incorporating HA2 and/or M2e epitopes are under development, including fusion proteins with bacterial enterotoxins, flagellin, *Neisseria meningititis* outer membrane protein complex or *Mycobacterium tuberculosis* heat-shock protein 70, virus-like particles, bacterial outer membrane vesicles, bacteriophages, liposomes, immune stimulating complexes (ISCOM), bacterial or viral vectored vaccines, DNA or RNA vaccines, organic polymers such as chitosan, poly(lactic-*co*-glycolic acid) or poly-γ-glutamic acid particles and inorganic nanoparticles such as gold nanoparticles (5, 7–15). These vaccine candidates were shown to provide protection against homologous and/or heterologous IAV challenges in pre-clinical trials. Whereas anti-HA1 antibodies block viral entry into host cells by inhibiting the interaction between HA1 and sialic acid residues on cellular receptors, anti-HA2 antibodies neutralize infection at other stages of the virus life cycle, including the fusion step between viral and endosomal membranes. The HA2-specific antibodies also operate by engaging Fc-mediated effector functions including antibody-dependent cellular phagocytosis (ADCP) or antibody-dependent cell-mediated cytotoxicity (ADCC) (4, 6, 8). Vaccines incorporating a linear contiguous fragment of HA2, the long alpha helix (LAH), elicited protective LAH-specific humoral responses in mouse studies (16–18). M2e is sparsely expressed at the surface of the virus but is abundant at the surface of infected cells. M2e-specific antibodies are non-neutralizing but exhibit Fc-mediated protective effector functions (4, 6–8). The protective potential of HA2- and M2e-based vaccines also correlates with the generation of specific cell-mediated immune responses (7, 8). Although vaccine trials with HA2- or M2e-based formulations gave encouraging results in mouse or ferret models, inconsistent results have been obtained in poultry (5, 9, 11, 12, 19–21).

A growing body of evidence emphasizes the importance of mucosal vaccination in the fight against IAV (15, 22–24). Current mucosal anti-IAV vaccines licensed in humans are intranasal cold-adapted live attenuated influenza vaccines (LAIV) displaying limited replication at high temperatures of the lower respiratory tract, but efficient replication at lower temperatures of the upper respiratory tract. Alternative attenuation strategies for the generation of LAIV under development in mammals and birds include the use of non-structural protein 1 (NS1) deficient, altered or truncated viruses, codon deoptimized viruses, or single-cycle infectious viruses obtained after mutation, deletion or substitution of viral components such as the transmembrane and cytoplasmic domains of M2 protein (5, 25, 26). LAIV have the potential to

generate local and systemic humoral and cell-mediated immune responses and provide broad protection against IAV infections. However, some drawbacks have been associated with the use of LAIV such as safety issues related to the possible reversion of the vaccine strains into virulent strains by mutations or genetic reassortment with other circulating strains (27). Besides LAIV, mucosal inactivated subunit vaccines are being developed. To ensure the immuno-availability and the immuno-stimulating capacity of the IAV antigen(s), innovative delivery/adjuvant systems for subunit vaccines have been successfully developed in pre-clinical and clinical tests, including micro/nanosized particulate carriers associated or not with immunopotentiators such as agonists of pattern recognition receptors (PRRs) including Toll-like receptors (TLRs) (15). These formulations boost the magnitude, the duration and/or the breadth of the immune responses directed against the IAV antigen(s) (15). In this context, we previously fused three tandem repeats of M2e peptide to a ring nanoplatform based on recombinant nucleoprotein (N) of the respiratory syncytial virus (RSV), which self-assembled in homogenous rings of about 15 nm diameter when expressed in *Escherichia coli* ("N-3M2e nanorings") (28). Mice immunized intranasally with these nanorings developed potent M2e-specific local and systemic humoral responses and were significantly protected against homologous IAV challenge (28). Recent studies have focused on the P97 protein of *Mycoplasma hyopneumoniae*, the etiological agent of porcine enzootic pneumonia, which plays a major role in the bacterial adhesion to the respiratory epithelium and stimulates the production of pro-inflammatory cytokines during infection (29). The fusion of the C-terminal end of P97 protein (P97c) to viral proteins boosted the anti-viral immune responses in mice (30), and the adjuvant effect of P97c may be mediated through its interaction with TLR-5 (29).

The goal of this study is to evaluate the immunogenicity and the protective potential of chimeric nanorings bearing 3M2e and LAH epitopes in fusion or not with P97c as universal mucosal anti-IAV vaccines in mice and chickens.

MATERIALS AND METHODS

Plasmid Constructions

The M2e (GenBank accession number BAV59614.1, 1-24 aa) and LAH (GenBank accession number CAA24272.1, 420-474 aa) sequences derived from A/Puerto Rico/8/1934 (H1N1) (PR8) strain, the M2e (GenBank accession number AGY42150.1, 1-24 aa) and LAH (GenBank accession number AGY42146.1, 418-468 aa) sequences derived from A/mallard/Sweden/49/2002 (H5N9) strain, and the P97c sequence derived from *M. hyopneumoniae* 232 strain (GenBank accession #U50901.1, 799-1108 aa) were used in this study. The two cysteine residues of the M2e sequence (aa 17 and 19) were replaced by two serine residues to avoid formation of a disulfide bond that could perturb the assembly of nanorings (28). The pET-N-Sac plasmid was obtained from the pET-N plasmid, which contained the full-length coding sequence of N derived from RSV Long strain (ATCC VR-26, GenBank accession number AY911262.1), by introducing a SacI restriction enzyme site in frame and at the C-terminal end of the N sequence (28). The pET-N-3M2e plasmid containing three repetitions of the PR8 M2e sequence in frame and the C-terminal end of the N sequence was obtained previously (28). To obtain the pET-N-3M2e plasmid containing three repetitions of the H5N9 M2e sequence, the synthesized pUC57-3M2e plasmid (ProteoGenix, Schiltigheim, France) containing the H5N9 3M2e sequence was used as a template to amplify the 3M2e sequence by PCR using the Phusion high-fidelity DNA polymerase (Thermo Fisher Scientific, Waltham, MA, USA) with gene-specific primers flanked with SacI/SacI (forward primer/reverse primer) sites. The PCR-amplified 3M2e sequence was then digested by SacI enzyme and inserted into the pET-N-Sac plasmid using the same restriction site. The pET-LAH plasmid was obtained by inserting the PR8 LAH sequence between NdeI and XhoI sites into a pET-22 vector. The pET-N-LAH plasmid was obtained by inserting the PR8 or H5N9 LAH sequence containing a linker sequence GCCGGAGCA at its N-terminal end between the SacI and XhoI sites into the pET-N-Sac plasmid. The pET-N-P97c plasmid was obtained by inserting the P97c sequence containing a linker sequence GGCGGAAGC at its N-terminal end between the SacI and EcoRI sites into the pET-N-Sac plasmid. The pET-N-3M2e-P97c plasmid was obtained by inserting the PR8 3M2e sequence at the SacI site into the pET-N-P97c plasmid. The pET-N-P97c-3M2e plasmid was obtained by inserting the P97c sequence containing a linker sequence GGCGGAAGC at its N-terminal end at the SacI site into the pET-N-3M2e plasmid. The pET-N-LAH-P97c and pET-N-P97c-LAH plasmids were obtained by inserting the PR8 LAH and P97c sequences at the SacI site into the pET-N-P97c and pET-N-LAH plasmids, respectively. The LAH-P97c and P97c-LAH gene fragments were PCR-amplified using the pET-N-LAH-P97c and pET-N-P97c-LAH plasmids as templates and gene-specific primers flanked with NdeISacI/XhoI and NdeI/SacIXhoI sites, respectively. NdeI/XhoI-digested LAH-P97c and P97c-LAH PCR products were finally inserted into a pET-22 vector identically treated with restriction enzymes to generate the pET-LAH-P97c and pET-P97c-LAH plasmids, respectively. The PCR-amplified PR8 3M2e sequence flanked with SacI/SacI site was digested by SacI and inserted into either the SacI-digested pET-LAH-P97c plasmid to generate the pET-3M2e-P97c plasmid, or into the SacI-digested pET-P97c-LAH plasmid to generate the pET-P97c-3M2e plasmid. The primers and the restriction enzymes were purchased from Sigma-Aldrich (Saint-Louis, MO, USA) and Thermo Fisher Scientific, respectively. The entire coding sequences of all plasmid constructions were validated on both strands by DNA sequencing. All sequences and primers are available upon request.

Expression and Purification of Proteins

The purification of nanorings depends upon specific interactions between the C-terminus of the phosphoprotein P of RSV (161-241 aa) (PCT) fused to glutathione *S*-transferase and the N protein, as previously described (31). Briefly, *E. coli* Rosetta 2 (DE3) competent cells (Novagen, Madison, WI, USA) co-transformed with the pGEX-PCT plasmid and either the

pET-N-Sac, pET-N-P97c, pET-N-LAH, pET-N-3M2e, pET-N-LAH-P97c, pET-N-P97c-LAH, pET-N-3M2e-P97c or pET-N-P97c-3M2e plasmid were grown at 37°C for 8 h in Luria-Bertani (LB) medium containing 100 µg/ml ampicillin, 50 µg/ml kanamycin and 40 µg/ml chloramphenicol. The protein expression was induced by adding 0.8 mM isopropyl-β-D-thio-galactoside (IPTG) to the medium and bacteria were incubated overnight at 28°C. Bacterial pellets were then incubated for 1 h on ice in lysis buffer (50 mM Tris-HCl pH 8, 60 mM NaCl, 1 mM EDTA, 2 mM dithiothreitol (DTT), 0.2% Triton X-100, 1 mg/ml lysozyme) supplemented with complete protease inhibitor cocktail (Roche, Basel, Switzerland), then sonicated, and finally centrifuged at 4°C for 30 min at 10,000 × *g*. Supernatants were incubated overnight with glutathione-sepharose 4B beads (GE Healthcare, Chicago, IL, USA). Beads were then washed three times in lysis buffer and three times in phosphate-buffer saline (PBS), and incubated with thrombin (Novagen) overnight at 20°C. Recombinant nanorings separated from the beads were finally loaded onto a HiLoad Superdex 200 column (GE Healthcare) using 20 mM Tris-HCl (pH 8.5) and 150 mM NaCl as the eluent.

The purification of LAH, LAH-P97c, P97c-LAH, 3M2e-P97c or P97c-3M2e relied on the presence of a 6xHis-tag located at the C-terminal end of the coding sequence. *E. coli* competent cells transformed with the pET-LAH, pET-LAH-P97c, pET-P97c-LAH, pET-3M2e-P97c or pET-P97c-3M2e plasmid were grown at 37°C for 8 h in LB medium containing 100 µg/ml ampicillin and 40 µg/ml chloramphenicol. After protein expression, bacterial pellets were re-suspended in lysis buffer (20 mM Tris-HCl pH 8, 500 mM NaCl, 0.1% Triton X-100, 10 mM imidazole, 1 mg/ml lysozyme) supplemented with complete protease inhibitor cocktail, incubated for 1 h on ice, sonicated, and then centrifuged at 4°C for 30 min at 10,000 × *g*. Supernatants were then loaded onto a HiTrap immobilized metal ion affinity chromatography (IMAC) column (GE Healthcare) charged with 0.2 M $NiSO_4$. The column was washed in the washing buffer (20 mM Tris-HCl pH 8.5, 500 mM NaCl, 50 mM imidazole) and proteins were eluted in the same buffer with 500 mM imidazole before being loaded onto a HiLoad Superdex 200 column using 20 mM Tris-HCl (pH 8.5) and 150 mM NaCl as the eluent. P97c and 3M2e peptides were synthesized by ProteoGenix. The absence of endotoxin was tested by a Limulus amebocyte lysate (LAL) endotoxin quantification kit (Thermo Fisher Scientific) with a sensitivity limit of 0.1 endotoxin unit/ml.

SDS-PAGE and Western Blot Assays

Proteins were prepared in Laemmli buffer (62.5 mM Tris-HCl pH 6.8, 5% β-mercaptoethanol, 2% sodium dodecyl sulfate (SDS), 20% glycerol, 0.01% bromophenol blue) and denatured 5 min at 95°C. Samples were then run on 12.5% SDS-polyacrylamide gels with to ProSieve Prestained protein ladder and detected by Coomassie brilliant blue staining. Alternatively, gels were electroblotted onto a nitrocellulose membrane for 1 h at 20 V. Membranes were blocked with PBS containing 5% skim milk during 1 h at room temperature (RT) and then incubated overnight at 4°C with either a rabbit anti-N polyclonal sera (Pab) (1:5,000) (32), a mouse anti-M2 monoclonal antibody (Mab) (1:5,000; clone 14C2) (Santa Cruz Biotechnology, Dallas, TX, USA) or a mouse anti-P97c Mab (1:3,000; clone 8H4-G6) (30) in PBS with 0.3% Tween 20 (PBS-T 0.3%) and 5% skim milk. Membranes were washed in PBS-T 0.3% and finally incubated 1 h at RT with relevant peroxidase-conjugated secondary antibodies (SeraCare, Milford, MA, USA) diluted in blocking solution. Proteins were visualized by chemiluminescence with Clarity Western ECL substrate (Bio-Rad, Hercules, CA, USA).

Size Measurements of Nanorings by Dynamic Light Scattering (DLS)

Size measurements with the Zetasizer Nano series (Malvern Panalytical, Malvern, UK) based on the principle of DLS, were made at 20°C using a helium-neon laser wavelength of 633 nm and detection angle of 173°. The results were presented as size distribution by volume calculated from the Malvern software (28).

Visualization of Nanorings by Transmission Electron Microscope (TEM)

Electron micrographs were acquired using a CM12 TEM (Royal Philips Electronics, Amsterdam, Netherlands) at 80 kV excitation voltage. Samples at 0.05-1 mg/ml were applied onto an airglow- discharged carbon-coated 200-mesh copper grid and stained with a 2% uranyl acetate aqueous solution (28).

In Vivo Experiments in Mice

Six to 7-week-old female BALB/c mice were purchased from Janvier Labs (Le Genest-Saint-Isle, France) and housed under specific-pathogen-free (SPF) conditions in a biosafety level 2 facility (IERP, INRAE, Jouy-en-Josas, France) with access to food and water *ad libitum*. All mouse experiments were carried out in accordance with INRAE guidelines, which are compliant with the European animal welfare regulation. The protocols were approved by the Animal Care and Use Committee at the Centre de Recherche de Jouy-en-Josas (COMETHEA) under relevant institutional authorization (Ministère de l'éducation nationale, de l'enseignement supérieur et de la recherche; authorization number 2015100910396112v1, APAFIS number 1487).

Three sets of experiments were conducted to evaluate the immunogenicity of vaccine candidates bearing PR8 epitopes and the immunostimulatory effect of nanorings and P97c. In the first set of experiments, mice were anesthetized with a solution of ketamine and xylazine (50 and 10 mg/kg of body weight, respectively) and immunized three times, at 2-week intervals, by intranasal instillation of 50 µl of endotoxin-free PBS containing 20 µg of nanorings bearing PR8 epitopes in fusion or not to P97c (N-LAH, [n = 10]; N-3M2e, [n = 8]; N-LAH-P97c, [n = 9]; N-P97c-LAH, [n = 9]; N-3M2e-P97c, [n = 9]). Control groups received intranasal administrations of 20 µg of free PR8 peptides (LAH, [n = 8]; 3M2e, [n = 7]) or PR8 peptides fused to P97c (LAH-P97c, [n = 9]; P97c-LAH, [n = 9]; 3M2e-P97c, [n = 10]; P97c-3M2e, [n = 9]). Preparations which did not contain P97c were adjuvanted with 5% MG (SEPPIC, Air Liquide, La Garenne-Colombes, France). Negative control groups received preparations without PR8 epitopes (P97c (20 µg), [n = 5]; N (20 µg) + MG, [n = 8]; N-P97c (20 µg), [n = 10]; MG, [n = 5]). The antigen dose was selected according to previous studies (28). On day 42, sera were isolated

from blood samples collected *via* cheek puncture. Mice were then sacrificed and bronchoalveolar lavage fluids (BAL) were collected by flushing the lungs *via* tracheal puncture with 1 ml PBS and clarified by centrifugation. In the second set of experiments, mice were immunized three times, at 2-week intervals, by intranasal instillation of 50 µl of endotoxin-free PBS containing nanorings bearing PR8 epitopes (N-LAH (20 µg) + MG, [n = 5]; N-3M2e (20 µg) + MG, [n = 5]). Control groups received intranasal administrations of free PR8 peptides (LAH (20 µg) + MG, [n = 5]; 3M2e (20 µg) + MG, [n = 5]) or subcutaneous injections of an equivalent of 100 lethal dose 50 (LD_{50}) of UV-inactivated PR8 strain (iPR8, [n = 4]) admixed with MG. This latter group has been included in the study as an experimental control representative of current anti-IAV vaccines which are mainly inactivated viruses administered *via* the parenteral route (15). Negative control group received MG (n = 4). On day 42, spleens were collected to evaluate LAH- or M2e-specific cellular responses. In the last set of experiments, mice were immunized three times, at 2-week intervals, by intranasal instillation of 50 µl of endotoxin-free PBS containing nanorings bearing PR8 administered alone (N-LAH (20 µg) + MG, [n = 7]; N-3M2e (20 µg) + MG, [n = 7]), or in combination (N-3M2e (20 µg) + N-LAH (20 µg) + MG, [n = 8]). Control groups received intranasal administrations of free PR8 peptides (LAH (20 µg) + MG, [n = 7]; 3M2e (20 µg) + MG, [n = 7]) or MG (n = 4), or subcutaneous injections of [iPR8 + MG] (n = 7). On day 42, spleens (n = 4 for MG and [iPR8 + MG] groups; n = 5 for [N-LAH + MG] and [N-3M2e + MG] groups), sera and BAL were collected.

A final set of experiments aimed at evaluating the protective potential of nanorings bearing PR8 epitopes against an experimental homologous IAV infection. In a first stage, mice received three administrations of vaccine formulations or vehicle as described above (N-LAH + MG, [n = 10]; N-3M2e + MG, [n = 10]; N-3M2e + N-LAH + MG, [n = 10]; LAH + MG, [n = 10]; 3M2e + MG, [n = 10]; MG, [n = 9]). Two weeks after the last immunization, mice were anesthetized and inoculated intranasally with 15 LD_{50} of PR8 strain in 50 µl endotoxin-free PBS. Mice immunized with [iPR8 + MG] (n = 8) were included as a positive control group because conventional vaccination with inactivated virus is known to confer protection against homologous challenge with the induction of neutralizing anti-HA antibodies contributing critically to viral clearance (15, 28). Body weight and mortality of each mouse were monitored daily until 14 days post-infection (p.i.). Mice that had lost 20% or more of their initial weight were euthanized according to ethical endpoints. In a second stage, mice received three administrations of vaccine formulations or vehicle and were then infected with 15 LD_{50} of PR8 strain as described above. Four days after infection, individual viral loads were measured from lung homogenates (N-LAH + MG, [n = 4]; N-3M2e + MG, [n = 5]; N-LAH + N-3M2e + MG, [n = 4]; LAH + MG, [n = 5]; 3M2e + MG, [n = 5]; iPR8 + MG, [n = 4]; MG, [n = 5]) by quantitative real-time polymerase chain reaction (qRT-PCR).

In Vivo Experiments in Chickens

Experimentations were conducted in accordance with the European Council Directive CEE86/609 and animal protocols approved by the Ethics Committee "Sciences et santé animale", committee number 115. Three-week-old white Leghorn chickens were purchased from the Plateforme d'Infectiologie Expérimentale (INRAE, Nouzilly, France) and housed under SPF conditions in a biosafety level 2 facility at the National Veterinary School of Toulouse (France) (experimental unit agreement number C3155527) with access to food and water *ad libitum*. Birds were transferred in biosafety level 3 cabinets (I-Box; Noroit, Nantes, France) under negative pressure with HEPA-filtered air before experimental AIV infection. Chickens were immunized three times at 2-week intervals with a combination of two chimeric nanorings bearing H5N9 LAH and 3M2e epitopes. The first group received 100 µl of endotoxin-free PBS containing 50 µg of each chimeric nanorings adjuvanted with 70% Montanide™ ISA 71 VG (ISA) (SEPPIC) intramuscularly (N-LAH + N-3M2e + ISA, [n = 15]). ISA is a blend of oil and an ester from mannitol sugar and oleic fatty acid (anhydromannitol octadecenoate ether) with specific emulsifying properties due to its sugar polar head, its non-ionicity and the specificity of fatty acid chains of the surfactant system, which is extensively used in parenteral vaccination in chickens. The second group received 100 µl of endotoxin-free PBS containing 25 µg of each chimeric nanorings adjuvanted with MG by choanal route in addition to 40 µl of endotoxin-free PBS containing 25 µg of each chimeric nanorings adjuvanted with MG by eye drop (20 µl/eye) (N-LAH + N-3M2e + MG, [n = 15]). Non-vaccinated control group received PBS (n = 16). On day 46, sera were isolated from blood samples collected *via* jugular vein punction and tears were obtained by sprinkling salt in an eye of each bird (n = 3-5 per group) and collecting the fluid with a micropipette (33). On day 49, chickens were inoculated *via* the choanal route with 5 LD_{50} of HPAIV A/duck/Tarn/RG/2016 (H5N8) strain in 100 µl endotoxin-free PBS and the mortality was recorded daily until 7 days p.i.

Antigen-Specific Antibody Titration by ELISA

Microtiter plates (Immulon 2HB, Thermo Fisher Scientific) were coated overnight at 4°C with synthesized LAH or M2e (ProteoGenix) derived from PR8 (for the analysis of mouse samples) or H5N9 (for the analysis of chicken samples) strains (200 ng per well in 100 µl carbonate-bicarbonate buffer 0.1 M pH 9.5). Plates were washed five times with PBS-T 0.05% between each step of the assay. After coating, the plates were blocked with PBS-T 0.05% and 5% skim milk for 2 h at RT. Sera, BAL and LS were serially diluted (2-fold dilutions) in PBS-T 0.05% and 5% skim milk (starting at 1:3 for LS and at 1:50 for serum/BAL) and incubated for 1 h at RT. Negative wells contained only PBS-T 0.05% and 5% skim milk. Antigen-bound mouse antibodies were detected using peroxidase-conjugated goat anti-mouse IgG (H+L) (1:5,000) (KPL, Gaithersburg, MD, USA), IgA (1:5,000) (Southern Biotech, Birmingham, AL, USA), IgG2b (1:1,000) (Southern Biotech), or IgG3 (1:1,000) (Southern Biotech), or peroxidase-conjugated rat anti-mouse IgG1 (1:1,000) (BD Biosciences, Franklin Lakes, NJ, USA) or IgG2a (1:1,000) (BD Biosciences). Antigen-bound chicken antibodies were detected using peroxidase-conjugated goat anti-chicken IgG (Fc) (1:50,000 or 1:10,000 for sera or LS, respectively) (Bio-Rad) or IgA (1:10,000) (Bio-Rad). After incubation for 1 h at RT, plates

were developed with 3,3',5,5'-tetramethylbenzidine (TMB) substrate (KPL), and the enzyme reaction was stopped by addition of 1 M H_2SO_4. Absorbance was read at 450 nm with an Infinite 200 Pro microplate reader (Tecan, Männedorf, Switzerland). The reciprocal of the last sample dilution that resulted in an optical density at 450 nm (OD_{450}) ≤ twice the OD_{450} of negative wells (cutoff) was considered the titer of that sample. When the OD_{450} of the first dilution of a sample was lower than the cutoff, its titer was arbitrarily fixed to 3 or 50 for LS or sera/BAL, respectively. Optimal dilutions of the coating antigen (LAH or M2e) and peroxidase-conjugated anti-mouse or anti-chicken antibodies were determined during preliminary standardizations.

Preparation of Mouse Spleen Cells

Individual spleens were mechanically disrupted in sterile RPMI-1640 medium (Thermo Fisher Scientific) supplemented with 10% heat-inactivated fetal calf serum (FCS, Eurobio Scientific, Les Ulis, France) and filtered through a 100 µm nylon filter. After incubation with NH_4Cl lysing buffer (Sigma-Aldrich) to remove red blood cells, total spleen cells were adjusted to 5 x 10^6 viable cells/ml in complete medium consisting of RPMI-1640 medium supplemented with 10% FCS, 2 mM L-glutamine, 50 µM β-mercaptoethanol and 100 U/ml penicillin-streptomycin (Thermo Fisher Scientific) and were re-stimulated *ex vivo* to evaluate specific cellular immune responses by ELISA and ELISpot assay (see below). All solutions were tested for the absence of endotoxin by the LAL test. Any possible residual endotoxin during cell stimulation was controlled by the addition of polymyxin B sulfate (MilliporeSigma, Burlington, MA, USA) at 20 µg/ml (34).

Cytokine Quantification by ELISA

Mouse spleen cells were distributed in 96-well flat-bottom cell culture plates (5×10^5 cells/well) and incubated in triplicate with synthesized LAH or M2e (2 µg/well) as activators or with complete medium as negative control. Cell cultures were incubated at 37°C in 5% CO_2 for 72 h, and supernatants were harvested. Levels of interferon gamma (IFN-γ), interleukin-17A (IL-17A), IL-4, IL-5, IL-6 and IL-10 were measured from supernatants by sandwich ELISA using pair-matched antibodies from eBioscience (San Diego, CA, USA) (IFN-γ, IL-4, IL-5, IL-6, IL-10) or BD Biosciences (IL-17A). Two-fold dilutions of recombinant mouse cytokines were used to generate standard curves. Sample dilutions giving OD_{450} readings in the linear portion of the appropriate standard curve were used to quantify the levels of each cytokine.

ELISpot Assay

Ninety-six-well $MultiScreen_{HTS}$-IP polyvinylidene fluoride membrane plates (MilliporeSigma) were coated overnight at 4°C with capture anti-mouse IFN-γ Mab (clone R4-6A2, BD Biosciences) or IL-17A Mab (clone TC11-18H10) (1 µg per well in 100 µl PBS). Plates were then washed three times with sterile PBS and blocked with complete medium for 2 h at 37°C. Mouse spleen cells were serially diluted (two-fold dilution) in complete medium (starting at a concentration of 5×10^6 cells/ml) and 100 µl/well of each dilution was incubated with synthesized LAH or M2e (2 µg/well) for 24 h at 37°C.

Negative control wells were coated wells containing complete medium or uncoated wells containing 5×10^5 cells. Subsequently, plates were washed in PBS-T 0.05% and incubated with 100 µl/well of biotinylated rat anti-mouse IFN-γ Mab (clone XMG1.2) or IL-17A Mab (clone TC11-8H4) at 2 µg/ml in PBS-T 0.05% supplemented with 1% BSA for 2 h at 37°C. After further washes and 45 min incubation with streptavidin-alkaline phosphatase at 1 µg/ml (Mabtech, Nacka Strand, Sweden), IFN-γ- or IL-17A-secreting cells were visualized by adding BCIP-NBT (5-bromo-4-chloro-3-indolyl-phosphate/nitro blue tetrazolium; Thermo Fisher Scientific) substrate for 30 min. The spots were counted using the iSPOT reader from AID Autoimmun Diagnostica GmbH (Straßberg, Germany). The background from the negative wells was subtracted and the results were expressed as the number of spot-forming cells per 5×10^5 input cells. Optimal dilutions of coating antibodies and biotinylated anti-mouse antibodies were determined during preliminary standardizations.

Determination of Pulmonary Viral Loads by qRT-PCR

Total RNA was extracted from mouse lung homogenates using the RNeasy Plus Mini Kit (Qiagen, Venlo, Netherlands) and 100 ng of RNA samples were reverse-transcribed with SuperScript II Reverse Transcriptase (Thermo Fisher Scientific) using the specific IAV M1 primer: 5'-TCT AAC CGA GGT CGA AAC GTA-3' (35). Resulting cDNA samples were mixed with iTaq universal SybR green PCR supermix (Bio-Rad) and primers targeting a conserved region of the PR8 M1 gene (sense: 5'-TCT AAC CGA GGT CGA AAC GTA-3'; antisense: 5'-AGG GCA TTT TGG ACA AAG CGT CTA-3'). The qRT-PCR program was run on the MasterCycler R realplex (Eppendorf, Montesson, France) as follows: an initial DNA denaturation step at 95°C for 3 min, then 40 cycles composed firstly of a denaturation step at 95°C for 15 s, then an annealing step at 64°C for 15 s, and finally an extension step at 72°C for 30 s. Each cDNA sample and non-template controls were run in triplicate. To ensure that primers produced a single and specific PCR amplification product, a dissociation curve was performed at the end of the PCR cycle. In each assay, serial ten-fold dilutions of the pPOLI-M/PR8 plasmid (Pr. Ervin Fodor, University of Oxford, UK) were run in duplicate, allowing to quantify the number of M1 gene copies generated from unknown samples by comparison of the cycle threshold values using the Realplex software (Eppendorf). Results were expressed as the number of copies of M1 RNA per 100 ng of input total lung RNA.

Statistical Data Analysis

The log-rank (Mantel-Cox) test was used to compare the survival rates between the mouse groups. Otherwise, differences between the experimental groups were analyzed for significance using the Mann-Whitney rank sum test. All analyses were done using the Sigma Plot system v11.0 (Systat Software, San Jose, CA, USA). A P value < 0.05 was considered statistically significant.

RESULTS

Biochemical and Biophysical Characterization of LAH- and M2e-Based Fusion Proteins

In this study, we explored the adjuvant potential of N nanorings and P97c for the development of efficient anti-IAV vaccine formulations containing conserved IAV epitopes. To this end, we produced a series of chimeric nanorings with PR8 (H1N1) epitopes linked alone or in combination with P97c at the C-terminal end of the N sequence exposed at the surface of nanorings (36). Different combinations of PR8 epitopes and P97c were conceived because the fusion protein orientation could influence the characteristics of the humoral response generated against the viral epitopes (30). M2e-based constructions were designed with three M2e copies to increase the immunogenicity of the peptide (28). Five different chimeric nanorings were thus created, namely N-LAH, N-3M2e, N-LAH-P97c, N-P97c-LAH and N-3M2e-P97c. In parallel, we produced LAH-P97c, P97c-LAH, 3M2e-P97c and P97c-3M2e fusion proteins. Naked nanorings (N) and nanorings bearing P97c (N-P97c) were generated as controls. Due to very low production yield, N-P97c-3M2e nanorings were excluded from the study. Analysis by SDS-PAGE followed by Coomassie blue staining revealed the presence of a unique band at the expected theorical molecular weight for each sample (**Figure 1A**). Western blot assays using specific antibodies confirmed the identity and antigenicity of each preparation (**Figure 1B**). The presence of LAH epitopes was validated by liquid chromatography coupled with tandem mass spectrometry (data not shown). Observation by TEM showed that nanorings carrying IAV and/or P97c epitopes formed similar ring-like structures as those previously observed with N or N-3M2e nanorings (28) (**Figure 1C**). DLS analysis indicated that N and N-3M2e nanoring preparations were mainly composed of a homogenous population with a hydrodynamic radius of 17 nm and 18 nm, respectively, in accordance with previous observations (28, 31). A similar DLS profile with a hydrodynamic radius of 18 nm was obtained with the N-LAH nanoring preparation (**Supplemental Figure 1**). The size of the particles was increased after the fusion of P97c to

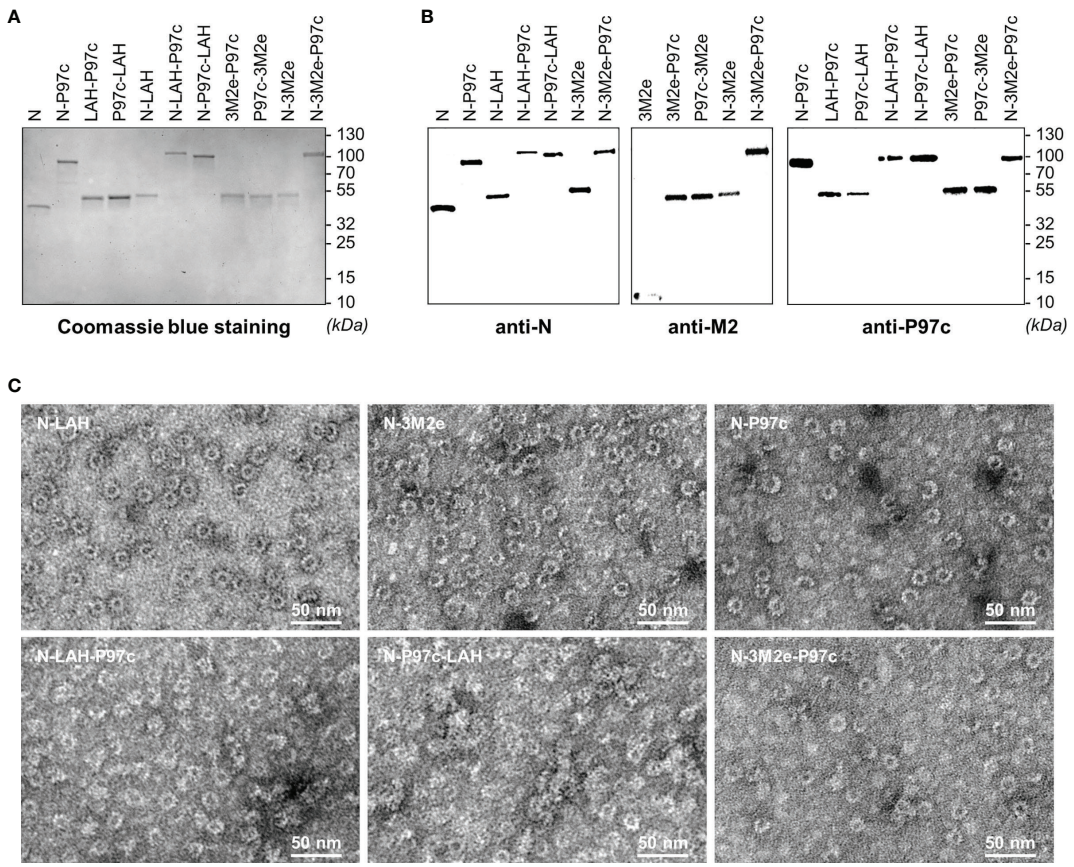

FIGURE 1 | Biochemical and biophysical characterization of LAH- and 3M2e-based fusion proteins. Recombinant nanorings bearing PR8 epitopes in fusion or not with P97c (N-LAH, N-3M2e, N-LAH-P97c, N-P97c-LAH, N-3M2e-P97c), fusion proteins composed of PR8 epitopes and P97c (LAH-P97c, P97c-LAH, 3M2e-P97c, P97c-3M2e), nanorings bearing P97c (N-P97c) and naked nanorings (N) were produced and purified as described in "Materials and Methods" and then analyzed by **(A)** SDS-PAGE followed by Coomassie blue staining and **(B)** Western blot assay with (**B**, left panel) N-specific Pab, (**B**, central panel) M2-specific Mab and (**B**, right panel) P97c-specific Mab. **(C)** Nanorings were negatively stained and observed by transmission electron microscopy.

nanorings, and a major population with a hydrodynamic radius of 25 nm, 41 nm, 32 nm and 34 nm was detected with N-P97c, N-LAH-P97c, N-P97c-LAH and N-3M2e-P97c samples, respectively. Therefore, nanorings are versatile nanoplatforms on which different IAV epitopes can be grafted alone or in combination with adjuvant sequence (P97c) without affecting the self-assembly and the structural integrity of nanorings.

Evaluation of the Immunopotentiator Effect of Nanorings and P97c on LAH- and M2e-Specific Systemic and Mucosal Humoral Responses in Mice

In a first set of experiments, we evaluated the immunopotentiator effect of nanorings and P97c on the development of humoral immunity directed against IAV epitopes in mice. Animals received three intranasal administrations of LAH or 3M2e peptides derived from PR8 strain fused to nanorings and/or P97c. Vaccine preparations which did not contain P97c were admixed with MG, a commercial adjuvant efficient in mucosal immunization (28). The magnitude and composition of systemic and local antibody responses directed against LAH or M2e were evaluated (**Figure 2**).

Concerning LAH-specific humoral responses, mice vaccinated with [LAH + MG] did not present significant systemic (**Figure 2A**) or mucosal (**Figures 2C, E**) antibody titers. In contrast, mice immunized with P97c-LAH or LAH-P97c fusion proteins developed a potent systemic IgG response, and the antibody titers were significantly higher in the P97c-LAH group than in the LAH-P97c group (**Figure 2A**). Nonetheless, although IgG were detected in the BAL of the P97c-LAH group, overall mice presented low to negligible IgA titers, and the mucosal humoral response of [LAH-P97c]-instilled mice was not significantly different from negative control groups (**Figures 2C, E**). The LAH-specific humoral response of mice immunized with N-LAH-P97c or N-P97c-LAH nanorings was only composed of serum IgG, whose titers were not increased in comparison to mice immunized with LAH-P97c or P97c-LAH fusion proteins, respectively, and no significant mucosal antibody titers could be measured (**Figures 2C, E**). Finally, the [N-LAH + MG] formulation triggered the strongest humoral responses, composed of serum IgG as well as local IgG and IgA.

Regarding M2e-specific humoral responses, mice vaccinated with [3M2e + MG] exhibited significant systemic IgG titers (**Figure 2B**) and local IgG (**Figure 2D**) and IgA (**Figure 2F**) titers in contrast with [3M2e-P97c]- or [P97c-3M2e]-vaccinated mice. There was a tendency towards higher levels of antibodies in serum and BAL in the [N-3M2e + MG] group compared to the [3M2e + MG] group, however these differences were not statistically significant (**Figures 2B, D, F**). N-3M2e-P97c nanorings induced modest serum IgG titers (**Figure 2B**) but no mucosal Ig were detected (**Figures 2D, F**).

To summarize, while fusion of P97c to LAH boosted LAH-specific systemic humoral responses, no adjuvant effect of P97c could be observed towards 3M2e. The fusion of LAH to nanorings boosted both systemic and local LAH-specific antibody responses, whereas the carrier effect of nanorings was less pronounced towards 3M2e. Chimeric proteins composed of the IAV epitopes fused to P97c either administered alone or in fusion with nanorings were unable to trigger potent mucosal humoral responses and were thus excluded from the following experiments. In contrast, preparations incorporating N-LAH or N-3M2e nanorings admixed with MG were shown to be efficient mucosal vaccine formulations.

Evaluation of the Immunopotentiator Effect of Nanorings on LAH- and 3M2e-Specific Cell-Mediated Immune Responses in Mice

Both humoral and cellular immune defenses are involved in the fight against IAV infections. Accordingly, we analyzed the characteristics of LAH- and M2e-specific cell-mediated immunity generated in [N-LAH + MG]- and [N-3M2e + MG]-vaccinated mice, respectively. The carrier effect of nanorings was investigated and the cellular response of mice immunized with the inactivated homologous IAV strain (iPR8) *via* the parenteral route was analyzed in parallel. We focused our study on prototypical type 1 (IFN-γ), type 2 (IL-4, IL-5 and IL-10), and type 17 (IL-17A) cytokines and on IL-6, a pleiotropic cytokine with multiple immunoregulatory effects including the promotion of T helper (Th) 2 and Th17 responses as well as antibody responses and mucosal IgA immunity (37).

Mice vaccinated with [LAH + MG] developed LAH-specific cellular responses with type 1 and type 17 cytokine profiles as seen by the detection of IFN-γ (**Figure 3A**) and IL-17A (**Figure 3B**) in culture supernatants of LAH-restimulated spleen cells, respectively. Low levels of IL-5 (**Figure 3D**) and IL-6 (**Figure 3E**) were also measured, whereas there were no differences in the levels of IL-4 or IL-10 between LAH-restimulated cells isolated from [LAH + MG]- and MG-instilled mice (**Figures 3C, F**). The cell-mediated immune response of mice vaccinated with [N-LAH + MG] exhibited similar cytokine profiles, with higher levels of secreted IFN-γ, IL-6 and IL-17A than [LAH + MG]-immunized mice. Mice vaccinated with [3M2e + MG] developed M2e-specific cellular responses with type 1 (**Figure 4A**) and type 17 (**Figure 4B**) cytokine profiles. While M2e-restimulated cells isolated from [3M2e + MG]-vaccinated mice secreted significant levels of IL-10 (**Figure 4F**) and IL-6 (**Figure 4E**), the cells released low levels of IL-5 (**Figure 4D**) and no significant amount of IL-4 could be detected (**Figure 4C**). The M2e-specific cellular responses were generally similar in [3M2e + MG] and [N-3M2e + MG] groups. High levels of IFN-γ, IL-4, IL-5, IL-6, and IL-10 and low levels of IL-17A were detected in culture supernatants of spleen cells isolated from [iPR8 + MG]-vaccinated mice (**Figures 3**, **4**). However, no differences were obtained between cells restimulated with PR8 peptides and non-restimulated cells. Thus, no cell-mediated immunity specifically directed against LAH or M2e epitopes could be measured in the spleen of mice immunized with [iPR8 + MG]. The quantification of LAH- (**Supplemental Figure 2A**) or M2e- (**Supplemental Figure 2B**) specific IFN-γ-secreting cells by ELISpot assay led to the same conclusions as those obtained with ELISA. An immunostimulatory effect of nanorings on 3M2e was nevertheless observed in ELISpot

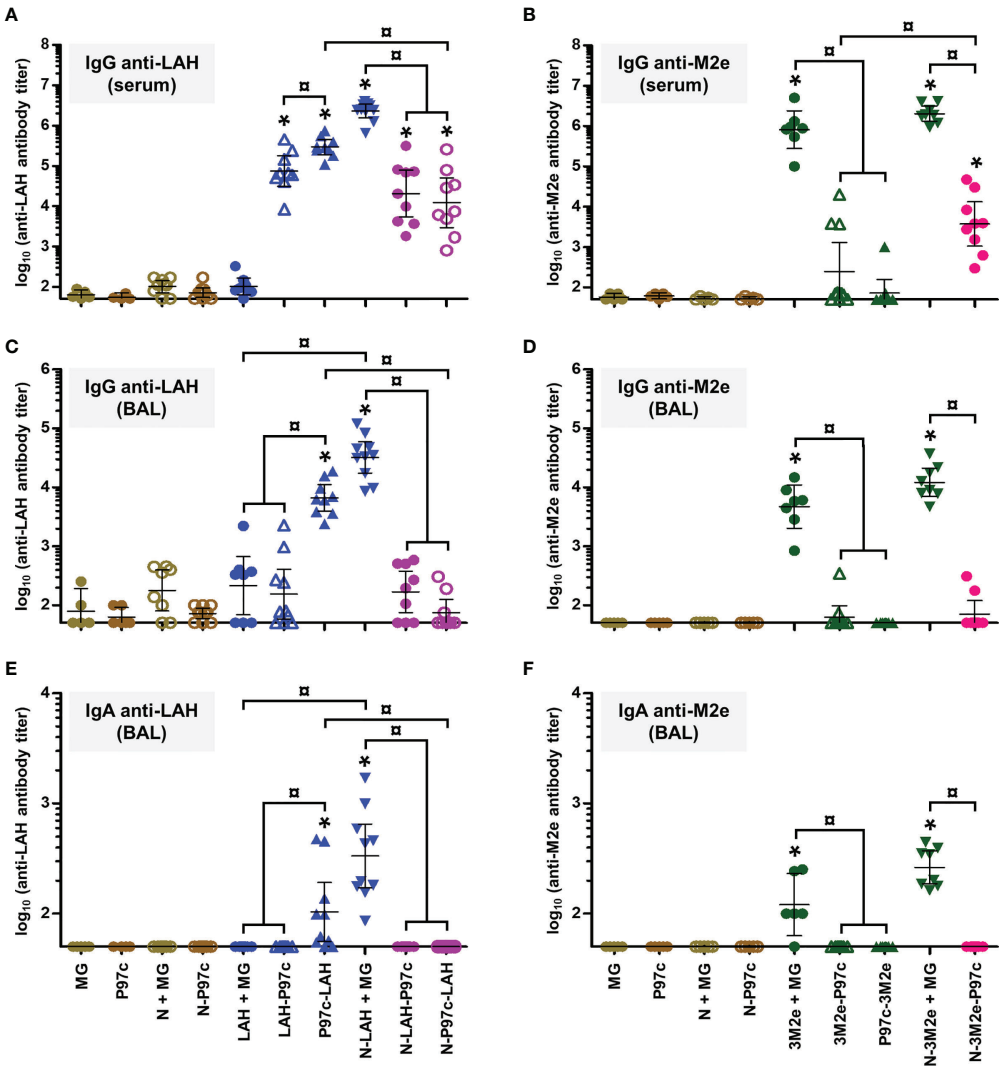

FIGURE 2 | Evaluation of the immunopotentiator effect of nanorings and P97c on LAH- and M2e-specific systemic and mucosal humoral responses in mice. Mice received at 2-week intervals three intranasal administrations of LAH or 3M2e peptides fused to nanorings and/or P97c or, as controls, free LAH or 3M2e peptides. Preparations without P97c were admixed with Montanide™ gel (MG). Mice receiving P97c nanorings (N-P97c), naked nanorings (N + MG), P97c or MG were included as negative control groups. Two weeks after the third immunization, **(A)** anti-LAH or **(B)** anti-M2e IgG titers in the serum, and anti-LAH **(C)** IgG and **(E)** IgA or anti-M2e **(D)** IgG and **(F)** IgA titers in the bronchoalveolar lavage fluids (BAL) were determined by ELISA. The titer of each mouse sample is presented, including the geometric mean with 95% confidence interval. *, statistically significant difference ($P < 0.05$) in comparison to the respective negative control groups (MG, P97c, N + MG, N-P97c). ¤, statistically significant difference ($P < 0.05$) between the indicated groups.

assay, which reported a higher frequency of M2e-specific IFN-γ-secreting cells in the [N-3M2e + MG] group than in the [3M2e + MG] group (**Supplemental Figure 2B**).

Thus, administration of [N-LAH + MG] and [N-3M2e + MG] promoted the development of LAH- and M2e-specific cellular responses in mice, respectively, which were dominated by type 1 and type 17 cytokine profiles. In contrast, the inactivated homologous IAV strain was unable to trigger specific responses against the two conserved IAV epitopes. Nanorings exerted a potent immunostimulatory effect on the formation of LAH-specific cellular immunity, whereas the carrier effect of nanorings was less pronounced towards 3M2e.

Nasal Immunization With Bi-Component Vaccine Formulations Incorporating LAH- and 3M2e-Bearing Nanorings Admixed With MG Promoted the Development of a Potent, Multi-Factorial and Multi-Compartmental Immunity Directed Against Both IAV Epitopes and Protected Mice Against H1N1 Challenge

In light of the promising immunogenicity results obtained with [N-LAH + MG] and [N-3M2e + MG] formulations, we evaluated the protective potential of these preparations administered separately or in combination against a homologous H1N1 challenge in mice.

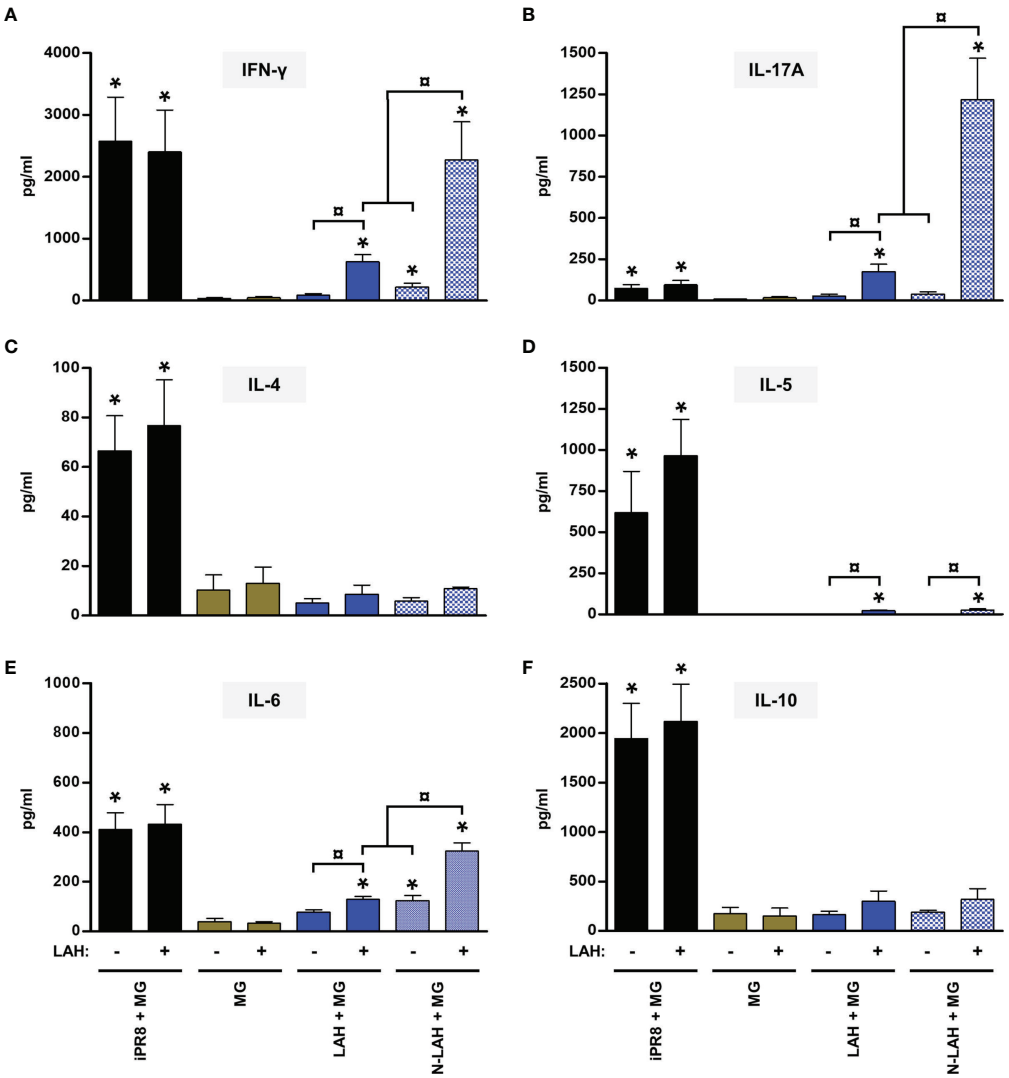

FIGURE 3 | Evaluation of the immunopotentiator effect of nanorings on LAH-specific cellular responses in mice. Mice received at 2-week intervals three intranasal administrations of LAH peptide fused to nanorings admixed with Montanide™ gel (MG). Experimental control groups received intranasal administrations of free LAH peptide admixed with MG or subcutaneous administrations of UV-inactivated PR8 strain (iPR8) admixed with MG. Vaccine vehicle (MG) was intranasally administered to the negative control group. Two weeks after the third immunization, spleen cells from individual mice were restimulated *ex vivo* for 72 h in presence ('+') or absence ('-') of synthesized LAH peptide. The levels of secreted **(A)** IFN-γ, **(B)** IL-17A, **(C)** IL-4, **(D)** IL-5, **(E)** IL-6 and **(F)** IL-10 in the culture supernatants were quantified by ELISA. Data are presented as arithmetic means with SEM of 4-5 individual spleens. *, statistically significant difference ($P < 0.05$) in comparison to MG group. ¤, statistically significant difference ($P < 0.05$) between the indicated groups.

Firstly, we compared the characteristics of LAH- and M2e-specific immune responses between mice immunized with [N-3M2e + MG] or [N-LAH + MG] and mice immunized with [N-3M2e + N-LAH + MG]. The addition of N-3M2e nanorings to the [N-LAH + MG] formulation partially reduced the magnitude of LAH-specific systemic **(Figure 5A)** and local **(Figures 5C, E)** humoral responses. In contrast, addition of N-3M2e nanorings to the [N-LAH + MG] formulation did not impede the generation of M2e-specific humoral responses **(Figures 5B, D, F)**. The serum IgG response generated by the chimeric nanorings was composed of both type 1 (IgG2a, IgG2b) **(Figures 6B, C, 7B, C)** and type 2 (IgG1) **(Figures 6A, 7A)** IgG subclasses. M2e-specific IgG3 titers were also detected in mice immunized with [N-3M2e + MG] and [N-3M2e + N-LAH + MG] **(Figure 7D)**, and low levels of LAH-specific IgG3 titers were measured in [N-3M2e + N-LAH + MG]-vaccinated mice **(Figure 6D)**. Mice parenterally vaccinated with [iPR8 + MG] developed a LAH-specific IgG response detectable only in the serum **(Figure 5)** and composed of both type 1 and type 2 IgG subclasses **(Figure 6)**, but were unable to mount a M2e-specific humoral response **(Figures 5, 7)**. Whereas the addition of N-3M2e nanorings to the [N-LAH + MG] formulation did not impact the generation of LAH-specific IFN-γ-secreting cells **(Figure 8A)**,

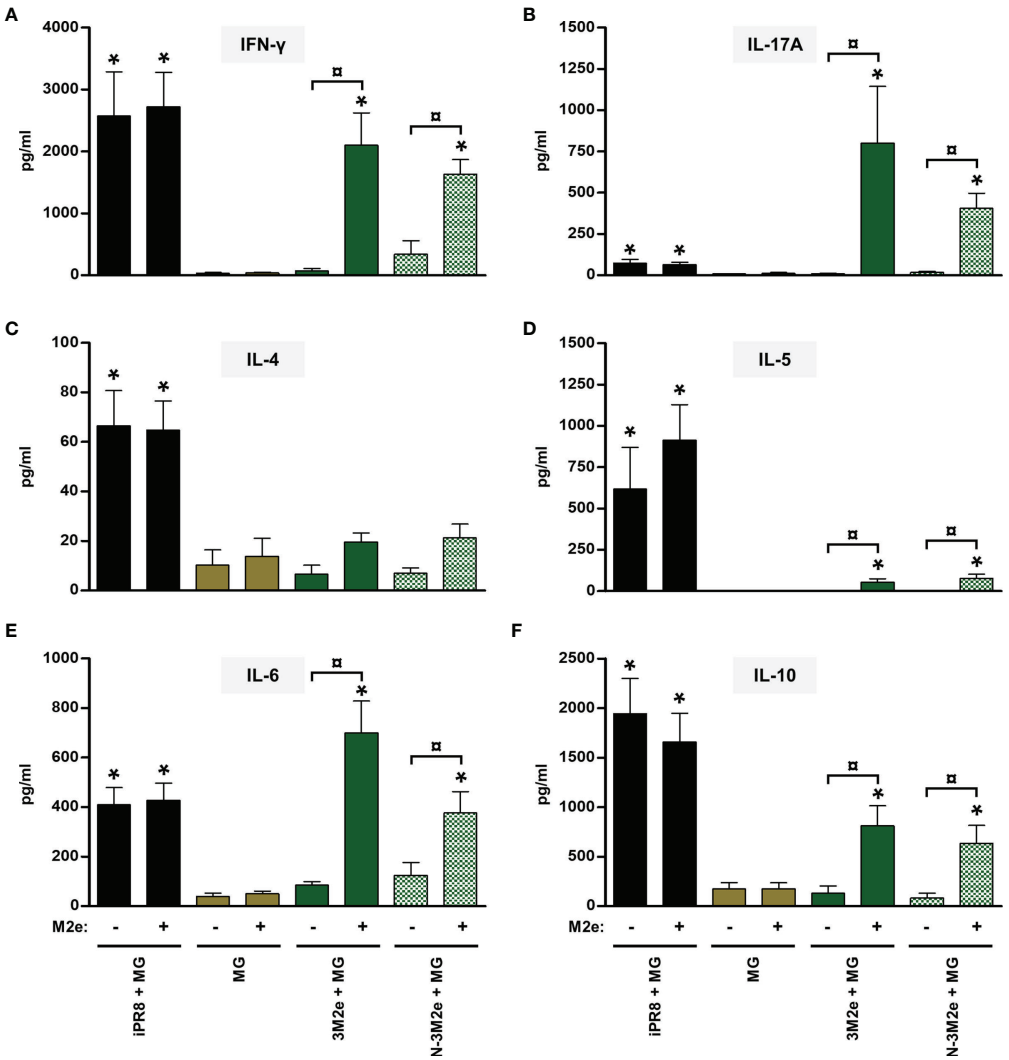

FIGURE 4 | Evaluation of the immunopotentiator effect of nanorings on M2e-specific cellular responses in mice. Mice received at 2-week intervals three intranasal administrations of 3M2e peptide fused to nanorings admixed with Montanide™ gel (MG). Experimental control groups received intranasal administrations of free 3M2e peptide admixed with MG or subcutaneous administrations of UV-inactivated PR8 strain (iPR8) admixed with MG. Vaccine vehicle (MG) was intranasally administered to negative control group. Two weeks after the third immunization, spleen cells from individual mice were restimulated *ex vivo* for 72 h in presence ('+') or absence ('-') of synthesized M2e peptide. The levels of secreted **(A)** IFN-γ, **(B)** IL-17A, **(C)** IL-4, **(D)** IL-5, **(E)** IL-6 and **(F)** IL-10 in the culture supernatants were quantified by ELISA. Data are presented as arithmetic means with SEM of 4-5 individual spleens. *, statistically significant difference ($P < 0.05$) in comparison to MG group. ¤, statistically significant difference ($P < 0.05$) between the indicated groups.

it reduced the frequency of LAH-specific IL-17A-secreting cells in the spleen (**Figure 8C**). In contrast, the addition of N-LAH nanorings to the [N-3M2e + MG] formulation resulted in an increase in the frequency of M2e-specific IFN-γ- and IL-17A-secreting cells (**Figures 8B, D**). The frequency of cells secreting type 2 cytokines was not significantly different between mice immunized with the different preparations and mice instilled with MG after restimulation with LAH or M2e peptides (data not shown).

Two weeks after the third immunization, mice were challenged with 15 LD_{50} of PR8 strain and monitored daily for mortality (**Figure 9A**) and weight loss (**Figures 9B–D**). Only one out of nine mice instilled with MG survived the infection after having lost 19% of its initial weight at day 6 p.i. In contrast, all mice immunized with [iPR8 + MG] survived the challenge with minor weight loss (mean percentage of initial weight of 92% at day 7 p.i.). The LAH peptide administered free or in fusion with nanorings with MG conferred a partial protection, and a similar clinical picture was observed for both groups (survival rate of 50% in [LAH + MG] and [N-LAH + MG] groups). The 3M2e peptide administered free or in fusion to nanorings conferred a significant protection (survival rates of 80% and 100% in [3M2e + MG] and [N-3M2e + MG] groups, respectively) with little weight loss (mean percentage of initial weight of 88% at day 7 and day 6 p.i. in [3M2e + MG] and [N-3M2e + MG] groups, respectively). Finally, all mice immunized

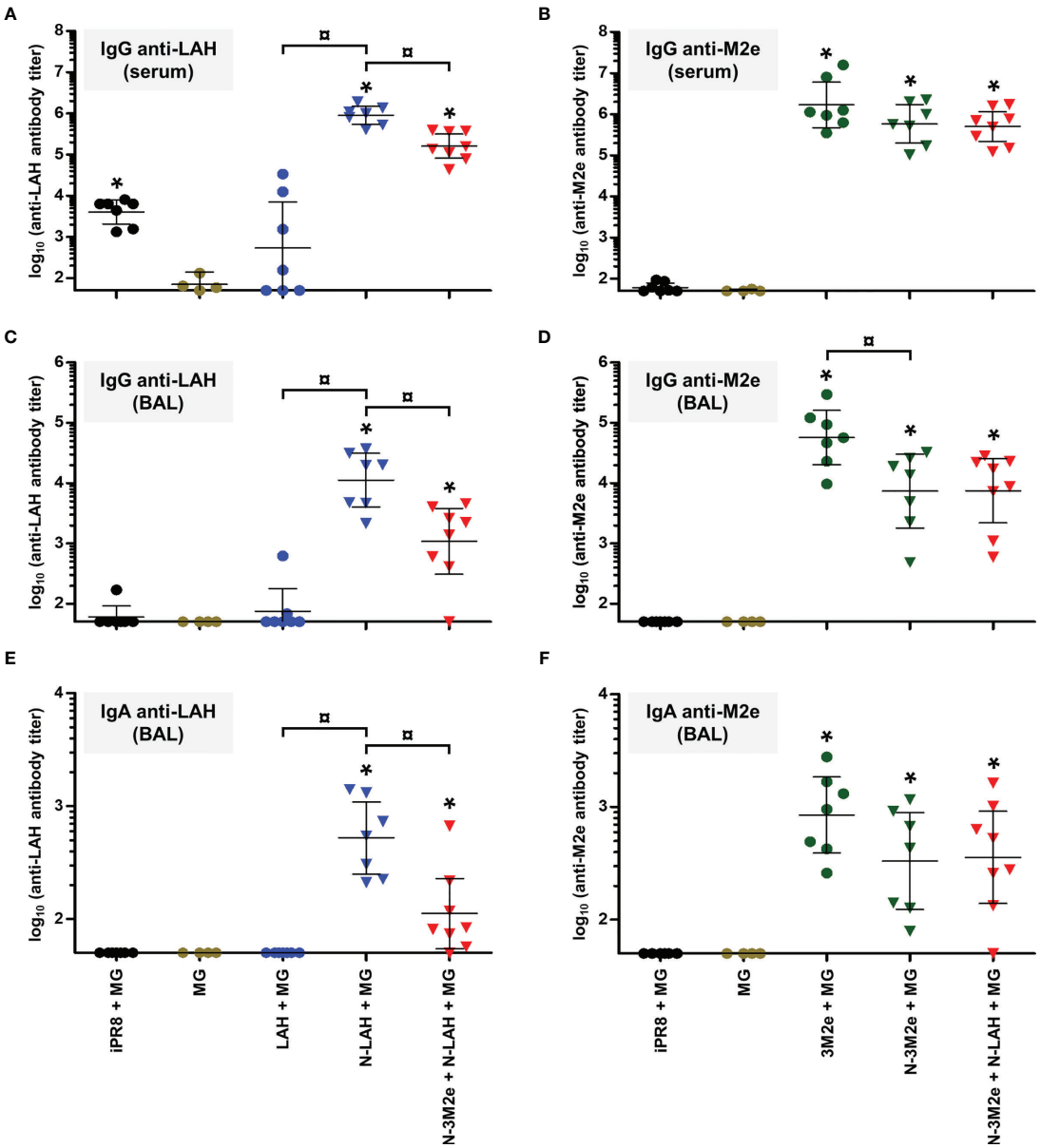

FIGURE 5 | Comparison of specific serum and mucosal humoral responses in mice immunized with LAH- and M2e-bearing nanorings instilled separately or in combination. Mice received at 2-week intervals three intranasal administrations of N-LAH and N-3M2e nanorings admixed with Montanide™ gel (MG) instilled separately or in combination. Control groups received intranasal administrations of free LAH or 3M2e peptides admixed with MG or vaccine vehicle (MG), or subcutaneous administrations of UV-inactivated PR8 strain (iPR8) admixed with MG. Two weeks after the third immunization, **(A)** anti-LAH or **(B)** anti-M2e IgG titers in the serum, and anti-LAH **(C)** IgG and **(E)** IgA or anti-M2e **(D)** IgG and **(F)** IgA titers in the bronchoalveolar lavage fluids (BAL) were determined by ELISA. The titer of each mouse sample is presented, including the geometric mean with 95% confidence interval. *, statistically significant difference ($P < 0.05$) in comparison to MG group. ¤, statistically significant difference ($P < 0.05$) between the indicated groups.

with [N-3M2e + N-LAH + MG] survived infection and presented a transient reduction of weight (mean percentage of initial weight of 88% at day 5 p.i.). These mice showed a faster weight recovery than mice immunized with [N-3M2e + MG] or [iPR8 + MG] between day 6 and day 10 p.i. (**Figure 9D**). Virus quantification in the lung homogenates at day 4 p.i. (**Figure 10**) revealed no major decrease in viral loads between MG-instilled mice and [LAH + MG] or [N-LAH + MG] groups, the latter showing nevertheless statistically lower viral loads than the MG group. In contrast, the administration of [N-3M2e + MG] induced more than 1-log decrease in viral loads in comparison to MG instillation, and statistically less viral copies were measured in the lungs isolated from mice vaccinated with [N-3M2e + MG] than those vaccinated with [3M2e + MG]. Finally, mice immunized with [N-3M2e + N-LAH + MG] displayed an

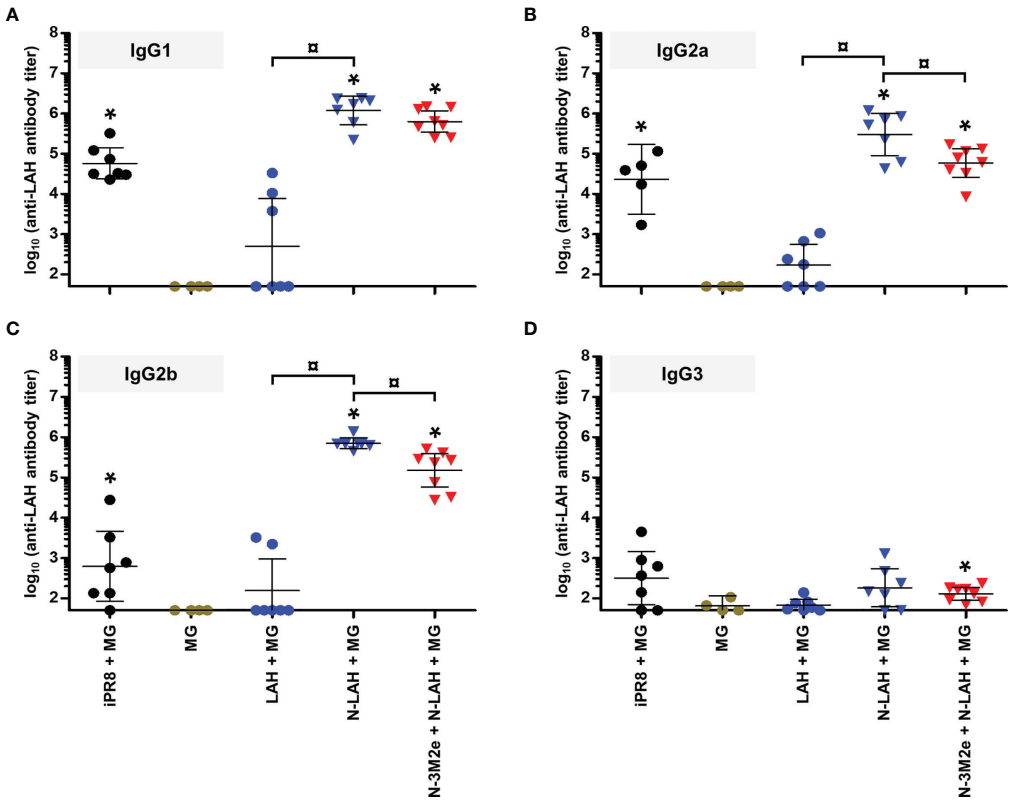

FIGURE 6 | IgG subclass composition of LAH-specific serum humoral response in mice immunized with N-LAH nanorings instilled alone or in combination with N-3M2e nanorings. Mice received at 2-week intervals three intranasal administrations of N-LAH nanorings admixed with Montanide™ gel (MG) instilled alone or in combination with N-3M2e nanorings. Control groups received intranasal administrations of free LAH peptide admixed with MG or vaccine vehicle (MG), or subcutaneous administrations of UV-inactivated PR8 strain (iPR8) admixed with MG. Two weeks after the third immunization, serum anti-LAH **(A)** IgG1, **(B)** IgG2a, **(C)** IgG2b, and **(D)** IgG3 titers were determined by ELISA. The titer of each mouse sample is presented, including the geometric mean with 95% confidence interval. *, statistically significant difference ($P < 0.05$) in comparison to MG group. ¤, statistically significant difference ($P < 0.05$) between the indicated groups.

almost 2-log reduction in viral loads *versus* the MG group and significantly less viral copies than mice immunized with [N-3M2e + MG]. Mice which received [iPR8 + MG] had more than 2-log decrease in viral loads *versus* the MG group and there were no statistical differences between [N-3M2e + N-LAH + MG]- and [iPR8 + MG]-immunized groups.

Overall, these results demonstrate that the [N-3M2e + N-LAH + MG] formulation elicited humoral responses composed of serum type 1/type 2 IgG and mucosal IgG and IgA as well as cellular responses dominated by type 1/type 17 cytokine profiles, and conferred clinical and virological protection against H1N1 homologous infection in mice.

Evaluation of the Immunogenicity and Protective Potential of LAH- and 3M2e-Bearing Chimeric Nanorings Against Heterosubtypic HPAIV H5N8 Infection in Chickens

Experiments in mice have shown that intranasal vaccination of a combination of N-LAH and N-3M2e nanorings admixed with MG generated a protective immunity against homologous IAV infection. In a final set of experiments, we evaluated the immunogenicity of this vaccine formulation in chickens, as well as its cross-protective potential against heterosubtypic HPAIV infection. H5N9 LAH and 3M2e peptides fused to nanorings were administered to birds either mucosally with MG or parenterally with ISA adjuvant. The stability of nanorings mixed with ISA was confirmed previously (38). The non-vaccinated control group received only PBS. Eighteen days after the third immunization, anti-M2e- and anti-LAH antibodies were dosed in the serum (**Figures 11A, B**) and in the LS (**Figures 11C, D**) to analyze systemic and mucosal humoral responses, respectively. Chickens immunized with [N-3M2e + N-LAH + ISA] developed LAH- and M2e-specific serum IgG responses. In contrast, [N-3M2e + N-LAH + MG]-immunized birds exhibited a lower, albeit significant, M2e-specific serum IgG response, and no anti-LAH IgG were detected in the serum (**Figures 11A, B**). In addition, no significant differences were found in M2e- or LAH-specific IgG or IgA titers in LS between [N-3M2e + N-LAH + MG]- and PBS-instilled chickens (**Figures 11C, D**). Three weeks after the third immunization, chickens were challenged with 5 LD_{50} of HPAIV

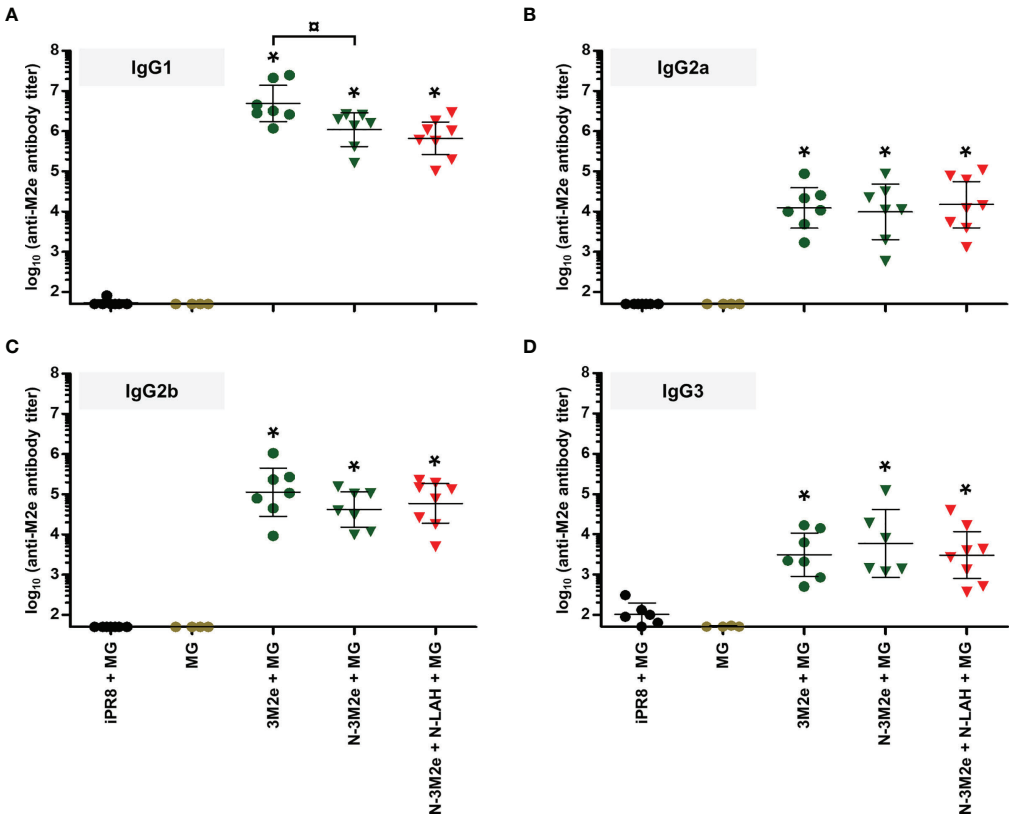

FIGURE 7 | IgG subclass composition of M2e-specific serum humoral response in mice immunized with N-3M2e nanorings instilled alone or in combination with N-LAH nanorings. Mice received at 2-week intervals three intranasal administrations of N-3M2e nanorings admixed with Montanide™ gel (MG) instilled alone or in combination with N-LAH nanorings. Control groups received intranasal administrations of free 3M2e peptide admixed with MG or vaccine vehicle (MG), or subcutaneous administrations of UV-inactivated PR8 strain (iPR8) admixed with MG. Two weeks after the third immunization, serum anti-M2e **(A)** IgG1, **(B)** IgG2a, **(C)** IgG2b, and **(D)** IgG3 titers were determined by ELISA. The titer of each mouse sample is presented, including the geometric mean with 95% confidence interval. *, statistically significant difference ($P < 0.05$) in comparison to MG group. ¤, statistically significant difference ($P < 0.05$) between the indicated groups.

H5N8 strain and the mortality was monitored daily (**Figure 11E**). Neither chickens from the [N-3M2e + N-LAH + MG] group, nor chickens from the non-vaccinated group survived the infection (100% mortality within 5 days for both groups). Notwithstanding the presence of elevated specific serum antibody titers, all chickens vaccinated with [N-3M2e + N-LAH + ISA] died within 6 days. No correlation was found between the magnitude of the specific humoral response and the survival time (data not shown). Because of the high mortality rate and the fast kinetics of the infection, pharyngeal or cloacal viral shedding were not analyzed.

DISCUSSION

Faced with the pressing challenge posed by the high variability associated with IAV which requires surveillance monitoring of circulating strains and regular updating of the composition of current vaccines, novel immunization strategies which include the use of conserved "universal" viral epitopes are urgently needed. In the present study, we evaluated the ability of various intranasal M2e- and LAH-based vaccine formulations to trigger specific antibody- and cell-mediated immunity, two critical adaptive immune arms in the fight against IAV infections, and to confer protection against an experimental IAV challenge in mice and chickens.

M2e and LAH peptides are poorly immunogenic *per se*. Therefore, they have to be administered in association with adjuvant/delivery systems to induce robust immune responses in the host, including ligands of PRRs, bacterial toxins and derivatives, lipid-based particles, virus-like particles, organic and inorganic polymers and bacterial or viral vectored vaccines (5, 7–15). In this study, we have used innovative nanostructures developed in our research unit named "nanorings" as a mucosal vaccine delivery platform. Nanorings are composed of 10-11 N_{RSV} protomers entrapping random stretches of bacterial RNA (36) and are readily internalized by antigen-presenting cells (APCs) (39). Nanorings also stimulate expression of co-stimulatory molecules as well as secretion of type I interferons by APCs (Riffault S., personal communication). We demonstrated that LAH fused to nanorings elicited higher LAH-specific humoral responses, both at systemic and mucosal

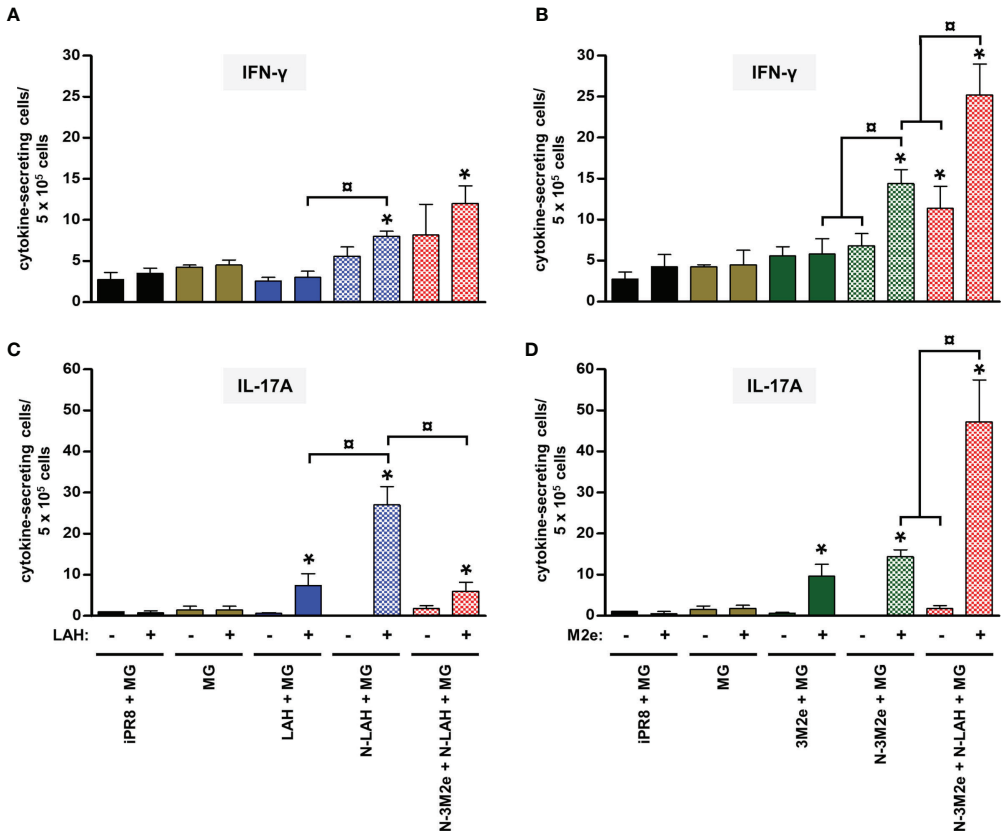

FIGURE 8 | Comparison of specific cellular responses in mice immunized with LAH- and M2e-bearing nanorings instilled separately or in combination. Mice received at 2-week intervals three intranasal administrations of N-LAH and N-3M2e nanorings admixed with Montanide™ gel (MG) instilled separately or in combination. Control groups received intranasal administrations of free LAH or 3M2e peptides admixed with MG or vaccine vehicle (MG), or subcutaneous administrations of UV-inactivated PR8 strain (iPR8) admixed with MG. Two weeks after the third immunization, spleen cells from individual mice were restimulated *ex vivo* for 24 h in presence ('+') or absence ('-') of synthesized **(A, C)** LAH or **(B, D)** M2e peptide and the frequency of LAH-specific **(A)** IFN-γ- and **(C)** IL-17A-secreting cells or M2e-specific **(B)** IFN-γ- and **(D)** IL-17A-secreting cells was monitored by ELISpot assay. Data are presented as arithmetic means with SEM of 4-5 individual spleens. *, statistically significant difference ($P < 0.05$) in comparison to MG group. ¤, statistically significant difference ($P < 0.05$) between the indicated groups.

levels, as well as higher cellular responses than those observed in mice receiving free LAH peptide. The immunopotentiator properties of nanorings may be conferred by the single-stranded bacterial RNA fragment of 70 to 77 bases and/or the nanoparticle architecture of the rings. Such a marked adjuvant effect of nanorings was not observed for the 3M2e epitope, which could be related to our immunization protocol. Indeed, 20 μg of 3M2e peptides contain more M2e epitopes than 20 μg of N-3M2e nanorings (molecular ratio of 1/6 for N-3M2e/3M2e). In addition, mice immunized with N-3M2e nanorings exhibited significantly higher titers of serum anti-M2e IgG than 3M2e-immunized mice after two immunizations (data not shown), as previously described (28), and thus the third immunization may have masked the adjuvant potential of the nanoring platform.

The fusion in tandem of P97c to LAH also boosted immunogenicity of the viral epitope, and the fusion orientation greatly influenced the features of the LAH-specific antibody response. The serum IgG titers were more elevated in the P97c-LAH group than in [LAH-P97c]-instilled mice. Similarly, P97c was shown to enhance the magnitude of the antibody response directed against the capsid protein of the porcine circovirus type 2 only when it was fused at the N-terminal end of the viral epitope (30). A recent *in vitro* study indicated that P97c stimulated innate immune responses through activation of TLR-5 (29). TLR-5 agonists, such as flagellin, are potent and safe adjuvants for influenza vaccines administered *via* parenteral or mucosal routes in both animals and humans. The mucosal adjuvant properties of TLR-5 ligands rely on an enhancement of transepithelial transport of co-administered antigens by the follicle-associated epithelium of the mucosa-associated lymphoid tissues, as well as on the stimulation of the migration of APCs into the follicle-associated epithelium (15). These ligands also stimulate the uptake of vaccine antigens by APCs and promote the activation and the maturation of APCs *in vitro* (15). Nonetheless, P97c remains a poor mucosal adjuvant and low to non-significant specific IgA titers were detected in the BAL of mice immunized with chimeric proteins composed of IAV epitopes fused to P97c either administered alone or in fusion

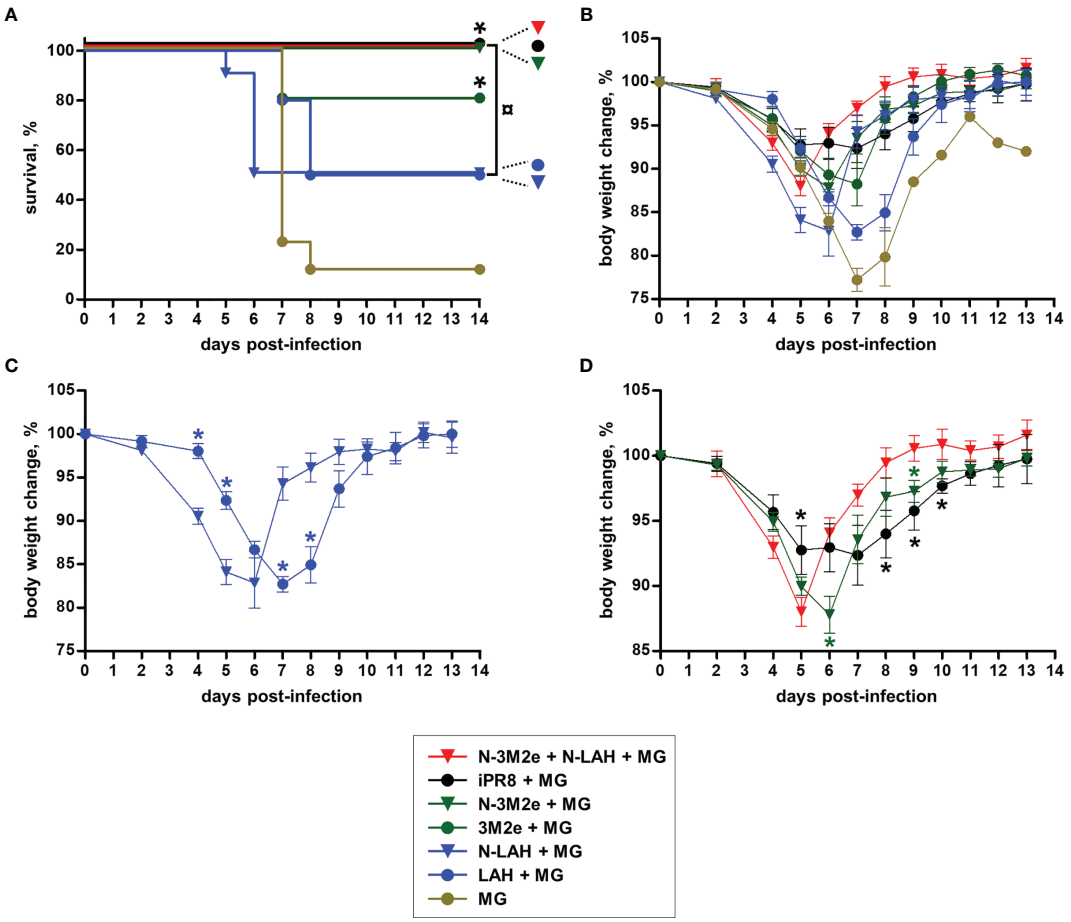

FIGURE 9 | Evaluation of the clinical protection conferred by LAH- and 3M2e-bearing nanorings against homologous H1N1 infection in mice. Mice received at 2-week intervals three intranasal administrations of N-LAH and N-3M2e nanorings admixed with Montanide™ gel (MG) instilled separately or in combination. Experimental control groups received intranasal administrations of free LAH or 3M2e peptides admixed with MG. Mice receiving subcutaneous administrations of UV-inactivated PR8 strain (iPR8) admixed with MG or intranasal administrations of vaccine vehicle (MG) were included as positive or negative control groups, respectively. Two weeks after the third immunization, all mice were challenged with 15 LD_{50} of PR8 strain and monitored daily for **(A)** mortality and **(B–D)** body weight loss. **(A)** Survival curves of infected mice are expressed as the percentages of surviving mice. The log-rank (Mantel-Cox) test was used to compare survival curves. *, statistically significant difference ($P < 0.05$) in comparison to MG group. ¤, statistically significant difference ($P < 0.05$) between the indicated groups. **(B–D)** Weight curves of infected mice are expressed as the arithmetic mean (with SEM) of the percentages of body weight changes between the examined day and the day of infection (day 0). *, statistically significant difference ($P < 0.05$) in comparison to [N-LAH + MG] (panel **C**) or [N-3M2e + N-LAH + MG] groups (panel **D**).

to nanorings. In contrast, N-3M2e and N-LAH nanorings admixed with MG induced a significant mucosal humoral immunity specifically directed against IAV epitopes. MG is a polymeric aqueous adjuvant based on a dispersion of a high-molecular-weight polyacrylic polymer in water whose safety and efficacy have been proven in the context of a mucosal vaccination. However, the mechanisms of action associated with MG are still poorly characterized.

All mice vaccinated with [N-3M2e + N-LAH + MG] survived infection and presented significantly reduced pulmonary viral loads, and various immune defense mechanisms could be engaged. Passive transfer experiments in mice showed that antibodies directed against M2e or LAH mediated resistance against IAV infection (16, 17, 40, 41). An *in vitro* study demonstrated that anti-LAH antibodies exerted broad neutralizing activities against H3 strains and inhibited the conformational change of the HA stalk domain during the fusion step between viral and endosomal membranes (18). However, no functional activity was detected with the serum or BAL of mice vaccinated with our H1 LAH-based formulations using standard microneutralization assay (data not shown). Similarly, a norovirus P particle displaying H1 and H3 LAH epitopes elicited neutralizing antibodies against H3 but not H1 strains, and differences in the conformational flexibility of the two epitopes or in the time of exposure of the epitopes during membrane fusion may explain this result (42, 43). Other effector functions exerted by anti-LAH antibodies may be involved, such as Fc-mediated mechanisms or complement activation (44). Anti-M2e antibodies restricted viral replication by the elimination of infected cells *via* Fc-mediated effector functions

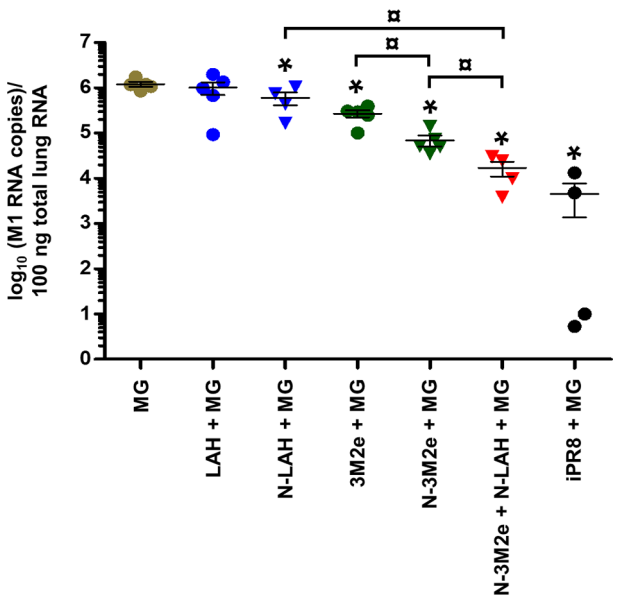

FIGURE 10 | Evaluation of the virological protection conferred by LAH- and 3M2e-bearing nanorings against homologous H1N1 infection in mice. Mice received at 2-week intervals three intranasal administrations of N-LAH and N-3M2e nanorings admixed with Montanide™ gel (MG) instilled separately or in combination. Experimental control groups received intranasal administrations of free LAH or 3M2e peptides admixed with MG. Mice receiving subcutaneous administrations of UV-inactivated PR8 strain (iPR8) admixed with MG or intranasal administrations of vaccine vehicle (MG) were included as positive or negative control groups, respectively. Two weeks after the third immunization, all mice were challenged with 15 LD_{50} of PR8 strain and four days after challenge, mice were sacrificed, and individual viral loads were measured from lung homogenates by qRT-PCR. The number of M1-specific RNA copies for 100 ng total lung RNA was determined against a standard curve using a plasmid encoding PR8 M1 gene. The number of viral copies of each mouse lung sample is presented, including the arithmetic mean with SEM. *, statistically significant difference ($P < 0.05$) in comparison to MG group. ¤, statistically significant difference ($P < 0.05$) between the indicated groups.

mobilizing alveolar macrophages and natural killer cells (7), and both type 1 and type 2 IgG were associated with protection conferred by anti-M2e antibodies (45, 46). Further investigations on the functionality of anti-LAH and anti-M2e antibodies generated by our vaccine preparations are required.

Beside humoral responses, various type 1-, type 2- and type 17-cytokine secreting $CD4^+$ (47, 48) and $CD8^+$ (49, 50) T cell subsets contribute to anti-IAV immunity by limiting the duration and severity of the disease *via* multiple synergistic effector mechanisms. IAV-specific $CD8^+$ T cells are mainly involved in the direct killing of infected cells, and $CD4^+$ T cells provide helper functions to B cells and $CD8^+$ T cells, regulate the response of innate immune cells, and exert direct cytotoxic functions (51). Both major histocompatibility complex class I- and class II-restricted epitopes are found in LAH and M2e peptides (52–55), and LAH- or M2e-specific $CD4^+$ or $CD8^+$ T cells secreting type 1, type 2 or type 17 cytokines can be generated by subunit vaccines in mice (40, 54, 56–58). Some studies also indicated a protective role of M2e-specific $CD4^+$ T cells (40, 54). We detected LAH- and M2e-specific type 1-, type 2-, and type 17-secreting cells in the spleen of mice immunized with N-LAH and/or N-3M2e nanorings admixed with MG, and the cell subsets engaged in these responses need to be identified.

Various experiments in mice demonstrated that M2e- and LAH-based vaccines conferred better clinical and virological protection against IAV when they were administered mucosally instead of parenterally, and this was correlated with the ability to induce local IgA (28, 59–61). Secretory IgA, which are polymeric IgA produced by B cells in the lamina propria and secreted to mucosal surfaces, are one of the first lines of defense against respiratory pathogens. They neutralize viral infection of respiratory epithelial cells *via* extracellular and intracellular immune exclusion and also exhibit FcαR-mediated effector functions (15, 62). IgA display a broad spectrum of reactivity against heterovariant and heterosubtypic IAV strains, and are thus an essential defensive front line against highly variable IAV (15). Whereas IgA prevent infections of the upper respiratory system, IgG, which are secreted systemically and diffuse in mucosal tissues, are mainly involved in the defense of the lower respiratory tract by decreasing viral pneumonia (15). Mucosal vaccination is also prone to generate tissue-resident memory T cells in the respiratory tract, which was shown to mediate optimal (cross-) resistance against IAV infections (15, 54). Further analyses on the features of the humoral response in the upper respiratory tract, on the functionality of the mucosal antibody response as well as on the characteristics of cellular immunity in the respiratory mucosa of mice immunized with N-LAH and/or N-3M2e admixed with MG are thus necessary.

The protection conferred by the [N-3M2e + N-LAH + MG] preparation in mice was enhanced in comparison to [N-LAH + MG] or [N-3M2e + MG] preparations. Other studies demonstrated that the combination of LAH and M2e epitopes in vaccine preparations increased immunogenic and protective properties (63–65). This is likely due to the cooperation of both LAH- and M2e-specific effector functions. In addition, the supplementation of [N-3M2e + MG] with N-LAH nanorings raised the number of M2e-specific spleen cells secreting type 1 and type 17 cytokines. Memory M2e-specific $CD4^+$ T cells have been shown previously to boost the generation of HA-specific IgG responses (54). Additional studies are required to evaluate whether LAH-specific immune mediators can influence the generation of M2e-specific immunity. Ongoing experiments are evaluating the immunogenicity and protective efficacy of chimeric nanorings bearing M2e and LAH epitopes simultaneously (N-3M2e-LAH, N-LAH-3M2e).

In this study, the efficacy of nanoring-based vaccines in chickens was evaluated for the first time. In stark contrast with the potent protective effect conferred by the combination of N-3M2e and N-LAH nanorings in the mouse model, none of the chickens vaccinated with the formulation administered *via* the mucosal or parenteral routes survived a HPAIV infection.

Some studies demonstrated that parenteral or mucosal administrations of M2e epitopes under various vaccine

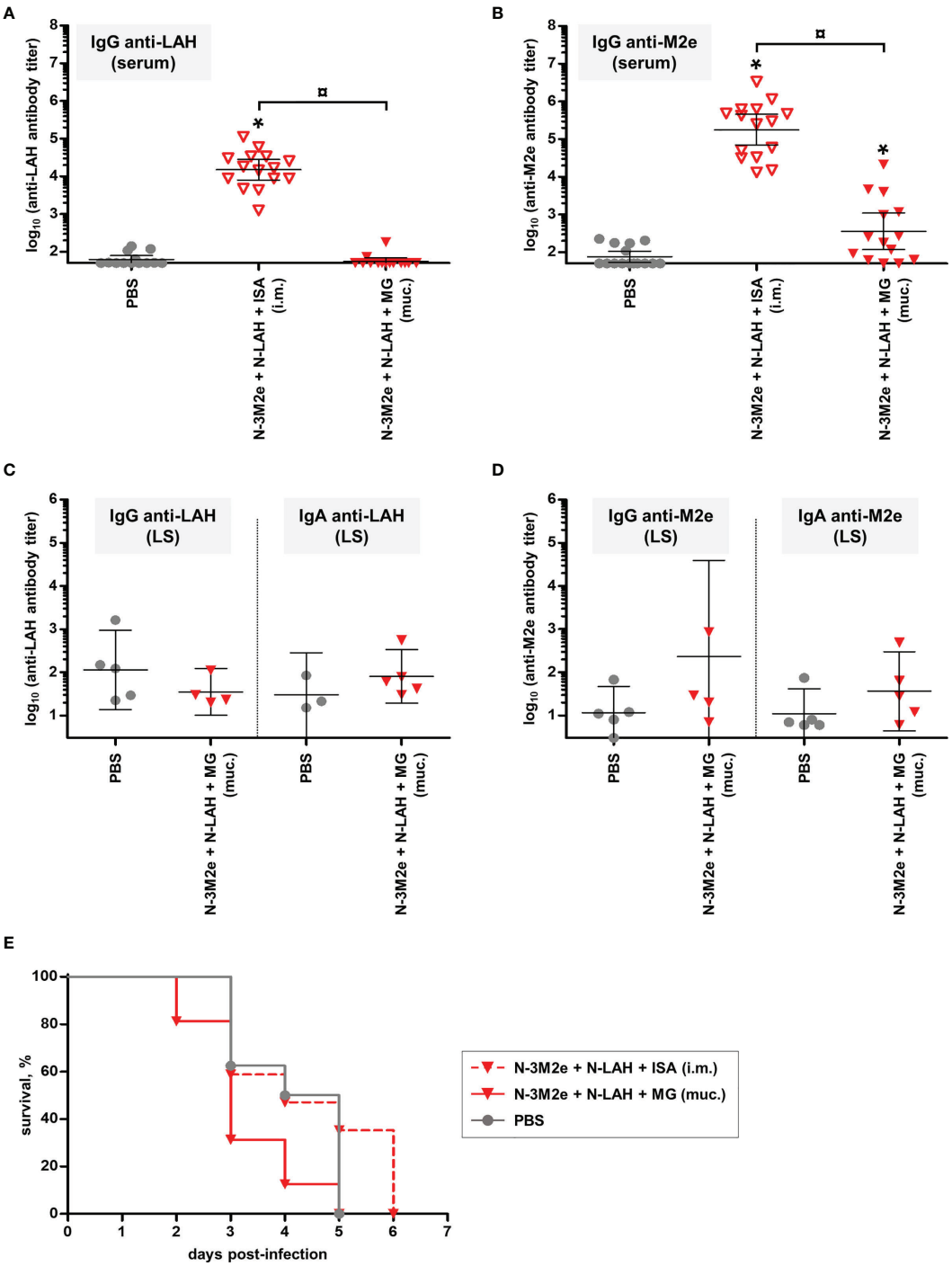

FIGURE 11 | Evaluation of the immunogenicity and protective potential of LAH- and 3M2e-bearing nanorings against heterosubtypic H5N8 HPAIV infection in chickens. Chickens received at 2-week intervals three intranasal administrations of H5N9 LAH and 3M2e peptides fused to nanorings either mucosally ('muc.') with Montanide™ gel (MG) or intramuscularly ('i.m.') with Montanide™ ISA (ISA). The non-vaccinated control group received only PBS. Eighteen days after the third immunization, serum **(A)** anti-LAH or **(B)** anti-M2e IgG titers or mucosal **(C)** anti-LAH IgG and IgA or **(D)** anti-M2e IgG or IgA titers in the lachrymal secretions (LS) were dosed. The titer of each chicken sample is presented, including the geometric mean with 95% confidence interval. *, statistically significant difference ($P < 0.05$) in comparison to PBS group. ¤, statistically significant difference ($P < 0.05$) between the indicated groups. **(E)** Three weeks after the third immunization, all chickens were challenged with 5 LD_{50} of H5N8 strain and the mortality was monitored daily. Survival curves of infected chickens are expressed as the percentages of surviving chickens.

formats, including a fusion protein with TLR agonists, nanoparticles or a bacterial vector, reduced, and sometimes even totally abrogated, viral shedding and the severity of clinical signs or lung lesions after homologous or heterologous LPAIV challenges in chickens (13, 14, 21, 66, 67). The association of M2e with other viral epitopes such as LAH and NA increased the protective potential of these vaccine formulations (12, 68). In contrast, the effectiveness of a stand-alone M2e vaccine remained limited against HPAIV infections (11, 69–71), and only incorporation of other IAV epitopes such as LAH enabled chickens to present significant survival rates (19). Nonetheless, not all chickens immunized with the combination of M2e and LAH epitopes survived the infection and the virus shedding from the respiratory and digestive tracts remained elevated (19). Although vaccinated chickens developed M2e- and/or LAH-specific humoral and cellular immune responses in these studies, the cellular and molecular mechanisms involved, as well as the respective engagement of mucosal and systemic immune compartments in the resistance against LPAIV and HPAIV, remain largely unknown. Further examination of the characteristics and the functionality of the antibody and cell-mediated responses generated in chickens vaccinated with N-LAH and N-3M2e nanorings are needed for a comprehensive interpretation of the lack of protection observed in our study.

While subunit vaccines incorporating universal epitopes did not provide an adequate protection against HPAIV infections, recent studies indicated that M2e and/or LAH-based vaccines improved the (cross-) protective effects of inactivated IAV vaccines in chickens (11, 20, 72). For example, all chickens co-immunized with a recombinant baculovirus expressing LAH, M2e and nucleoprotein epitopes and an H5N1 inactivated vaccine survived a heterologous HPAIV H5N1 challenge and no longer spread the virus in contrast with chickens immunized with the inactivated vaccine alone (72). The supplementation of inactivated IAV vaccines with M2e-based nanoparticles enhanced protection against H5N1 homologous and H5N8 heterologous HPAIV infections (11), as well as against heterologous LPAIV infection (20). Thus, further studies are warranted to evaluate the beneficial effects of N-LAH and N-3M2e nanorings as supplements to current IAV inactivated vaccines in chickens, and especially in broadening the resistance against vaccine-escape viruses.

DATA AVAILABILITY STATEMENT

The raw data supporting the conclusions of this article will be made available by the authors, without undue reservation.

ETHICS STATEMENT

The animal study was reviewed and approved by Animal Care and Use Committee at the Centre de Recherche de Jouy-en-Josas (COMETHEA) authorization number 2015100910396112v1, APAFIS number 1487 (mouse experiments); European Council Directive CEE86/609 and animal protocols approved by the Ethics Committee "Sciences et santé animale", committee number 115 (chicken experiments).

AUTHOR CONTRIBUTIONS

ChC, DA, SB, RG, and CyC conceived and designed the study. CyC, MM, MT, QV, AM, LS, P-LH, and ChC produced vaccine candidates. CyC, MM, MT, QV, JM, LS, RG, and ChC performed mouse experiments. TF, PB, RV, MD, CyC, MM, and MT performed chicken experiments. CyC and ChC performed data analysis. CyC and ChC wrote the manuscript. CyC, ChC, RG, DA, and SB reviewed and edited the manuscript. All authors contributed and approved the submitted version of the manuscript.

FUNDING

This work was supported by a grant from the Livestock Vaccine Innovation Fund (International Development Research Centre, Bill & Melinda Gates Foundation, Global Affairs Canada) to ChC and DA (Project ID 108517).

ACKNOWLEDGMENTS

We thank Mathilde Bauducel, Marlène Hery, Kathleen Auger, Roxane Trepier, André Tiffoche and Jérôme Pottier (IERP-UE907, INRAE, Jouy-en-Josas) for technical assistance in animal experiments. We thank Christine Longin (Plateforme Microscopie et Imagerie des Micro-organismes, Animaux et Aliments, INRAE, Jouy-en-Josas) for performing TEM analysis and Céline Henry and Lydie Correia (PAPPSO, MICALIS, INRAE, Jouy-en-Josas) for performing LC-MS/MS analysis. We thank Dr Isabelle Schwartz-Cornil, Dr Delphyne Descamps and Vincent Pietralunga (VIM, INRAE, Jouy-en-Josas) for providing us with ELISA reagents and for technical help with the iSPOT reader. We thank Dr Jean-François Eléouet (VIM, INRAE, Jouy-en-Josas) and Sébastien Deville (SEPPIC) for providing us with N-specific Pab and Montanide™ adjuvants, respectively. We thank Bruno Da Costa for technical help with the production of the stock of PR8 virus. We thank Dr. Charles-Adrien Richard (VIM, INRAE, Jouy-en-Josas) for technical help with the Äkta-Purifier 100 FPLC system. We thank Dr. Jean Millet (VIM, INRAE, Jouy-en-Josas) for critical reading of the manuscript. The authors thank Dr Sabine Riffault (VIM, INRAE, Jouy-en-Josas) for helpful discussions and the critical reading of the manuscript.

SUPPLEMENTARY MATERIAL

The Supplementary Material for this article can be found online at: https://www.frontiersin.org/articles/10.3389/fimmu.2021.772550/full#supplementary-material

Supplementary Figure 1 | Molecular size distribution by volume as detected by dynamic light scattering for the different nanoring preparations. d.nm: hydrodynamic diameter in nanometers.

Supplementary Figure 2 | Evaluation of the immunopotentiator effect of nanorings on the frequency of LAH- and M2e-specific IFN-γ-secreting cells in mice. Mice received at 2-week intervals three intranasal administrations of LAH or 3M2e peptides fused to nanorings admixed with Montanide™ gel (MG). Experimental control groups received intranasal administrations of free LAH or 3M2e peptides admixed with MG or subcutaneous administrations of UV-inactivated PR8 strain (iPR8) admixed with MG. Vaccine vehicle (MG) was intranasally administered to negative control group. Two weeks after the third immunization, spleen cells from individual mice were restimulated *ex vivo* for 24 h in presence ('+') or absence ('-') of synthesized LAH or M2e peptides. The frequency of **(A)** LAH- or **(B)** M2e-specific IFN-γ-secreting cells was monitored by ELISpot assay. Data are presented as arithmetic means with SEM of 4-5 individual spleens. *, statistically significant difference ($P < 0.05$) in comparison to MG group. ¤, statistically significant difference ($P < 0.05$) between the indicated groups.

REFERENCES

1. World Health Organization. *Influenza (Avian and Other Zoonotic)* (2018). Available at: https://wwwwhoint/news-room/fact-sheets/detail/influenza-(avian-and-other-zoonotic).
2. Pantin-Jackwood MJ, Swayne DE. Pathogenesis and Pathobiology of Avian Influenza Virus Infection in Birds. *Rev Sci Tech* (2009) 28:113–36. doi: 10.20506/rst.28.1.1869
3. Krammer F. The Human Antibody Response to Influenza A Virus Infection and Vaccination. *Nat Rev Immunol* (2019) 19:383–97. doi: 10.1038/s41577-019-0143-6
4. Rajao DS, Perez DR. Universal Vaccines and Vaccine Platforms to Protect Against Influenza Viruses in Humans and Agriculture. *Front Microbiol* (2018) 9:123. doi: 10.3389/fmicb.2018.00123
5. Swayne DE, Kapczynski DR. Vaccines and Vaccination for Avian Influenza in Poultry. In: DE Swayne, editor. *Animal Influenza*. Ames, IA: Wiley-Backwell. (2016). p. 378–434.
6. Krammer F, Palese P. Advances in the Development of Influenza Virus Vaccines. *Nat Rev Drug Discovery* (2015) 14:167–82. doi: 10.1038/nrd4529
7. Kolpe A, Schepens B, Fiers W, Saelens X. M2-Based Influenza Vaccines: Recent Advances and Clinical Potential. *Expert Rev Vaccines* (2017) 16:123–36. doi: 10.1080/14760584.2017.1240041
8. Kostolansky F, Tomcikova K, Briestenska K, Mikusova M, Vareckova E. Universal Anti-Influenza Vaccines Based on Viral HA2 and M2e Antigens. *Acta Virol* (2020) 64:417–26. doi: 10.4149/av_2020_408
9. Hajam IA, Senevirathne A, Hewawaduge C, Kim J, Lee JH. Intranasally Administered Protein Coated Chitosan Nanoparticles Encapsulating Influenza H9N2 HA2 and M2e mRNA Molecules Elicit Protective Immunity Against Avian Influenza Viruses in Chickens. *Vet Res* (2020) 51:37. doi: 10.1186/s13567-020-00762-4
10. Watkins HC, Pagan CL, Childs HR, Posada S, Chau A, Rios J, et al. A Single Dose and Long Lasting Vaccine Against Pandemic Influenza Through the Controlled Release of a Heterospecies Tandem M2 Sequence Embedded Within Detoxified Bacterial Outer Membrane Vesicles. *Vaccine* (2017) 35:5373–80. doi: 10.1016/j.vaccine.2017.08.013
11. Song BM, Kang HM, Lee EK, Jung SC, Kim MC, Lee YN, et al. Supplemented Vaccination With Tandem Repeat M2e Virus-Like Particles Enhances Protection Against Homologous and Heterologous HPAI H5 Viruses in Chickens. *Vaccine* (2016) 34:678–86. doi: 10.1016/j.vaccine.2015.11.074
12. Elaish M, Xia M, Ngunjiri JM, Ghorbani A, Jang H, Kc M, et al. Protective Immunity Against Influenza Virus Challenge by Norovirus P Particle-M2e and HA2-AtCYN Vaccines in Chickens. *Vaccine* (2019) 37:6454–62. doi: 10.1016/j.vaccine.2019.08.082
13. Hajam IA, Kim J, Lee JH. *Salmonella Gallinarum* Delivering M2eCD40L in Protein and DNA Formats Acts as a Bivalent Vaccine Against Fowl Typhoid and H9N2 Infection in Chickens. *Vet Res* (2018) 49:99. doi: 10.1186/s13567-018-0593-z
14. Yang WT, Yang GL, Zhao L, Jin YB, Jiang YL, Huang HB, et al. *Lactobacillus Plantarum* Displaying Conserved M2e and HA2 Fusion Antigens Induces Protection Against Influenza Virus Challenge. *Appl Microbiol Biotechnol* (2018) 102:5077–88. doi: 10.1007/s00253-018-8924-6
15. Calzas C, Chevalier C. Innovative Mucosal Vaccine Formulations Against Influenza A Virus Infections. *Front Immunol* (2019) 10:1605. doi: 10.3389/fimmu.2019.01605
16. Wang TT, Tan GS, Hai R, Pica N, Ngai L, Ekiert DC, et al. Vaccination With a Synthetic Peptide From the Influenza Virus Hemagglutinin Provides Protection Against Distinct Viral Subtypes. *Proc Natl Acad Sci USA* (2010) 107:18979–84. doi: 10.1073/pnas.1013387107
17. Chen S, Zheng D, Li C, Zhang W, Xu W, Liu X, et al. Protection Against Multiple Subtypes of Influenza Viruses by Virus-Like Particle Vaccines Based on a Hemagglutinin Conserved Epitope. *BioMed Res Int* (2015) 2015:901817. doi: 10.1155/2015/901817
18. Gong X, Yin H, Shi Y, Guan S, He X, Yang L, et al. Conserved Stem Fragment From H3 Influenza Hemagglutinin Elicits Cross-Clade Neutralizing Antibodies Through Stalk-Targeted Blocking of Conformational Change During Membrane Fusion. *Immunol Lett* (2016) 172:11–20. doi: 10.1016/j.imlet.2016.02.006
19. Li J, Helal Z, Ladman B, Karch C, Gelb J, Burkhard P, et al. Nanoparticle Vaccine for Avian Influenza Virus: A Challenge Study Against Highly Pathogenic H5N2 Subtype. *J Virol Antivir Res* (2018) 7:1. doi: 10.4172/2324-8955.1000179
20. Elaish M, Ngunjiri JM, Ali A, Xia M, Ibrahim M, Jang H, et al. Supplementation of Inactivated Influenza Vaccine With Norovirus P Particle-M2e Chimeric Vaccine Enhances Protection Against Heterologous Virus Challenge in Chickens. *PloS One* (2017) 12:e0171174. doi: 10.1371/journal.pone.0171174
21. Elaish M, Kang KI, Xia M, Ali A, Shany SA, Wang L, et al. Immunogenicity and Protective Efficacy of the Norovirus P Particle-M2e Chimeric Vaccine in Chickens. *Vaccine* (2015) 33:4901–9. doi: 10.1016/j.vaccine.2015.07.049
22. Hoft DF, Lottenbach KR, Blazevic A, Turan A, Blevins TP, Pacatte TP, et al. Comparisons of the Humoral and Cellular Immune Responses Induced by Live Attenuated Influenza Vaccine and Inactivated Influenza Vaccine in Adults. *Clin Vaccine Immunol* (2017) 24:e00414–16. doi: 10.1128/CVI.00414-16
23. Zens KD, Chen JK, Farber DL. Vaccine-Generated Lung Tissue-Resident Memory T Cells Provide Heterosubtypic Protection to Influenza Infection. *JCI Insight* (2016) 1:e85832. doi: 10.1172/jci.insight.85832
24. Wang T, Wei F, Liu J. Emerging Role of Mucosal Vaccine in Preventing Infection With Avian Influenza A Viruses. *Viruses* (2020) 12:862. doi: 10.3390/v12080862
25. Blanco-Lobo P, Nogales A, Rodriguez L, Martinez-Sobrido L. Novel Approaches for the Development of Live Attenuated Influenza Vaccines. *Viruses* (2019) 11:190. doi: 10.3390/v11020190
26. Sarawar S, Hatta Y, Watanabe S, Dias P, Neumann G, Kawaoka Y, et al. M2SR, a Novel Live Single Replication Influenza Virus Vaccine, Provides Effective Heterosubtypic Protection in Mice. *Vaccine* (2016) 34:5090–8. doi: 10.1016/j.vaccine.2016.08.061
27. Jang YH, Seong BL. Immune Responses Elicited by Live Attenuated Influenza Vaccines as Correlates of Universal Protection Against Influenza Viruses. *Vaccines (Basel)* (2021) 9:353. doi: 10.3390/vaccines9040353
28. Herve PL, Raliou M, Bourdieu C, Dubuquoy C, Petit-Camurdan A, Bertho N, et al. A Novel Subnucleocapsid Nanoplatform for Mucosal Vaccination Against Influenza Virus That Targets the Ectodomain of Matrix Protein 2. *J Virol* (2014) 88:325–38. doi: 10.1128/JVI.01141-13
29. Gauthier L, Babych M, Segura M, Bourgault S , Archambault D. Identification of a Novel TLR5 Agonist Derived From the P97 Protein of *Mycoplasma Hyopneumoniae*. *Immunobiol* (2020) 225:151962. doi: 10.1016/j.imbio.2020.151962
30. Roques E, Girard A, Gagnon CA, Archambault D. Antibody Responses Induced in Mice Immunized With Recombinant Adenovectors Expressing Chimeric Proteins of Various Porcine Pathogens. *Vaccine* (2013) 31:2698–704. doi: 10.1016/j.vaccine.2013.03.068

31. Tran TL, Castagne N, Bhella D, Varela PF, Bernard J, Chilmonczyk S, et al. The Nine C-Terminal Amino Acids of the Respiratory Syncytial Virus Protein P Are Necessary and Sufficient for Binding to Ribonucleoprotein Complexes in Which Six Ribonucleotides Are Contacted Per N Protein Protomer. *J Gen Virol* (2007) 88:196–206. doi: 10.1099/vir.0.82282-0
32. Castagne N, Barbier A, Bernard J, Rezaei H, Huet JC, Henry C, et al. Biochemical Characterization of the Respiratory Syncytial Virus P-P and P-N Protein Complexes and Localization of the P Protein Oligomerization Domain. *J Gen Virol* (2004) 85:1643–53. doi: 10.1099/vir.0.79830-0
33. Ganapathy K, Cargill PW. Jones RC. A Comparison of Methods of Inducing Lachrymation and Tear Collection in Chickens for Detection of Virus-Specific Immuoglobulins After Infection With Infectious Bronchitis Virus. *Avian Pathol* (2005) 34:248–51. doi: 10.1080/03079450500112344
34. Calzas C, Goyette-Desjardins G, Lemire P, Gagnon F, Lachance C, Van Calsteren MR, et al. Group B *Streptococcus* and *Streptococcus Suis* Capsular Polysaccharides Induce Chemokine Production by Dendritic Cells *via* Toll-Like Receptor 2- and MyD88-Dependent and -Independent Pathways. *Infect Immun* (2013) 81:3106–18. doi: 10.1128/IAI.00113-13
35. Le Goffic R, Bouguyon E, Chevalier C, Vidic J, Da Costa B, Leymarie O, et al. Influenza A Virus Protein PB1-F2 Exacerbates IFN-Beta Expression of Human Respiratory Epithelial Cells. *J Immunol* (2010) 185:4812–23. doi: 10.4049/jimmunol.0903952
36. Tawar RG, Duquerroy S, Vonrhein C, Varela PF, Damier-Piolle L, Castagne N, et al. Crystal Structure of a Nucleocapsid-Like Nucleoprotein-RNA Complex of Respiratory Syncytial Virus. *Science* (2009) 326:1279–83. doi: 10.1126/science.1177634
37. Murakami M, Kamimura D, Hirano T. Pleiotropy and Specificity: Insights From the Interleukin 6 Family of Cytokines. *Immunity* (2019) 50:812–31. doi: 10.1016/j.immuni.2019.03.027
38. Riffault S, Meyer G, Deplanche M, Dubuquoy C, Durand G, Soulestin M, et al. A New Subunit Vaccine Based on Nucleoprotein Nanoparticles Confers Partial Clinical and Virological Protection in Calves Against Bovine Respiratory Syncytial Virus. *Vaccine* (2010) 28:3722–34. doi: 10.1016/j.vaccine.2010.03.008
39. Roux X, Dubuquoy C, Durand G, Tran-Tolla TL, Castagne N, Bernard J, et al. Sub-Nucleocapsid Nanoparticles: A Nasal Vaccine Against Respiratory Syncytial Virus. *PloS One* (2008) 3:e1766. doi: 10.1371/journal.pone.0001766
40. Lee YN, Lee YT, Kim MC, Hwang HS, Lee JS, Kim KH, et al. Fc Receptor Is Not Required for Inducing Antibodies But Plays a Critical Role in Conferring Protection After Influenza M2 Vaccination. *Immunology* (2014) 143:300–9. doi: 10.1111/imm.12310
41. Neirynck S, Deroo T, Saelens X, Vanlandschoot P, Jou WM, Fiers W. A Universal Influenza A Vaccine Based on the Extracellular Domain of the M2 Protein. *Nat Med* (1999) 5:1157–63. doi: 10.1038/13484
42. Gong X, Yin H, Shi Y, He X, Yu Y, Guan S, et al. Evaluation of the Immunogenicity and Protective Effects of a Trivalent Chimeric Norovirus P Particle Immunogen Displaying Influenza HA2 From Subtypes H1, H3 and B. *Emerg Microbes Infect* (2016) 5:e51. doi: 10.1038/emi.2016.51
43. Mallajosyula VV, Citron M, Lu X, Meulen JT, Varadarajan R, Liang X. *In Vitro* and *In Vivo* Characterization of Designed Immunogens Derived From the CD-Helix of the Stem of Influenza Hemagglutinin. *Proteins* (2013) 81:1759–75. doi: 10.1002/prot.24317
44. Tomcikova K, Vareckova E. Different Mechanisms of the Protection Against Influenza A Infection Mediated by Broadly Reactive HA2-Specific Antibodies. *Acta Virol* (2019) 63:347–65. doi: 10.4149/av_2019_408
45. Mozdzanowska K, Zharikova D, Cudic M, Otvos L, Gerhard W. Roles of Adjuvant and Route of Vaccination in Antibody Response and Protection Engendered by a Synthetic Matrix Protein 2-Based Influenza A Virus Vaccine in the Mouse. *Virol J* (2007) 4:118. doi: 10.1186/1743-422X-4-118
46. El Bakkouri K, Descamps F, De Filette M, Smet A, Festjens E, Birkett A, et al. Universal Vaccine Based on Ectodomain of Matrix Protein 2 of Influenza A: Fc Receptors and Alveolar Macrophages Mediate Protection. *J Immunol* (2011) 186:1022–31. doi: 10.4049/jimmunol.0902147
47. Brown DM, Lee S, Garcia-Hernandez Mde L, Swain SL. Multifunctional CD4 Cells Expressing Gamma Interferon and Perforin Mediate Protection Against Lethal Influenza Virus Infection. *J Virol* (2012) 86:6792–803. doi: 10.1128/JVI.07172-11
48. McKinstry KK, Strutt TM, Buck A, Curtis JD, Dibble JP, Huston G, et al. IL-10 Deficiency Unleashes an Influenza-Specific Th17 Response and Enhances Survival Against High-Dose Challenge. *J Immunol* (2009) 182:7353–63. doi: 10.4049/jimmunol.0900657
49. Cerwenka A, Morgan TM, Harmsen AG, Dutton RW. Migration Kinetics and Final Destination of Type 1 and Type 2 CD8 Effector Cells Predict Protection Against Pulmonary Virus Infection. *J Exp Med* (1999) 189:423–34. doi: 10.1084/jem.189.2.423
50. Hamada H, Garcia-Hernandez Mde L, Reome JB, Misra SK, Strutt TM, McKinstry KK, et al. Tc17, a Unique Subset of CD8 T Cells That Can Protect Against Lethal Influenza Challenge. *J Immunol* (2009) 182:3469–81. doi: 10.4049/jimmunol.0801814
51. Jansen JM, Gerlach T, Elbahesh H, Rimmelzwaan GF, Saletti G. Influenza Virus-Specific CD4+ and CD8+ T Cell-Mediated Immunity Induced by Infection and Vaccination. *J Clin Virol* (2019) 119:44–52. doi: 10.1016/j.jcv.2019.08.009
52. Gianfrani C, Oseroff C, Sidney J, Chesnut RW, Sette A. Human Memory CTL Response Specific for Influenza A Virus Is Broad and Multispecific. *Hum Immunol* (2000) 61:438–52. doi: 10.1016/s0198-8859(00)00105-1
53. Jameson J, Cruz J, Ennis FA. Human Cytotoxic T-Lymphocyte Repertoire to Influenza A Viruses. *J Virol* (1998) 72:8682–9. doi: 10.1128/JVI.72.11.8682-8689.1998
54. Eliasson DG, Omokanye A, Schon K, Wenzel UA, Bernasconi V, Bemark M, et al. M2e-Tetramer-Specific Memory CD4 T Cells Are Broadly Protective Against Influenza Infection. *Mucosal Immunol* (2018) 11:273–89. doi: 10.1038/mi.2017.14
55. Stanekova Z, Adkins I, Kosova M, Janulikova J, Sebo P, Vareckova E. Heterosubtypic Protection Against Influenza A Induced by Adenylate Cyclase Toxoids Delivering Conserved HA2 Subunit of Hemagglutinin. *Antiviral Res* (2013) 97:24–35. doi: 10.1016/j.antiviral.2012.09.008
56. Stepanova LA, Kotlyarov RY, Kovaleva AA, Potapchuk MV, Korotkov AV, Sergeeva MV, et al. Protection Against Multiple Influenza A Virus Strains Induced by Candidate Recombinant Vaccine Based on Heterologous M2e Peptides Linked to Flagellin. *PloS One* (2015) 10:e0119520. doi: 10.1371/journal.pone.0119520
57. Lee YN, Kim MC, Lee YT, Hwang HS, Cho MK, Lee JS, et al. AS04-Adjuvanted Virus-Like Particles Containing Multiple M2 Extracellular Domains of Influenza Virus Confer Improved Protection. *Vaccine* (2014) 32:4578–85. doi: 10.1016/j.vaccine.2014.06.040
58. Stepanova LA, Mardanova ES, Shuklina MA, Blokhina EA, Kotlyarov RY, Potapchuk MV, et al. Flagellin-Fused Protein Targeting M2e and HA2 Induces Potent Humoral and T-Cell Responses and Protects Mice Against Various Influenza Viruses A Subtypes. *J BioMed Sci* (2018) 25:33. doi: 10.1186/s12929-018-0433-5
59. De Filette M, Ramne A, Birkett A, Lycke N, Lowenadler B, Min Jou W, et al. The Universal Influenza Vaccine M2e-HBc Administered Intranasally in Combination With the Adjuvant CTA1-DD Provides Complete Protection. *Vaccine* (2006) 24:544–51. doi: 10.1016/j.vaccine.2005.08.061
60. Zheng D, Chen S, Qu D, Chen J, Wang F, Zhang R, et al. Influenza H7N9 LAH-HBc Virus-Like Particle Vaccine With Adjuvant Protects Mice Against Homologous and Heterologous Influenza Viruses. *Vaccine* (2016) 34:6464–71. doi: 10.1016/j.vaccine.2016.11.026
61. Qi M, Zhang XE, Sun X, Zhang X, Yao Y, Liu S, et al. Intranasal Nanovaccine Confers Homo- and Hetero-Subtypic Influenza Protection. *Small* (2018) 14:e1703207. doi: 10.1002/smll.201703207
62. Mullarkey CE, Bailey MJ, Golubeva DA, Tan GS, Nachbagauer R, He W, et al. Broadly Neutralizing Hemagglutinin Stalk-Specific Antibodies Induce Potent Phagocytosis of Immune Complexes by Neutrophils in an Fc-Dependent Manner. *mBio* (2016) 7:e01624–16. doi: 10.1128/mBio.01624-16
63. Ni Y, Guo J, Turner D, Tizard I. Development of a Novel Dual-Domain Nanoparticle Antigen Construct for Universal Influenza Vaccine. *Vaccine* (2017) 35:7026–32. doi: 10.1016/j.vaccine.2017.10.051
64. Tsybalova LM, Stepanova LA, Shuklina MA, Mardanova ES, Kotlyarov RY, Potapchuk MV, et al. Combination of M2e Peptide With Stalk HA Epitopes of Influenza A Virus Enhances Protective Properties of Recombinant Vaccine. *PloS One* (2018) 13:e0201429. doi: 10.1371/journal.pone.0201429
65. Deng L, Kim JR, Chang TZ, Zhang H, Mohan T, Champion JA, et al. Protein Nanoparticle Vaccine Based on Flagellin Carrier Fused to Influenza Conserved Epitopes Confers Full Protection Against Influenza A Virus Challenge. *Virology* (2017) 509:82–9. doi: 10.1016/j.virol.2017.06.001

66. Babapoor S, Neef T, Mittelholzer C, Girshick T, Garmendia A, Shang H, et al. A Novel Vaccine Using Nanoparticle Platform to Present Immunogenic M2e Against Avian Influenza Infection. *Influenza Res Treat* (2011) 2011:126794. doi: 10.1155/2011/126794
67. Dabaghian M, Latify AM, Tebianian M, Nili H, Ranjbar AR, Mirjalili A, et al. Vaccination With Recombinant 4 X M2e.HSP70c Fusion Protein as a Universal Vaccine Candidate Enhances Both Humoral and Cell-Mediated Immune Responses and Decreases Viral Shedding Against Experimental Challenge of H9N2 Influenza in Chickens. *Vet Microbiol* (2014) 174:116–26. doi: 10.1016/j.vetmic.2014.09.009
68. Kim JH, Hajam IA, Lee JH. Oral Immunization With a Novel Attenuated *Salmonella Typhimurium* Encoding Influenza HA, M2e and NA Antigens Protects Chickens Against H7N9 Infection. *Vet Res* (2018) 49:12. doi: 10.1186/s13567-018-0509-y
69. Zhang X, Liu M, Liu C, Du J, Shi W, Sun E, et al. Vaccination With Different M2e Epitope Densities Confers Partial Protection Against H5N1 Influenza A Virus Challenge in Chickens. *Intervirology* (2011) 54:290–9. doi: 10.1159/000319440
70. Reese KA, Lupfer C, Johnson RC, Mitev GM, Mullen VM, Geller BL, et al. A Novel Lactococcal Vaccine Expressing a Peptide From the M2 Antigen of H5N2 Highly Pathogenic Avian Influenza A Virus Prolongs Survival of Vaccinated Chickens. *Vet Med Int* (2013) 2013:316926. doi: 10.1155/2013/316926
71. Layton SL, Kapczynski DR, Higgins S, Higgins J, Wolfenden AD, Liljebjelke KA, et al. Vaccination of Chickens With Recombinant Salmonella Expressing M2e and CD154 Epitopes Increases Protection and Decreases Viral Shedding After Low Pathogenic Avian Influenza Challenge. *Poult Sci* (2009) 88:2244–52. doi: 10.3382/ps.2009-00251
72. Zhang Z, Zhang J, Zhang J, Li Q, Miao P, Liu J, et al. Coimmunization With Recombinant Epitope-Expressing Baculovirus Enhances Protective Effects of Inactivated H5N1 Vaccine Against Heterologous Virus. *Vet Microbiol* (2017) 203:143–8. doi: 10.1016/j.vetmic.2017.03.004

Conflict of Interest: The authors declare that the research was conducted in the absence of any commercial or financial relationships that could be construed as a potential conflict of interest.

frontiers in Immunology

ORIGINAL RESEARCH
published: 13 January 2022
doi: 10.3389/fimmu.2021.768144

HPV-16 E7-Specific Cellular Immune Response in Women With Cervical Intraepithelial Lesion Contributes to Viral Clearance: A Cross-Sectional and Longitudinal Clinical Study

Lina Zhang[1], Xinyi Shi[2], Qing Zhang[2], Zhilei Mao[1], Xiaoyu Shi[1], Jun Zhou[1], Aili Jian[2,3], Renying Zhu[2], Shisong Jiang[4] and Wenshu Lu[2,4,5]**

[1] Center for Diagnosis and Treatment of Cervical Diseases, Changzhou Maternal and Child Health Care Hospital, Nanjing Medical University, Changzhou, China, [2] R & D Department, Oxford Vacmedix (Changzhou) Co. Ltd., Changzhou, China, [3] Department of Microbiology and Immunology, School of Basic Medicine, Dali University, Dali, China, [4] Department of Oncology, University of Oxford, Oxford, United Kingdom, [5] R & D Department, Shanghai Jia Wen (JW) Inflinhix Co. Ltd., Shanghai, China

OPEN ACCESS

Edited by:
Cornelis Joseph Melief, Leiden University, Netherlands

Reviewed by:
Osaretin Emmanuel Asowata, Population Council, United States
Duo Xu, University of California, Riverside, United States

***Correspondence:**
Shisong Jiang
shisong.jiang@oncology.ox.ac.uk
Wenshu Lu
wenshu.lu@oncology.ox.ac.uk

Specialty section:
This article was submitted to Vaccines and Molecular Therapeutics, a section of the journal Frontiers in Immunology

Received: *31 August 2021*
Accepted: *17 December 2021*
Published: *13 January 2022*

Citation:
Zhang L, Shi X, Zhang Q, Mao Z, Shi X, Zhou J, Jian A, Zhu R, Jiang S and Lu W (2022) HPV-16 E7-Specific Cellular Immune Response in Women With Cervical Intraepithelial Lesion Contributes to Viral Clearance: A Cross-Sectional and Longitudinal Clinical Study. Front. Immunol. 12:768144. doi: 10.3389/fimmu.2021.768144

High-risk human papillomavirus (HPV) infection is the cause of almost all cervical cancers. HPV16 is one of the main risk subtypes. Although screening programs have greatly reduced the prevalence of cervical cancer in developed countries, current diagnostic tests cannot predict if mild lesions may progress into invasive lesions or not. In the current cross-sectional and longitudinal clinical study, we found that the HPV16 E7-specific T cell response in peripheral blood mononuclear cells of HPV16-infected patients is related to HPV16 clearance. It contributes to protecting the squamous interaepithelial lesion (SIL) from further malignant development. Of the HPV16 infected women enrolled (n = 131), 42 had neither intraepithelial lesion nor malignancy (NILM), 33 had low-grade SIL, 39 had high-grade SIL, and 17 had cervical cancer. Only one of 17 (5.9%) cancer patients had a positive HPV16 E7-specific T cell response, dramatically lower than the groups of precancer patients. After one year of follow-up, most women (28/33, 84.8%) with persistent HPV infection did not exhibit a HPV16 E7-specific T cell response. Furthermore, 3 malignantly progressed women, one progressed to high-grade SIL and two progressed to low-grade SIL, were negative to the HPV16 E7-specific T cell response. None of the patients with a positive HPV16 E7-specific T cell response progressed to further deterioration. Our observation suggests that HPV16 E7-specific T cell immunity is significant in viral clearance and contributes in protection against progression to malignancy.

Keywords: recombinant overlapping peptide, human papillomavirus, cervical intraepithelial neoplasia, immune responses, cervical cancer

INTRODUCTION

Cervical cancer is a malignant tumor that seriously threatens the life and health of women. Globally, approximately 500,000 women are diagnosed with cervical cancer every year and of these 280,000 women die from cervical cancer (1). It is an accepted fact that high-risk human papillomavirus (HR-HPV) infection is the main risk factor for the occurrence, persistence, and development of cervical cancer (2). For disease control, hybrid capture 2 (HC-2) or HPV-DNA typing combined with cytology examination are the diagnostic methods used to detect cervical cancer (3). However, these methods cannot distinguish invasive lesions from noninvasive lesions, nor do they provide any prognostic value for patients. In fact, only about 1% of women infected with HR-HPV will gradually develop cervical cancer (4, 5). HPV infection in most women is only temporary or does not lead to cervical cancer even if HPV persists. Currently once HPV-infected lesions have been diagnosed, patients are often over treated with unnecessary medical procedures including surgical interventions (1). To avoid over treatment, it is important to understand the mechanisms of viral clearance followed by developing practical methods to monitor the process. If the viral clearance mechanism exists, it may not be urgent for HPV-infected women to undergo surgery.

HPV-related carcinogenesis is not a uniform process. The "integration" of the virus into the host cell increases gene instability, marking the beginning of malignant transformation (2). It takes approximately 10 years from HR-HPV infection to develop cervical carcinogenesis (6). HPV infection triggers a series of immune responses, namely, innate and adaptive immune responses. Consequently, the occurrence of cervical cancer is the result of the struggle between foreign HPV infection and self-immunological defense (4). In most circumstances, the body's own immune function will resolve the infection, prevent further viral invasion and pathogenesis, eliminate damaged or aging cells, and address abnormal transformed cells in the body. However, when the immune surveillance function of the body is compromised or dysfunctional, it will result in a decrease in the ability to eradicate abnormal transformed cells. This will lead to high-level lesions and perhaps the occurrence of a malignant tumor (4, 7).

Among all high-risk HPVs, more than half of cervical cancer patients around the world are infected with HPV16 (8). The responses of cytotoxic lymphocytes (CTL) to E6/E7 appeared to be important in the prevention of squamous interaepithelial lesions (SILs) (9, 10). Strict conservation of HPV16 E7 is critical for HPV16 carcinogenesis (11). Therefore, effectively detecting an HPV16 E7-specific immune response may act as an immune control mechanism to prevent persistent HPV infection and to predict the progress of the disease. Thus, immune function, especially T cell-based immunity, is at least one of the key factors that are relevant to the prognosis of HPV infection and its malignancy. However, there is no commercially available test for monitoring T cell immunity.

In this study, we used the recombinant overlapping peptide protein of HPV16 E7 (ROP-HPV16 E7) and the E7 overlapping polypeptides as stimulants in the Enzyme-linked immunospot (ELISPOT) assay to evaluate the HPV16E7 specific-T lymphocyte response in peripheral blood mononuclear cells (PBMCs) of patients. The results showed that the low HPV16 specific T cell response in peripheral blood was significantly correlated with persistent viral infection. Our study suggests that the HPV16-specific T cell response in peripheral blood can effectively predict clinical outcome.

RESULTS

Effective Detection of HPV16-Specific T Lymphocytes in the Peripheral Blood

In our previous study, ROP-HPV16E7 effectively stimulated the HPV16 E7-specific T cell response in mice immunized with the HPV protein (12). In this study, using patient PBMCs infected with HPV16, we compared the ability of ROP-16 E7 with a pool of HPV16 E7 overlapping peptides to simulate the specific T cell response against HPV16 E7. ROP-16E7 stimulation mimicked that of pooled HPV16 E7 peptides to effectively stimulate HPV16 E7-specific T cells in patients infected with HPV16 (**Figure 1**). No significant difference was found between ROP-16 E7 and HPV16 E7 pooled peptides. Therefore, ROP-16E7, a recombinant protein that can be easily and abundantly expressed and purified from *E. coli*, is able to replace the costly, and difficult to manufacture, quality-controlled pool of HPV16 E7 peptides, in the interferon-γ release assay (IGRA).

Recruitment of Patients and Their HPV16 E7-Specific T Lymphocyte Response at Study Entry

A total of 131 female patients with HPV16 (type 16) infection was recruited for the study. At the time of enrollment, the IGRA-based HPV16 E7-specific T cell response of PBMCs was assessed

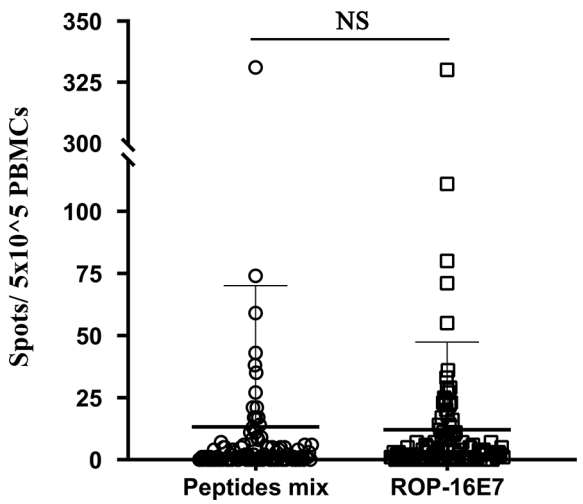

FIGURE 1 | IFN-γ release assay of patient-derived PBMC cultures that recognize HPV16-specific peptide pools (peptides mix) and ROP-16 E7. NS, no significance.

and cervical biopsy diagnosis was performed. There were 42 patients without intraepithelial lesions or malignant lesions (NILM), 33 patients with low-grade SIL (LSIL), 39 patients with high-grade SIL (HSIL), and 17 patients with cervical cancer (**Table 1**). Patients in the NILM, LSIL, and HSIL groups were followed for a period of 12 months. Their HPV genotyping results and clinical histological results were also collected at study entry and at the end of the study.

We first performed an HPV type16 E7 ROP-based IGRA to assess the status of HPV-related T cell immunity. In the NILM group, 11 patients (26.2%) tested positive for HPV16 E7-specific T cell response and 31 patients (73.8%) had a negative response. In the LSIL group, 14 patients (42.4%) tested positive and 19 patients (57.6%) tested negative for the HPV16-specific T cell response. In the HSIL group, 15 patients (38.5%) were positive and 24 (61.5%) negative for the HPV16 E7 T cell response. All HSIL patients underwent surgery to remove the local pathological lesions. Of the 17 cervical cancer patients, only 1 (5.9%) patient showed a positive HPV16 E7-specific T cell response, and 16 (94.1%) patients presented a negative response (**Table 2**).

The Low HPV16-Specific T Cell Response in Peripheral Blood is Relevant to the Persistence of HPV Infection

To determine whether the HPV or HPV peptide-specific T cell response was relevant to the clearance of the persistent HPV infection in different pathogenetic groups, at the end of the one-year follow-up period, HPV genotyping was performed on cervical exfoliated cell samples. In the NILM group, only 2 of 11 patients (18.2%) with a positive HPV16 E7-specific T cell response at the start of the study sustained HPV16 infection. However, 11 of 31 patients (35.5%) who were negative for the HPV16 ROP-specific T cell response harbored a persistent infection. The persistent infection rate was 1.95 times higher than that of patients with positive responses (P = 0.005). In the LSIL group, 2 of 14 patients (14.3%) with a positive HPV16 ROP-specific T cell response sustained a HPV16 infection, while 12 of 19 patients (63.2%) with a negative HPV16-specific T cell response were persistently infected. The persistent infection rate was 4.42 times higher than that of patients with positive response (P <0.0001). In the HSIL group, 39 patients with HPV16 virus infection and high lesions were diagnosed at the time of enrollment, and all these patients underwent surgery. After one year, only 1 of 15 patients (6.7%) with a positive HPV16 specific T cell response sustained HPV16 infection, but 8 of 24 patients (33.3%) with a negative T cell response sustained HPV16 infection. The persistent infection rate was 4.97 times higher than in patients with positive HPV16-specific T cell response (P <0.0001) (**Table 3**). Therefore, the low HPV16 specific T cell response is highly correlated with the persistence of HPV16 infection.

TABLE 1 | Clinical characteristics of enrolled patients at study entry (n = 134).

Characteristic	N
Median age	41
Age range	23–67
Pathological diagnosis of HPV infected	
NILM	42 (31.3%)
LSIL	33 (24.6%)
HSIL	39 (29.1%)
Cancer	17 (12.7%)
HPV status	
HPV 16 positive	131
HPV negative	3

NILM, negative for intraepithelial lesion or malignancy; LSIL, low-grade squamous intraepithelial lesion; HSIL, high-grade squamous intraepithelial lesion; HPV, human papilloma virus.

The HPV16 E7 ROP-Specific T Cell Response is Associated With Histological Regression

To study the influence of the T-cell immunity response on HPV pathogenesis, at the end of this study, a cervical biopsy was performed. The results showed that in all three groups (NILM, LSIL, HSIL), none of the patients with positive specific T cell response against HPV16 E7 presented any further disease deterioration (**Table 4**). Specifically, in the NILM group, 25.8% of patients with negative T cell response retained the same lesion features by pathohistological examination, which was 1.42-fold higher than that of patients who were T cell positive (18.2%) against HPV ROP. The histological regression rate among patients with positive T cells for HPV16 E7 ROP was 81.7%, which was 1.26-fold higher than that of the negative T cell response (64.5%). Three of 31 patients (9.7%) with negative specific T cell response against HPV16 E7 ROP progressed pathologically (P = 0.001); the histological results are shown in **Figure 2**. Among the patients in the LSIL group (n = 33), 31.6% of patients with a negative T cell response to HPV16 E7 ROP maintained the same lesion characteristics on pathohistological examination, which was 2.21-fold higher than that of patients with a positive T cell response (14.3%). The regression rate in T cell negative patients (68.4%) was less (0.8-fold) than those with a positive T cell response (85.7%) (P = 0.002). In the HSIL group (n = 39), at the end of the 12-month study, the 15 patients with positive specific T cell response against HPV16 E7 ROP are in stable condition without histologically observed recurrence (100% regressed); although 1 of the 24 patients with a negative response experienced disease recurrence (P = 0.043) (**Table 4**). Of note, all patients in the HSIL group received surgery before the study had started. This could have contributed to the higher regression rate in this group.

The HPV16 E7 ROP-Specific T Cell Response is Relevant for the Clinical Outcome

A total of 114 women completed the 12-month study. At the beginning of their hospital visit, all were positive for HPV16 infection by PCR test. Forty patients (35.1%) were positive for the HPV16 E7 ROP-specific T cell response. The remaining 74 patients (64.9%) were negative for the T cell response (**Table 5**). At the most recent follow-up visit, 78 of 114 patients (68.4%) had cleared the HPV16 infection, 3 patients (2.6%) had persistent HPV16 infection and progressed histologically, the remaining 33 patients (28.9%) had persistent HPV16 infection. All 3 progressed patients were negative for the HPV16 E7 ROP-specific T cell

TABLE 2 | Results of HPV16 E7-specific T lymphocyte response at study entry.

Pathological diagnosis	T+	T–
NILM (n = 42)	11 (26.2%)	31 (73.8%)
LSIL (n = 33)	14 (42.4%)	19 (57.6%)
HSIL (n = 39)	15 (38.5%)	24 (61.5%)
Cancer (n = 17)	1 (5.9%)	16 (94.1%)

T+, positive HPV16 E7-specific T lymphocyte response;
T–, negative HPV16 E7-specific T lymphocyte response.

response. Only 5/33 (15.2%) HPV16 persistently infected patients had a positive HPV16 E7 specific T cell response, while 28/33 (84.8%) had a negative response. Among patients who were positive for the HPV16 E7 ROP-specific T cell response (n = 40), 87.5% of the patients cleared HPV16 infection, 12.5% had persistent infection and none of them progressed after 12 months. While in patients with a negative HPV16 E7 ROP-specific T cell response (n = 74), 43 of 74 (58.1%) patients had cleared HPV16 infection, 31 of 74 (41.9%) persistently infected, and 3 of persistently infected patients histologically progressed (**Table 5**).

We also performed flow cytometry using PBMCs of 32 patients and 3 non-infected controls, detecting the proportion of $CD8^+$ T cells, $CD4^+$ T cells, $CD4^+$:$CD8^+$ ratio, $CD8^+$ T cells expressing PD-1 and regulatory T cells expressing Foxp3. The results showed no correlation with prognosis (**Figure 3**). The detailed gating information of flow cytometry data can be found in **Supplementary Figures 1** and **2**.

DISCUSSION

The purpose of this study was to evaluate the role of HPV specific T cell immunity in the clinical outcome of HPV infected patients. We used ROP-HPV E7, LRMK-linked overlapping peptides covering the HPV E7 sequence (12) as the antigenic agent to test the specific T cell activity of the patient. This study evaluated cellular immunity specific to HPV16 E7 in 131 women with HPV16 infection. Only one of 17 (5.9%) patients with cervical cancer had a positive HPV16 E7-specific T cell response, dramatically lower than the precancer patient groups (26.5% in NILM, 42.4% in LSIL, and 38.5% in HSIL). Our data are consistent with others who have shown that immunosuppressed humans or animals have increased risks of HPV infection and associated dysplasia (13, 14), suggesting that immune reactivity is associated with virus elimination and disease clearance.

The progression from HPV infection to malignant tumor requires viral escape from host immunity (15). With a properly functioning immune system, up to 80–90% of HPV infection was cleared in two years (16). This has raised a dilemma in the management of HPV infection, that is, whether costly, complicated, and invasive medical surgical intervention should be provided to an HPV infected patient once diagnosed as HPV-positive, or should this wait until the cancer is developed? A valid prognostic method is an unmet need and will be helpful for clinicians and patients for clinical decision-making. Most current clinically available diagnostic methods focus on either detecting the presence of virus by PCR or detecting tumor presence by histological examination. There is no good prognosis method available to monitor HPV-associated human immune responses. Consequently, patients may either undergo unnecessary surgery if the decision is made based only on PCR findings or patients may receive intervention when it is too late to achieve effective treatment. Unfortunately, in many cases no action has been taken because clinicians take for granted that most HPV infections resolved automatically. Our results support that the monitoring of T cell-based immunity may be a suitable approach for prognostic purposes. The results of this pilot study suggest that if good T cell immunity is detected, then it is likely that HPV infection will be cleared. In the absence of T cell immunity, interventions should be taken to stop the malignant progression.

The WHO proposes 3 tiers of management for HPV related diseases. Tier 1: prophylactic vaccines for individuals without HPV infection; Tier 2: therapy for HPV-infected individuals who have not progressed to malignancy; Tier 3: therapies for HPV-infected individuals who have progressed to a late malignant stage. The findings from this study are relevant to the development of T cell-based therapeutic vaccines for Tier 2 and 3 therapies. Although prophylactic vaccines against HPV are available, these vaccines are not effective for those who have already been infected with HPV (17). The fact that T cell immunity is important for resolving HPV infection indicates that a T cell-based vaccine strategy will be feasible and beneficial to HPV-infected individuals having low immunity. Indeed, there are several promising clinical trials evaluating the role of enhanced T cell-based immunity (4). For example, synthetic long overlapping peptides (SLP) derived from HPV E6 and E7 are in a Phase II clinical trial in HPV-infected high-grade vulvar intraepithelial neoplasia have shown an 80% partial effect response and 47% complete regression (18). The combination of SLP with anti-PD-1 antibody has shown a achieve of a

TABLE 3 | Results of HPV test from women with HPV16 E7-specific T lymphocyte response at study entry and exit.

		Entry		Exit		P-Value
		HPV positive	HPV negative	HPV positive	HPV negative	
NILM (n = 42)	T+	11 (26.2%)	0	2 (18.2%)	9 (81.8%)	0.005
	T–	31 (73.8%)	0	11 (35.5%)	20 (64.5%)	
LSIL (n = 33)	T+	14 (42.4%)	0	2 (14.3%)	12 (85.7%)	<0.0001
	T–	19 (57.6%)	0	12 (63.2%)	7 (36.8%)	
HSIL (n = 39)	T+	15 (38.5%)	0	1 (6.7%)	14 (93.3%)	<0.0001
	T–	24 (61.5%)	0	8 (33.3%)	16 (66.7%)	

TABLE 4 | Results of cervical biopsy test from women with HPV16 E7-specific T lymphocyte response at study exit.

			Cervical biopsies			P-value
			Progressors	Persistors	Regressors	
NILM (n = 42)	T+	11 (26.2%)	0	2 (18.2%)	9 (81.7%)	0.001
	T–	31 (73.8%)	3 (9.7%)	8 (25.8%)	20 (64.5%)	
LSIL (n = 33)	T+	14 (42.4%)	0	2 (14.3%)	12 (85.7%)	0.002
	T–	19 (57.6%)	0	6 (31.6%)	13 (68.4%)	
HSIL (n = 39)	T+	15 (38.5%)	0	0	15 (100%)	0.043
	T–	24 (61.5%)	0	1 (4.2%)	23 (95.8%)	

The NILM, LSIL and HSIL cohorts were classified as Progressors, Persistors or Regressors after 1-year observation.

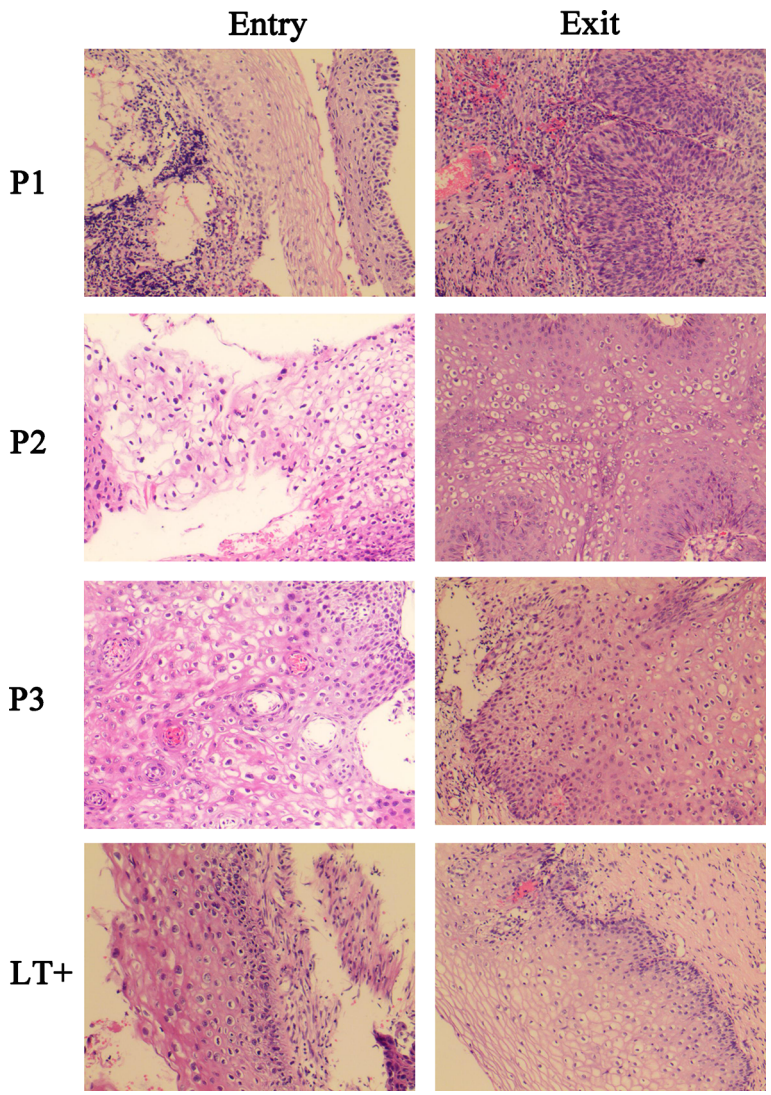

FIGURE 2 | Histological images of three progressed patients and a regressed representative patient. P1, P2, P3, were HPV16-infected patients in NILM cohorts at the study entry. At study exit, P1 progressed to HSIL, and P2, P3 progressed to LSIL. LT+, is a regressed representative of patients positive for the HPV16 E7 specific T lymphocyte response, who was LSIL at study entry and completely regressed at study exit.

TABLE 5 | Clinical outcomes of patients with HPV16 E7-specific T cell response.

Entry	Exit			P-value
HPV16 Positive (n = 114)	**Clearance (n = 78)**	**Persistence (n = 33)**	**Progression (n = 3)**	
T+ (n = 40, 35.1%)	35 (87.5%)	5 (12.5%)	0	<0.0001
T– (n = 74, 64.9%)	43 (58.1%)	28 (37.8%)	3 (4.1%)	

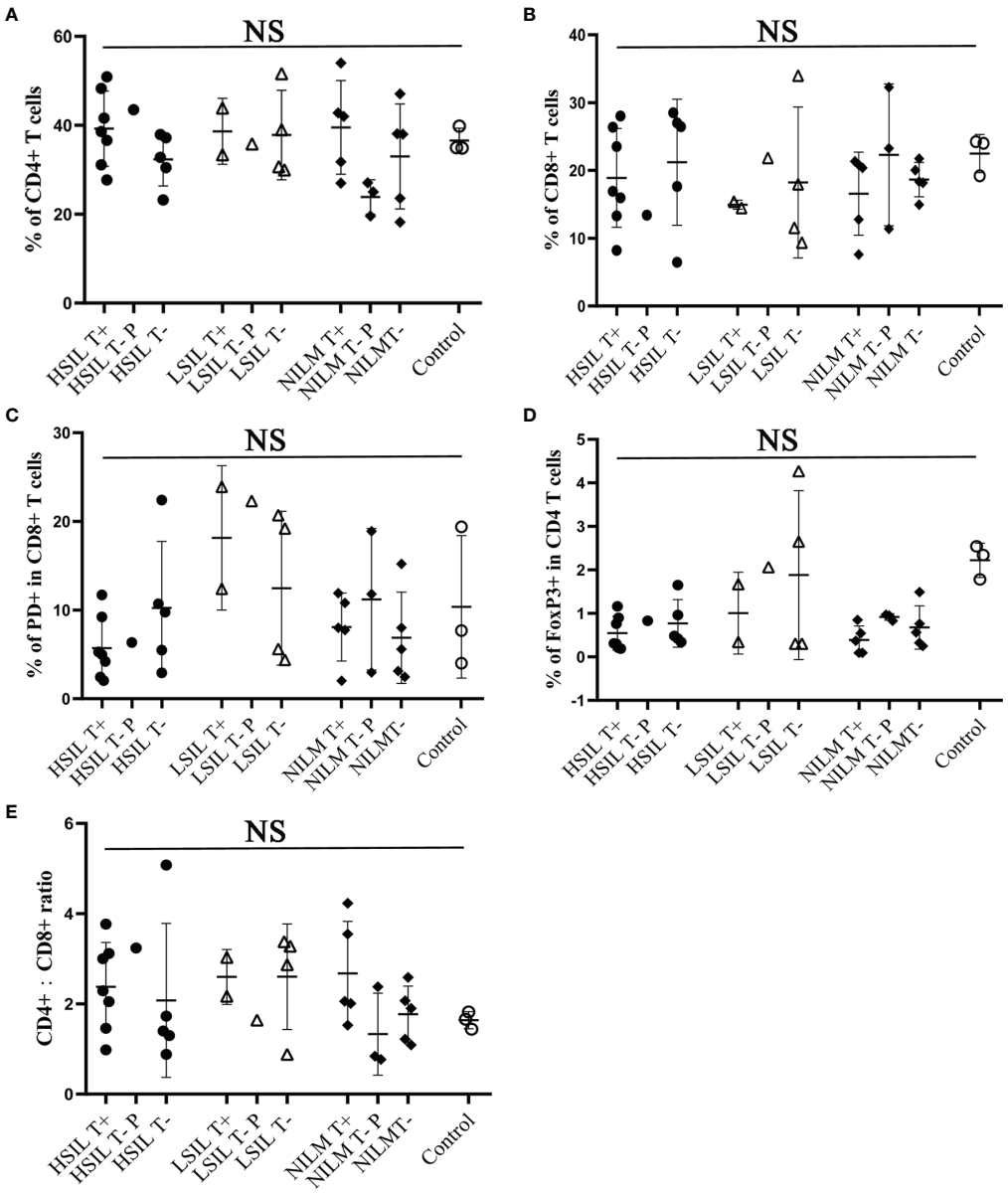

FIGURE 3 | Flow cytometric analysis of CD8, CD4, CD4/CD8 ratio, PD-1 and FoxP3 from peripheral blood $CD3^+$ T cells of HPV 16 infected cohorts. In total 32 patients were analyzed. **(A, B)** Frequency of CD8 or CD4 expression on $CD3^+$ T cells. **(C)** Frequency of PD-1 expression on $CD8^+/CD3^+$ T cells. **(D)** Frequency of FoxP3 expression on $CD4^+/CD3^+$ T cells. **(E)** CD4:CD8 ratio. T+, sample with positive HPV16-specific T cell response; T–, sample with negative HPV16-specific T cell response; P, persistent HPV16 infection; Control, samples from 3 women with no history of HPV16 infection. NS, no significance.

synergetic effect in incurable HPV 16-related cancer (19). Together with these promising trials, our data support the hypothesis that T-cell-based immunity plays an instrumental role in the containment of HPV infection.

METHODS

Patients

Women with HPV16 infection aged 23 to 67 years attending routine cervical cancer screening at the Changzhou Maternity and Child Health Care Hospital affiliated with Nanjing Medical University were asked to enroll in the study after giving their written informed consent. The study was approved by the Internal Review Board. Exclusion criteria were unwillingness or unavailability to follow up 12 months after recruitment. The patients enrolled were not pregnant and had no prior medical history of immune disorders. At the beginning of the study, a cervico-vaginal sample was collected from each participating subject for cytological testing and HPV DNA genotyping. Women positive for HPV 16 genotyping were recruited and referred for colposcopy and biopsy. Blood samples from enrolled patients were collected for the ELISPOT test. Patients would be recalled every 6 months. At the end of the study, 114 HPV 16 positively infected patients completed the 12-month follow-up study.

Histology

HPV16-positive patients were referred to colposcopy biopsy. Cervical or vaginal wall biopsy tissues were formalin-fixed, paraffin-embedded, and stored at room temperature. The tissue size was at least 3 mm for manual slicing with a rotary slicer. Serial sections were cut and stained with hematoxylin and eosin (HE). All images used in this study were acquired using an Olympus BX45 microscope equipped with 20× objective (Olympus, America). All histological sections were reviewed by a single histopathologist for the purpose of this study, who was blinded to other clinical information. The cases were classified as NILM, LSIL, HSIL, or cancer.

Mixed HPV16 E7 Peptides and ROP-HPV16 E7

Four synthetic overlapping peptides covering the entire sequence of the HPV16 E7 protein were synthesized (Ontores Biotech, China): Peptide 1, I R T L E D L L M G T L G I V C P I C S Q K P; peptide 2, M H G D T P T L H E Y M L D L Q P E T T D L Y C Y E Q L N D S S E E E; peptide 3, E Q L N D S S E E E D E I D G P A G Q A E P D R A H Y N I V T F C C K; and peptide 4, H Y N I V T F C C K C D S T L R L C V Q S T H V D I R T L E D L L M G.

The ROP-HPV16 E7 recombinant overlapping peptide is an artificial protein that contains E7 overlapping peptides linked to LRMK (a cathepsin S cleavage site). ROP-HPV16 E7 were expressed and purified as described elsewhere (12). Briefly, BL21 transformed with ROP-HPV16 E7 (DE3) was cultured in LB broth (50 μg/ml Kanamycin) overnight at 37°C and was then diluted with fresh LB broth and cultured until the OD600 reached 0.6. Cells were harvested 16 h after induction with IPTG (0.5 mM). Cell pellets were resuspended in lysis buffer (25 mM TrisHCl, 200 mM NaCl, 2% Triton X-100, 10 mM imidazole, pH8.0) and lysed by sonication. Soluble fractions were collected. The Ni-NTA resin was then added to the soluble fractions for 30 min, followed by washing with 30 resin volumes of lysis buffer and eluted with lysis buffer containing 200 mM imidazole. The eluted protein was dialyzed at 4°C in PBS buffer containing 10% glycerol.

Isolation of Human Peripheral Blood Mononuclear Cells

Heparin-treated human blood (10 ml) from patients was carefully added to the lymphocyte-separation medium (density = 1.077) and centrifuged at 1,500×*g* for 25 min. The PBMC layer was transferred to a new tube and was washed twice with RPMI 1640 medium.

Enzyme-Linked Immunospot Assay

The assays were performed using ELISPOT kits (Mabtech, Sweden). PBMCs (5×10^5 cells/well) were stimulated overnight with 2 μM ROP-HPV16 E7 or with mixed E7 peptides in anti-IFN-γ-Ab precoated plates (Millipore, Bedford, MA). Cells were discarded and biotinylated anti-IFNγ antibodies were added for 2 h at room temperature, followed by an additional 1 h incubation at room temperature with enzyme-labeled strepavidin. After the color developed, the reaction was stopped by washing the plates with tap water, and the plates were air dried. Spots were counted with an Elispot reader (Autoimmun Diagnostike, Strasburg, Germany).

Flow Cytometry Analysis

PBMCs were washed once with 1 ml ice-cold FACS buffer (2% FCS in PBS) and the cell density was adjusted to 1×10^6 cells/100 μl. APC-conjugated anti-human CD3 monoclonal antibody (BD, USA), FITC-conjugated anti-human CD8 (BD, USA), PE-conjugated anti-human CD279 monoclonal antibody (BD, USA) and FVS620 (BD, USA) were added and incubated in the dark for 15 min at room temperature. For FoxP3 staining, PBMCs were first stained with FITC-conjugated anti-Human CD4 monoclonal antibody (BD, USA), APC-conjugated anti-Human CD25 monoclonal antibody (BD, USA) and FVS620 (BD, USA) for 15 min in the dark at room temperature. After fixation and permeabilization, the cells were stained with PE-conjugated anti-human FoxP3 monoclonal antibody (BD, USA) overnight at 4°C. The cells were then washed three times with 1 ml of FACS buffer, resuspended in 0.5 ml of FACS fixing buffer (BD, USA) and acquired using CytoFLEX S flow cytometer (Beckman, USA). The data was analyzed by FlowJo software version VX (ThreeStar, San Carlos, CA, USA).

Statistical Analysis

We used the *t*-test for continuous variables and Chi-square test for categorical variables. A P-value <0.05 in the two-sided test was considered statistically significant. Statistical analyses were performed using IBM SPSS Statistics version 25 (SPSS, Chicago, USA). **Figures 1** and **3** were generated and analyzed using GraphPad Prism version 8 (GraphPad Software Inc.).

DATA AVAILABILITY STATEMENT

The original contributions presented in the study are included in the article/**Supplementary Material**. Further inquiries can be directed to the corresponding authors.

ETHICS STATEMENT

The studies involving human participants were reviewed and approved by the Ethics Committee of Changzhou Maternal and Child Health Hospital. The patients/participants provided their written informed consent to participate in this study.

AUTHOR CONTRIBUTIONS

SJ and WL designed and wrote the manuscript. LZ collected patient samples and performed most of the experiments. XinS and WL carried out ELISPOT analysis. QZ performed flow cytometry assays. ZM and XiaS helped to collect patient samples. ZM and AJ participated in the statistical analysis; RZ and JZ participated in the experimental design and project management. All authors contributed to the article and approved the submitted version.

FUNDING

This research was supported by grants from the general scientific research project of Jiangsu Provincial Health Commission (H2018018).

ACKNOWLEDGMENTS

We thank all the study participants.

SUPPLEMENTARY MATERIAL

The Supplementary Material for this article can be found online at: https://www.frontiersin.org/articles/10.3389/fimmu.2021.768144/full#supplementary-material

REFERENCES

1. Hu Z, Ma D. The Precision Prevention and Therapy of HPV-Related Cervical Cancer: New Concepts and Clinical Implications. *Cancer Med* (2018) 7:5217–36. doi: 10.1002/cam4.1501
2. Morrow MP, Kraynyak KA, Sylvester AJ, Dallas M, Knoblock D, Boyer JD, et al. Clinical and Immunologic Biomarkers for Histologic Regression of High-Grade Cervical Dysplasia and Clearance of HPV16 and HPV18 After Immunotherapy. *Clin Cancer Res* (2018) 24:276–94. doi: 10.1158/1078-0432.CCR-17-2335
3. Choi YJ, Park JS. Clinical Significance of Human Papillomavirus Genotyping. *J Gynecol Oncol* (2016) 27:e21. doi: 10.3802/jgo.2016.27.e21
4. Lee SJ, Yang A, Wu TC, Hung CF. Immunotherapy for Human Papillomavirus-Associated Disease and Cervical Cancer: Review of Clinical and Translational Research. *J Gynecol Oncol* (2016) 27:e51. doi: 10.3802/jgo.2016.27.e51
5. Josefsson AM, Magnusson PK, Ylitalo N, Sorensen P, Qwarforth-Tubbin P, Andersen PK, et al. Viral Load of Human Papilloma Virus 16 as a Detetmination for Development of Cervical Carcinoma Insitu:a Nested Case Control Study. *Lancet* (2000) 355:2189–93. doi: 10.1016/S0140-6736(00)02401-6
6. Xie JY, Xie JN, Yu KJ, Dong GQ, Cai CL, Xu GH, et al. The Relationship Between the Load and Duration of High-Risk Human Papillomavirus and Cervical Lesion in Pregnant Women. *Chin J Clin Obstet Gynecol* (2015) 16:550–2. doi: 10.13390/j.issn.1672-1861.2015.06.022
7. Shalapour S, Karin M. Immunity, Inflammation, and Cancer: An Eternal Fight Between Good and Evil. *J Clin Invest* (2015) 125:3347–55. doi: 10.1172/JCI80007
8. Sarkara AK, Tortolero-Luna G, Follen M, Sastry KJ. Inverse Correlation of Cellular Immune Responses Specific to Synthetic Peptides From the E6 and E7 Oncoproteins of HPV-16 With Recurrence of Cervical Intraepithelial Neoplasia in a Cross-Sectional Study. *Gynecol Oncol* (2005) 99:S251–61. doi: 10.1016/j.ygyno.2005.07.099
9. Nakagawa M, Stites DP, Palefsky JM, Kneass Z, Moscicki AB. CD4-Positive and CD8-Positive Cytotoxic T Lymphocytes Contribute to Human Papillomavirus Type 16 E6 and E7 Responses. *Clin Diagn Lab Immunol* (1999) 6:494–8. doi: 10.1128/CDLI.6.4.494-498.1999
10. Nakagawa M, Stites DP, Patel S, Farhat S, Scott M, Hills NK, et al. Persistence of Human Papillomavirus Type 16 Infection is Associated With Lack of Cytotoxic T Lymphocyte Response to the E6 Antigens. *J Infect Dis* (2000) 182:595–8. doi: 10.1086/315706
11. Mirabello L, Yeager M, Yu K, Clifford GM, Xiao Y, Zhu B, et al. HPV16 E7 Genetic Conservation Is Critical to Carcinogenesis. *Cell* (2017) 170:1164–74. doi: 10.1016/j.cell.2017.08.001
12. Cai L, Zhang J, Zhu R, Shi W, Xia X, Edwards M, et al. Protective Cellular Immunity Generated by Cross-Presenting Recombinant Overlapping Peptide Proteins. *Oncotarget* (2017) 8:76516–24. doi: 10.18632/oncotarget.20407
13. Ahdieh L, Muñoz A, Vlahov D, Trimble CL, Timpson LA, Shah K. Cervical Neoplasia and Repeated Positivity of Human Papillomavirus Infection in Human Immunodeficiency Virus-Seropositive and -Seronegative Women. *Am J Epidemiol* (2000) 151:1148–57. doi: 10.1093/oxfordjournals.aje.a010165
14. Jain S, Moore RA, Anderson DM, Gough GW, Stanley MA. Cell-Mediated Immune Responses to COPV Early Proteins. *Virology* (2006) 356:23–34. doi: 10.1016/j.virol.2006.07.032
15. Smola S. Immunopathogenesis of HPV-Associated Cancers and Prospects for Immunotherapy. *Viruses* (2017) 9:254. doi: 10.3390/v9090254
16. Moscicki AB, Shiboski S, Hills NK, Powell KJ, Jay N, Hanson EN, et al. Regression of Low-Grade Squamous Intra-Epithelial Lesions in Young Women. *Lancet* (2004) 364:1678–83. doi: 10.1016/S0140-6736(04)17354-6
17. Hildesheim A, Herrero R, Wacholder S, Rodriguez AC, Solomon D, Bratti MC, et al. Effect of Human Papillomavirus 16/18 L1 Viruslike Particle Vaccine Among Young Women With Preexisting Infection: A Randomized Trial. *JAMA* (2007) 298:743–53. doi: 10.1001/jama.298.7.743
18. Kenter GG, Welters MJ, Valentijn AR, Lowik MJ, Berends-van der Meer DM, Vloon AP, et al. Vaccination Against HPV-16 Oncoproteins for Vulvar Intraepithelial Neoplasia. *N Engl J Med* (2009) 361:1838–47. doi: 10.1056/NEJMoa0810097
19. Massarelli E, William W, Johnson F, Kies M, Ferrarotto R, Guo M, et al. Combining Immune Checkpoint Blockade and Tumor-Specific Vaccine for Patients With Incurable Human Papillomavirus 16–Related Cancer A Phase 2 Clinical Trial. *JAMA Oncol* (2019) 5:67–73. doi: 10.1001/jamaoncol.2018.4051

Conflict of Interest: Authors XinS, QZ, AJ and RZ were employed by company Oxford Vacmedix Co. Ltd. Author WL was employed by company Oxford Vacmedix Co. Ltd. and Shanghai JW Inflinhix Co. Ltd.

The remaining authors declare that the research was conducted in the absence of any commercial or financial relationships that could be construed as a potential conflict of interest.

Publisher's Note: All claims expressed in this article are solely those of the authors and do not necessarily represent those of their affiliated organizations, or those of the publisher, the editors and the reviewers. Any product that may be evaluated in

this article, or claim that may be made by its manufacturer, is not guaranteed or endorsed by the publisher.

frontiers in Immunology

ORIGINAL RESEARCH
published: 14 March 2022
doi: 10.3389/fimmu.2022.768569

A Systematic Immuno-Informatic Approach to Design a Multiepitope-Based Vaccine Against Emerging Multiple Drug Resistant *Serratia marcescens*

Marcelo Silva Folhas Damas[1†], *Fernando Gabriel Mazur*[1†], *Caio Cesar de Melo Freire*[1], *Anderson Ferreira da Cunha*[1] and *Maria-Cristina da Silva Pranchevicius*[1,2*]

[1] Departamento de Genética e Evolução, Universidade Federal de São Carlos, São Carlos, Brazil, [2] Centro de Ciências Biológicas e da Saúde, Biodiversidade Tropical – BIOTROP, Universidade Federal de São Carlos, São Carlos, Brazil

OPEN ACCESS

Edited by:
Shisong Jiang,
University of Oxford, United Kingdom

Reviewed by:
Wayne Robert Thomas,
University of Western Australia, Australia
Rupert Laurenz Mayer,
VIB-UGent Center for Medical Biotechnology, Belgium

***Correspondence:**
Maria-Cristina da Silva Pranchevicius
mcspranc@gmail.com

[†]These authors have contributed equally to this work

Specialty section:
This article was submitted to Vaccines and Molecular Therapeutics, a section of the journal Frontiers in Immunology

Received: 31 August 2021
Accepted: 14 February 2022
Published: 14 March 2022

Citation:
Damas MSF, Mazur FG, Freire CCM, Cunha AF and Pranchevicius MC (2022) A Systematic Immuno-Informatic Approach to Design a Multiepitope-Based Vaccine Against Emerging Multiple Drug Resistant Serratia marcescens. Front. Immunol. 13:768569. doi: 10.3389/fimmu.2022.768569

Serratia marcescens is now an important opportunistic pathogen that can cause serious infections in hospitalized or immunocompromised patients. Here, we used extensive bioinformatic analyses based on reverse vaccinology and subtractive proteomics-based approach to predict potential vaccine candidates against *S. marcescens*. We analyzed the complete proteome sequence of 49 isolate of *Serratia marcescens* and identified 5 that were conserved proteins, non-homologous from human and gut flora, extracellular or exported to the outer membrane, and antigenic. The identified proteins were used to select 5 CTL, 12 HTL, and 12 BCL epitopes antigenic, non-allergenic, conserved, hydrophilic, and non-toxic. In addition, HTL epitopes were able to induce interferon-gamma immune response. The selected peptides were used to design 4 multi-epitope vaccines constructs (SMV1, SMV2, SMV3 and SMV4) with immune-modulating adjuvants, PADRE sequence, and linkers. Peptide cleavage analysis showed that antigen vaccines are processed and presented *via* of MHC class molecule. Several physiochemical and immunological analyses revealed that all multiepitope vaccines were non-allergenic, stable, hydrophilic, and soluble and induced the immunity with high antigenicity. The secondary structure analysis revealed the designed vaccines contain mainly coil structure and alpha helix structures. 3D analyses showed high-quality structure. Molecular docking analyses revealed SMV4 as the best vaccine construct among the four constructed vaccines, demonstrating high affinity with the immune receptor. Molecular dynamics simulation confirmed the low deformability and stability of the vaccine candidate. Discontinuous epitope residues analyses of SMV4 revealed that they are flexible and can interact with antibodies. In silico immune simulation indicated that the designed SMV4 vaccine triggers an effective immune response. In silico codon optimization and cloning in expression vector indicate that SMV4 vaccine can be efficiently expressed in *E. coli* system. Overall, we showed that SMV4 multi-epitope vaccine successfully elicited antigen-specific humoral and cellular immune responses and

may be a potential vaccine candidate against *S. marcescens*. Further experimental validations could confirm its exact efficacy, the safety and immunogenicity profile. Our findings bring a valuable addition to the development of new strategies to prevent and control the spread of multidrug-resistant Gram-negative bacteria with high clinical relevance.

Keywords: *Serratia marcescens*, reverse vaccinology, multidrug resistance, computational approaches, subtractive proteomics

INTRODUCTION

The spread of antimicrobial resistance (AMR) is urgent, especially regarding bacteria (1). Once resistant strains emerge, the options for effective antibiotic therapy become limited and their alarming spread around the globe has not been followed by the development of novel antibiotics (2, 3). AMR produces significant impacts on human health around the world, causing troublesome levels of morbidity and mortality leading to dramatic economic consequences (4). It has been estimated that 10 million lives a year will be lost to AMR by 2050, and cumulative loss of world economies might be as high as $100 trillion (2, 5). AMR is a serious issue that demands an organized global action plan (4, 6, 7). Developing novel and integrated strategies are paramount to effectively fight AMR; these strategies include the development of monoclonal antibodies, new antibiotics, new diagnostics, new vaccines that target antibiotic-resistant bacteria, and increasing coverage of existing vaccines (3, 4, 8).

Serratia spp. is within the World Health Organization (9) global priority list of multidrug-resistant (MDR) bacteria that poses a major threat to human health around the world. Hence, there is an urgent need to development new and effective treatments and prevention strategies. *Serratia marcescens* is a Gram-negative *Enterobacteriaceae* species that has emerged as a neglected opportunistic human pathogen (10). This species can cause a variety of infections, including respiratory, bloodstream, skin, ocular, urinary, and catheter-related infections, as well as meningitis and sepsis in immunocompromised or critically ill patients, especially those in intensive care units (ICUs) and neonatal intensive care units (NICU). Studies have reported an increase in the number, and it of multidrug-resistant *S. marcescens* strains worldwide (11) and this increase has been related to severe outcomes (12) and a high mortality rate (13, 14).

Several studies and medical experiments have supported that *S. marcescens* may be promising for vaccine development. For instance, Field et al. (15) immunized adult mice with lipopolysaccharide (LPS) somatic antigen, or a heat-killed vaccine of *Serratia marcescens* and observed a rapid presence of specific antibody-forming cells in the spleen, in the mesenteric nodes, and in the thymus. Kreger et al. (16) showed that the severity of experimentally induced corneal disease by *S. marcescens* is considerably reduced by immunization against either the lipopolysaccharide endotoxins or the proteases of the bacteria. Kumagai et al. (17) showed that the protection against an experimental *Serratia marcescens* infection in mice was enhanced by prior injection of formalin-killed or viable bacteria of the same strain. They suggested that the humoral immunity and T-cell-mediated immunity were associated with protection against systemic *Serratia* infection. Shi et al. (18) reported that *S. marcescens* vaccine was effective for malignant pleural effusion and presented tolerable toxic effects. In the late 19th century, William Coley developed a formulation containing *Streptococcus pyogenes* and *S. marcescens* called by various names, such as Coley's fluid, Coley's vaccine, mixed bacterial vaccine (MBV), Coley's toxins, and Vaccineurin. This formulation was used to treat sarcoma in many countries until 1990 (19–21). In the 1970s, Coley's mixture (MBV) was further investigated, and it has been used in clinical trials against different types of cancer presenting variable results (22–27). The recent interest in MBV is motivated by humoral and cellular immunity to cancer antigens, which has the ability to spontaneous induce antibody responses. The stimulation of the innate immune system produces a complex cascade of cytokines that contribute to the immune recognition of cancer, possibly inducing apoptosis (22).

Vaccination is one of the most effective means to efficiently, rapidly and affordably improve public health; it is also the most feasible way to eradicate a variety of infectious diseases (28). Current vaccine research has mostly focused on peptide and subunit vaccines instead of whole organism vaccines. This is because subunit vaccines contain specific immunogenic components of the pathogens responsible for the infection rather than the whole pathogen. Traditional approaches for vaccine production have also been considered less efficient than computational approaches for a variety of reasons, including inaccuracy, safety, stability, high cost, hypersensitivity, and specificity.

Reverse vaccinology (RV), subtractive proteomics (SP), and genomics studies have emerged as powerful computational tools that have revolutionized the identification of drug targets and potential vaccine candidates (29). These methodologies are able to identify *in silico* the complete repertoire of immunogenic antigens and druggable targets that an organism is capable of expressing without the need of culturing the microorganism (30). In addition, it reduces the dependence on conventional animal testing based screening for getting a potentially suitable candidate, minimizing the time consuming and cost of the vaccine and drug development processes (31). Since the first application of reverse vaccinology that was used to development of a vaccine against serogroup B *Neisseria meningitidis* (MenB) (32), this tool has been used in the identification of numerous promising vaccine candidates against many bacterial pathogens, including *Mycoplasma pneumoniae* (33),

Pseudomonas aeruginosa (34), *Mycobacterium tuberculosis* (30), *Acinetobacter baumannii* (35), and *Neisseria meningitidis* (36).

In this study, we have applied RV and SP based computational strategies and selected a new multi epitope-based vaccine candidate against *Serratia marcescens*, which can be used in further experiments to validate its efficacy, safety, and immunogenic profile.

MATERIAL AND METHODS

Subtractive proteomics and reverse vaccinology approaches were used to identify potential vaccine candidates against the *S. marcescens* strain. A flowchart summarizing the methodology is shown in **Figure 1**.

Data Collection of Proteome and Selection of Core Proteins

The proteome sequences of 49 *S. marcescens* were downloaded from the Genome Project database of the National Center for Biotechnology Information (NCBI) (https://www.ncbi.nlm.nih.gov/genbank/). Out of these proteomic sequences, one corresponded to the representative proteome of *Serratia marcescens* subsp. *marcescens* Db11 and 48 sequences were from *S. marcescens* associated with human infections. Bacterial Pan Genome Analysis (BPGA) tool (37) version 1.3 was used to identify core (conserved) protein families (**Supplementary Data Sheet 2**). BPGA uses USEARCH as a default protein clustering tool with an identity cut off = 50%. Strain names, source of isolation, country, RefSeq assembly accession numbers, assembly levels, and references are shown in **Supplementary File Table S1**.

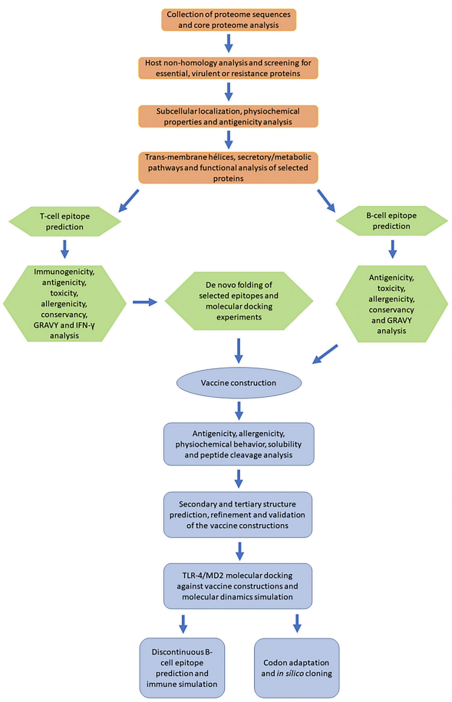

FIGURE 1 | A schematic flowchart diagram showing the procedure used in the current study. Orange: subtractive proteome analysis. Green: identification, characterization, and selection of peptide epitopes. Blue: construction and analysis of the multiepitope vaccine.

Screening of Essential Proteins, Virulence Factors and Resistance Proteins

The identified core protein families related to 49 bacteria species were subjected to BLASTp searches against the Database of Essential Genes (DEG 10) providing the essential information of the proteins (35, 38–42). DEG is a database for essential genes that is frequently updated (43, 44). The parameters of the analysis were E-value ≤ 10^{-4} and bitscore ≥ 100 (**Supplementary Data Sheet 3**). The core proteins of *S. marcescens* were also subjected to BLASTp search against Virulence Factor database (VFdb) (http://www.mgc.ac.cn/VFs/) (45) and Microbial virulence DataBase (MvirDB) (http://mvirdb.llnl.gov/) **Supplementary Data Sheet 4** (46). In both databases, the E-value cut-off was set to ≤ 10^{-4} and bitscore ≥ 100. The resistance associated proteins were found through a BLASTp against two databases, ARG-ANNOT (Antibiotic Resistance Gene-ANNOTation), which provides protein sequences associated with antibiotic (47), and CARD (Comprehensive Antibiotic Resistance Database), a database of peer-reviewed antibiotic resistance determinants (**Supplementary Data Sheet 5**) (48). The E-value cut-off for both antibiotic resistance analyses was ≤ 10^{-4}.

Subtracting Gut-Human Homologous and Human Non-Homology Proteins

The identified essential, virulent or resistance associated proteins were filtered against the proteome of host *Homo sapiens* (taxid:9606), using BLASTp with E-value of ≤ 10^{-4} (**Supplementary Data Sheet 6**). The host non-homologue proteins were filtered against a custom protein database containing 79 human gut floral species [see supplementary Text 1 from (44, 49)]. For subtraction of homologous sequence between gut microbiota and *S. marcescens*, we carried out BLASTp analysis. The obtained hits with an E-value of ≤ 10^{-4} and similarity ≥ 50% were considered as gut-flora homologous proteins and excluded from further analyses (**Supplementary Data Sheet 7**).

Prediction of Subcellular Localization

Prediction of selected proteins subcellular localization was done by using two different web servers: PSORTb v3.0.2 (50) algorithm (https://www.psort.org/psortb/) that determines different subcellular localization like cytoplasmic membrane, outer membrane, periplasm, extracellular, cytoplasmic, and unknown; and CELLO v2.5 (http://cello.life.nctu.edu.tw) (51), a web-based system which is also used for predicting protein subcellular localization.

Physicochemical Property and Antigenicity Analysis of Proteins

Physicochemical properties such as number of amino acids and molecular weight were examined on the online servers Expasy

ProtParam (52) (https://web.expasy.org/protparam/) and UniProt (https://www.uniprot.org/). Antigenicity of proteins was predicted using two online servers: VaxiJen v2.0 (53), (http://www.ddg-pharmfac.net/vaxijen/VaxiJen/VaxiJen.html) which predicts whether a protein could be a protective antigen based on physicochemical properties of amino acid sequence and has a threshold value ≥ 0.5; and AntigenPRO (http://scratch.proteomics.ics.uci.edu/), an alignment-free, sequence-based and pathogen-independent predictor of protein antigenicity with 79% accuracy and an area under curve (AUC) of 0.89 (54).

Identification of Trans-Membrane Alpha-Helices and Secretory Pathway Analysis

To assess the proteins getting embedded in the plasma membrane and to subtract those being exported, we submitted the amino acid sequences from the outer membrane, periplasm and extracellular proteins of *S. marcescens* to the TMHMM v.2.0 (https://services.healthtech.dtu.dk/service.php?TMHMM-2.0) server, which predicted the topology of these proteins by the Markov method (55). Secretory pathway was analyzed using SignalP 5.0 (https://services.healthtech.dtu.dk/service.php?SignalP-5.0), a server based on deep neural network method that predicts signal peptide (SP) sequences and discriminates among three main types of SPs (56).

Pathogen-Specific Pathways and Functionality Analysis of Selected Proteins

The comparison between metabolic pathways of *S. marcescens* and human pathways was done manually, using KEGG (Kyoto encyclopedia of gene and genome) pathway database. Proteins that play a role in unique and shared pathways in both pathogen and host were enlisted (**Table S2**) (35). Protein function prediction was made by three different servers: UniProt, KEGG Genes Database, and InterPro (https://www.ebi.ac.uk/interpro/), a server that provides family classification, biological process and molecular function of the protein (57).

Prediction of T Cell and B Cell Epitope

The prediction of MHC-I epitopes was performed by three servers: IEDB Tepitool prediction (http://tools.iedb.org/tepitool/) server (58), NetMHCpan 4.1 BA (https://services.healthtech.dtu.dk/service.php?NetMHCpan-4.1), and NetCTLpan 1.1 (https://services.healthtech.dtu.dk/service.php?NetCTLpan-1.1). In the IEDB server, 27 different alleles that cover more than 97% of the global population were selected for MHC class I predictions (59). Identified T-cell epitopes having alleles with IC50 value ≤ 50 nM were considered of high binding affinity. The default prediction method was set as the IEDB recommended that uses the Consensus method consisting of ANN (Artificial neural network, also called as NetMHC, version 3.4), SMM (Stabilized matrix method), CombLib (Scoring Matrices derived from Combinatorial Peptide Libraries), and NetMHCpan (version 2.8). NetMHCpan 4.1 server predicts binding of peptides to any MHC molecule of a known sequence using artificial neural networks (ANNs). We used a threshold value IC50 ≤ 50 nM and a percentile rank ≤ 0.20 (34). NetCTLpan 1.1 server performs integrate prediction of peptide MHC class I binding, proteasomal C terminal cleavage, and TAP transport efficiency. In this analysis, the threshold value was set as 0.75 (35).

Predictions of MHC class II epitopes or HTL epitopes were made by Tepitool, using the IEDB recommended method. A set of the 26 most frequent human class II alleles from DP, DQ, and DR loci was used. Selection criteria was peptides with binding affinity ≤ 50nM for IC50. Prediction of linear B-cell epitopes or BCL epitopes for proteins was achieved by using IEDB server, ABCpred, and Bcepred. IEDB server predicted epitopes based on antigenicity (60), accessibility (61), linear epitope (Bepipred-1.0) (62) and sequential/conformational epitope (BepiPred-2.0) (63). ABCpred (https://webs.iiitd.edu.in/raghava/abcpred/) uses Artificial Neural Network (ANN) machine-learning to predict B-cell epitopes and has an accuracy of 65.93%. In this server, parameters were set to default. Bcepred (https://webs.iiitd.edu.in/raghava/bcepred/bcepred_instructions.html) predicted B-cell epitopes based on four amino acid properties (hydrophilicity, flexibility, polarity and exposed surface). We used a threshold of 2.38 that predicts epitopes with 58.7% accuracy

MHC Class I Immunogenicity Determination

The MHC I immunogenicity prediction were assessed by the IEDB server (64) (http://tools.immuneepitope.org/immunogenicity/). A high score suggests a higher probability of stimulating an immune response. The epitopes with positive immunogenicity value were selected for further studies.

Antigenicity, Toxicity, Allergenicity of Selected Epitopes

The epitopes of MHC Class I, MHC Class II and LB were screened for their antigenic properties by VaxiJen2.0. The threshold for MHC class I and MHC class II epitopes was set to ≥ 0.5, and to ≥ 0.70 for the B-cell epitopes (53). The antigenic B-Cell epitopes obtained, with 9 or more amino acids in length and those that overlapped with the amino acids sequences found in IEDB, ABCpred and Bcepred tools were selected for toxicity and allergenicity analyses. The toxicity prediction was carried out using ToxinPred (http://www.imtech.res.in/raghava/toxinpred/index.html), keeping all the parameters to default. This tool predicts the antigenic behavior of epitopes through their physicochemical properties and confirms that the specific immune responses in the host cell will only target the bacteria rather and not host tissue (65). Allergenicity analysis was conducted with AllerTOP v2.0 server (https://www.ddg-pharmfac.net/AllerTOP/feedback.py). This is a server based on the main physicochemical properties of proteins (66), presenting an accuracy of 88.7% (67).

Conservancy, Hydrophobicity and IFN-Inducing Validation of Selected Epitopes

The conservancy of MHC Class I and MHC Class II selected epitopes within protein sequences were predicted using IEDB web server (68). For calculating the conservancy score, the

sequence identity threshold was kept at 100%. Grand average of hydropathicity of MHC Class I. MHC Class II and LB epitopes were done using ProtParam (52) server. The GRAVY value is described by the sum of hydropathy values of all amino acids divided by the protein's length (34). A negative value implies that protein contains hydrophilic properties whereas a positive GRAVY value indicates that the protein is hydrophobic (35). For further refinements, we investigated whether Helper T cell (HTL) epitope can induce IFN gamma immune response using the IFN epitope server (69) (http://crdd.osdd.net/raghava/ifnepitope/), an online tool with 82.10% accuracy. The server constructs overlapping sequences from which the IFN-γ epitopes are predicted. The default prediction method was set as "Motif and Support Vector Machine (SVM) hybrid" and "IFN-gamma vs. Non-IFN-gamma" model to predict IFN-γ-inducing peptides based on score. The higher the score, the higher the chance of inducing IFN-γ (70). Although the IFN epitope server has limitations regarding the number of residues that can be used for prediction (71), it is a common online prediction server used for vaccine design (70, 72–74). Therefore, the epitopes with positive results for the IFN-γ response were selected for further prediction.

Predicting Three Dimensional (3D) Epitope Structure and Molecular Docking of the Selected Epitopes

The best-selected MHC class I and MHC class II epitopes were submitted to PEP-FOLD3 server (http://bioserv.rpbs.univ-paris-diderot.fr/services/PEP-FOLD3/), an online tool for generating *de novo* peptide 3D structure (75). The docking experiments were made using PatchDock (https://bioinfo3d.cs.tau.ac.il/PatchDock/php.php) tool. The obtained models were refined and re-scored by FireDock server (http://bioinfo3d.cs.tau.ac.il/FireDock/), that ranks the docked models by their global energy, and the lowest global energy represented the best prediction (76). The MHC class I epitopes were docked with HLA-A*0101 (PDB: 6AT9), HLA-A*0201 (PDB: 3UTQ), HLA-B*1501 (PDB: 1XR8), HLA-B*3501 (PDB: 1ZSD), HLA-B*3901 (PDB: 4O2E), HLA-B*5301 (PDB: 1A1M), HLA-B*5801 (PDB: 5IM7), HLA-B*4403 (PDB: 1SYS) alleles. The alleles used to MHC Class II epitopes were: HLA-DRB1*0101 (PDB: 2FSE), HLA-DRB1*0301 (PDB: 1A6A), HLA-DRB1*0401 (PDB: 2SEB), HLA-DRB1*1501 (PDB: 1BX2), HLA-DRB3*0101 (PDB: 2Q6W), HLA-DRB3*0202 (PDB: 3C5J) and HLA-DRB5*0101 (PDB: 1H15). The docked structures were visualized using PyMol tool (https://pymol.org/pymol.html?) (67). The epitopes that showed the best binding affinity were selected for vaccine construction.

Vaccine Construction

Best binding peptides were selected for potential vaccine candidate. To construct the vaccine, CTL, HTL and BCL epitopes were linked together by GGGS, GPGPG and KK linkers. GGGS linkers were used to conjugate the Universal Pan HLA DR sequence (PADRE) sequence with CTL epitopes and the CTL epitopes among themselves. GPGPG linkers were used to conjugate the CTL epitopes with HTL epitopes and also the HTL epitopes with the other HTL. KK linkers were used to attach the HTL and BCL epitopes as well as the BCL epitopes among themselves (67). Adjuvants sequences were linked with the help of EAAAK linkers at both N- and C-terminus, and EAAAK linkers were also used to conjugate the PADRE sequence (AKFVAAWTLKAAA) (35). Five different adjuvant sequences were used to attach the PADRE sequence: 50s ribosomal L7/L12 protein (77), beta-defensin (78), HBHA protein (*M. tuberculosis*, accession number: AGV15514.1), and HBHA conserved sequence (79).

Antigenicity and Allergenicity of Vaccine Constructs

VaxiJen 2.0 and ANTIGENpro server were used to determine the antigenicity of the vaccine constructs. AllerTOP and AlgPred (http://crdd.osdd.net/raghava/algpred/) servers were used to evaluate the allergen potential of the multi-epitope vaccine construct. Allergen prediction is based on similarity of known epitope of any of the known region of the protein. It uses MAST to search MEME/MAST allergen motifs and predict the allergen if it has a motif. AlgPred is an SVM module based program which uses amino acid or dipeptide composition for the prediction of allergen. The parameters (IgE epitope + MAST + SVM + ARPs BLAST) were combined to predict the allergenicity of vaccine constructs (35, 80).

Solubility Prediction and Physiochemical Behavior Analysis of Vaccine Constructs

SOLpro of Scratch Protein predictor was used for vaccine solubility estimation. SOLpro performs a two-stage SVM architecture method based on multiple representations of the primary sequence (81). The overall accuracy of SOLpro is estimated in over 74% using multiple runs of ten-fold cross-validation (81). Vaccine constructs physiochemical properties were analyzed using Expasy ProtParam server, which determined the number of amino acids, molecular weight, theoretical isoelectric point (PI), instability and aliphatic index, and hydropathicity GRAVY values.

Peptide Cleavage Analysis

Proteasomal cleavage is important for T Cell epitope presentation. This was analyzed by NetChop 3.1 (http://www.cbs.dtu.dk/services/NetChop/), a neural network-based method trained on MHC class I ligands produced by the human proteasomes (**Supplementary Data Sheet 8**) (82). Since cathepsins cleavage sites may play a vital role in the immune antigen presentation, cathepsin specific peptidase activity was analyzed with the SitePrediction (http://www.dmbr.ugent.be/prx/bioit2-public/SitePrediction/index.php) server for MHC class II epitopes (83).

Secondary and Tertiary Structure Prediction of the Vaccine Constructs

The secondary structures of the multi-epitope vaccine constructs were generated using online tool PSIPRED 4.0 (http://bioinf.cs.ucl.ac.uk/psipred/), a web-based freely accessible online server that also predicts the transmembrane topology, transmembrane helix, fold and domain recognition (74). PSIPRED 4.0 has a Q3

secondary structure prediction precision of 84.2% (84). The 3D structures of multi-epitope vaccine constructs were predicted using the I-TASSER (Iterative Threading ASSEmbly Refinement) server (https://zhanglab.ccmb.med.umich.edu/I-TASSER/). I-TASSER is an integrated platform for automated protein structure and function prediction based on the sequence-to-structure-to-function paradigm. I-TASSER initial creates three-dimensional (3D) atomic models from several threading alignments and iterative structural assembly simulations starting from an amino acid sequence. In five community wide CASP (Critical Assessment of techniques for Structure Prediction) experiments, I-TASSER has been ranked best server for protein 3D structure prediction (70). Pymol program was used to visualize the modeled 3D structures.

Refinement and Validation of Vaccines Constructs

The 3D structures of the constructed vaccines were refined using 3Drefine server (http://sysbio.rnet.missouri.edu/3Drefine/). 3Drefine server is based in optimization of the hydrogen bonding network and composite physics and knowledge-based force fields to give atomic-level energy minimization using the MESHI molecular modeling framework (85, 86). The validation process was performed using the PROCHECK's Ramachandran plot analysis (https://servicesn.mbi.ucla.edu/PROCHECK/) (87) that analyzes the geometry of the refined vaccine construct and predict the best stereochemical quality of the construct (88); ProSA (https://prosa.services.came.sbg.ac.at/prosa.php) (89) that computes the overall quality score (Z score) for a specific 3D structure (90); and ERRAT server (http://services.mbi.ucla.edu/ERRAT/) (91) that analyzes the statistics of non-bonded interactions between different atom types (92).

Protein-Protein Docking

Each vaccine construct was docked against TLR4-MD2 complex (PDB:3FXI). The docking experiments were made using ClusPro 2.0 (https://cluspro.bu.edu/login.php) and PatchDock (https://bioinfo3d.cs.tau.ac.il/PatchDock/php.php). ClusPro 2.0 ranks the cluster of docked complexes based on their center and lowest energy scores (93). PatchDock algorithm divides the Connolly dot surface representation of the molecules into concave, convex, and flat patches (94). ClusPro 2.0 and PatchDock were further analyzed by the PRODIGY tool of HADDOCK server (https://haddock.science.uu.nl/) and FireDock server (http://bioinfo3d.cs.tau.ac.il/FireDock/php.php), respectively. The PRODIGY server produces binding affinity score (95) and the FireDock server accesses the global energy of the docked complexes.

Molecular Dynamic Simulation

After performing the protein-protein molecular docking, the best-scored vaccine construction (SMV4) complexed with TLR4-MD2 was subjected to molecular dynamic simulation by the online server iMODS (http://imods.chaconlab.org/) (96), using the parameters as default. This server predicts the dynamics simulation of the protein complex in terms of atomic B-factors, eigenvalue variance, deformability, elastic network, and covariance map. The deformability of a given protein mostly relies on the capability of each of its residues to deform. The eigenvalue is related with the energy that is required to deform the given structure; the lower the eigenvalue value, the easier the deformability of the complex (67, 97). Moreover, the eigenvalue of the given protein complex provides its motion stiffness (79).

Discontinuous B Cell Epitopes

SMV4 vaccine construction selected was submitted to ElliPro server (http://tools.iedb.org/ellipro/) that predicts epitopes based upon solvent-accessibility and flexibility (98). The algorithms implemented in this analysis were approximation of the protein shape as an ellipsoid (99), protrusion index (PI) of residue (100), and neighboring residues clustering based on their PI values. The conformational B-cell epitopes with minimum score value set at 0.70 while the maximum distance was set as default.

Immune Simulation of the Vaccine Construct

C-ImmSim server (http://150.146.2.1/C-IMMSIM/index.php?page=1) was used for the immune simulation study. It uses position-specific scoring matrix for immune epitope forecast and machine learning techniques to estimate immune interactions (101). The three mammalian anatomical regions to get simulated by the server were thymus (T cell), bone marrow (lymphoid and myeloid cell), and a lympathic organ to exhibit immune response (102). All parameters were kept as default at the time of vaccine introduction, and three injections were administered with the recommended intervals of 30 days. The time steps followed for three injections were 1, 90 and 180. The volume of simulation and the steps of the simulation were set at 10 and 600, respectively (103).

Codon Adaptation and *In Silico* Cloning

Reverse translation and codon optimization were performed using Java Codon Adaptation Tool (JCat) server (http://www.prodoric.de/JCat) (104). The JCat output includes the codon adaptation index (CAI) and percentage GC content, which can be used to assess protein expression levels. CAI provides information on codon usage biases; CAI score >0.8 is considered a good score (105). The ideal GC content of a sequence should range between 30–70% (80). The *E. coli* strain K12 was chosen as host for cloning our vaccine construct. We avoided rho-independent transcription termination, prokaryote ribosome binding site, and restriction enzymes cleavage sites. Vaccine construct was cloned in pET28a (+) plasmid vector by adding XhoI and NdeI restriction sites at C and N terminus, respectively. The optimized sequence of the vaccine was inserted into the expression vector [pET-28a (+)] using Benchling webserver (https://www.benchling.com/).

RESULTS

Pre-Screening of Primary Data

Primarily, we selected representative proteomes of 48 *S. marcescens* associated with human infections, and a *Serratia marcescens* subsp. marcescens Db11 as a reference strain for our vaccine prediction.

The proteomes of all *S. marcescens* strains were retrieved from Genome Project database of the National Center for Biotechnology Information (NCBI). With the help of Bacterial Pan Genome Analysis (BPGA) tool the number of core proteins found from analyzing of the 49 proteomes was 2832 proteins.

Screening of Essential, Virulence, Resistance and Non-Homology Against Human and Gut Flora Proteins

All the 2832 proteins were subsequently analyzed for essential, virulent and resistance functions. The analyses of the non-redundant proteins resulted in 1815 proteins. Of these proteins, we have found 879 essential proteins, 155 proteins contained virulence property, 98 were resistant proteins, 370 proteins were found to be virulence and essential, 70 were resistant and essential, 42 resistant and virulence, and 201 proteins were related with essential, virulence and resistance functions, 1106 were non-homologous with human proteins. Of these 1106 proteins, 20 were gut flora non-homologous proteins, and were used for subsequent analysis

Subcellular Localization, Identification of Essential Proteins, Virulence Factors and Resistant Determinants

Next, the subcellular localization of 20 gut flora non-homologous proteins revealed that 2 proteins were outer membrane proteins, 6 periplasmic, and 2 extracellular (**Table 1**). Of these 10 proteins, 4 protein were essential (D-alanyl-D-alanine carboxypeptidase, 51.35 kDa; patatin-like phospholipase, 35.68 kDa; lipoprotein 11.82 kDa; helix-turn-helix domain-containing protein, 10.66 kDa), 4 virulence (phospholipase C, 79.68 kDa; spore coat U domain-containing protein, 33.28 kDa; protein of avirulence locus ImpE, 29.48 kDa; NADPH-dependent FMN reductase, 19.24 kDa; 1 was related to resistance (TonB-dependent receptor, 76.90 kDa), and 1 protein presented essential and virulent functions (MoaF domain-containing protein, 16.27 kDa) (**Table 1**).

Peptide Signal, Trans-Membrane, and Antigenicity Prediction

Of these 10 proteins selected, analyses of presence of signal peptide/anchor resulted into 3 proteins with secretory signal peptides that are transported by the Sec translocon and cleaved by Signal Peptidase I (Sec/SPI), 2 proteins having lipoprotein signal peptides transported by the Sec translocon and cleaved by Signal Peptidase II (Sec/SPII), and 1 protein with Tat signal peptides transported by the Tat translocon and cleaved by Signal Peptidase I (Tat/SPI). Only 1 protein (MoaF domain-containing protein) contained 1 transmembrane helix (**Table 1**). VaxiJen v2.0 and AntigenPRO tools reveled 7 and 8 proteins with a good antigenic nature (>0.50) (**Table 1**), respectively. Of these, 2 essential proteins (D-alanyl-D-alanine carboxypeptidase, patatin-like phospholipase family protein), 2 virulent proteins (Phospholipase C, phosphocholine specific; spore coat U domain-containing protein), and 1 resistant protein (TonB-dependent receptor) presented antigenicity profile, had extracellular domain or were proteins located in the outer membrane. Therefore, these 5 protein were considered for further prediction of vaccine targets (**Table 1**).

MHC Class-I Epitopes Prediction and Immunogenicity, Antigenicity, Toxicity, Hydropathicity and Conservancy Analysis of Selected Epitopes

The prediction of T-cell epitopes of MHC class-I of the 5 proteins (D-alanyl-D-alanine carboxypeptidase, patatin-like phospholipase family protein, Phospholipase C phosphocholine specific, spore coat U domain-containing protein, TonB-dependent receptor) had the sequence length 9 residues. Among the 284 predicted epitopes, the 123 common epitopes found in three servers were selected for immunogenicity analysis and resulted in 59 epitopes. From these, 31 epitopes were found to be antigenic and we found no epitopes with toxicity. Out of 31, 17 epitopes were non-allergenic. Epitope conservancy analysis found 14 peptides with a score of more than 50%. GRAVY analysis resulted in 7 peptides with negative value score, which suggests hydrophilic nature of peptides. For further analysis, we selected 7 MHC class-I epitopes (TPFGAGWSW, LEDRLVETL, SSNVNFPLY, FTIPLPGDR, QTYGAKIAR, SEYVWNYEL, YQFLKGWEL) that were found to be immunogenic, antigenic, non-allergenic, non-toxic, conserved, and with negative hydropathicity (**Table 2).** We excluded the patatin-like phospholipase family protein because its prediction analysis did not reach all the recommended parameters (**Table 2**).

MHC-II Epitopes and Antigenicity, Toxicity, Conservancy, Hydropathicity, IFN-γ Analysis

The MHC-II binding prediction of the 5 proteins (D-alanyl-D-alanine carboxypeptidase, patatin-like phospholipase family protein, Phospholipase C phosphocholine specific, spore coat U domain-containing protein, TonB-dependent receptor) resulted in 415 MHC-II epitopes with higher affinity. From these, 196 were antigenic, and all were subjected to toxicity and allergenicity prediction. According with results, all selected epitopes were non-toxic and 114 had non-allergic nature. Conservancy analysis showed that 93 epitopes had score more than 50%, and GRAVY analysis revealed that 70 epitopes had a hydrophilic nature. Additionally, the 31 the best resultant epitopes of all analyses conducted were analyzed for their IFN-γ inducing. A total of 16 epitopes (4 from D-alanyl-D-alanine, 1 from patatin-like phospholipase family protein, 2 from Phospholipase C phosphocholine specific, 2 from spore coat U domain-containing protein and 7 from TonB-dependent receptor) had a IFN-γ inducing profile and were selected for molecular docking analysis (**Table 3**).

B-Cell Epitope Prediction and Antigenicity, Toxicity, Allergenicity and Hydropathicity Analysis

The prediction of linear B-cell epitopes for D-alanyl-D-alanine carboxypeptidase, patatin-like phospholipase family protein, Phospholipase C, TonB-dependent receptor and spore coat U

TABLE 1 | Predicted subcellular localization, physicochemical, antigenicity, trans-membrane alpha-helices and peptide signal analysis.

Ref. Sequence (1)	Protein name (2)	Length (amino acid) (3)	Mol. Wt kDa (4)	Signal peptide (5)	Localization (6)	Functional Discription (7,8,9)	TMHMM (10)	Antigenicity (11,12)
	Essential proteins							
WP_041033700.1	* D-alanyl-D-alanine carboxypeptidase/D-alanyl-D-alanine-endopeptidase	489	51.35	Sec/SPIICleavage site (17 and 18, LAG-CS)	Outer membrane/ Periplasm	Penicilin-binding protein/ Serine endopeptidase activity	0	0.5856, 0.5066
WP_084827239.1	* Patatin-like phospholipase Family protein	323	35.68	Not identified	Outer membrane	Hydrolase activity/lipid catabolic process	0	0.6024, 0.8235
WP_004939944.1	Lipoprotein	108	11.82	Sec/SPIICleavage site (16 and 17, LSA-CA)	Periplasm	Lipoprotein with MoaF domain	0	0.5595, 0.4857
WP_047571040.1	Helix-turn-helix domain-containing protein	92	10.66	No identified	Periplasm	Uncharacterized conserved protein with HTH_43 domain	0	0.2089, 0.2900
	Virulent proteins							
WP_141960268.1	* Phospholipase C, phosphocholine-specific	715	79.68	Tat/SPICleavage site (31 and 32, (ALA-IP)	Extracellular	Membrane damaging toxin, phosphoric-diester hydrolase	0	0.4097, 0.6277
WP_048321499.1	* Spore coat U domain-containing protein	311	33.28	Sec/SPICleavage site (23 and 24, AFA-DC)	Extracellular	Involved in motility and biofilm formation	0	0.6887, 0.8719
WP_148123533.1	Protein of avirulance locus ImpE	273	29.48	Not identified	Periplasm	Signaling, type VI secretion system component	0	0.5895, 0.7594
WP_004940045.1	NADPH-dependent FMN reductase	183	19.24	Not identified	Periplasm	Electron transfer activity/ FMN binding	0	0.4056, 0.7386
	Resistance protein							
WP_033636744.1	* TonB-dependent receptor	697	76.90	Sec/SPICleavage site (44 and 45, VNA-AE)	Outer membrane	Iron complex receptor protein, channel transporter of siderophores	0	0.6847, 0.7910
	Essential and virulent protein							
WP_099783007.1	MoaF domain-containing protein	150	16.27	Sec/SPICleavage site (26 and 27, ATA-AQ)	Periplasm	Exported protein with MoaF domain	1	0.5896, 0.9631

*All data were analyzed using various server: 1, 2, 3 = NCBI/UniProt; 4 = Expasy; 5 = SignalP5.0; 6 = PSORTb/CELLO; 7, 8, 9 = Uniprot/KEGG/InterPro; 10 = TMHMM; 11 = Vaxijen, 12 = AntigenPRO. * proteins considered for further analysis.*

domain-containing protein is showed in **Figure S1**. Antigenicity scale, and the most potent regions in epitopes found is showed in yellow (**Figure S1**). A total of 503 B cell epitopes were predicted by three servers, of which 236 epitopes were found to be antigenic. From these antigenic epitopes, we manually selected 23 epitopes that had regions overlapping with the amino acids sequences found in IEDB, ABCpred and Bcepred tools. These epitopes were subsequently tested to toxicity, allergenicity, conservancy and hydropathicity. This analysis resulted in 12 epitopes (TGEQRGDTL, SGDPTLHPDDL, GRKTQGKGD, QREVYSHRTTPRM, SSQRINTRTLGLRLDS, MAVANTDGSGD, TTVWDSTNKQSGAGT, QPEVRLRPTG, FAAQRHESVGN, AETKSNETYQD, DRQRRRSEADL, RLEREHRRRDG) non-allergen, non-toxic, conserved and having hydrophilic nature. All 12 epitopes were selected for further analysis and vaccine construction (**Table 4**).

Peptide Modeling and Molecular Docking Analysis

All the 7 MHC class I and 16 MHC class II T-cell epitopes were subjected to 3D structure generation by the PEP-FOLD3 server, and the predicted 3D structures found were docked with 8 MHC class I alleles and 7 MHC class II alleles, respectively. Among the epitopes, 5 MHC class I and 12 class II epitopes showed the best result with the lowest global energy of -34.89 and -70.54, respectively (**Table 5**) and were used in multi-peptide vaccine construction.

Construction of Multi-Epitope Peptide Vaccine, Physiochemical Properties and Antigenicity, Allergenicity, Solubility Analysis of Different Vaccine Constructs

We combined an adjuvant, PADRE sequence, CTL epitopes (MHC-I epitopes), HTL epitopes (MHC-II epitopes) and BCL epitopes (B-cell epitopes) in a sequential manner, and constructed four vaccines candidates, named SMV1, SMV2, SMV3 and SMV4. All designed vaccine proteins contained 5 CTL epitopes, 12 HTL, and 12 BCL epitopes. The vaccines differed each other only by adjuvant sequence, and the adjuvants used were 50s ribosomal L7/L12 protein, beta defensin, HBHA conserved sequence and HBHA protein (*M. tuberculosis*, accession number: AGV15514.1) (**Table 6**). For vaccine construction, the adjuvant sequence was linked with PADRE sequence by EAAAK linker, GGGS linkers were used to join the PADRE sequence with the CTL epitopes and the CTL epitopes with the other CTL epitopes, GPGPG were used to linked the CTL epitopes with the HTL epitopes and also the HTL

TABLE 2 | Predicted MHC class-I epitopes and immunogenicity, antigenicity, toxicity, allergenicity, conservancy and hydropathicity analysis.

No.	Protein ID (1), name (2)	Start (3 4,5)	End (3,4,5)	Epitope (3,4,5)	Tepitool Alleles (3)	NetMHCpan Alleles (4)	NetCTLpan Alleles (5)	Immunogenicity (6)	Antigenicity (7)	Toxicity (8)	Allergenicity (9)	Conservancy (10)	Hydropathicity (11)
1	WP_041033700.1; D-alanyl-D-alanine carboxypeptidase/ endopeptidase	156	164	TPFGAGWSW	HLA-B*53:01	HLA-B*53:01	HLA-B*35:01, HLA-B*53:01	0.23238	0.5798	Non-toxin	Non-allergen	100%	-0.12
		471	479	LEDRLVETL	HLA-B*40:01	HLA-B*40:01	HLA-B*40:01	0.19452	0.7321	Non-toxin	Non-allergen	100%	-0.01
3	WP_141960268.1; Phospholipase C, phosphocholine-specific	74	82	FTIPLPGDR	HLA-A*68:01	HLA-A*68:01	HLA-A*68:01	0.05236	0.739	Non-toxic	Non-allergen	97.96%	-0.13
4	WP_048321499.1; spore coat U domain-containing protein	127	135	SSNVNFPLY	HLA-A*30:02	HLA-A*30:02	HLA-A*01:01, HLA-A*11:01, HLA-A*30:02	0.1275	0.983	Non-toxin	Non-allergen	63.27%	-0.08
5	WP_033636744.1; TonB-dependent receptor	469	477	QTYGAKIAR	HLA-A*68:01	HLA-A*31:01, HLA-A*68:01	HLA-A*68:01	0.00318	1.2908	Non-toxin	Non-allergen	100%	-0.69
		499	507	SEYWNYEL	HLA-B*40:01	HLA-B*40:01	HLA-B*40:01, HLA-B*44:03	0.30533	1.4052	Non-toxin	Non-allergen	100%	-0.76
		608	616	YQFLKGWEL	HLAA*02:01, HLA-A*02:06	HLA-A*02:01, HLA-A*02:06	HLA-A*02:01, HLA-A*02:06	0.09418	0.561	Non-toxin	Non-allergen	100%	-0.34

All data were analyzed using various server: 1, 2 = NCBI/UniProt; 3 = IEDB Tepitool; 4 = NetMHCpan 4.1; 5 = NetCTLpan 1.1; 6 = IEDB server; 7 = VaxiJen 2.0; 8 = ToxinPred; 9 = AllerTOP v2.0; 10 = IEDB, 11 = GRAVY ProtParam.

epitopes among themselves, and KK linkers were used to conjugate HTL with the BCL epitopes, the BCL with the other BCL epitopes, and BCL with the PADRE sequence. Each vaccine construct was finished by an additional GGGS linker.

Each designed vaccine construct contained 668 (SMV1), 659 (SMV2), 554 (SMV3) and 639 (SMV4) residues long, while the molecular weight of each construction was found to be 70.335, 69.217, 57.867 and 66.147 kDa respectively. The theoretical pI of each construct ranged from 9.85 to 10.36, suggesting that the constructions have a negative charge if the pH is above the isoelectric point and vice versa. The computed instability index of constructions varied from 28.01 to 35.66 representing the stable nature of the vaccine proteins. The high aliphatic index range (66.68 to 74.19) of all vaccine constructs suggest the protein stability in several temperatures. The negative GRAVY value of the vaccine constructs revealed that all of them has a hydrophilic in nature. All four vaccine constructs showed good solubility (>0.873) during its heterologous expression in the *E. coli*. Therefore, all of the vaccine constructs showed be antigenic, non-allergenic, hydrophilic, stable and soluble. The sequence of vaccine constructs and their physiochemical properties are showed in **Table 6**.

Peptide Cleavage Analysis

We investigated both proteasomal and cathepsin specific peptidase activity on the vaccine constructs. NetChop 3.1 server detected 17 proteasomal sites, which majority of them were close to the linkers. SitePrediction server provided 1 peptidase and 14 peptidase links with 99.9% and 99% specificity for cathepsin B, respectively; 1 peptidase and 2 peptidase links with 99.9% and 99% specificity for cathepsin D, respectively; 8 and 3 peptidase links with 99% specificity for cathepsins E and G, respectively; 2 peptidase links with 99.9% and 4 peptidase links with 99% specificity for cathepsin K, and 1 peptidase link with 99% specificity for cathepsin L. Our results indicates that these multi-epitope vaccine constructs might be processed and presented in context of MHC class molecule.

Secondary Structure Prediction of the Constructed Vaccines

The analyze of the secondary structure of vaccine constructs showed that SMV1 had 48.35% of amino acids in coil structure, 40.12% of amino acids in alpha helix, and the lowest percentage of the amino acids in beta sheet formation (11.23%). SMV2 had 49.75% of amino acids in coil structure, 38.56% in alpha helix region, and 11.69% of the amino acids in the beta sheet formation. SMV3 had the highest percentage of coil structure (55.05%), 27.62% of the amino acids in alpha helix region, and the highest percentage of the amino acids in the beta sheet formation (17.33%). SMV4 presented coil structure in 54.23%, 30.05% of alpha helix region, and 15.72% of the amino acids in the in beta sheet formation (**Figure 2**).

3D Structure Prediction of the Constructed *S. marcescens*

The 3D structure was obtained by threading using I-TASSER web server. For each vaccine sequence was predicted five 3D models, and the first model of each construction was selected. All

TABLE 3 | Identification of MHC-II epitopes and antigenicity, toxicity, conservancy, hydropathicity and IFN-γ inducing profile prediction.

No.	Protein ID (1); name (2)	Start (3)	End (3)	Epitope (3)	Alleles (3)	Antigenicity (4)	Toxicity (5)	Allergenicity (6)	Conservancy (7)	Hydropathicity (8)	IFN-γ inducing (9)
1	WP_041033700.1; D-alanyl-D-alanine carboxypeptidase/ endopeptidase	7	21	WLLPAILALAGCSSS	HLA-DRB1*01:01	10.376	Non-toxin	Non-allergen	83.67%	-0.93	0.476
		170	184	AFAAPISALNYAFTP	HLA-DRB1*01:01	0.6842	Non-toxin	Non-allergen	75.51%	-0.89	0.228
		197	211	PGARAGAPGRVSFYP	HLA-DQA1*05:01/DQB1*03:01	10.191	Non-toxin	Non-allergen	61.22%	-0.1	0.329
		451	465	PLAFAIISNNYLVPG	HLA-DRB1*04:05/HLA-DRB1*04:01/HLA-DRB1*15:01HLA-DRB1*07:01/HLA-DRB1*01:01/HLA-DRB1*13:02	0.5584	Non-toxin	Non-allergen	100%	-0.92	0.089
2	WP_084827239.1; patatin-like phospholipase family protein	40	54	SGASAGAIAALLVGL	HLA-DQA1*05:01/DQB1*03:01	0.8684	Non-toxin	Non-allergen	100%	-0.71	0.416
3	WP_141960268.1; Phospholipase C, phosphocholine-specific	243	257	RQYRAASIQVGNPAR	HLA-DRB1*01:01	0.5796	Non-toxin	Non-allergen	97.96%	-0.93	0.131
		452	466	EKRFQVHEPNISAWR	HLA-DRB1*01:01	0.8644	Non-toxin	Non-allergen	100%	-1.34	0.673
4	WP_048321499.1; spore coat U domain-containing protein	117	131	SLNLLSLILISSNVN	HLA-DRB1*01:01	0.6343	Non-toxin	Non-allergen	97.96%	-0.82	0.041
		121	135	LSLILISSNVNFPLY	HLA-DRB1*13:02/HLA-DRB1*01:01	0.5934	Non-toxin	Non-allergen	63.27%	-1.05	0.41
5	WP_033636744.1; TonB-dependent receptor	125	139	NVGANAFLSGTRPRL	HLA-DRB5*01:01	0.7968	Non-toxin	Non-allergen	87.76%	-0.11	0.314
		129	143	NAFLSGTRPRLNLSL	HLA-DRB5*01:01, HLA-DRB1*01:01, HLA-DRB1*11:01	0.8159	Non-toxin	Non-allergen	87.76%	-0.03	0.136
		339	353	TDFNINRPTAYNIQY	HLA-DRB3*02:02, HLA-DRB1*13:02	0.6574	Non-toxin	Non-allergen	87.76%	-0.93	0.154
		372	386	ADSRLHGLAGLRYFH	HLA-DRB1*01:01	0.5227	Non-toxin	Non-allergen	100%	-0.27	0.494
		565	579	RWDFELFGNLGLLKT	HLA-DRB1*01:01	0.5005	Non-toxin	Non-allergen	87.76%	-0.03	0.108
		595	609	ARAPAYTANMGAKYQ	HLA-DRB3*02:02	0.9467	Non-toxin	Non-allergen	87.76%	-0.65	0.04
		606	620	AKYQFLKGWELSSNV	HLA-DRB1*01:01	0.7445	Non-toxin	Non-allergen	87.76	-0.41	0.63

All data were analyzed using various server: 1, 2 = NCBI/UniProt; 3 = IEDB Tepitool; 4 = VaxiJen 2.0; 5 = ToxinPred; 6 = AllerTop v2.0; 7 = IEDB; 8 = GRAVY ProtParam; 9 = IFN epitope.

TABLE 4 | Identification of B-cell epitopes and antigenicity, toxicity, allergenicity and hydropathicity prediction of selected epitopes.

No.	Protein ID (1); name (2)	Start	End	Lenght	Epitopes (3,4,5)	Antigenicity (6)	Toxicity (7)	Allergenicity (8)	Hydropathicity (9)	Conservancy (10)
1	WP_041033700.1; D-alanyl-D-alanine carboxypeptidase/ endopeptidase	100	108	9	TGEQRGDTL	1.4316	Non-toxin	Non-allergen	1.49	51.02%
		117	127	11	SGDPTLHPDDL	0.7116	Non-toxin	Non-allergen	-1.02	100%
		331	339	9	GRKTQGKGD	2.7203	Non-toxin	Non-allergen	2.36	89,80%
2	WP_084827239.1; patatin-like phospholipase family protein	147	159	13	QREVYSHRTTPRM	0.7944	Non-toxin	Non-allergen	-2.05	100%
		214	229	16	SSQRINTRTLGLRLDS	17.872	Non-toxin	Non-allergen	-0.77	71.43%
3	WP_141960268.1; Phospholipase C, phosphocholine-specific	620	629	10	QPEVRLRPTG	1.3449	Non-toxin	Non-allergen	-1.23	93.88%
4	WP_048321499.1; spore coat U domain-containing protein	81	91	11	MAVANTDGSGD	1.8801	Non-toxin	Non-allergen	-0.28	63.27%
		263	277	15	TTVWDSTNKQSGAGT	1.023	Non-toxin	Non-allergen	-0.97	61.22%
5	WP_033636744.1; TonB-dependent receptor	5	15	11	FAAQRHESVGN	0.8087	Non-toxin	Non-allergen	-0.80	97.96%
		45	55	11	AETKSNETYQD	1.6267	Non-toxin	Non-allergen	-2.10	100%
		233	243	11	DRQRRRSEADL	1.2989	Non-toxin	Non-allergen	-2.47	87.86%
		429	439	11	RLEREHRRRDG	1.6679	Non-toxin	Non-allergen	-2.98	87.86%

All data were analyzed using various on line server: 1, 2 = NCBI/UniProt; 3, 4, 5 = ABCPred, Bcepred, IEDB; 6 = VaxiJen 2.0; 7 = ToxinPred; 8 = AllerTOP v2.0; 9 = GRAVY ProtParam; 10 = IEDB.

the model was ranked on their C-scores values, which measure similarity between the query and template based on the significance of threading template alignment and the query coverage parameters. C-score values ranges between -5 and 2, and a higher value represents a model with a higher confidence and correct topology. SMV1 presented a Z-Score ranging from 0.64 to 2.42 and a C-Score of -2.41. SMV2 showed a Z-Score ranging from 0.65 to 2.39 and a C-Score of -2.41. SMV3 had a C-Score of -1.92 and a Z-Score ranging from 1.08 to 3.43. SMV4 exhibited a Z-Score of 1.06 to 5.61 and the highest C-Score, -1.34 (**Figure 3A**). In addition to C and Z score, I-TASSER predicted the TM-score, a metric for measuring the similarity of two protein structures, and the root mean square deviation (RMSD) of atomic positions. TM-score obtained in vaccines constructs ranged from 0.43 ± 0.14 to 0.55 ± 0.15. SMV4 had a TM-score more than 0.5, indicating a higher accuracy in topology. For all vaccines tested the RMSD ranged from 11.1 ± 4.6Å to 14.0 ± 3.9 Å (**Figures 3A, B**).

3D Structure Refinement and Validation

The 4 vaccine constructs 3D model were refined using the 3Drefine server. 3Drefine server provided five refined models with different parameters, including the 3D refined score, GDT-TS, GDTHA, RMSD, MolProbity, and RWPlus. Higher GDT-TS, GDT-HA, and RMSD values, and lower 3D refine Score, RWplus, and MolProbity values indicate a higher quality for the models. The models number 1 in all 4 vaccine constructs presented lowest MolProbity score, which ranged from 3.454 to 3.565 (**Figure 4A**). Therefore, these were validated by PROCHECK's Ramachandran plot, ERRAT and ProSA webserver. ERRAT score for 3D models of four vaccines were calculated as 88.601, 85.162, 79.607, and 84.751, respectively (**Figure 4A**). The ProSA Z-Score for SMV1, SMV2, SMV3 and SMV4 were -4.60, -4.42, -2.02 and -5.16 respectively, indicating models were within the range of scores typically found for the native proteins of similar size (**Figures 4A, B**). Ramachandran plot analysis showed 97.1%, 97.4%, and 97.6% residues in allowed region for vaccine SMV1, SMV3 and SMV4, respectively. The SMV2 vaccine had 98.1% of residues in the allowed regions (**Figure 4C**). These analyses authenticated the reliability and stability of the predicted structures.

Protein-Protein Docking

Docking analysis was performed between SMV1, SMV2, SMV3 and SMV4 vaccine constructs and TLR4-MD2 complex (PDB:3FXI), in order to find out the best constructed *S. marcescens* vaccine. SMV4 showed binding affinity -28.3 kcal/mol, a K_d of 1.1E-20 at 37°C, a global energy of -55.38, and an HB energy of -12.81 (**Figure 5A**). Since SMV4 showed superior results in the protein-protein docking study, it was considered as the best vaccine construct among the four constructed vaccines (**Figure 5B**).

Molecular Dynamics Simulation

The molecular dynamics simulation and normal mode analysis (NMA) of SMV-4-TLR4 docked complex is showed in **Figure 6A**. Deformability graphs of the complex illustrates the peaks in the graphs, having regions of the proteins with high deformability (**Figure 6B**). The B-Factor graphs of the complexes provide easy understanding and visualization of the comparison

TABLE 5 | Molecular docking of epitopes with HLA.

MHC Class I

No.	Protein ID, name	Epitope	Global Energy								
			HLA-A*0101 (PDB: 6AT9)	HLA-A*0201 (PDB: 3UTQ)	HLA-B*1501 (PDB: 1XR8)	HLA-B*3501 (PDB: 1ZSD)	HLA-B*3901 (PDB: 4O2E)	HLA-B*4403 (PDB: 1SYS)	HLA-B*5301 (PDB: 1A1M)	HLA-B*5801 (PDB: 5IM7)	Average
1	WP_041033700.1 D-alanyl-D-alanine carboxypeptidase/ endopeptidase	**TPFGAGWSW**	-54.89	-18.06	-34.65	-42.60	-13.15	-43.74	-38.83	-33.18	-34.89
		LEDRLVETL	-41.35	-22.48	-43.79	-24.36	-35.34	-16.97	-38.40	-23.62	-30.79
2	WP_141960268.1 Phospholipase C, phosphocholine-specific	**FTIPLPGDR**	-46.08	-24.55	-15.99	-24.14	-6.21	-15.41	-33.75	-23.74	-23.73
3	WP_048321499.1 spore coat U domain-containing protein	**SSNVNFPLY**	-56.28	-23.22	-32.65	-9.88	-19.00	-36.62	-37.51	-30.24	-30.68
4	WP_033636744.1 TonB-dependent receptor	**QTYGAKIAR**	-43.86	-4.69	-22.38	-19.36	-15.90	-25.60	-18.49	-26.75	-22.13
		SEYVWNYEL	-40.96	-17.05	-33.96	-25.68	-8.14	-15.25	-42.89	-39.22	-27.89
		YQFLKGWEL	-49.03	-18.24	-15.98	-8.29	-15.5	-25.71	-47.98	-35.74	-27.06

MHC Class II

No.	Protein ID, name	Epitope	Global Energy							
			HLA-DRB1*0101 (PDB: 2FSE)	HLA-DRB1*0301 (PDB: 1A6A)	HLA-DRB1*0401 (PDB: 2SEB)	HLA-DRB1*1501 (PDB: 1BX2)	HLA-DRB3*0101 (PDB: 2Q6W)	HLA-DRB3*0202 (PDB: 3C5J)	HLA-DRB5*0101 (PDB: 1H15)	Average
1	WP_041033700.1 D-alanyl-D-alanine carboxypeptidase/ endopeptidase	**WLLPAILALAGCSSS**	-89.74	-79.65	-74.83	-68.81	-65.01	-43.20	-72.52	-70.54
		PGARAGAPGRVSFYP	-74.58	-62.83	-62.02	-62.94	-41.19	-30.71	-64.83	-57.01
		LAVTFLKVSNNGYGE	-66.12	-73.03	-51.81	-54.69	-36.28	-30.34	-61.55	-53.40
		PLAFAIISNNYLVPG	-72.3	-57.61	-55.05	-62.76	-58.5	-47.77	-89.92	-63.42
2	WP_084827239.1 patatin-like phospholipase family protein	**SGASAGAIAALLVGL**	-58.55	-72.12	-64.58	-75.20	-59.65	-41.55	-64.48	-62.30
3	WP_141960268.1 Phospholipase C. phosphocholine-specific	**RQYRAASIQVGNPAR**	-61.17	-55.80	-47.44	-47.05	-13.96	-30.96	-69.12	-46.50
		EKRFQVHEPNISAWR	-38.13	-38.77	-45.12	-8.34	-16.93	-24.41	-27.34	-28.43
4	WP_048321499.1 spore coat U domain-containing protein	**SLNLLSLILISSNVN**	-88.21	-56.66	-52.15	-68.53	-29.65	-50.10	-89.29	-62.08
		LSLILISSNVNFPLY	-93.62	-65.33	-50.97	-82.72	-16.16	-46.28	-45.35	-57.20
5	WP_033636744.1 TonB-dependent receptor	**NVGANAFLSGTRPRL**	-65.95	-52.33	-55.04	-61.88	-20.96	-31.18	-58.32	-49.38
		NAFLSGTRPRLNLSL	-74.06	-48.43	-59.42	-37.86	-35.10	-31.70	-35.66	-46.03
		TDFNINRPTAYNIQY	-42.87	-44.67	-49.32	-32.67	-13.94	-34.32	-43.83	-37.37
		ADSRLHGLAGLRYFH	-62.54	-47.66	-53.30	-61.08	-24.56	-25.95	-58.13	-47.60
		RWDFELFGNLGLLKT	-45.56	-55.26	-56.56	-51.49	-16.14	-32.27	-63.07	-45.76
		ARAPAYTANMGAKYQ	-45.59	-44.37	-51.96	-44.44	-22.36	-29.58	-34.58	-38.98
		AKYQFLKGWELSSNV	-54.33	-61.70	-39.90	-59.14	-18.93	-25.68	-38.05	-42.53

3D structures were generated by the PEP-FOLD3 server. The docking was performed using PatchDock online tool and the results were refined by FireDock online server.

TABLE 6 | Characteristics of the constructed vaccines against *S. marcescens* strains.

Vaccine name/adjuvant	Sequence	Antigenicity (1, 2)	Allergenicity (3,4)	Amino acids length (5)	Mol. weight kDa (5)	pI (5)	Instability index (5)	Aliphatic index (5)	GRAVY (5)	SOLpro (6)
SMV1/(HBHA)	**EAAAK**MAENPNIDDLPAPLLAALGAADLALATVNDLIANLRERAEE TRAETRTRVEERRARLTKFQEDLPEQFIELRDKFTTEELRKAAEGY LEAATNRYNELVERGEAALQRLRSQTAFEDASARAEGYVDQAVELT QEALGTVASQTRAVGERAAKLVGIEL**EAAAK***AKFVAAWTLKAAA***G GGS**TPFGAGWSW**GGGS**LEDRLVETL**GGGS**SSNVNFPLY**GGGS**S EYVWNYEL**GGGS**YQFLKGWEL**GPGPG**WLLPAILALAGCSSS**GPG PG**AFAAPISALNYAFTP**GPGPG**PGARAGAPGRVSFYP**GPGPG**PLA FAIISNNYLVPG**GPGPG**SGASAGAIAALLVGL**GPGPG**RQYRAASIQ VGNPAR**GPGPG**SLNLLSLILISSNVN**GPGPG**LSLILISSNVNFPLY**G PGPG**NVGANAFLSGTRPRL**GPGPG**NAFLSGTRPRLNLSL**GPGP G**ADSRLHGLAGLRYFH**GPGPG**RWDFELFGNLGLLKT**KK**TGEQR GDTL**KK**SGDPTLHPDDL**KK**GRKTQGKGD**KK**QREVYSHRTTPRM **KK**SSQRINTRTLGLRLDS**KK**MAVANTDGSGD**KK**TTVWDSTNKQ SGAGT**KK**QPEVRLRPTG**KK**FAAQRHESVGN**KK**AETKSNETYQD **KK**DRQRRRSEADL**KK**RLEREHRRRDG**KK***AKFVAAWTLKAA A***GGGS**	Vaxijen: 1.0377 ANTIGENpro: 0.835	Non-allergen	668	70.335	9.91	33.33	72.46	-0.525	0.967
SMV2/(HBHA Conserved Sequence)	**EAAAK**MAENSNIDDIKAPLLAALGAADLALATVNELITNLRERAEE TRRSRVEESRARLTKLQEDLPEQLTELREKFTAEELRKAAEGYLEA ATSELVERGEAALERLRSQQSFEEVSARAEGYVDQAVELTQEALG TVASQVEGRAAKLVGIEL**EAAAK***AKFVAAWTLKAAA***GGGS**TPFG AGWSW**GGGS**LEDRLVETL**GGGS**SSNVNFPLY**GGGS**SEYVWNY EL**GGGS**YQFLKGWEL**GPGPG**WLLPAILALAGCSSS**GPGPG**AFA APISALNYAFTP**GPGPG**PGARAGAPGRVSFYP**GPGPG**PLAFAIISN NYLVPG**GPGPG**SGASAGAIAALLVGL**GPGPGR**QYRAASIQVGNP AR**GPGPG**SLNLLSLILISSNVN**GPGPG**LSLILISSNVNFPLY**GPGP G**NVGANAFLSGTRPRL**GPGPG**NAFLSGTRPRLNLSL**GPGPG**ADS RLHGLAGLRYFH**GPGPG**RWDFELFGNLGLLKT**KK**TGEQRGDTL **KK**SGDPTLHPDDL**KK**GRKTQGKGD**KK**QREVYSHRTTPRM**KK**S SQRINTRTLGLRLDS**KK**MAVANTDGSGD**KK**TTVWDSTNKQSGA GT**KK**QPEVRLRPTG**KK**FAAQRHESVGN**KK**AETKSNETYQD**KK**D RQRRRSEADL**KK**RLEREHRRRDG**KK***AKFVAAWTLKAAA***GGGS**	Vaxijen: 1.0449 ANTIGENpro: 0.851	Non-allergen	659	69.217	9.86	35.66	73.87	-0.510	0.974
SMV3/(β-Defensin)	**EAAAK**GIINTLQKYYCRVRGGRCAVLSCLPKEEQIGKCSTRGRKC CRRKK**EAAAK***AKFVAAWTLKAAA***GGGS**TPFGAGWSW**GGGS**LE DRLVETL**GGGS**SSNVNFPLY**GGGS**SEYVWNYEL**GGGS**YQFLKGW EL**GPGPG**WLLPAILALAGCSSS**GPGPG**AFAAPISALNYAFTP**GPG PG**PGARAGAPGRVSFYP**GPGPG**PLAFAIISNNYLVPG**GPGPG**SG ASAGAIAALLVGL**GPGPG**RQYRAASIQVGNPAR**GPGPG**SLNLLSL ILISSNVN**GPGPG**LSLILISSNVNFPLY**GPGPG**NVGANAFLSGTRPR L**GPGPG**NAFLSGTRPRLNLSL**GPGPG**ADSRLHGLAGLRYFH**GPG PG**RWDFELFGNLGLLKT**KK**TGEQRGDTL**KK**SGDPTLHPDDL**KK** GRKTQGKGD**KK**QREVYSHRTTPRM**KK**SSQRINTRTLGLRLDS**K K**MAVANTDGSGD**KK**TTVWDSTNKQSGAGT**KK**QPEVRLRPTG**K K**FAAQRHESVGN**KK**AETKSNETYQD**KK**DRQRRRSEADL**KK**RLE REHRRRDG**KK***AKFVAAWTLKAAA***GGGS**	Vaxijen: 1.1417 ANTIGENpro: 0.827	Non-allergen	554	57.867	10.36	31.21	66.68	-0.547	0.873
SMV4/(50s ribosomal L7/L12 protein)	**EAAAK**MAKLSTDELLDAFKEMTLLELSDFVKKFEETFEVTAAAPVA VAAAGAAPAGAAVEAAEEQSEFDVILEAAGDKKIGVIKVVREIVSGLG LKEAKDLVDGAPKPLLEKVAKEAADEAKAKLEAAGATVTVK**EAAAK**	Vaxijen: 1.0210	Non-allergen	639	66.147	9.85	28.01	74.19	-0.389	0.957

(Continued)

TABLE 6 | Continued

Vaccine name/adjuvant	Sequence	Antigenicity (1, 2)	Allergenicity (3,4)	Amino acids length (5)	Mol. weight kDa (5)	pI (5)	Instability index (5)	Aliphatic index (5)	GRAVY (5)	SOLpro (6)
	*AKFVAAWTLKAAA***GGGS**TPFGAGWSW**GGGS**LEDRLVETL**GGG** **S**SSNVNFPLY**GGGS**SEYVWNYEL**GGGS**YQFLKGWEL**GPGPG**W LLPAILALAGCSSS**GPGPG**AFAAPISALNYAFTP**GPGPG**PGARAG APGRVSFYP**GPGPG**PLAFAISNNYLVPG**GPGPG**SGASAGAIAALL VGL**GPGPG**RQYRAASIQVGNPAR**GPGPG**SLNLLSLILISSNVN**G** **PGPG**LSLILISSNVNFPLY**GPGPG**NVGANAFLSGTRPRL**GPGPG**N AFLSGTRPRLNLSL**GPGPG**ADSRLHGLAGLRYFH**GPGPG**RWDF ELFGNLGLLKT**KK**TGEQRGDTL**KK**SGDPTLHPDDL**KK**GRKTQGK GD**KK**QREVYSHRTTPRM**KK**SSQRINTRTLGLRLDS**KK**MAVANT DGSGD**KK**TTWWDSTNKQSGAGT**KK**QPEVRLRPTG**KK**FAAQRH ESVGN**KK**AETKSNETYQD**KK**DRQRRRSEADL**KK**RLEREHRRRD G**KK***AKFVAAWTLKAAA***GGGS**	ANTIGENpro: 0.818								

The bolded sequence represent the linker sequences. The Italic regions characterize PADRE sequences. 1, 2: VaxiJen 2.0, ANTIGENpro; 3, 4: AlgPred,AllerTOP v2.0; 5, 6: ProtParam Expasy; 6: SOLPro. SMV, Serratia marcescens vaccine.

between NMA and the PDB field of the docked complex (**Figure 6C**). The SMV4-TLR4 docked complex suggested that docked complex should be quite stable and should have relatively less chance of deformability (**Figures 6B, D**). In the variance graph (**Figure 6E**), red colored bars shows the individual variance and green colored bars represent the cumulative variance. Co-variance map of the complex showed a good amount of amino acid pairs in the correlated motion (**Figure 6F).** The elastic map (**Figure 6G**) of the complex describes the connection between atoms and darker gray regions shows stiffer regions.

Discontinuous B Cell Epitopes

Eight discontinuous B-cell epitopes with scores ranging from 0.713 to 0.872 were predicted by Ellipro online tool at IEDB. Shortest and longest discontinuous B cell epitope ranged from 3 to 63 residues long respectively (**Figure 7A**). The amino acid residues present in conformational epitopes, the number of residues, their scores, and the 3D representation of conformational B-cell epitopes are shown in **Figure 7A, B**.

Immune Simulation for Vaccine Efficacy

The vaccine primary response was characterized by high levels of IgM, while the secondary and tertiary responses were higher than the primary reaction and distinguished by greater IgM + IgG, IgG1 + IgG2, IgG1 antibodies level, and a rapid clearance in antigen concentration (**Figure 8A**). B cell activation were found high, particularly B isotype IgM and IgG1, with prominent memory cell development (**Figure 8B**). The cell population of TH (helper) and TC (cytotoxic) cells were also found high along with memory development (**Figures 8C, D**). A significant levels of T regulatory (Treg cells) cells was found in the exposure to the SMV4, and a Treg cell reduction few days after antigen exposure (**Figure 8E**). The vaccine can induce both IFN-γ and IL-2 with a suitable Simpson Index (D) (**Figure 8F**), which is a measure of diversity.

Codon Adaptation of the Final Vaccine Construct

Codons of SMV4 construct were adapted as per codon utilization of *E. coli* expression system, and JCAT server was used to optimize the SMV4 codons according to *E. coli* K12. The optimized SMV4 construct had a length of 1917 pb; an ideal range of GC content 54.17% (30–70%), showing good probable expression of the vaccine candidate in the *E. coli* K12; and CAI value 0.958 (0.8–1.0), indicating a high gene expression potential. In the next step, the SMV4 sequence was cloned between XhoI and NdeI restriction sites at the multiple cloning-site of the pET28a(+) vector. The clone had a total length of 7212 bp (**Figure 9**).

DISCUSSION

Vaccine development is one of greatest advances to prevent global morbidity and mortality; not only does it halt the onset of

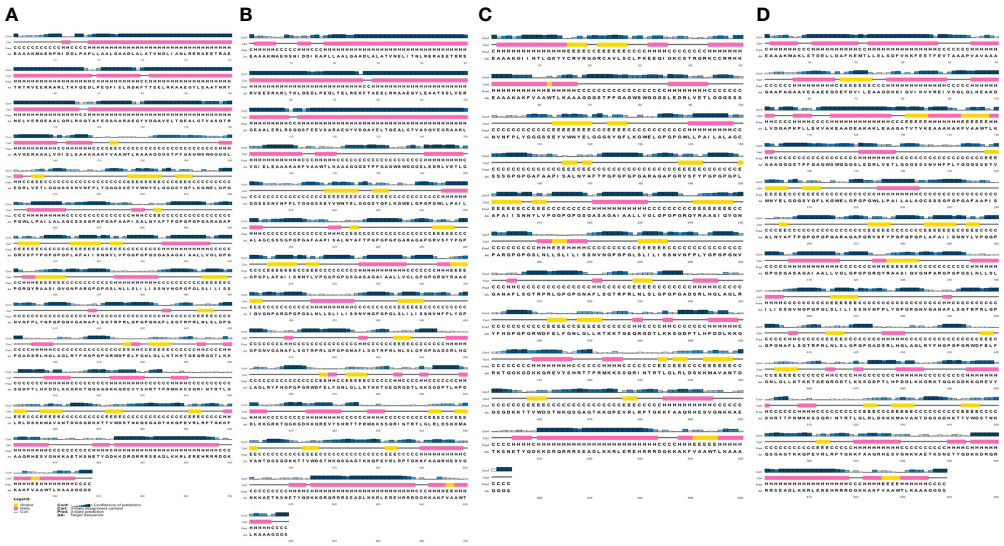

FIGURE 2 | Secondary structure prediction of the constructed *S. marcescens* vaccines using PESIPRED 4.0 server. **(A)** SMV1, **(B)** SMV2, **(C)** SMV3, **(D)** SMV4.

A

Vaccine name	C-Score	TM-Score	RMSD	Z-Score
SMV1	-2.41	0.43±0.14	14.0±3.9 Å	0.64 to 2.42
SMV2	-2.41	0.43±0.14	13.9±3.9 Å	0.65 to 2.39
SMV3	-1.92	0.48±0.15	12.2±4.4 Å	1.08 to 3.43
SMV4	-1.34	0.55±0.15	11.1±4.6 Å	1.06 to 5.61

B

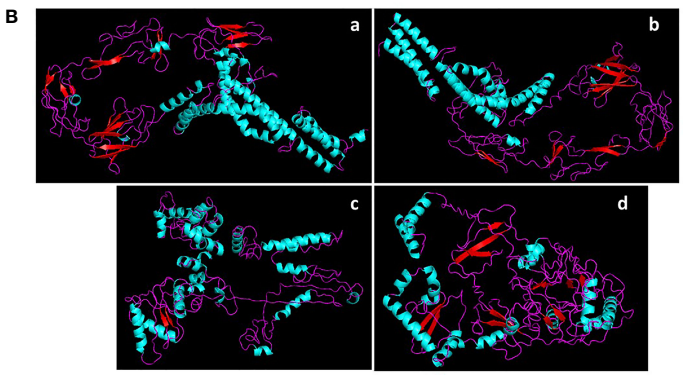

FIGURE 3 | **(A)** Characteristics and **(B)** 3D structure prediction of the constructed S. marcescens vaccines using I-TASSER server. a SMV1, b SMV2, c SMV3, d SMV4.

different diseases, but it also labels a gateway for its elimination while reducing toxicity (74). Vaccines that prevent infections caused by MDR bacterial species have a number of potential benefits. They can be used prophylactically reducing antibiotic use, emergence and spread of AMR, incidence of sensitive and resistant infections, severity life-threatening diseases, sequelae remaining after infection resolution, and health care costs (3, 4, 8).

The main strategy in the present study was to design and construct a multiepitope-based vaccine against *S. marcescens*, a gram-negative rod frequently involved in diverse nosocomial infections and with systemic mortality rate in immunocompromised and intensive care patients (11, 13).

Using computational subtractive analysis, we enrolled non-redundant proteome of *S. marcescens* to find proteins which had essential, virulent, and resistance profile and, at the same time, were non-homologous from human and gut flora, antigenic, had extracellular domain and/or were secreted. The antigens used in vaccines do not need to be virulence factors, although virulence gene products are often immunogenic and responsible for

A

Vaccine name	MolProbity Score	Quality Factor	Aminoacids in the allowed regions	Aminoacids in the disallowed regions	Pro-SA web Z-Score
SMV1	3.454	88.601	97.1%	2.9%	-4.60
SMV2	3.565	85.162	98.1%	1.9%	-4.42
SMV3	3.554	79.607	97.4%	2.6%	-2.02
SMV4	3.455	84.751	97.6%	2.4%	-5.16

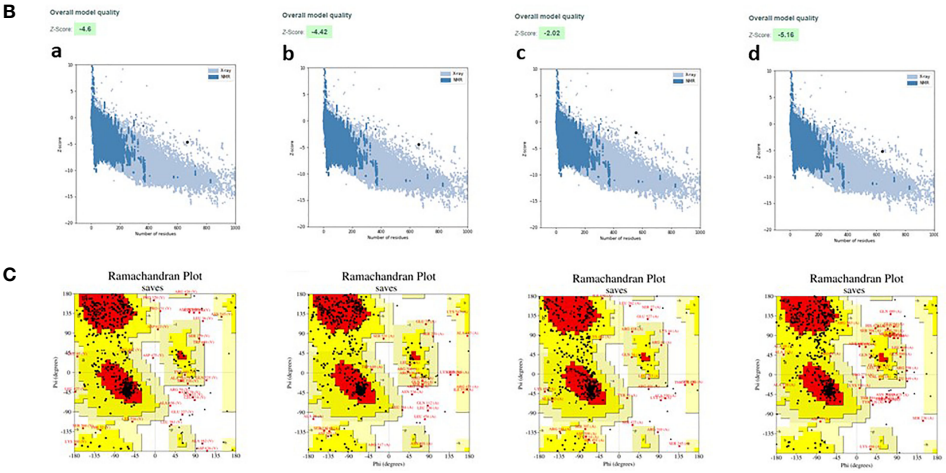

FIGURE 4 | Refinement and validations characteristics of *S. marcescens* vaccine constructs **(A)** ProSA Z-score (highlighted as a black dot) **(B)** is displayed in a plot that contains the Z-scores of all experimentally determined protein chains currently available in the Protein Data Bank; Ramachandran plotanalysis **(C)**, indicating residues in the favored regions (red), allowed regions (yellow), generously allowed regions (light yellow) and disallowed regions (white). a: SMV1, b: SMV2, c: SMV3, d: SMV4.

A

Vaccine name	Global Energy	HB	Binding Affinity ΔG kcal/mol	K_d (M) at 37.0º C
SMV1	-29.19	-4.15	-22.5	1.4E-16
SMV2	-13.40	-5.31	-26.2	3.4E-19
SMV3	-34.88	-0.21	-25.0	2.6E-18
SMV4	-55.38	-12.81	-28.3	1.1E-20

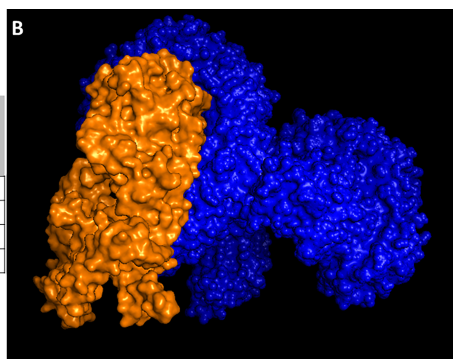

FIGURE 5 | **(A)** Docking analysis of vaccine constructs. **(B)** 3D representation of SMV4 vaccine construct and TLR4-MD2 complex. The SMV4 vaccine construct is represented by orange color, and TLR4-MD2 complex is in blue. The docking was carried out by ClusPro 2.0 and PatchDock servers, and refined and re-scored by the PRODIGY tool of HADDOCK server, and FireDock server, respectively.

acquired immunity that protects against the disease (106, 107). The exclusion of human and gut flora homologs is necessary to prevent autoimmunity in the host and to protect the symbiotic environment of the gut flora (44). Antigenicity of a protein means the potential to generate immune response against the organism to which the protein belongs, an essential factor to use the protein as a vaccine (82). Bacterial cell surface and secreted proteins are of interest for their potential as vaccine candidates because they are easily accessible and can significantly improve therapeutic target identification (39, 108).

After shortlisting, we identified five novel antigenic proteins of *S. marcescens* that were taken as suitable vaccine candidates. The first filtered antigenic protein was D-alanyl-D-alanine carboxypeptidase/endopeptidase, an essential membrane-associated protein and member of the penicillin binding proteins (PBPs), a family of proteins inhibited by ß-lactam

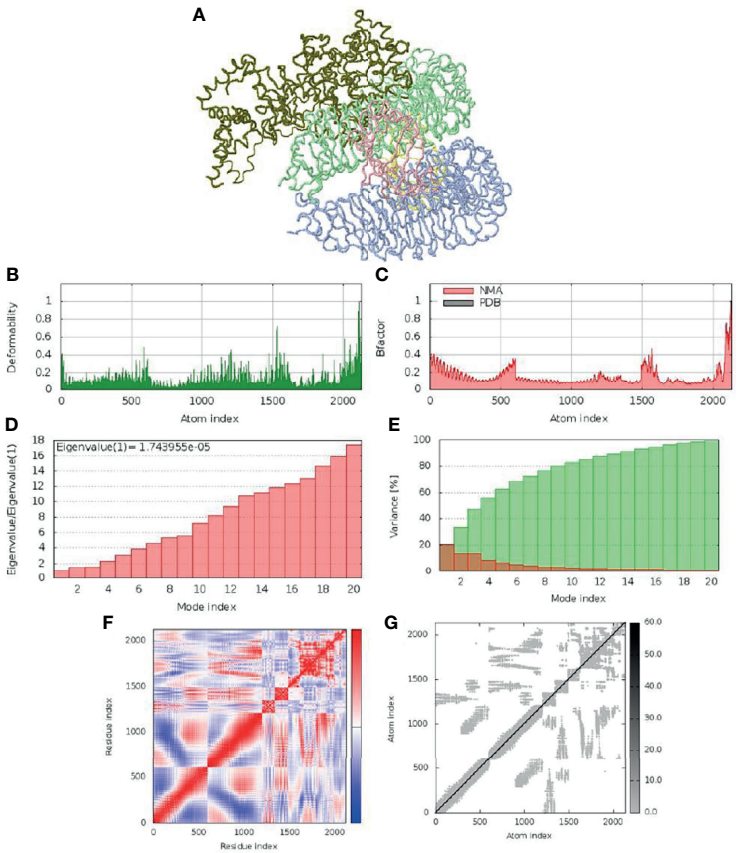

FIGURE 6 | Molecular dynamic simulation of SMV4 and TLR4 docked complex. **(A)** NMA mobility. **(B)** deformability. **(C)** B-Factor. **(D)** eigenvalue. **(E)** variance (red: individual variance, green: cumulative variance). **(F)** co-variance map (correlated in red, uncorrelated in white, and anti-correlated in blue). **(G)** elastic network.

A

ID	Residues	N. residues	Score
A	V:T548, V:N549, V:K550, V:Q551, V:S552, V:G553, V:A554, V:G555, V:T556, V:K557, V:R565, V:T586, V:K587, V:S588, V:N589, V:E590, V:T591, V:Y592, V:Q593, V:D594, V:K595, V:K596, V:D597, V:R598, V:R600, V:R602, V:S603, V:E604, V:A605, V:D606, V:L607, V:S608, V:K609, V:R610, V:L611, V:E612, V:R613, V:E614, V:H615, V:R616, V:R617, V:R618, V:D619, V:G620, V:K621, V:K622, V:A623, V:K624, V:F625, V:V626, V:A627, V:A628, V:W629, V:T630, V:L631, V:K632, V:A633, V:A634, V:A635, V:G636, V:G637, V:G638, V:S639	63	0.872
B	V:A49, V:A50, V:S51, V:A52, V:A53, V:P54, V:A55, V:S56, V:A57, V:A58, V:V59, V:E60, V:A61, V:A62, V:E63, V:E64, V:I71, V:L72, V:E73, V:A74, V:A75, V:G76, V:D77, V:K78, V:K79, V:I80, V:G81, V:V82, V:I83	29	0.841
C	V:A3, V:M6, V:A7, V:K8, V:L9, V:S10, V:T11, V:D12, V:E13, V:L14, V:L15, V:D16, V:A17, V:F18, V:K19, V:E20, V:M21, V:T22, V:L23, V:L24, V:E25, V:L26, V:S27, V:D28, V:F29, V:V30, V:K31, V:K32, V:F33, V:E35, V:T36, V:F37, V:K96, V:K99, V:D100, V:V102, V:D103, V:G104, V:A105, V:P106, V:K107, V:P108, V:L109, V:L110, V:E111, V:K112, V:K115, V:E116	48	0.825
D	V:G181, V:S183, V:S184, V:S185, V:N186, V:V187, V:N188, V:F189, V:P190, V:L191, V:Y192, V:G193, V:G194, V:G195	14	0.763
E	V:Y326, V:R327, V:L347	3	0.762
F	V:K150, V:A152, V:A153, V:G154, V:G155, V:G156, V:S157, V:T158, V:P159, V:F160, V:G161, V:W164, V:S165, V:W166, V:G167, V:G168, V:G169	17	0.739
G	V:E177, V:F245, V:A246, V:A247, V:P248, V:D249, V:S250, V:A251, V:L252, V:N253, V:Y254, V:A255, V:F256, V:T257, V:P258, V:G259, V:P260, V:G261, V:P262, V:G263, V:P264, V:G265, V:A266, V:R267, V:A268, V:G269, V:A270, V:P271, V:G272, V:R273, V:V274, V:S275, V:F276, V:Y277, V:P278, V:G279	36	0.722
h	V:G379, V:P380, V:G381, V:P382, V:G383, V:N384, V:V385, V:G386, V:S407, V:S408, V:G409, V:T410, V:R411, V:P412	14	0.713

B

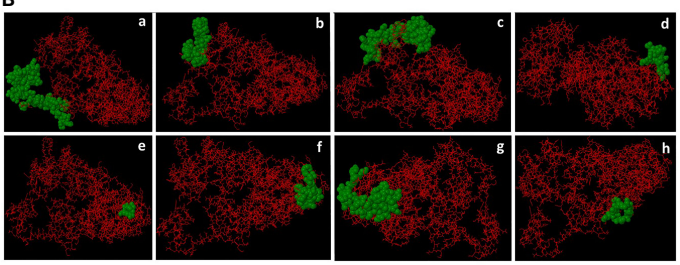

FIGURE 7 | Conformational B-cell epitopes prediction. **(A)** Amino acid residues present in conformational epitopes, the number of residues and their scores. ID: Identification of Epitopes. **(B) a-h**: 3D representation of conformational B-cell epitopes of protein. The predicted epitope residues are represented by green color, and the bulk of the polyprotein is represented in red color.

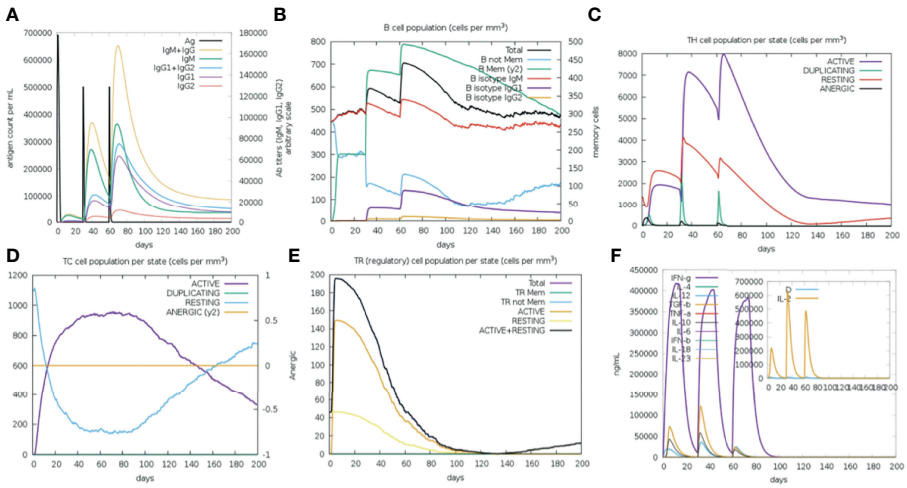

FIGURE 8 | Immune Simulation with the SMV4 vaccine candidate using C-ImmSim server. **(A)** Immunoglobulin production in response to antigen injections; specific subclasses are showed as colored peaks. **(B)** B-cell populations after the three injections. **(C)** Generations of T-helper cells. **(D)** Generation of T-cytotoxic cell populations. The resting state characterizes cells not presented to the antigen, the anergic state indicates tolerance of the T-cells to the antigen. **(E)** Levels of T regulatory cells. **(F)** The main plot shows cytokine levels after the injections. The insert plot shows IL-2 level with the Simpson index, **(D)** shown by the dotted line. **(D)** is a measure of diversity. Increase in **(D)** over time indicates emergence of different epitope-specific dominant clones of T-cells. The smaller the **(D)** value, the lower the diversity.

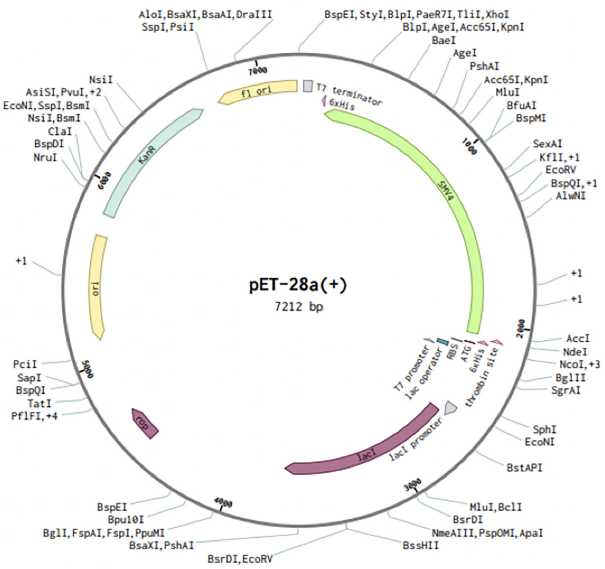

FIGURE 9 | *In silico* restriction cloning of the multi-epitope vaccine sequence (SMV4) into the pET28a (+) expression vector. Green arrow represents the vaccine's gene coding. The His-tag is located at the N-terminal end.

antibiotics involved in peptidoglycan synthesis and remodeling (109). The second identified protein was patatin-like phospholipase family protein, an essential protein that has been associated with infection in host cells and phagosome escape of various pathogenic bacteria (110, 111). The third selected protein was phospholipase C, phosphocholine-specific (PLC-PC). PLCs are considered an important virulence factor that can be exported out of the cytoplasm to their functional locality through Tat or Sec pathway (112). In bacteria, PLCs have been related in a wide variety of cellular function during infection, including membrane lysis, intracellular signaling, lipid metabolism and/or pathogenicity-associated activity (113, 114). The fourth protein was also antigenic and identified like spore coat U domain-containing protein, a domain found in a bacterial family of the secreted pili proteins involved in motility and biofilm formation (115, 116). The fifth and last selected protein was TonB-dependent receptor, a family of beta barrel proteins located in the outer membrane that is associated to progressive antibiotic resistance, transport ferric–siderophore complexes, vitamins, nickel complexes, and carbohydrates (117–121).

Prado et al. (122) introduced seven proteins that can be considered as vaccine candidates against *S. marcescens* using reverse vaccinology and subtractive genomic approaches. Prediction of these proteins was based on non-host homologous proteins, subcellular localization (putative surface exposed, secreted; membrane), transmembrane helix, Signal IP, MHC-I and MHC-II adhesion probability, and essentiality. Some features are required to select a potential vaccine candidate, such as sub-cellular localization; presence of a signal peptide; transmembrane domain; and antigenic epitopes. In addition to recognizing antigenic and virulence factors, one of the main strategies behind identifying potential vaccine candidates is predicting epitopes that are likely to bind to major histocompatibility complex molecules on the antigen presenting cells within the host (123). Therefore, mapping of T-cell derived B-cell epitopes for antigenic proteins is a critical step for designing vaccines (39).

In addition to selecting five novel proteins as potential vaccine candidates against *S. marcescens*, we used the sequence these proteins to predict MHC-class-I, MHC class-II allele and B cell epitopes that would be capable of inducing effective cellular and humoral immunity. All selected antigenic epitopes were antigenic, so they could induce antigenic response; non-allergenic in nature, thus not be able to induce any allergenic reaction; conserved epitopes, which is an important feature for designing a broad spectrum vaccine; hydrophilic in nature, hence able to interact with water molecules; and non-toxic. We selected the IFN-γ inducing Helper T cell (HTL) epitopes since this cytokine plays a significant role in innate and adaptive immune responses, stimulates macrophages and natural killer cells, and provides an enhanced response to MHC antigens (124).

In addition to *S. marcescens* having extracellular proliferation, this bacterium is able to invade nonphagocytic cells, such as epithelial cells (125–127). After internalization, *S. marcescens* can control the autophagic traffic, generating an appropriate niche for survival and replication inside the host cell (126, 128). Efficient protection against intracellular pathogens is dependent on the induction of cellular immunity, including pathogen-specific cytotoxic T cell responses (129, 130). CTL epitopes are essential for coherent vaccine design (131, 132). Thus, we analyzed the immunogenicity of CD8+ T cell epitopes to ensure that the epitope vaccine could effectively activate CD8 T cell-mediated immune response. In humans, MHC molecules are known as human leukocyte antigens (HLAs), as they are highly polymorphic; the frequency of expression of diverse HLA alleles varies in ethnically different populations (28). Thus, the HLA specificity of T-cell epitopes must be an important criterion for epitopes selection (133). We used the molecular docking simulation to delineate the interactions between the targeted T cell epitopes and their respective HLA alleles. In the docking results, five MHC class-I and twelve MHC class-II epitopes produced global energies. This means they had the capacity to bind specifically with their targets.

A total of 4 multi-epitope vaccines (SMV1, SMV2, SMV3, SMV4) were constructed using five MHC class-I, twelve MHC class-II and twelve B cell epitopes; four different adjuvants HBHA protein (*M. tuberculosis*), HBHA conserved sequence, beta-defensin, L7/L12 ribosomal protein (13) along with PADRE; and four different linkers EAAAK, GGGS, GPGPG and KK, which were used to bind the adjuvant, CTL, HTL and B-cell epitopes, respectively. Adjuvant HBHA and L7/L12 ribosomal protein are agonists to the TLR4/MD2 complex while beta-defensin adjuvant can act as an agonist to TLR1, TLR2, and TLR4 (134). The PADRE peptide induces CD4+ T-cells that increase efficacy and potency of peptide vaccine (135). It also overcomes the problems caused by highly polymorphic HLA alleles (88). Linkers ensure effective separation of individual epitopes *in vivo* (136). After that, several predicted physiochemical and immunological properties showed that all the vaccine constructions were safe with no possible allergenicity, had the capability to induce immunity with high antigenicity, were hydrophilic and soluble during its heterologous expression in *E. coli*, which is important to many biochemical and functional studies (137), and had negative charge. Neutral or negatively charged molecules are preferred and a balance between its hydrophobicity and hydrophilicity is important in designing vaccine candidates (138). The molecular weight range (57.867 to 70.335) and the high pI value range (9.85 to 10.36) indicated the efficacy and stability of the vaccine constructs (138). In addition to evaluating the vaccine efficacy, the epitopes separated by linker were sensitive to both degradation proteasomal and cathepsin specific peptidase activity. Hence, our data showed that the chosen linkers and their distribution were suitable, and the epitope produced could be presented in the host immune system, processed, and induced in the host humoral and cellular immune pathway (139).

Secondary and tertiary structures are necessary for designing a vaccine candidate (140). Analyses of the secondary structure of all vaccine constructs showed that all the proteins mainly contained amino acids in coil, and in alpha helix structure. Natively unfolded protein regions and α-helical coiled-coils peptides have been identified as important "structural antigen" forms (70). After 3D modeling, the structure of the vaccine was refined, displaying suitable characteristics and high-quality structure.

Molecular docking is a widely used computer simulation approach to explore the binding affinity with a protein, a strategic tool in vaccine design (141). Our findings showed stable interaction and high affinity between the vaccine construct SMV4 and the TLR-4/MD2 complex. The interaction between the TLR4 and adjuvant enhance the immune response, while TLR3, TLR4 and TLR9 agonists have been used to improve vaccines against HBV, influenza, malaria and anthrax (142). Furthermore, the physical movement and stabilization of the docked complex were assessed by molecular dynamics simulation, which confirmed that SMV4-TLR-4/MD2 complex has low deformability and remains stable in a biological environment.

Various discontinuous epitope residues were predicted from SMV4 vaccine sequence and revealed that they can interact with antibodies. The most B-cell epitopes are discontinuous epitopes composed of amino acid residues located on separate regions of the protein, joined together by the folding of the chain (143). Thus, analysis of discontinuous epitope in the final vaccine construct is essential (88).

Immune simulation through repeated exposure to the antigen showed a consistent increase in the generated immune responses. There was a notable generation of T- cells as well as memory B cells, which is required for immunity, supporting a humoral response (124). The levels of IFN-γ and IL-2 increased after the first injection and got induced following repeated exposures to the antigen, which also contribute to the subsequent immune response after vaccination (144). Interleukin induction is needed for any kind of cellular immunity and the vaccine satisfies this criterion having good induction potentiality (82). Considering the designed vaccine is constituted of sufficient B- and T-cell epitopes, the Simpson index (D) value suggests that the vaccine can stimulate a large and diverse immune response.

When designing a multi-epitope vaccine candidate, the efficacious cloning and expression in a suitable vector is a critical stage (145). Codon optimization is essential because the

genetic code's degeneracy allows most of the amino acids to be encoded by multiple codons (70). In this context, codon optimization and in silico cloning were performed, and our data showed expression and translation efficiency of the SMV4 vaccine using pET-28a (+).

In conclusion, our study identified a potential SMV4 vaccine candidate against *S. marcescens* with the ability to stimulate both cellular and humoral immunity. The epitopes used in the vaccine construct are antigenic, non-toxic, and non-allergic. The SMV4 vaccine candidate were highly immunogenic, safe, non-toxic, stable, and had high affinity and stability of binding to TLR4 innate immune receptor, which is vital in recognition and processing by the host immune system. Altogether, our findings have the potential to provide a novel strategy for the protection against multidrug resistant Gram negative infection. Future experimental validation of the proposed vaccine candidate is required to establish its potency as well efficacy and safety.

DATA AVAILABILITY STATEMENT

The original contributions presented in the study are included in the article/**Supplementary Material**, further inquiries can be directed to the corresponding author.

AUTHOR CONTRIBUTIONS

M-CP, MD, and FM conceived this project. M-CP, MD, FM, CF, and AC aided with edition of the manuscript and analyzed data. M-CP and MD wrote the manuscript. All authors contributed to the article and approved the submitted version.

FUNDING

This work was supported by Fundação de Amparo à Pesquisa do Estado de São Paulo-Brazil (FAPESP grants 2020/11964-4 and 2022/01316-0 to M-CP, and FAPESP grants 2018/20697-0 to AC). This study was partially financed by the Fundação de Amparo à Pesquisa do Estado de São Paulo-Brazil (FAPESP) as a fellowship to MD (FAPESP fellowship 2018/24213-7).

SUPPLEMENTARY MATERIAL

The Supplementary Material for this article can be found online at: https://www.frontiersin.org/articles/10.3389/fimmu.2022.768569/full#supplementary-material

Supplementary Data Sheet S2 | Core protein sequences.

Supplementary Data Sheet S3 | Essential protein sequences.

Supplementary Data Sheet S4 | Virulence protein sequences.

Supplementary Data Sheet S5 | Resistance protein sequences.

Supplementary Data Sheet S6 | Human non-homologue protein sequences.

Supplementary Data Sheet S7 | Gut flora non-homologue protein sequences.

Supplementary Data Sheet S8 | Cleavage sites predicted by NetChop 3.1.

REFERENCES

1. Prestinaci F, Pezzotti P, Pantosti A. Antimicrobial Resistance: A Global Multifaceted Phenomenon. *Pathog Global Health* (2015) 109:309–18. doi: 10.1179/2047773215Y.0000000030
2. Jansen KU, Anderson AS. The Role of Vaccines in Fighting Antimicrobial Resistance (AMR). *Hum Vaccines Immunother* (2018) 14:2142–9. doi: 10.1080/21645515.2018.1476814
3. Micoli F, Bagnoli F, Rappuoli R, Serruto D. The Role of Vaccines in Combatting Antimicrobial Resistance. *Nat Rev Microbiol* (2021) 19:287–302. doi: 10.1038/s41579-020-00506-3
4. Bloom DE, Black S, Salisbury D, Rappuoli R. Antimicrobial Resistance and the Role of Vaccines. *Proc Natl Acad Sci USA* (2018) 115:12868–71. doi: 10.1073/pnas.1717157115
5. AMR Review. *Antimicrobial Resistance: Tackling a Crisis for the Health and Wealth of Nations* (2014). Available at: https://amr-review.org/sites/default/files/AMR%20Review%20Paper%20-%20Tackling%20a%20crisis%20for%20the%20health%20and%20wealth%20of%20nations_1.pdf (Accessed February 6, 2022).
6. Murray CJ, Ikuta KS, Sharara F, Swetschinski L, Robles Aguilar G, Gray A, et al. Global Burden of Bacterial Antimicrobial Resistance in 2019: A Systematic Analysis. *Lancet* (2022) 399:629–55. doi: 10.1016/s0140-6736(21)02724-0
7. World Health Organization (WHO). *Antimicrobial Resistance* (2021). Available at: https://www.who.int/news-room/fact-sheets/detail/antimicrobial-resistance (Accessed February 6, 2022).
8. López-Siles M, Corral-Lugo A, McConnell MJ. Vaccines for Multidrug Resistant Gram Negative Bacteria: Lessons From the Past for Guiding Future Success. *FEMS Microbiol Rev* (2021) 45:fuaa054. doi: 10.1093/femsre/fuaa054
9. World Health Organization (WHO). *Global Priority List of Antibiotic-Resistant Bacteria to Guide Research, Discovery, and Development of New Antibiotics* (2017). Available at: https://www.who.int/medicines/publications/WHO-PPL-Short_Summary_25Feb-ET_NM_WHO.pdf?ua=1 (Accessed February 6, 2022).
10. Cristina ML, Sartini M, Spagnolo AM. Serratia Marcescens Infections in Neonatal Intensive Care Units (NICUs). *Int J Environ Res Public Health* (2019) 16:610. doi: 10.3390/ijerph16040610
11. Ferreira RL, Rezende GS, Damas MSF, Oliveira-Silva M, Pitondo-Silva A, Brito MCA, et al. Characterization of KPC-Producing Serratia Marcescens in an Intensive Care Unit of a Brazilian Tertiary Hospital. *Front Microbiol* (2020) 11:956. doi: 10.3389/fmicb.2020.00956
12. Kim B, Jeon YD, Kim JH, Kim JK, Ann HW, Choi H, et al. Risk Factors for Mortality in Patients With Serratia Marcescens Bacteremia. *Yonsei Med J* (2015) 56:348–54. doi: 10.3349/ymj.2015.56.2.348
13. Khanna A, Khanna M, Aggarwal A. Serratia Marcescens- A Rare Opportunistic Nosocomial Pathogen and Measures to Limit Its Spread in Hospitalized Patients. *J Clin Diagn Res* (2013) 7:243–6. doi: 10.7860/JCDR/2013/5010.2737
14. Engel HJ, Collignon PJ, Whiting PT, Kennedy KJ. Serratia Sp. Bacteremia in Canberra, Australia: A Population-Based Study Over 10 Years. *Eur J Clin Microbiol Infect Dis* (2009) 28:821–4. doi: 10.1007/s10096-009-0707-7
15. Field C, Allen JL, Friedman H. The Immune Response of Mice to Serratia Marcescens LPS or Intact Bacteria. *J Immunol (Baltimore Md : 1950)* (1970) 105:193–203.
16. Kreger AS, Lyerly DM, Hazlett LD, Berk RS. Immunization Against Experimental Pseudomonas Aeruginosa and Serratia Marcescens Keratitis.

Vaccination With Lipopolysaccharide Endotoxins and Proteases. *Invest Ophthalmol Visual Sci* (1986) 27:932–9.
17. Kumagai Y, Okada K, Sawae Y. The Effect of Humoral and Cell-Mediated Immunity in Resistance to Systemic Serratia Infection. *J Med Microbiol* (1992) 36:245–9. doi: 10.1099/00222615-36-4-245
18. Shi H, Zhu Y, Xu L, Liu Z, You Y, Meng Q, et al. Serratia Marcescens Vaccine in the Treatment of Malignant Pleural Effusion. *Zhonghua zhong liu za zhi [Chin J Oncol]* (2002) 24:188–90.
19. Woodward H. A Case of Infection in Man by the Bacterium Prodigiosum. *Lancet* (1913) 181:314–5. doi: 10.1016/S0140-6736(00)76133-2
20. Kleef R, Hager ED. Fever, Pyrogens and Cancer. In: *Hyperthermia in Cancer Treatment: A Primer*. Boston, MA: Springer US (2006). p. 276–337. doi: 10.1007/978-0-387-33441-7_21
21. Mahlen SD. Serratia Infections: From Military Experiments to Current Practice. *Clin Microbiol Rev* (2011) 24:755–91. doi: 10.1128/CMR.00017-11
22. Karbach J, Neumann A, Brand K, Wahle C, Siegel E, Maeurer M, et al. Phase I Clinical Trial of Mixed Bacterial Vaccine (Coley's Toxins) in Patients With NY-ESO-1 Expressing Cancers: Immunological Effects and Clinical Activity. *Clin Cancer Res* (2012) 18:5449–59. doi: 10.1158/1078-0432.CCR-12-1116
23. Kempin S, Cirrincione C, Straus DS. Improved Remission Rate and Duration in Nodular Non-Hodgkin Lymphoma (NNHL) With the Use of Mixed Bacterial Vaccine (MBV). *Proc Am Assoc Cancer Res* (1981) 22:514–4.
24. Kempin S, Cirrincione C, Myers J. Combined Modality Therapy of Advanced Nodular Lymphomas (NL): The Role of Nonspecific Immunotherapy (MBV) as an Important Determinant of Response and Survival. *Proc Am Soc Clin Oncol* (1983) 24:56.
25. Kölmel KF, Vehmeyer K, Göhring E, Kuhn B, Wieding JU. Treatment of Advanced Malignant Melanoma by a Pyrogenic Bacterial Lysate. A Pilot Study. *Onkologie* (1991) 14:411–7. doi: 10.1159/000217017
26. Tang ZY, Zhou HY, Zhao G, Chai LM, Zhou M, Lu JZ, et al. Preliminary Result of Mixed Bacterial Vaccine as Adjuvant Treatment of Hepatocellular Carcinoma. *Med Oncol Tumor Pharmacother* (1991) 8:23–8. doi: 10.1007/BF02988567
27. Vas HFH, Axelrod RS, Burns MM, Murasko D, Goonewardene M. Clinical Results and Immunologic Effects of a Mixed Bacterial Vaccine in Cancer Patients. *Med Oncol Tumor Pharmacother* (1993) 10:145–58. doi: 10.1007/BF02989663
28. Lata KS, Kumar S, Vaghasia V, Sharma P, Bhairappanvar SB, Soni S, et al. Exploring Leptospiral Proteomes to Identify Potential Candidates for Vaccine Design Against Leptospirosis Using an Immunoinformatics Approach. *Sci Rep* (2018) 8:1–15. doi: 10.1038/s41598-018-25281-3
29. Moxon R, Reche PA, Rappuoli R. Editorial: Reverse Vaccinology. *Front Immunol* (2019) 10:2776. doi: 10.3389/fimmu.2019.02776
30. Monterrubio-López GP, González-Y-Merchand JA, Ribas-Aparicio RM. Identification of Novel Potential Vaccine Candidates Against Tuberculosis Based on Reverse Vaccinology. *BioMed Res Int* (2015) 2015:11–4. doi: 10.1155/2015/483150
31. Naz A, Obaid A, Shahid F, Dar HA, Naz K, Ullah N, et al. *Reverse Vaccinology and Drug Target Identification Through Pan-Genomics*. London, GB: Elsevier Inc (2020) p. 317–33. doi: 10.1016/b978-0-12-817076-2.00016-0
32. Pizza M, Scarlato V, Masignani V, Giuliani MM, Aricò B, Comanducci M, et al. Identification of Vaccine Candidates Against Serogroup B Meningococcus by Whole-Genome Sequencing. *Science* (2000) 287:1816–20. doi: 10.1126/science.287.5459.1816
33. Rodrigues TCV, Jaiswal AK, De Sarom A, Oliveira LDC, Oliveira CJF, Ghosh P, et al. Reverse Vaccinology and Subtractive Genomics Reveal New Therapeutic Targets Against Mycoplasma Pneumoniae: A Causative Agent of Pneumonia. *R Soc Open Sci* (2019) 6:190907. doi: 10.1098/rsos.190907
34. Solanki V, Tiwari M, Tiwari V. Prioritization of Potential Vaccine Targets Using Comparative Proteomics and Designing of the Chimeric Multi-Epitope Vaccine Against Pseudomonas Aeruginosa. *Sci Rep* (2019) 9:1–19. doi: 10.1038/s41598-019-41496-4
35. Solanki V, Tiwari V. Subtractive Proteomics to Identify Novel Drug Targets and Reverse Vaccinology for the Development of Chimeric Vaccine Against Acinetobacter Baumannii. *Sci Rep* (2018) 8:1–19. doi: 10.1038/s41598-018-26689-7
36. Serruto D, Bottomley MJ, Ram S, Giuliani MM, Rappuoli R. The New Multicomponent Vaccine Against Meningococcal Serogroup B, 4cmenb: Immunological, Functional and Structural Characterization of the Antigens. *Vaccine* (2012) 30:B87–97. doi: 10.1016/j.vaccine.2012.01.033
37. Chaudhari NM, Gupta VK, Dutta C. BPGA-An Ultra-Fast Pan-Genome Analysis Pipeline. *Sci Rep* (2016) 6:1–10. doi: 10.1038/srep24373
38. Luo H, Lin Y, Gao F, Zhang CT, Zhang R. DEG 10, an Update of the Database of Essential Genes That Includes Both Protein-Coding Genes and Noncoding Genomic Elements. *Nucleic Acids Res* (2014) 42:574–80. doi: 10.1093/nar/gkt1131
39. Hassan A, Naz A, Obaid A, Paracha RZ, Naz K, Awan FM, et al. Pangenome and Immuno-Proteomics Analysis of Acinetobacter Baumannii Strains Revealed the Core Peptide Vaccine Targets. *BMC Genomics* (2016) 17:732. doi: 10.1186/s12864-016-2951-4
40. Rashid MI, Rehman S, Ali A, Andleeb S. Fishing for Vaccines Against Vibrio Cholerae Using *In Silico* Pan-Proteomic Reverse Vaccinology Approach. *PeerJ* (2019) 7:e6223. doi: 10.7717/peerj.6223
41. Asad Y, Ahmad S, Rungrotmongkol T, Ranaghan KE, Azam SS. Immuno-Informatics Driven Proteome-Wide Investigation Revealed Novel Peptide-Based Vaccine Targets Against Emerging Multiple Drug Resistant Providencia Stuartii. *J Mol Graphics Modell* (2018) 80:238–50. doi: 10.1016/j.jmgm.2018.01.010
42. Vilela Rodrigues TC, Jaiswal AK, de Sarom A, de Castro Oliveira L, Freire Oliveira CJ, Ghosh P, et al. Reverse Vaccinology and Subtractive Genomics Reveal New Therapeutic Targets Against Mycoplasma Pneumoniae : A Causative Agent of Pneumonia. *R Soc Open Sci* (2019) 6:190907. doi: 10.1098/rsos.190907
43. Peng C, Lin Y, Luo H, Gao F. A Comprehensive Overview of Online Resources to Identify and Predict Bacterial Essential Genes. *Front Microbiol* (2017) 8:2331. doi: 10.3389/fmicb.2017.02331
44. Naz K, Naz A, Ashraf ST, Rizwan M, Ahmad J, Baumbach J, et al. PanRV: Pangenome-Reverse Vaccinology Approach for Identifications of Potential Vaccine Candidates in Microbial Pangenome. *BMC Bioinf* (2019) 20:1–11. doi: 10.1186/s12859-019-2713-9
45. Chen L, Xiong Z, Sun L, Yang J, Jin Q. VFDB 2012 Update: Toward the Genetic Diversity and Molecular Evolution of Bacterial Virulence Factors. *Nucleic Acids Res* (2012) 40:641–5. doi: 10.1093/nar/gkr989
46. Zhou CE, Smith J, Lam M, Zemla A, Dyer MD, Slezak T. MvirDB - A Microbial Database of Protein Toxins, Virulence Factors and Antibiotic Resistance Genes for Bio-Defence Applications. *Nucleic Acids Res* (2007) 35:391–4. doi: 10.1093/nar/gkl791
47. Gupta SK, Padmanabhan BR, Diene SM, Lopez-Rojas R, Kempf M, Landraud L, et al. ARG-Annot, a New Bioinformatic Tool to Discover Antibiotic Resistance Genes in Bacterial Genomes. *Antimicrob Agents Chemother* (2014) 58:212–20. doi: 10.1128/AAC.01310-13
48. Alcock BP, Raphenya AR, Lau TTY, Tsang KK, Bouchard M, Edalatmand A, et al. CARD 2020: Antibiotic Resistome Surveillance With the Comprehensive Antibiotic Resistance Database. *Nucleic Acids Res* (2020) 48:D517–25. doi: 10.1093/nar/gkz935
49. Jadhav A, Shanmugham B, Rajendiran A, Pan A. Unraveling Novel Broad-Spectrum Antibacterial Targets in Food and Waterborne Pathogens Using Comparative Genomics and Protein Interaction Network Analysis. *Infect Genet Evol* (2014) 27:300–8. doi: 10.1016/j.meegid.2014.08.007
50. Yu NY, Wagner JR, Laird MR, Melli G, Rey S, Lo R, et al. PSORTb 3.0: Improved Protein Subcellular Localization Prediction With Refined Localization Subcategories and Predictive Capabilities for All Prokaryotes. *Bioinformatics* (2010) 26:1608–15. doi: 10.1093/bioinformatics/btq249
51. Yu C-S, Lin C-J, Hwang J-K. Predicting Subcellular Localization of Proteins for Gram-Negative Bacteria by Support Vector Machines Based on N -Peptide Compositions. *Protein Sci* (2004) 13:1402–6. doi: 10.1110/ps.03479604
52. Wilkins MR, Gasteiger E, Bairoch A, Sanchez JC, Williams KL, Appel RD, et al. Protein Identification and Analysis Tools in the ExPASy Server. *Methods Mol Biol (Clifton NJ)* (1999) 112:531–52. doi: 10.1385/1-59259-584-7:531
53. Doytchinova IA, Flower DR. VaxiJen: A Server for Prediction of Protective Antigens, Tumour Antigens and Subunit Vaccines. *BMC Bioinf* (2007) 8:1–7. doi: 10.1186/1471-2105-8-4

54. Magnan CN, Zeller M, Kayala MA, Vigil A, Randall A, Felgner PL, et al. High-Throughput Prediction of Protein Antigenicity Using Protein Microarray Data. *Bioinformatics* (2010) 26:2936–43. doi: 10.1093/bioinformatics/btq551
55. Krogh A, Larsson B, Von Heijne G, Sonnhammer ELL. Predicting Transmembrane Protein Topology With a Hidden Markov Model: Application to Complete Genomes. *J Mol Biol* (2001) 305:567–80. doi: 10.1006/jmbi.2000.4315
56. Almagro Armenteros JJ, Tsirigos KD, Sønderby CK, Petersen TN, Winther O, Brunak S, et al. SignalP 5.0 Improves Signal Peptide Predictions Using Deep Neural Networks. *Nat Biotechnol* (2019) 37:420–3. doi: 10.1038/s41587-019-0036-z
57. Mitchell AL, Attwood TK, Babbitt PC, Blum M, Bork P, Bridge A, et al. InterPro in 2019: Improving Coverage, Classification and Access to Protein Sequence Annotations. *Nucleic Acids Res* (2019) 47:D351–60. doi: 10.1093/nar/gky1100
58. Paul S, Sidney J, Sette A, Peters B. TepiTool: A Pipeline for Computational Prediction of T Cell Epitope Candidates. *Curr Protoc Immunol* (2016) 114:18.19.1–18.19.24. doi: 10.1002/cpim.12
59. Fleri W, Paul S, Dhanda SK, Mahajan S, Xu X, Peters B, et al. The Immune Epitope Database and Analysis Resource in Epitope Discovery and Synthetic Vaccine Design. *Front Immunol* (2017) 8:278. doi: 10.3389/fimmu.2017.00278
60. Kolaskar AS, Tongaonkar PC. A Semi-Empirical Method for Prediction of Antigenic Determinants on Protein Antigens. *FEBS Lett* (1990) 276:172–4. doi: 10.1016/0014-5793(90)80535-Q
61. Emini EA, Hughes JV, Perlow DS, Boger J. Induction of Hepatitis A Virus-Neutralizing Antibody by a Virus-Specific Synthetic Peptide. *J Virol* (1985) 55:836–9. doi: 10.1128/jvi.55.3.836-839.1985
62. Larsen JEP, Lund O, Nielsen M. Improved Method for Predicting Linear B-Cell Epitopes. *Immunome Res* (2006) 2:2. doi: 10.1186/1745-7580-2-2
63. Jespersen MC, Peters B, Nielsen M, Marcatili P. BepiPred-2.0: Improving Sequence-Based B-Cell Epitope Prediction Using Conformational Epitopes. *Nucleic Acids Res* (2017) 45:W24–9. doi: 10.1093/nar/gkx346
64. Calis JJA, Maybeno M, Greenbaum JA, Weiskopf D, De Silva AD, Sette A, et al. Properties of MHC Class I Presented Peptides That Enhance Immunogenicity. *PloS Comput Biol* (2013) 9:e1003266. doi: 10.1371/journal.pcbi.1003266
65. Gupta S, Kapoor P, Chaudhary K, Gautam A, Kumar R, Raghava GPS. In Silico Approach for Predicting Toxicity of Peptides and Proteins. *PloS One* (2013) 8:e73957. doi: 10.1371/journal.pone.0073957
66. Dimitrov I, Bangov I, Flower DR, Doytchinova I. AllerTOP V.2 - A Server for *In Silico* Prediction of Allergens. *J Mol Model* (2014) 20:2278. doi: 10.1007/s00894-014-2278-5
67. Ullah MA, Sarkar B, Islam SS. Exploiting the Reverse Vaccinology Approach to Design Novel Subunit Vaccines Against Ebola Virus. *Immunobiology* (2020) 225:151949. doi: 10.1016/j.imbio.2020.151949
68. Dash R, Das R, Junaid M, Akash MFC, Islam A, Hosen SMZ. *In Silico*-Based Vaccine Design Against Ebola Virus Glycoprotein. *Adv Appl Bioinf Chem* (2017) 10:11–28. doi: 10.2147/AABC.S115859
69. Dhanda SK, Vir P, Raghava GPS. Designing of Interferon-Gamma Inducing MHC Class-II Binders. *Biol Direct* (2013) 8:1–15. doi: 10.1186/1745-6150-8-30
70. Bibi S, Ullah I, Zhu B, Adnan M, Liaqat R, Kong WB, et al. In Silico Analysis of Epitope-Based Vaccine Candidate Against Tuberculosis Using Reverse Vaccinology. *Sci Rep* (2021) 11:1–16. doi: 10.1038/s41598-020-80899-6
71. Shey RA, Ghogomu SM, Shintouo CM, Nkemngo FN, Nebangwa DN, Esoh K, et al. Computational Design and Preliminary Serological Analysis of a Novel Multi-Epitope Vaccine Candidate Against Onchocerciasis and Related Filarial Diseases. *Pathogens* (2021) 10:99. doi: 10.3390/pathogens10020099
72. Mahmud S, Rafi M, Paul GK, Promi MM, Shimu M, Biswas S, et al. Designing a Multi-Epitope Vaccine Candidate to Combat MERS-CoV by Employing an Immunoinformatics Approach. *Sci Rep* (2021) 11:15431. doi: 10.1038/s41598-021-92176-1
73. Behbahani M. In Silico Design of Novel Multi-Epitope Recombinant Vaccine Based on Coronavirus Surface Glycoprotein. *bioRxiv* (2020). doi: 10.1101/2020.03.10.985499
74. McGuffin LJ, Bryson K, Jones DT. The PSIPRED Protein Structure Prediction Server. *Bioinformatics* (2000) 16:404–5. doi: 10.1093/bioinformatics/16.4.404
75. Lamiable A, Thévenet P, Rey J, Vavrusa M, Derreumaux P, Tufféry P. PEP-FOLD3: Faster De Novo Structure Prediction for Linear Peptides in Solution and in Complex. *Nucleic Acids Res* (2016) 44:W449–54. doi: 10.1093/nar/gkw329
76. Sarkar B, Ullah MA, Araf Y, Islam NN, Zohora US. Immunoinformatics-Guided Designing and in Silico Analysis of Epitope-Based Polyvalent Vaccines Against Multiple Strains of Human Coronavirus (HCoV). *Expert Rev Vaccines* (2021) 00:1–21. doi: 10.1080/14760584.2021.1874925
77. Lee SJ, Shin SJ, Lee MH, Lee MG, Kang TH, Park WS, et al. A Potential Protein Adjuvant Derived From Mycobacterium Tuberculosis Rv0652 Enhances Dendritic Cells-Based Tumor Immunotherapy. *PloS One* (2014) 9:1–11. doi: 10.1371/journal.pone.0104351
78. Mei H-F, Jin X-B, Zhu J-Y, Zeng A-H, Wu Q, Lu X-M, et al. Defensin 2 as an Adjuvant Promotes Anti-Melanoma Immune Responses and Inhibits the Growth of Implanted Murine Melanoma *In Vivo*. *PloS One* (2012) 7:e31328. doi: 10.1371/journal.pone.0031328
79. Sarkar B, Ullah M. Designing Novel Subunit Vaccines Against Herpes Simplex Virus-1 Using Reverse Vaccinology Approach. *bioRxiv* (2020). doi: 10.1101/2020.01.10.901678
80. Ali M, Pandey RK, Khatoon N, Narula A, Mishra A, Prajapati VK. Exploring Dengue Genome to Construct a Multi-Epitope Based Subunit Vaccine by Utilizing Immunoinformatics Approach to Battle Against Dengue Infection. *Sci Rep* (2017) 7:1–13. doi: 10.1038/s41598-017-09199-w
81. Magnan CN, Randall A, Baldi P. SOLpro: Accurate Sequence-Based Prediction of Protein Solubility. *Bioinformatics* (2009) 25:2200–7. doi: 10.1093/bioinformatics/btp386
82. Chaudhuri D, Datta J, Majumder S, Giri K. In Silico Designing of Peptide Based Vaccine for Hepatitis Viruses Using Reverse Vaccinology Approach. *Infect Genet Evol* (2020) 84:104388. doi: 10.1016/j.meegid.2020.104388
83. Verspurten J, Gevaert K, Declercq W, Vandenabeele P. SitePredicting the Cleavage of Proteinase Substrates. *Trends Biochem Sci* (2009) 34:319–23. doi: 10.1016/j.tibs.2009.04.001
84. Buchan DWA, Jones DT. The PSIPRED Protein Analysis Workbench: 20 Years on. *Nucleic Acids Res* (2019) 47:W402–7. doi: 10.1093/nar/gkz297
85. Shuid AN, Kempster R, Mcguffin LJ. ReFOLD: A Server for the Refinement of 3D Protein Models Guided by Accurate Quality Estimates. *Nucleic Acids Res* (2017) 45:W422–8. doi: 10.1093/nar/gkx249
86. Kalisman N, Levi A, Maximova T, Reshef D, Zafriri-Lynn S, Gleyzer Y, et al. MESHI: A New Library of Java Classes for Molecular Modeling. *Bioinformatics* (2005) 21:3931–2. doi: 10.1093/bioinformatics/bti630
87. Laskowski RA, Hutchinson EG, Michie AD, Wallace AC, Jones ML, Thornton JM. PDBsum: A Web-Based Database of Summaries and Analyses of All PDB Structures. *Trends Biochem Sci* (1997) 22:488–90. doi: 10.1016/S0968-0004(97)01140-7
88. Khan MT, Islam R, Jerin TJ, Mahmud A, Khatun S, Kobir A, et al. Immunoinformatics and Molecular Dynamics Approaches: Next Generation Vaccine Design Against West Nile Virus. *PloS One* (2021) 16:1–27. doi: 10.1371/journal.pone.0253393
89. Wiederstein M, Sippl MJ. ProSA-Web: Interactive Web Service for the Recognition of Errors in Three-Dimensional Structures of Proteins. *Nucleic Acids Res* (2007) 35:407–10. doi: 10.1093/nar/gkm290
90. Sanami S, Azadegan-Dehkordi F, Rafieian-Kopaei M, Salehi M, Ghasemi-Dehnoo M, Mahooti M, et al. Design of a Multi-Epitope Vaccine Against Cervical Cancer Using Immunoinformatics Approaches. *Sci Rep* (2021) 11:1–15. doi: 10.1038/s41598-021-91997-4
91. Colovos C, Yeates TO. Verification of Protein Structures: Patterns of Nonbonded Atomic Interactions. *Protein Sci* (1993) 2:1511–9. doi: 10.1002/pro.5560020916
92. Khatoon N, Pandey RK, Prajapati VK. Exploring Leishmania Secretory Proteins to Design B and T Cell Multi-Epitope Subunit Vaccine Using Immunoinformatics Approach. *Sci Rep* (2017) 7:1–12. doi: 10.1038/s41598-017-08842-w
93. Kozakov D, Hall DR, Xia B, Porter KA, Padhorny D, Yueh C, et al. The ClusPro Web Server for Protein-Protein Docking. *Nat Protoc* (2017) 12:255–78. doi: 10.1038/nprot.2016.169

94. Sarkar B, Ullah MA, Araf Y. A Systematic and Reverse Vaccinology Approach to Design Novel Subunit Vaccines Against Dengue Virus Type-1 (DENV-1) and Human Papillomavirus-16 (HPV-16). *Inf Med Unlocked* (2020) 19:100343. doi: 10.1016/j.imu.2020.100343
95. Xue LC, Rodrigues JP, Kastritis PL, Bonvin AM, Vangone A. PRODIGY: A Web Server for Predicting the Binding Affinity of Protein-Protein Complexes. *Bioinformatics* (2016) 32:3676–8. doi: 10.1093/bioinformatics/btw514
96. López-Blanco JR, Aliaga JI, Quintana-Ortí ES, Chacón P. IMODS: Internal Coordinates Normal Mode Analysis Server. *Nucleic Acids Res* (2014) 42:271–6. doi: 10.1093/nar/gku339
97. Islam R, Parvez MSA, Anwar S, Hosen MJ. Delineating Blueprint of an Epitope-Based Peptide Vaccine Against the Multiple Serovars of Dengue Virus: A Hierarchical Reverse Vaccinology Approach. *Inf Med Unlocked* (2020) 20:100430. doi: 10.1016/j.imu.2020.100430
98. Ponomarenko J, Bui HH, Li W, Fusseder N, Bourne PE, Sette A, et al. ElliPro: A New Structure-Based Tool for the Prediction of Antibody Epitopes. *BMC Bioinf* (2008) 9:1–8. doi: 10.1186/1471-2105-9-514
99. Taylor WR, Thornton JM, Turnell WG. An Ellipsoidal Approximation of Protein Shape. *J Mol Graphics* (1983) 1:30–8. doi: 10.1016/0263-7855(83)80001-0
100. Thornton JM, Edwards MS, Taylor WR, Barlow DJ. Location of "Continuous" Antigenic Determinants in the Protruding Regions of Proteins. *EMBO J* (1986) 5:409–13. doi: 10.1002/j.1460-2075.1986.tb04226.x
101. Sanches RCO, Tiwari S, Ferreira LCG, Oliveira FM, Lopes MD, Passos MJF, et al. Immunoinformatics Design of Multi-Epitope Peptide-Based Vaccine Against Schistosoma Mansoni Using Transmembrane Proteins as a Target. *Front Immunol* (2021) 12:621706. doi: 10.3389/fimmu.2021.621706
102. Rapin N, Lund O, Bernaschi M, Castiglione F. Computational Immunology Meets Bioinformatics: The Use of Prediction Tools for Molecular Binding in the Simulation of the Immune System. *PloS One* (2010) 5:e9862. doi: 10.1371/journal.pone.0009862
103. Qamar MTU, Shokat Z, Muneer I, Ashfaq UA, Javed H, Anwar F, et al. Multiepitope-Based Subunit Vaccine Design and Evaluation Against Respiratory Syncytial Virus Using Reverse Vaccinology Approach. *Vaccines* (2020) 8:1–27. doi: 10.3390/vaccines8020288
104. Grote A, Hiller K, Scheer M, Münch R, Nörtemann B, Hempel DC, et al. JCat: A Novel Tool to Adapt Codon Usage of a Target Gene to Its Potential Expression Host. *Nucleic Acids Res* (2005) 33:526–31. doi: 10.1093/nar/gki376
105. Morla S, Makhija A, Kumar S. Synonymous Codon Usage Pattern in Glycoprotein Gene of Rabies Virus. *Gene* (2016) 584:1–6. doi: 10.1016/j.gene.2016.02.047
106. Delany I, Rappuoli R, Seib KL. Vaccines, Reverse Vaccinology, and Bacterial Pathogenesis. *Cold Spring Harbor Perspect Med* (2013) 3:a012476. doi: 10.1101/cshperspect.a012476
107. Wassenaar TM, Gaastra W. Bacterial Virulence: Can We Draw the Line? *FEMS Microbiol Lett* (2001) 201:1–7. doi: 10.1016/S0378-1097(01)00241-5
108. Shanmugham B, Pan A. Identification and Characterization of Potential Therapeutic Candidates in Emerging Human Pathogen Mycobacterium Abscessus: A Novel Hierarchical *In Silico* Approach. *PloS One* (2013) 8:e59126. doi: 10.1371/journal.pone.0059126
109. Rioseras B, Yagüe P, López-Garciá MT, Gonzalez-Quinõnez N, Binda E, Marinelli F, et al. Characterization of SCO4439, a D-Alanyl-D-Alanine Carboxypeptidase Involved in Spore Cell Wall Maturation, Resistance, and Germination in Streptomyces Coelicolor. *Sci Rep* (2016) 6:1–15. doi: 10.1038/srep21659
110. Cui Z, Dang G, Song N, Cui Y, Li Z, Zang X, et al. Rv3091, An Extracellular Patatin-Like Phospholipase in Mycobacterium Tuberculosis, Prolongs Intracellular Survival of Recombinant Mycolicibacterium Smegmatis by Mediating Phagosomal Escape. *Front Microbiol* (2020) 11:532371. doi: 10.3389/fmicb.2020.532371
111. Gaspar AH, Machner MP. VipD is a Rab5-Activated Phospholipase A1 That Protects Legionella Pneumophila From Endosomal Fusion. *Proc Natl Acad Sci USA* (2014) 111:4560–5. doi: 10.1073/pnas.1316376111
112. Sinha AK, Dutta A, Chandravanshi M, Kanaujia SP. An Insight Into Bacterial Phospholipase C Classification and Their Translocation Through Tat and Sec Pathways: A Data Mining Study. *Meta Gene* (2019) 20:100547. doi: 10.1016/j.mgene.2019.100547
113. Dedieu L, Serveau-Avesque C, Kremer L, Canaan S. Mycobacterial Lipolytic Enzymes: A Gold Mine for Tuberculosis Research. *Biochimie* (2013) 95:66–73. doi: 10.1016/j.biochi.2012.07.008
114. Schmiel DH, Miller VL. Bacterial Phospholipases and Pathogenesis. *Microbes Infect* (1999) 1:1103–12. doi: 10.1016/S1286-4579(99)00205-1
115. Tomaras AP, Dorsey CW, Edelmann RE, Actis LA. Attachment to and Biofilm Formation on Abiotic Surfaces by Acinetobacter Baumannii: Involvement of a Novel Chaperone-Usher Pili Assembly System. *Microbiology* (2003) 149:3473–84. doi: 10.1099/mic.0.26541-0
116. Gollop R, Inouye M, Inouye S. Protein U, a Late-Developmental Spore Coat Protein of Myxococcus Xanthus, Is a Secretory Protein. *J Bacteriol* (1991) 173:3597–600. doi: 10.1128/jb.173.11.3597-3600.1991
117. Li W, Zhao Y, Yu J, Lin L, Ramanathan S, Wang G, et al. TonB-Dependent Receptors Affect the Spontaneous Oxytetracycline Resistance Evolution in Aeromonas Hydrophila. *J Proteome Res* (2021) 20:154–63. doi: 10.1021/acs.jproteome.9b00708
118. Zhang Z, Jiang S, Liu Y, Sun Y, Yu P, Gong Q, et al. Identification of Irea, 0007, 0008, and 2235 as TonB-Dependent Receptors in the Avian Pathogenic Escherichia Coli Strain DE205B. *Vet Res* (2020) 51:1–10. doi: 10.1186/s13567-020-0734-z
119. Gómez-Santos N, Glatter T, Koebnik R, Świątek-Połatyńska MA, Søgaard-Andersen L. A TonB-Dependent Transporter Is Required for Secretion of Protease PopC Across the Bacterial Outer Membrane. *Nat Commun* (2019) 10:1360. doi: 10.1038/s41467-019-09366-9
120. Schalk IJ, Mislin GLA, Brillet K. *Structure, Function and Binding Selectivity and Stereoselectivity of Siderophore-Iron Outer Membrane Transporters*. London, GB: Elsevier (2012). p. 37–66. doi: 10.1016/B978-0-12-394390-3.00002-1
121. Koebnik R, Locher KP, Van Gelder P. Structure and Function of Bacterial Outer Membrane Proteins: Barrels in a Nutshell. *Mol Microbiol* (2000) 37:239–53. doi: 10.1046/j.1365-2958.2000.01983.x
122. Prado LC da S, Giacchetto Felice A, Rodrigues TCV, Tiwari S, Andrade BS, Kato RB, et al. New Putative Therapeutic Targets Against Serratia Marcescens Using Reverse Vaccinology and Subtractive Genomics. *J Biomolec Struct Dynam* (2021) 30:1–16. doi: 10.1080/07391102.2021.1942211
123. Leow CY, Kazi A, Ismail CMKH, Chuah C, Lim BH, Leow CH, et al. Reverse Vaccinology Approach for the Identification and Characterization of Outer Membrane Proteins of Shigella Flexneri as Potential Cellular-and Antibody-Dependent Vaccine Candidates. *Clin Exp Vaccine Res* (2020) 9:15–25. doi: 10.7774/cevr.2020.9.1.15
124. Shey RA, Ghogomu SM, Esoh KK, Nebangwa ND, Shintouo CM, Nongley NF, et al. *In-Silico* Design of a Multi-Epitope Vaccine Candidate Against Onchocerciasis and Related Filarial Diseases. *Sci Rep* (2019) 9:1–18. doi: 10.1038/s41598-019-40833-x
125. Barchiesi J, Castelli ME, di Venanzio G, Colombo MI, García Véscovi E. The PhoP/PhoQ System and Its Role in Serratia Marcescens Pathogenesis. *J Bacteriol* (2012) 194:2949–61. doi: 10.1128/JB.06820-11
126. Fedrigo G v, Campoy EM, di Venanzio G, Colombo MI, García Véscovi E. Serratia Marcescens Is Able to Survive and Proliferate in Autophagic-Like Vacuoles Inside Non-Phagocytic Cells. *PloS One* (2011) 6:e24054. doi: 10.1371/journal.pone.0024054
127. Hertle R, Schwarz H. Serratia Marcescens Internalization and Replication in Human Bladder Epithelial Cells. *BMC Infect Dis* (2004) 4:16. doi: 10.1186/1471-2334-4-16
128. Xiong Q, Yang M, Li P, Wu C. Bacteria Exploit Autophagy For Their Own Benefit. *Infect Drug Resist* (2019) 12:3205–15. doi: 10.2147/IDR.S220376
129. Ozawa Y, Suda T, Nagata T, Hashimoto D, Nakamura Y, Enomoto N, et al. Mucosal Vaccine Using CTL Epitope-Pulsed Dendritic Cell Confers Protection for Intracellular Pathogen. *Am J Respir Cell Mol Biol* (2009) 41:440–8. doi: 10.1165/rcmb.2008-0446OC
130. Kaufmann SHE. Recent Findings in Immunology Give Tuberculosis Vaccines a New Boost. *Trends Immunol* (2005) 26:660–7. doi: 10.1016/j.it.2005.09.012
131. Nain Z, Karim MM, Sen MK, Adhikari UK. Structural Basis and Designing of Peptide Vaccine Using PE-PGRS Family Protein of Mycobacterium

Ulcerans—An Integrated Vaccinomics Approach. *Mol Immunol* (2020) 120:146–63. doi: 10.1016/j.molimm.2020.02.009
132. Chaudhri G, Quah BJ, Wang Y, Tan AHY, Zhou J, Karupiah G, et al. T Cell Receptor Sharing by Cytotoxic T Lymphocytes Facilitates Efficient Virus Control. *Proc Natl Acad Sci* (2009) 106:14984–9. doi: 10.1073/pnas.0906554106
133. Shi J, Zhang J, Li S, Sun J, Teng Y, Wu M, et al. Epitope-Based Vaccine Target Screening Against Highly Pathogenic MERS-CoV: An *In Silico* Approach Applied to Emerging Infectious Diseases. *PloS One* (2015) 10:1–16. doi: 10.1371/journal.pone.0144475
134. Azim KF, Hasan M, Hossain MN, Somana SR, Hoque SF, Bappy MNI, et al. *Immunoinformatics Approaches for Designing a Novel Multi Epitope Peptide Vaccine Against Human Norovirus (Norwalk Virus)*. Elsevier B.V (2019). p. 103936. doi: 10.1016/j.meegid.2019.103936
135. Ghaffari-Nazari H, Tavakkol-Afshari J, Jaafari MR, Tahaghoghi-Hajghorbani S, Masoumi E, Jalali SA. Improving Multi-Epitope Long Peptide Vaccine Potency by Using a Strategy That Enhances CD4+ T Help in BALB/c Mice. *PloS One* (2015) 10:1–12. doi: 10.1371/journal.pone.0142563
136. Hajighahramani N, Nezafat N, Eslami M, Negahdaripour M, Rahmatabadi SS, Ghasemi Y. Immunoinformatics Analysis and *In Silico* Designing of a Novel Multi-Epitope Peptide Vaccine Against Staphylococcus Aureus. *Infect Genet Evol* (2017) 48:83–94. doi: 10.1016/j.meegid.2016.12.010
137. Chen Z, Zhu Y, Sha T, Li Z, Li Y, Zhang F, et al. Design of a New Multi-Epitope Vaccine Against Brucella Based on T and B Cell Epitopes. *Epidemiol Infect* (2021) 149:E136. doi: 10.1017/S0950268821001229
138. Chukwudozie OS, Gray CM, Fagbayi TA, Chukwuanukwu RC, Oyebanji VO, Bankole TT, et al. Immuno-Informatics Design of a Multimeric Epitope Peptide Based Vaccine Targeting SARS-CoV-2 Spike Glycoprotein. *PloS One* (2021) 16:1–25. doi: 10.1371/journal.pone.0248061
139. Couto J, Seixas G, Stutzer C, Olivier NA, Maritz-Olivier C, Antunes S, et al. Probing the Rhipicephalus Bursa Sialomes in Potential Anti-Tick Vaccine Candidates: A Reverse Vaccinology Approach. *Biomedicines* (2021) 9:1–18. doi: 10.3390/biomedicines9040363
140. Majid M, Andleeb S. Designing a Multi-Epitopic Vaccine Against the Enterotoxigenic Bacteroides Fragilis Based on Immunoinformatics Approach. *Sci Rep* (2019) 9:1–15. doi: 10.1038/s41598-019-55613-w
141. Alom MW, Shehab MN, Sujon KM, Akter F. Exploring E, NS3, and NS5 Proteins to Design a Novel Multi-Epitope Vaccine Candidate Against West Nile Virus: An *In-Silico* Approach. *Inf Med Unlocked* (2021) 25:100644. doi: 10.1016/j.imu.2021.100644
142. Toussi DN, Massari P. Immune Adjuvant Effect of Molecularly-Defined Toll-Like Receptor Ligands. *Vaccines* (2014) 2:323–53. doi: 10.3390/vaccines2020323
143. Palatnik-de-Sousa CB, Soares I da S, Rosa DS. Editorial: Epitope Discovery and Synthetic Vaccine Design. *Front Immunol* (2018) 9:826. doi: 10.3389/fimmu.2018.00826
144. Rahman MS, Hoque MN, Islam MR, Akter S, Ul Alam ASMR, Siddique MA, et al. Epitope-Based Chimeric Peptide Vaccine Design Against S, M and E Proteins of SARS-CoV-2, the Etiologic Agent of COVID-19 Pandemic: An in Silico Approach. *PeerJ* (2020) 8:e9572. doi: 10.7717/peerj.9572
145. Obaidullah AJ, Alanazi MM, Alsaif NA, Albassam H, Almehizia AA, Alqahtani AM, et al. Immunoinformatics-Guided Design of a Multi-Epitope Vaccine Based on the Structural Proteins of Severe Acute Respiratory Syndrome Coronavirus 2. *RSC Adv* (2021) 11:18103–21. doi: 10.1039/d1ra02885e

Conflict of Interest: The authors declare that the research was conducted in the absence of any commercial or financial relationships that could be construed as a potential conflict of interest.

Publisher's Note: All claims expressed in this article are solely those of the authors and do not necessarily represent those of their affiliated organizations, or those of the publisher, the editors and the reviewers. Any product that may be evaluated in this article, or claim that may be made by its manufacturer, is not guaranteed or endorsed by the publisher.

Advantages of publishing in Frontiers

OPEN ACCESS
Articles are free to read for greatest visibility and readership

FAST PUBLICATION
Around 90 days from submission to decision

HIGH QUALITY PEER-REVIEW
Rigorous, collaborative, and constructive peer-review

TRANSPARENT PEER-REVIEW
Editors and reviewers acknowledged by name on published articles

Frontiers
Avenue du Tribunal-Fédéral 34
1005 Lausanne | Switzerland

Visit us: www.frontiersin.org
Contact us: frontiersin.org/about/contact

REPRODUCIBILITY OF RESEARCH
Support open data and methods to enhance research reproducibility

DIGITAL PUBLISHING
Articles designed for optimal readership across devices

FOLLOW US
@frontiersin

IMPACT METRICS
Advanced article metrics track visibility across digital media

EXTENSIVE PROMOTION
Marketing and promotion of impactful research

LOOP RESEARCH NETWORK
Our network increases your article's readership